THE UNIVERSITY *of* EDINBURGH

This thesis has been submitted in fulfilment of the requirements for a postgraduate degree (e. g. PhD, MPhil, DClinPsychol) at the University of Edinburgh. Please note the following terms and conditions of use:

- This work is protected by copyright and other intellectual property rights, which are retained by the thesis author, unless otherwise stated.
- A copy can be downloaded for personal non-commercial research or study, without prior permission or charge.
- This thesis cannot be reproduced or quoted extensively from without first obtaining permission in writing from the author.
- The content must not be changed in any way or sold commercially in any format or medium without the formal permission of the author.
- When referring to this work, full bibliographic details including the author, title, awarding institution and date of the thesis must be given.

In vivo investigation of component-specific functions of the Hippo pathway

Susanna Elizabeth Riley (BA, MScR)

A thesis submitted for the degree of

Doctor of Philosophy

October 2023

School of Clinical Sciences

College of Medicine and Veterinary Medicine

University of Edinburgh

Table of Contents

LIST OF TABLES 5

LIST OF FIGURES 6

ABSTRACTS 9

Scientific Abstract **9**

Lay Abstract **10**

ACKNOWLEDGEMENTS 11

DECLARATION 12

ABBREVIATIONS AND ACRONYMS 13

1 INTRODUCTION 14

1.1 The Hippo pathway **14**

1.2 Studying the Hippo pathway *in vivo* **16**

1.3 The Hippo pathway and zebrafish development **18**

1.4 Regeneration and the Hippo pathway **21**

1.5 The Hippo pathway in immunity **21**

1.6 Yap1 and Taz: differences and similarities in function **23**

1.7 CRISPR/Cas9 genome editing technology **26**

1.8 Summary **28**

1.9 Hypothesis and aims **28**

1.9.1 Hypothesis 28

1.9.2 Aims 28

2 MATERIALS AND METHODS 30

2.1 CRISPant generation **30**

2.2 Stable mutant generation **33**

2.3 DNA sequencing **34**

2.3.1 gDNA sequencing of F2 fish 34

2.3.2 cDNA sequencing 35

2.3.3 Homozygous fish screening 35

2.4 *ctgfa*:GFP reporter transgenic generation **36**

2.5 gDNA extraction **36**

2.6 Restriction enzyme analysis of CRISPR guide efficiency **37**

2.7 RNA extraction **37**

2.7.1 Method ‘a’ 37

2.7.2 Method ‘b’ 38

2.7.3 Method ‘c’ (for RNAseq analysis) 38

2.8 cDNA preparation **39**

2.9 RT-qPCR 39
2.10 Western blotting/PhosTag 39
2.10.1 Sample preparation 39
2.10.2 Blotting protocol 40
2.10.3 Western blot quantification 41
2.11 96hpf imaging and quantification 41
2.12 Tail fin regeneration and quantification 42
2.12.1 Tail fin regeneration measurements in the CRISPR/Cas9 screen 42
2.12.2 Tail fin regeneration measurements for in depth tracking 42
2.13 Neuromast regeneration and imaging 43
2.14 Juvenile zebrafish imaging and quantification 43
2.15 Immunofluorescence 44
2.16 HCR RNA-FISH imaging 45
2.17 Confocal imaging 46
2.17.1 Live imaging (single timepoint) 46
2.17.2 Live imaging (timelapse) 46
2.17.3 Fixed imaging (unstained) 47
2.17.4 Opera imaging 47
2.18 RNA sequencing analysis 47
2.18.1 Sample collection and sequencing (severe injury only) 47
2.18.2 Sample processing 48
2.18.3 Analysis 49
2.19 General zebrafish husbandry and analysis 50
2.20 Quantification and statistics 51
2.21 Use of Artificial Intelligence 51
2.22 Materials 53
3 CHAPTER 1: A CRISPR/CAS9 SCREEN TARGETING HIPPO PATHWAY COMPONENTS IN ZEBRAFISH EMBRYOS IDENTIFIES COMPONENT-SPECIFIC DEVELOPMENTAL AND REGENERATIVE PHENOTYPES 56
3.1 Optimisation of CRISPR/Cas9 mutagenesis mix generation 56
3.1.1 Microinjection mix generation is optimal at room temperature 56
3.1.2 The ideal microinjection mix volume is 2nl per embryo 58
3.2 Validation of successful CRISPR/Cas9 mutagenesis using *yap1* CRISPants 58
3.2.1 *yap1* CRISPR/Cas9 guide RNAs had high DNA mutagenesis efficiency 58
3.2.2 RT-qPCR during zebrafish embryo development was possible and showed specific patterns in mRNA expression 60

3.2.3 Optimisation of Western and PhosTag blotting of zebrafish embryos showed effective CRISPR mutagenesis 64
3.2.4 Optimisation of developmental and regenerative CRISPR/Cas9 screen assays 67
3.2.5 *tp53* CRISPants are not an appropriate negative control for the CRISPR/Cas9 screen 82
3.3 Summary of a CRISPR/Cas9 screen to identify developmental and regenerative phenotypes 85
3.4 Design and testing of highly efficient CRISPR/Cas9 guides 85
3.5 Developmental phenotypes of 13 Hippo pathway-associated CRISPants 90
3.5.1 Embryonic development phenotypes in CRISPants had a general pattern of developmental disruption 90
3.5.2 Juvenile developmental phenotypes in *yap1* and *wwtr1* CRISPants were limited 95
3.6 Regenerative phenotypes of 13 Hippo pathway-associated CRISPants 95
3.6.1 Neuromast development and regeneration 95
3.6.2 Tail fin development and regeneration 101
3.7 Summary and comparison of screen parameters 106
4 CHAPTER 2: GENERATION AND CHARACTERISATION OF TRANSGENIC AND STABLE MUTANT ZEBRAFISH LINES 111
4.1 *ctgfa*:GFP reporter fish as a readout of Yap1 and Taz activity during tail fin regeneration 111
4.2 Stable *yap1* and *wwtr1* mutants mostly, but not completely, phenocopy *yap1* and *wwtr1* CRISPants 117
4.2.1 Mutations induced by CRISPR/Cas9 injection 117
4.2.2 Adult survival of homozygous mutants 119
4.2.3 Embryonic developmental phenotypes of homozygous mutants 119
4.2.4 Embryonic regenerative phenotypes of homozygous mutants 123
5 CHAPTER 3: INVESTIGATION OF *YAP1* AND *WWTR1* CRISPANT TAIL FIN REGENERATION PHENOTYPES 129
5.1 Differences in *yap1* and *wwtr1* CRISPant tail fin regeneration phenotypes 129
5.2 Transcriptome changes upon early mild tail fin injury 131
5.3 Severe tail fin injury and CRISPR mutagenesis alters the transcriptome 137
5.3.1 Overview of gene expression changes after injury 137
5.3.2 GO term analysis after severe tail fin injury 141
5.3.3 Transcriptomic changes in uninjured fish 142
5.3.4 Transcriptomic changes in injured fish 145
5.3.5 Direct comparison of genotypes upon injury 151
5.3.6 Changes in the Hippo signalling pathway upon mutagenesis and injury 157
5.3.7 Changes in the Wnt signalling pathway upon *yap1* mutagenesis 160
5.4 *yap1* and *wwtr1* mRNA expression at baseline in the larval tail fin 162

5.5 *yap1* and *wwtr1* CRISPR mutagenesis affects *yap1* and *wwtr1* mRNA abundance during regeneration but does not have any clear localisation patterns 166
5.6 *yap1* and *wwtr1* mRNA localisation in a *ctgfa*:GFP transgenic after injury showed slight mutagenesis-induced changes 169
5.7 Abundance and localisation of blastema markers at 48 hours post injury is unchanged in CRISPants 172
5.8 CRISPants have reduced proliferation in the tail fin 176
5.9 Immune cells during development 178
5.10 RNAseq analysis of immune markers after tail fin injury 184
5.11 Neutrophils during tail fin regeneration 187
5.12 Macrophages during tail fin regeneration 193
6 DISCUSSION 198
6.1 Flexibility, utility, and limitations of CRISPR/Cas9 mutagenesis in the embryonic zebrafish to study development and regeneration 198
6.1.1 Optimisation of a CRISPR/Cas9 zebrafish screen 198
6.1.2 A CRISPR/Cas9 screen of Hippo pathway components showed a range of phenotypes that inform knowledge on Hippo pathway function in development and regeneration 200
6.1.3 Limitations of the CRISPR/Cas9 screen 203
6.1.4 Comparison of CRISPant and stable mutant phenotypes 204
6.2 The role of Taz in embryonic zebrafish 205
6.2.1 *wwtr1* CRISPR-mediated disruption caused specific defects in severe tail fin injury regeneration 205
6.2.2 Future elucidation of a cell intrinsic versus cell extrinsic role of Taz 207
6.2.3 Yap1 and Taz cannot be considered to be one entity as they have differing functions in the embryonic zebrafish 208
6.3 Hippo pathway function in innate immune cell dynamics 209
6.4 Comparing mild and severe tail fin injury paradigms 211
6.5 Linking the Hippo pathway's role in regeneration and cancer: potential therapeutic insights 213
7 BIBLIOGRAPHY 215
8 APPENDIX 231

List of Tables

Table 2.1: CRISPR/Cas9 guide RNA sequences.....31
Table 2.2: CRISPR/Cas9 guide RNA analysis primers.....32
Table 2.3: Microinjection mix concentrations.....33
Table 2.4: gDNA sequencing primers.....35
Table 2.5: cDNA sequencing primers.....35
Table 2.6: Restriction enzymes used and parameters for guide RNA efficiency analysis.....38
Table 2.7: RT-qPCR primer sequences.....40
Table 2.8: HCR RNA-FISH targets and amplifiers.....45
Table 2.9: Number of clusters passing quality filters per library.....48
Table 2.10: Hippo gene signature used in RNAseq analysis.....50
Table 5.1: Differentially expressed genes when compared between WT and CRISPants.....154
Table 5.2: Differentially expressed immune-associated genes when compared between WT and CRISPants.....185

List of Figures

Figure 1.1: The Hippo pathway signalling cascade 16
Figure 1.2: Human and zebrafish Hippo pathway orthology comparisons show a high degree of similarity 19
Figure 2.1: T7E1 and RE digest overview 30
Figure 2.2: Overview of stable mutant generation 34
Figure 2.3: Summary of *ctgfa*:GFP transgenic line generation 37
Figure 2.4: Tail fin measurements used in the CRISPR/Cas9 screen 43
Figure 2.5: Tail fin measurements used in detailed tracking of tail fin regeneration 44
Figure 2.6: Areas used for quantification of immunofluorescence staining and immune cells 44
Figure 3.1: Optimisation of microinjection mix generation temperature 57
Figure 3.2: Optimisation of microinjection mix volume 59
Figure 3.3: *yap1* CRISPR guide testing 60
Figure 3.4: RT-qPCR of selected Hippo pathway-associated genes across early development and upon mutagenesis 63
Figure 3.5: Optimisation of Western blotting and PhosTag electrophoresis in zebrafish embryos and verification of CRISPR mutagenesis 66
Figure 3.6: Developmental timing in *yap1* CRISPants at 6hpf and 96hpf 68
Figure 3.7: Developmental defects in *yap1* CRISPants at 96hpf 72
Figure 3.8: Differences in *yap1* CRISPant phenotype severity 73
Figure 3.9: Developmental phenotypes in *yap1* CRISPants at 1 month post fertilisation 75
Figure 3.10: *yap1* CRISPant tail fin development and regeneration 77
Figure 3.11: *yap1* CRISPant neuromast development and regeneration 80
Figure 3.12: *tp53* CRISPants as a negative control 84
Figure 3.13: Overview of the optimised CRISPR/Cas9 screen 85
Figure 3.14: Restriction enzyme digestion of CRISPR guides targeting Hippo pathway components 89
Figure 3.15: Embryonic development phenotypes of Hippo pathway-associated CRISPants 91
Figure 3.16: Juvenile development phenotypes of *yap1* and *wwtr1* CRISPants 96

Figure 3.17: Neuromast regeneration phenotypes of Hippo pathway-associated CRISPants 100
Figure 3.18: Tail fin regeneration phenotypes of Hippo pathway-associated CRISPants 105
Figure 3.19: Plots of average developmental and regenerative phenotypes of Hippo pathway-associated CRISPants 108
Figure 4.1: *ctgfa*:GFP signal in uninjured WT and CRISPant embryos 113
Figure 4.2: *ctgfa*:GFP signal after mild tail fin injury in WT and CRISPant embryos 115
Figure 4.3: *ctgfa*:GFP signal after severe tail fin injury in WT and CRISPant embryos 116
Figure 4.4: Sequencing of a F1 *yap1* stable mutant line 119
Figure 4.5: Sequencing of a F1 *wwtr1* stable mutant line 121
Figure 4.6: Proportion of stable mutant line genotypes 121
Figure 4.7: 96hpf phenotypes of stable mutants and CRISPants 123
Figure 4.8: Neuromast regeneration phenotypes in stable mutants and CRISPants 126
Figure 4.9: Tail fin regeneration phenotypes in stable mutants and CRISPants 128
Figure 5.1: Regeneration after mild tail fin injury is impaired in *yap1* but not *wwtr1* CRISPants 131
Figure 5.2: Regeneration after severe tail fin injury is impaired in *yap1* CRISPants from 6hpi and *wwtr1* CRISPants at 48hpi 133
Figure 5.3: Bulk RNAseq data in WT fish after mild tail fin injury 135
Figure 5.4: Overview of bulk RNAseq data after severe tail fin injury 140
Figure 5.5: GO term analysis after severe tail fin injury 142
Figure 5.6: Transcriptomic changes in uninjured CRISPant embryos 148
Figure 5.7: Transcriptomic changes in CRISPant embryos following severe tail fin injury 151
Figure 5.8: Comparison of differentially expressed genes after injury between WT and CRISPants 152
Figure 5.9: Alterations in Hippo gene signature after mutagenesis and after severe tail fin injury 159
Figure 5.10: Wnt signalling is altered in uninjured *yap1* CRISPants 161
Figure 5.11: *yap1* and *wwtr1* CRISPR mutagenesis has limited impacts on *yap1* and *wwtr1* mRNA fluorescence during embryonic development 164
Figure 5.12: Specific reductions in *yap1* and *wwtr1* mRNA in CRISPants during severe tail fin regeneration 168

Figure 5.13: Labelling of endogenous GFP signal can be quantified and colocalised with other markers, showing mutagenesis-induced changes 171
Figure 5.14: Abundance and localisation of blastema markers following severe injury showed no obvious malformations 174
Figure 5.15: Reduced proliferation in the tail fin at baseline and after severe injury 178
Figure 5.16: Macrophage and neutrophil characteristics in the developing WT and CRISPant embryo 180
Figure 5.17: RNAseq analysis of immune markers after tail fin injury 184
Figure 5.18: Neutrophil infiltration following tail fin injury 190
Figure 5.19: Macrophage infiltration following tail fin injury.....193
Figure 5.20: Macrophage subtypes are altered after severe tail fin injury 196

Abstracts

Scientific Abstract

The Hippo pathway is a kinase signalling cascade involved in the regulation of organ size, tissue homeostasis, and stem cell proliferation. Dysfunction of this pathway is associated with carcinogenesis, fibrosis, and defects in development and regeneration. The key effectors of the Hippo pathway are YAP and TAZ, which translocate to the nucleus, bind to transcription factors, and induce transcription when Hippo signalling is off. The wide-ranging role of the Hippo pathway means that it must be strictly regulated, and so context-dependent molecular understanding is needed for it to be manipulated therapeutically. However, the function of individual components of the pathway is not well understood, and a direct comparison of the different roles of Hippo pathway components has so far mainly been carried out *in vitro*.

To study these functions *in vivo*, a range of zebrafish Hippo pathway CRISPR mutants (CRISPants) were generated and analysed as part of a medium-throughput screen to identify regenerative and developmental phenotypes. Many developmental phenotypes were identified and quantified that match those reported in previous publications, as well as multiple novel findings. Neuromast and tail fin regeneration phenotypes were also identified. Notable phenotypes include differences between *yap1* and *wwtr1* CRISPants, and a selective reduction in severe tail fin regeneration in *wwtr1* CRISPants but no consistent phenotype in any other developmental or regenerative parameter.

Preliminary analysis of molecular and cellular drivers of this tail fin regeneration was performed, including the analysis of RNAseq data, immunofluorescence labelling of both proteins and mRNA, and live imaging of multiple transgenic lines after tail fin injury. These enabled a separation of *yap1* and *wwtr1* CRISPant phenotypes at a molecular and cellular level. The generation and characterisation of a *ctgfa*:GFP reporter transgenic line and Yap1 and Taz stable mutant lines are also reported.

Overall, the project provides insights into Hippo component-specific regulation of development and regeneration in both teleosts and mammals.

Lay Abstract

Roughly 330 billion times every day, one cell in the human body will turn into two, known as cell proliferation to allow the body to maintain normal function. After injury, the same cells can proliferate at a much higher rate to replace their dead or damaged neighbours. This leads to tissue regeneration, such as the regrowth of skin after a cut. However, proliferation can also be too high. If mutations in the proteins that regulate proliferation occur, it becomes uncontrolled, potentially resulting in a tumour.

This link between regeneration and cancer is a big hurdle in the development of both cancer treatments and regenerative therapies. Chemotherapy drugs target highly proliferating cells, so, as well as killing cancer cells, it also destroys regenerating cells. These include cells in the hair follicle, causing hair loss, and immune cells, increasing the risk of infection. Conversely, regeneration-promoting treatments such as stem cell therapy are limited by the risk of tumour-promoting side effects. This report focusses on a group of proteins linked to these processes, collectively known as the Hippo pathway. These proteins are present in most organisms, where they regulate how often cells grow in response to outside stimuli. In fact, reduced activity of some of these proteins has been associated with both increased regeneration and increased incidence of certain cancers.

In this project I closely focussed on these proteins using zebrafish and the gene editing technique CRISPR. This allowed me to change the function of many different proteins within the Hippo pathway group and measure the results. Zebrafish are a useful model to study this because, as well as getting cancer, they can regenerate to a much greater extent than mammals, making regeneration of everything from skin to spine easy to study. It was discovered that disrupting individual Hippo proteins gives specific defects, including differences in the activity of immune cells in response to injury. This suggests that each Hippo pathway protein may have a unique role in cell function and so may impact on regeneration and cancer in different ways. Therefore, targeted treatments that alter the activity of some Hippo proteins but not others may allow us to create better and kinder cancer treatments that don’t alter regeneration, and vice versa.

Acknowledgements

Scientific research is a fundamentally collaborative endeavour, and my project has been no different. I have been lucky enough to learn from many people during my PhD, both personally and scientifically, and I would like to begin to thank some of them here. First of all, I would like to thank my supervisors Dr Carsten Gram Hansen and Dr Yi Feng. Their guidance throughout my project has been vital for its success. I also want to thank all past and present members of the Hansen and Feng groups for their insight, particularly Dr Richard Cunningham, Michaela Nosková, and Shijia Xia for their practical help.

Guidance from my thesis committee has been invaluable, thank you Prof Julia Dorin and Dr James Minchin for our interesting discussions. Further, my work has been made much easier by many technicians and administrators, so thank you Dr Carl Tucker, Kelly Douglas, Dr Marieke Hoeve, Dr Rolly Wiegand, Dr Justyna Cholewa-Waclaw, and all the zebrafish facility technicians.

I am so grateful for an amazing group of family and friends. Thank you to my family, for instilling in me a fascination with science that has propelled through my whole academic career but also giving me reality checks when they were much needed.

The past 16 years have been immeasurably improved by Gina's stalwart friendship. Although hundreds of miles often separate us, their voice down the phone is always a joy to hear. Thank you for the years of "such fun".

And because organised fun is sometimes the best kind, I would like to thank Matt M. and Brennan for introducing me to a new hobby that has given me hundreds of hours of enjoyment. And thanks to Evelyn, Eimear, Matt S., Olly, and Ana for indulging me with this, it has been a brilliant distraction.

And finally, thank you Eoin for being my greatest supporter. So much of what I have accomplished would not have been possible without you.

Declaration

I declare that this thesis has been written by me and not submitted for any other degree or qualification. The experimental work described within is my own work, with collaborative contributions from others clearly acknowledged at the appropriate points. I declare that all due references have been provided for supporting literature and resources. Parts of the introduction refer to my published literature review, where I am the first author and wrote the manuscript, apart from small edits from the other authors. This review is inserted at the end of this thesis as an appendix.

Abbreviations and Acronyms

Abbreviation/Acronym	Meaning
BMP	Bone Morphogenetic Protein
bp	Base pairs
Cas	CRISPR-associated
CHT	Caudal haematopoietic tissue
CRISPant	CRISPR-mutagenised fish
CRISPR	Clustered Regularly Interspaced Short Palindromic Repeats
DE	Differentially expressed
dpf	Days post fertilisation
ECM	Extracellular matrix
EMT	Epithelial-mesenchymal transition
F0	Founder generation (CRISPants)
Fgf	Fibroblast growth factor
FW	Forward
gDNA	Genomic DNA
GO	Gene ontology
gRNA	Guide RNA
hpf	Hours post fertilisation
hpi	Hours post injury
IF	Immunofluorescence
IFN	Interferon
KO	Knock-out
mpf	Months post fertilisation
PAGE	Polyacrylamide gel electrophoresis
pH3	Phosphohistone H3
PTU	N-phenylthiourea
RE	Restriction enzyme
REV	Reverse
ROS	Reactive oxygen species
RT	Room temperature
SB	Swim bladder
SNP	Single nucleotide polymorphisms
Taz	Transcriptional coactivator with PDZ-binding motif
TLR	Toll-like receptor
TNFα	Tumour necrosis factor alpha
T7E1	T7 Endonuclease I
WT	Wild-type
wwtr1	WW domain containing transcription regulator 1 (gene encoding Taz)
Yap1	Yes-associated protein

1 Introduction

1.1 The Hippo pathway

The development and function of all animals requires extensive but appropriate tissue growth. The mechanisms that control this growth are not fully elucidated, including how cells "know" when to start and stop dividing during development and how they sense and respond to injury. The first evidence that an organ may possess intrinsic mechanisms to determine its size was provided in 1931. Limb transplantation studies in salamanders showed that transplantation of embryonic leg tissues between salamander species with different leg sizes resulted in legs the size of the donor species rather than the recipient[1]. Similarly, also in 1931, a surgically resected rat liver was observed to regrow within one week, but stopped when it reached its original size[2]. These suggested that the cells within a tissue must communicate to coordinate its growth, and so investigation into the processes underlying this began.

One signalling pathway associated with organ growth is the Hippo pathway. This was first identified as having a role in growth control using genetic screens of the fruit fly *Drosophila melanogaster*[3–5]. In fact, the Hippo pathway is so named as *Drosophila* mutants for a key upstream kinase (*Hpo*) had a tissue overgrowth phenotype where the head resembled hippopotamus hide[6]. The overgrowth was due to mutant cells having defects in regulation of both cell proliferation and apoptosis: cells proliferated at a higher rate, failed to stop proliferating once the tissue had reached a normal size, and were resistant to pro-apoptotic signals (reviewed in[3,7,8]). A similar response was seen after mutation of another kinase *Wts*, which forms a signalling module with Hpo and the scaffolding protein Sav to regulate organ size (reviewed in[3,7,8]). Investigation into other Wts binding partners identified Yki as a protein inactivated by Wts[5]. Yki was required for normal tissue development, and its overexpression phenocopied loss of function mutations in *Hpo* or *Wts*[5].

Further studies identified the Hippo pathway in both *Drosophila* and mammals, the core components of which form a serine/threonine kinase phosphorylation cascade (Figure 1.1). In contrast to many other well-known signalling pathways, the Hippo pathway does not respond to a dedicated signalling molecule or receptor. Instead, the pathway responds to a range of inputs. These include cell shape, metabolism, extracellular matrix (ECM) components

and mechanical properties, G-protein coupled receptor ligands, and more[9–17]. When the Hippo pathway is “on”, the integration of these inputs results in the activation of MST1/2 (Hpo orthologs), STK25, and MAP4K kinases, which activate LATS1/2 (Wts orthologs) kinases via phosphorylation[9,16,18–20]. These LATS1/2 kinases in turn phosphorylate YAP1 and TAZ (Yki orthologs), the core transcriptional co-activators of the Hippo pathway[9,12,19,21,22]. When phosphorylated, YAP1 and TAZ either undergo ubiquitin-mediated degradation or bind to protein 14-3-3, causing them to remain in the cytoplasm, and thus preventing transcription[9,12,21–23]. If these phosphorylations do not occur, i.e. when the Hippo pathway is “off”, YAP1 and TAZ can translocate to the nucleus, where they bind to TEAD1-4 transcription factors[9,24–27]. This promotes transcription of genes known to promote processes such as proliferation and dedifferentiation/stemness, including *CTGF* and *CYR61*[9,10,15,24–26,28–30].

Most work has focussed on the role of phosphorylation and ubiquitination post-translational modifications in Hippo pathway component regulation (reviewed elsewhere[31,32]) as described above. However, YAP function has been shown to also be regulated through other post-translational modifications, including sumoylation, methylation, and acetylation. For example, sumoylation of YAP after DNA damage by the promyelocytic protein results in YAP stabilisation and subsequent increased p73-dependent apoptosis[33]. Similarly, DNA damage results in YAP acetylation, which reduces YAP phosphorylation to promote its nuclear translocation[34]. YAP methylation has diverse effects on cell and YAP function, dependent on the methylated residue location and the methyltransferase acting on YAP. For example, methylation of lysine 494 by SETD7 following high cell-cell contact promotes YAP cytoplasmic retention[35]. Conversely, methylation of lysine 342 by SET1A in response to factors such as high glucose and Wnt signalling promotes YAP nuclear localisation by blocking its nuclear export[36]. The opposing effects of YAP methylation is also reflected in carcinogenesis. YAP methylation has been shown to both inhibit and promote breast cancer cell metastasis[37], and high levels of SET1A-mediated YAP methylation can predict poor prognosis in lung and colorectal cancers[36].

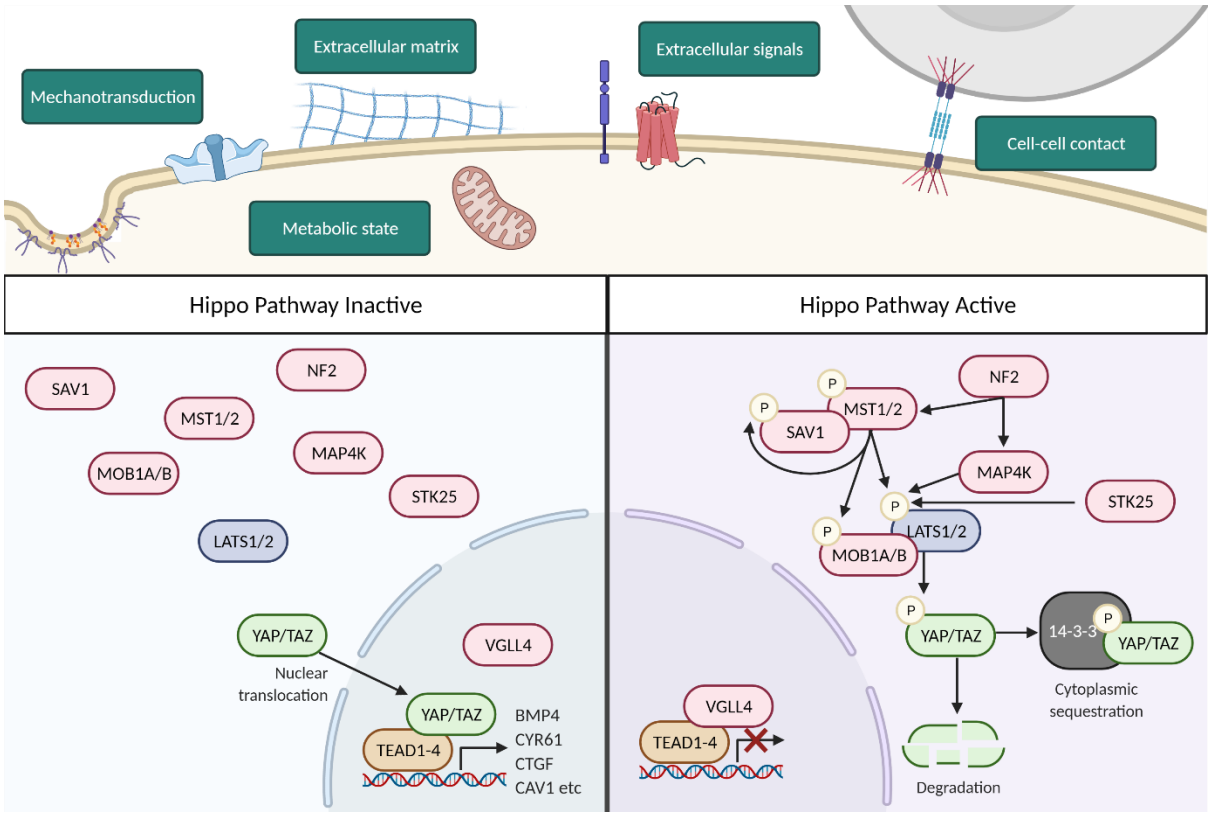

Figure 1.1: The Hippo pathway signalling cascade
Activation of the Hippo pathway by a range of stimuli triggers a phosphorylation cascade that leads to the phosphorylation of the Hippo pathway effectors YAP/TAZ. Phosphorylation of YAP/TAZ redistributes YAP/TAZ to the cytoplasm, preventing TEAD-mediated gene expression. Hippo pathway inactivation prevents YAP/TAZ phosphorylation, allowing their nuclear translocation and hence TEAD-mediated gene expression by activation of transcription. From Riley et. al., 2022[38].

1.2 Studying the Hippo pathway *in vivo*

Drosophila continues to be a powerful model system in which to study the Hippo pathway, regeneration, and development, due to their low cost, ease of culture and genetic modification, and large numbers of offspring. However, where many organisms have two distinct proteins YAP1 and TAZ, *Drosophila* only has one ortholog, Yki. This is also the case for other Hippo pathway components such as LATS1 and LATS2 (Wts). Therefore, in order to study the function of individual Hippo pathway components that are found in the human, many labs instead utilise gene editing approaches *in vitro* (for example in[18,39,40]) or have turned to the mouse as an *in vivo* model. However, *Yap1* knockout (KO) mice die by E8.5 with multiple severe developmental defects[41], and although *Wwtr1* (gene encoding Taz) KO mice are viable, they have high early mortality with pulmonary and kidney disease[42–45], so studying the impact of removing these proteins in the germline is difficult in the mouse.

However, cell- and tissue-specific Hippo pathway mouse mutants have proved powerful in investigations of Hippo pathway function in mammalian homeostasis, cancer, and regeneration[7,8,15,46–48]. One of the first organs studied in this regard was the murine liver. *Yap1* overexpression in the liver resulted in an organ with a large increase in cell number and so liver mass[49,50]. Interestingly, halting *Yap1* overexpression caused the liver to revert to a normal size, suggesting the activation of intrinsic size control mechanisms that were dysregulated following YAP1 activity manipulation[50]. A role for the Hippo pathway is also found in liver regeneration. After a range of liver injuries in humans and mice, YAP1 expression is enhanced in bile ducts and hepatocytes respectively[51,52]. Liver-specific *Yap1* deletion resulted in impaired liver regeneration following both partial hepatectomy and bile duct ligation, with decreased hepatocyte and bile duct cell proliferation and increased hepatocyte necrosis[51,53]. Interestingly, activation of YAP1/TAZ signalling by knockdown or pharmacological inhibition of MST1/MST2 promoted regeneration after both acute and chronic injury by enhancing hepatocyte proliferation[54,55]. These experiments all suggest a key role for YAP1 in promoting liver regeneration.

Another organ with development and regeneration potential impacted by the Hippo pathway is the murine heart. Deletion of *Yap1* in the embryonic heart gave cardiac defects and often early mortality[56,57]. In contrast, cardiac-specific *Wwtr1* deletion gave no cardiac developmental phenotypes, unless combined with a heterozygous deletion of *Yap1*[57]. Therefore, the effect of deleting *Yap1* on heart regeneration could not be investigated in full. However, YAP1/TAZ activation via expression of a constitutively active YAP1 or by conditional deletion of *Lats1/2* or *Sav1* promoted cardiac regeneration through enhanced cardiomyocyte proliferation or reactivation of embryonic signalling pathways[57–61], suggesting a key role for YAP1/TAZ signalling in promoting heart regeneration.

Intestine regeneration has also been associated with Hippo pathway signalling in model organisms. Mice with intestine-specific *Yap1* or *Yap1*/*Wwtr1* deletion show no change in intestine development or homeostasis[62,63]. The intestine usually has very high regenerative capacity, with designated intestinal stem cells that maintain homeostasis. In *Drosophila* midgut, the proliferation of these stem cells is normally suppressed by the inhibition of Yki via Hpo[64–66]. Inactivation of *Hpo* subsequently triggers intestinal stem cell proliferation[64–66]. Similarly, hyperactivation of *Yap1* in the mouse results in an enlargement of the intestinal

stem cell compartment, partly due to inhibition of differentiation[49,50,62]. Following injury of the murine intestine, YAP1 levels increase to far above homeostatic levels[62,67,68]. However, the function of YAP1 in regeneration is unclear. A mouse model of intestinal-specific *Yap1* deletion shows both inhibition[62] and promotion[68] of regeneration following two different injury paradigms (dextran sulphate sodium administration and irradiation respectively). The mechanism behind this discrepancy is unclear but may be due to the experimental setup and timepoints analysed. Another potential reason is the interaction of the Hippo pathway with the Wnt signalling pathway[46]. Following irradiation (which results in increased regeneration following *Yap1* deletion), Wnt target genes are upregulated[68], which is critical for intestinal regeneration[69,70]. YAP1 has been shown to transiently inactivate Wnt signalling in intestinal stem cells following injury[67], and so deletion of *Yap1* may promote Wnt signalling to enhance regeneration.

However, mouse experiments are expensive, lengthy, and often low-throughput. In addition, systemic therapies based on tissue-specific animal models may result in unexpected off-target effects. Some labs have, therefore, moved to using the zebrafish to study the function of the Hippo pathway. Of note, many human Hippo pathway genes have zebrafish orthologs with a high sequence similarity (Figure 1.2). Coupled with rapid external development, ease of genetic manipulation, conservation of genes underlying human disease, robust regeneration, and transparent juveniles[71], this highlights that the zebrafish may be an appropriate and powerful model to study the function of Hippo pathway genes. Some studies have begun to report on the effect of disrupting Hippo pathway function in the embryonic and adult zebrafish, particularly in development and regeneration, which is described below.

1.3 The Hippo pathway and zebrafish development

Hippo signalling dysregulation is associated with varied developmental defects in the zebrafish. General developmental defects include reduced survival in *yap1*, *wwtr1*, *sav1*, *stk3*, and *lats2*-disrupted embryos[72–76] and developmental delay in *yap1*, *wwtr1*, *amotl2*, *lats1*, and *lats2*-disrupted embryos[72,73,77–81]. Defects in organogenesis were observed, with incorrect heart looping in *yap1* and *wwtr1*-disrupted embryos[82]. Alterations in dorsoventral patterning in these embryos were also observed after disruption of the Yap1/Taz target genes *amotl2* and *cav-1α/β*[72,82–85]. Reduced size can also be seen (both overall length and for specific

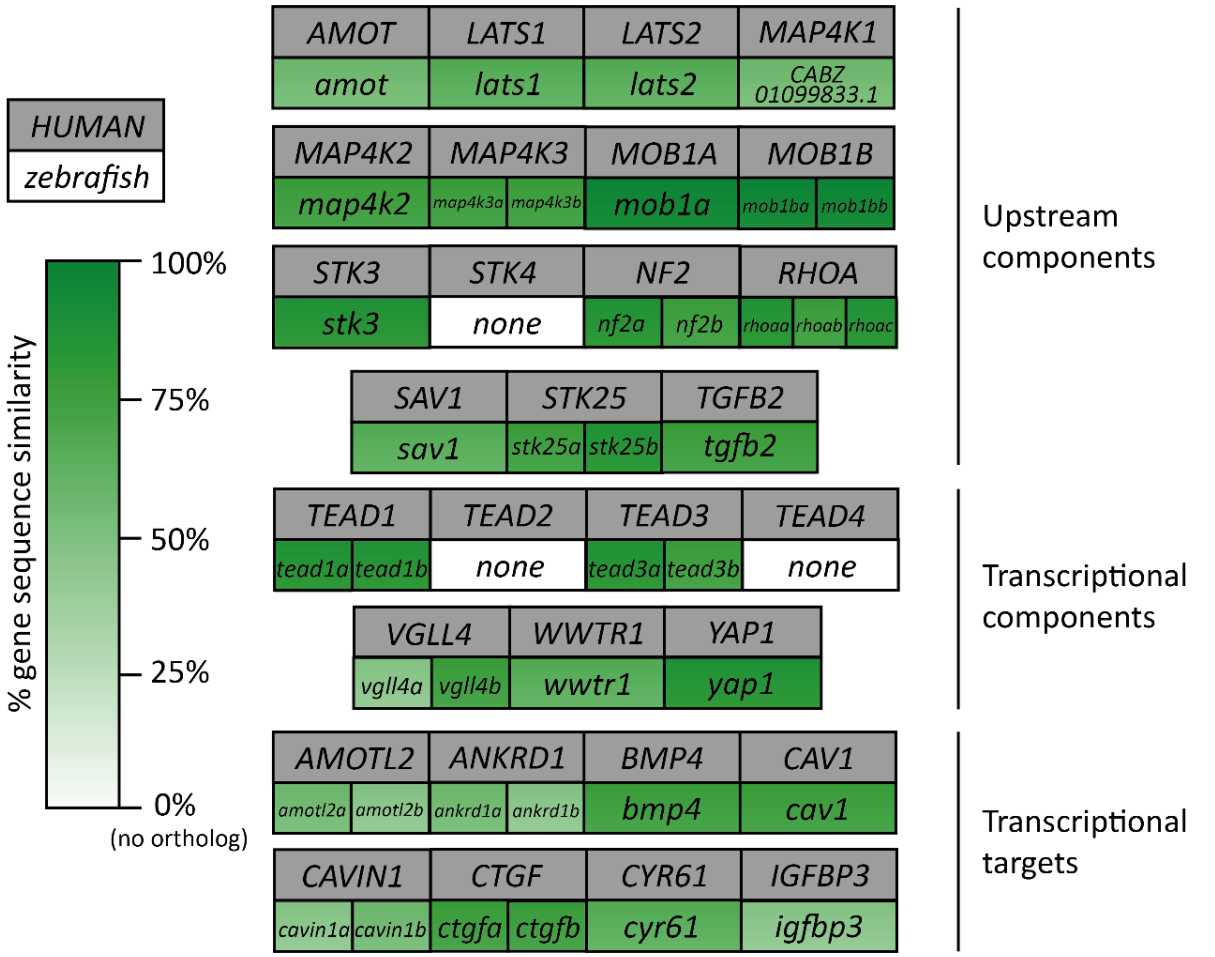

Figure 1.2: Human and zebrafish Hippo pathway orthology comparisons show a high degree of similarity

WWTR1 encodes TAZ, *STK4* encodes MST1 and *STK3* encodes MST2. *CYR61* is also known as *CCN1* and *CTGF* as *CCN2*. % gene sequence similarity identified using ensembl.org under orthology tab or manual BLAST comparison of genomic sequence (from GRCz11) if not present. From Riley et. al., 2022[38].

organs) in *yap1*, *wwtr1*, *cyr61*, *cav-1α/β*, *ctgfa*, *amotl2*, *mst2*, and *cavin-1*-disrupted embryos[72,77,83,85–95]. This size dysregulation is reported in other Hippo-disrupted organisms (e.g. mouse[49,50]), but the extent varies depending on the study, with some reporting no phenotype in Hippo pathway mutants[96–99].

Reduced embryonic length in the zebrafish is a characteristic of a deformed notochord[90,100,101]. The notochord is a rod-like support structure that reaches along the midline of the zebrafish embryo and is present in all members of the Chordata phylum. This structure has two key functions: a signalling centre to provide fate and locational information, and a structural support[101]. Cells within the notochord have a unique structure that aids in the mechanical function of the notochord – they are highly vacuolated and press against a stiff extracellular sheath. This creates a high amount of pressure within the notochord,

forming a stiff rod that can also bend in any direction as cells move over each other. The Hippo pathway is associated with notochord function, as *ctgf*, *yap1*, *wwtr1*, *cav-1*, and *cavin1*-disrupted embryos show notochord defects or are expressed in the notochord[85,86,93,95,102–105]. This Hippo pathway role may be linked to caveolae[29], mechanotransducive plasma membrane invaginations present at a very high density in the notochord[95], which provide a buffering capacity to the cell after mechanical stress[10]. This includes the mechanical stress within notochord cells after movement in the embryo, which causes notochord lesions when *cavin-1ƀ* is disrupted[95]. Caveolae are composed of Hippo-associated cavins (e.g. *cavin-1*) and caveolins (e.g. *cav-1*)[10,29]. Disruption of *yap1*/*wwtr1*, *cavin-1*, *cav-1*, and *cav-3* all result in a reduced caveolae density[29,86,103], further supporting a role for Hippo pathway activity in correct formation and function of this structure.

In agreement with a global role of the Hippo pathway in cell function, the central nervous system is often abnormal in Hippo-disrupted zebrafish embryos. This includes structural defects in the brain, such as neural ventricle defects in *cav-1α*/*ƀ*-disrupted embryos[90], reduced cerebrum development in *ctgf*-knockdown lines[88], defects in brain vascular development after *amotl2a* dysregulation[106], and reduced forebrain size in *nf2a* morphants[107]. Eye defects are also seen, including coloboma[97], reduced eye size or a lack of eyes[77,89,93,108], pigmentation defects[74,92], and an abnormal retinal pigmented epithelium. Some of these eye defects may be a result of altered biomechanical properties in the zebrafish eye, which has been shown to disrupt eye morphogenesis[109]. Others may be due to altered progenitor cell function, for example an inability of optic vesicle progenitors to adopt a retinal pigmented epithelium identity after Hippo pathway dysfunction[80,86,90,92,97].

Defects in the development of the cardiovascular system are also observed in Hippo pathway-disrupted zebrafish. One obvious phenotype seen in mutant embryos is a pericardial oedema, which has been reported in *yap1*, *wwtr1*, *cavin-1*, *cav-1α*, *sav1*, and *amotl2*-disrupted embryos[73,74,80,86,87,97,108,110–114]. The oedema can be a result of cardiac dysfunction[113,115], which is seen in the form of improper heart formation (including cardia bifida, incorrect heart looping, abnormal trabeculation, and defects in outflow tract valvulogenesis)[86,116–118] and abnormal vasculature sprouting, stabilisation, and maintenance[79,87,88,90,97,106,114,119–123]. This may be a result of cell defects in the Hippo pathway mutants, which includes cardiomyocyte, epicardial cell, endothelial cell, and haematopoietic stem and progenitor cell

dysfunction[79,88,98,118,124–126]. Some of this dysfunction may also result from changes in biomechanical signalling within the zebrafish heart, which has been associated with both Yap1 and Caveolin-1 signalling[126,127].

The Hippo pathway is also associated with the development of the lateral line, a mechanosensitive organ in amphibians consisting of small clusters of cells (neuromasts) along the head and trunk (posterior lateral line)[128]. Neuromasts contain hair cells with stereocilia projecting into the external water, allowing the detection of, and orientation in, currents and aiding feeding and social behaviour. Surrounding the hair cells are interdigitating supporting cells and mantle cells, and the whole structure is innervated by afferent sensory neurons[128]. The development of the lateral line has been associated with the Hippo pathway, as disruption of *yap1* and *cav-1α* is linked to a reduced number of neuromasts and, for *yap1*, a reduction in hair cell number specifically[77,86,99,129,130].

1.4 Regeneration and the Hippo pathway

The Hippo pathway has many functions in regeneration, including some published in the zebrafish. These studies mainly focus on the role of Yap1. Hippo pathway regeneration in the zebrafish is summarised in the published review article incorporated into this thesis in the Appendix (material from[38]: Riley, S.E., Feng, Y., and Hansen, C.G., Hippo-Yap/Taz signalling in zebrafish regeneration, *npj* Regenerative Medicine, published 2022 in partnership with Australian Regenerative Medicine Institute). This review concludes that Hippo pathway signalling, particularly via increases in Yap1 and Ctgfa activity, promotes regeneration in a range of contexts, including tail fin and lateral line regeneration. This role may be via sensing changes in the injury microenvironment, promoting proliferation, scar resolution, epithelial-to-mesenchymal transition, progenitor cell function, and crosstalk with a range of other signalling pathways, including Bmp, Wnt, and Fgf. However, the roles of many different Hippo pathway components, prior to this thesis, have not been carefully investigated.

1.5 The Hippo pathway in immunity

The immune system is often vital for tissue repair and regeneration. The inflammatory response must be tightly regulated, with the innate immune cell response being required for different types of regeneration, but prolonged inflammation also inhibiting regeneration[131].

This is seen in many animal models, including the zebrafish, and is regulated by a range of signalling pathways. One such pathway is the Hippo signalling pathway[132], although limited work has been published on this in the zebrafish. The Hippo pathway is both modulated by and modulates many of the key innate immune signalling pathways. This is reviewed elsewhere[132,133], and includes toll-like receptor (TLR), type I interferon (IFN), reactive oxygen species (ROS), NF-κB, and tumour necrosis factor alpha (TNFα) signalling. For example, MST1 promotes TLR3/4-linked IFN-β production through IRAK1 inhibition in macrophages[134], whilst TLR2 activates MST1/2 after *Mycobacterium tuberculosis* infection to promote the production of inflammatory cytokines[135]. Similarly, ROS production is increased after Mst1/2 activation[136], whilst high ROS levels activates MST1 by enhancing MST1-TRAF2 binding[137] and increases YAP expression independent of the canonical Hippo pathway[138].

Hippo signalling is also linked to injury-induced inflammation in mammals[139]. This includes an association with a range of pathologies, including inflammatory bowel disease, pulmonary disease, stroke, and atherosclerosis. One mechanism by which the Hippo pathway may impact immunity is via alterations in the tissue microenvironment, such as through regulation of cell density and ECM composition and stiffness, which modulates immune cell function. For example, YAP1 mediates macrophage activation *in vitro* via sensing microenvironment stiffness[140].

The innate immune system mainly consists of macrophages and neutrophils, which show high levels of similarity in zebrafish and mammals[141–143]. These cells have multiple functions. Neutrophils are the most prevalent innate immune cell in zebrafish larvae from 2dpf[144], and recognise and perform the earliest response to infection or injury, including phagocytosis, NETosis, and induction of inflammation[141–143]. Macrophages respond slightly later, regulating this inflammation via cytokine production and phagocytosis, and so promoting repair[141–143]. Both macrophages and neutrophils develop from a common myeloid progenitor at 12hpf[141,145–147], when a combination of genes regulate whether they become a neutrophil (requiring low but present Spi1b, Csf3/Gcsf, and Csf3r/Gcsfr[141,147–150]) or a macrophage (requiring continual Spi1b and Irf8[141,147,149,151]). By 30hpf, both functional neutrophils and macrophages are present, found in peripheral tissues and the caudal hematopoietic tissue (CHT, the haematopoietic cell niche) from 72hpf onwards[142].

Some work has been published on the function of innate immune cells after tail fin injury in the embryonic zebrafish. In these studies, both neutrophils and macrophages respond to injury, migrating to the transection plane via a chemoattractant gradient[143] and performing varied functions[152]. In the first 6 hours post mild tail fin injury, neutrophils are the primary scavenging cells, removing debris at the wound in a similar manner to mammalian neutrophils[152–154]. However, this function is short-lived, and neutrophils quickly undergo apoptosis and are cleared by phagocytes such as macrophages[153,154], or migrate away from the wound[143,155,156]. Unexpectedly, experimental ablation of these neutrophils does not impair fin regeneration[153], suggesting that these cells are not essential for regeneration. No prior investigation into the role of the Hippo pathway in the neutrophil response to zebrafish tail fin injury could be found.

Published works have also focussed on macrophage function after larval tail fin injury, albeit without investigating the role of Hippo signalling in this process. Macrophage number increases during the regeneration timecourse[154], where from 6hpi they are the dominant scavengers to aid in resolving inflammation and facilitating regeneration[153]. Ablation of these macrophages impairs regeneration, suggesting an essential role for macrophages in lateral line regeneration[157] and caudal fin regeneration[142,152,153,158,159]. This may be through providing a favourable environment for the blastema, formation of which has been shown to be dependent on myeloid cells[142,158,160]. Macrophages have also been shown to clear apoptotic neutrophils[143,144], and downregulate pro-inflammatory cytokines Il1b and Tnfα to promote late healing[158,160,161]. However, more studies are desirable to investigate the role of the Hippo pathway in both zebrafish innate immunity and regeneration.

1.6 Yap1 and Taz: differences and similarities in function

YAP1 and TAZ are the core transcriptional effectors of the Hippo pathway, phosphorylation of which determines the transcriptional output of the entire signalling cascade[21,23]. However, many studies focus on YAP1 alone, or consider YAP1 and TAZ to have greatly overlapping functions. Relatively few papers focus on TAZ alone, and even fewer actively compare the functions of YAP1 and TAZ. Despite originating from one gene (as evidenced by a single YAP1/TAZ ortholog in invertebrates such as Yki in *Drosophila*), functional differences and similarities can be observed when comparing YAP1 and TAZ *in vitro* or *in vivo*[162]. For example,

a dramatic phenotypic difference is observed between mouse *Yap1* or *Wwtr1* KO, as described in 1.2 above. However, a double *Yap1*/*Wwtr1* KO mouse embryo has a more severe defect than either KO mouse alone, with embryos dying before reaching the morula stage[163]. This suggests some level of functional redundancy between the two proteins.

Although human YAP1 and TAZ have a high sequence similarity (60%), there are some key structural differences in vital functional protein domains. This includes (in the most prominent splice isoforms[164,165]) the number of WW domains (YAP1 = 2; TAZ = 1) and the presence of a proline-rich domain in the N-terminus of YAP1 which is associated with pre-mRNA splicing[44,162,166]. YAP1 also contains a SRC homology 3 domain-binding motif that is not present in TAZ[162]. This domain expands the number of potential YAP1-binding partners, as this domain can bind to complementary domains on several different proteins, including tyrosine, YES, and SRC kinases[162,167]. Differently from YAP1, TAZ contains an additional GSK3β-responsive phosphodegron that results in TAZ degradation through a $SCF^{\beta\text{-}TrCP}$ ubiquitylation pathway and subsequently a more dynamic regulation than YAP1, potentially accounting for the overall lower stability of TAZ relative to YAP1[23,44,162,168]. Key TEAD-interacting residues in the TEAD-binding domain are also conserved between YAP1 and TAZ, which show similar interaction and affinity with TEAD proteins[169], but there are some differences in the domain[44]. One such difference is the potential of TAZ only to form a TAZ-TEAD heterotetramer complex that may affect the selectivity of TAZ for binding to specific target genes[170]. Other evidence shows that key TEAD protein interactions are made through different residues in YAP1 and TAZ[170]. Finally, structural differences in YAP1 and TAZ alter their ability to complex with themselves and each other. This includes the ability of YAP1 and TAZ to heterodimerise, but only TAZ has the ability to form a homodimer[162,171]. These differences in structure result in differences in interactions and subsequently regulation of multiple signalling pathways[162]. For example, only YAP1 interacts with SMAD1[172] and ERBB4[173,174] to promote the transcriptional response of the BMP and EGFR signalling pathways respectively. On the other hand, only TAZ inhibits PPARγ whilst activating RUNX to promote osteogenic differentiation from mesenchymal stem cells[110].

When directly comparing YAP1, TAZ, and YAP1/TAZ KO HEK293 cells, Plouffe et. al. found that although there is some functional redundancy, there are distinct differences, most notably observed as TAZ is unable to compensate for a loss of YAP1 after individual component KO[44].

Cellular physiology was affected to a much greater extent after YAP1 KO compared to after TAZ KO, including in measurements of cell size, proliferation, migration, and glucose uptake[44]. YAP1 KO cells were more similar to YAP1/TAZ KO cells than TAZ KO[44], confirming that TAZ could not compensate for the loss of YAP1, and that YAP1 has a greater role in cellular function than TAZ. This was also reflected in transcriptomic analyses, including in the expression of key Hippo pathway target genes *CTGF* (*CCN2*) and *CYR61* (*CCN1*)[44]. Finally, Hansen et. al., found that YAP1 KO cells had more severe loss of the amino acid transporter SLC7A5 than TAZ KO cells, while YAP1/TAZ double KO cells had an even greater loss, suggesting some functional redundancy[39].

Some similarities and differences between YAP1 and TAZ function have also been observed in cancer studies. For example, chemotherapy resistance has been linked to both YAP1 and TAZ activation[175,176]. One potential cause of chemotherapy resistance is the presence of cancer stem cells, a small subpopulation of tumour cells that have a high rate of self-renewal and the ability to differentiate into many cell types[177]. TAZ was expressed at higher levels than YAP1 in mammary cancer stems cells *in vitro* and regulated their self-renewal and tumour-initiation properties[178]. However, YAP1 was not enriched in these cells[178], despite other studies linking YAP1 to promoting cancerous properties in many other cell types (reviewed elsewhere[7]). This suggests a specific role for TAZ in mammary cancer stem cell function. Cancer cells also show differences in YAP1 and TAZ regulation. For example, in prostate cancer cells, the androgen receptor regulates YAP1 translation but TAZ transcription[179]. YAP1 and TAZ also respond differently to hypoxia[180]. In epithelial ovarian cancer cells, hypoxic conditions resulted in increased TAZ phosphorylation but decreased YAP1 phosphorylation and overall level[180].

Comparison of YAP1 and TAZ function is clearly complex, notably due to a level of feedback between the two proteins, and the Hippo pathway in general[181]. This includes both positive and negative feedback. Positive feedback interactions include findings such as YAP1 being required for TAZ protein stability in prostate cancer cells[179]. In addition, *SGK1*, a YAP1 target gene, stabilises TAZ by inhibiting GSK3β-mediated ubiquitin degradation in human mammary epithelial cells[182]. Similarly, the TAZ-specific target gene *ITGAV* maintains YAP1/TAZ activity such that perturbation of *ITGAV* diminishes nuclear YAP1/TAZ protein levels in hepatocellular carcinoma cells[183]. Negative feedback interactions include YAP1/TAZ promoting LATS1/LATS2

activation, either directly (LATS2 only) or indirectly via NF2, in both mouse tissue and cultured cells[184,185]. Finally, Yap1 overexpression in the mouse results in downregulation of both YAP1 and TAZ[186]. Downregulation of TAZ in particular promotes adipose stem cell differentiation, resulting in the commonly observed Yap1 overexpression phenotype of obesity[186].

There has been limited investigation into these functional similarities and diversity in the zebrafish. Most investigations into the Hippo pathway in zebrafish has focussed on the role of Yap1[38]. As described above, *yap1* mutants have established wide-ranging defects in regeneration and development, whilst *wwtr1* mutants are much less well-studied, with the few papers published showing defects in kidney structure and function[187], alterations in heart development and blood vessel patterning[73,87,118], and general reductions in size and survival[73,87]. A direct comparison between Yap1 and Taz function in the zebrafish could only be found in one paper. Ren et. al.[188] found that *stk3* mutants had renal dysfunction that was alleviated by disruption of *wwtr1*, but not *yap1*, suggesting a specific role for Taz in kidney function and so a difference in Yap1 and Taz roles in zebrafish development. There is a clear interest therefore in investigating more differences and similarities in Yap1 and Taz function in the zebrafish.

1.7 CRISPR/Cas9 genome editing technology

Clustered Regularly Interspaced Short Palindromic Repeat (CRISPR) sequences were first described in a 1987 report about repetitive DNA sequences in a bacterial genome, commonly found together with genes encoding CRISPR-associated (Cas) proteins[189]. These have a role in bacterial adaptive immunity, where invading viral DNA and RNA are recognised and destroyed by Cas-mediated cleavage[190–193]. This naturally-occurring phenomenon was then adapted for scientific use, allowing the precise modification of cellular DNA sequences[194–197].

These modifications are often performed by a CRISPR/Cas9 protein complexed with a guide RNA. The exact mechanism is reviewed elsewhere (for example in[195–198]). In brief, the guide RNA is designed to complement a specific target DNA sequence of scientific or therapeutic interest. The target must be adjacent to a short protospacer adjacent motif, which triggers the binding of the guide RNA to the DNA. A spacer region in the guide RNA then creates an R-loop structure which directs the CRISPR/Cas9 complex to cleave the DNA, creating a double-

stranded DNA break. This break is then repaired by endogenous repair pathways, including nonhomologous end joining, microhomology-mediated end joining pathways, or homology-directed repair. The repair is unlikely to perfectly recreate the original DNA sequence, and instead induces mutations that could disrupt the function of the protein. This allows for straightforward and efficient gene editing on a much shorter timescale than previous technologies allowed, thereby revolutionising the ability to perform, for example, screens *in vitro* and *in vivo*[197].

The protospacer adjacent motif requirement of the Cas9 nuclease limits its ability to target any DNA sequence. Therefore, some modifications of the nuclease have been optimised to allow for more precise control over both target sequence and the nature of the induced mutation (reviewed in[195–197]). This will allow even greater applications of this technique, such as for therapies targeting a range of monogenic disorders, including sickle cell anaemia, cystic fibrosis, and Duchenne muscular dystrophy, amongst others[197,198].

The zebrafish is of particular utility in the performance of CRISPR/Cas9 screens, where they reside between the high-throughput but lacking in translatability *in vitro* screens and the low-throughput but informative mammalian *in vivo* screens[199]. The relative low cost and high sample numbers possible in the zebrafish, coupled with an *in vivo* system that shares over 80% of disease-causing genes with the human[200] and ease of genetic manipulation, means that the zebrafish has often been used for CRISPR/Cas9 screens. This includes the study of regeneration of the lateral line[201] and the spinal cord[202,203] in both adults and embryos.

The wealth of published work describing zebrafish CRISPR/Cas9 mutagenesis, including in screens, has revealed key points required to ensure a successful CRISPR/Cas9 screen experiment. This includes a high rate of mutagenesis that results in the removal of the protein of interest, ease of microinjection mix generation and injection to allow for a high number of mutagenised embryos to be produced, the ability to quickly and robustly investigate resulting phenotypes, and the recapitulation of stable mutant phenotypes. Precisely how these criteria are met differ between published screens, and so some optimisation was required to ensure that appropriate assays were developed for the screen in this project.

1.8 Summary

In summary, the Hippo pathway has been linked to both development and regeneration. However, much of the work investigating this in the zebrafish has focussed on Yap1, disruption of which gives developmental phenotypes that may be a cause of the regenerative defects also observed. This is due to the wide-ranging effects of the Hippo pathway, which can impact cell proliferation, progenitor cell function, and response to mechanical forces. The regeneration-promoting effect of Yap1 signalling in the zebrafish is however of great interest, suggesting some therapeutic potential in this pathway. Before this can be done, the Hippo pathway must be studied in more depth to elucidate more clearly the roles of the different Hippo pathway components in these processes. This will aim to identify individual Hippo pathway components that can be precisely therapeutically targeted to utilise the regeneration-promoting effect without any effects on development or normal function.

More studies are also required as pathological hyperactivation of YAP1/TAZ is associated with fibrosis and carcinogenesis in many solid tumours[7,30,204]. This tumorigenesis is associated with the Hippo pathway's role in cell proliferation, stemness, and therapeutic resistance, amongst others. Therefore, pro-regenerative therapies that enhance YAP1/TAZ activity may increase cancer risk, and cancer therapies that inhibit YAP1/TAZ may also impact on highly proliferative regenerating cells (such as those in the hair follicles and intestines)[46]. Therefore, for kinder and more effective therapies, more research is needed on the Hippo pathway *in vivo*.

1.9 Hypothesis and aims

1.9.1 Hypothesis

Specific Hippo pathway components have distinct roles in developmental and regenerative processes.

1.9.2 Aims

1. To use *yap1* to optimise a CRISPR/Cas9 screen for the elucidation of the Hippo pathway's role in zebrafish development and regeneration
2. To screen other Hippo pathway components for their roles in zebrafish embryonic development and regeneration

3. To investigate underlying roles of Hippo pathway components identified as being of interest during Aim 2

2 Materials and Methods

2.1 CRISPant generation

CRISPR/Cas9 guide RNAs were designed by C. Hansen (*yap1*) and S. Riley (remainder) using gene sequences imported from Ensembl (ensembl.org) into Benchling software[205]. Benchling was used to identify predicted efficient CRISPR/Cas9 guide RNAs, which were then validated and ordered via IDT (custom or predesigned Alt-R CRISPR-Cas9 gRNA, cRNA 10nmol) (for sequence, see

Table 2.1). Primers used to determine guide RNA cleavage were designed using NCBI PrimerBlast[206] with sequences imported from Benchling (Table 2.2). Primers were chosen with a Tm of 52-58°C, between 150 and 250 base pairs (bp) amplicon length, based on their area of amplification – with the putative guide RNA cleavage site being as close to the centre of the amplicon as possible, and without including the cleavage site of any coinjected guide RNAs. The latter parameter was not applied when guide RNAs targeted different restriction enzyme (RE) digest sites (excluding T7 endonuclease I (T7E1) digest) (Figure 2.1).

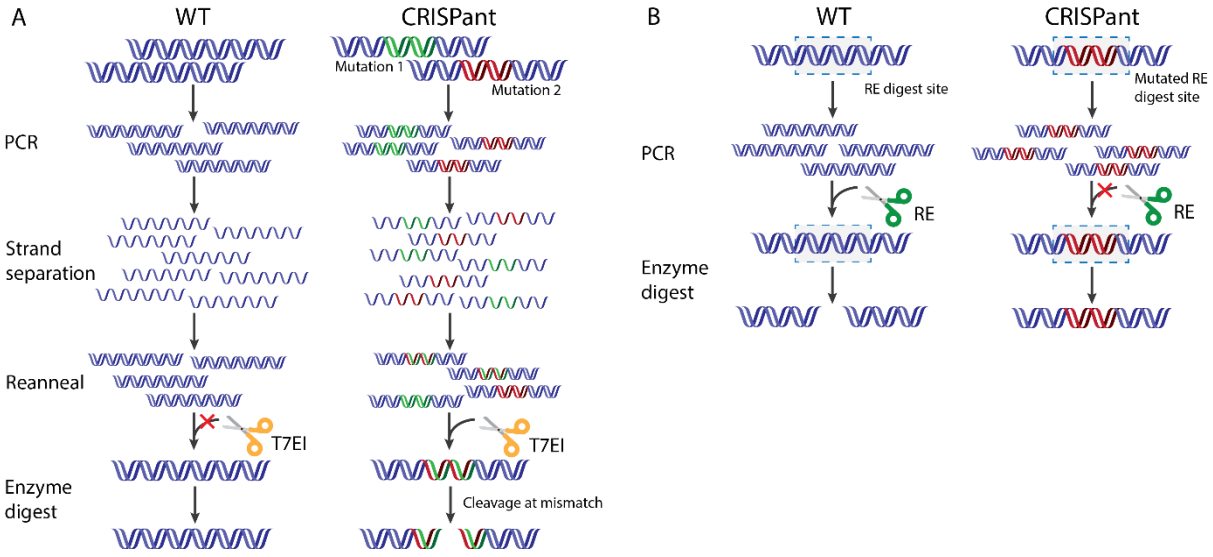

Figure 2.1: T7E1 and RE digest overview
(A) Overview of mechanism of action of T7EI for WT and CRISPant DNA. CRISPR mutagenesis will likely induce different mutations in the different chromosomes. PCR and strand separation generates multiple single-stranded DNA sequences. Reannealing these strands does not always match the same mutations in the double-stranded DNA, creating mismatches. Digestion with T7E1 cleaves the mismatched strands. The same occurs in heterozygotes. **(B)** Overview of mechanism of action of RE for WT and CRISPant DNA. CRISPR guides were designed to cause mutations at the RE digest site such that the RE could no longer recognise the digest site and therefore not cleave DNA in the CRISPant.

Table 2.1: CRISPR/Cas9 guide RNA sequences

Gene	Ensembl ID	Guide	Sequence
ctgfa	ENSDARG00000042934	*ctgfa* guide 1	5'-GCU UAC ACC AGG UGA ACA CU-3'
		ctgfa guide 2	5'-CUG UGC AGA CAC CAA UAC GA-3'
ctgfb	ENSDARG00000104292	*ctgfb* guide 1	5'-CAG GGA UCU GGA CAC GUC GT-3'
		ctgfb guide 2	5'-CCA CGA CGU GUC CAG AUC CC-3'
cyr61	ENSDARG00000023062	*cyr61* guide 1	5'-CGC UGC AGA CCC ACU CCU GG-3'
		cyr61 guide 2	5'-CUG CGA CCA CAG CAA GGG CC-3'
lats1	ENSDARG00000003751	*lats1* guide 1	5'-CAA CAG GAU AAA CUU CCA GG-3'
		lats1 guide 2	5'-GCC CAC GAC AGC UCC UCC AG-3'
lats2	ENSDARG00000078864	*lats2* guide 1	5'-UAG UUG UUA AAC UUC UGG GG-3'
		lats2 guide 2	5'-CUA CAG GAU CUG GUC AAU GC-3'
nf2a	ENSDARG00000020204	*nf2a* guide 1	5'-AAA UGG GAC UCU CUC UUC GG-3'
		nf2a guide 2	5'-AAC ACU AUA GGC UCC UCU UU-3'
nf2b	ENSDARG00000025567	*nf2b* guide 1	5'-GAC CUG GUA UGC CGG ACC AU-3'
		nf2b guide 2	5'-UAA AGU CAA AGU CAG CAC UA-3'
tp53	ENSDARG00000035559	*tp53* guide 1	5'-CCA AGA GUU CGC GGA GCU CU-3'
		tp53 guide 2	5'-CAG CUA CAU UAC GAC CUG AG-3'
wwtr1	ENSDARG00000067719	*wwtr1* guide 1	5'-UGG CGA CAU GGA UCA CCU GG-3'
		wwtr1 guide 2	5'-CCG GCA CCA GUC CUG CGA UG-3'
yap1	ENSDARG00000068401	*yap1* guide 1	5'-GUU AAA AAG AGC CUC CAG AU-3'
		yap1 guide 2	5'-GAU GAC AUG CCG CUG CCC CC-3'
Synthetic crRNA sequence (IDT standard)			5'-GUU UUA GAG CUA UGC UGU UUU G-3'

A microinjection mix was generated at concentrations shown in Table 2.3 with all reagents diluted in phenol red to aid visualisation of injection. Optimisation of mix temperature was performed at room temperature (RT), 95°C, and 60°C (as a mid-point between the two). At RT and 60°C, components were mixed and incubated for 5 minutes at the desired temperature. At 95°C (protocol from Dewari et. al.[207] and Essner[208]), guide RNAs and tracrRNA were mixed and heated at 95°C for 5 minutes before incubation at RT for 30 minutes. Cas9 nuclease was added and the reaction mix was incubated at RT for 10 minutes. Microinjection mixes were stored at 4°C for a maximum of 1 week before use. Three microinjection groups were analysed: Cas9-only injected fish (Cas9 and tracrRNA), gRNA-only injected fish (gRNAs and tracrRNA), and embryos injected with the full Cas9-gRNA complex (Cas9, gRNAs, and tracrRNA). Mixes were injected at 0.5nl into one-cell stage embryos (see Table 2.3 for concentration). Needles were pulled from a glass capillary using a Flaming/Brown Micropipette puller P-97 (Sutter instruments) using the following settings: heat=580; pull=250; vel=50; time=125. Microinjection mix was loaded into the needle using Eppendorf

Table 2.2: CRISPR/Cas9 guide RNA analysis primers

Construct	FW/REV	WT product length (bp)	Sequence
ctgfa guide 1	FW	150	5'-TGG AGC TCT TTA GCA AAT GT-3'
	REV		5'-CCC ACA GGT GTC CAG AA-3'
ctgfa guide 2	FW	160	5'-AGA ACG AGA TGT TTG CGA C-3'
	REV		5'-AAG ATT GTT TAC AAT TCT GAC TCT-3'
ctgfb guide 1 and 2	FW	220	5'-GAT CTG GGT GGT GTG ATT TA-3'
	REV		5'-GAC TGG AAG GTG TCT TCT TG-3'
cyr61 guide 1	FW	180	5'-TAT CCT CCA GCT GCC C-3'
	REV		5'-CCC CAT AGT TGC ACT CCA-3'
cyr61 guide 2	FW	150	5'-GTG CTC CTG TGC TCC-3'
	REV		5'-GTG GCT GGC CCC ATA-3'
lats1 guide 1	FW	160	5'-ATG TGA TCA ATG CAA TGT GG-3'
	REV		5'-TTA ATA ATG CCT ACC CGC TT-3'
lats1 guide 2	FW	190	5'-GAT GAG TCC AGA CAG CAA-3'
	REV		5'-CTG CAT TAC CTC ATC AAA GC-3'
lats2 guide 1	FW	180	5'-GAG TCA GGC ACT TCA TGG-3'
	REV		5'-ACC TGA ATC ATT GGC ATA GG-3'
lats2 guide 2	FW	195	5'-ATG CCA ATG ATT CAG GTC C-3'
	REV		5'-TCA AGT TAC TGT TGA CTA CAA TTC-3'
nf2a guide 1	FW	210	5'-TGT AGC TTT TAA GCA GAG AGG-3'
	REV		5'-GAA CTC CAA ATC AGC ATC CA-3'
nf2a guide 2	FW	190	5'-AAG CAG AGT GCA ACA CTT AT-3'
	REV		5'-AAA ATC ATC CTG AGC CAG TG-3'
nf2b guide 1	FW	230	5'-GTG TCT GTC TGA TTC TGT GT-3'
	REV		5'-TGG GAA CAG ATT TTA GGC TC-3'
nf2b guide 2	FW	175	5'-AAT TAT TTG TGT TTT CAG GTG T-3'
	REV		5'-GGA CAC AGA ATC AGA CAG AC-3'
tp53 guide 1	FW	185	5'-CCC CCA GGT TTT TAT GAC TT-3'
	REV		5'-GAC ATG GCT GCT AAC AAA AA-3'
tp53 guide 2	FW	170	5'-CTG GGA CCA AAC GTA GTA AG-3'
	REV		5'-GTA AAG ATC TCC TCA TCG CT-3'
wwtr1 guide 1	FW	150	5'-AGT TTG TTT TGA CCA TGA GC-3'
	REV		5'-GCA TAT CCT TGT TCC TCC AG-3'
wwtr1 guide 2	FW	200	5'-GTT CTC TCC CGC CGA G-3'
	REV		5'-GAG AAA GTA CTT CTG GCC GT-3'
yap1 guide 1	FW	400	5'-GGT GTT TTT GGC AAG CAG CA-3'
	REV		5'-GGA GTG GGA CCT TGG CTC TG-3'
yap1 guide 2	FW	440	5'-CAG ATG CAG GTA CTG CTG GTA-3'
	REV		5'-TGC CTT CAT CAT GTA AAT GAA CTG C-3'

microloader tips and mounted onto a PV820 PicoPump microinjector rig (WPI). Injection parameters optimised to give a bolus of the desired size (using $V = \frac{4}{3}\pi r^3$, where V = volume and r = radius) on a 1mm graticule with a droplet of mineral oil, viewed through a light microscope. Embryos were lined along the edge of a glass microscope slide in a petri dish lid. The CRISPR mix was injected into the yolk into the single zygote cell, as close to the cell as possible without damaging it.

After establishing that RT was the optimal temperature for mix generation (3.1), optimisation of dosage was then performed using microinjection mixes generated at RT. Mixes were injected at 0.5nl, 2nl, and 4nl total volume (approximate, to the nearest 0.5nl) into one-cell stage embryos. The final optimised microinjection mix was generated by mixing components at RT and incubating for 5 minutes. 2nl was then injected into one-cell stage embryos. Resulting embryos were used for all further analyses.

Table 2.3: Microinjection mix concentrations

Reagent	Concentration	0.5nl volume (pg)	2nl volume (pg)	4nl volume (pg)
Cas9	500ng/µl	250	1000	2000
guide RNAs (each)	25ng/µl	12.5	50	100
tracrRNA	100ng/µl	50	200	400

2.2 Stable mutant generation

To generate stable mutants, CRISPants (F0) were grown to adulthood through standard zebrafish husbandry (summarised in Figure 2.2). Once breeding age was reached, F0 fish were crossed with WT fish and half of the offspring were genotyped (as described in 2.6) in bulk where possible to confirm that the F0 founder contained a mutation. The remaining offspring (F1) were grown to adulthood then genotyped individually using PCR and Sanger sequencing (as described in 2.3). Heterozygotes of interest were then outcrossed (bred with a different strain, in this thesis WT – WIK strain) to generate F2 offspring, which were genotyped using DNA obtained from fin clips at adulthood to identify F2 heterozygotes. These F2 heterozygotes were incrossed (bred with siblings) and the resulting F3 offspring were grown to adulthood. DNA was extracted from fin clips, and homozygous F3 fish were identified by PCR (see 2.3.3).

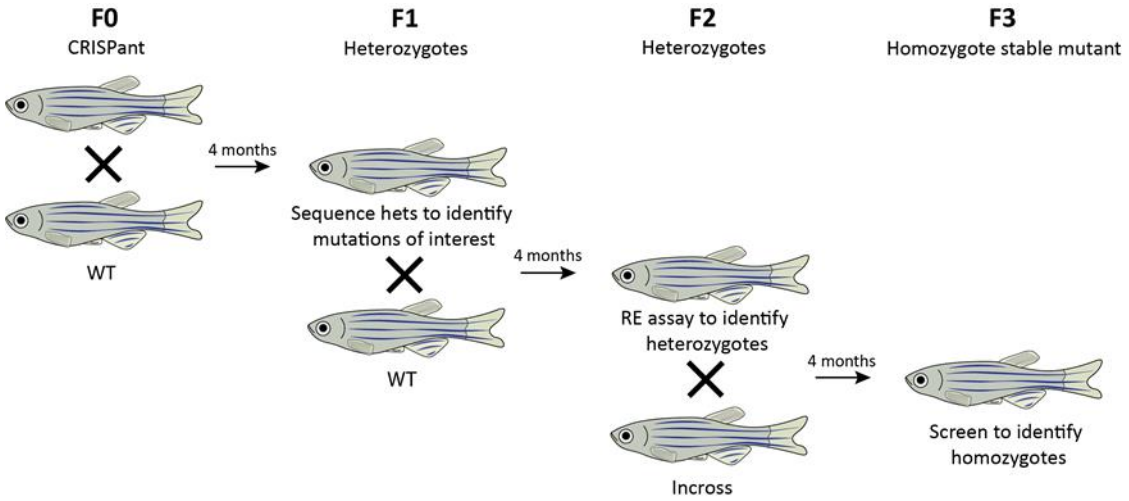

Figure 2.2: Overview of stable mutant generation
Schematic showing the generations required to generate homozygous stable mutants from a CRISPant founder. The CRISPant founder was outcrossed with a WT to generate heterozygous offspring. These heterozygotes were sequenced to identify fish with key mutations where the gene of interest was sufficiently disrupted, which were then outcrossed again to ensure only the mutations of interest were propagated. The resulting mixed heterozygous/WT population were analysed by restriction enzyme digest to identify heterozygotes, which were incrossed to generate a mixed homozygous/heterozygous/WT population. The homozygotes were the final stable mutants, and the WT fish were also kept to act as a sibling control.

2.3 DNA sequencing

2.3.1 gDNA sequencing of F2 fish

Fin clipping of adult fish was performed in accordance with Home Office Regulations. gDNA extracted from fin clips as described in 2.5, and Taq PCR (PCR settings: 95°C 30 sec, 30 cycles at 95°C 15 sec, 50°C 15 sec, 68°C 30 sec, final extension 68°C 5 min) was performed using primers shown in Table 2.4, designed to amplify an approximately 150bp long region around the CRISPR target site. These sequences were then inserted into a pSC vector, transformed into bacteria using SOC medium, and amplified according to the Strataclone PCR Cloning Kit instructions. Positive colonies were selected for overnight liquid culture, from which DNA was extracted using an E.Z.N.A. Plasmid DNA Mini Kit I, diluted to 100ng/µl, and sent to Source BioScience for Sanger sequencing with an M13R primer. Sequences were cleaned in the FinchTV app and aligned to published sequences (from ensembl.org) using Clustal Omega (ebi.ac.uk/Tools/msa/clustalo).

Table 2.4: gDNA sequencing primers

Construct	FW/REV	Sequence
wwtr1 guide 1	FW	5'-AAA ACT CTC CAA ACT CCA CG-3'
	REV	5'-AGC GAA AGT GGA CCC TC-3'
wwtr1 guide 2	FW	5'-GAT CTG GAG GCT CTT TTT AAC TC-3'
	REV	5'-GTA TGC ACT CCA CTA ACT GGT AA-3'
yap1 guide 1	FW	5'-GAG GGC TGT GAT TTT CAA TG-3'
	REV	5'-GCA GGA AAA GTT TGT GGA AA-3'
yap1 guide 2	FW	5'-CCT GTG GGG TAT TTG CTT TA-3'
	REV	5'-TGC AGT TTA CAC AGA GTT GA-3'

2.3.2 cDNA sequencing

Sequencing of cDNA of the *yap1* and *wwtr1* gene was performed on F1 heterozygotes to identify the full mutant sequence. Fin clipping of adult fish was performed in accordance with Home Office Regulations. RNA was extracted from the fin clip as described in 2.7.3, and cDNA generated from this RNA as described in 2.8. Taq PCR was performed using primers shown in Table 2.5. *wwtr1* primers span the entirety of the gene, whilst *yap1* needed two primer sets, one to amplify the first half of the gene (A), and another to amplify the second (B). Sequences were then inserted into a pSC vector, transformed, amplified, and DNA was extracted and diluted as described in 2.3.1. Samples were sent to Source BioScience for Sanger sequencing with M13R and T7F primers. Sequences were cleaned in the FinchTV app and aligned to published sequences (from ensembl.org) using Clustal Omega (ebi.ac.uk/Tools/msa/clustalo).

Table 2.5: cDNA sequencing primers

Construct	FW/REV	Sequence
wwtr1	FW	5'-ATG AGC GGT AAT CCT CTC CA-3'
	REV	5'-CTA GAG CCA GGT GAG GAA G-3'
yap1	FW A	5'-ATG GAT CCG AAC CAG CA-3'
	REV A	5'-TTG TTT CCA CTC ATC ACT CC-3'
	FW B	5'-GAA TTT CCC AGA GTG CCC-3'
	REV B	5'-CTA TAG CCA GG TTA GAA AGT T-3'

2.3.3 Homozygous fish screening

F3 offspring (mix of WT, heterozygotes and homozygotes) were grown to adulthood. Fin clipping of adult fish was performed in accordance with Home Office Regulations. gDNA was extracted as described in 2.5. For *wwtr1* mutants, screening was performed using PCR and digestion via the SexAI restriction enzyme, as the mutant had a disrupted SexAI recognition

site (Figure 2.1B). This allowed the distinguishing of WT, heterozygous, and homozygous fish. For *yap1* mutants, PCR and T7 endonuclease I (T7E1) digestion was performed using the *yap1* guide 1 primer described in Table 2.2. This identified heterozygotes. The remaining fish were outcrossed with WT fish, and the resulting embryos underwent gDNA extraction, PCR, and T7E1. T7E1-positive embryos were assumed to come from homozygous parents (as an outcross would give heterozygous offspring).

2.4 *ctgfa*:GFP reporter transgenic generation

A Tol2-ctgf(-1kb)-d2GFP-pA (referred to throughout as *ctgfa*:GFP) reporter plasmid was kindly donated by Prof. B. Link (Medical College of Wisconsin) (first reported in Miesfeld et. al.[97]). *CTGF* is a well characterised YAP/TAZ-TEAD target gene[209]. Therefore, in this *ctgfa*:GFP reporter, GFP expression correlates with *ctgfa* expression as a marker for Hippo pathway transcriptional activity at *ctgfa*. 25ng/µl plasmid was co-injected into 1 cell stage embryos as a 1nl bolus with 25ng/µl Tol2 mRNA (generated in the Y. Feng lab, University of Edinburgh) diluted in phenol red. F0 embryos were screened at 48 hours post injury (hpf) and embryos with GFP fluorescence in the heart and trunk were grown to adulthood. These F0 were then outcrossed with WT fish and GFP-positive F1 embryos were again screened. Batches where 50% F1 embryos were GFP-positive were grown to adulthood before themselves being outcrossed with WT fish, screened for 50% heart and trunk fluorescence at 48hpf (F2), and grown to adulthood. This was repeated to generate F3 adults that were assumed to contain a single stable GFP insertion. These F3 adults were then incrossed and the F4 GFP-positive offspring (heterozygotes and homozygotes) grown to adulthood. F4 homozygous adults were identified by outcrossing with WT fish and screening the offspring to identify the percentage of GFP-positive embryos, with homozygotes giving 100% GFP-positive F5 offspring, and heterozygotes giving 50% GFP-positive F5 offspring (summarised in Figure 2.3).

2.5 gDNA extraction

Whole embryos at 24hpf (for RE analysis) or fin clips from adult fish (for DNA sequencing) were incubated at 95°C for 20 minutes in 50mM NaOH. 10% 1M Tris was added before tubes were spun down at 14,000xg for 10 minutes and supernatant transferred to a fresh tube. Volumes added were dependent on the number of embryos from which DNA was extracted

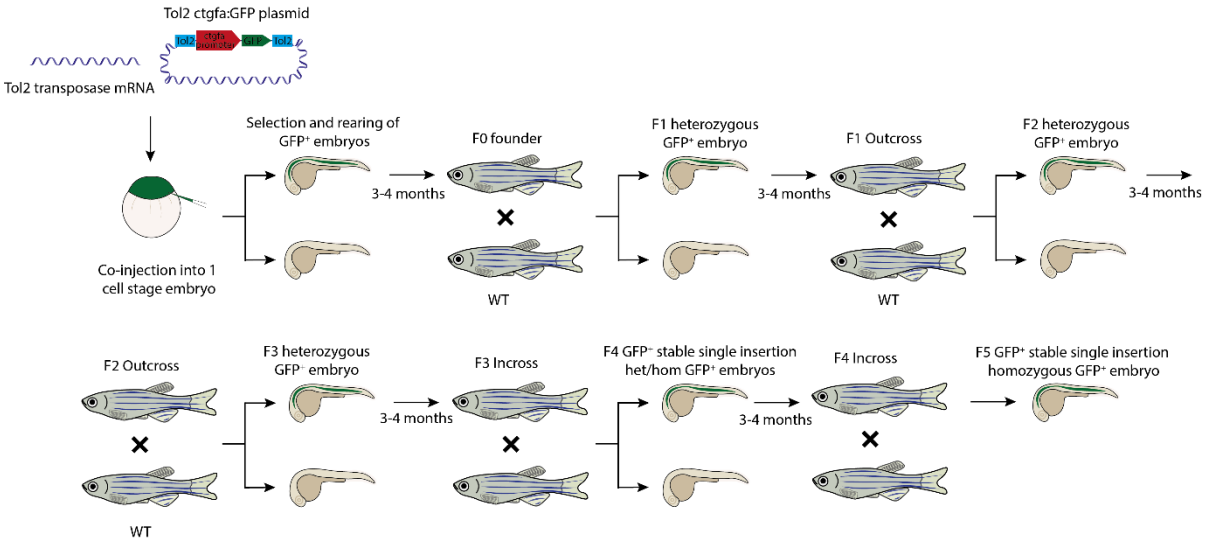

Figure 2.3: Summary of *ctgfa*:GFP transgenic line generation
Schematic showing the generations required to generate a stable single insertion homozygous GFP$^+$ embryo. The Tol2 *ctgfa*:GFP plasmid was coinjected with Tol2 transposase mRNA into a one-cell stage WT embryo. GFP$^+$ embryos were selected from those injected and grown as F0 founders. These fish were then outcrossed with WT fish for three generations, selectively rearing the GFP$^+$ offspring, to ensure a single insertion of the GFP cassette. The F3 heterozygotes were then incrossed and the mixed heterozygous/homozygous GFP$^+$ offspring were reared. These F4 fish were then outcrossed to identify homozygous fish (where all the offspring would be GFP$^+$) and these homozygotes could be incrossed to generate a F5 stable homozygous line

for 1 embryo (for analysis of guide cleavage efficiency), 50µl NaOH/5µl Tris was used, for more embryos and fin clips, 100µl/10µl used.

2.6 Restriction enzyme analysis of CRISPR guide efficiency

gDNA was amplified using PrimeSTAR Max premix (PCR settings: 30 cycles at 98°C 10 sec, 55°C 5 sec, 72°C 10 sec) with primers as shown in Table 2.2 (correct amplification was confirmed by running on a 1% agarose gel) then digested using various restriction enzymes (**Figure 2.1**). Different parameters and buffers were used depending on the restriction enzyme used for digestion (Table 2.6). Once digested, DNA was visualised on a 1.5-2% agarose gel using gel red.

2.7 RNA extraction

2.7.1 Method 'a'

Embryos were collected and added to 500µl TRIzol before storage in -80°C overnight (approx. 100 embryos per sample). Samples were homogenised using a fine-gauged needle, 100µl

Table 2.6: Restriction enzymes used and parameters for guide RNA efficiency analysis

Restriction enzyme	Buffer	Guide cleavage site targeted	Parameters
BstXI	3.1	*ctgfb* guide 2	Digestion at 37°C for 15 min
Bsu36I	CutSmart	*tp53* guide 1	Digestion at 37°C for 15 min
EcoO109I	CutSmart	*cyr61* guide 2	Digestion at 37°C for 15 min
Hpy99I	CutSmart	*ctgfb* guide 1	Digestion at 37°C for 1 hour
PfoI	Tango	*cyr61* guide 1	Digestion at 37°C for 1 hour
SacI	1.1	*tp53* guide 2	Digestion at 37°C for 15 min
SexAI	rCutSmart	*wwtr1* guide 1	Digestion at 37°C for 1 hour
T7	2	*ctgfa* guide 2 *lats1* guide 1 and 2 *lats2* guide 1 and 2 *wwtr1* guide 2 *yap1* guide 1 and 2 *nf2a* guide 1 and 2 *nf2b* guide 1 and 2	Annealing at 95°C for 5 min, then reduced to 25°C over 20 min Digestion at 37°C for 15 min
XcmI	2.1	*ctgfa* guide 1	Digestion at 37°C for 1 hour

chloroform was added, the mixture incubated for 5 minutes, and then centrifuged for 15 minutes at 12,000xg and 4°C. 250µl propan-2-ol was added to the aqueous phase, incubated for 10 minutes, and centrifuged for 10 minutes at 12,000xg and 4°C. The pellet was resuspended in 500µl 75% ethanol before vortexing and centrifugation for 5 minutes at 7,500xg and 4°C. The RNA pellet was air dried for 5-10 minutes before resuspension in RNase-free water and incubation at 55°C for 10 minutes.

2.7.2 Method 'b'

Embryos were collected and added to 500µl TRIzol before storage at -80°C overnight (approx. 35 taken at 24hpf). Samples were homogenised using a fine-gauged needle, then 100µl chloroform was added, incubated for 5 minutes, and centrifuged for 15 minutes at 12,000xg and 4°C. 200µl 70% ethanol was added to the aqueous phase and samples were processed using a RNeasy plus Mini prep kit.

2.7.3 Method 'c' (for RNAseq analysis)

Uninjured and injured samples were collected from 50 embryos. For injured samples, fish were injured at 3dpf using the severe tail fin injury paradigm, then left to recover for 24 hours in 0.3X Danieau's solution. Both uninjured and injured tail fin was removed caudal to the end

of the dorsal vein (at the beginning of the pigment gap). Tissue was collected in chilled PBS and kept on ice for a maximum of one hour before extraction. RNA extraction was performed using the Qiagen RNeasy micro kit and initial quality check and sample concentration determined by nanodrop. Some samples were prepared with help from M. Nosková.

2.8 cDNA preparation

RNA was diluted to 100ng/µl and cDNA generated using the High Capacity cDNA Reverse Transcription Kit with the following PCR settings: 25°C 10 minutes, 37°C 2 hours, 85°C 5 seconds.

2.9 RT-qPCR

10ng of cDNA was added to qPCR master mix, diluted with SYBR green master mix and transferred into a 96/364 well qPCR plate. 2µM gene-specific primers were added to each well and run on a qPCR machine (95°C 180 seconds, 95°C 5 seconds, 60°C 10 seconds, 40 cycles). *ef1α* was used as a housekeeping control for normalisation. Relative abundance and quantifications were calculated using $2^{-\Delta\Delta Ct}$.

Primers were taken from papers or designed using NCBI PrimerBlast (sequences shown in Table 2.7). For primers designed using PrimerBlast, mRNA accession values were imported from relevant NCBI gene pages (ncbi.nlm.nih.gov/gene) into PrimerBlast software, with Tm of 57-63°C, 100-200 base pair amplicon length, and spanning an intron.

2.10 Western blotting/PhosTag

2.10.1 Sample preparation

Numbers of embryos pooled and used per sample: 24hpf – 25; 48hpf – 20; 72hpf – 10; 96hpf – 10; 120hpf – 20.

2.10.1.1 Yolk removal protocol

Embryos were deyolked using a protocol adapted from Link et al.[210]. Embryos were dechorionated (removal of the chorion, the outermost embryonic membrane) if needed then mixed with 100µl deyolking buffer (1/2 concentration Ginzberg Fish Ringer) and homogenised

Table 2.7: RT-qPCR primer sequences

Target	FW/REV	Sequence
cav1	FW	5'-CGA TGT GGT GAA GGT GGA CTT T-3'
	REV	5'-TCA GCA GCC TGT AGC ACC AAT-3'
cav2	FW	5'-CGA ACG TGT ATT CGG AGG TT-3'
	REV	5'-GTG GTG AGG ATC CGG TAG AA-3'
cavin1a	FW	5'-GGA CTT GGA GAA GCA AGT GG-3'
	REV	5'-TTC AGA GGC ATG CTC TTC CT-3'
cavin1b	FW	5'-AAA CGT CTG GAG AGC AAC GAG A-3'
	REV	5'-GCC ACA TTC ACT TTC GAA CCC-3'
ctgfa	FW	5'-CTG CAC AGC CAG AGA TG-3'
	REV	5'-CAC TTC CCS GGC ACT TT-3'
cyr61	FW	5'-CCG TGT CCA CAT GTA CAT GGG-3'
	REV	5'-GGT GCA TGA AAG CTC GTC-3'
ef1α	FW	5'-TCT CTC AAT CTT GAA ACT TAT CAA TCA-3'
	REV	5'-AAC ACC CAG GCG TTAC TTG AA-3'
lats2	FW	5'-CTC CGA GAG ATC CGC AAG TC-3'
	REV	5'-CAC GTA CAA TCT GTT CAG TGT G-3'
wwtr1	FW	5'-GCA TCC AGA TGG AGA GAG AG-3'
	REV	5'-GCT GTT ATT GGG CAT GTT TC-3'
yap1	FW	5'-CCA GAC AAG CCA GTA CAG AT-3'
	REV	5'-GAA GTA TCT CTG TCC CGA AGG-3'

by vortexing. Samples were spun down and supernatant discarded before being dissolved in 50µl 2X SDS-PAGE loading buffer and incubated at 95°C for 5 minutes. Samples were spun down again and supernatant transferred to a fresh tube.

2.10.1.2 Yolk retained protocol

Embryos were dechorionated if needed and lysed in 60µl of cell lysis buffer with protease and phosphatase inhibitors. Samples were stored overnight at -80°C, then homogenised using a fine gauged needle and centrifuged at 14,000xg for 10 minutes at 4°C. 20µl of 4X SDS-PAGE loading buffer was added to the supernatant and samples heated for 10 minutes at 95°C.

2.10.2 Blotting protocol

10µl samples were loaded into a 10% polyacrylamide/PhosTag gel[211] and run for 1.5/2.5 hours respectively then transferred to a nitrocellulose membrane at 0.5A for 80 minutes. Membranes were incubated in Ponceau solution for 5 minutes, imaged, then destained in 5% milk at RT for a minimum of 30 minutes before incubation in primary antibody (1:1,000 in 5%

BSA) overnight at 4°C. Membranes were then washed 3 times in TBST, probed with an HRP-conjugated secondary antibody (1:10,000 in 5% milk) at RT for 1 to 2 hours, then washed again. Proteins were visualised using Immobilon reagent onto X-ray films.

2.10.3 Western blot quantification

ImageJ was used to quantify Western blots[212]. Loading was determined by analysing the peak height between ~55-100 kDa (where possible) of a Ponceau blot. Values for bands of interest were then normalised to loading values, and these values for injected groups were then normalised to WT values and plotted for each independent replicate.

2.11 96hpf imaging and quantification

96hpf embryos were lightly anaesthetised using tricaine (until no motor response but heart rate was maintained), mounted with a left (lateral) view in 2-3% methylcellulose, and imaged in brightfield using a Leica M205 FCA microscope and LAS X software. Images were quantified in ImageJ by S. Riley (except for *nf2a*, *nf2b*, and one repeat of *nf2a*/*nf2b* CRISPants, which was performed by S. Xia) by outlining areas of interest and calculating length/area as required. See Figure 3.7A for a schematic overview of parameters measured at this timepoint. Data was presented as either raw values or as a proportion of the area of the whole left side of the embryo (excluding fins, traced manually).

Embryo length was quantified by measuring the length of a line manually drawn along the length of the embryo's body from the tip of the head, along the notochord, and ending at the tip of the body (excluding the tail fin). Standard length was not used due to the twisting of the body of some CRISPants, which would have skewed length measurements.

Developmental stage was quantified by using the circle tool in ImageJ to outline the swim bladder and the area of the circle was measured. Visual classification of early developmental stage (described in section 3.2.4.1) showed high variability even amongst controls and so were not used. Other measures of development, such as the head-trunk angle, were considered but not brought forward in the screen due to the high levels of twisting/defective midline development that may skew this measurement and the ease of measuring swim

bladder area. Experimental ease was a large consideration as many embryos needed to be quantified to reach suitable statistical power.

Eye size was quantified by using the circle tool in ImageJ to outline the embryo eye on the left (lateral) side and the area of the circle measured. Yolk size was quantified by manually tracing the full circumference of yolk, using the pigmentation line along the centre of the embryo body as the internal border and measuring the area of the resulting shape. Heart size was quantified by manually outlining the protruding area rostral to the yolk, using the slightly darker head and yolk and the pigmentation line along the centre of the embryo as borders, and measuring the area of the resulting shape.

FishInspector software[213] was investigated to measure these parameters, and more, in an automated fashion. However, the high levels of oedema seen in many of the CRISPants meant that it was not possible to image these fish using a capillary-based imaging system with a fixed diameter, which is required for the software to function properly.

2.12 Tail fin regeneration and quantification

2.12.1 Tail fin regeneration measurements in the CRISPR/Cas9 screen

72hpf embryos were anaesthetised using tricaine and a portion of the caudal tail was excised using a sharp scalpel. Embryos were imaged then separated into individual wells of a 24 well plate and left for 48 hours to recover before imaging again. The same process was followed for analysis of baseline growth, except without caudal fin excision. The area of tail fin was measured as outlined in Figure 2.4, and fin growth was compared between individual fish. If embryos died or were dying (heartbeat was still present but the tail fin reduced in size over the 48 hours post injury (hpi) and embryos looked extremely unhealthy), the embryo was excluded from statistical analyses.

2.12.2 Tail fin regeneration measurements for in depth tracking

72hpf embryos were anaesthetised using tricaine and a portion of the caudal tail was excised using a sharp scalpel. Tail fin area was measured whilst analysing the embryo for other assays, such as immune cell infiltration or after immunofluorescence. Fin area was measured at 4, 6,

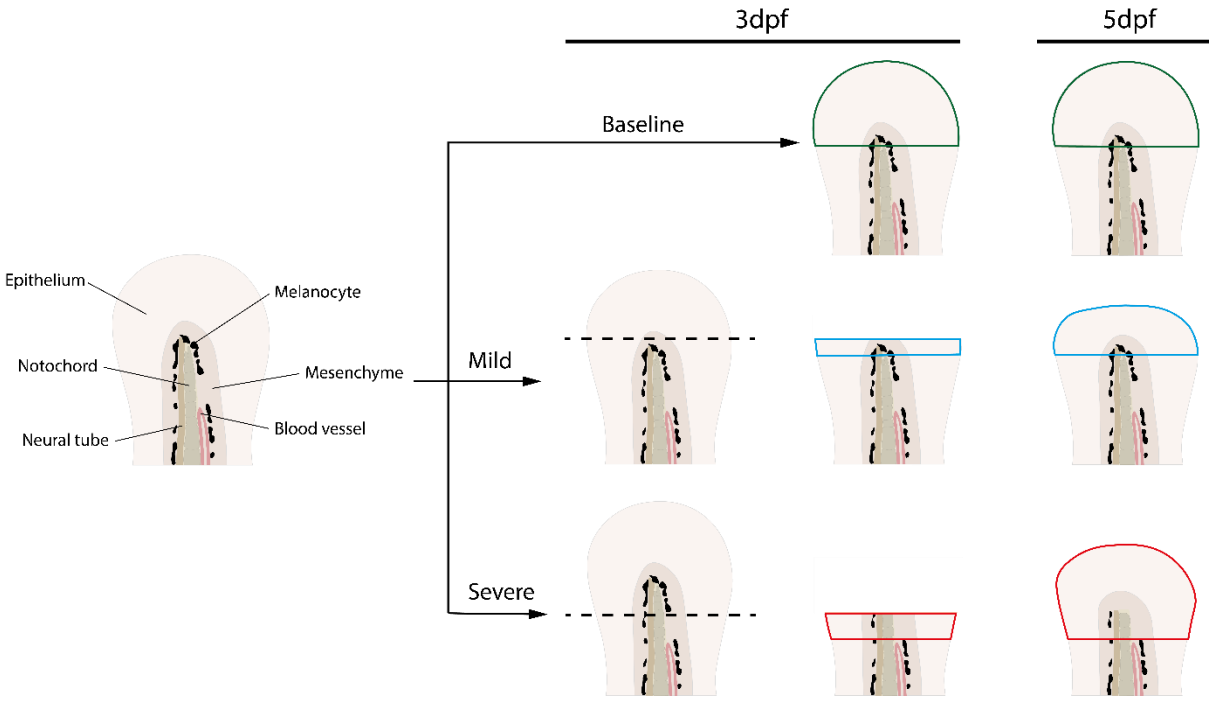

Figure 2.4: Tail fin measurements used in the CRISPR/Cas9 screen
Schematic of the types of measurements taken to analyse tail fin regeneration and baseline growth in the CRISPR/Cas9 screen. Area was measured in the outlined region (green=uninjured, blue=mild injury, red=severe injury), and the area at 3dpf is subtracted from the area at 5dpf.

24, and 48hpi after both mild and severe tail fin injury. Tail fin area was measured as outlined in Figure 2.5.

2.13 Neuromast regeneration and imaging

72hpf embryos were injured by incubation in 10µM copper (II) sulphate (diluted in 0.3X Danieau's solution) for 2 hours at 28.5°C. For imaging, embryos were incubated for 10 minutes in prewarmed 1mM DASPEI (diluted in 0.3X Danieau's solution) then imaged using an mCherry filter on a Leica M205 FCA microscope and LAS X software at 24hpi and 48hpi. Analysis was performed by isolating the posterior lateral line then thresholding and measuring the number and area of particles between 50-500µm using ImageJ.

2.14 Juvenile zebrafish imaging and quantification

28-35dpf juvenile fish were anaesthetised using tricaine (MS222), mounted with a dorsal view in 2-3% methylcellulose, and imaged in brightfield using a Leica M205 FCA microscope and LAS X software. Images were quantified in ImageJ by outlining areas of interest and calculating length/area as required. Data was presented as either raw values or as a proportion of the area of the whole side of the embryo (excluding fins).

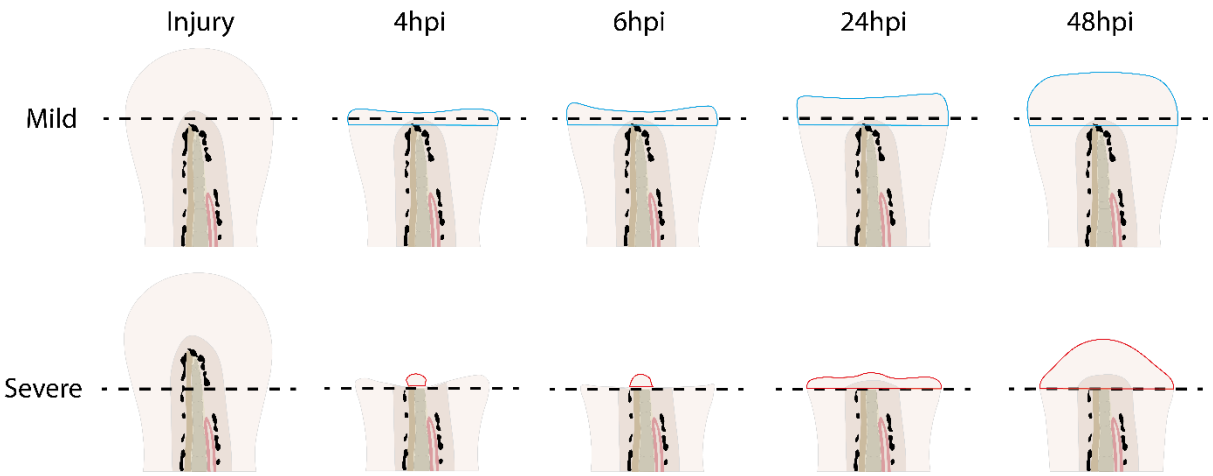

Figure 2.5: Tail fin measurements used in detailed tracking of tail fin regeneration
Schematic of the types of measurements taken to analyse mild (top) and severe (bottom) tail fin regeneration in detail in 5.1. Area is measured in the outlined region. Dotted line denotes transection plane.

2.15 Immunofluorescence

Embryos were fixed in 4% PFA/PBS overnight at 4°C or for a minimum of 2 hours at RT, washed in PBST, then transferred to 100% freezer cold methanol and stored at -20°C for a maximum of 1 month. Samples were washed in PDT (PBS, 1% DMSO, 0.3% Triton X100), then blocked in blocking buffer (PBST, 10% goat serum, 2% w/v BSA) at RT for 3 hours. Embryos were incubated in primary antibodies (1:200 in blocking buffer) overnight at 4°C. Samples then underwent ten 15-minute washes in PDT before incubation in secondary antibodies (1:250 in blocking buffer) for 2 hours at RT and further washes in PDT as before. Samples were incubated in DAPI (1:1000 in PDT) before washes in PDT and dehydration in increasing concentrations of glycerol in PBS, and storage either in 80% glycerol or antifade mountant at 4°C overnight. If DAPI staining was not performed, samples were stored in ProLong Diamond Antifade mountant with DAPI. Embryos were then mounted onto glass slides and imaged

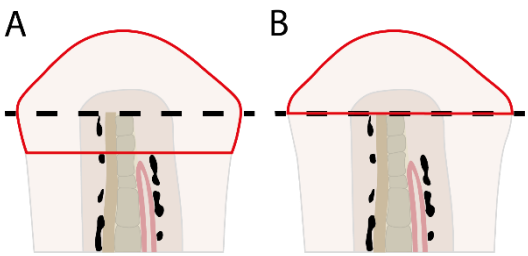

Figure 2.6: Areas used for quantification of immunofluorescence staining and immune cells
Schematic of the areas in which to analyse pH3 staining (5.8) and immune cell infiltration (5.11-5.12) after tail fin injury. Stained cells were counted either in the region caudal to the start of the pigment gap **(A)**, or in the regenerate **(B)**. Number of positive cells were measured in the outlined region. Dotted line denotes severe injury transection plane.

using a Leica Sp8 confocal microscope (20X air objective), using LASX software and ensuring no saturation of pixels. Samples were quantified as described in Figure 2.6.

2.16 HCR RNA-FISH imaging

Casper, WT, or *ctgfa*:GFP embryos (incubated in 0.003% PTU to inhibit melanogenesis if needed) were injected with *yap1* or *wwtr1* CRISPR or left uninjected. Embryos underwent severe tail fin injury at 3dpf and fixed at either 24hpi or 48hpi. Uninjured embryos were fixed at 96hpf or 120hpf.

The protocol "HCR RNA-FISH protocol for whole-mount zebrafish embryos and larvae (*Danio rerio*)", revision number 9, from Molecular Instruments was followed. This involved fixation in PFA overnight then dehydration and permeabilisation in methanol for storage before rehydration in PBST, treatment with proteinase K and postfixation with intermediate wash steps. Samples were then pre-hybridised in probe hybridisation buffer for 30 mins at 37°C before addition of the probe solution and incubation overnight at 37°C. Multiple washes in probe wash buffer and SSCT were then performed, followed by pre-amplification in amplification buffer for 30 mins at RT whilst the HCR hairpins were heated to 95°C for 90 secs and cooled to RT in the dark. Hairpin solution was then added to the samples and incubated overnight at RT in the dark. Hairpin solution was removed by washes in SSCT and samples mounted for imaging using anti-fade mountant.

Table 2.8: HCR RNA-FISH targets and amplifiers

Target	Amplifier
aldh1a2 mRNA	B4-594
col9a2 mRNA	B1-514
Donkey anti-Rabbit anti-GFP	B2-488
inhbaa mRNA	B2-488
wwtr1 mRNA	B5-647
yap1 mRNA	B3-546

A slight modification from the protocol-recommended 30µg/ml Proteinase K for 45 mins to 8µg/ml for 15 mins was used, as optimised for other experiments by Dr. J. Johansson (Feng lab). Initial attempts to use an anti-GFP antibody (#2956, Cell Signalling Technology) coupled with HCR protocol "HCR 2° IHC + HCR RNA-FISH protocol for sample in solution" did not give useable results, so endogenous GFP signal was utilised, with no amplification as the signal

was found to survive the normal HCR protocol. Imaging was performed on a Leica Sp8 confocal microscope (20X air objective or 40X oil objective). Post-imaging processing of spectral unmixing (initially set up by Dr. R. Wiegand, QMRI CALM imaging facility using preset Alexa fluorophores) was performed where required to separate the fluorophores.

2.17 Confocal imaging

Both live and fixed confocal imaging of established transgenic lines was performed. These lines include Tg(*ctgfa*:GFP)^{ed237}, Tg(*lysC*:dsRed)^{nz50} (neutrophil reporter), Tg(*lysC*-NLS:mScarlet)^{ed229} (neutrophil nuclear marker), *Tg(mpeg*:mCherry)^{gl23} (macrophage marker), Tg(*mpeg*-NLS:mScarlet)^{ed230} (macrophage nuclear marker), Tg(*mpeg*:eGFP) (macrophage marker), and TgBAC(*tnfα*:GFP)^{pd1028} (M1 macrophage marker).

2.17.1 Live imaging (single timepoint)

Embryos were anaesthetised using tricaine in 0.3X Danieau's solution (diluted from 30X: 1740mM NaCl, 21mM KCl, 12mM $MgSO_4 \cdot 7H_2O$, 18mM $Ca(NO_3)_2$, 150mM HEPES) and mounted in a glass-bottomed imaging chamber using heated 1% low melting point agarose. When set, agarose was covered with ½ strength tricaine in 0.3X Danieau's solution. Samples were imaged live using a Leica Sp5 confocal microscope (20X air objective) ensuring no pixel saturation.

2.17.2 Live imaging (timelapse)

Embryos were anaesthetised using tricaine in 0.3X Danieau's solution and mounted in a glass-bottomed imaging chamber using heated 0.7% low melting point agarose. When set, agarose was removed from the tail of the embryo using a scalpel. Fish were then covered with ¼ strength tricaine in 0.3X Danieau's solution. Samples were imaged live using a Leica Sp5 confocal microscope (20X air objective) ensuring no pixel saturation. Images were initially taken every 10 minutes from 30 minutes post injury to approximately 5 hours post injury, when images were taken every 30 minutes until 24 hours post injury. GFP fluorescence was quantified in the central blastema, then corrected for fluorescence in a non-regenerating area of the fin (dorsal to the caudal vein), and for autofluorescence in a non-GFP fish.

2.17.3 Fixed imaging (unstained)

Embryos were fixed in 4% PFA/PBS either for 2h at RT or overnight at 4°C, then briefly washed in PBST and mounted onto glass slides using 80% glycerol. Embryos were imaged using a Leica Sp8 confocal microscope (20X air objective) ensuring no pixel saturation.

2.17.4 Opera imaging

lysC-NLS:mScarlet and *mpeg*:eGFP fish were incrossed, and the resulting embryos incubated in 0.003% PTU from 0dpf, with microinjection of *yap1* or *wwtr1* CRISPR as required. At 3dpf, embryos were screened and placed individually in a specialised 96 well imaging plate (ZF plate, Fukanoshi) in 0.3X Danieau's solution with 0.003% PTU and tricaine. Fish were aligned into imaging window just before imaging by spinning down at 1000rpm for 1 minute and manual adjustment. Embryos were imaged using the Opera high-throughput imaging system, using automatic detection of the whole body (optimised by Dr. J. Cholewa-Waclaw, IRR imaging facility). Images were taken through 300µm of the embryo depth (z-stack size=1µm). Stitching and processing of the images and writing of the analysis scripts to quantify cell number in the whole fish was performed by Dr. J. Cholewa-Waclaw. Quantification of cells in the CHT was performed manually in QuPath, with the CHT defined from end of the yolk extension and reaching along the trunk of the embryo to the start of the pigment gap.

2.18 RNA sequencing analysis

Two different types of RNA sequencing were performed and are described below. Previously published data from Lin *et. al*, (2021)[214] was utilised to investigate mild tail fin injury in WT fish at 4hpi. Samples were generated to investigate severe tail fin injury in WT, *yap1* CRISPant, and *wwtr1* CRISPant fish at 24hpi.

2.18.1 Sample collection and sequencing (severe injury only)

RNA extraction was performed as described in 2.7.3. Samples were submitted for RNA sequencing to the Genetics Core, Wellcome Trust Clinical Research Facility Edinburgh. Libraries were prepared using the NEBNext Single Cell/Low Input RNA Library Prep Kit for Illumina according to the provided protocol. Paired-end sequencing was performed on the NextSeq 2000 platform (Illumina Inc, #20038897) using NextSeq 2000 P3 Reagents (200

Cycles). Basecall data was uploaded to BaseSpace and converted into FASTQ files. It is expected to see an average of 63M reads per sample. The number of clusters passing quality filters per sample are shown in Table 2.9.

Table 2.9: Number of clusters passing quality filters per library

Genotype	Injury	Sample ID	Number of clusters
WT	Uninjured	1	51,077,217
		2	77,942,506
		3	102,193,167
	Injured	1	61,680,360
		2	92,764,429
		3	50,509,202
yap1 CRISPant	Uninjured	1	71,681,254
		2	75,366,505
		3	53,443,758
	Injured	1	86,251,076
		2	54,226,186
		3	49,066,003
		4	44,194,080
wwtr1 CRISPant	Uninjured	1	88,271,055
		2	57,452,280
		3	56,997,850
	Injured	1	36,621,711
		2	53,494,456
		3	61,033,837

2.18.2 Sample processing

2.18.2.1 Mild tail fin injury

Previously published bulk RNAseq raw data was obtained from Lin *et. al*, (2021)[214] (only WT untreated samples). Raw fastq files were reanalysed using protocols from the Data Carpentry workshop "RNAseq analysis with R", using self-generated code in Git Bash, Ubuntu, and Eddie, the University of Edinburgh High Performance Computing Cluster (Linux), via MobaXterm. A Fastqc[215] module was used throughout for quality control of samples and to confirm adapter removal. Trimmomatic[216] was used to remove adapters (TruSeq). Burrows-Wheeler Aligner-MEM[217] was used to align trimmed fastq files, creating sam files. SAMtools[218] was used to convert files to bam files and sort by coordinates. HTSeq[219] was used via anaconda[220] to generate count tables for downstream analysis. The reference genome utilised was GRCz11, downloaded from ensembl.org.

2.18.2.2 Severe tail fin injury

Fastq files were downloaded from BaseSpace and analysed using protocols from the Data Carpentry workshop "RNAseq analysis with R", using self-generated code in Eddie, the University of Edinburgh High Performance Computing Cluster (Linux), via MobaXterm. Analysis was performed as described in 2.18.2.1 above, except Trim Galore[221] was used to remove adapters (Illumina and GCT AAT CAT TGC AAG CAG TGG TAT CAA CGC AGA GTA CAT).

2.18.3 Analysis

Data was analysed and visualised using R. Differential expression analysis was performed by the DESeq2 package[222,223]. Significant genes were subset for those with an adjusted p-value of <0.05, and with a log2 fold change as detailed in the relevant sections in 5.2 and 5.3. Data from DESeq analysis was transformed using the rlog function of the rld package[224] before plotting. Annotation was provided by the AnnotationDbi package[225]. Gene names were matched to Ensembl IDs using biomart data from ensembl.org. Heatmaps were generated using the pheatmap package[226], and volcano plots using the ggplot2 package[227].

GO term analysis was performed using the enrichGO function of the clusterProfiler package[228], with genome-wide zebrafish annotation from org.Dr.eg.db package[229]. Significant values were determined to have p<0.05 and a log2 fold change of >0.6 or <-0.6 for an increase or reduction in enrichment respectively. The top 30 most enriched terms (or all enriched terms if fewer than 30) were shown in the graphs, generated by ggplot2[227].

RNAseq differential expression data was filtered by specific gene signatures to elucidate the activity of particular signalling pathways or processes. The Hippo gene signature was generated from lab discussions and the 22 Hippo gene signature described by Wang et. al[230], and is summarised in Table 2.10. The Wnt pathway gene signature was taken from the GO term "Wnt Signalling" GO0016055, and the immune gene signature was taken from the GO term "Immune System Process" GO0002376, both identified using zfin.org. Support for coding throughout was provided by Dr. R. Cunningham (Hansen lab).

Table 2.10: Hippo gene signature used in RNAseq analysis

Gene name	ENSDARG	Gene name	ENSDARG
amot	ENSDARG00000078335	*map4k3a*	ENSDARG00000087742
amotl2a	ENSDARG00000061923	*map4k3b*	ENSDARG00000071357
amotl2b	ENSDARG00000061948	*mob1a*	ENSDARG00000102320
ankrd1a	ENSDARG00000075263	*mob1ba*	ENSDARG00000009169
ankrd1b	ENSDARG00000076192	*mob1bb*	ENSDARG00000012953
arhgef17	ENSDARG00000101644	*myof*	ENSDARG00000006112
asap1a	ENSDARG00000029463	*myofl*	ENSDARG00000017128
asap1b	ENSDARG00000039729	*nf2a*	ENSDARG00000020204
axl	ENSDARG00000112045	*nf2b*	ENSDARG00000025567
bmp4	ENSDARG00000019995	*nt5e*	ENSDARG00000071017
cav1	ENSDARG00000103747	*nuak2*	ENSDARG00000063661
cavin1a	ENSDARG00000076411	*rbms3*	ENSDARG00000044574
cavin1b	ENSDARG00000059362	*rhoaa*	ENSDARG00000026845
crim1	ENSDARG00000029668	*rhoab*	ENSDARG00000094673
ctgfa	ENSDARG00000042934	*rhoac*	ENSDARG00000116058
ctgfb	ENSDARG00000104292	*sav1*	ENSDARG00000006196
cyr61	ENSDARG00000023062	*stk25a*	ENSDARG00000002210
dock5	ENSDARG00000001968	*stk25b*	ENSDARG00000039022
f3a	ENSDARG00000099124	*stk3*	ENSDARG00000011312
fjx1	ENSDARG00000035873	*tead1a*	ENSDARG00000028159
foxp1a	ENSDARG00000004843	*tead1b*	ENSDARG00000059483
foxp1b	ENSDARG00000014181	*tead3a*	ENSDARG00000074321
gadd45aa	ENSDARG00000043581	*tead3b*	ENSDARG00000063649
gadd45ab	ENSDARG00000104571	*tgfb2*	ENSDARG00000027087
igfbp3	ENSDARG00000099144	*vgll4a*	ENSDARG00000094332
lats1	ENSDARG00000003751	*vgll4b*	ENSDARG00000103730
lats2	ENSDARG00000078864	*wwtr1*	ENSDARG00000067719
map4k1	ENSDARG00000114026	*yap1*	ENSDARG00000068401
map4k2	ENSDARG00000001234		

2.19 General zebrafish husbandry and analysis

All zebrafish embryos and adult fish were maintained in the Bioresearch and Veterinary Services (BVS) Aquatic facility in the Queen's Medical Research Institute, the University of Edinburgh, in accordance with UK Home Office Regulations (Guidance on the Operations of Animals, Scientific Procedures Act, 1986). Animal use was reviewed by the Wellcome Trust and conducted with local ethical approval from the University of Edinburgh. Experiments were undertaken under PPL PP1975958 or PEE579666 and PIL I0890B33A. Help was provided for stock maintenance by animal technicians and M. Nosková.

Day-to-day care was performed by trained animal technicians. Fish were maintained in a 14/10 hour light/dark cycle with a water temperature of 28.5°C, pH between 7-7.5, and daily control of water quality, hardness and conductivity. Embryos were obtained through natural matings, were not sorted by sex, and were staged referring to development at 28.5°C. Unless otherwise stated, all fish, including WT, had a WIK background. Adult fish were kept at approximately equal stocking densities throughout. Embryonic survival was calculated as the percentage of embryos that survived from successful fertilisation to 100hpf. Juvenile survival was calculated as the percentage of embryos that survived from 120hpf (i.e. being put into tanks) to 28-35dpf.

"Disrupted" embryos investigated in 3.2.4.2 were defined as embryos that were visually classified as being abnormal in two or more parameters as measured in 96hpf analysis. Remaining embryos were classified as "normal".

2.20 Quantification and statistics

Parameters were quantified using FIJI/ImageJ or QuPath and tabulated with Microsoft Excel 2013. For the screen, CRISPant values were normalised to a gRNA-only control for each gene for each experimental repeat. The average of this normalisation was then transformed by taking the natural log to generate heat map summaries. Screen data was visualised and statistical analyses performed using self-generated R code, except for heat maps, which were generated in GraphPad Prism. RNAseq data visualisation was performed exclusively in R. General R coding was performed using ggplot2[231], tidyverse[227], ggrepel[232], extrafont[233], RColorBrewer[234], and viridis[235] packages. Visualisation and statistical testing for the remaining experiments were performed in GraphPad Prism. Normality calculations were performed using the D'Agostino and Pearson test, unless the sample size was smaller than required for this test, where the Shapiro-Wilk test was used. The term "experimental repeats", used throughout this thesis, is used to mean fish samples generated from a new injection day or breeding, and an independent experiment performed as described.

2.21 Use of Artificial Intelligence

ChatGPT (OpenAI) was used in this thesis for code troubleshooting and initial investigations of differentially expressed genes in the RNAseq analysis (5.2 and 5.3). A list of top DE genes

was given to the interface and asked to determine overall functions of the genes, sorting them into functional groups. This was then confirmed and referenced manually.

2.22 Materials

Reagent	Cat. #/Supplier
2X Brilliant III SYBR Green QPCR Master Mix	600882/Agilent
6X Blue/Orange Loading dye	G190A/Promega
Acetone	20066.321/VWR
Acrylamide (40%)	BP1408-1/Fisher
Agarose	A9539/Sigma
Alexa Fluor 488 goat anti-rabbit 2° Ab	A11088/Invitrogen
Alexa Fluor 555 goat anti-rabbit 2° Ab	A21428/Invitrogen
Ammonium persulfate (APS)	10396503/Fisher Scientific UK
BcgI with NEB buffer 3.1	R0545S/NEB
BD Microlance Needle (25G x 1" – Nr.18)	300400/BD
Bovine Serum Albumin (BSA)	BP9700/Fisher Scientific
BstXI with NEB buffer 3.1	R0113S/NEB
Bsu36I with NEB buffer 1.1 (10X)	R0524S/NEB
Calcium chloride dihydrate ($CaCl_2 \cdot 2H_2O$)	208291/Merck Life Sciences
Calcium Nitrate Tetrahydrate ($Ca(NO_3)_2 \cdot 4H_2O$)	C1396/Sigma
Capillary glass (1.2mm outer diameter, 0.68mm inner diameter, 10.16cm length, with filament)	1B120F-4/World Precision Instruments
Cas9 nuclease	1081059/IDT
Cell lysis buffer	9803S/Cell signalling technologies
Chloroform	C2432/Honeywell
CitiFluor AF1 Mountant Solution	17970-100/Electron Microscopy Sciences
Copper (II) sulphate	451657/Sigma-Aldrich
CRISPR constructs and primers	Various/IDT
DAPI	D9542/Sigma
DASPEI	D0815/Sigma-Aldrich
DMSO	276855/Sigma
DNA ladder	N0467S/NEB
E.Z.N.A. Plasmid DNA Mini Kit I	D6942-02/Omega Bio-Tek
EcoO109I with Neb CutSmart buffer	R0503S/NEB
Ethanol	E/0650DF/17/Fisher
Filter Papers (Western Blotting)	88600/Fisher Scientific
Gapdh 1° Ab	sc25778/Santa Cruz Biotechnology
Gel red	BT41003/Scientific laboratory supplies ltd.
GFP 1° Ab	2956S/Cell signalling
Glucose	G8270/Sigma
Glycerol	BP229-1/Fisher
Goat serum	G9023/Sigma
HCR Probe Buffers (Amplification, Wash, and Hybridisation), amplifiers, and probes	No cat. #/Molecular Instruments
HEPES	H3375/Sigma
High Capacity cDNA Reverse Transcription Kit	4368814/Thermo Fisher Scientific
Hpy99I with NEB CutSmart buffer	R0615S/NEB
HRP 2° substrates	Various/Millipore
Immobilon Western Chemiluminescent HRP substrate	WBKLS0500/Millipore
Low melting point (LMP) agarose	16500/Invitrogen
Magnesium chloride ($MgCl_2$)	M8266/Sigma

Magnesium chloride hexahydrate ($MgCl_2 \cdot 6H_2O$)	12288.36/VWR
Magnesium sulphate ($MgSO_4$)	M2643/Sigma
Manganese(II) chloride (MnCl)	CHE2476/Scientific Laboratory Supplies
Methanol	M/4000/17/Fisher
Methyl cellulose	M0387/Merck Life Sciences
Microloader tips (0.5-20µl)	F5242956003/SLS
NEB buffer 2 (10X)	B70025/NEB
NEBNext Single Cell/Low Input RNA Library Prep Kit	E6420/NEB
NextSeq 2000 P3 Reagents	20040560/NEB
N-Phenylthiourea (PTU)	L06690.09/VWR
One*Taq* Hot Start DNA Polymerase	M0481G/NEB
PageRuler Prestained Protein Ladder	26616/ Thermo Scientific
PFA	28908/Life Technologies
PfoI with Tango buffer	10568350/Fisher Scientific UK
pH3 1° Ab for IF	3377T/Cell signalling
Phenol Red	P0290/Sigma
Phosstop tablets	04906837001/Roche
PhosTag reagent	304-93521/Alpha Laboratories
Ponceau S solution	P7170/Sigma
Potassium chloride (KCl)	P9541/Sigma
PrimeSTAR Max Premix (2x)	R045/TaKaRa
ProLong Diamond Antifade Mountant with DAPI	P36962/Life Technologies
Propan-2-ol	20842.323/VWR chemicals
Protease inhibitors	4693124001/Sigma-Aldrich
qPCR primers	Various/IDT
RNeasy plus micro kit	74034/Qiagen
RNeasy plus mini kit	74136/Qiagen
SacI with NEB CutSmart buffer (10X)	R0156S/NEB
Saline-sodium citrate (SSC)	MB-045-4000/Cambridge Bioscience Ltd
Scalpel (No. 23)	0510/Swann-Morton
SexAI with NEB rCutSmart buffer (10X)	R0605S/NEB
Sodium bicarbonate (NaHCO3)	S6014/Sigma
Sodium chloride (NaCl)	S7653/Sigma
Sodium dodecyl sulphate (SDS)	L3771/Sigma
Sodium hydroxide (NaOH)	S5881/Sigma
StrataClone PCR Cloning Kit	240205/Agilent
T7 Endonuclease	M03025/NEB
Taz 1° Ab for WB and IF	cs8418/Cell signalling
TEMED	17919/Thermo Scientific
tracrRNA	1073190/IDT
Triton X-100	X100/Sigma Aldrich
Trizma base	T6066/Sigma
TRIzol	15596026/Ambion
Tryptone	1279-7099/Fisher Scientific
Tween-20	P1379/Sigma
UltraPure Distilled Water DNase/RNase Free	10977-049/Invitrogen
XcmI with NEB buffer 2.1	R0533S/NEB
X-gal	16495/Cambridge BioScience
X-ray films	MOL7016/Scientific Laboratory Supplies
Yap1 1° Ab for IF	13584-1-AP/ProteinTech

Yap1 1° Ab for WB	cs4912/Cell signalling
Yeast extract	8013-01-2/Acros Organics
ZF imaging plate	HDK-ZFA101-02a/Funakoshi Co.

3 Chapter 1: A CRISPR/Cas9 screen targeting Hippo pathway components in zebrafish embryos identifies component-specific developmental and regenerative phenotypes

3.1 Optimisation of CRISPR/Cas9 mutagenesis mix generation

In order to establish the functional importance of Hippo pathway components *in vivo*, we decided to use the freshwater teleost *Danio rerio* (zebrafish) to perform a CRISPR/Cas9 screen. Multiple Hippo pathway components were targeted, including core components, upstream regulators, and established target genes. The resulting embryos were put through a range of regenerative and developmental assays. However, it was initially vital to optimise the conditions of the CRISPR mutagenesis mix.

A wide variety of dosages and methods to generate the CRISPR/Cas9 mutagenesis microinjection mix in zebrafish can be found from even the briefest of literature searches. For this reason, multiple parameters needed to be optimised for a CRISPR/Cas9 screen of Hippo pathway components. *yap1* CRISPR mutagenesis was utilised for this optimisation, as multiple phenotypes have been previously published for comparison against (see 1.3), including reduced eye size[104,116,236], delayed development[72], and shortened body length[72]. To analyse these in the screen, gross phenotypes were measured at 96hpf, including embryo length, swim bladder inflation (a measure of developmental stage, as the swim bladder inflates in WT embryos at 72hpf[237]), and eye size. These descriptors were used to determine optimal microinjection mix parameters where a clear phenotype was observed in *yap1* CRISPR-mutagenised embryos (CRISPants), without any off-target effects on Cas9-only injected embryos (Cas9) or gRNA-only injected embryos (gRNA).

3.1.1 Microinjection mix generation is optimal at room temperature

CRISPR microinjection mix has been generated at a range of temperatures in multiple publications. Some papers report generating the mix at 95°C[207,208], whilst others specify being generated at room temperature (RT)[238] or components were described as coinjected[73,118,119], suggesting that no heating was performed, and thus can be treated as being generated at RT. Therefore, these two temperatures and a mix generated at 60°C (as an approximate midpoint

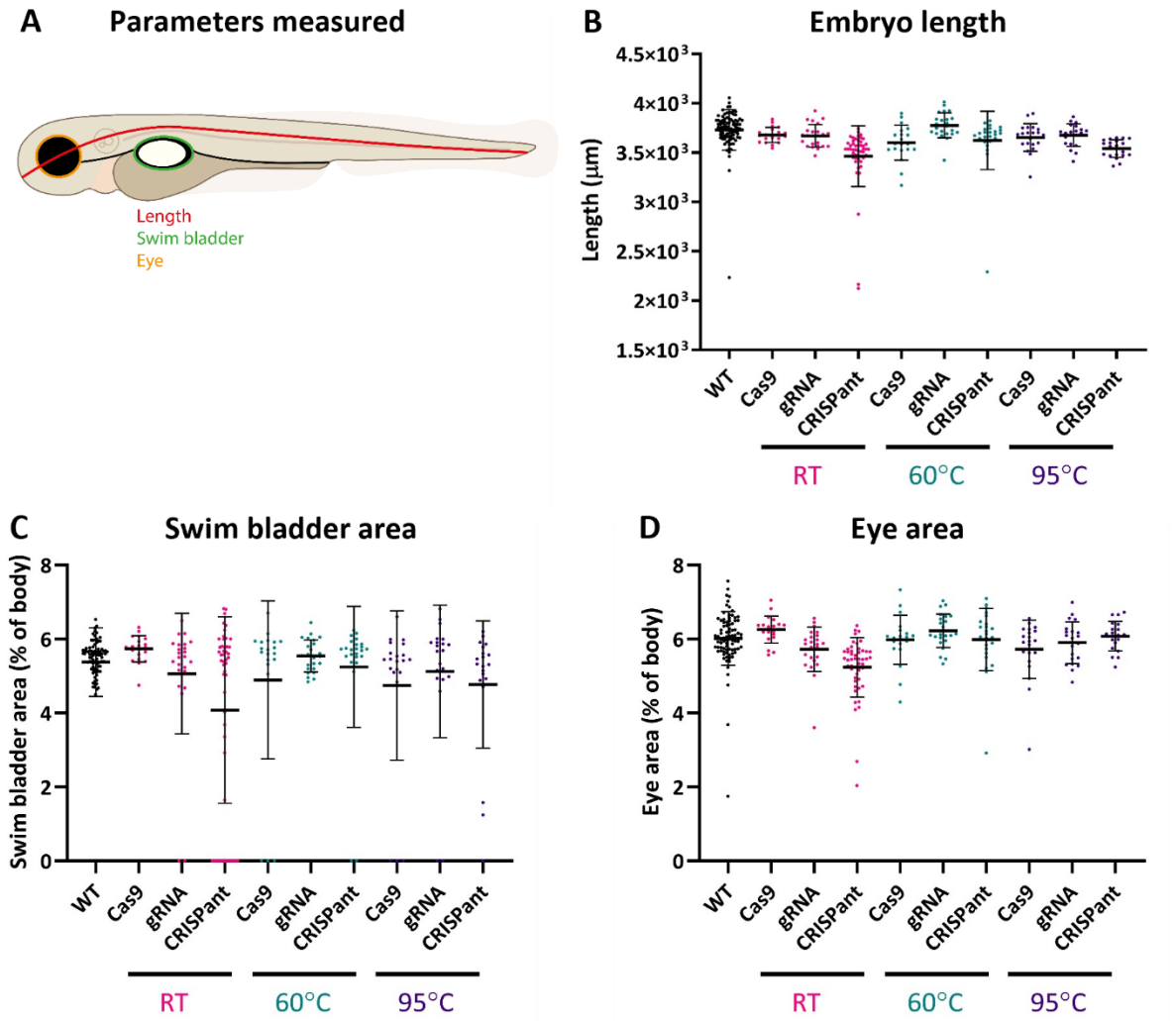

Figure 3.1: Optimisation of microinjection mix generation temperature

(A) Schematic of measured parameters. **(B)** Quantification of embryo length in CRISPants and controls with microinjection mixes generated at RT, 60°C, and 95°C. Embryo length of *yap1* CRISPant and controls showed little difference upon changing temperature. **(C)** Quantification of swim bladder area (as percentage of whole-body area) in CRISPants and controls with microinjection mixes generated at RT, 60°C, and 95°C. Swim bladder area became more altered in controls from WT as temperature increases. **(D)** Quantification of eye area (as percentage of whole-body area) in CRISPants and controls with microinjection mixes generated at RT, 60°C, and 95°C. Only mix generated at RT had a specific CRISPant-associated phenotype of reduced eye size.

Significance not shown for clarity of graphs, as many groups required comparison. Bars show mean±SD. Data from one independent experimental repeat. Each dot represents one embryo. RT=room temperature; Cas9=Cas9-only injected fish; gRNA=*yap1* CRISPR guide RNA-only injected fish; CRISPant=*yap1* CRISPR-mutagenised fish. Injection of a 1nl bolus.

between RT and 95°C) were tested to optimise this critical step of the mutagenesis protocol (see 2.1 for more detail). Assuming accuracy of previously published papers, *yap1* CRISPR mutagenesis was expected to show reduced length, reduced swim bladder (SB) size (i.e. delayed development), and reduced eye area[72,77–79,92,104,108]. Only embryos injected with a mix generated at RT gave a consistent phenotype solely in CRISPants (Figure 3.1). In *yap1* CRISPants generated at RT, trends towards the expected reduction in length (Figure 3.1B), swim bladder area (Figure 3.1C), and eye area (Figure 3.1D) was observed. This data, combined with the ease of generating the microinjection mix at this temperature, suggests that the mix should be generated at RT before injection.

3.1.2 The ideal microinjection mix volume is 2nl per embryo

A range of volumes and doses of the CRISPR microinjection mix have been reported (e.g.[73,75,201,239]), so this was also optimised. For this study, 0.5nl, 2nl, and 4nl volumes were injected using a microinjection mix generated at RT, at a concentration of 500ng/µl Cas9, 25ng/µl each guide RNA, and 100ng/µl tracrRNA (for the total amount that these represent see Table 2.3). The data from this optimisation showed that injection of 2nl and 4nl volumes gave the expected CRISPant phenotype for all parameters analysed (Figure 3.2). However, 4nl volume gave apparent off-target effects in Cas9 and gRNA-only injected groups, suggesting that the microinjection mix became toxic at a higher dose and/or volume. For the remainder of the screen, a 2nl bolus was injected.

3.2 Validation of successful CRISPR/Cas9 mutagenesis using *yap1* CRISPants

3.2.1 *yap1* CRISPR/Cas9 guide RNAs had high DNA mutagenesis efficiency

CRISPR-mediated *yap1* DNA mutagenesis was confirmed using T7E1 digestion (see Figure 2.1 for summary of its function). This enzyme cleaves DNA mismatches, giving distinct DNA bands when run on an agarose gel, and so indicating successful CRISPR mutagenesis. When applied to gDNA extracted from embryos injected with one of two *yap1*-targeting CRISPR guides (sequences in

Table 2.1) and relevant controls, this showed mutagenesis for both guides in the CRISPant embryos only (Figure 3.3). The control samples from guide 2 (Figure 3.3B) also showed some banding, suggesting the presence of single nucleotide polymorphisms (SNPs) in the control population. However, the CRISPant sample

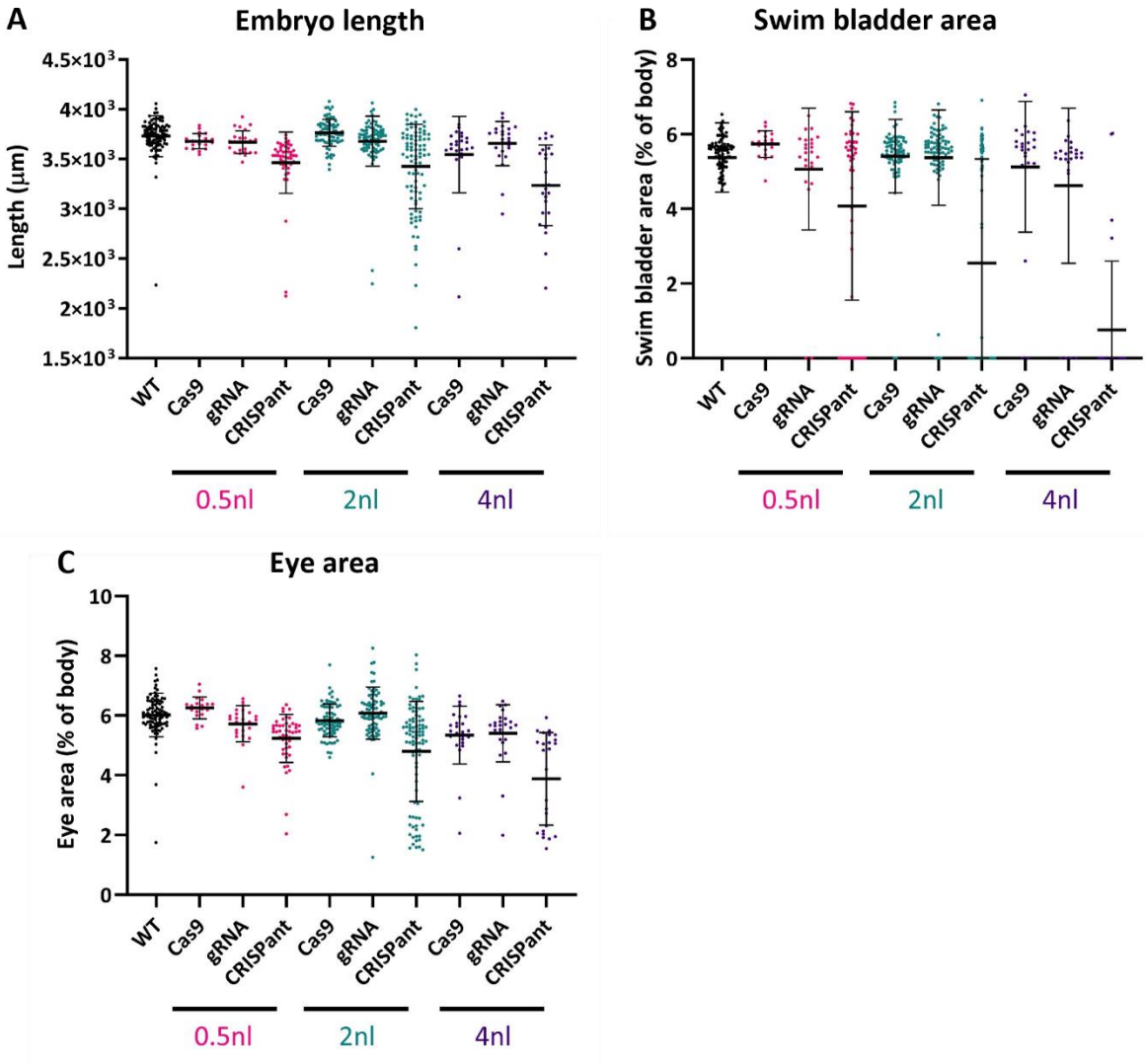

Figure 3.2: Optimisation of microinjection mix volume

(A) Quantification of embryo length in CRISPants and controls with microinjection mixes injected at doses of 0.5nl, 2nl, and 4nl. A CRISPant-specific length reduction was observed that becomes more prominent with increasing volume. **(B)** Quantification of swim bladder area (as percentage of whole-body area in CRISPants and controls with microinjection mixes injected at doses of 0.5nl, 2nl, and 4nl. The area had more prominent reductions with increasing volume. Controls began to show the expected *yap1* disruption-associated phenotypes at 4nl volume. **(C)** Quantification of eye area (as percentage of whole-body area in CRISPants and controls with microinjection mixes injected at doses of 0.5nl, 2nl, and 4nl. Eye size had more prominent defects with increasing volume. Controls began to show the expected *yap1* disruption-associated phenotypes at 4nl volume.

Significance not shown for clarity of graphs, as many groups required comparison. Bars show mean±SD. Data from one independent experimental repeat, except 2nl, where at least three experimental repeats were performed (this data is also shown in Figure 3.7). Each dot represents one embryo. Cas9=Cas9-only injected fish; gRNA=*yap1* CRISPR guide RNA-only injected fish; CRISPant=*yap1* CRISPR-mutagenised fish.

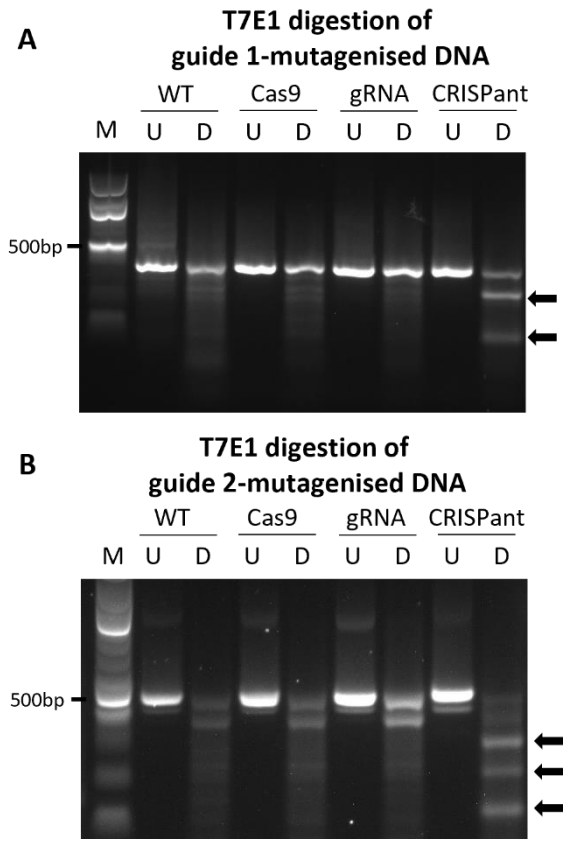

Figure 3.3: *yap1* CRISPR guide testing
DNA agarose gels of pooled *yap1* CRISPants and associated controls treated with T7 endonuclease I shows specific DNA mutagenesis. **(A)** T7 endonuclease I digestion of the region targeted by *yap1* CRISPR guide 1. Only the CRISPant group showed mutagenesis. **(B)** T7 endonuclease I digestion of the region targeted by *yap1* CRISPR guide 2. Only the CRISPant group showed mutagenesis.
Banding indicates gDNA mutations. U=undigested gDNA; D=digested gDNA; M=100bp marker; Cas9=Cas9-only injected fish; gRNA=*yap1* CRISPR guide RNA-only injected fish; CRISPant=*yap1* CRISPR-mutagenised fish. Arrows denote cleaved bands that represent mutagenesis. Undigested bands expected at ~400bp (guide 1) and ~440bp (guide 2).

had a noticeably different banding pattern to controls, suggesting mutagenesis outside these SNPs. To ensure total gene disruption going forward, both guides were injected together to create *yap1* CRISPants.

3.2.2 RT-qPCR during zebrafish embryo development was possible and showed specific patterns in mRNA expression

Molecular studies of CRISPR mutants are desirable to ensure that CRISPR mutagenesis disrupts the gene/protein of interest and to elucidate the molecular mechanisms that underlie any phenotype measured from the above functional and developmental assays. One key area of study for this was the analysis of mRNA levels in CRISPant embryos via RT-qPCR.

RNA isolation using a protocol based on the TRIzol reagent user guide extraction (method 'a', see 2.7.1) yielded RNA with a low purity, particularly at early developmental time points, as shown by the 260/280 absorbance ratio being lower than the desired value of 2 (Figure 3.4A). Therefore, RNA isolation was trialled using a Qiagen RNeasy mini kit (method 'b', see 2.7.2). This approach gave significantly higher 260/280 absorbance ratios than samples from extraction method 'a' and were closer to the desired value of 2. Therefore, this method was used for RNA extraction going forward.

RNA extraction and RT-qPCR analysis were performed during embryogenesis (1-120hpf) for the Hippo pathway components *yap1*, *wwtr1*, *lats2*, and the Yap1/Taz target genes *cyr61*, *ctgfa*, *cav1*, and *cavin1a*[9,10] (Figure 3.4B-H). Note that, in mammals, LATS2 is also a YAP/TAZ target gene and part of a negative feedback loop[240]. All selected genes were expressed at detectable levels throughout embryogenesis. Expression levels were dynamic and followed two notable patterns: one where the expression levels decreased after 1hpf and did not increase to above that level throughout development (for *yap1* and *cyr61*), and one where expression increased during development, peaking at 72hpf (*wwtr1* and *ctgfa*). This shows that RNA can be isolated, and these Hippo pathway-associated genes can be analysed at a range of time points during embryogenesis.

A range of timepoints were also taken to analyse mRNA expression in *yap1* CRISPants: 24hpf, 48hpf, and 96hpf (Figure 3.4I-L). These showed that *yap1* mRNA expression was reduced at both 24hpf and 48hpf, though only significantly at 24hpf (Figure 3.4I), suggesting that CRISPant cells might be outcompeted at later developmental timepoints. Alternatively, CRISPR mutagenesis may not affect mRNA levels, as mRNA could still be generated, but be altered through post-transcriptional processes such as the introduction of an early stop codon that does not become apparent until translation. There were also no changes in mRNA of select other Hippo pathway components, including the *yap1* paralogue *wwtr1*. For all groups and genes, there was a much higher variability in CT values at 96hpf. Therefore, RNA should preferentially be extracted at early time points to confirm that CRISPR-mediated mutagenesis impacts on mRNA levels. Data for 24hpf *yap1* samples are shown in Figure 3.4M, this time normalised to gRNA-only injected controls. The same pattern of *yap1* mRNA reduction but not *wwtr1* mRNA or Yap1/Taz downstream target mRNA was observed. This pattern was

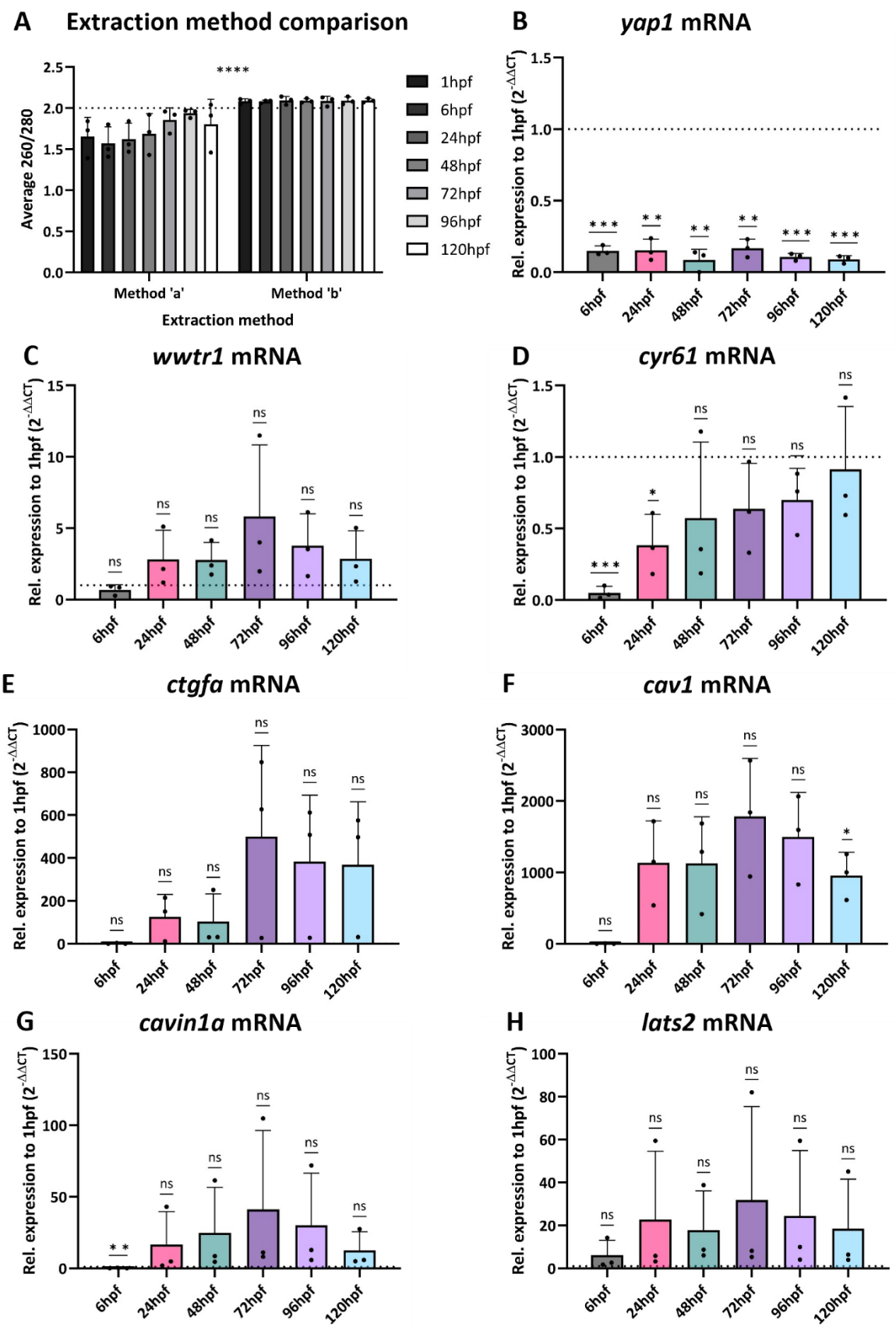
A
Extraction method comparison
Average 260/280
Extraction method
Method 'a'
Method 'b'
****
1hpf
6hpf
24hpf
48hpf
72hpf
96hpf
120hpf
B
yap1 mRNA
C
wwtr1 mRNA
D
cyr61 mRNA
E
ctgfa mRNA
F
cav1 mRNA
G
cavin1a mRNA
H
lats2 mRNA
Rel. expression to 1hpf (2-ΔΔCT)
6hpf
24hpf
48hpf
72hpf
96hpf
120hpf
ns

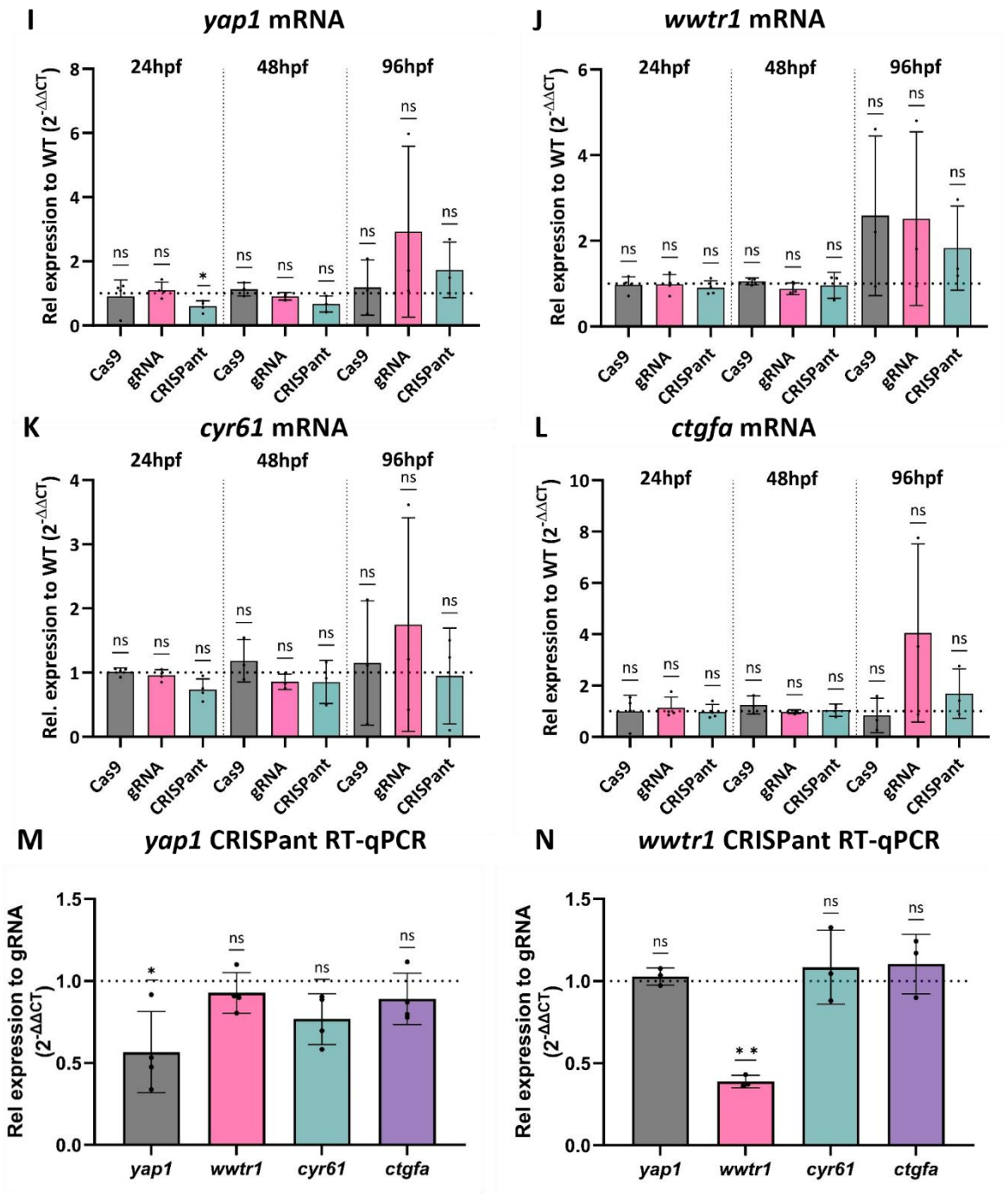

Figure 3.4: RT-qPCR of selected Hippo pathway-associated genes across early development and upon mutagenesis

(A) 260/280 values of RNA extracted over development by RNA extraction methods 'a' and 'b'. Method 'b' had the more consistent quality throughout (2-way ANOVA, comparison of extraction method). **(B)** *yap1* mRNA levels during embryogenesis measured by RT-qPCR. **(C)** *wwtr1* mRNA levels during embryogenesis measured by RT-qPCR. **(D)** *cyr61* (*ccn1*) mRNA levels during embryogenesis measured by RT-qPCR. **(E)** *ctgfa* (*ccn2a*) mRNA levels during embryogenesis measured by RT-qPCR. **(F)** *cav1* mRNA levels during embryogenesis measured by RT-qPCR. **(G)** *cavin1a* mRNA levels during embryogenesis measured by RT-qPCR. **(H)** *lats2* mRNA levels during embryogenesis measured by RT-qPCR. **(I)** *yap1* mRNA levels after *yap1* CRISPR mutagenesis measured by RT-qPCR at 24hpf, 48hpf, and 96hpf. *yap1* mRNA was specifically reduced in CRISPants at 24hpf only. **(J)** *wwtr1* mRNA levels after

yap1 CRISPR mutagenesis measured by RT-qPCR at 24hpf, 48hpf, and 96hpf. No change was observed. **(K)** *cyr61* mRNA levels after *yap1* CRISPR mutagenesis measured by RT-qPCR at 24hpf, 48hpf, and 96hpf. No change was observed. **(L)** *ctgfa* mRNA levels after *yap1* CRISPR mutagenesis measured by RT-qPCR at 24hpf, 48hpf, and 96hpf. No change was observed. **(M)** RT-qPCR of 24hpf *yap1* CRISPant mRNA abundance relative to gRNA control. *yap1* mRNA was significantly reduced, whilst *wwtr1*, *cyr61*, and *ctgfa* mRNA levels are unchanged. **(N)** RT-qPCR of 24hpf *wwtr1* CRISPant mRNA abundance relative to gRNA control. *wwtr1* mRNA was significantly reduced, whilst *yap1*, *cyr61*, and *ctgfa* mRNA levels are unchanged.
Data for B-H is normalised to housekeeping gene *ef1α* and shown relative to 1hpf values. Data for I-L is normalised to *ef1α* and shown relative to WT values. Data for M+N is normalised to *ef1α* and shown relative to gRNA values. Cas9=Cas9-only injected fish; gRNA=*yap1* CRISPR guide RNA-only injected fish; CRISPant=*yap1* CRISPR-mutagenised fish. Data from at least three experimental repeats, each dot represents one repeat. Bars represent mean±SD. Note the y-axis is different for each gene. Significance calculated by one-sample t-test unless otherwise stated (μ=1). *p<0.05; **p<0.01; ns= not significant.

---

wwtr1 mRNA only (Figure 3.4N) (see below for investigation of *wwtr1* CRISPants). This confirms the specificity of the CRISPR/Cas9 mutagenesis technique at early timepoints.

3.2.3 Optimisation of Western and PhosTag blotting of zebrafish embryos showed effective CRISPR mutagenesis

Most antibodies that are used in research are raised against human or mouse proteins. Therefore, the use of antibodies in zebrafish is notorious in its unreliability and low specificity, meaning that few robust antibodies are available. Luckily, there are antibodies available that reportedly target zebrafish Yap1 and Taz. However, due to the paucity of effective zebrafish antibodies, Western blotting protocols for zebrafish samples are few and varied, so this technique required optimisation. One key interfering variable in the analysis of (particularly early) zebrafish embryos is the presence of the protein-rich yolk, which provides nutrients to the developing embryo. To reduce the impact of this, two sample preparation protocols were followed: one to remove the yolk before lysate preparation (to remove any interfering yolk components[210]) and another to create lysates that retained the yolk (see 2.10.1). The resulting western blots are shown in Figure 3.5A and B and suggest that removing the yolk creates a more consistent and specific band at the correct size. In yolk-retained samples, no protein was seen at later timepoints and there were non-specific bands at early timepoints, suggesting yolk proteins interfere with western blotting. The absence of interfering proteins in yolk-removed samples can be observed in the Ponceau blot of early embryo samples, where the yolk-retained samples showed a “smearing” of protein that was absent in yolk-

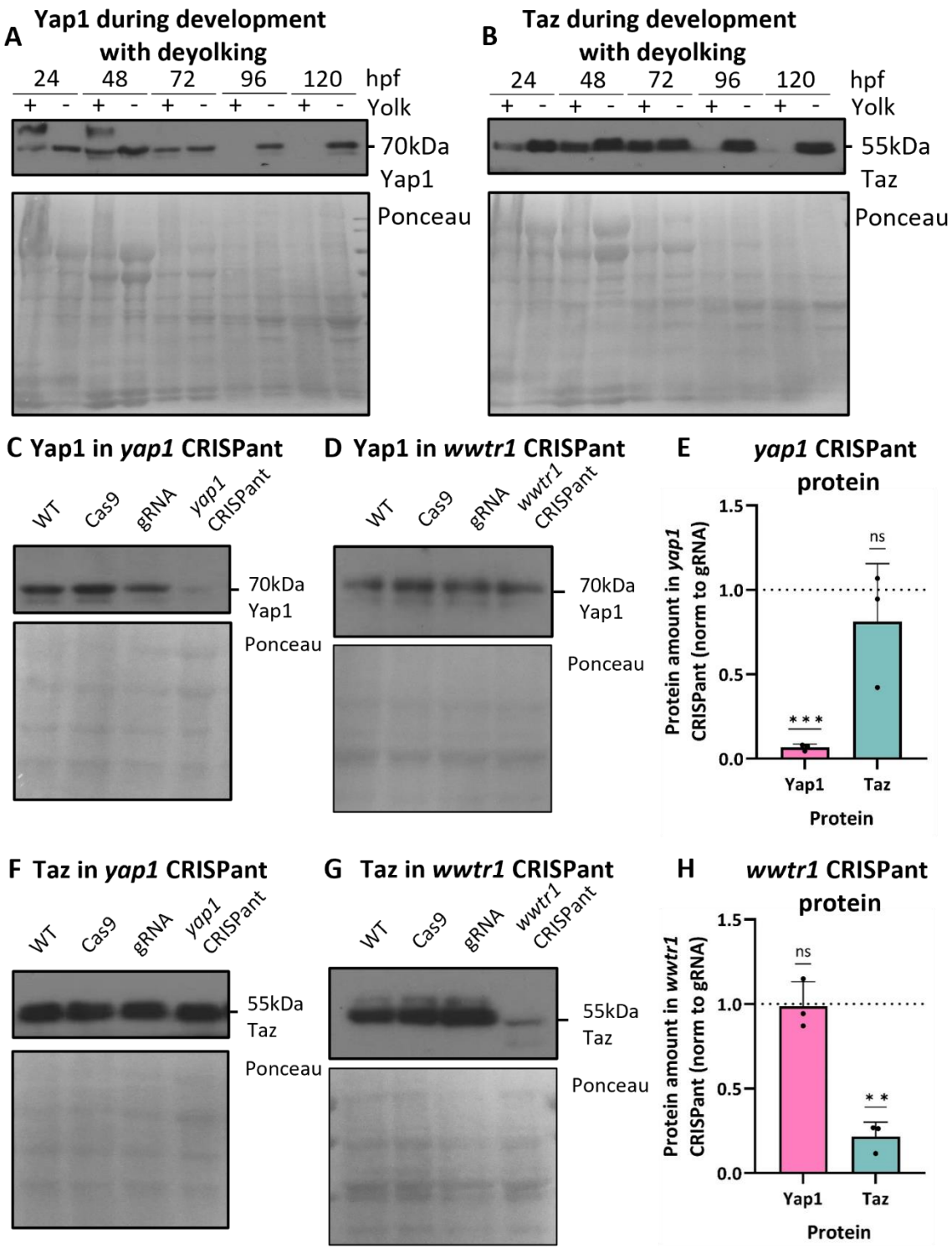
A
Yap1 during development with deyolking
24 48 72 96 120 hpf
+ - + - + - + - + - Yolk
70kDa Yap1
Ponceau
B
Taz during development with deyolking
24 48 72 96 120 hpf
+ - + - + - + - + - Yolk
55kDa Taz
Ponceau
C Yap1 in yap1 CRISPant
WT Cas9 gRNA yap1 CRISPant
70kDa Yap1
Ponceau
D Yap1 in wwtr1 CRISPant
WT Cas9 gRNA wwtr1 CRISPant
70kDa Yap1
Ponceau
E yap1 CRISPant protein
Protein amount in yap1 CRISPant (norm to gRNA)
1.5
1.0
0.5
0.0
ns
***
Yap1 Taz
Protein
F Taz in yap1 CRISPant
WT Cas9 gRNA yap1 CRISPant
55kDa Taz
Ponceau
G Taz in wwtr1 CRISPant
WT Cas9 gRNA wwtr1 CRISPant
55kDa Taz
Ponceau
H wwtr1 CRISPant protein
Protein amount in wwtr1 CRISPant (norm to gRNA)
1.5
1.0
0.5
0.0
ns
**
Yap1 Taz
Protein
I Taz PhosTag
24 48 72 96 120 hpf
Inactive Taz
Active Taz

Figure 3.5: Optimisation of Western blotting and PhosTag electrophoresis in zebrafish embryos and verification of CRISPR mutagenesis

(A) Yap1 western blot during development of WT fish with yolk retained (+) and yolk removed (-). Deyolked samples had a stronger and more consistent Yap1 band at all timepoints. **(B)** Western blot during development of WT fish with yolk retained (+) and yolk removed (-). Deyolked samples had a stronger and more consistent Taz band at all timepoints. **(C)** Western blot probed for Yap1 in 72hpf *yap1* CRISPants and controls. An absence of Yap1 was only seen in CRISPants. **(D)** Western blot probed for Yap1 in 72hpf *wwtr1* CRISPants and controls. No change was seen. **(E)** Western blot quantification of *yap1* CRISPant samples. *yap1* CRISPants had reduced Yap1 but not Taz. **(F)** Western blot probed for Taz in 72hpf *yap1* CRISPants and controls. No change was seen. **(G)** Western blot probed for Taz in 72hpf *wwtr1* CRISPants and controls. A marked reduction of Taz protein was only seen in *wwtr1* CRISPants. **(H)** Western blot quantification of *wwtr1* CRISPant samples. *wwtr1* CRISPants had reduced Taz but not Yap1. **(I)** Sample Taz PhosTag of WT samples during development. It was difficult to visualise any robust changes in phosphorylation status.

Cas9=Cas9-only injected fish; gRNA=*yap1* CRISPR guide RNA-only injected fish; CRISPant=CRISPR-mutagenised fish. Ponceau stain of membrane was used as a loading control. Samples were pooled from individual larvae under the same experimental conditions (for numbers, see 2.10). Bars show mean±SD. Significance calculated by one-sample t-test (μ=1). Data (E+H) from three independent experimental repeats, each dot represents one repeat. **p<0.01; ***p<0.001

removed samples. Therefore, in subsequent protein analyses the yolk was removed before western blotting/PhosTag samples were prepared.

The Yap1 antibody was tested in *yap1* CRISPants, showing a clear reduction in Yap1 signal and demonstrating the efficiency of this method of mutagenesis and the specificity of the antibody (Figure 3.5C). There was no change in Yap1 protein in *wwtr1* CRISPants, showing the specificity of both the antibody and the CRISPR technique (Figure 3.5D). Accordingly, the Taz antibody showed a reduction in Taz protein in *wwtr1* CRISPants but not in *yap1* CRISPants (Figure 3.5F and G). These antibodies also created blots that could be quantified and that supported this finding (Figure 3.5E and H).

PhosTag PAGE is a variant of SDS-PAGE where proteins are separated predominantly according to their phosphorylation state rather than molecular weight[211,241]. This is a key technique often used *in vitro* to analyse Hippo pathway activity as the Hippo pathway is a phosphorylation cascade, where the activity of the main effectors YAP/TAZ is regulated by their phosphorylation status (inactive when phosphorylated and active when dephosphorylated) (Figure 1.1). We therefore attempted to utilise this technique to analyse the activity of the upstream Hippo pathway kinases in zebrafish samples. This is of particular utility as these kinases do not have confirmed antibodies in the zebrafish and would allow the

indirect measurement of Yap1/Taz activity, rather than abundance as measured by Western blotting.

Running a PhosTag gel and probing for Taz showed that phosphorylation of a key Hippo pathway effector can be detected at a range of developmental timepoints in the zebrafish. Therefore, this may be a useful tool to analyse the effects of Hippo pathway components upstream of Yap1/Taz (Figure 3.5I). No changes in phosphorylation status were observed. However, this blot was unclear compared to those generated from *in vitro* samples (for example, in Cunningham et. al.[242]), with a "wavy" pattern and poorly defined protein bands. This could be a result of interfering components within the sample, but further investigation as to the cause was not performed. A Yap1 PhosTag could also not be performed, limiting this technique's utility in these studies. This technique will therefore not be brought forward for further analysis.

3.2.4 Optimisation of developmental and regenerative CRISPR/Cas9 screen assays

3.2.4.1 Developmental phenotypes are best measured at 96hpf

As described in 1.3, many phenotypes associated with *yap1* mutagenesis include a delay or defect in development. This includes reduced size with curved body axis[72,77,78,80,92,108], developmental delay[72,77,78], decreased eye size and other craniofacial defects[72,77,104,108], reduced survival[72], and cardiovascular deformations such as heart oedema[80,97,108] and vascular defects[79,97,119]. Multiple potential ways to measure these parameters in the CRISPR screen were investigated. Firstly, measurements of early developmental stages were performed at 6hpf. Embryos were imaged and the developmental stage was visually categorised from stages defined in Kimmel *et. al.*, 1995[243]. This showed a significant difference when all groups were compared (Figure 3.6A), with a trend for CRISPants to be developmentally delayed. However, this significance was maintained when the CRISPant group was excluded from the analysis, suggesting that this method is not accurate enough to show a specific CRISPant phenotype, or that the mechanical stress of injection impacts on very early development. This method is also subjective, as some embryos showed unclear developmental stages. Therefore, this analysis was not brought forward in the screen. Developmental delay was then measured at the later time point of 96hpf. This time point was chosen as the WT zebrafish embryo swim bladder inflates at around 72hpf[243]. Therefore, by

imaging the embryos at the later time point of 96hpf, the size of the swim bladder can be measured and used as a proxy for developmental stage. As expected, *yap1* CRISPants showed a significant reduction in swim bladder size at 96hpf (Figure 3.6B-C), suggesting a developmental delay. This timepoint was therefore carried forward for the screen.

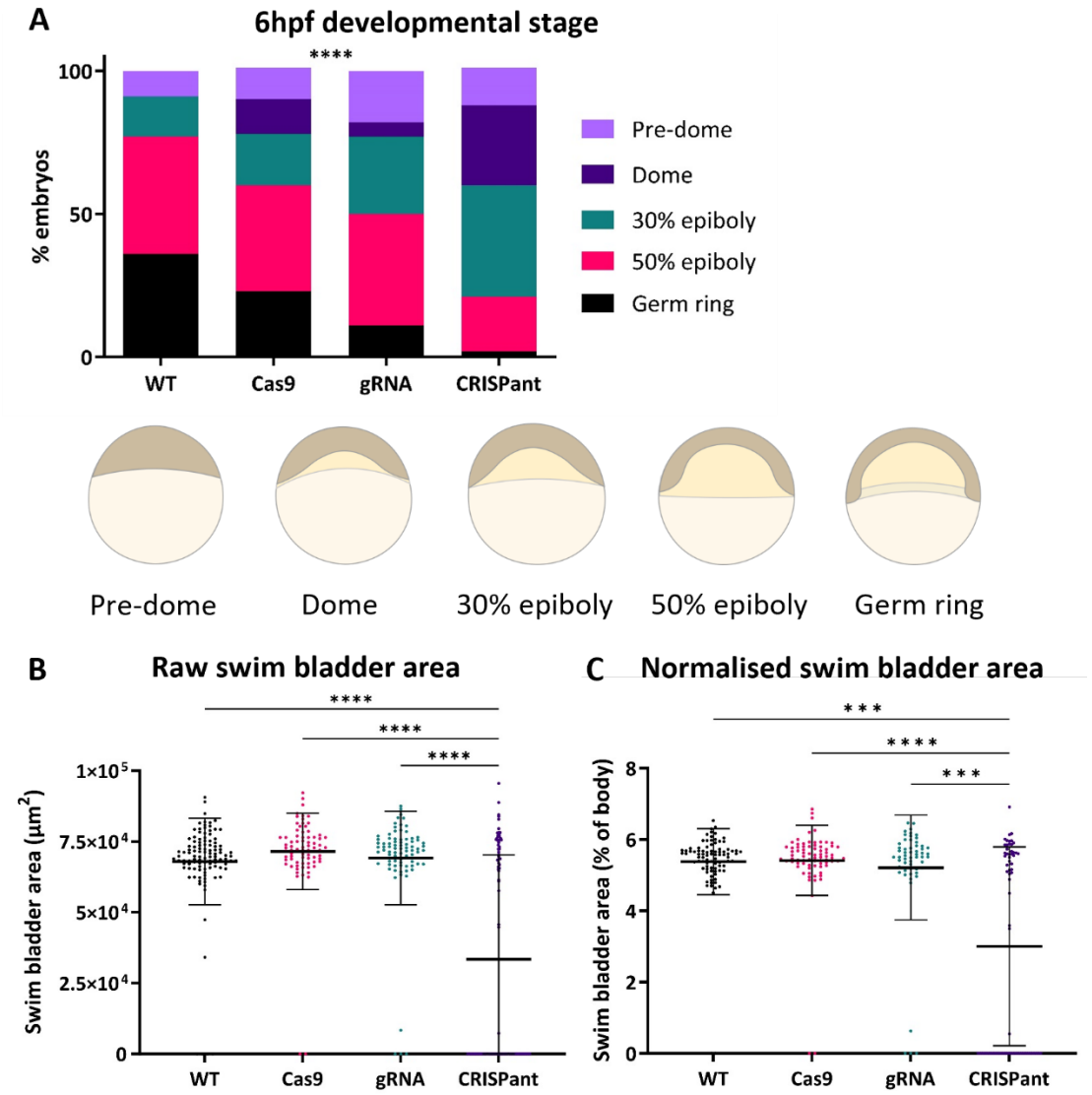

Figure 3.6: Developmental timing in *yap1* CRISPants at 6hpf and 96hpf
(A) Proportion of embryos at each developmental stage at 6hpf (chi-squared test), scored according to images in Kimmel et. al., 1995[243] (n=20-40). Schematics depict each developmental stage. This showed significant differences across all groups. **(B)** Quantification of raw swim bladder area at 96hpf. Only *yap1* CRISPants showed a significant decrease. **(C)** Quantification of swim bladder area as a percentage of body size at 96hpf. Only *yap1* CRISPants showed a significant decrease.
Cas9=Cas9-only injected fish; gRNA=*yap1* CRISPR guide RNA-only injected fish; CRISPant=*yap1* CRISPR-mutagenised fish. Bars show mean±SD. Significance for B+C calculated by Kruskal-Wallis test, with multiple comparisons. Data from at least three independent experimental repeats. Each dot represents one embryo. ***p<0.001; ****p<0.0001.

Imaging was also used to analyse a range of other gross developmental phenotypes at this timepoint. A schematic representation of these is shown in Figure 3.7A and analysis involves measurements of length, body area, eye area, cardiac oedema, and yolk oedema. Representative images are shown in Figure 3.7B. These showed the expected *yap1* CRISPant phenotypes, including reduced body length (Figure 3.7C), decreased eye area (suggesting organ size dysregulation) (Figure 3.7D), and increased heart (Figure 3.7E) and yolk-associated oedema (Figure 3.7F) (suggesting general developmental defects). Measurement of overall body size showed there was no significant change in CRISPants (Figure 3.7G). However, parameters were calculated as a percentage of whole body size to determine which would be a clearer measure of gross phenotypes. Similar results to those seen for raw values were observed (Figure 3.7H-J). This is likely due to body area being unchanged from controls (Figure 3.7G). However, other CRISPants could have altered body size that may confound other results. Consequently, the area as a percentage of whole body size was used to reduce the impact of confounding variables on other measurements.

In measurements of embryo twisting (indicative of defective midline development[244]), a significant increase in the proportion of embryos that were visually classified as twisted was observed (Figure 3.7K). Twisted embryos were defined as those without a trunk that points only slightly downwards from the head. The *yap1* CRISPant image in Figure 3.7B would be classified as twisted whilst the controls would not. As for 6hpf analyses, this significance was maintained when the CRISPant group was removed from the analysis. This suggests that this is not an appropriate method to analyse CRISPR mutagenesis, potentially due to its subjective nature or the mechanical trauma of microinjection.

A trend towards a reduction in survival in microinjected embryos was seen over the first 100 hours of development (Figure 3.7L). However, this was not significant or specific to CRISPants as Cas9 and gRNA controls also showed a reduction in survival, suggesting that this may be due to the mechanical trauma of injection. The majority of embryo death occurred in the first 48 hours post injection. Therefore, for analysis of survival in the CRISPR screen, survival was only noted at one timepoint: 96hpf, for experimental ease.

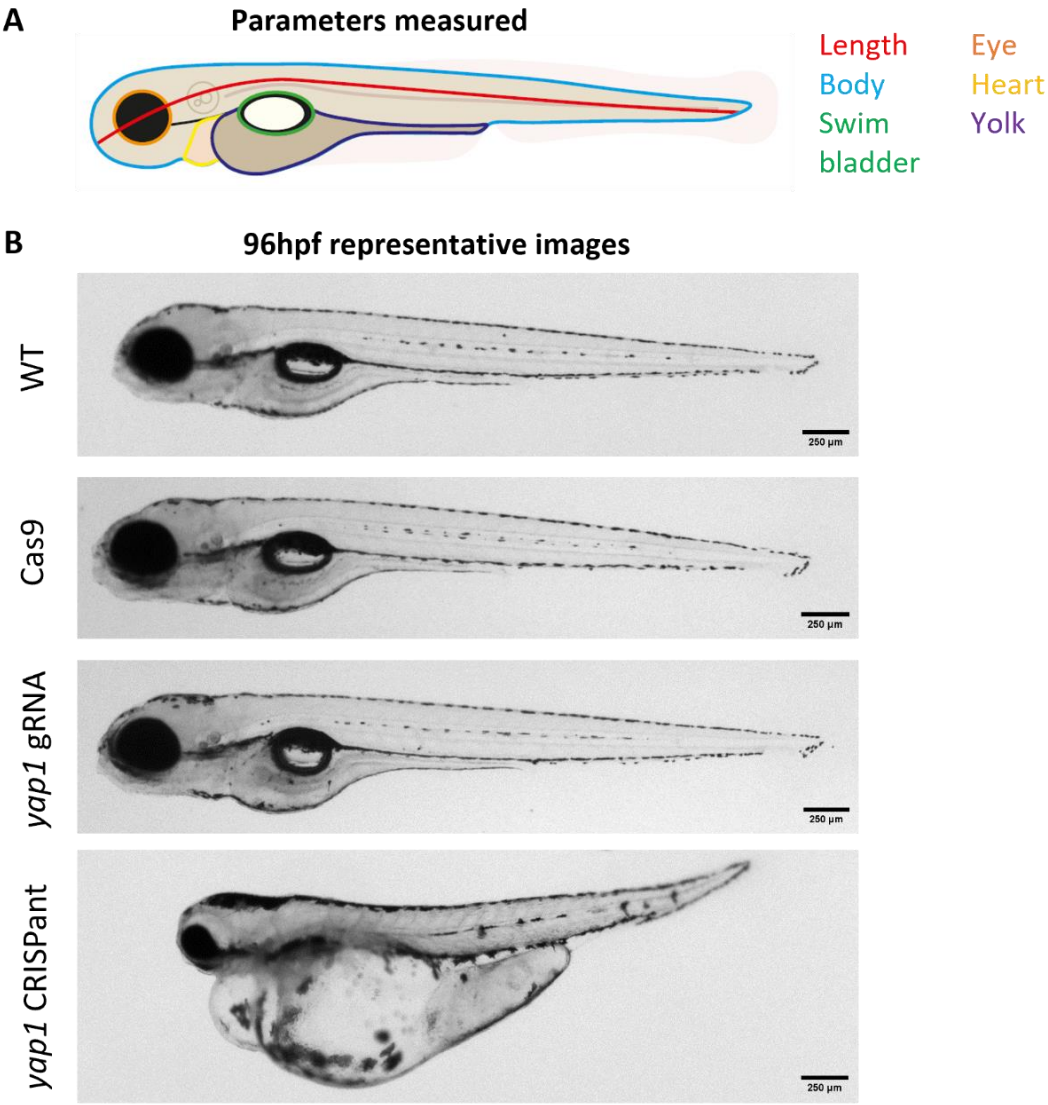
A
Parameters measured
Length
Body
Swim bladder
Eye
Heart
Yolk
B
96hpf representative images
WT
Cas9
yap1 gRNA
yap1 CRISPant
250 µm
C
Embryo length
Length (µm)
4500
4000
3500
3000
2500
2000
1500
****
****
ns
WT
Cas9
gRNA
CRISPant
D
Eye area
Eye area (µm²)
1.25×10⁵
1×10⁵
7.5×10⁴
5×10⁴
2.5×10⁴
0
****
****
****
WT
Cas9
gRNA
CRISPant

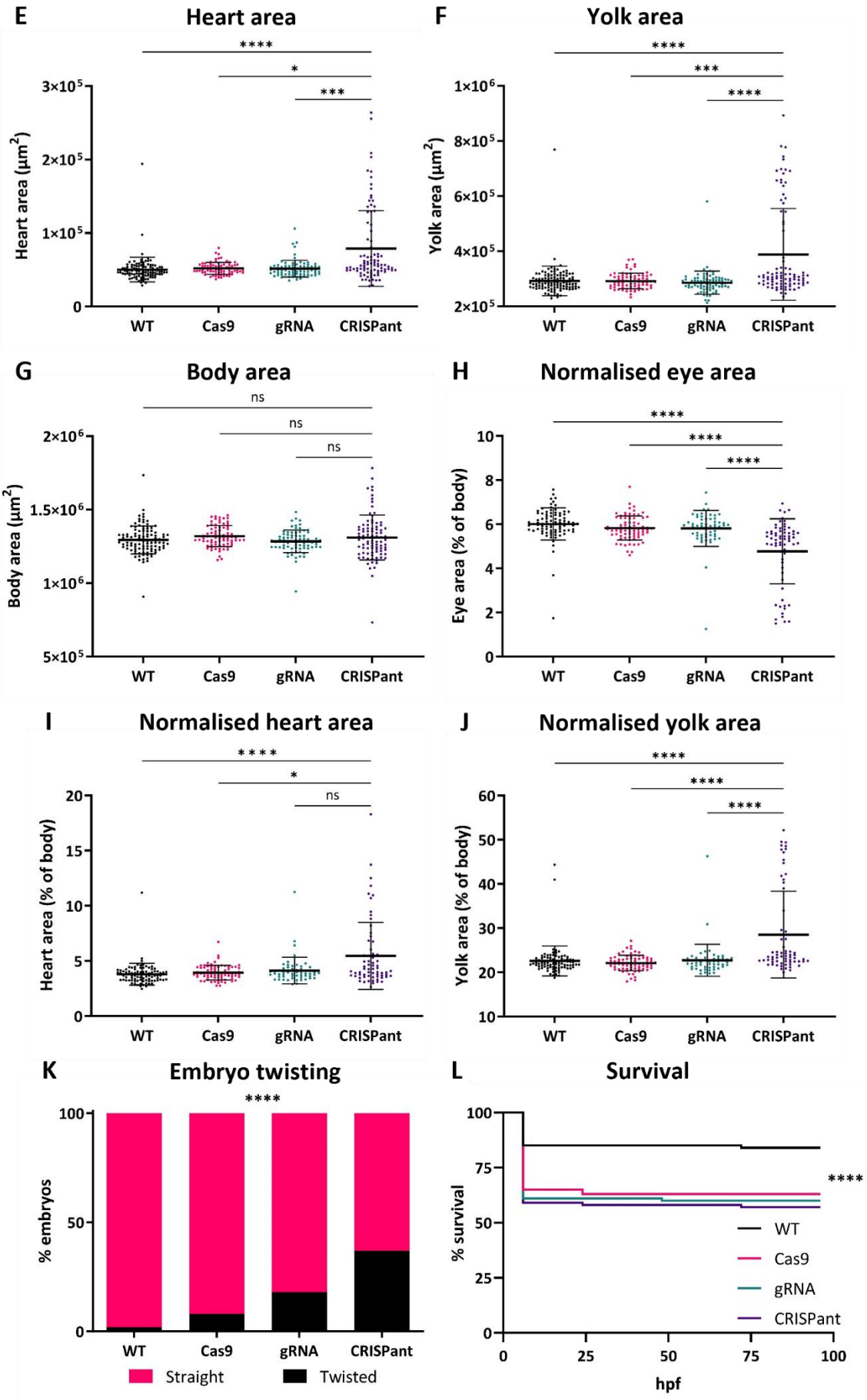
E
Heart area
Heart area (µm²)
3×10⁵
2×10⁵
1×10⁵
0
****
*
***
WT
Cas9
gRNA
CRISPant
F
Yolk area
Yolk area (µm²)
1×10⁶
8×10⁵
6×10⁵
4×10⁵
2×10⁵
****
***
****
WT
Cas9
gRNA
CRISPant
G
Body area
Body area (µm²)
2×10⁶
1.5×10⁶
1×10⁶
5×10⁵
ns
ns
ns
WT
Cas9
gRNA
CRISPant
H
Normalised eye area
Eye area (% of body)
10
8
6
4
2
0
****
****
****
WT
Cas9
gRNA
CRISPant
I
Normalised heart area
Heart area (% of body)
20
15
10
5
0
****
*
ns
WT
Cas9
gRNA
CRISPant
J
Normalised yolk area
Yolk area (% of body)
60
50
40
30
20
10
****
****
****
WT
Cas9
gRNA
CRISPant
K
Embryo twisting
% embryos
100
50
0
****
WT
Cas9
gRNA
CRISPant
Straight
Twisted
L
Survival
% survival
100
75
50
25
0
****
WT
Cas9
gRNA
CRISPant
0
25
50
75
100
hpf

Figure 3.7: Developmental defects in *yap1* CRISPants at 96hpf
(A) Schematic overview of parameters measured at 96hpf. **(B)** Representative images of 96hpf controls and *yap1* CRISPant embryos. **(C)** Quantification of embryo length at 96hpf. Length was reduced in *yap1* CRISPants when compared to all controls except gRNA. **(D)** Quantification of eye area at 96hpf. Eye area was reduced in *yap1* CRISPants when compared to controls. **(E)** Quantification of heart area at 96hpf. Heart area was increased in *yap1* CRISPants when compared to controls. **(F)** Quantification of yolk area at 96hpf. Yolk area was increased in *yap1* CRISPants when compared to controls. **(G)** Quantification of body area at 96hpf. Body area was unchanged between groups. **(H)** Quantification of eye area as a percentage of body size at 96hpf. Eye area was decreased in *yap1* CRISPants when compared to controls. **(I)** Quantification of heart area as a percentage of body size at 96hpf. Heart area was increased in *yap1* CRISPants when compared to all controls except gRNA. **(J)** Quantification of yolk area as a percentage of body size at 96hpf. Yolk area was increased in *yap1* CRISPants when compared to controls. **(K)** Number of twisted embryos (classified visually as those without a straight body) expressed as a proportion of total embryos. Proportion increases after injection, with most disruption in *yap1* CRISPants. WT n=87; Cas9 n=76; gRNA n=79; CRISPant n=91. **(L)** Embryo survival to 100hpf. Injection reduces survival, with the most death at early timepoints. Percentage calculated from WT n=466; Cas9 n=448; gRNA n=545; CRISPant n=566.
Cas9=Cas9-only injected fish; gRNA=*yap1* CRISPR guide RNA-only injected fish; CRISPant=*yap1* CRISPR-mutagenised fish. Bars show mean±SD. Significance calculated by Kruskal-Wallis test unless otherwise stated, with multiple comparisons. Data from at least three independent experimental repeats. Each dot represents one embryo. *p<0.05; **p<0.01; ***p<0.001; ****p<0.0001; ns= not significant.

3.2.4.2 Different phenotype severities did not have different DNA mutagenesis efficiency or protein abundance

From the developmental analyses of *yap1* CRISPants (3.2.4.1), a clear separation of CRISPant phenotypes can be observed, with some embryos having a phenotype similar to controls ("normal"), and others having a more severe phenotype ("disrupted") (Figure 3.8A). One hypothesis is that the CRISPR guide mutagenesis efficiency is variable and so a proportion of the embryos are not mutagenised, suggesting that only the most severe phenotypes should be analysed. However, this does not appear to be the case, as T7E1 digestion (Figure 3.8B) showed that separated "normal" and "disrupted" samples had no differences in DNA mutagenesis. There was a marginal increase in Yap1 protein when analysed by western blot in normal samples (Figure 3.8C), but Yap1 levels were still much lower than controls. Therefore, it is assumed that these different phenotypes are due to natural variation or due to different types of mutations within the same population, such as null and nonsense mutations. Therefore, CRISPant embryos with a range of phenotype severities were analysed together in the screen.

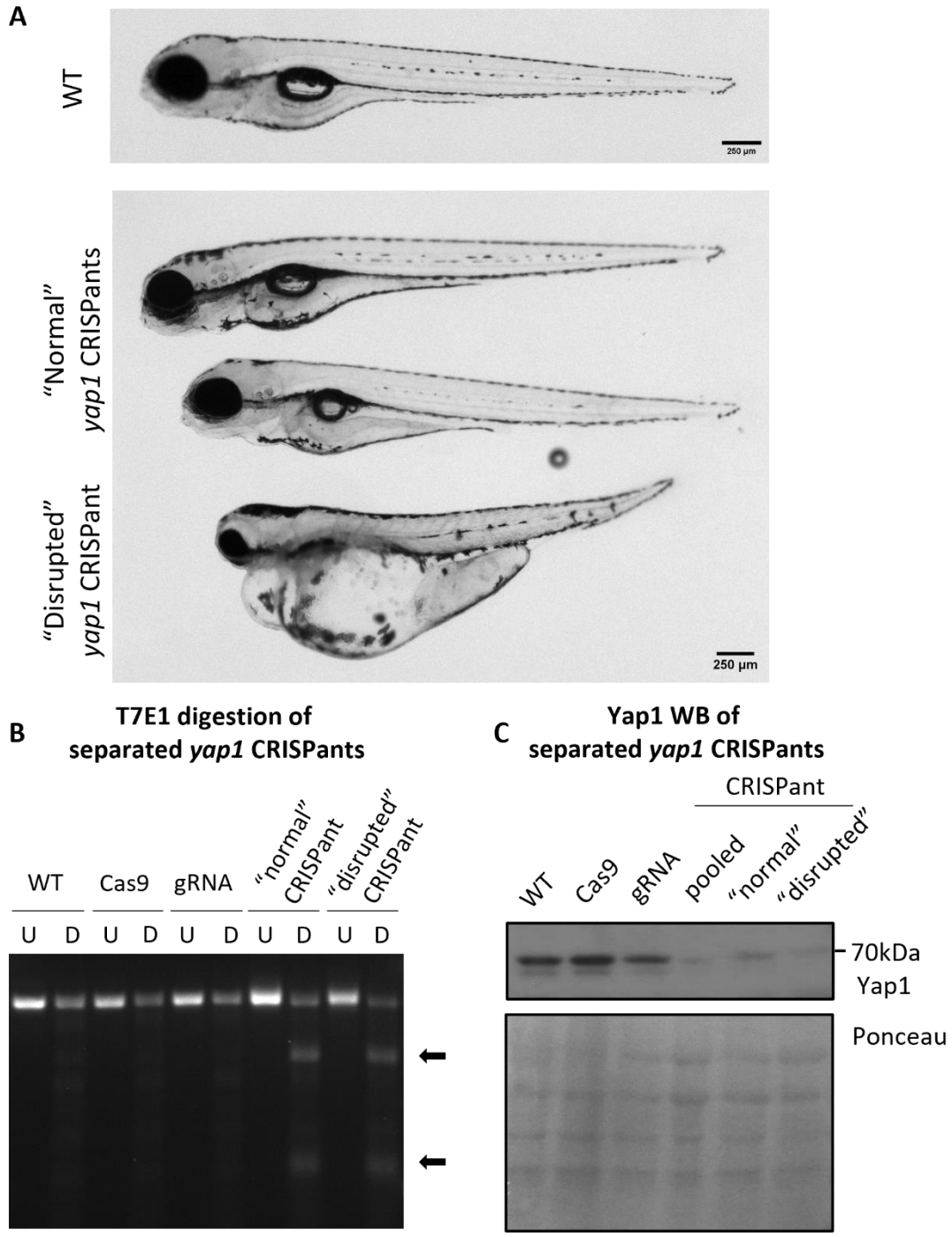

Figure 3.8: Differences in *yap1* CRISPant phenotype severity

(A) Representative images of WT embryos and "normal" and "disrupted" phenotype *yap1* CRISPants from the same experimental repeat. **(B)** DNA gel showing a T71 endonuclease assay of controls and *yap1* CRISPant embryos, separated into "normal" and "disrupted" phenotypes. Both CRISPant groups showed the same DNA mutagenesis. U=undigested sample; D=digested sample (with T7E1). Arrows show band shift indicative of efficient *yap1* mutagenesis. **(C)** Yap1 Western blot of controls and *yap1* CRISPant embryos, separated into "normal" and "disrupted" phenotypes, and a "pooled" sample with no separation. There was little difference between CRISPant groups. Loading control was a ponceau stain.

Cas9=Cas9-only injected fish; gRNA=*yap1* CRISPR guide RNA-only injected fish; CRISPant=*yap1* CRISPR-mutagenised fish. Data from one experimental repeat.

3.2.4.3 yap1 CRISPants have no phenotypes at the juvenile stage

Phenotypes at the later juvenile developmental stage of 1 month post fertilisation (mpf) were then measured. As these fish are no longer transparent, a reduced number of parameters (length, body area, and eye area) could be measured. These parameters are summarised in Figure 3.9A and representative images of WT and *yap1* CRISPant fish are shown in Figure 3.9B. A trend towards a reduction in survival was seen for *yap1* CRISPants (Figure 3.9C). Although this was not significant due to large inter-batch variability, this reduction in survival may represent the death of the CRISPants with the most deleterious *yap1* mutations, as the most disrupted embryos were observed to be most likely to die at embryonic stages. The adult *yap1* CRISPants had no significant differences in overall or eye size (Figure 3.9D-F). Cas9- and gRNA-only injected fish showed only slight variations in parameters measured. Therefore, as these fish become protected under ASPA post 5dpf, become more expensive to keep, and are subject to the 'Reduce' principle of animal research, these control groups were not carried forward for further investigation. In the screen, this experiment was therefore only performed in CRISPants that had an interesting embryonic phenotype and which were grown to a stable mutant. This reduced the number of adult animals required for this study.

3.2.4.4 Tail fin development and regeneration can be analysed using two different injury paradigms

The zebrafish caudal tail fin is an area used commonly to study epimorphic regeneration[38,142,245,246]. Yap1-disrupted fish have been shown to have defective regeneration after tail fin injury in the adult[247,248]. However, this fin regeneration assay can also be performed in the zebrafish embryo, which will be suitable for the CRISPR/Cas9 screen described here. In order to optimise this assay for use in the screen, tail fin amputations of varying severity was performed at 3dpf, either transecting the notochord (severe) or just the fin fold (mild) (Figure 3.10A). These two injury paradigms were chosen as papers focussing on embryonic tail fin regeneration use either of these, without known direct comparisons of the two methods. It is assumed that the mild tail fin injury denotes a quicker regrowth of the epithelium that is based on compensatory uninjured cell proliferation, whilst the severe tail fin regeneration occurs through the formation of a blastema, requiring dedifferentiation and proliferation. These injury paradigms should therefore not be assumed to require the same

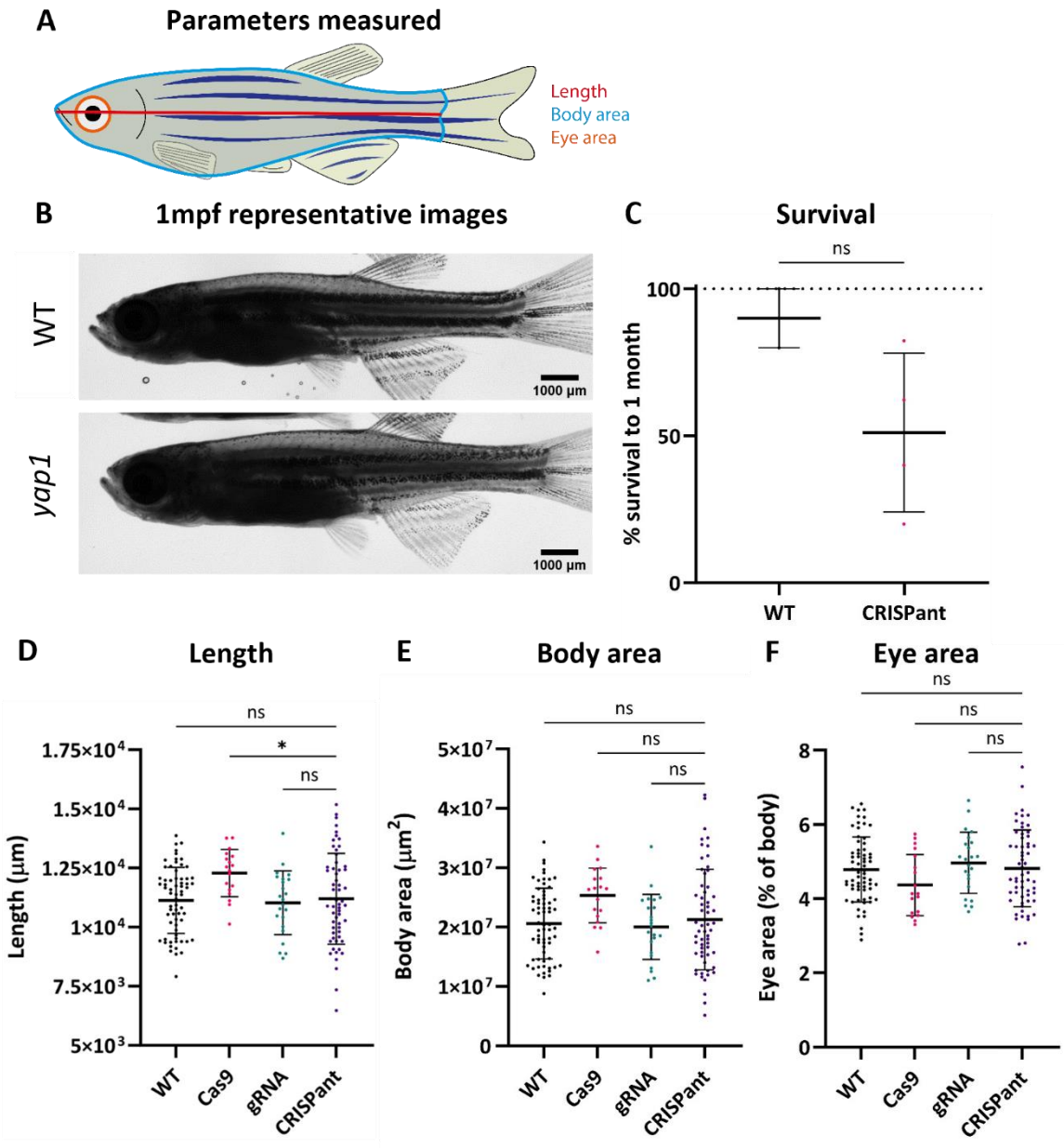

Figure 3.9: Developmental phenotypes in *yap1* CRISPants at 1 month post fertilisation
(A) Schematic overview of parameters measured at 1 month post fertilisation (mpf). **(B)** Representative images of juvenile WT and *yap1* CRISPant zebrafish at 1mpf. **(C)** Quantification of survival to 1mpf of WT and *yap1* CRISPant fish. CRISPants showed a non-significant decrease in survival (WT n=67; CRISPant n=60). **(D)** Quantification of 1mpf length of *yap1* CRISPants and controls. CRISPants had reduced length relative to Cas9 only. **(E)** Quantification of 1mpf body area of *yap1* CRISPants and controls. No significant change in CRISPants was observed. **(F)** Quantification of 1mpf eye area (as percentage of body area) of *yap1* CRISPants and controls. No significant change in CRISPants was observed.
Cas9=Cas9-only injected fish; gRNA=*yap1* CRISPR guide RNA-only injected fish; CRISPant=*yap1* CRISPR-mutagenised fish. Bars show mean±SD. Significance calculated using unpaired t-test (C) or one-way ANOVA with multiple comparisons (D-F). Cas9 and gRNA data from one experimental repeat, WT and CRISPant from three independent experimental repeats. Each dot represents one embryo (D-F), or independent repeats (C). *p<0.05; ns=not significant.

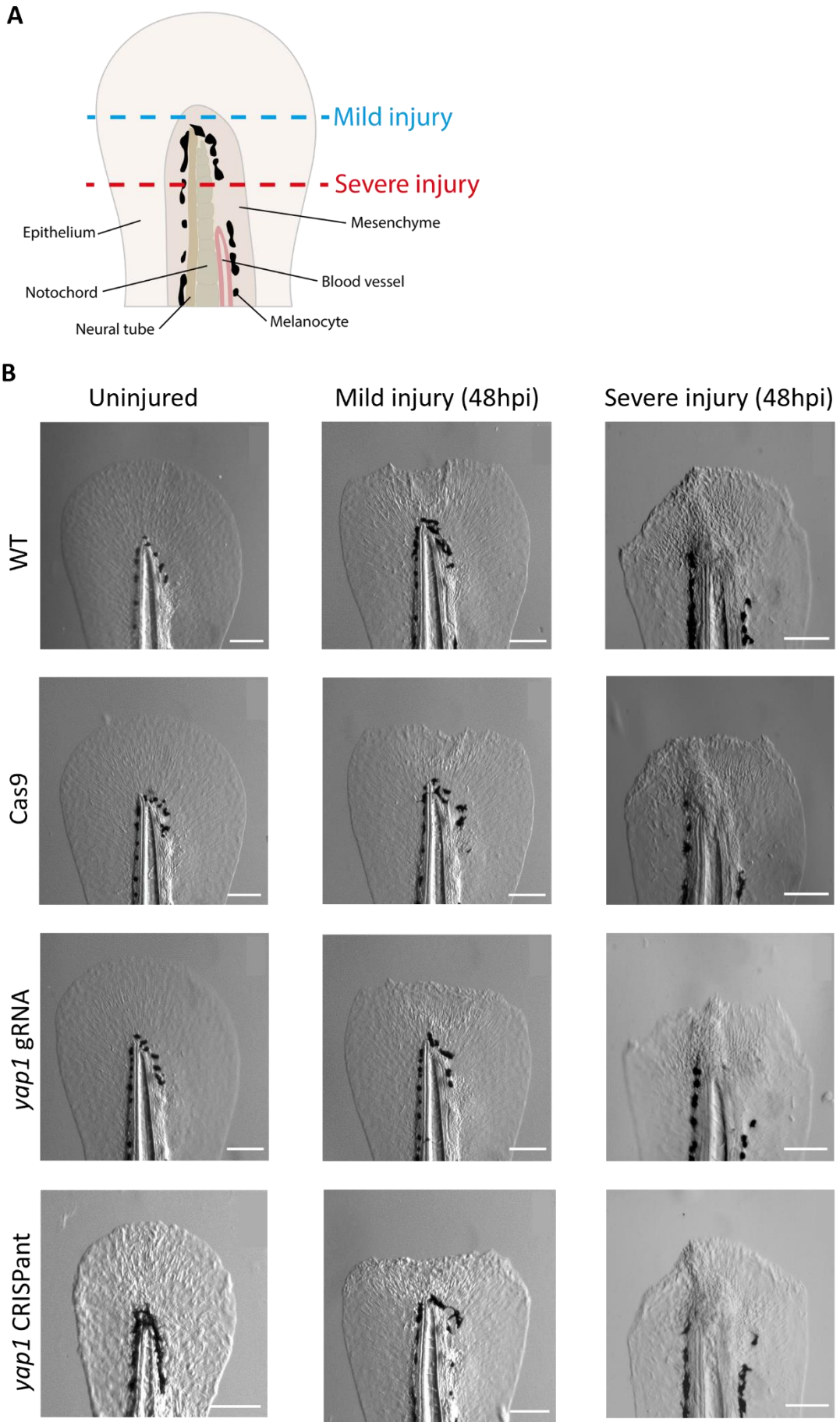
A
Mild injury
Severe injury
Epithelium
Mesenchyme
Notochord
Blood vessel
Neural tube
Melanocyte
B
Uninjured
Mild injury (48hpi)
Severe injury (48hpi)
WT
Cas9
yap1 gRNA
yap1 CRISPant

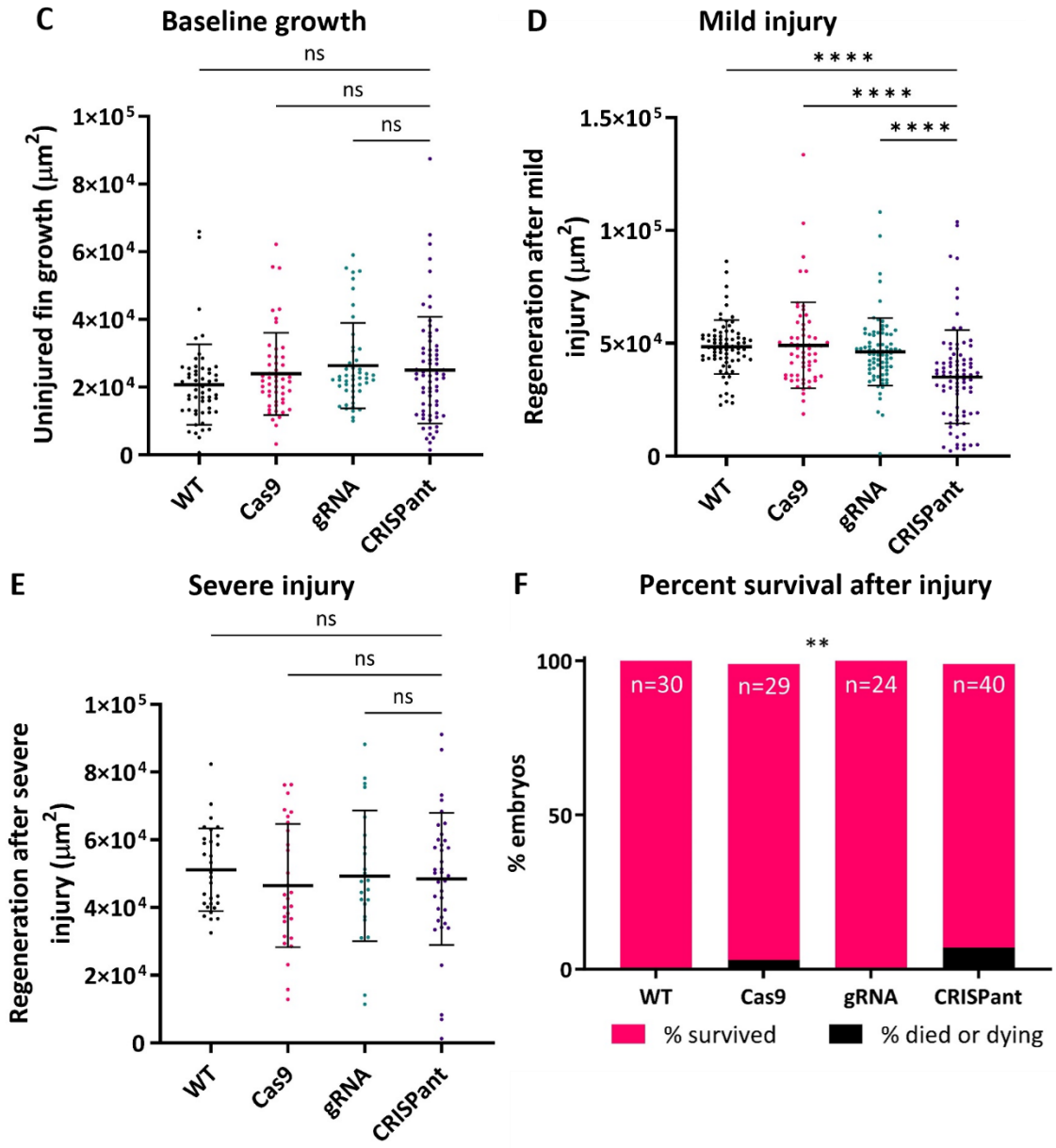

Figure 3.10: *yap1* CRISPant tail fin development and regeneration

(A) Schematic of injury points of a 3dpf embryo tail fin. Red dotted line = severe injury amputation plane; Blue dotted line = mild injury amputation plane. **(B)** Representative images of uninjured growth, and mild and severe tail fin regeneration in *yap1* CRISPants and controls. **(C)** Quantification of the uninjured (baseline) growth of the tail fin in *yap1* CRISPants and controls. No significant changes were observed upon mutagenesis. **(D)** Quantification of fin regeneration after mild tail fin injury. *yap1* CRISPants had a significant decrease in regeneration when compared to controls. **(E)** Quantification of fin regeneration after severe tail fin injury. No significant changes were observed upon mutagenesis. **(F)** Quantification of percentage survival after severe tail fin injury. Survival was significantly altered (Chi-squared test).

Area quantified at 0hpi and 48hpi from the beginning of the pigment gap, as described in Figure 2.4. Cas9=Cas9-only injected fish; gRNA=*yap1* CRISPR guide RNA-only injected fish; CRISPant=*yap1* CRISPR-mutagenised fish. Significance calculated by Kruskal-Wallis test (C+D) or one-way ANOVA (E) with multiple comparisons. Bars show mean±SD. Data from at least three independent experimental repeats. Each dot represents one embryo. **p<0.01; ****p<0.0001; ns=not significant.

pathways, and so the screen includes both types of injury, allowing a direct comparison of the injury types.

Representative images of uninjured fin growth and mild and severe regeneration 48 hours post injury (hpi) are shown in Figure 3.10B. Uninjured growth showed no significant change in *yap1* CRISPants compared to controls (Figure 3.10C). After mild tail fin injury, CRISPants did show a significant reduction in regeneration (Figure 3.10D), whilst after severe injury, there appeared to be no significant change (Figure 3.10E). This was unexpected, as *yap1* disruption has been linked to many different regenerative defects and impaired cell proliferation and dedifferentiation[72,247,249], both of which are expected to be vital for severe tail fin regeneration. One explanation for this may be that the more severely disrupted embryos did not tolerate the injury well, with many of them dying at a higher rate than controls (Figure 3.10F). These embryos had to be excluded from the analyses, which may skew the results. However, this rate was still not high so there may be other conditions affecting this.

3.2.4.5 Hair cell development and regeneration in the lateral line can be analysed

Another regenerative assay in the embryonic zebrafish is hair cell regeneration of the lateral line. Hair cell injury is performed by administration of heavy metals (in this case, $Cu(II)SO_4$) which are taken up by the cells and result in cell death[250]. Unlike the inner ear hair cells of mammals, which do not regenerate, lateral line hair cells can robustly regenerate[251]. This process can be visualised by DASPEI dye administration, which is taken up by hair cell mitochondria[252] and is commonly used to study lateral line development and regeneration (reviewed in[253,254]) (Figure 3.11A). Yap1 signalling has been associated with both the development and regeneration of the lateral line, with signalling disruption resulting in impaired regeneration[249] and reduced lateral line size[77,99,129,130].

Lateral line regeneration was imaged and quantified in WT fish after injury over a 48-hour period. Analysis included both the number of neuromasts per fish and the average area of this fluorescence (taken to be a proxy for number of hair cells in each neuromast) (Figure 3.11B-C). Analysis of neuromast number (Figure 3.11B) revealed a sharp decline in neuromast number and area immediately post injury, showing that the drug administration successfully

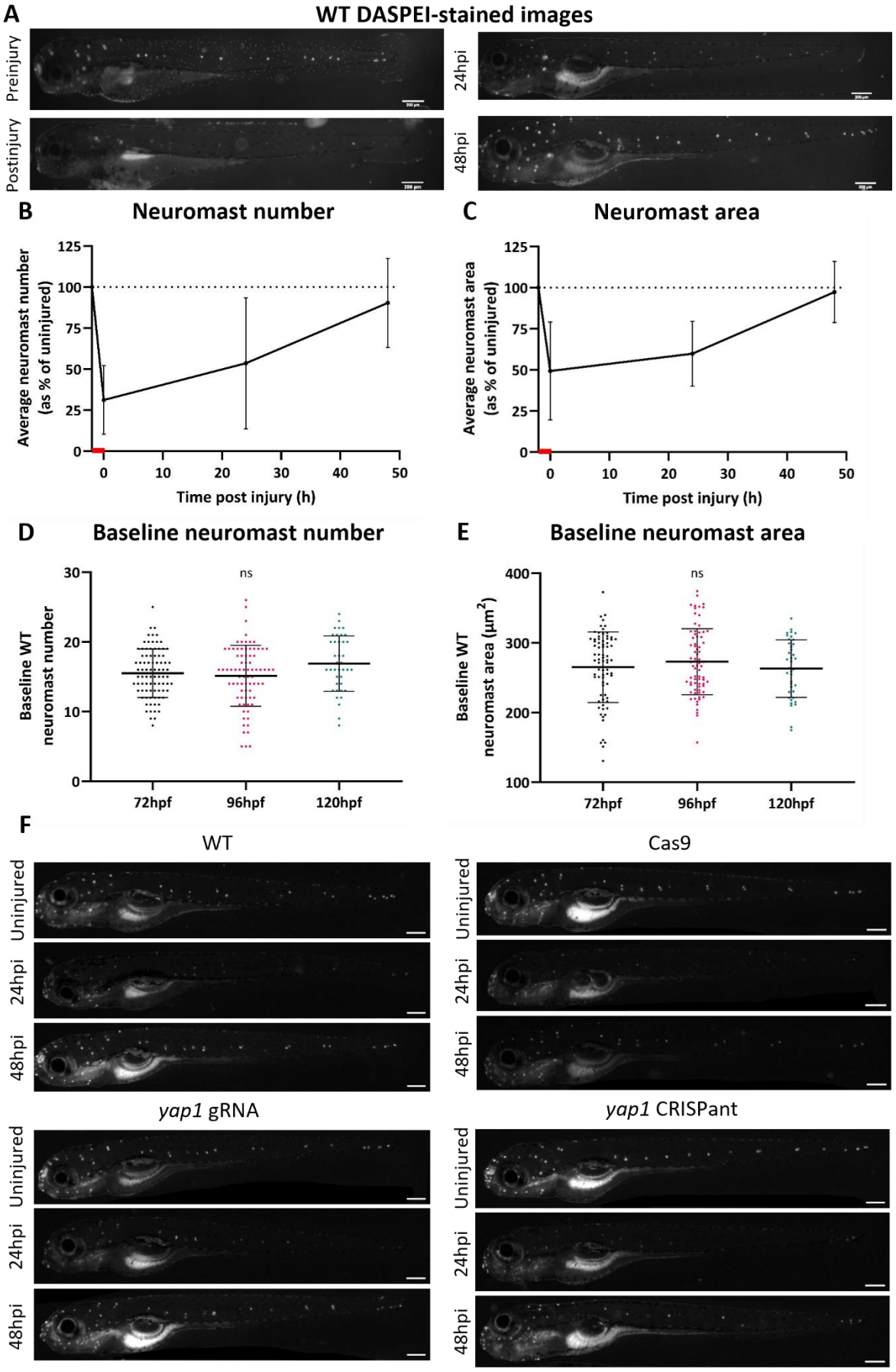
A
WT DASPEI-stained images
Preinjury
Postinjury
24hpi
48hpi
B
Neuromast number
Average neuromast number (as % of uninjured)
Time post injury (h)
C
Neuromast area
Average neuromast area (as % of uninjured)
Time post injury (h)
D
Baseline neuromast number
Baseline WT neuromast number
ns
72hpf
96hpf
120hpf
E
Baseline neuromast area
Baseline WT neuromast area (µm²)
ns
72hpf
96hpf
120hpf
F
WT
Cas9
yap1 gRNA
yap1 CRISPant
Uninjured
24hpi
48hpi

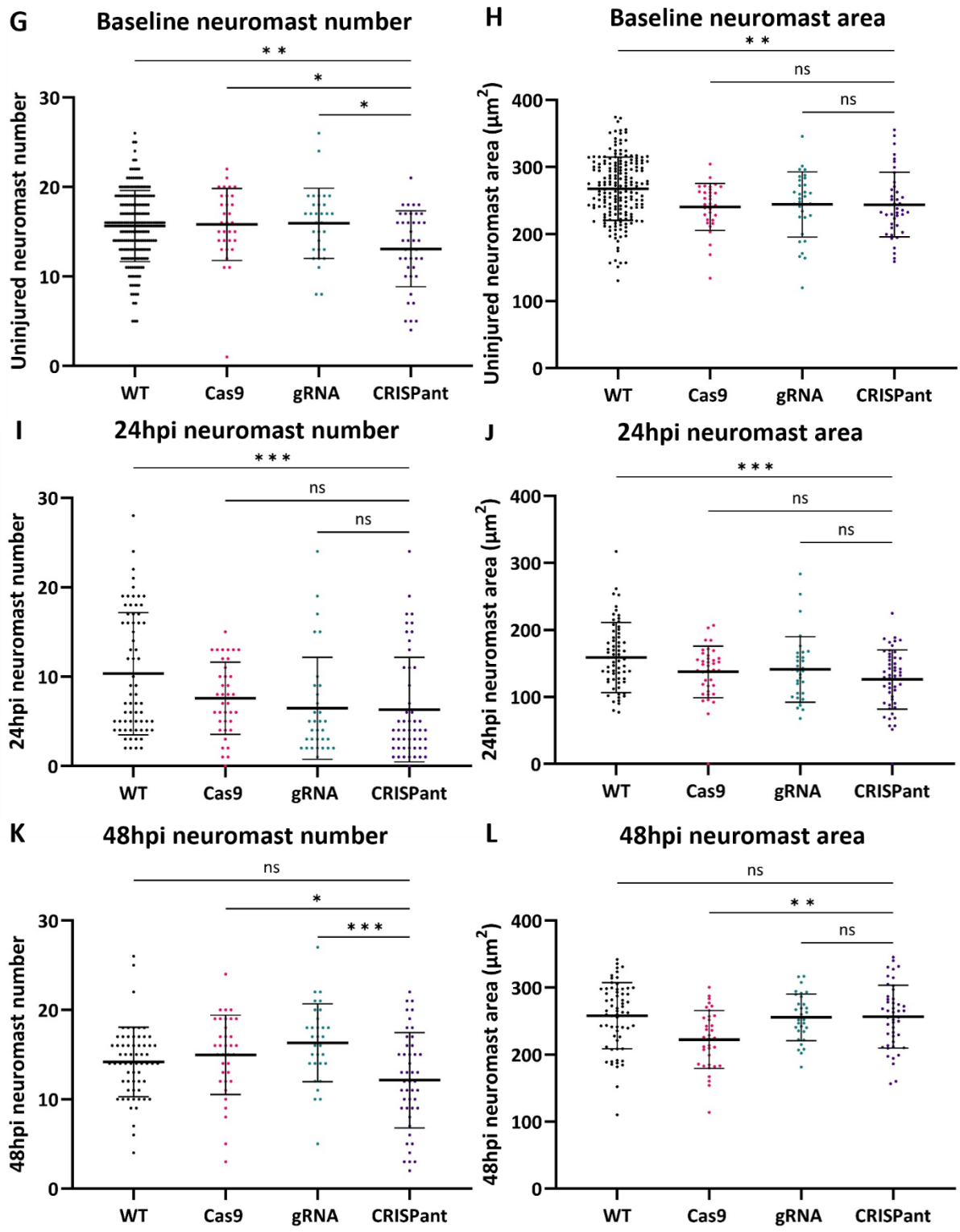

Figure 3.11: *yap1* CRISPant neuromast development and regeneration

(A) Sample images of WT embryos stained with DASPEI before and during neuromast regeneration. Note the absence of any DASPEI-positive puncta immediately post injury which recover at later timepoints. **(B)** Time course of WT mean neuromast number after injury as a percentage of mean uninjured number. Neuromast number showed a large reduction quickly following injury that recovered to uninjured levels by 48hpi. Red bar denotes period of injury. n=31-51. **(C)** Time course of

WT mean neuromast area after injury as a percentage of mean uninjured area. Neuromast area showed a large reduction quickly following injury that recovered to uninjured levels by 48hpi. Red bar denotes period of injury. n=31-67. **(D)** Quantification of baseline (uninjured) neuromast number at 72hpf, 96hpf, and 120hpf. No significant change in number was observed. **(E)** Quantification of baseline (uninjured) neuromast area at 72hpf, 96hpf, and 120hpf. Baseline neuromast area was unchanged. **(F)** Representative images of neuromast regeneration in *yap1* CRISPants and controls. **(G)** Quantification of baseline neuromast number in *yap1* CRISPants and controls. *yap1* CRISPants had decreased uninjured number relative to controls. **(H)** Quantification of baseline neuromast area in *yap1* CRISPants and controls. *yap1* CRISPants had decreased uninjured number relative to WT controls. **(I)** Quantification of 24hpi neuromast number in *yap1* CRISPants and controls. *yap1* CRISPants had decreased number relative to WT and Cas9 controls. **(J)** Quantification of 24hpi neuromast area in *yap1* CRISPants and controls. *yap1* CRISPants had decreased area relative to WT controls. **(K)** Quantification of 48hpi neuromast number in *yap1* CRISPants and controls. *yap1* CRISPants had decreased number relative to Cas9 and gRNA controls. **(L)** Quantification of 48hpi neuromast area in *yap1* CRISPants and controls. *yap1* CRISPants had increased area relative to Cas9 controls.
Cas9=Cas9-only injected fish; gRNA=*yap1* CRISPR guide RNA-only injected fish; CRISPant=*yap1* CRISPR-mutagenised fish. Bars represent mean±SD. Significance calculated using one-way ANOVA (D+E) or Kruskal-Wallis test (G-L) with multiple comparisons. Data from at least three independent experimental repeats, except for injured at 0hpi timepoints in B+C, where data was from two experimental repeats. Each dot represents one embryo. Scale bar represents 200µm. *p<0.05; **p<0.01; ***p<0.001; ns=not significant.

injures hair cells. The number of hair cells returned to preinjury levels by 48hpi. Analysis of WT neuromast area over the 48hpi showed a similar pattern, with a decline in neuromast area immediately post injury and a gradual return to baseline levels by 48hpi (Figure 3.11C). Therefore, to streamline the CRISPR screen, imaging will not be performed immediately after injury, which would likely not show genotype-specific phenotypes.

An accurate determination of baseline (uninjured) neuromast area and number is required for reliable analyses of neuromast regeneration. To do this, optimisation of the timing of imaging uninjured embryos was performed (Figure 3.11D-E). Imaging of both uninjured neuromast number and area at 72hpf, 96hpf, and 120hpf (the 48-hour time course the experiment takes place over) showed no significant differences. This suggests that, to streamline the CRISPR screen, only one uninjured time point is required. For experimental ease, this was selected to be 96hpf.

Representative images of *yap1* CRISPants and controls during neuromast regeneration are shown in Figure 3.11F. *yap1* CRISPants had reduced number and area at baseline and 24hpi (Figure 3.11G-J), particularly when compared to WT fish. However, there was no consistent significant reduction at 48hpi area or number (Figure 3.11K+L), suggesting that there may be a time-dependent effect of *yap1* on neuromast regeneration.

3.2.5 *tp53* CRISPants are not an appropriate negative control for the CRISPR/Cas9 screen

To attempt to create a negative control that complements the positive *yap1* control to confirm that CRISPR mutagenesis itself does not inherently impact on development and regeneration, *tp53* (zebrafish ortholog of the human *P53* gene) CRISPants were investigated. In the zebrafish, *tp53*-disruption has been previously shown to have adult cancer-associated phenotypes and only minor embryonic phenotypes, including delayed hatching, reduced swimming behaviour, and decreased apoptosis[255,256].

However, phenotypes were observed when *tp53* CRISPant embryos underwent the screen. Representative images of embryonic fish are shown in Figure 3.12A. When CRISPant values were normalised to *tp53* gRNA controls from the same experiment (so gRNA control = 1), *tp53* CRISPants showed significant embryonic developmental phenotypes (Figure 3.12B) similar to *yap1* CRISPants but less severe, suggesting that there was in fact an embryonic developmental phenotype. Representative images of juvenile fish are shown in Figure 3.12C. Similarly to embryonic stages, *tp53* CRISPants showed juvenile growth defects, with a reduction in both length and body area (Figure 3.12D and E respectively), and an increase in eye area (Figure 3.12F).

Despite these developmental phenotypes, there were only limited neuromast regeneration phenotypes in *tp53* CRISPants (Figure 3.12G-I). A small increase in neuromast area was observed at baseline and at 24hpi, but no change was found at 48hpi or in neuromast number. Interestingly, an increase in baseline tail fin growth rate was observed in CRISPants, but no other tail fin regeneration defects (Figure 3.12J and K). This could suggest a role for Tp53, and so apoptosis, in the normal development of the tail fin, potentially by limiting its overgrowth.

The developmental phenotypes in these CRISPants could be a result of a general survival issue or because of the impact of CRISPR mutagenesis on apoptotic cell death, which Tp53 has a key role in and which is vital in normal embryonic development[255]. Therefore, these *tp53* CRISPants were not appropriate negative controls, and therefore not included in the screen. Due to time constraints, and the realisation that different CRISPants included in the screen gave distinct gene-specific phenotypes (including no phenotype), additional negative control CRISPants were not investigated.

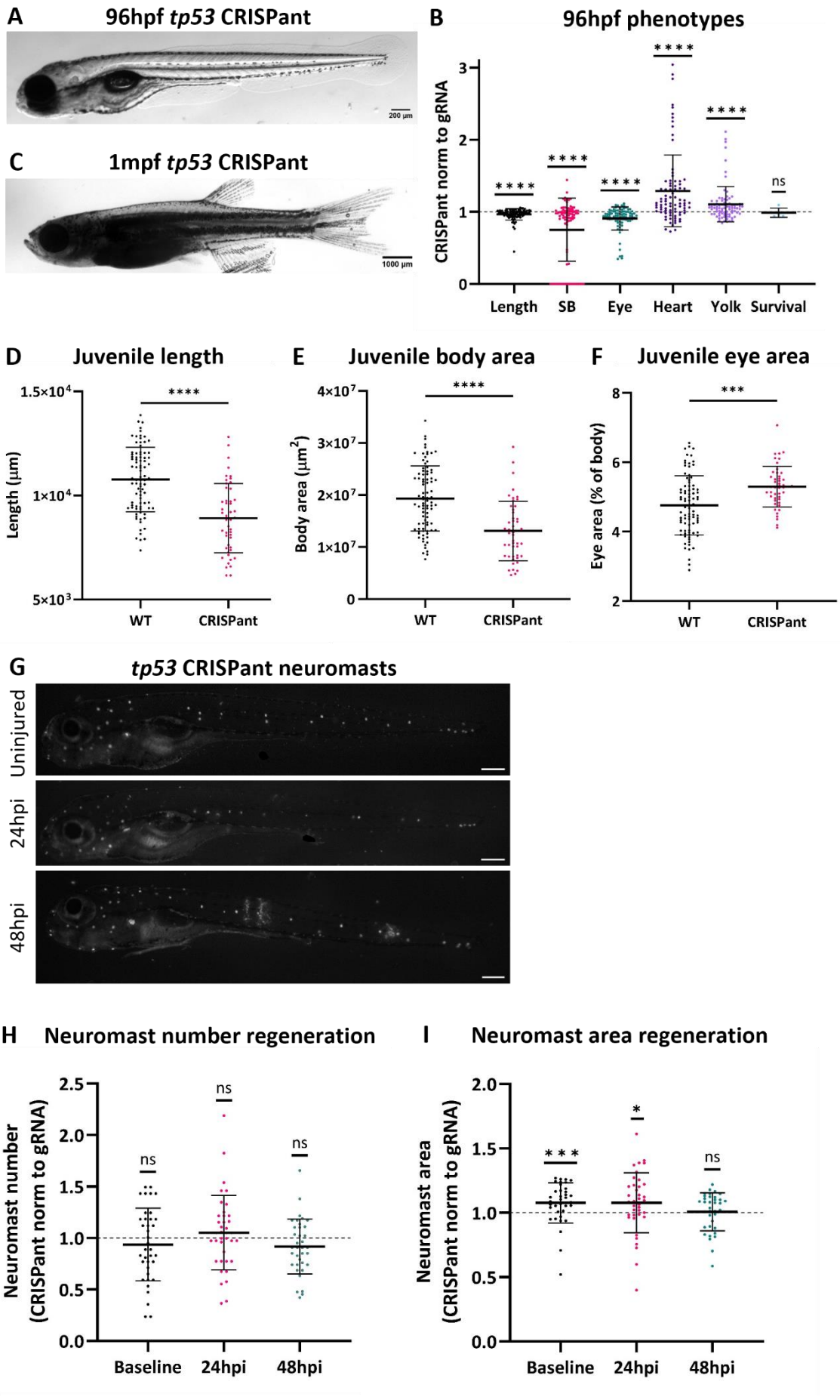
A
96hpf tp53 CRISPant
200 µm
C
1mpf tp53 CRISPant
1000 µm
B
96hpf phenotypes
CRISPant norm to gRNA
****
****
****
****
ns
Length
SB
Eye
Heart
Yolk
Survival
D
Juvenile length
Length (µm)
****
WT
CRISPant
E
Juvenile body area
Body area (µm²)
****
WT
CRISPant
F
Juvenile eye area
Eye area (% of body)
***
WT
CRISPant
G
tp53 CRISPant neuromasts
Uninjured
24hpi
48hpi
H
Neuromast number regeneration
Neuromast number (CRISPant norm to gRNA)
ns
ns
ns
Baseline
24hpi
48hpi
I
Neuromast area regeneration
Neuromast area (CRISPant norm to gRNA)
***
*
ns
Baseline
24hpi
48hpi

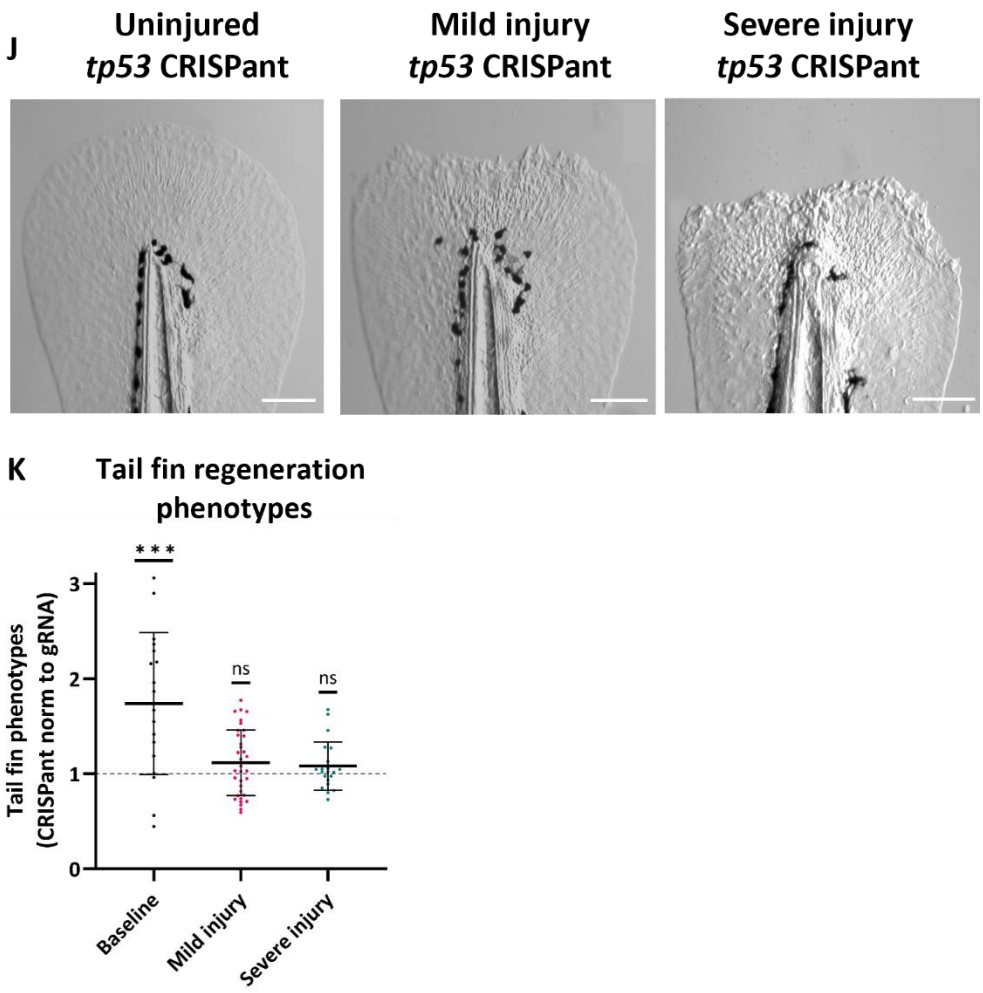

Figure 3.12: *tp53* CRISPants as a negative control

(A) Representative image of *tp53* CRISPant embryo at 96hpf. **(B)** Quantification of 96hpf phenotypes of *tp53* CRISPants, normalised to *tp53* gRNA-only injected fish. Multiple significant disruption-associated phenotypes were observed (one sample Wilcoxon test, μ=1). **(C)** Representative images of juvenile (1mpf) *tp53* CRISPant zebrafish. **(D)** Quantification of juvenile fish length in WT and *tp53* CRISPants. CRISPants had decreased length (Mann-Whitney test). **(E)** Quantification of juvenile body area in WT and *tp53* CRISPants. CRISPants had decreased body area (Mann-Whitney test). **(F)** Quantification of juvenile eye area (as a percentage of body area) in WT and *tp53* CRISPants. CRISPants had increased eye area (unpaired t-test). **(G)** Representative images of neuromast regeneration in *tp53* CRISPant. **(H)** Quantification of neuromast number when uninjured and during regeneration, normalised to gRNA controls. Neuromast number was unchanged at all timepoints (one sample Wilcoxon test, μ=1). **(I)** Quantification of neuromast area when uninjured and during regeneration, normalised to gRNA controls. Area was increased at baseline and at 24hpi but unchanged at 48hpi (one sample Wilcoxon test, μ=1). **(J)** Representative images of tail fin regeneration and baseline growth in *tp53* CRISPant at 48hpi. **(K)** Quantification of tail fin growth at baseline and during mild and severe tail fin regeneration in *tp53* CRISPants, normalised to gRNA controls. Baseline growth was increased but mild and severe tail fin regeneration was unchanged (one sample t test, μ=1).

gRNA=*tp53* CRISPR guide RNA-only injected fish; CRISPant=*tp53*-mutagenised CRISPant. Data from at least three independent experimental repeats, except juvenile analyses, which is from two independent experimental repeats. All data, except for juvenile analyses, is normalised to *tp53* gRNA controls performed during the same independent experiment. Each dot represents one embryo. Bars show mean±SD. *p<0.05; ***p<0.001; ****p<0.0001; ns=not significant.

3.3 Summary of a CRISPR/Cas9 screen to identify developmental and regenerative phenotypes

An overview of the optimised CRISPR/Cas9 screen is shown in Figure 3.13. This shows the timeline for one repeat of the CRISPR screen. Only genotypes of particular interest are continued past 5dpf, to support the "Reduce" principle of animal research. gDNA and RNA is extracted at 24hpf and protein at 72hpf for molecular analyses. Injury for tail fin and neuromast regeneration was performed at 72hpf. For the tail fin assay, uninjured growth and regeneration after both mild and severe injury was measured at 48hpi (120hpf). For the neuromast assay, regeneration was measured at 24hpi (96hpf) and 48hpi (120hpf) and uninjured size and number at 96hpf. Embryonic development and survival were measured at 96hpf. The screen was performed a minimum of 3 times for all genotypes and all assays, unless otherwise stated. Some experiments involving *nf2a*, *nf2b*, and *nf2a*/*nf2b* CRISPants were performed by S. Xia (MScR student with supervision by S. Riley).

3.4 Design and testing of highly efficient CRISPR/Cas9 guides

Two CRISPR/Cas9 guides were co-injected per gene targeted in the screen. These were analysed either through T7E1 endonuclease digestion, or other restriction enzymes where an appropriate cleavage site in the gene could be disrupted (more information in 2.6). The resulting DNA gels are shown in Figure 3.14. Mutagenised genes were (in addition to *yap1* and *tp53*): *wwtr1*, *lats1*, *lats2*, *nf2a*, *nf2b*, *ctgfa*, *ctgfb*, and *cyr61*. Only guides that caused 100% efficient mutagenesis when tested on individual embryos were taken forward in the screen. The guides targeting *nf2a* and *nf2b* were designed by S. Riley but injected and tested by S. Xia, and the DNA gels depicting their cleavage are shown in S. Xia's MScR thesis.

Figure 3.13: Overview of the optimised CRISPR/Cas9 screen
Microinjection mix was injected at the one cell stage. RNA and DNA was extracted for molecular analyses at 1dpf. Protein levels were analysed at 3dpf. Embryonic phenotypes and survival were measured at 96hpf. Neuromast injury was performed at 3dpf, with follow-up imaging of injured fish at 4dpf and 5dpf, and uninjured imaging at 4dpf. Tail fin injury was performed at 3dpf with initial imaging at 0hpi, then follow-up imaging of regeneration at 5dpf. Juvenile imaging was performed at approximately 1mpf. Generation of stable mutants began at 4mpf.

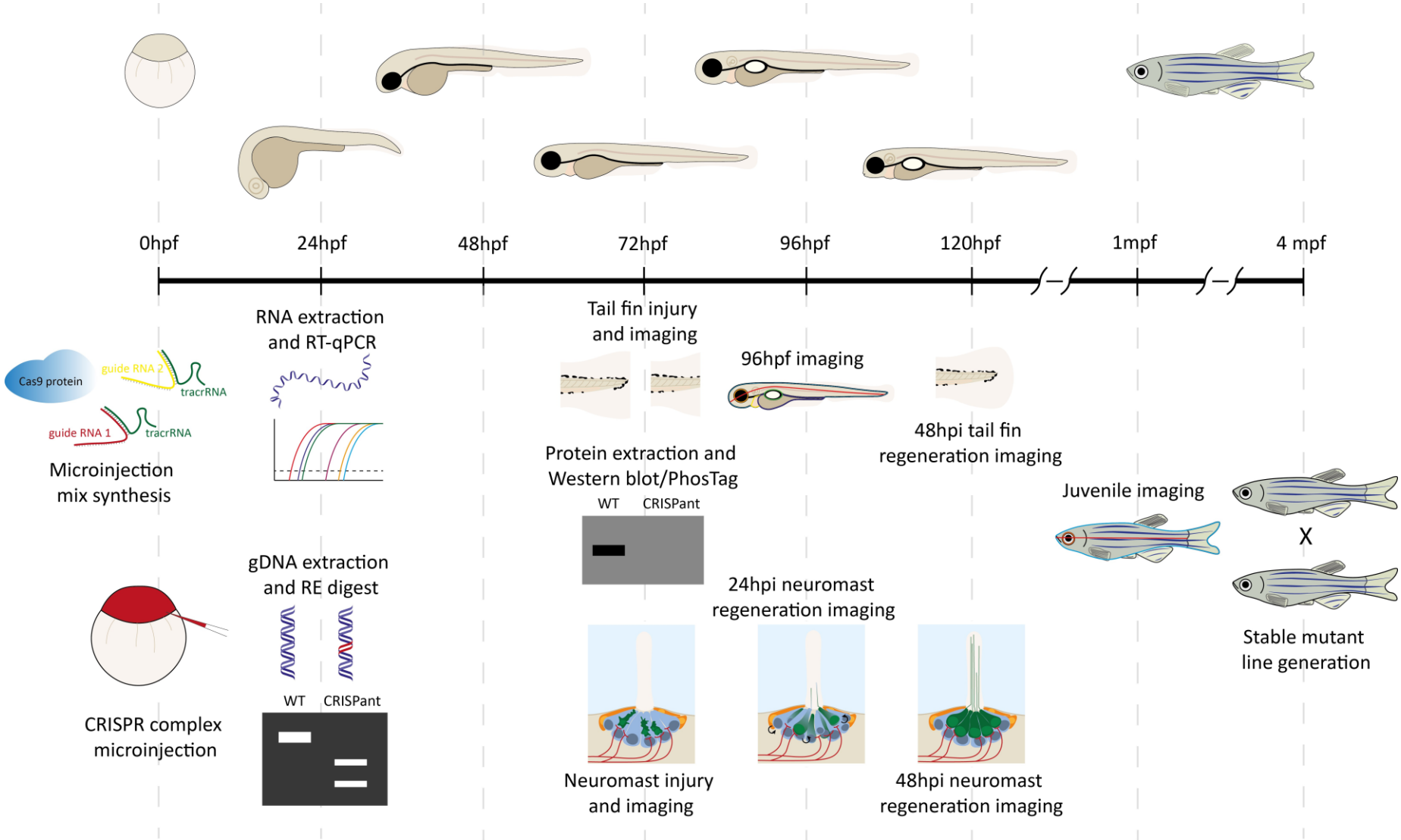
0hpf
24hpf
48hpf
72hpf
96hpf
120hpf
1mpf
4 mpf
Cas9 protein
guide RNA 2
tracrRNA
guide RNA 1
tracrRNA
Microinjection mix synthesis
RNA extraction and RT-qPCR
Tail fin injury and imaging
96hpf imaging
48hpi tail fin regeneration imaging
Protein extraction and Western blot/PhosTag
WT
CRISPant
Juvenile imaging
X
Stable mutant line generation
gDNA extraction and RE digest
WT
CRISPant
CRISPR complex microinjection
24hpi neuromast regeneration imaging
Neuromast injury and imaging
48hpi neuromast regeneration imaging

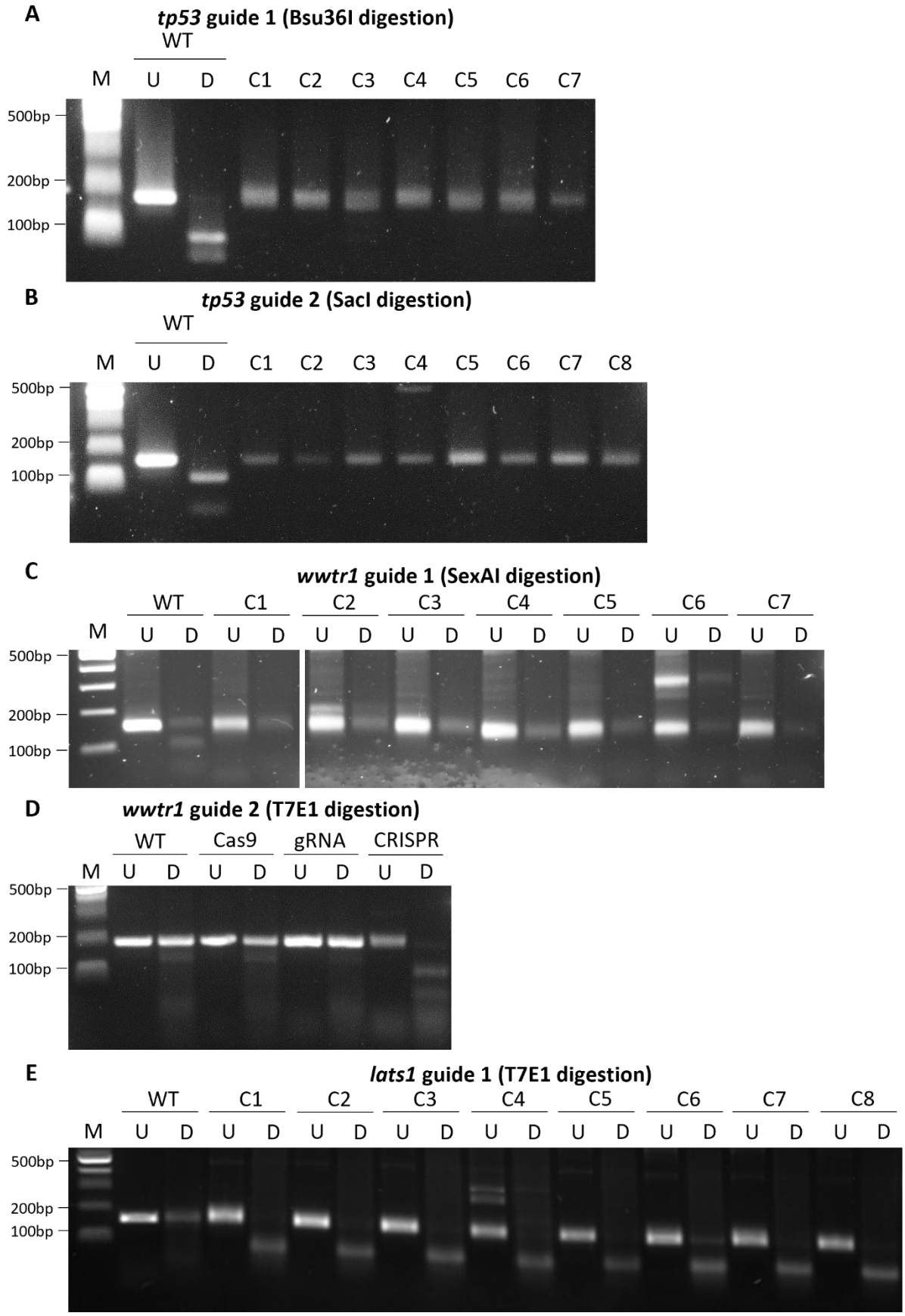
A
tp53 guide 1 (Bsu36I digestion)
WT
M U D C1 C2 C3 C4 C5 C6 C7
500bp
200bp
100bp
B
tp53 guide 2 (SacI digestion)
WT
M U D C1 C2 C3 C4 C5 C6 C7 C8
500bp
200bp
100bp
C
wwtr1 guide 1 (SexAI digestion)
WT C1 C2 C3 C4 C5 C6 C7
M U D U D U D U D U D U D U D U D
500bp
200bp
100bp
D
wwtr1 guide 2 (T7E1 digestion)
WT Cas9 gRNA CRISPR
M U D U D U D U D
500bp
200bp
100bp
E
lats1 guide 1 (T7E1 digestion)
WT C1 C2 C3 C4 C5 C6 C7 C8
M U D U D U D U D U D U D U D U D U D
500bp
200bp
100bp

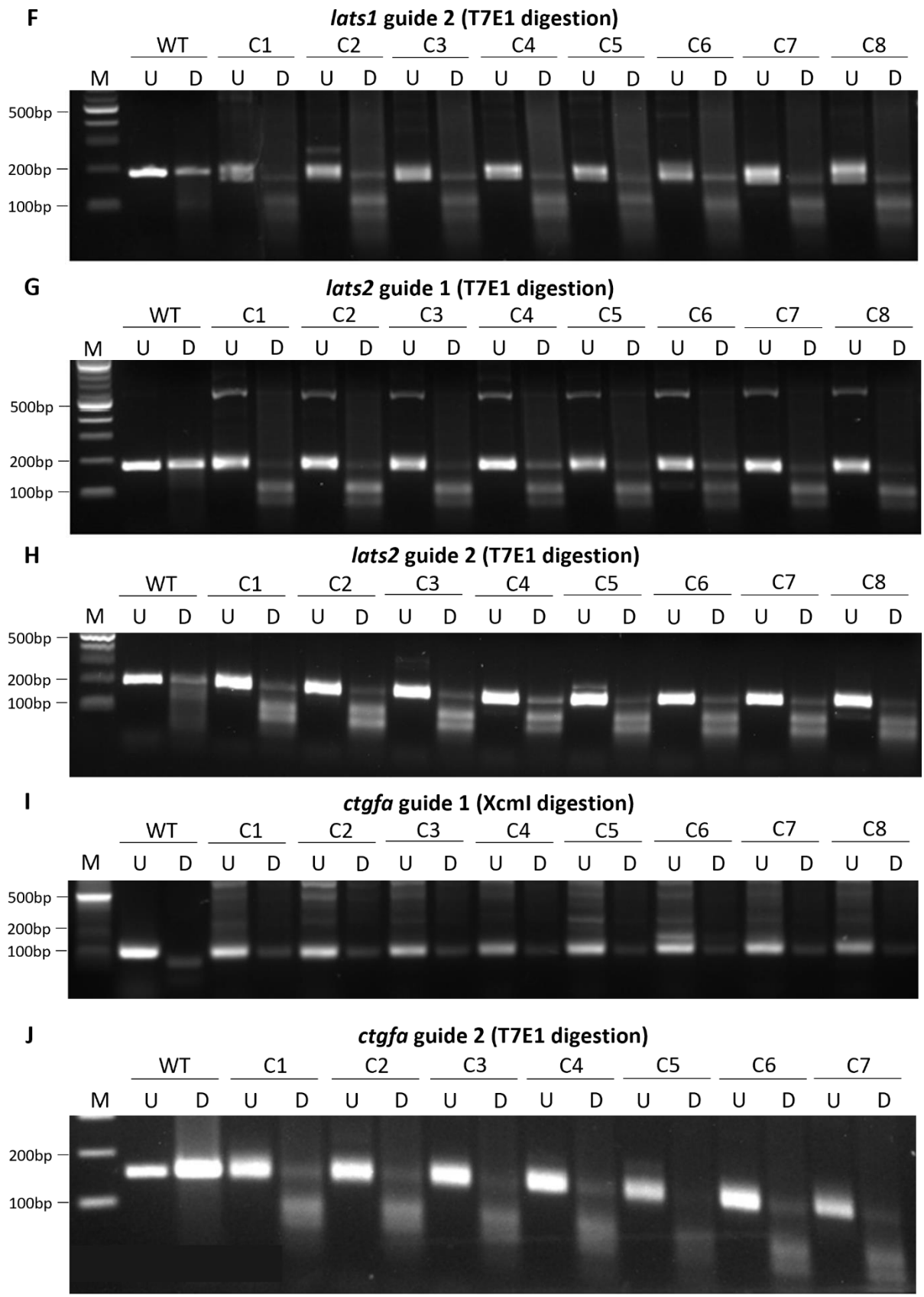
F
lats1 guide 2 (T7E1 digestion)
WT C1 C2 C3 C4 C5 C6 C7 C8
M U D U D U D U D U D U D U D U D U D
500bp
200bp
100bp
G
lats2 guide 1 (T7E1 digestion)
WT C1 C2 C3 C4 C5 C6 C7 C8
M U D U D U D U D U D U D U D U D U D
500bp
200bp
100bp
H
lats2 guide 2 (T7E1 digestion)
WT C1 C2 C3 C4 C5 C6 C7 C8
M U D U D U D U D U D U D U D U D U D
500bp
200bp
100bp
I
ctgfa guide 1 (XcmI digestion)
WT C1 C2 C3 C4 C5 C6 C7 C8
M U D U D U D U D U D U D U D U D U D
500bp
200bp
100bp
J
ctgfa guide 2 (T7E1 digestion)
WT C1 C2 C3 C4 C5 C6 C7
M U D U D U D U D U D U D U D U D U D
200bp
100bp

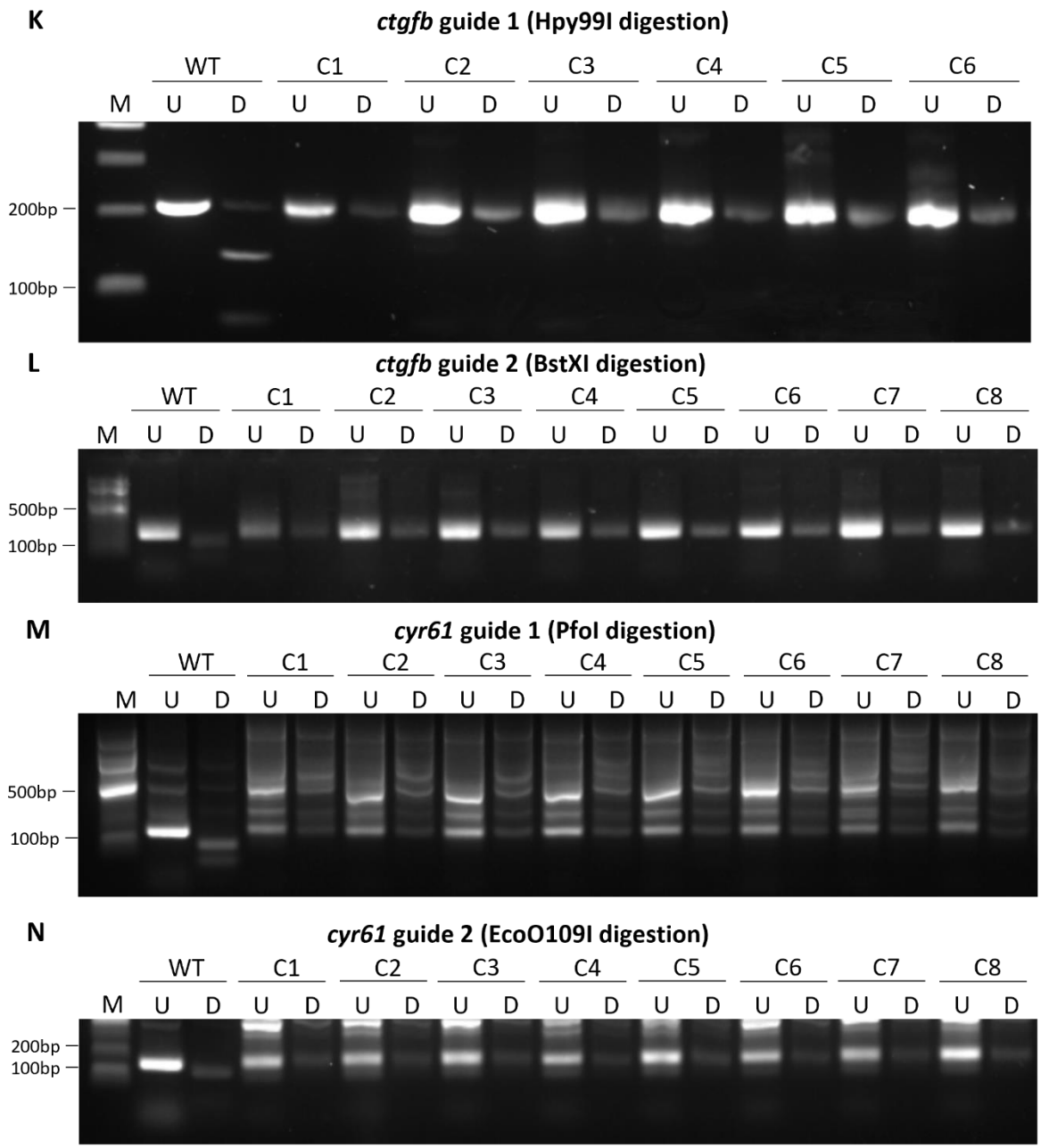

Figure 3.14: Restriction enzyme digestion of CRISPR guides targeting Hippo pathway components

DNA agarose gels of 24hpf CRISPant gDNA extracted from individual embryos (except D), digested by restriction enzymes (RE) or T7 endonuclease I (T7E1) to show mutagenesis efficiency. Mutagenesis is indicated by banding in T7E1-digested samples, or resistance to digest in RE-digested samples (see summary in Figure 2.1). **(A)** Bsu36I digestion of *tp53* guide 1-targeted region. *tp53* guide 1 CRISPants resisted RE digest. Band expected at ~185bp. **(B)** SacI digestion of *tp53* guide 2-targeted region. *tp53* guide 2 CRISPants resisted RE digest. Band expected at ~170bp. **(C)** SexAI digestion of *wwtr1* guide 1-targeted region. *wwtr1* guide 1 CRISPants resisted RE digest. Band expected at ~150bp. **(D)** T7E1 digestion of *wwtr1* guide 2-targeted region. *wwtr1* guide 2 CRISPants showed T7E1 digestion. Band expected at ~200bp. Pooled samples are used as bands for individual embryos are very faint. **(E)** T7E1 digestion of *lats1* guide 1-targeted region. *lats1* guide 1 CRISPants showed T7E1 digestion. Band expected at ~160bp. **(F)** T7E1 digestion of *lats1* guide 2-targeted region. *lats1* guide 2 CRISPants showed T7E1 digestion. Band expected at ~190bp. **(G)** T7E1 digestion of *lats2* guide 1-targeted region.

lats2 guide 1 CRISPants showed T7E1 digestion. Band expected at ~180bp. **(H)** T7E1 digestion of *lats2* guide 2-targeted region. *lats2* guide 2 CRISPants showed T7E1 digestion. Band expected at ~195bp. **(I)** XcmI digestion of *ctgfa* guide 1-targeted region. *ctgfa* guide 1 CRISPants resisted RE digest. Band expected at ~150bp. **(J)** T7E1 digestion of *ctgfa* guide 2-targeted region. *ctgfa* guide 2 CRISPants showed T7E1 digestion. Band expected at ~160bp. **(K)** Hpy99I digestion of *ctgfb* guide 1-targeted region. *ctgfb* guide 1 CRISPants resisted RE digest. Band expected at ~220bp. **(L)** BstXI digestion of *ctgfb* guide 2-targeted region. *ctgfb* guide 2 CRISPants resisted RE digest. Band expected at ~220bp. **(M)** PfoI digestion of *cyr61* guide 1-targeted region. *cyr61* guide 1 CRISPants resisted RE digest. Band expected at ~180bp. **(N)** EcoO109I digestion of *cyr61* guide 2-targeted region. *cyr61* guide 2 CRISPants resisted RE digest. Band expected at ~150bp.
Enzymes and digestion conditions used for each guide are described in Table 2.6. C=CRISPant; M=100bp marker; U=undigested; D=digested by enzyme.

3.5 Developmental phenotypes of 13 Hippo pathway-associated CRISPants

3.5.1 Embryonic development phenotypes in CRISPants had a general pattern of developmental disruption

The developmental phenotypes in 13 CRISPants are shown in Figure 3.15. These CRISPants include those described in 3.4, as well as the double CRISPants *yap1*/*wwtr1*, *nf2a*/*nf2b*, *lats1*/*lats2*, and *ctgfa*/*ctgfb*. Representative images of all embryos are shown in Figure 3.15A. To more clearly display the large amount of data generated in this screen, values were normalised to gRNA controls analysed in the same independent experimental repeat. Therefore, significance was calculated as difference from 1. A range of phenotypes are shown: length (Figure 3.15B), swim bladder area (Figure 3.15C), eye area (Figure 3.15D), yolk area (Figure 3.15E), heart area (Figure 3.15F), and survival (Figure 3.15G). *yap1* CRISPants had a consistent phenotype compared to that described during optimisation (Figure 3.7). Interestingly, previous work posits that *yap1* and *wwtr1* overall have similar functions, with some emerging evidence also suggesting different functions[44]. A difference in function was supported *in vivo* in the zebrafish as *wwtr1* CRISPants showed limited robust developmental phenotypes, suggesting that Taz does not have a key role in embryonic development. RT-qPCR and western blots performed previously (Figure 3.4N, and Figure 3.5D) showed that this was not due to a compensatory increase in *yap1* mRNA or Yap1 protein levels, although an increase in Yap1 activity was possible. Despite this, a double CRISPant for *yap1* and *wwtr1* showed a more severe developmental phenotype than *yap1* or *wwtr1* alone, with reduced length, survival, and eye area, a mostly absent swim bladder, and severe heart and yolk oedema (Figure 3.15B-G). This highlights that *wwtr1* has some effects on development. In the single *wwtr1* CRISPant, normal Yap1 levels and activity may be enough without compensatory

Figure 3.15: Embryonic development phenotypes of Hippo pathway-associated CRISPants
(A) Representative images of CRISPant embryos at 96hpf. Scale bar represents 200µm. **(B)** Quantification of embryo length in CRISPants, normalised to gRNA controls. Embryo length both increased and decreased following CRISPR mutagenesis. **(C)** Quantification of swim bladder area (as a percentage of body area) in CRISPants, normalised to gRNA controls. Swim bladder size decreased following the majority of CRISPR mutagenesis. **(D)** Quantification of eye area (as a percentage of body area) in CRISPants, normalised to gRNA controls. Eye area was increased following mutagenesis of individual upstream Hippo pathway kinases but decreased in double CRISPants and in many downstream components, notably except in *wwtr1* CRISPants. **(E)** Quantification of yolk area (as a percentage of body area) in CRISPants, normalised to gRNA controls. Yolk oedema was increased in multiple CRISPants, particularly in double CRISPants and *yap1* CRISPants. **(F)** Quantification of heart area (as a percentage of body area) in CRISPants, normalised to gRNA controls. Heart oedema was often increased in CRISPants, particularly in double CRISPants and *yap1* CRISPants. **(G)** Quantification of survival to 96hpf, normalised to gRNA controls. No significant changes were observed. **(H)** Dot plots of normalised values from B-F, plotting phenotypes against each other. CRISPants disrupted in one phenotype are often disrupted in another.
Significance calculated by Wilcoxon test (µ=1). Data from at least three independent experimental repeats. Each dot represents one embryo, except in (G), where it represents an independent experimental repeat. All values normalised to the average value for gRNA controls from the same independent repeat. *p<0.05; **p<0.01; ***p<0.001; ****p<0.0001; ns=not significant.

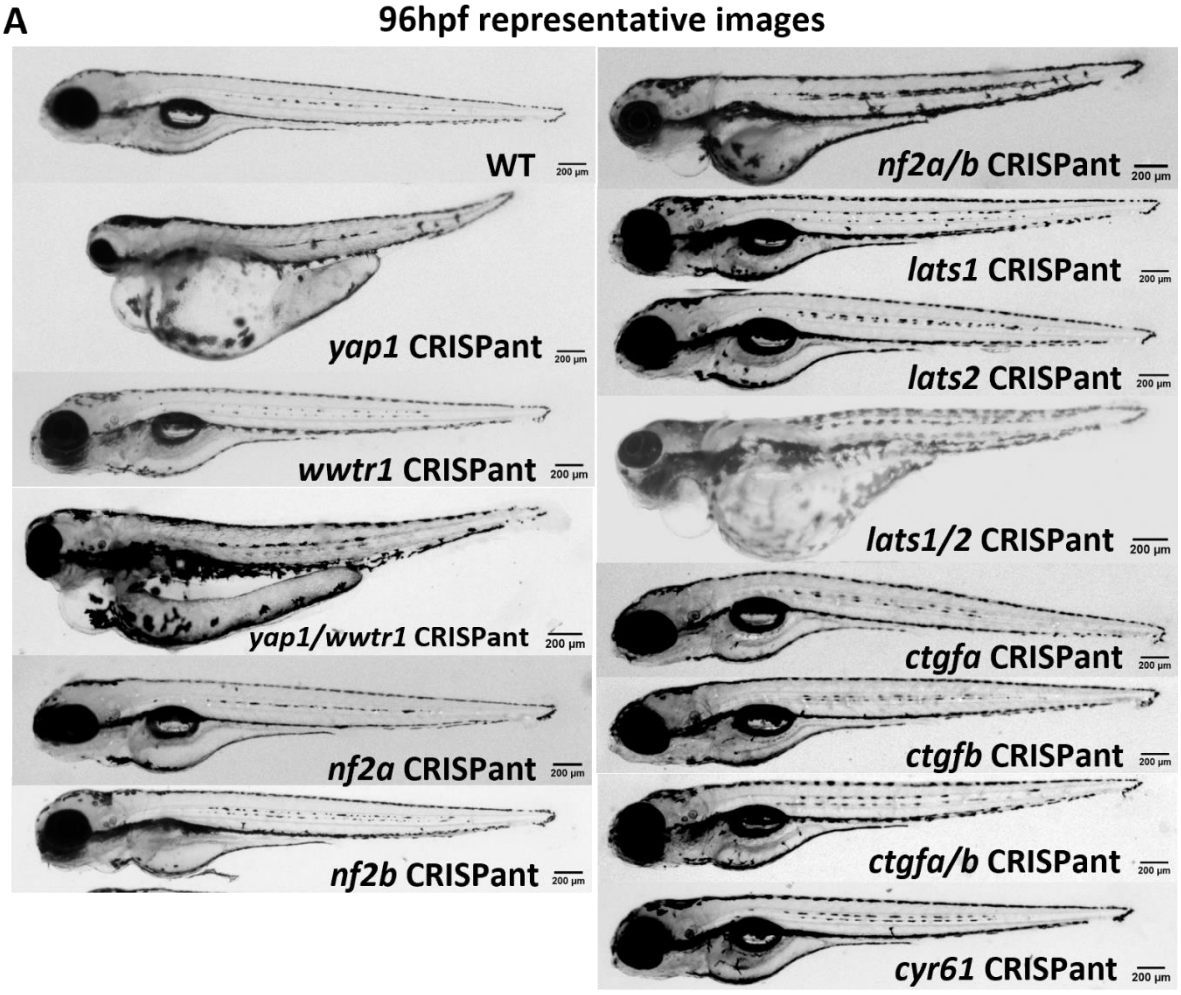

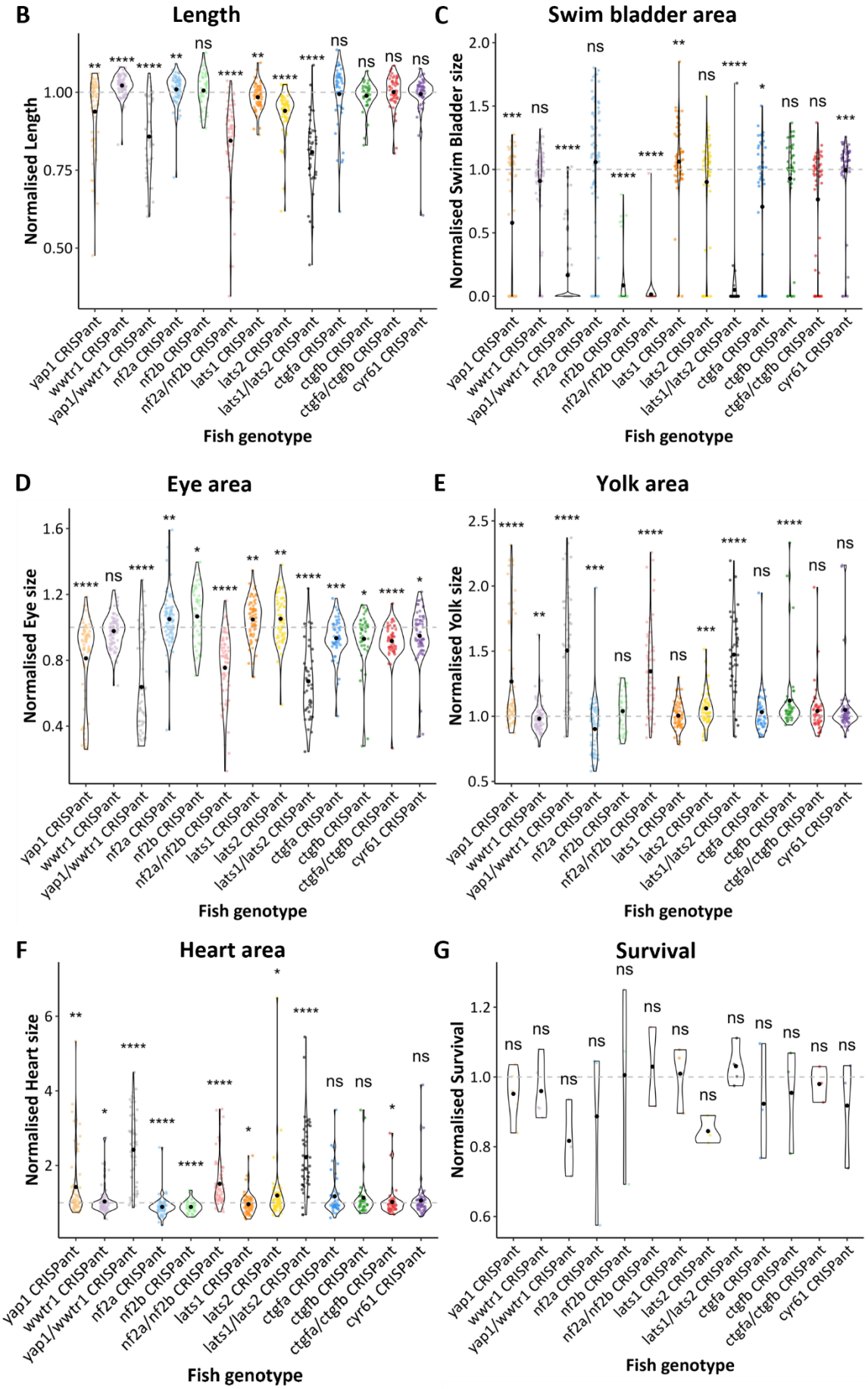
B
Length
Normalised Length
1.00
0.75
0.50
C
Swim bladder area
Normalised Swim Bladder size
2.0
1.5
1.0
0.5
0.0
D
Eye area
Normalised Eye size
1.6
1.2
0.8
0.4
E
Yolk area
Normalised Yolk size
2.5
2.0
1.5
1.0
0.5
F
Heart area
Normalised Heart size
6
4
2
G
Survival
Normalised Survival
1.2
1.0
0.8
0.6
yap1 CRISPant
wwtr1 CRISPant
yap1/wwtr1 CRISPant
nf2a CRISPant
nf2b CRISPant
nf2a/nf2b CRISPant
lats1 CRISPant
lats2 CRISPant
lats1/lats2 CRISPant
ctgfa CRISPant
ctgfb CRISPant
ctgfa/ctgfb CRISPant
cyr61 CRISPant
Fish genotype

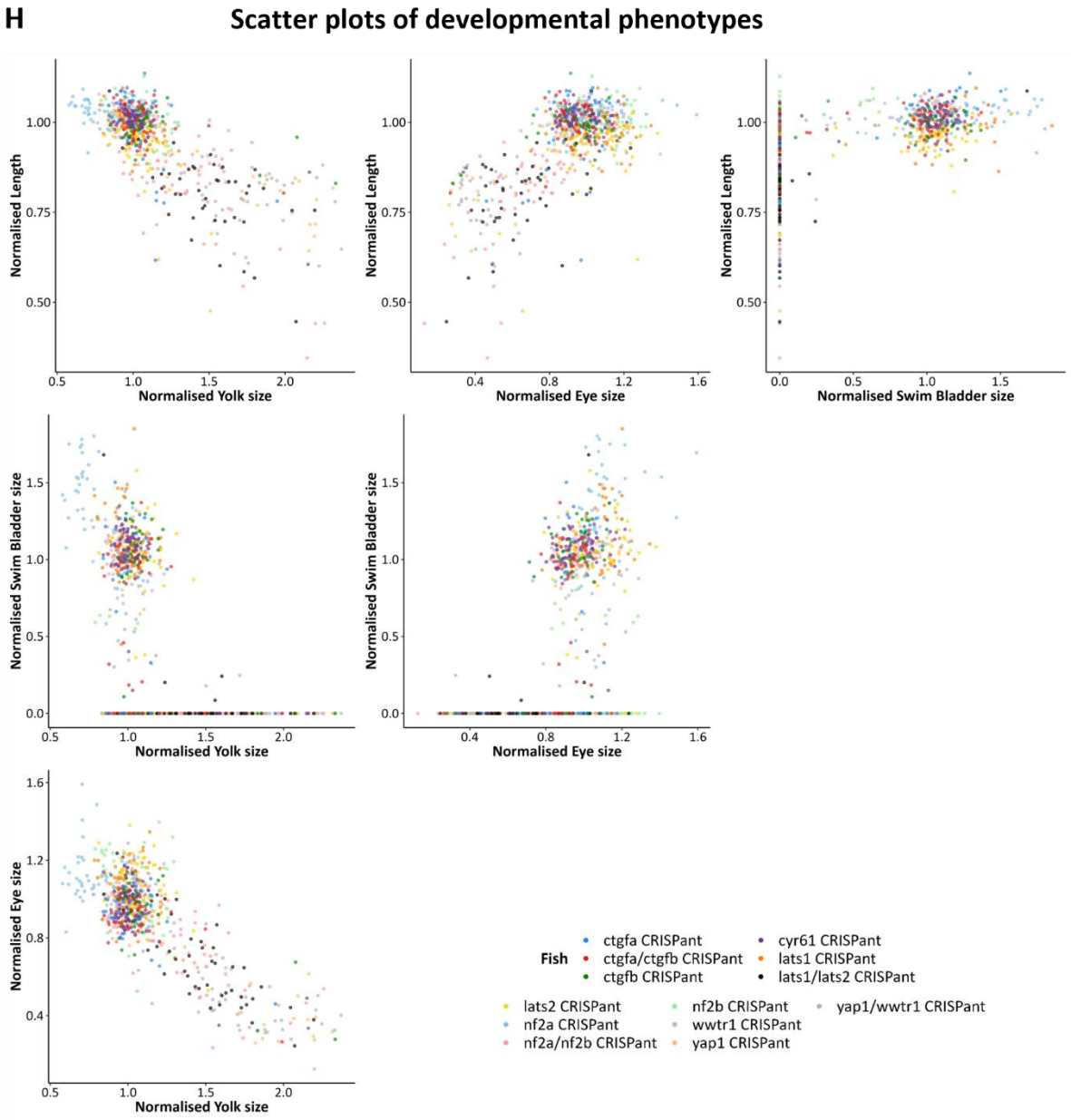

increase, whilst Taz activity alone was not enough to compensate for *yap1* disruption in the single *yap1* CRISPant.

Upstream components *lats1*, *lats2*, *nf2a*, and *nf2b* were also investigated. These components would usually inhibit Yap1/Taz activity (Figure 1.1). Therefore, their mutagenesis is predicted to increase Yap1/Taz activity. *nf2a* and *nf2b* single CRISPants, and one repeat of the double CRISPants were performed by S. Xia under the supervision of S. Riley (which is continued in regeneration analyses). Single CRISPants of these four genes had opposing phenotypes to those seen in *yap1* CRISPants, suggesting an increase in Yap1 (and potentially Taz) activity. This included an increased swim bladder (*lats1*), increased eye area (*lats1*, *lats2*, *nf2a*, and

nf2b), increased length (*nf2a*), and reduced oedema (*nf2a* and *nf2b*). Conversely, there were some phenotypes that were similar to *yap1* CRISPants, including slight oedema in *lats2* CRISPants, and an absent swim bladder in *nf2b* CRISPants. However, double *nf2a*/*nf2b* and *lats1*/*lats2* CRISPants were extremely disrupted to a comparable extent as *yap1*/*wwtr1* double CRISPants and would likely be non-viable to adulthood. This is potentially due to the large number of signalling pathways that these components contribute to, in addition to the detrimental effect of constitutively high Yap1/Taz activity. The findings also highlight a level of compensation between the paralogues.

A small selection of Yap1/Taz target genes[230] were also investigated: *ctgfa*, *ctgfb*, *cyr61*, and a double *ctgfa*/*ctgfb* CRISPant. These CRISPants had a similar, but less severe, phenotype to *yap1* CRISPants, likely indicating that a range of Yap1 target genes together produce the *yap1* CRISPant phenotype. All these CRISPants had reduced eye area (Figure 3.15D), *ctgfa* CRISPants showed reduced swim bladder (Figure 3.15C), and *ctgfb* increased yolk oedema (Figure 3.15E). The *ctgfa*/*ctgfb* double CRISPant did not have a more severe phenotype than each individual *ctgf* CRISPant, suggesting limited compensation between the two genes. Survival at 96hpf was also measured (Figure 3.15G), but significance was not observed, as only limited data points were available (three points denoting the three independent repeats). However, a similar trend to other phenotypes was observed, namely a more severe reduction in survival in double CRISPants.

Another method to visualise this data is shown in Figure 3.15H, where the (normalised) value for a selected parameter in each embryo was plotted against the others (excluding survival and heart area for simplicity). Most genotypes cluster with each other, except for those that create a "tail" denoting a more severe phenotype. These are mainly the double CRISPants that showed a severe phenotype in the other plots. All phenotypes roughly correlate with each other – i.e. those that are disrupted in one parameter are often disrupted in another. At the opposite end to the double CRISPant "tail", we also saw two CRISPant groups becoming more distinct: *nf2a* and, to a lesser extent, *lats1*. This might imply that these genotypes are most likely to reflect an increase in Yap1/Taz activity.

In conclusion, upstream kinase module CRISPants had overall opposing phenotypes to those seen in *yap1* CRISPants (Figure 3.15). This suggests that the phenotypes could be a result of

increasing Yap1 activity, as the upstream kinase cascade inhibits Yap1/Taz. However, these upstream component CRISPants clearly showed a high level of compensation as the double CRISPants were greatly developmentally deformed, so it is challenging to determine the exact impact of removing individual proteins. *yap1* CRISPants also had a very different phenotype pattern to the grossly normal *wwtr1* CRISPants, showing that these paralogues have markedly differing roles in development.

3.5.2 Juvenile developmental phenotypes in *yap1* and *wwtr1* CRISPants were limited

Apart from the *yap1* CRISPants described above in 3.2.4.3, only *wwtr1* CRISPants were brought forward for juvenile development imaging. Both groups were normalised to WT controls (rather than gRNA) to reduce the number of post-embryonic fish needed. Results of these analyses are shown in Figure 3.16. No general defects were apparent, and the only significant phenotype was a reduction in eye area in *wwtr1* CRISPants (Figure 3.16D). This suggests that embryonic and juvenile phenotypes are not closely linked, potentially due to the death of the more severely disrupted fish before they reach juvenile ages (observation, data not shown). The Hippo pathway could also have a time-dependent effect on development, with early defects becoming compensated for at later ages.

3.6 Regenerative phenotypes of 13 Hippo pathway-associated CRISPants

3.6.1 Neuromast development and regeneration

3.6.1.1 Uninjured neuromast development was mainly impaired in double CRISPants

Neuromasts regenerate through transdifferentiation after ablation of sensory hair cells[38]. These sensory cells can be injured through Cu^{2+} metal ion administration (representative images shown in Figure 3.17A), which are taken up by hair cells and destroy the cell[250,252]. This can be imaged through the application of a DASPEI dye which is also taken up by hair cells, causing the hair cell to become fluorescent to allow for imaging and quantification. The baseline, or uninjured, development of this organ was determined through the analysis of live larval neuromast area and number via quantification of $DASPEI^{+}$ puncta using a fluorescence microscope (Figure 3.17B+C respectively). As for the development analyses above, results are shown as CRISPants normalised to gRNA controls performed concurrently. At baseline, *yap1* CRISPants had a reduced number of neuromasts, whilst *wwtr1* CRISPants had no change in

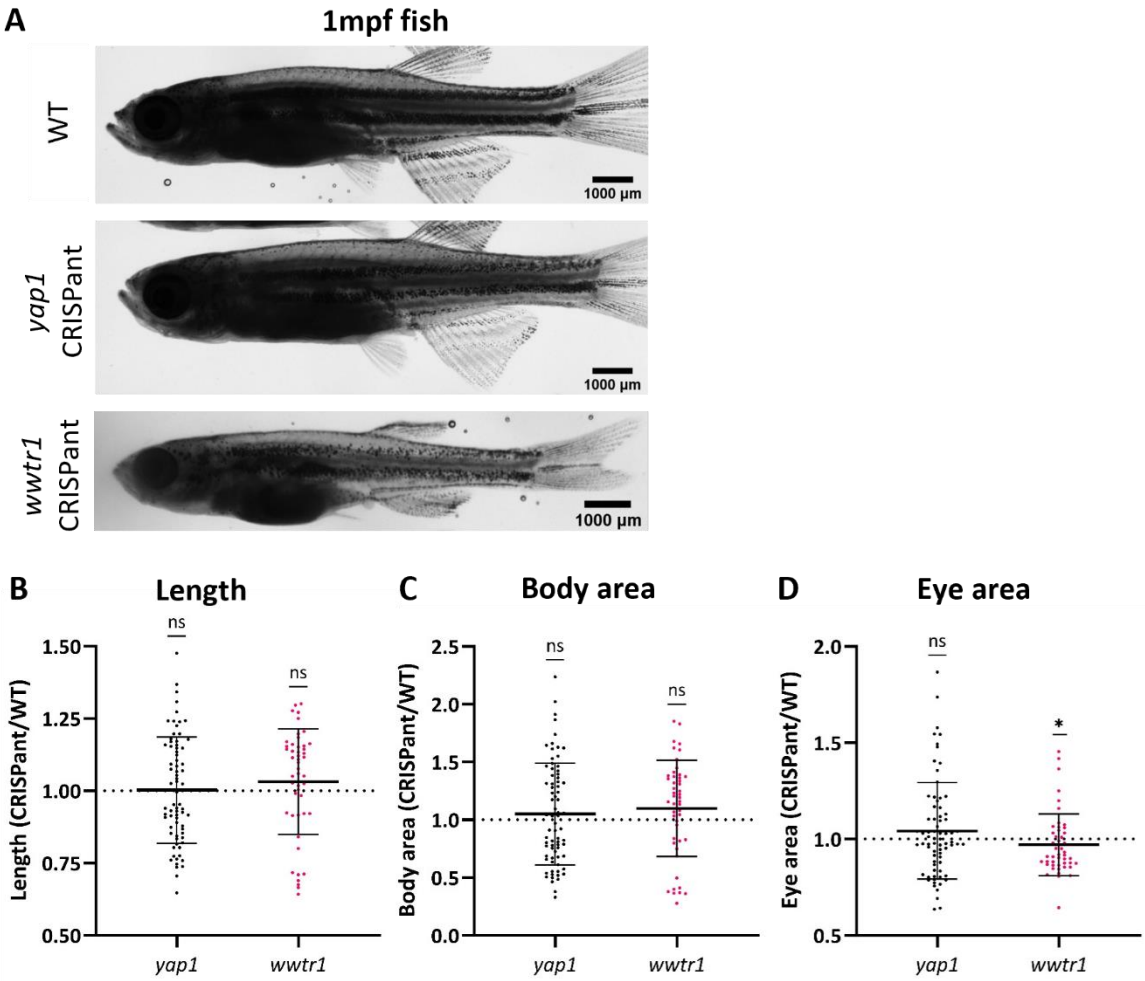

Figure 3.16: Juvenile development phenotypes of *yap1* and *wwtr1* CRISPants
(A) Representative images of WT, *yap1* CRISPant, and *wwtr1* CRISPant juveniles at 1mpf. WT and *yap1* CRISPant images are also shown in Figure 3.9. **(B)** Quantification of body length in *yap1* and *wwtr1* CRISPants, normalised to WT. CRISPant body length was unchanged. **(C)** Quantification of body area in *yap1* and *wwtr1* CRISPants, normalised to WT. CRISPant body area was unchanged. **(D)** Quantification of eye area in *yap1* and *wwtr1* CRISPants, normalised to WT. CRISPant eye size was unchanged in *yap1* CRISPants but reduced in *wwtr1* CRISPants relative to WT.
Scale bar represents 1000µm. Bars represent mean±SD. Significance calculated using one-sample t-test (B and C) or Wilcoxon test (D) (µ=1). Data from three independent experimental repeats. Each dot represents one embryo. All values normalised to the average value for WT controls. *p<0.05; ns=not significant.

either number or area. Like developmental phenotypes, the *yap1*/*wwtr1* double CRISPant had a more severe defect than either single CRISPant alone, with a significant reduction in both area and number. *nf2a* and *nf2b* CRISPants had no phenotype, but their double CRISPant had a significant reduction in both area and number, again like their developmental phenotypes and suggesting a level of compensation between the two paralogs. Similarly, the *lats1*/*lats2* double CRISPant had a more significant defect in neuromast development than either alone.

Finally, unlike developmental phenotypes, the double *ctgfa*/*ctgfb* CRISPant had a more severe defect in both number and area than either of the single CRISPants alone.

3.6.1.2 Neuromast regeneration showed diverse effects that differed from uninjured phenotypes

As described in 3.3, hair cells were injured at 72hpf, and regeneration was imaged and measured at 24 and 48hpi focussing on the size and number of neuromasts (Figure 3.17D-G). As may be expected from the uninjured phenotype, *yap1* CRISPants had reduced number at both timepoints, and a reduced area at 24hpi. Notably, *wwtr1* CRISPants had no striking phenotype, yet the double *yap1*/*wwtr1* CRISPant had a more significant defect than *yap1* CRISPant displays alone, indicating a potential compensatory role of Yap1 in the *wwtr1* CRISPant. Although the *nf2a* and *nf2b* CRISPants had no phenotype if unchallenged, during regeneration there was a reduced number at 24hpi, and a slight increase in number of *nf2a* CRISPants at 48hpi. However, the double *nf2a*/*nf2b* CRISPant had a larger reduction in number at 24hpi, and both area and number at 48hpi than the single CRISPants alone. *lats2* CRISPants had reduced number at baseline, and this was maintained throughout regeneration without a change in neuromast area. Conversely, *lats1* CRISPants had reduced neuromast area throughout regeneration, as well as a slight increase in number. This suggests different roles for these components in regeneration. However, the double *lats1*/*lats2* CRISPant had major defects in both area and number, to a greater extent than the single *lats1* or *lats2* CRISPants. Interestingly, the decrease in baseline neuromast number in *ctgfa* CRISPants was not maintained during regeneration, with no change in neuromast number or area after injury. However, the *ctgfb* CRISPant increase in baseline area was maintained at 48hpi only. This could suggest an anti-regenerative role for *ctgfb*, contrary to *ctgfa*, disruption of which has been shown to impair zebrafish regeneration[38,203,257,258]. The contrasting roles could be a result of differing regulation of the paralogues. Notably, double *ctgfa*/*ctgfb* CRISPants had no regenerative phenotype despite a reduction in baseline number and area. Finally, *cyr61* CRISPants had a slight increase in number at 24hpi and a decrease in area at 48hpi.

In conclusion, neuromast regeneration follows a similar pattern to developmental phenotypes. Double CRISPants often had a more severe phenotype than the single CRISPant,

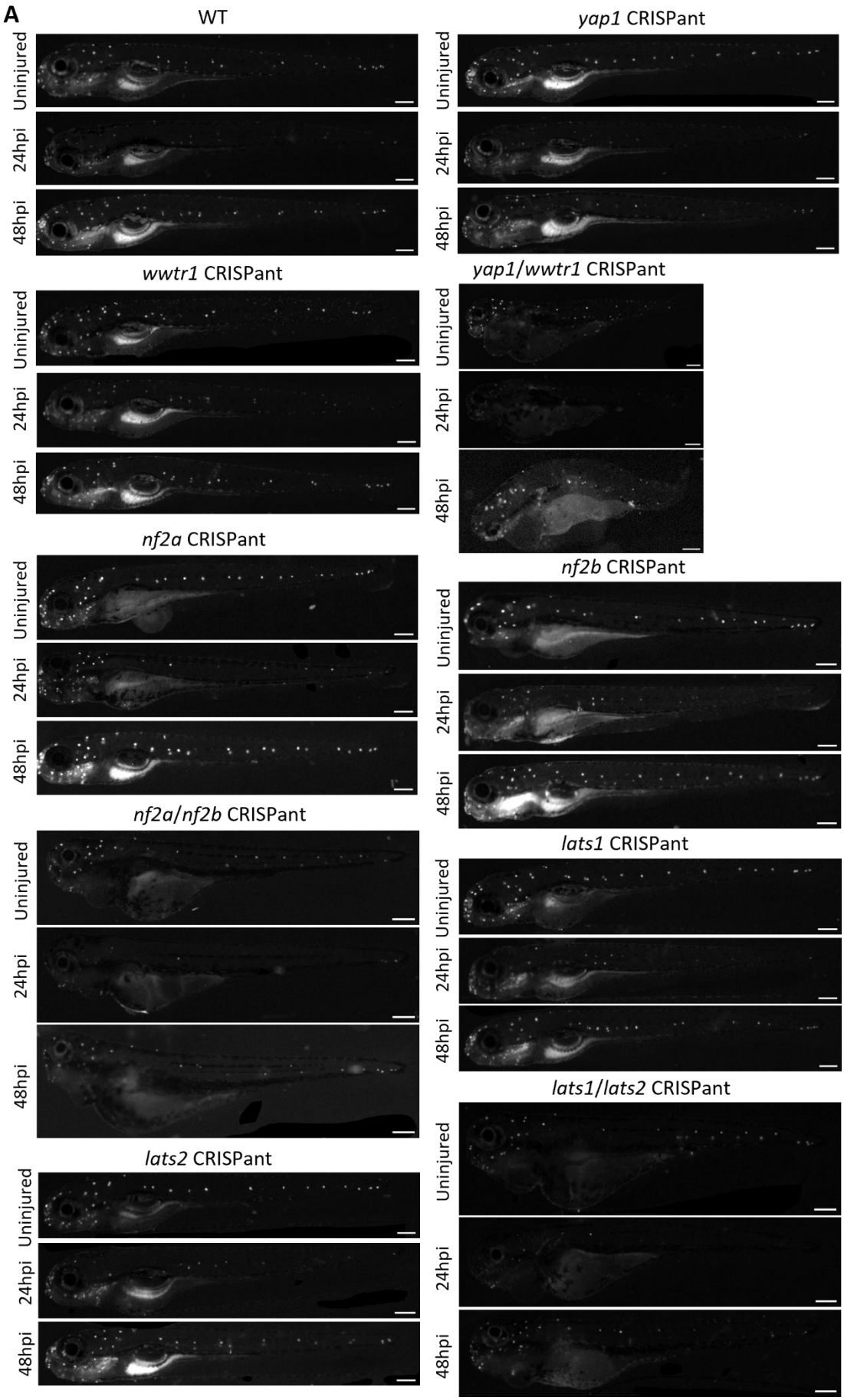
A
WT
Uninjured
24hpi
48hpi
yap1 CRISPant
wwtr1 CRISPant
yap1/wwtr1 CRISPant
nf2a CRISPant
nf2b CRISPant
nf2a/nf2b CRISPant
lats1 CRISPant
lats2 CRISPant
lats1/lats2 CRISPant

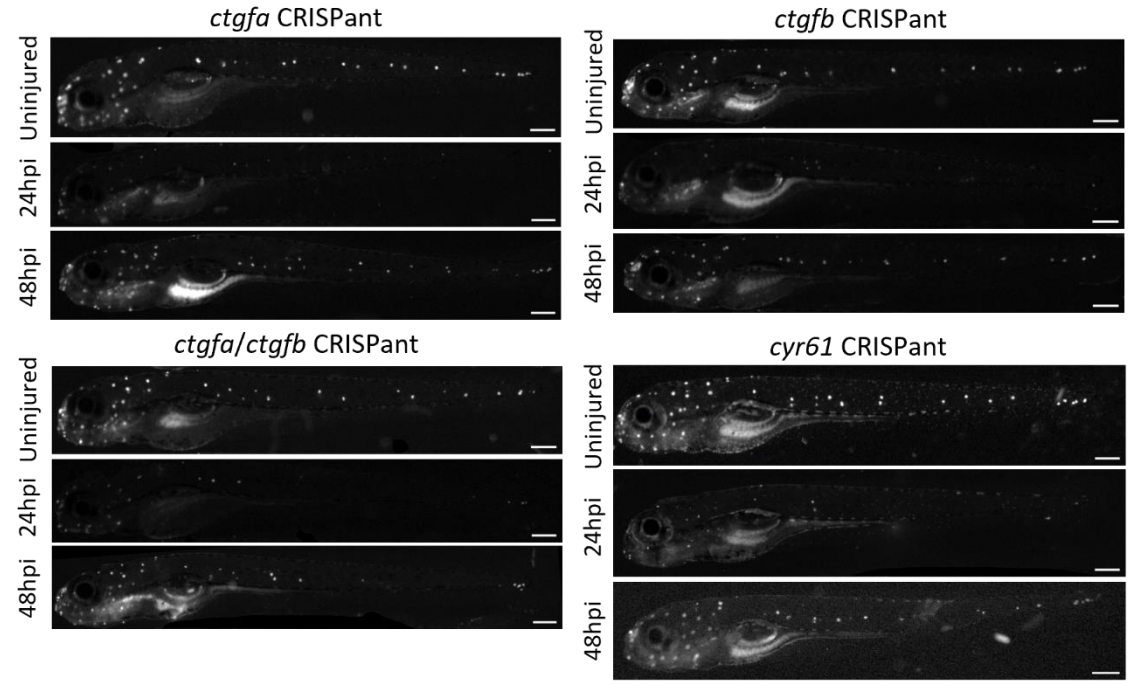
ctgfa CRISPant
ctgfb CRISPant
ctgfa/ctgfb CRISPant
cyr61 CRISPant
Uninjured
24hpi
48hpi

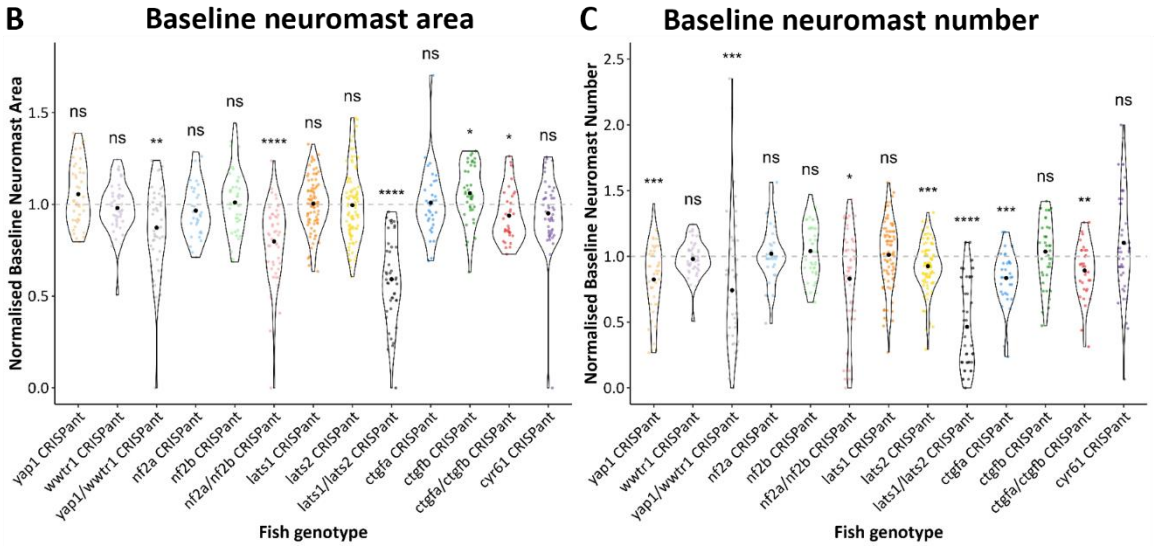
B
Baseline neuromast area
Normalised Baseline Neuromast Area
C
Baseline neuromast number
Normalised Baseline Neuromast Number
yap1 CRISPant
wwtr1 CRISPant
yap1/wwtr1 CRISPant
nf2a CRISPant
nf2b CRISPant
nf2a/nf2b CRISPant
lats1 CRISPant
lats2 CRISPant
lats1/lats2 CRISPant
ctgfa CRISPant
ctgfb CRISPant
ctgfa/ctgfb CRISPant
cyr61 CRISPant
Fish genotype

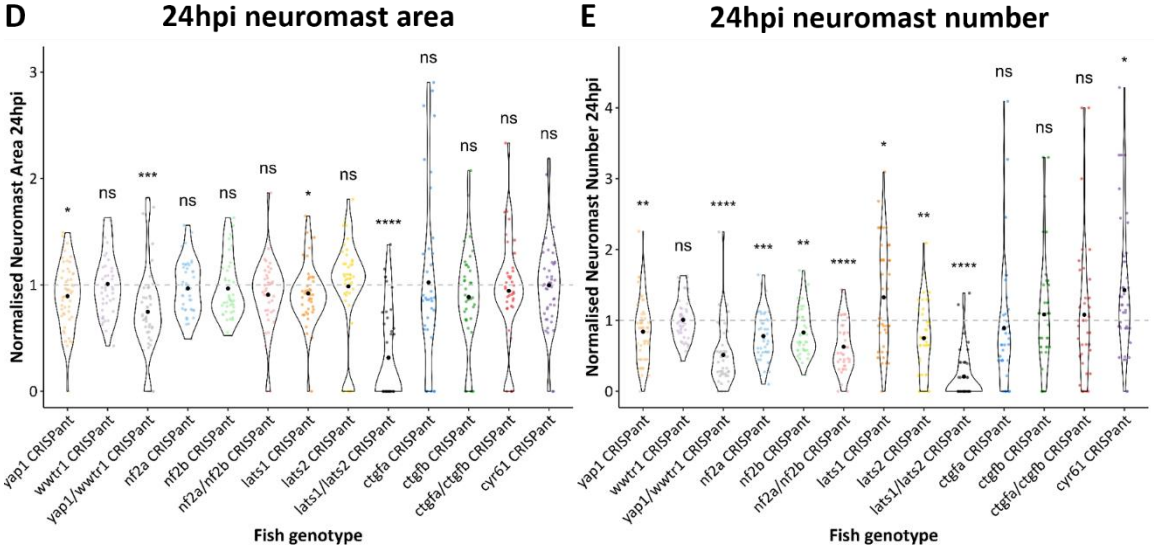
D
24hpi neuromast area
Normalised Neuromast Area 24hpi
E
24hpi neuromast number
Normalised Neuromast Number 24hpi
yap1 CRISPant
wwtr1 CRISPant
yap1/wwtr1 CRISPant
nf2a CRISPant
nf2b CRISPant
nf2a/nf2b CRISPant
lats1 CRISPant
lats2 CRISPant
lats1/lats2 CRISPant
ctgfa CRISPant
ctgfb CRISPant
ctgfa/ctgfb CRISPant
cyr61 CRISPant
Fish genotype

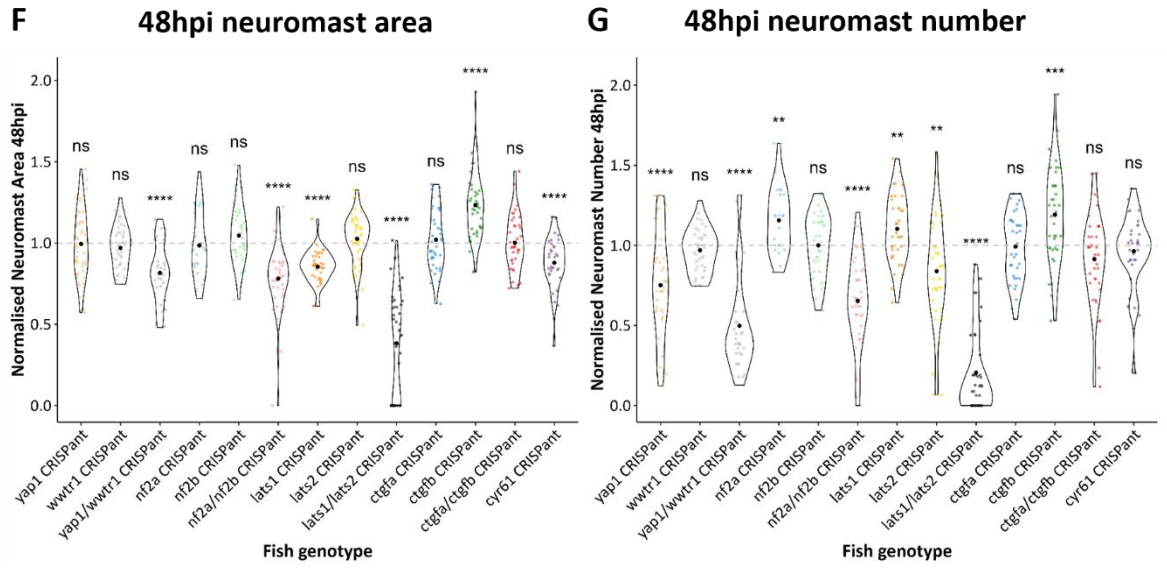

Figure 3.17: Neuromast regeneration phenotypes of Hippo pathway-associated CRISPants
(A) Representative images of DASPEI-labelled neuromasts in WT and CRISPants when uninjured and at 24hpi and 48hpi. Scale bar represents 200µm. **(B)** Quantification of uninjured neuromast area in CRISPants, normalised to gRNA controls. Baseline neuromast area was mainly reduced in double CRISPants. **(C)** Quantification of uninjured neuromast number in CRISPants, normalised to gRNA controls. Baseline neuromast number was reduced in multiple CRISPants. **(D)** Quantification of 24hpi neuromast area in CRISPants, normalised to gRNA controls. 24hpi neuromast area was reduced in *yap1*, *lats1*, and some double CRISPants. **(E)** Quantification of 24hpi neuromast number in CRISPants, normalised to gRNA controls. 24hpi neuromast number was reduced in multiple CRISPants but increased in *lats1* and *cyr61* CRISPants. **(F)** Quantification of 48hpi neuromast area in CRISPants, normalised to gRNA controls. 48hpi neuromast area was reduced in multiple CRISPants but increased in *ctgfb* CRISPants. **(G)** Quantification of 48hpi neuromast number in CRISPants, normalised to gRNA controls. 48hpi neuromast number was reduced in multiple CRISPants, but increased in *nf2a*, *lats1*, and *ctgfb* CRISPants.
Scale bar represents 200µm. Significance calculated by Wilcoxon test (µ=1). Data from at least three independent experimental repeats. Each dot represents one embryo. All values normalised to the average value for gRNA-only controls from the same independent repeat. *p<0.05; **p<0.01; ***p<0.001; ****p<0.0001; ns=not significant.

suggesting compensation. However, *ctgfa*/*ctgfb* CRISPants go against this trend. In addition, *yap1* CRISPants showed impaired regeneration whilst *wwtr1* CRISPants did not. However, there was no robust increase in regeneration in the upstream kinase CRISPants, suggesting that promoting Yap1/Taz activity alone is not sufficient to promote regeneration.

3.6.2 Tail fin development and regeneration

3.6.2.1 Uninjured fin growth showed gene-specific changes in CRISPants

A further regenerative process analysed in the CRISPant screen was that of tail fin regeneration (representative images in Figure 3.18A). Two paradigms were included: a mild injury that cuts only the fin fold, and a severe injury that cuts the notochord and neural tube (Figure 3.10A). Like neuromast regeneration (3.6.1), measurements of baseline (uninjured) tail fin growth were analysed (Figure 3.18B). Both increases and decreases in fin growth were seen. Notably, *yap1*, *wwtr1*, and *yap1/wwtr1* CRISPants had no baseline growth phenotypes. *nf2a* CRISPants showed an increase in fin growth from controls, whilst *nf2b* CRISPants had no change, and the *nf2a*/*nf2b* double CRISPants had a decrease. Similarly, *lats2* CRISPants had an increase in growth, whilst *lats1* CRISPants had no change, and the *lats1*/*lats2* double CRISPants showed a decrease. These suggest that a single CRISPant in both of these upstream inhibitory Hippo pathway components may be enough to enhance Yap1/Taz activity to promote growth, but the double CRISPants may have a plethora of other defects caused by a lack of compensation that prevent this from promoting growth. It is also possible that constitutively elevated Yap1/Taz activity is detrimental for normal fin growth, or that upstream kinase module components directly regulate Yap1/Taz-independent processes[259] that function during tail fin growth.

3.6.2.2 Mild tail fin regeneration was unchanged or reduced in all CRISPants

After mild tail fin injury, regeneration was measured at 48hpi (Figure 3.18C). Like neuromast regeneration, *yap1* CRISPants had reduced regeneration whilst *wwtr1* CRISPants did not. *yap1*/*wwtr1* double CRISPants also showed a decrease in regeneration, but to the same level as *yap1* CRISPant alone, highlighting that *wwtr1* does not play a significant role in this process. In accordance with the uninjured results, *nf2a*/*nf2b* double CRISPants and *ctgfb* CRISPants both had reduced regeneration. Although *lats2* CRISPants had increased uninjured growth, after injury these CRISPants had reduced regeneration, showing a specific phenotype for normal growth. *lats1*/*lats2* double CRISPants had reduced regeneration to a greater extent than *lats2* CRISPants alone, suggesting compensation is present between Lats family members.

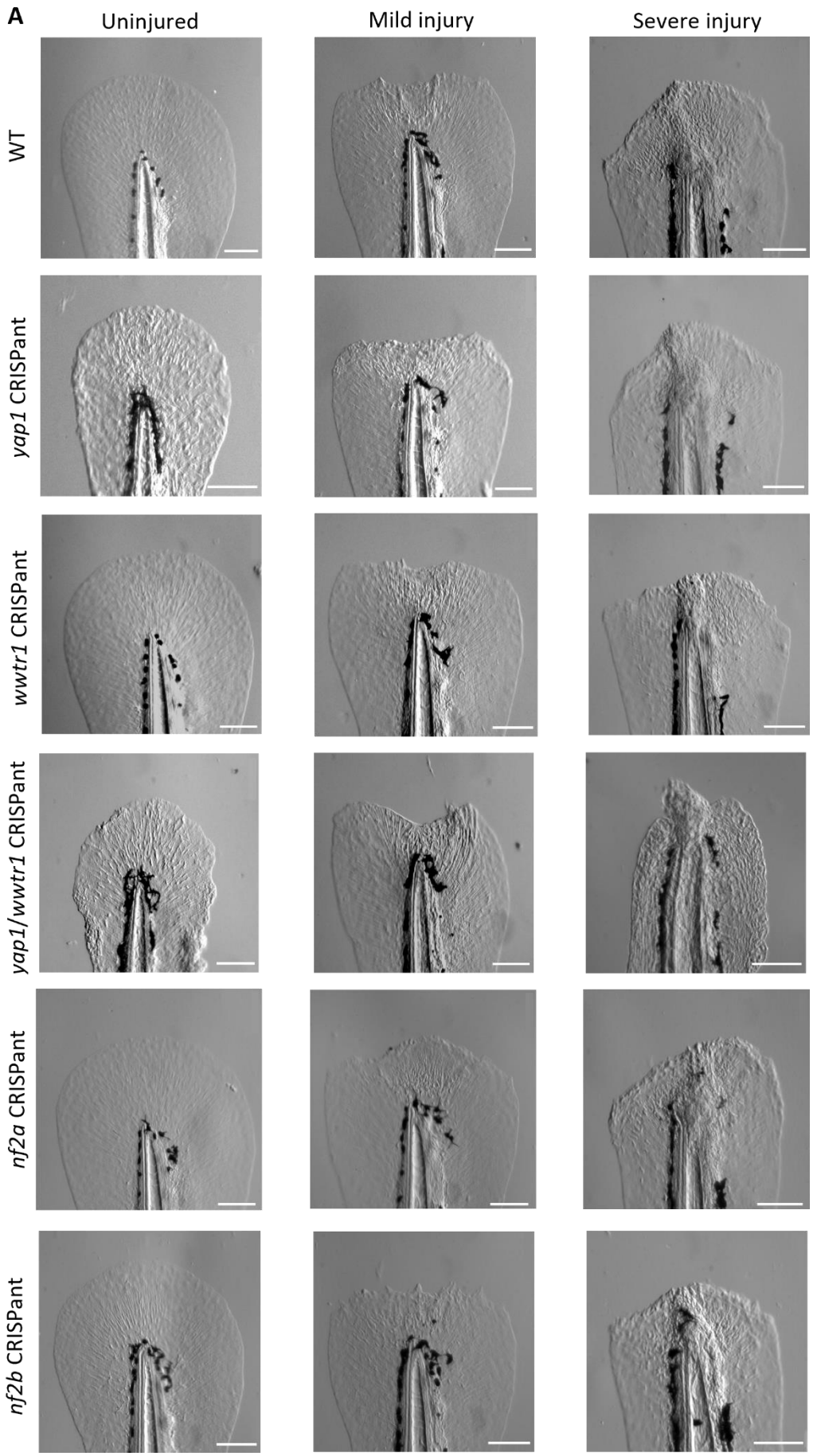
A
Uninjured
Mild injury
Severe injury
WT
yap1 CRISPant
wwtr1 CRISPant
yap1/wwtr1 CRISPant
nf2a CRISPant
nf2b CRISPant

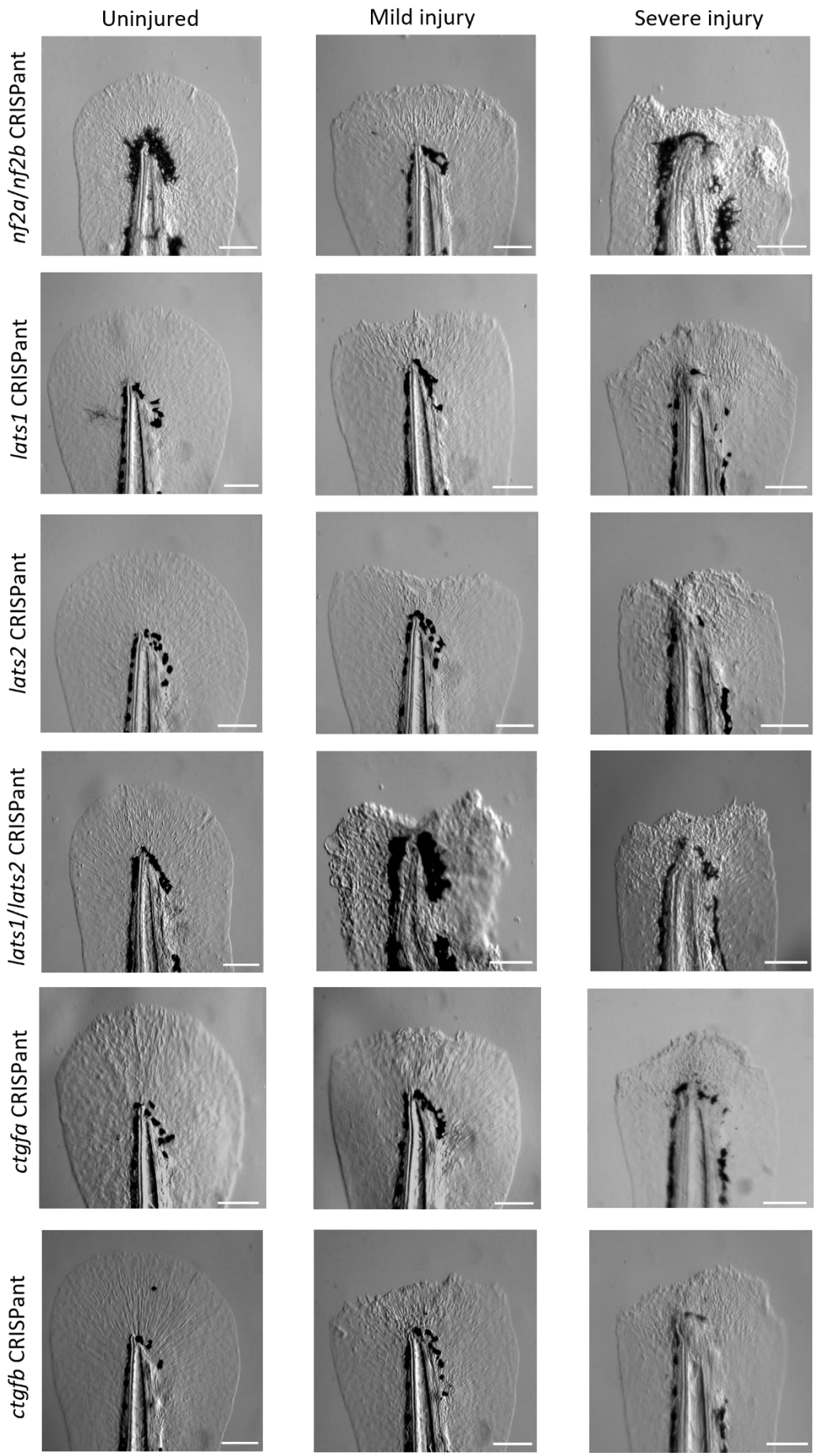
Uninjured
Mild injury
Severe injury
nf2a/nf2b CRISPant
lats1 CRISPant
lats2 CRISPant
lats1/lats2 CRISPant
ctgfa CRISPant
ctgfb CRISPant

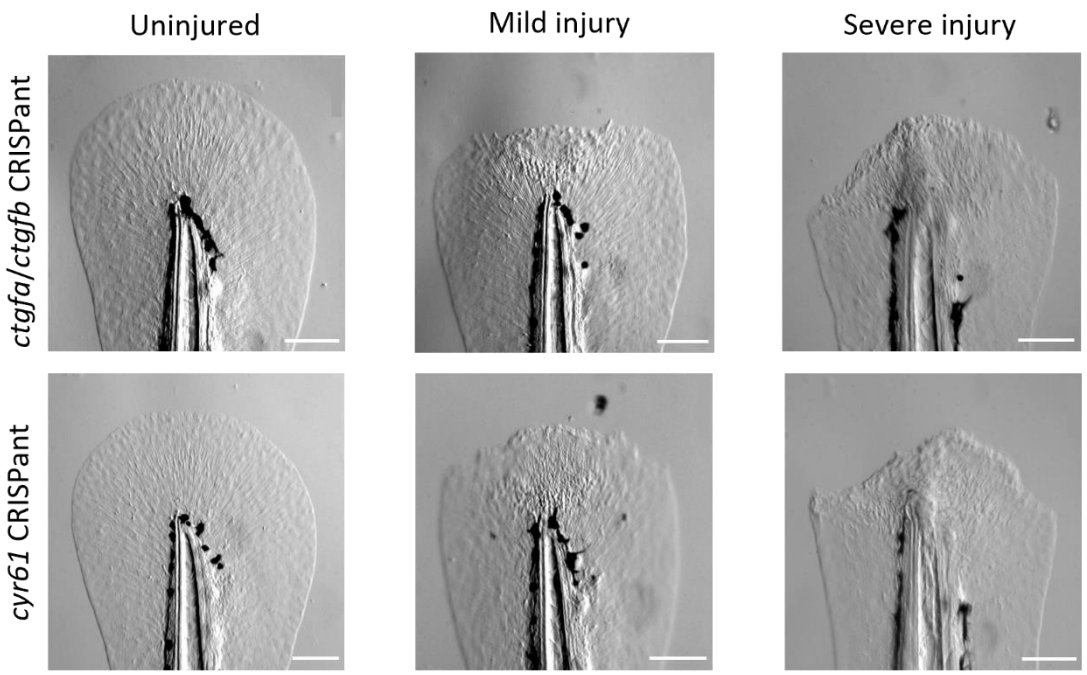
Uninjured
Mild injury
Severe injury
ctgfa/ctgfb CRISPant
cyr61 CRISPant

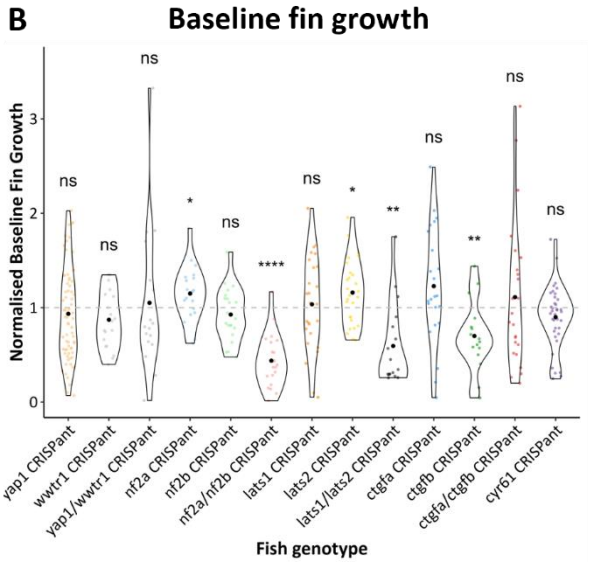
B
Baseline fin growth
Normalised Baseline Fin Growth
Fish genotype
yap1 CRISPant
wwtr1 CRISPant
yap1/wwtr1 CRISPant
nf2a CRISPant
nf2b CRISPant
nf2a/nf2b CRISPant
lats1 CRISPant
lats2 CRISPant
lats1/lats2 CRISPant
ctgfa CRISPant
ctgfb CRISPant
ctgfa/ctgfb CRISPant
cyr61 CRISPant

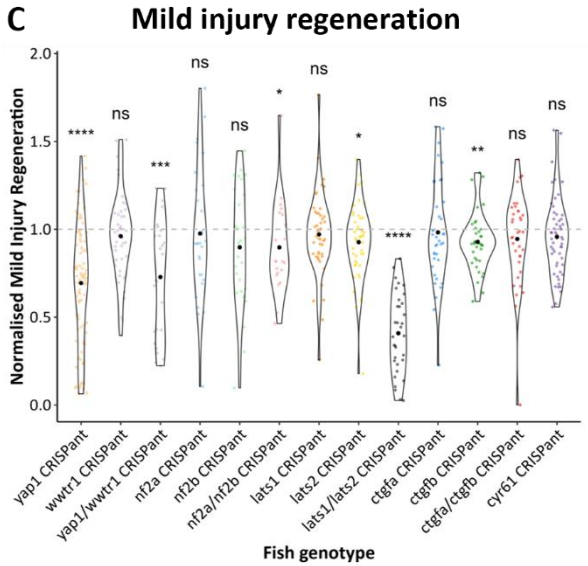
C
Mild injury regeneration
Normalised Mild Injury Regeneration
Fish genotype

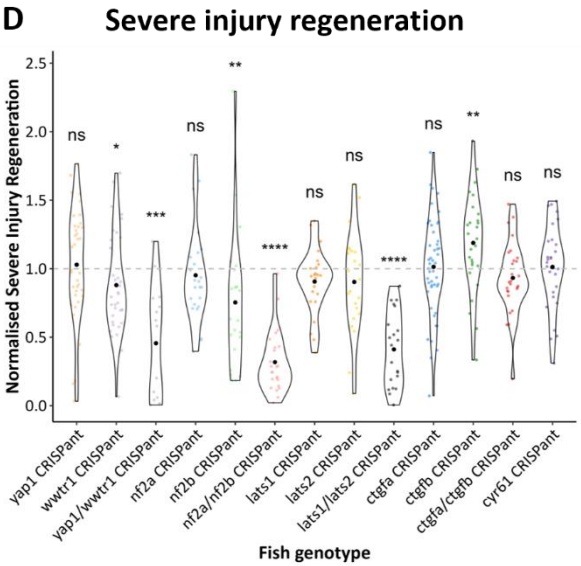
D
Severe injury regeneration
Normalised Severe Injury Regeneration
Fish genotype

Figure 3.18: Tail fin regeneration phenotypes of Hippo pathway-associated CRISPants
(A) Representative images of WT and CRISPant embryo tail fins when uninjured, 48 hours post mild injury, and 48 hours post severe injury. **(B)** Quantification of uninjured fin growth in CRISPants, normalised to gRNA controls. Baseline (uninjured) fin growth was altered in some CRISPant phenotypes, most severely in upstream component double CRISPants. **(C)** Quantification of regeneration following mild tail fin injury in CRISPants, normalised to gRNA controls. Regeneration was reduced in many CRISPants. **(D)** Quantification of regeneration following severe tail fin injury in CRISPants, normalised to gRNA controls. Regeneration was reduced in many CRISPants but increased in ctgfb CRISPants. Note the reduction in regeneration in *wwtr1* CRISPants, the only *wwtr1*-specific regeneration phenotype observed throughout the screen.
Scale bar represents 100μm. Significance calculated by Wilcoxon test (μ=1). Data from at least three independent experimental repeats. Each dot represents one embryo. All values normalised to the average value for gRNA-only controls from the same independent repeat. *p<0.05; **p<0.01; ***p<0.001; ****p<0.0001; ns=not significant.

3.6.2.3 Severe tail fin regeneration phenotypes were different to both uninjured growth and mild tail fin regeneration

Regeneration after severe tail fin injury was then analysed (Figure 3.18D). Interestingly, this highlights a marked change in *yap1* and *wwtr1* CRISPant phenotypes between the two tail fin regenerative paradigms. As discussed in 3.2.4.4, *yap1* CRISPants appeared not to have significant defects, although this may be explained by the higher death rate for the more disrupted embryos skewing the data. In fact, *yap1*/*wwtr1* double CRISPants had more severe defects than either *yap1* or *wwtr1* alone, highlighting that *yap1* does play a role. Despite having no other significant phenotypes in this screen, *wwtr1* CRISPants showed a defect in severe tail fin regeneration, which is of great interest. This specific phenotype suggests that the defect is not due to general developmental defects that might explain some of the *yap1* CRISPant and double CRISPant regenerative phenotypes. It could instead be a regenerative defect specific to severe tail fin regeneration. Despite having no uninjured or mild phenotype, *nf2b* CRISPants had a regeneration defect that was magnified when *nf2a* was also mutagenised in the double CRISPant, indicating compensation. *lats1*/*lats2* CRISPants also had a severe defect, in accordance with their developmental and other regenerative phenotypes. Finally, *ctgfb* CRISPants had an increase in severe tail fin regeneration in a similar manner to that seen in neuromast regeneration, despite having reduced general fin growth and mild tail fin regeneration. This suggests a potential inhibitory effect of Ctgfb in severe tail fin regeneration and neuromast regeneration at 48hpi, possibly through its role in the extracellular matrix[260]. In conclusion, the mild and severe injury paradigms have different effects on Hippo pathway CRISPants. Most notably, *wwtr1* CRISPants only showed a

regenerative phenotype after severe injury. This demonstrates a specific role for *wwtr1* in this process alone.

3.7 Summary and comparison of screen parameters

In order to directly compare the range of developmental and regenerative phenotypes measured in this study, the average normalised value for each CRISPant and each parameter was calculated and transformed using the natural log (ln) of the value. This transforms the average such that a negative number denotes a decrease in that parameter, and a positive number an increase. Figure 3.19A-D shows heat maps generated from these values. These show an overview of what is described in 3.5, 3.6.1, and 3.6.2, mainly the highly defective double CRISPants (excluding *ctgfa*/*ctgfb*) in all parameters. It is also clear that CRISPants defective in one parameter were more likely to be defective in another. This has also been reported in other CRISPR/Cas9 screens, which have shown, for example, that genes associated with one type of regeneration often also affect other types of regeneration[201].

A different way of illustrating the data is displayed in Figure 3.19E. For this, the natural log transformed values for a selected parameter were directly plotted against those in another parameter, for example, the swim bladder area in *yap1* CRISPants against neuromast number at 48hpi in *yap1* CRISPants etc. This approach allows us to visualise genotypes that behave obviously differently to others. Not all parameters were included for clarity. Genotypes that commonly deviate from others were mostly as expected, including *lats1*/*lats2* double CRISPants being defective in every parameter. This indicates the wide-ranging roles of these kinases, including potentially outside of Yap1/Taz regulation. *yap1*/*wwtr1* and *nf2a*/*nf2b* double CRISPants were similar but less consistent, suggesting potentially more specific roles for these components.

Some unexpected results were in the *lats* and *nf2* CRISPants. As these proteins act upstream of the Hippo pathway to inhibit Yap1/Taz activity, it might be expected that their CRISPants would give the opposite results to *yap1* and *wwtr1* CRISPants, namely enhancing regeneration or speeding up development. This was not consistently observed, with many phenotypes phenocopying those seen in *yap1* CRISPants. This might suggest that the activity level of Yap1/Taz needs to be under tight spatio-temporal control, and that either too much or

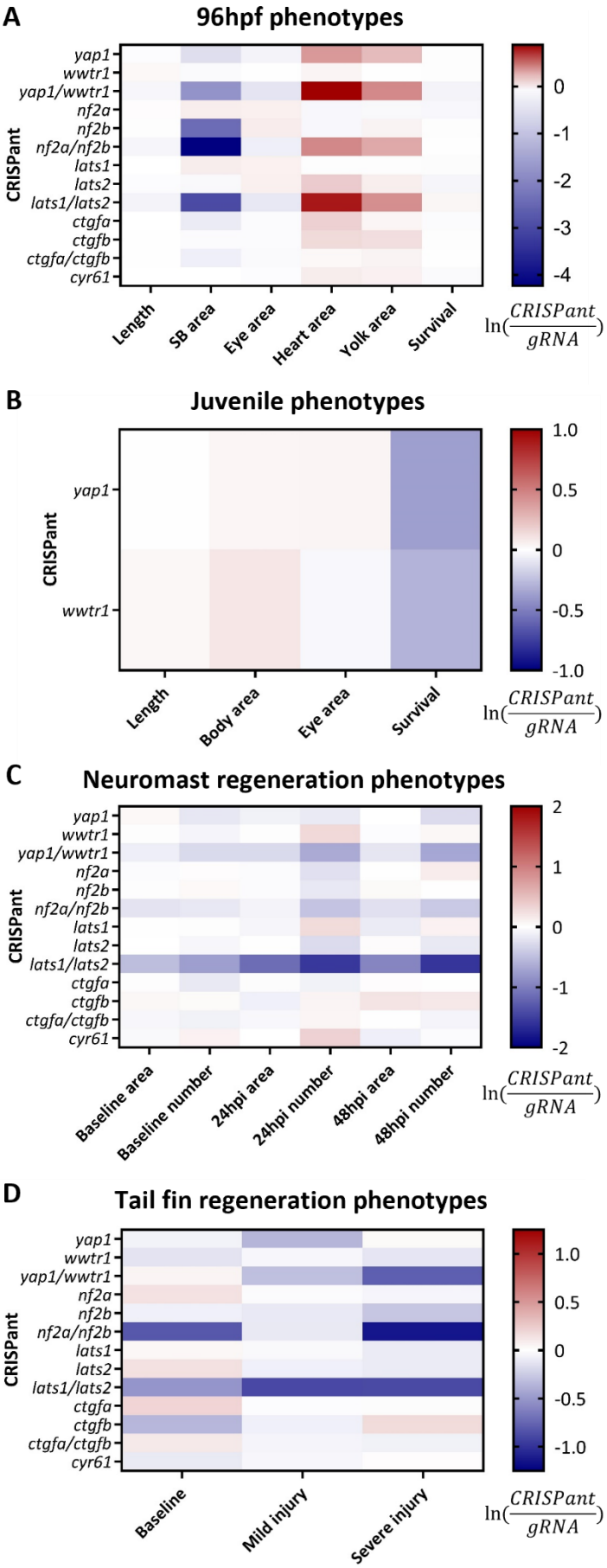
A
96hpf phenotypes
yap1
wwtr1
yap1/wwtr1
nf2a
nf2b
nf2a/nf2b
lats1
lats2
lats1/lats2
ctgfa
ctgfb
ctgfa/ctgfb
cyr61
CRISPant
Length
SB area
Eye area
Heart area
Yolk area
Survival
0
-1
-2
-3
-4
ln(CRISPant / gRNA)
B
Juvenile phenotypes
yap1
wwtr1
CRISPant
Length
Body area
Eye area
Survival
1.0
0.5
0
-0.5
-1.0
ln(CRISPant / gRNA)
C
Neuromast regeneration phenotypes
yap1
wwtr1
yap1/wwtr1
nf2a
nf2b
nf2a/nf2b
lats1
lats2
lats1/lats2
ctgfa
ctgfb
ctgfa/ctgfb
cyr61
CRISPant
Baseline area
Baseline number
24hpi area
24hpi number
48hpi area
48hpi number
2
1
0
-1
-2
ln(CRISPant / gRNA)
D
Tail fin regeneration phenotypes
yap1
wwtr1
yap1/wwtr1
nf2a
nf2b
nf2a/nf2b
lats1
lats2
lats1/lats2
ctgfa
ctgfb
ctgfa/ctgfb
cyr61
CRISPant
Baseline
Mild injury
Severe injury
1.0
0.5
0
-0.5
-1.0
ln(CRISPant / gRNA)

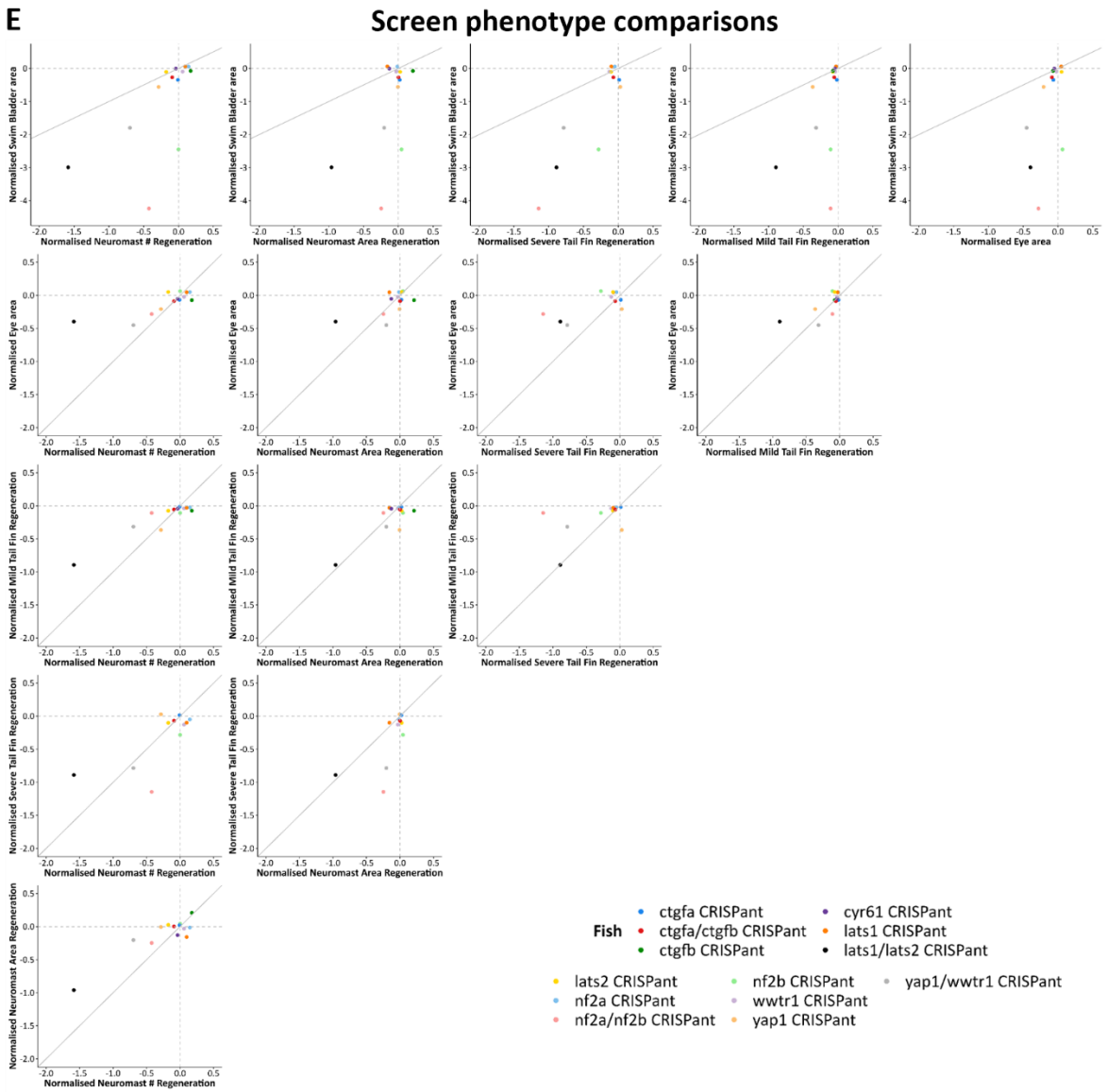

Figure 3.19: Plots of average developmental and regenerative phenotypes of Hippo pathway-associated CRISPants

(A) Heat map of average 96hpf phenotypes. Swim bladder (SB) area, heart area, and yolk area are often disrupted together, and double CRISPants are often more significantly disrupted than single CRISPants. **(B)** Heat map plot of average juvenile developmental phenotypes. No clear pattern is observed except a large reduction in survival. **(C)** Heat map of average neuromast regeneration phenotypes. *lats1/2* CRISPants had the most severe phenotypes overall, and CRISPants with a reduction in one parameter often are reduced in all others. **(D)** Heat map of average tail fin regeneration phenotypes. Double CRISPants had the most severe phenotypes overall, and CRISPants with a reduction in one parameter often are reduced in all others. **(E)** Comparative plots of ln values from select developmental and regenerative phenotypes. Most points lie on the y=x line, suggesting a similar degree of disruption in each phenotype. Note an exception was the swim bladder area. Each point denotes the average for each group. Solid line at y=x.

All values calculated by taking the natural log (ln) of the average normalised value for each CRISPant group. For A-D, any positive value (red) denotes an increase from controls, whilst a negative value (blue) denotes a reduction from controls.

too little activity is detrimental to this finely balanced process. An exception was embryonic eye area (Figure 3.15D), where the single *lats1*, *lats2*, *nf2a*, and *nf2b* CRISPants all showed increased eye size, suggesting enhanced organ growth in contrast to the reduced growth in *yap1* CRISPants. Increased regeneration was not observed, except an increase in neuromast number after injury in *lats1* CRISPants (Figure 3.17E and G). This shows that enhancing regeneration is not as simple as removing an expected inhibitory factor, and the impact of these factors on general development and other pathways will likely also affect regeneration.

One exception to this statement appeared to be the Yap1/Taz target gene Ctgfb. *ctgfb* CRISPants had enhanced regeneration after both severe tail fin injury (Figure 3.18D) and neuromast injury at 48hpi (Figure 3.17F and G). However, in other parameters, such as mild tail fin injury (Figure 3.18C), a reduction in regeneration was observed. This could imply that Ctgfb has highly specific inhibitory effect on regeneration, potentially through the extracellular matrix. Ctgfb's closely related paralog Ctgfa has been associated with regeneration in the zebrafish spinal cord[257], but by promoting regeneration rather than inhibiting it. This could suggest a widely differing role of the protein paralogs, but more investigation is required before any clearer conclusions can be drawn.

All double CRISPant phenotypes were more severe than single CRISPants, indicating a level of compensation or an additive effect in these closely related components. An exception is the *yap1*/*wwtr1* double CRISPant in mild tail fin injury where it phenocopied *yap1* CRISPants only. This highlights the distinct *yap1* and *wwtr1* roles. Often, these components are considered to have overlapping roles. Notably, Taz alone is not studied to the same extent as Yap1, and in some even recent papers Yap1 is studied as a transcriptional mediator of the Hippo pathway without investigation of Taz (e.g.[261–263]). In mice, a difference in phenotype can be seen between *Yap* and *Taz* knock-out (KO) mice (see 1.2). This suggests that Yap and Taz have differing functions in vivo, but studies are limited due to the early death of *Yap1* KOs. It is therefore of great interest to investigate these genes in the zebrafish as an *in vivo* model with higher survival. In this screen, *wwtr1* CRISPants had no phenotype, apart from severe tail fin regeneration defects. However, the *yap1*/*wwtr1* double CRISPant being more severe than the *yap1* CRISPant in most measurements suggests that Yap1 may be compensating for the loss of Taz in *wwtr1* CRISPants. However, a potential compensatory Yap1 upregulation was not supported by RT-qPCR (Figure 3.4M and N) or western blot (Figure 3.5D, E, G, H) analyses of

wwtr1 CRISPants, which showed no change in *yap1* mRNA or Yap1 protein. However, attempts to further determine Yap1 activity by PhosTag or immunofluorescence was not successful due to technical challenges. The exception to the more severe double *yap1*/*wwtr1* CRISPant phenotype was in mild tail fin injury, where the double CRISPant had the same severity of defect as the *yap1* CRISPant. This suggests that Taz does not have a role in mild tail fin regeneration. Conversely, Taz did show a phenotype in severe tail fin regeneration. This specific difference in phenotype is clearly of interest, and so warrants further investigation, and is an overall focus in the remainder of the thesis.

4 Chapter 2: Generation and characterisation of transgenic and stable mutant zebrafish lines

4.1 *ctgfa*:GFP reporter fish as a readout of Yap1 and Taz activity during tail fin regeneration

The optical transparency of the embryonic zebrafish lends itself particularly well to the use of transgenic fluorescent reporter lines as imaging can be easily performed in both live and fixed embryos. To take advantage of this, multiple transgenic lines were utilised in this thesis. One of particular interest is a *ctgfa*:GFP fluorescent reporter fish. *CTGF* is a well-established YAP/TAZ-TEAD target gene[26]. This zebrafish line expresses GFP under the *ctgfa* promoter and is therefore thought to give a readout of Yap1/Taz occupation of the *ctgfa* promoter, and so Yap1/Taz activity, rather than *ctgfa* expression directly. This line was first published by Miesfeld et. al.[97], who showed GFP expression in the eye, heart and trunk. In addition, constitutively active Yap1 overexpression increased *ctgfa*:GFP fluorescence in the retinal pigmented epithelium and neural retina of the eye[97]. These fish were established at the University of Edinburgh (see 2.4 for more details) for this thesis, using multiple outcrosses to ensure a single insertion was achieved. Representative images are shown in Figure 4.1A, which showed particularly strong GFP signal in the eye (although this may be autofluorescence), heart (masked in the representative image), and the notochord and surrounding musculature, comparable to the published pattern of expression[97].

As mentioned in 1.3, the link between Hippo signalling and notochord function has been previously investigated, where Yap1/Taz and target gene disruption is associated with notochord defects or are expressed in the notochord[85,86,93,95,102–105]. This link between Yap1/Taz activity and the notochord is consistent with increased *ctgfa*:GFP in the notochord and provides further proof that Yap1/Taz signalling is active in notochord cells (which are under high mechanical pressure[101]). These notochord cells have also been shown to be key in the secretion of Hedgehog ligands to promote regeneration[264]. In addition, GFP signal in the eye may further support the suggestion of a function for Hippo signalling in eye development, as indicated in the CRISPR screen (3.5.1).

However, the individual contribution of Yap1 or Taz to this expression is not clear by studying

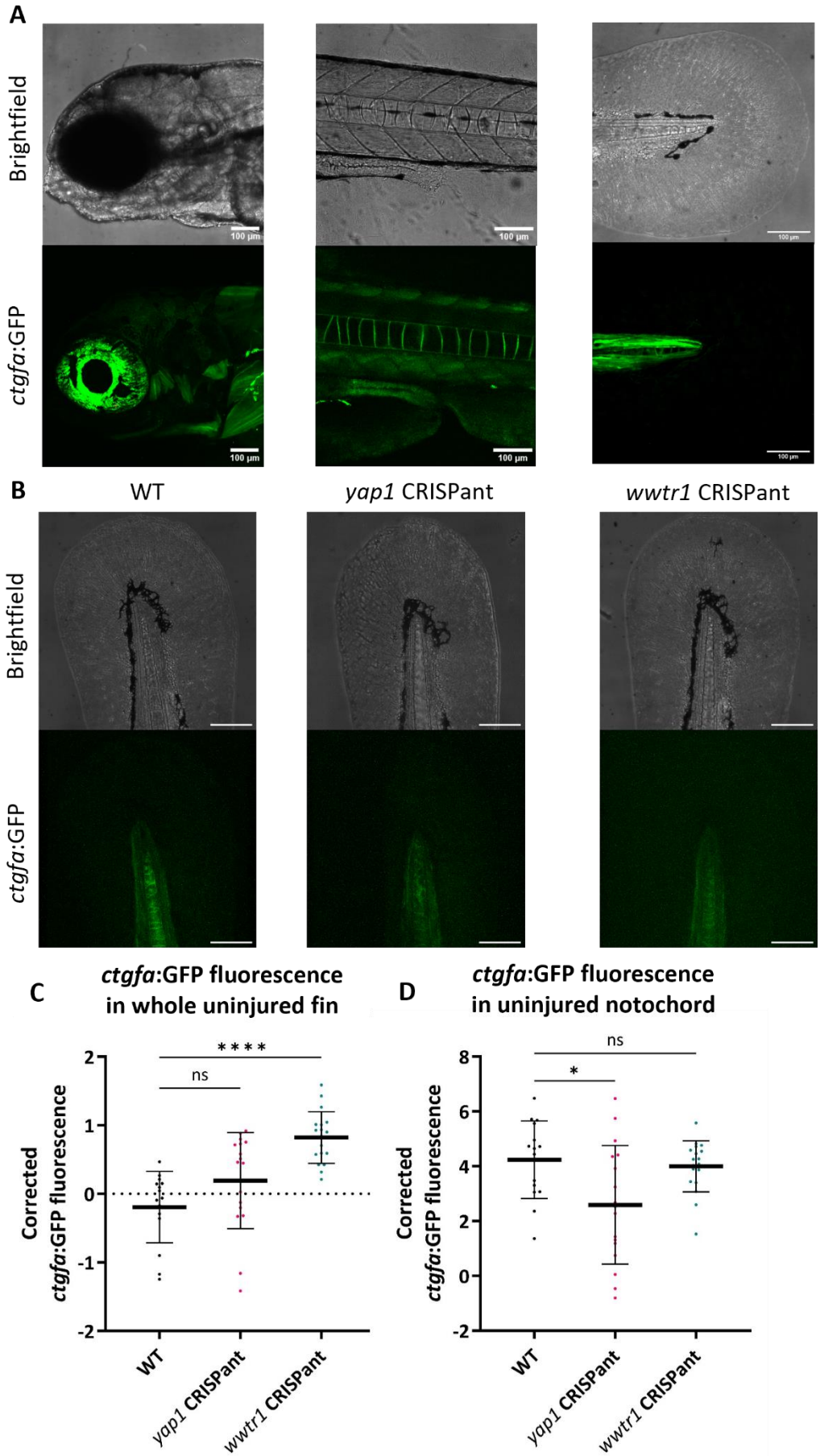
A
Brightfield
ctgfa:GFP
100 µm
B
WT
yap1 CRISPant
wwtr1 CRISPant
Brightfield
ctgfa:GFP
C
ctgfa:GFP fluorescence in whole uninjured fin
Corrected ctgfa:GFP fluorescence
****
ns
2
1
0
-1
-2
WT
yap1 CRISPant
wwtr1 CRISPant
D
ctgfa:GFP fluorescence in uninjured notochord
Corrected ctgfa:GFP fluorescence
ns
*
8
6
4
2
0
-2
WT
yap1 CRISPant
wwtr1 CRISPant

Figure 4.1: *ctgfa*:GFP signal in uninjured WT and CRISPant embryos
(A) Sample images of 96hpf WT *ctgfa*:GFP embryos, focussing on head, trunk cross-section, and tail fin. **(B)** Representative images of WT, *yap1* CRISPant, and *wwtr1* CRISPant tail fins when uninjured. **(C)** Quantification of mean corrected *ctgfa*:GFP fluorescence in the whole uninjured tail fin at 72hpf. *wwtr1* CRISPant GFP fluorescence was increased relative to WT. **(D)** Quantification of mean corrected *ctgfa*:GFP fluorescence in the tail fin notochord at 72hpf. *yap1* CRISPant GFP fluorescence was decreased relative to WT.
Scale bar denotes 100μm. Quantification of fluorescence corrected to remove autofluorescence. Each dot represents one embryo. Bars represent mean±SD. Data from three independent experimental repeats. Significance calculated by one-way ANOVA (C) or Kruskal-Wallis test (D) with multiple comparisons. *p<0.05; ****p<0.0001; ns=not significant.

only WT fish. To elucidate this, *yap1* and *wwtr1* CRISPR mutagenesis was performed in the *ctgfa*:GFP transgenic line (representative images are shown in Figure 4.1B). The resulting fluorescence was quantified and corrected for autofluorescence (Figure 4.1C-D). When quantified in the whole tail fin, there was an unexpected increase in fluorescence in the *wwtr1* CRISPant relative to WT (Figure 4.1C). However, this included the fin fold, which had very low levels of GFP signal which may bias this result. Therefore, fluorescence was quantified within the notochord only (Figure 4.1D). This gave higher fluorescence values than the fin fold and in all groups. Fluorescence was decreased in *yap1* CRISPants only, suggesting that Yap1 regulates *ctgfa* more strongly in the developing tail fin, or that Yap1 is more active during tail fin development compared to Taz.

GFP signal was also measured in CRISPants after mild tail fin injury (representative images in Figure 4.2A+B). This was quantified in the regenerated area, corrected for autofluorescence and with background (calculated from a non-regenerating region of the fin) removed. At 6hpi, there was no change in fluorescence between WT and CRISPants (Figure 4.2C). However, there was no significant increase in signal from the background level even in the WT fish, suggesting that this may be due to a lack of contribution of Yap1/Taz activity at this stage of mild tail fin regeneration. A later regeneration timepoint was therefore also investigated, 24hpi (Figure 4.2D). This did show a significant increase in signal from background ($p<0.0001$, Wilcoxon signed-rank test, $\mu=0$, significance not shown on figure), suggesting the activation of Yap1/Taz at this timepoint. However, the mutagenesis of *yap1* or *wwtr1* had no significant effect, although this may be due to the large SD in fluorescence values, suggesting that this analysis may be underpowered. This implies that Yap1/Taz activity is still limited at this timepoint, which is supported by the low fluorescence values, or may also imply some compensation for Yap1 or Taz loss. There may be other regulators of *ctgfa* expression, but

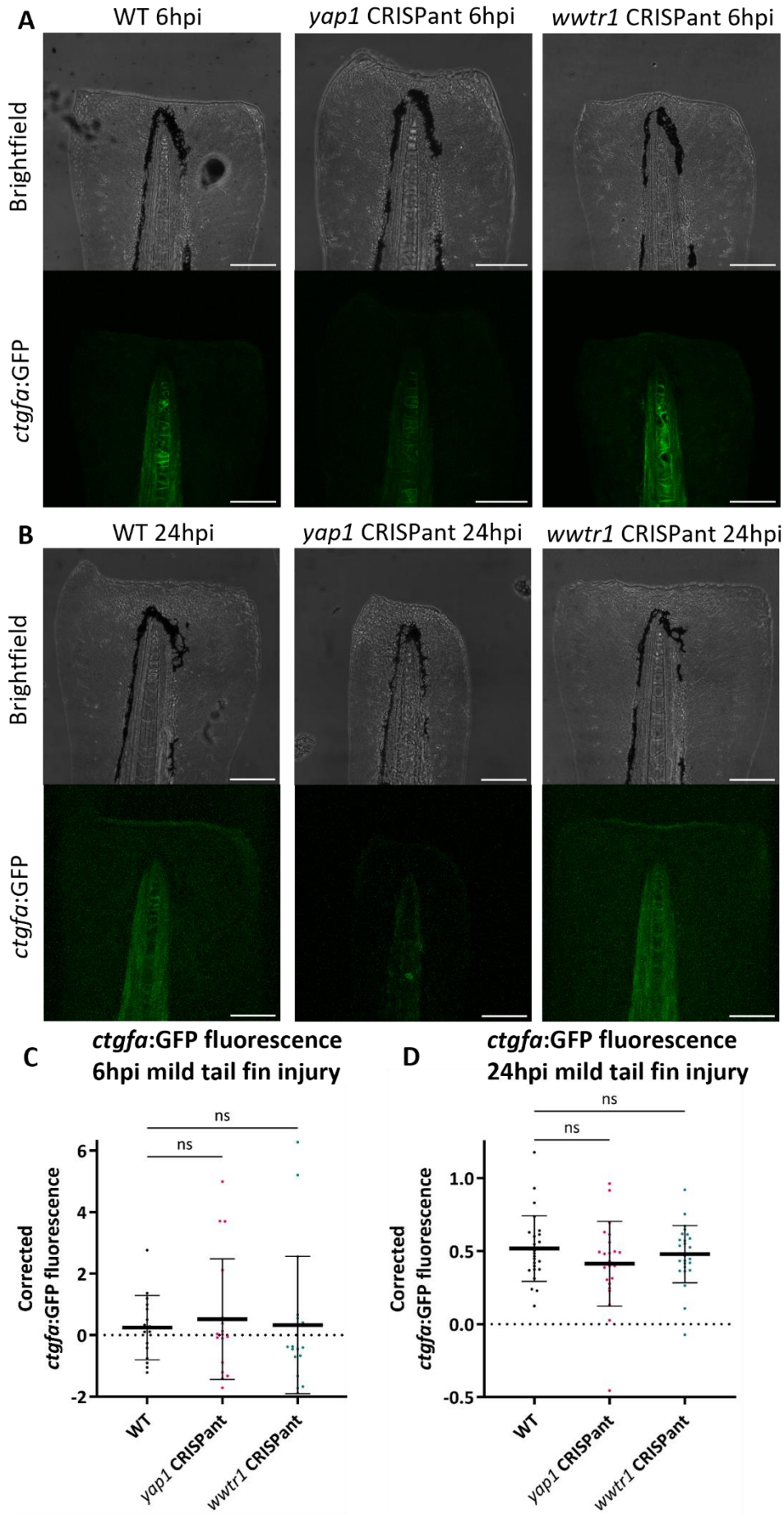
A
WT 6hpi
yap1 CRISPant 6hpi
wwtr1 CRISPant 6hpi
Brightfield
ctgfa:GFP
B
WT 24hpi
yap1 CRISPant 24hpi
wwtr1 CRISPant 24hpi
Brightfield
ctgfa:GFP
C
ctgfa:GFP fluorescence
6hpi mild tail fin injury
Corrected ctgfa:GFP fluorescence
ns
ns
6
4
2
0
-2
WT
yap1 CRISPant
wwtr1 CRISPant
D
ctgfa:GFP fluorescence
24hpi mild tail fin injury
Corrected ctgfa:GFP fluorescence
ns
ns
1.0
0.5
0.0
-0.5
WT
yap1 CRISPant
wwtr1 CRISPant

Figure 4.2: *ctgfa*:GFP signal after mild tail fin injury in WT and CRISPant embryos
(A) Representative images of *ctgfa*:GFP embryo tail fins at 6 hours post mild tail fin injury in WT, *yap1* CRISPants, and *wwtr1* CRISPants. **(B)** Representative images of *ctgfa*:GFP embryo tail fins at 24hpi in WT, *yap1* CRISPants, and *wwtr1* CRISPants. **(C)** Quantification of mean corrected *ctgfa*:GFP fluorescence in the regenerating tail fin at 6hpi. No change in CRISPants relative to WT was observed. **(D)** Quantification of mean corrected *ctgfa*:GFP fluorescence in the regenerating tail fin at 24hpi. No change in CRISPants relative to WT was observed.
Fluorescence corrected to remove background and autofluorescence. Scale bar denotes 100μm. Each dot represents one embryo. Bars represent mean±SD. Data from three independent experimental repeats. Significance calculated by one-way ANOVA (C) or Kruskal-Wallis test (D), with multiple comparisons. ns=not significant

there is also a limited role for Ctgfa in mild tail fin regeneration, as there were no tail fin regeneration phenotypes after *ctgfa* CRISPR mutagenesis (Figure 3.18), and so changes in *ctgfa* regulation might not be expected.

Analysis of the tail fin following severe injury was then performed (Figure 4.3). Representative images of the tail fin at 6hpi are shown in Figure 4.3A, and quantification of signal in the notochord bead (corrected for autofluorescence and background) in Figure 4.3B. This showed a reduction in signal in both *yap1* and *wwtr1* CRISPants, suggesting Yap1 and Taz activation following severe injury, and a role for both in the regulation of *ctgfa* expression. The reduction in signal in *wwtr1* CRISPants is of particular interest, as there was no change in signal in uninjured tail fins (Figure 4.1D).

As the severe injury paradigm was of particular interest, because *wwtr1* CRISPants showed a significant defect, more detailed imaging throughout the regenerative timecourse was desired. Timelapse imaging was performed throughout the first 24 hours post severe tail fin injury in WT and CRISPants, and GFP signal quantified as in Figure 4.3B (described in more detail in 2.17.2) (Figure 4.3C, representative timelapse videos not shown). WT GFP signal increased until approximately 8hpi, where it began to slowly decrease to the end of the imaging period. This suggests a consistent upregulation of Yap1/Taz activity throughout regeneration. Both *yap1* and *wwtr1* CRISPants showed a very slight increase in GFP signal following injury that plateaued at a significantly lower level than WT fish, further supporting a role for both Yap1 and Taz in severe tail fin injury.

In summary, the *ctgfa*:GFP transgenic line can demonstrate differential effects of Yap1 and Taz in embryonic development and tail fin regeneration. During development, GFP signal in the notochord was disrupted following *yap1* CRISPR only, suggesting that Yap1 is active and

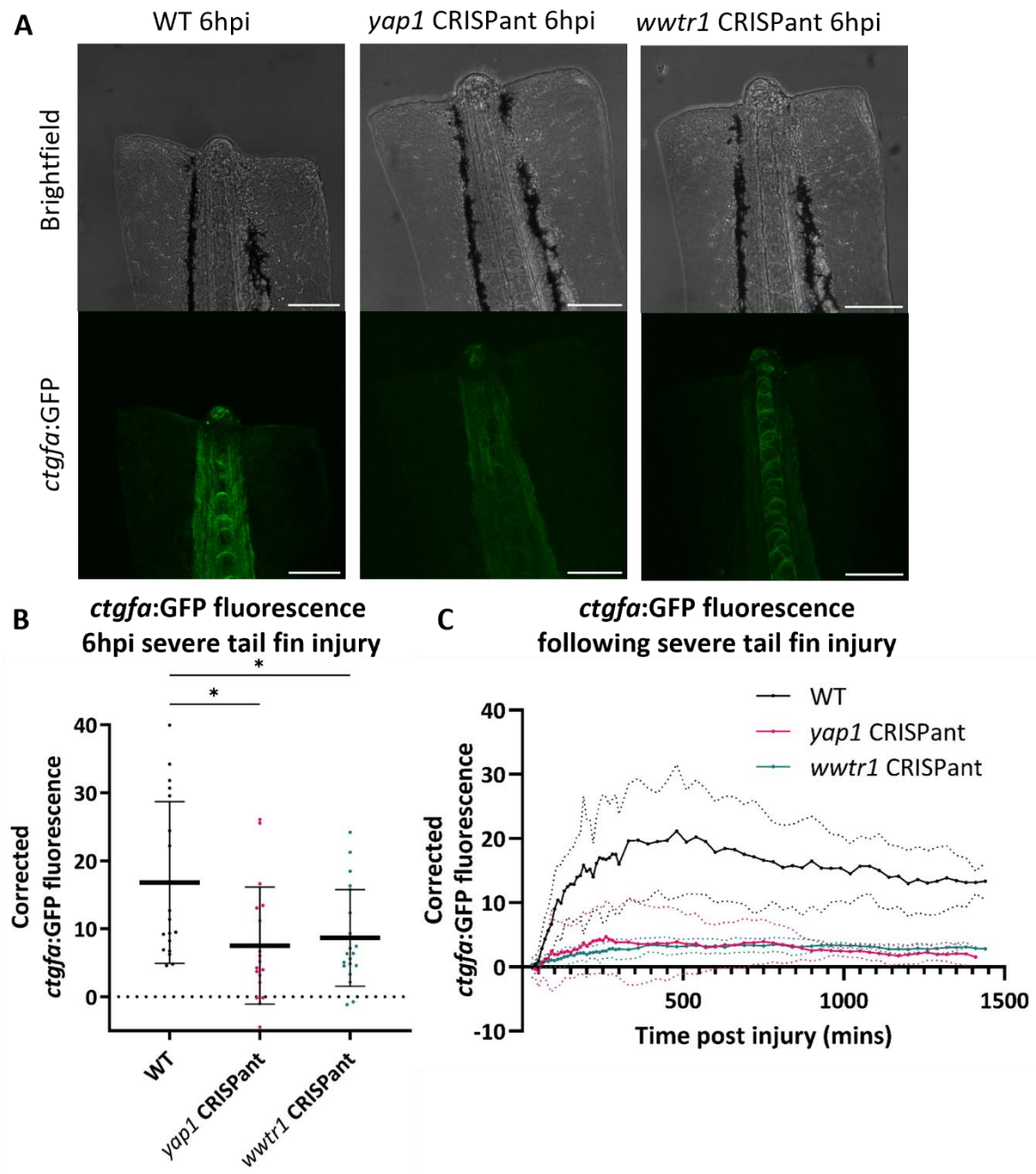

Figure 4.3: *ctgfa*:GFP signal after severe tail fin injury in WT and CRISPant embryos
(A) Representative images of *ctgfa*:GFP embryo tail fins at 6 hours post severe tail fin injury. **(B)** Quantification of mean corrected *ctgfa*:GFP fluorescence in the notochord bead at 6 hours post severe injury. GFP fluorescence was reduced in *yap1* and *wwtr1* CRISPants. Each dot represents one fish. Bars represent mean±SD. Significance calculated by one-way ANOVA with multiple comparisons. **(C)** Quantification of mean corrected *ctgfa*:GFP fluorescence in the notochord bead over the 24 hours post severe injury. Fluorescence was reduced in CRISPants relative to WT. Solid line represents the mean fluorescence for WT (black), *yap1* CRISPant (red), and *wwtr1* CRISPant (green) over time. Dotted line represents the SD for each genotype.
Fluorescence corrected to remove background and autofluorescence. Scale bar denotes 100µm. Data from three independent experimental repeats (B), or one experiment (C). *p<0.05.

promotes *ctgfa* expression in development, whilst Taz has no role. During mild tail fin regeneration, Yap1/Taz/Ctgfa appeared to have a limited role at 6hpi but were increased at 24hpi. However, this GFP signal at 24hpi was not affected by *yap1* or *wwtr1* mutagenesis, suggesting a continued limited role for Yap1, Taz, and Ctgfa at this timepoint. A much greater effect is seen after severe tail fin injury, with a significant induction of GFP signal at early timepoints in WT fish that was abolished upon mutagenesis of either *yap1* or *wwtr1*. This implies a key role of both Yap1 and Taz in severe tail fin regeneration.

4.2 Stable *yap1* and *wwtr1* mutants mostly, but not completely, phenocopy *yap1* and *wwtr1* CRISPants

4.2.1 Mutations induced by CRISPR/Cas9 injection

The interesting phenotypes observed in the screen for *yap1* and *wwtr1* CRISPants led to prioritising the development of stable mutant lines from these CRISPants. An overview of the breeding schedule for this is shown in Figure 2.3. Each fish harbours mutations that induce premature stop codons. The *yap1* stable mutant has a 5 nucleotide deletion at 70 base pairs (bp) from the beginning of exon 1 (induced by CRISPR guide 1) (Figure 4.4A) and an 11 nucleotide deletion at 140bp from the beginning of exon 2 (induced by CRISPR guide 2) (Figure 4.4B). These mutations translate to a greatly disrupted amino acid sequence as the deletions shift the reading frame (Figure 4.4C). Multiple early stop codons are induced, resulting in a dramatically truncated Yap1 protein that retains only the first 23 amino acids unchanged. Importantly, this disrupts the TEAD binding domain and loses key binding and phosphorylation residues as well as other important protein domains.

The *wwtr1* stable mutant has an 18 nucleotide insertion at 35bp from the start of exon 1 (induced by CRISPR guide 1) and a 5 nucleotide deletion at 321bp from the start of exon 1 (induced by CRISPR guide 2) (Figure 4.5A). The first insertion retains the reading frame but does create an early stop codon after 15 amino acids. Multiple stop codons are induced throughout the protein, resulting in a Taz protein that only contains 12 unchanged N-terminal amino acids (Figure 4.5B). In a similar manner to Yap1, this greatly truncated Taz protein disrupts the TEAD binding domain and loses key residues and other important protein domains.

A ***yap1* stable mutant Yap1 DNA sequence 1**

B ***yap1* stable mutant Yap1 DNA sequence 2**

C ***yap1* stable mutant Yap1 amino acid sequence**

Figure 4.4: Sequencing of a F1 *yap1* stable mutant line
(A) Aligned cDNA sequence for WT and *yap1* mutant fish, focussing on the target region for guide 1. Sequence begins at the start of exon 1. Red arrow denotes CRISPR guide target. CRISPR guide 1 has induced a 5 nucleotide deletion at 70bp from the beginning of the exon. **(B)** Aligned cDNA sequence for WT and *yap1* mutant fish, focussing on the target region for guide 2. The green line denotes the start of exon 2, blue arrow denotes CRISPR guide target. CRISPR guide 2 has induced an 11 nucleotide deletion at 140bp from the beginning of the exon. **(C)** Aligned Yap1 amino acid sequence derived from cDNA for WT and *yap1* mutant fish. CRISPR mutagenesis has induced multiple early stop codons (first one after 27 amino acids) which generates a truncated protein, retaining only the first 23 amino acids unchanged.

4.2.2 Adult survival of homozygous mutants

The above fish were bred to homozygosity (see 2.2 for more details). The proportion of the offspring of heterozygous parents is shown in Figure 4.6. For a non-deleterious mutation, a 1:2:1 split of WT:heterozygous:homozygous offspring would be expected. This split was not observed in the *yap1* mutant fish. The proportion of homozygous *yap1* stable mutants was significantly lower than expected, indicating reduced survival (Figure 4.6A), whilst there was no change in heterozygote survival as they were present at approximately double the rate of WT siblings. This reduction in *yap1* homozygote survival is not unexpected due to Yap1's roles in general survival and development seen at an embryonic level, and published work also showing reduced survival in *yap1* disruption (via morpholino[72] and in stable mutants[74]). A founder *yap1* homozygote pair was identified from this incross. Offspring from an incross of these fish were found to be smaller, with an increased likelihood of eye defects and spinal deformities (observational data, not quantified). These spinal deformities may be a result of notochord defects[265], which are found after *yap1* disruption in published works (1.3). The genotype proportions of *wwtr1* heterozygote offspring did not significantly differ from that expected (Figure 4.6B). The homozygote *wwtr1* stable mutants were grown to adulthood, but appeared smaller and took longer to reach breeding age than expected, despite being kept at approximately equal stocking density to other lines (observational data, not quantified).

4.2.3 Embryonic developmental phenotypes of homozygous mutants

Homozygous offspring of an incross of homozygous stable mutants were analysed using the same assays as utilised in the CRISPR screen (Figure 3.13). Results are shown normalised to WT controls run concurrently, which for *yap1* stable mutants were the offspring of their parent's WT siblings (and so "cousin" WTs), but for *wwtr1* stable mutants were unrelated WT

A ***wwtr1* stable mutant Taz DNA sequence**

```
WT       ATGAGCGGTAATCCTCTCCAGCCGATACGGGCCA----------------ACCAGGTG   42
Mutant   ATGAGCGGTAATCCTCTCCAGCCGATACCGGGCCACCATGTCACGTGACCAGGCCACGTG   60
         ********************************                   *** ***

WT       ATCCATGTCGCCAAAGACCTGGACACGGATCTGGAGGCTCTTTTTAACTCGGTCATGAAC  102
Mutant   ATCCATGTCGCCAAAGACCTGGACACGGATCTGGAGGCTCTTTTTAACTCGGTCATGAAC  120
         ************************************************************

WT       CCGAAACCGAGCTCCTGGAGGAACAAGGATATGCCGCAGTCTTTCTTCCAGGAGCCGGAC  162
Mutant   CCGAAACCGAGCTCCTGGAGGAACAAGGATATGCCGCAGTCTTTCTTCCAGGAGCCGGAC  180
         ************************************************************

WT       TCGGGCTCCCACTCCCGGCAGTCCAGCGCGGACTCCGGTTCTCTCCCGCCGAGGGTCCAC  222
Mutant   TCGGGCTCCCACTCCCGGCAGTCCAGCGCGGACTCCGGTTCTCTCCCGCCGAGGGTCCAC  240
         ************************************************************

WT       TTTCGCTCGCGCTCATCTCCGGCGTCCCTACAGCTGCCGGCGGGCTCCGTGAGCGGCCCG  282
Mutant   TTTCGCTCGCGCTCATCTCCGGCGTCCCTGCAGCTGCCGGCGGGCTCCGTGAGCGGCCCG  300
         *************************** ****************************

WT       AGCCCCGGGAGACTCCACTCCCACACCCGGCACCAGTCCTGCGATGTGGCCGAGGAGCTG  342
Mutant   AGCCCCGGGAGACTCCACCCCCACACCTGGCACCAGCC-----CTGTGGCCGAGGAGCTG  355
         ***************** ******* *********      ****************
```

B ***wwtr1* stable mutant Taz amino acid sequence**

```
WT       MSGNPLQPIPGHQ------VIHVAKDLDTDLEALFNSVMNPKPSSWRNKDMPQSFFQEPD   54
Mutant   MSGNPLQPIPGHHVT*PGHVIHVAKDLDTDLEALFNSVMNPKPSSWRNKDMPQSFFQEPD   59
         ***********:     ****************************************

WT       SGSHSRQSSADSGSLPPRVHFRSRSSPASLQLPAGSVSGPSPGRLHSHTRHQSCDVAEEL  114
Mutant   SGSHSRQSSADSGSLPPRVHFRSRSSPASLQLPAGSVSGPSPGRLHPHTWHQTCGRGAAA  119
         ******************************************** ** **:*. .

WT       PLPPGWEM-AFTPNGQKYFLNHIEKITTWHDPRKSMTPSVAQLSLHNQVSNTASIQQRSM  173
Mutant   A---PWVGDGLHPQRPEVL-------SQSH*EDHHMAR----------------PQEEHD  152
              *   .: *:  : :       :  *   : *:                 *:.

WT       ALSQPNLVL-NQQAHQQQQQHLQQQQQQVPVQVPVQAPQQQSSQPMMNLSAQQH-----Q  227
Mutant   ALGGPAEPP*SGLQHRQHPAALHGPLSAQPGAEPAGAPAAAAAPPAAAAAGPGASPGAGP  211
         **. *     .   *:*:   *:   .  *   *. **   :: *    :.

WT       QKMRLQRIQMERERIQRRQEELMRQEVALRQLPMDSDNLPPVAPAIGSPAMSAGNMPNNS  287
Mutant   SAAELSA-HDEPERAAAPAE---------DEAPAHPDGERAHPEETGGAHATGGGAPAAP  261
         .  .*.  : * **     *          : * . *.        *.   :.*. *

WT       ADPF--LNSGPYHSREQSTDSGLGLGCYSIPTTPEDFLNNMEDMDTGENMVPVSMN----  341
Mutant   RGL**SAASGSSHR-LSSDECGKHAQ*-QRRPLPQQWAVSLAGAEHRQWTRPGLLQHPDH  316
          .      **  *   .* :.*      .    *:::  .: . :  :   *  ::

WT       -------------------------VPPQSRFPDFLDSMPGTNVDLGTLEGT--DLMPI  373
Mutant   S*RLPQQHGGHGHRGKHGSCEHERPTTEPLPRLPGLH---AGHQRGPGHPGGYRPDAHPQ  372
                                  . *  *:*.:     * : . *   *   *  *

WT       LNDVESVLNKSEPFLTWL* 391
Mutant   RRRVGPEQERALPHLAL-- 389
          . *    ::: *.*:
```

Figure 4.5: Sequencing of a F1 *wwtr1* stable mutant line
(A) Aligned cDNA sequence for WT and *wwtr1* mutant fish, focussing on the first 340 bases. Sequence begins at the start of exon 1. Red arrow denotes CRISPR guide 1 target and blue arrow denotes CRISPR guide 2 target. CRISPR guide 1 has induced an 18 nucleotide insertion at 35bp from the beginning of the exon. CRISPR guide 2 has induced a 5 nucleotide deletion at 321bp from the beginning of the exon. **(B)** Aligned Taz amino acid sequence derived from cDNA for WT and *wwtr1* mutant fish. CRISPR mutagenesis has induced multiple early stop codons (first one after 15 amino acids) which generates a truncated protein, retaining only the first 12 amino acids unchanged.

fish (as WT siblings were lost due to husbandry error). CRISPant data from Chapter 1 is also included for ease of comparison and does not reflect a new experiment. Results from developmental analyses at 96hpf are shown in Figure 4.7. Normalised *yap1* stable mutants phenocopied *yap1* CRISPants in all parameters, showing reduced length (Figure 4.7B), reduced swim bladder size (indicating delayed development) (Figure 4.7C), reduced eye size (Figure 4.7D), increased heart and yolk oedema (Figure 4.7E+F), and reduced survival Figure 4.7G). Many of these parameters were more severely affected in the *yap1* stable mutants. This suggests that the *yap1* CRISPant is an appropriate model to study the loss of Yap1 protein, confirming the utility of the CRISPR/Cas9 system. However, this is not reflected in *wwtr1* stable mutants. Whilst *wwtr1* CRISPants had limited phenotypes, with only a small increase

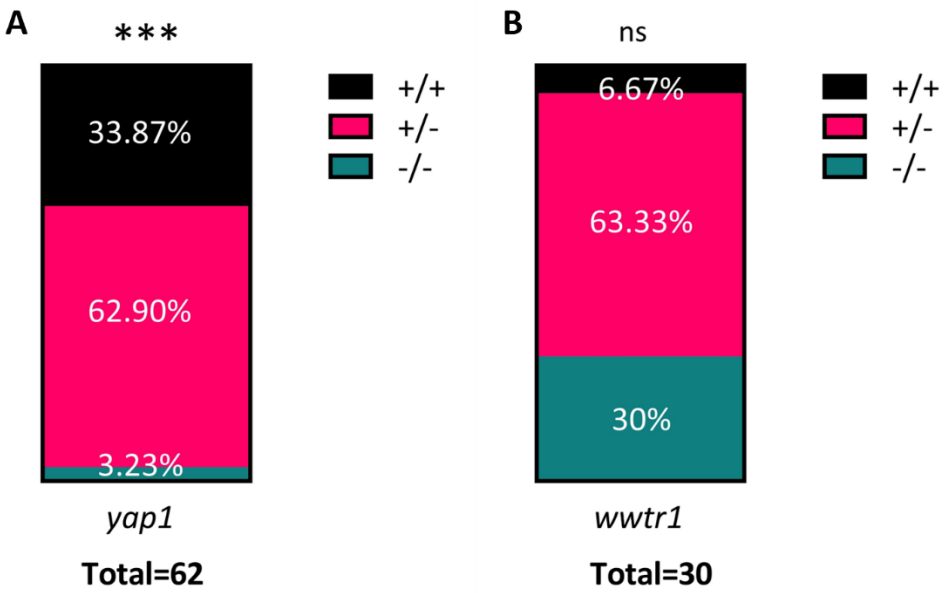

Figure 4.6: Proportion of stable mutant line genotypes
(A) Proportion at adulthood of offspring from an incross of *yap1* heterozygotes, shown as a proportion of the total number of fish genotyped. Survival differed significantly from the expected ratio. **(B)** Proportion at adulthood of offspring from an incross of *wwtr1* heterozygotes, shown as a proportion of the total number of fish genotyped. Survival was not significantly altered from the expected ratio. Significance calculated using Chi-squared test of an expected proportion of 25:50:25% (WT:het:hom). Text in white denotes percentage of embryos in each genotype. ***p<0.001; ns=not significant.

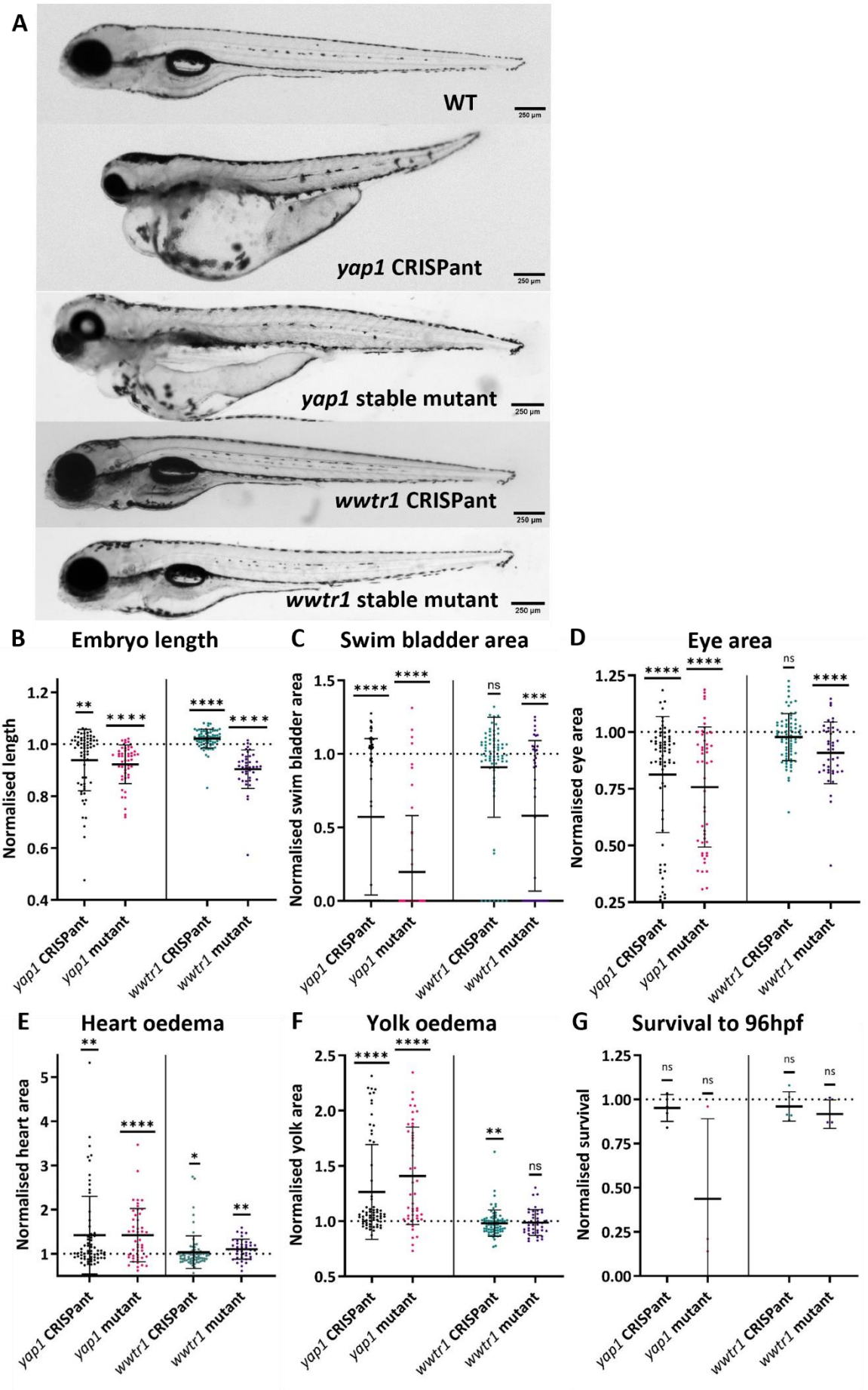
A
WT
250 µm
yap1 CRISPant
250 µm
yap1 stable mutant
250 µm
wwtr1 CRISPant
250 µm
wwtr1 stable mutant
250 µm
B
Embryo length
Normalised length
C
Swim bladder area
Normalised swim bladder area
D
Eye area
Normalised eye area
E
Heart oedema
Normalised heart area
F
Yolk oedema
Normalised yolk area
G
Survival to 96hpf
Normalised survival
yap1 CRISPant
yap1 mutant
wwtr1 CRISPant
wwtr1 mutant

Figure 4.7: 96hpf phenotypes of stable mutants and CRISPants
(A) Representative brightfield images of 96hpf WT, CRISPant, and stable mutant embryos. **(B)** Quantification of length of *yap1* and *wwtr1* CRISPants and stable mutants, normalised to controls. Length was reduced in both *yap1* CRISPants and stable mutants. Length of *wwtr1* CRISPants was increased but *wwtr1* stable mutant length was reduced. **(C)** Quantification of swim bladder area of *yap1* and *wwtr1* CRISPants and stable mutants, normalised to controls. Swim bladder area was reduced in both *yap1* CRISPants and stable mutants. Swim bladder area of *wwtr1* CRISPants was unchanged but decreased in *wwtr1* stable mutants. **(D)** Quantification of eye area of *yap1* and *wwtr1* CRISPants and stable mutants, normalised to controls. Eye area was reduced in both *yap1* CRISPants and stable mutants. Eye area of *wwtr1* CRISPants was unchanged but decreased in *wwtr1* stable mutants. **(E)** Quantification of heart oedema of *yap1* and *wwtr1* CRISPants and stable mutants, normalised to controls. Heart area was increased in all groups measured. **(F)** Quantification of yolk oedema of *yap1* and *wwtr1* CRISPants and stable mutants, normalised to controls. Yolk area was increased in both *yap1* CRISPants and stable mutants. Yolk area of *wwtr1* CRISPants was decreased but unchanged in *wwtr1* stable mutants. **(G)** Quantification of survival to 96hpf of *yap1* and *wwtr1* CRISPants and stable mutants, normalised to controls. Survival was unchanged in all groups measured. Each dot represents one embryo, except in (G) where it represents one repeat. Bars represent mean±SD. Data from at least three independent experimental repeats. Significance calculated by one-sample Wilcoxon test (μ=1). Data normalised to gRNA-only injected controls (for CRISPants), WT siblings (*yap1* stable mutants), or WT (*wwtr1* stable mutants) performed concurrently. WT and CRISPant images and data are also shown in Figure 3.15. *p<0.05; **p<0.01; ***p<0.001; ****p<0.0001; ns=not significant.

in length, slight increase in heart oedema, and slight decrease in yolk oedema, *wwtr1* stable mutants had a more severe defect similar to, but not to the same extent as, *yap1* stable mutants/CRISPants. This includes decreased length (Figure 4.7B), decreased swim bladder size (Figure 4.7C), reduced eye size (Figure 4.7D), and increased heart oedema (Figure 4.7E). This could be a result of the less appropriate controls to which the *wwtr1* stable mutants were normalised or could reflect a more deleterious mutation than the range of mutations induced in the CRISPants. It could also reflect the impact of mutant maternal mRNA on development. Although maternal mRNA is not present at 96hpf, the effect on very early embryonic development may be enough to impact later development in the *wwtr1* stable mutant. This may be considered a benefit of studying CRISPants, as WT maternal mRNA may allow for normal early development, and so the impact of removing Taz is only seen in regeneration. It does however show that there are limitations in the translatability between CRISPants and stable mutants, at least in developmental analyses.

4.2.4 Embryonic regenerative phenotypes of homozygous mutants

4.2.4.1 Neuromast regeneration

Measurements of neuromast regeneration were also performed (Figure 4.8), with the same

controls and comparisons as the developmental assays described above. *yap1* stable mutants again phenocopied *yap1* CRISPants, with no change in uninjured neuromast area but a decrease in uninjured neuromast number (Figure 4.8B+C), reduced neuromast area and number at 24hpi (Figure 4.8D+E), reduced area at 48hpi (Figure 4.8F), and unchanged number at 48hpi (Figure 4.8G). *wwtr1* stable mutants phenocopied the *wwtr1* CRISPants more closely than for developmental analyses but were altered in some parameters. Changes observed were an increase in uninjured neuromast numbers in stable mutants (decreased in CRISPants) (Figure 4.8C) and increased neuromast area at 24hpi in stable mutants (unchanged in CRISPants) (Figure 4.8D). The remaining parameters were equal in both CRISPants and stable mutants (no change in uninjured area, 48hpi area, and 48hpi number, and increased 24hpi number).

4.2.4.2 Tail fin regeneration

Finally, tail fin regeneration was analysed in stable mutants (Figure 4.9). *yap1* stable mutants showed more severe defects than *yap1* CRISPants, but generally followed the same pattern. This included a reduction in mild tail fin injury regeneration (Figure 4.9C) and severe tail fin regeneration (Figure 4.9D), which, despite the CRISPant screen not showing a clear impairment was in fact reduced in the *yap1* CRISPant (Figure 5.2). *yap1* stable mutants also showed a baseline growth defect (Figure 4.9B), whilst the *yap1* CRISPants did not, indicating a more severe phenotype in the stable mutants. Similarly, *wwtr1* stable mutants generally showed more severe defects than *wwtr1* CRISPants. Neither *wwtr1* stable mutants or CRISPants had altered uninjured tail fin growth (Figure 4.9B), and both showed a severe tail fin regeneration defect (Figure 4.9D). Of particular note is the reduction in mild tail fin injury regeneration in the *wwtr1* stable mutant (Figure 4.9C) not observed in the CRISPant.

In summary, in a similar manner to the developmental phenotypes, analyses of regeneration showed that *yap1* stable mutants generally phenocopied *yap1* CRISPants, albeit with a more significant defect in certain parameters such as uninjured fin growth (Figure 4.9B). However, this is less clear for *wwtr1* stable mutants, where most, but not all, parameters phenocopied *wwtr1* CRISPants. Differences were observed in uninjured neuromast number (Figure 4.8C), 24hpi neuromast area (Figure 4.8D), and mild tail fin regeneration (Figure 4.9C), suggesting a limited level of translatability, potentially as a result of the use of inappropriate controls. This

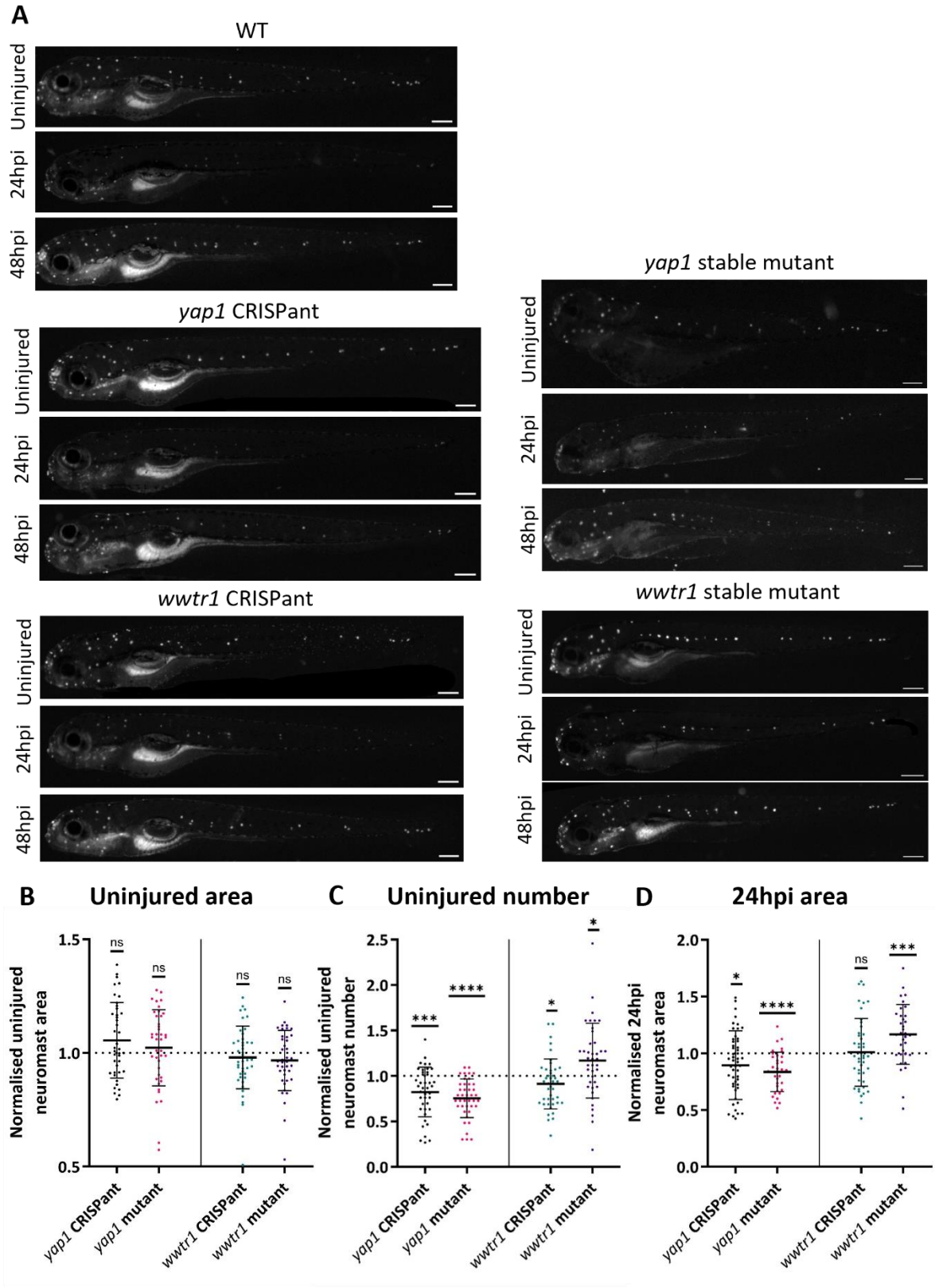
A
WT
Uninjured
24hpi
48hpi
yap1 CRISPant
yap1 stable mutant
wwtr1 CRISPant
wwtr1 stable mutant
B
Uninjured area
Normalised uninjured neuromast area
C
Uninjured number
Normalised uninjured neuromast number
D
24hpi area
Normalised 24hpi neuromast area
ns
*
***
****
yap1 CRISPant
yap1 mutant
wwtr1 CRISPant
wwtr1 mutant

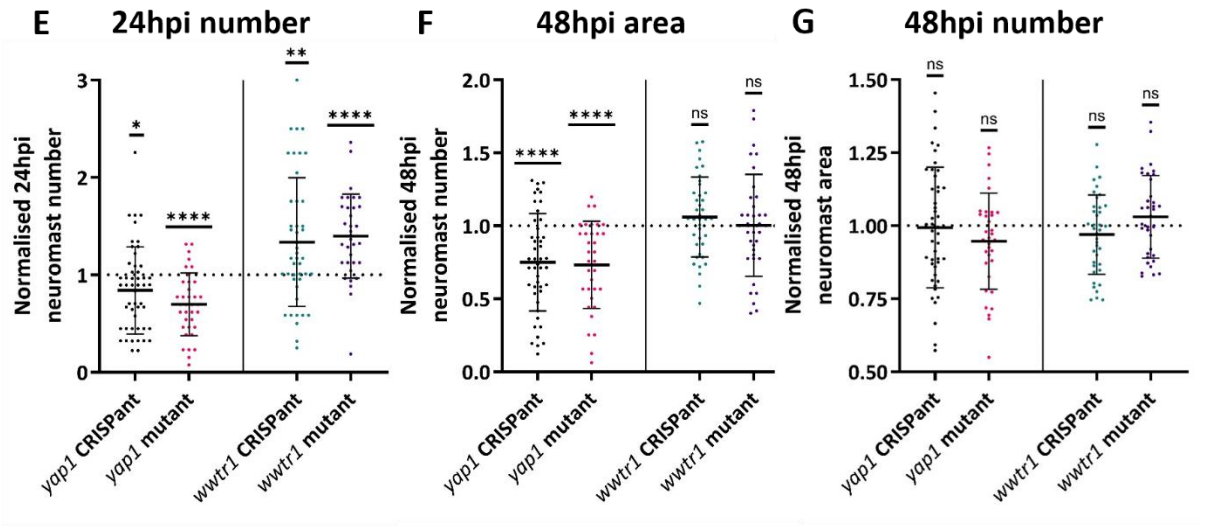

Figure 4.8: Neuromast regeneration phenotypes in stable mutants and CRISPants
(A) Representative images of DASPEI-incubated zebrafish (labelling neuromast hair cells) at baseline and at 24 hours and 48 hours post neuromast injury in WT, CRISPants, and stable mutants. **(B)** Quantification of uninjured neuromast area of *yap1* and *wwtr1* CRISPants and stable mutants, normalised to controls. Uninjured area was unchanged in all groups measured. **(C)** Quantification of uninjured neuromast number of *yap1* and *wwtr1* CRISPants and stable mutants, normalised to controls. Uninjured number was reduced in both *yap1* CRISPants and stable mutants and reduced in *wwtr1* CRISPants but increased in *wwtr1* stable mutants. **(D)** Quantification of 24hpi neuromast area of *yap1* and *wwtr1* CRISPants and stable mutants, normalised to controls. 24hpi area was reduced in both *yap1* CRISPants and stable mutants. Area was unchanged in *wwtr1* CRISPants and increased in *wwtr1* stable mutants. **(E)** Quantification of 24hpi neuromast number of *yap1* and *wwtr1* CRISPants and stable mutants, normalised to controls. 24hpi number was reduced in both *yap1* CRISPants and stable mutants. Number was increased in both *wwtr1* CRISPants and stable mutants. **(F)** Quantification of 48hpi neuromast area of *yap1* and *wwtr1* CRISPants and stable mutants, normalised to controls. 48hpi area was reduced in both *yap1* CRISPants and stable mutants. Area was increased in both *wwtr1* CRISPants and stable mutants. **(G)** Quantification of 48hpi neuromast number of *yap1* and *wwtr1* CRISPants and stable mutants, normalised to controls. 48hpi number was unchanged in all groups measured.
Each dot represents one embryo. Bars represent mean±SD. Data from at least three independent experimental repeats. Significance calculated by one-sample t-test (C-G) or one-sample Wilcoxon test (B) (μ=1). Data normalised to gRNA-only injected controls (for CRISPants), WT siblings (*yap1* stable mutants), or WT (*wwtr1* stable mutants) performed concurrently. Scale bar represents 200μm. WT and CRISPant images and data are also shown in Figure 3.17. *p<0.05; **p<0.01; ***p<0.001; ****p<0.0001; ns=not significant.

difference in mild tail fin regeneration is of particular concern, as it demonstrates that the specificity of the *wwtr1* CRISPant phenotype to severe injury, and the differential role of Yap1 and Taz may not be as clear cut as first expected. Stable mutants also had lower number of samples analysed than CRISPants, which could alter statistical power and therefore the outcome of the appropriate statistical tests. In addition, CRISPant and stable mutant experiments were not conducted at the same time, so may not be directly comparable due to potential differences in aquaculture conditions or in experimenter experience.

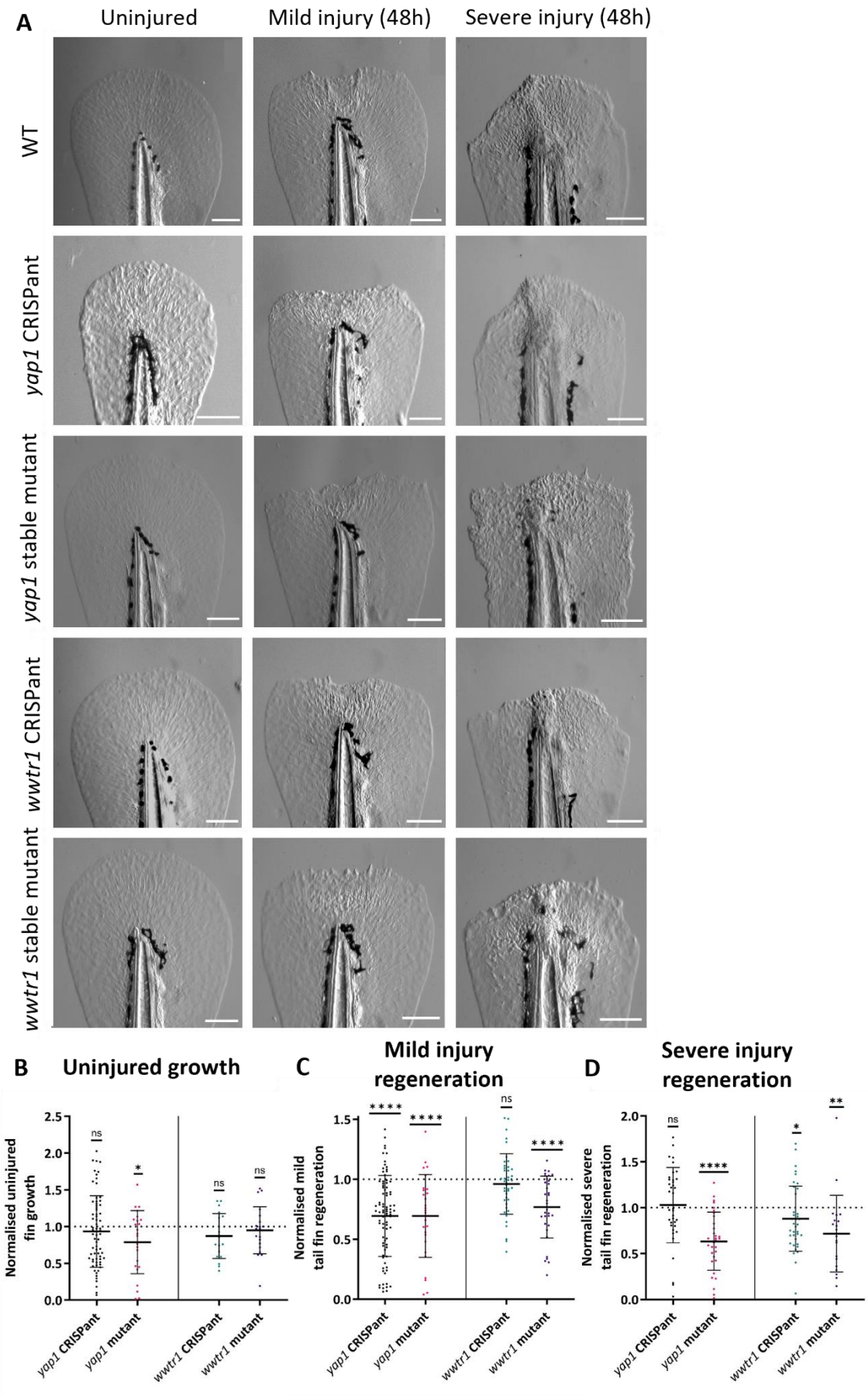
A
Uninjured
Mild injury (48h)
Severe injury (48h)
WT
yap1 CRISPant
yap1 stable mutant
wwtr1 CRISPant
wwtr1 stable mutant
B
Uninjured growth
Normalised uninjured fin growth
C
Mild injury regeneration
Normalised mild tail fin regeneration
D
Severe injury regeneration
Normalised severe tail fin regeneration
yap1 CRISPant
yap1 mutant
wwtr1 CRISPant
wwtr1 mutant
ns
*
**
****

Figure 4.9: Tail fin regeneration phenotypes in stable mutants and CRISPants

(A) Representative brightfield images of the tail fin when uninjured and at 48 hours post mild and severe tail fin injury in WT, *yap1* CRISPants, *yap1* stable mutants, *wwtr1* CRISPants, and *wwtr1* stable mutants. **(B)** Quantification of uninjured tail fin growth over 48 hours. Growth was unchanged in all groups except *yap1* stable mutants, where growth was reduced. **(C)** Quantification of fin growth over 48 hours post mild tail fin injury. Regeneration was reduced in *yap1* CRISPants, *yap1* stable mutants, and *wwtr1* stable mutants but unchanged in *wwtr1* CRISPants. **(D)** Quantification of fin growth over 48 hours post severe tail fin injury. Regeneration was unchanged in *yap1* CRISPants and reduced in all other groups.

Each dot represents one embryo. Bars represent mean±SD. Data from at least three independent experimental repeats. Significance calculated by one-sample t-test (B+C) or one-sample Wilcoxon test (D) (μ=1). Data normalised to gRNA-only injected controls (for CRISPants), WT siblings (*yap1* stable mutants), or WT (*wwtr1* stable mutants) performed concurrently. Scale bar represents 100μm. WT and CRISPant images and data are also shown in Figure 3.18. *p<0.05; **p<0.01; ****p<0.0001; ns=not significant.

5 Chapter 3: Investigation of *yap1* and *wwtr1* CRISPant tail fin regeneration phenotypes

5.1 Differences in *yap1* and *wwtr1* CRISPant tail fin regeneration phenotypes

The differences in tail fin injury regeneration shown in 3.6.2 are clearly of interest for further studies. *yap1* CRISPants showed a reduction in regeneration after mild tail fin injury but not severe tail fin injury, whilst *wwtr1* CRISPants had a reduction in regeneration after severe but not mild tail fin injury (Figure 3.18). It was thought that the *yap1* CRISPants did in fact have reduced regeneration after severe tail fin injury, but it was not seen in the screen as the more disrupted CRISPants were more likely to die following severe tail fin injury, and so were excluded from analysis. Therefore, more detailed analysis of both mild and severe tail fin injury over multiple time points was performed, with a high number of embryos closely followed. Analyses at 4 and 6hpi can be considered a "wound healing/wound response" time window, whilst from 24hpi is regenerative growth[266]. For the following experiments, WT fish (born at the same time as the CRISPants where possible) were used as controls rather than gRNA-only injected controls to streamline the assays with reduced group numbers.

Representative images of mild tail fin injury regeneration are shown in Figure 5.1A. At 4hpi there was no change in fin area between WT and CRISPants (Figure 5.1B). Interestingly, at 6hpi *yap1* CRISPants had significantly reduced fin area compared to WT (Figure 5.1C). This is still within the "wound response" time window, and therefore does not necessarily reflect impaired regeneration. Instead, it could reflect a change in the wound closure response. Immediately after wounding, epithelial cells surrounding the wound usually contract to close it[248]. Alterations in the ECM or in pathways regulating cell contractility in the *yap1* CRISPant may disrupt this process, potentially causing whole fin contraction. *yap1* CRISPants also had reduced regenerative outgrowth at 24 and 48hpi (Figure 5.1D+E), indicating a further defect in regeneration. *wwtr1* CRISPants had no change in area throughout the timecourse, recapitulating results seen in the screen.

Representative images of severe tail fin injury are shown in Figure 5.2A. Similar to mild tail fin injury, there was no change in fin area between WT and CRISPants at 4hpi (Figure 5.2B). At 6 and 24hpi, there was a reduction in area in *yap1* but not *wwtr1* CRISPants (Figure 5.2C-D). However, by 48hpi there was a reduction in area in both *yap1* and *wwtr1* CRISPants. This

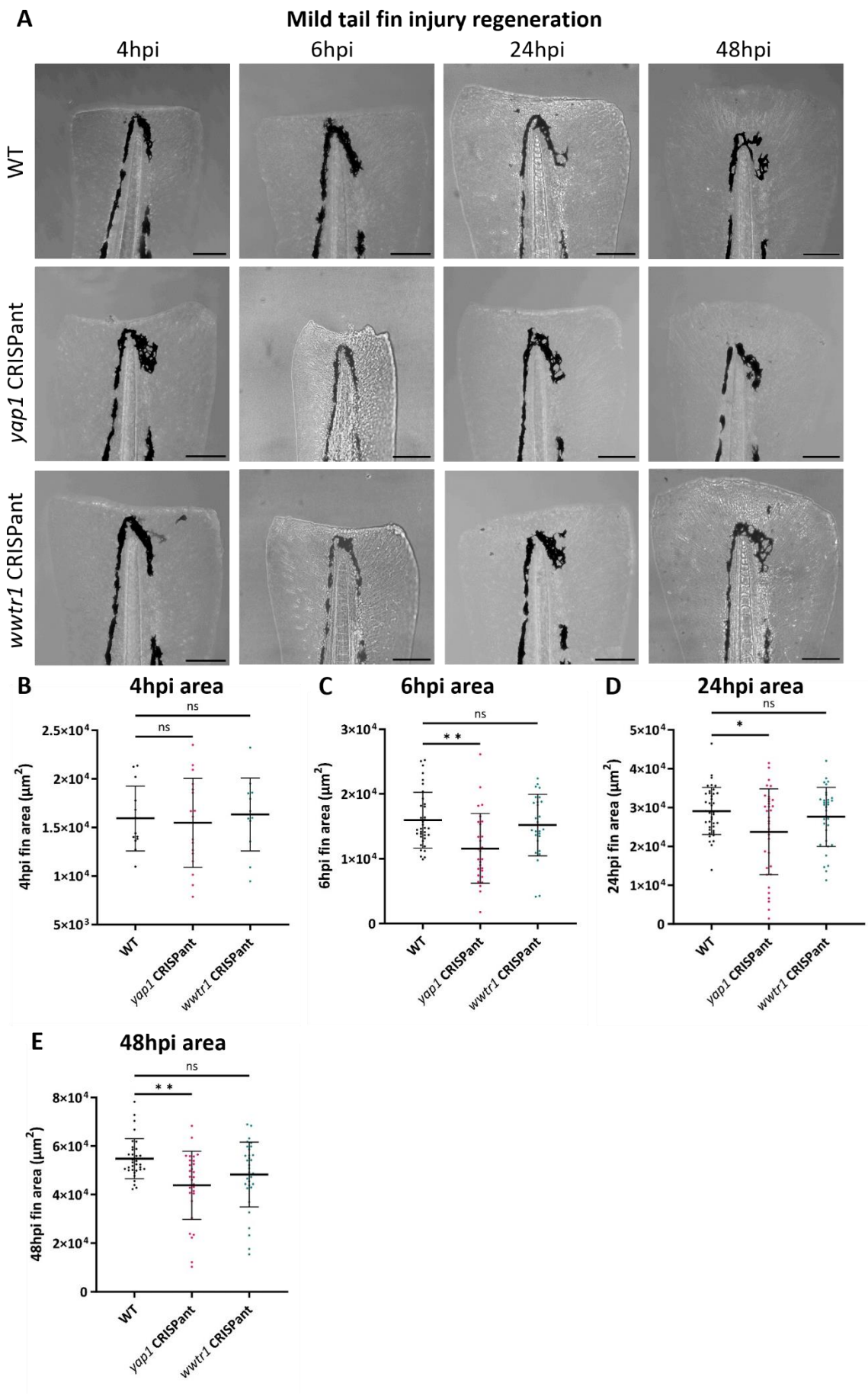
A
Mild tail fin injury regeneration
4hpi
6hpi
24hpi
48hpi
WT
yap1 CRISPant
wwtr1 CRISPant
B
4hpi area
4hpi fin area (µm²)
C
6hpi area
6hpi fin area (µm²)
D
24hpi area
24hpi fin area (µm²)
E
48hpi area
48hpi fin area (µm²)
ns
*
**
WT
yap1 CRISPant
wwtr1 CRISPant

Figure 5.1: Regeneration after mild tail fin injury is impaired in *yap1* but not *wwtr1* CRISPants
(A) Representative WT, *yap1* CRISPant, and *wwtr1* CRISPant images of the regenerating tail fin after mild injury at 4, 6, 24, and 48 hpi. Scale bar represents 100µm. **(B)** Quantification of fin area at 4 hours post mild tail fin injury. No change was seen in CRISPants. **(C)** Quantification of fin area at 6 hours post mild tail fin injury. Fin area was significantly reduced in *yap1* CRISPants only. **(D)** Quantification of fin area at 24 hours post mild tail fin injury. Fin area was significantly reduced in *yap1* CRISPants only. **(E)** Quantification of fin area at 48 hours post mild tail fin injury. Fin area was significantly reduced in *yap1* CRISPants only.
Fin area is measured from notochord tip by manually tracing the fin outline (see Figure 2.5). Significance is measured by one-way ANOVA (B-D) or Kruskal-Wallis test (E) with multiple comparisons. Each dot represents one fish. Results from at least three independent repeats. Bars represent mean±SD. *p<0.05; **p<0.01; ns=not significant.

suggests that Taz may modulate epithelial outgrowth at this later timepoint, whilst Yap1 has a broader function in maintaining tissue integrity. The detailed analysis indicates *yap1* CRISPants do have a severe tail fin regeneration defect (not observed in the screen), and confirms the defect observed in the *wwtr1* CRISPant screen.

The notochord bead of the tail fin will become a signalling centre that coordinates the development of the blastema and is required for proliferation[267], which can be seen in the images as the rounded structure that protrudes from the end of the cut plane (Figure 5.2A). The notochord bead consists of the vacuolated cells of the notochord surrounded by sheath cells[267]. The circularity of the notochord bead was measured at 4 and 6hpi (Figure 5.2F+G). At 4hpi and 6hpi, the *yap1* CRISPant notochord bead had significantly reduced circularity, suggesting an early defect in the formation of the blastema, and/or reflect changes in the mechanical properties of the vacuolated cells. In contrast, *wwtr1* CRISPants had no phenotype.

In conclusion, this shows that the original hypothesis that *yap1* CRISPants have a severe tail fin regeneration defect was correct and confirms that *wwtr1* CRISPants have a specific regenerative defect after severe tail fin injury only. This also confirms that mild and severe injury paradigms should be carefully compared as different proteins clearly impact on regeneration differently, a comparison that is generally lacking in the literature (see 6.4).

5.2 Transcriptome changes upon early mild tail fin injury

Although the previous data shown gives information on the phenotypes occurring upon tail fin injury, it does not indicate transcriptomic changes. Therefore, bulk RNAseq data obtained

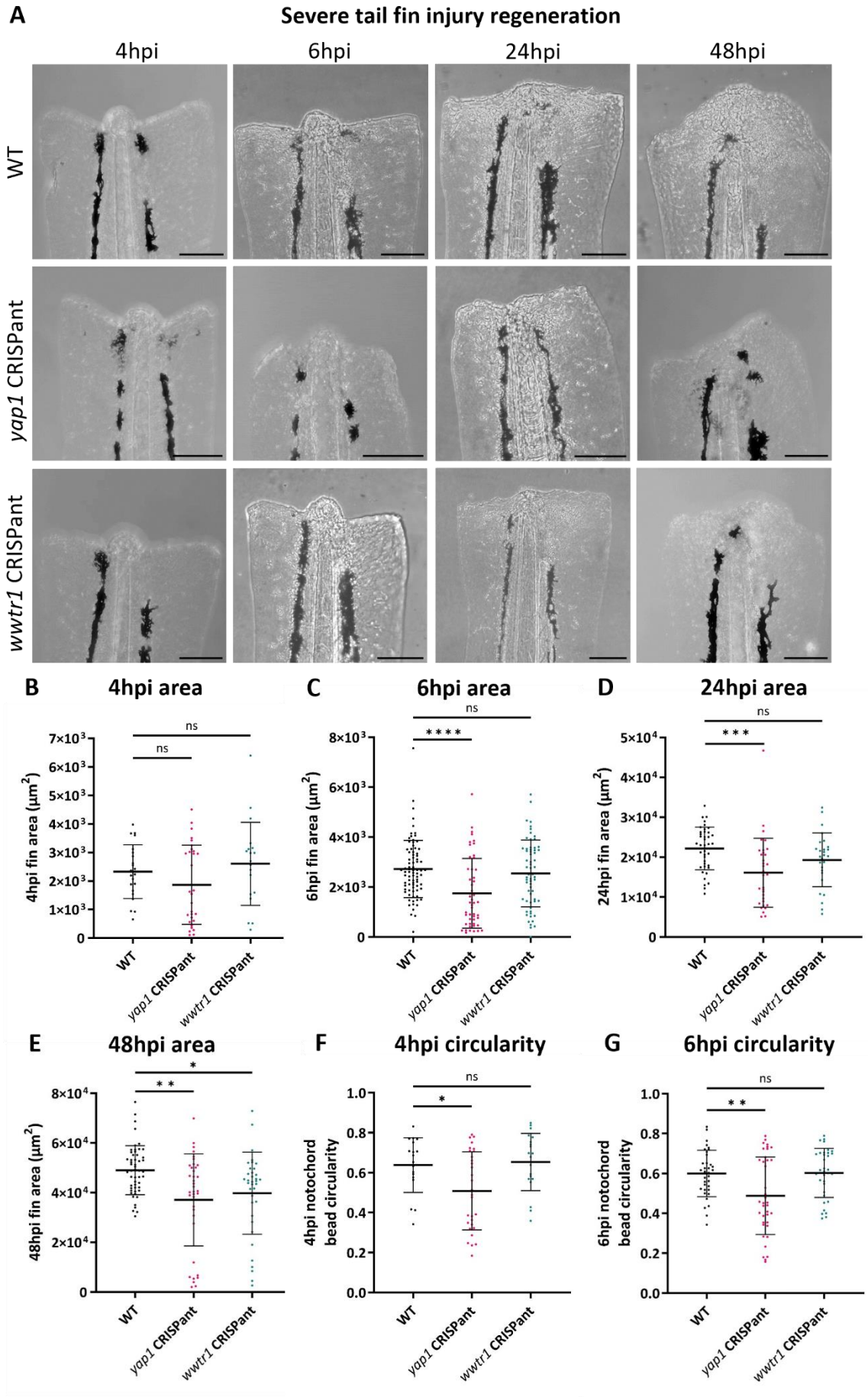
A
Severe tail fin injury regeneration
4hpi
6hpi
24hpi
48hpi
WT
yap1 CRISPant
wwtr1 CRISPant
B
4hpi area
4hpi fin area (µm²)
C
6hpi area
6hpi fin area (µm²)
D
24hpi area
24hpi fin area (µm²)
E
48hpi area
48hpi fin area (µm²)
F
4hpi circularity
4hpi notochord bead circularity
G
6hpi circularity
6hpi notochord bead circularity
ns
WT
yap1 CRISPant
wwtr1 CRISPant

Figure 5.2: Regeneration after severe tail fin injury is impaired in *yap1* CRISPants from 6hpi and *wwtr1* CRISPants at 48hpi

(A) Representative WT, *yap1* CRISPant, and *wwtr1* CRISPant images of the regenerating tail fin after severe injury at 4, 6, 24, and 48 hpi. Scale bar represents 100µm. **(B)** Quantification of fin area at 4 hours post severe tail fin injury. No change was seen in CRISPants. **(C)** Quantification of fin area at 6 hours post severe tail fin injury. Fin area was significantly reduced in *yap1* CRISPants only. **(D)** Quantification of fin area at 24 hours post severe tail fin injury. Fin area was significantly reduced in *yap1* CRISPants only. **(E)** Quantification of fin area at 48 hours post severe tail fin injury. Fin area was significantly reduced in both *yap1* and *wwtr1* CRISPants. **(F)** Quantification of notochord bead circularity at 4 hours post severe tail fin injury. Notochord bead circularity was significantly reduced in *yap1* CRISPants only. **(G)** Quantification of notochord bead circularity at 6 hours post severe tail fin injury. Notochord bead circularity was significantly reduced in *yap1* CRISPants only.

Fin area measured in the notochord bead at 4 and 6hpi, and from an approximate cut plane at 24 and 48hpi (see Figure 2.5). Significance is measured by Kruskal-Wallis test (D+E) or one-way ANOVA (remainder) with multiple comparisons and significance calculated relative to WT only. Each dot represents one fish. Results from at least three independent repeats. Bars represent mean±SD. *p<0.05; **p<0.01; ***p<0.001; ****p<0.0001; ns=not significant.

after injury was investigated. Raw files from 4 hours post mild tail fin injury in untreated WT fish were retrieved[214] and processed with no selection criteria (see 2.18.2.1). This early timepoint is assumed to reflect the local wound response, the missing fin fold tissue, and early recruitment of immune cells, rather than strictly regeneration.

Results from this analysis are summarised in Figure 5.3. The overall pattern of differentially expressed genes is shown in Figure 5.3A, which confirmed consistency between replicates, and also showed an expected pattern of both upregulation and downregulation of different genes upon injury. The top 25 most differentially expressed genes (ordered by largest difference in log2 fold change, with p(adj)<0.05) show multiple types of genes altered in response to injury (Figure 5.3B). As might be expected, there was a downregulation of genes expressed in fin development or in the fin fold in general (*and1* and *and3*)[268], and an upregulation of genes associated with fin regeneration (*mmp9, junba,* and *junbb*)[246,269–271]. There were also changes in genes associated with the extracellular matrix or cell adhesion[269,270,272–277]. These were both upregulated (*lama1* and *mmp9*) and downregulated (*col4a3*, *matn4*, *nid1b*, and *lamb2l*), suggesting that there are major changes in the extracellular matrix and general mechanical properties of the fin fold following amputation. There was also an upregulation of genes associated with DNA transcription and the cell cycle[278–280] (*fosl2*, *junba*, and *junbb*), and apoptosis[281] (*npm1a*), suggesting an increase in both cell proliferation and cell death. Finally, there was an upregulation of genes associated with the immune response[282–284] (*il6st*/*gp130* and *adam8b*).

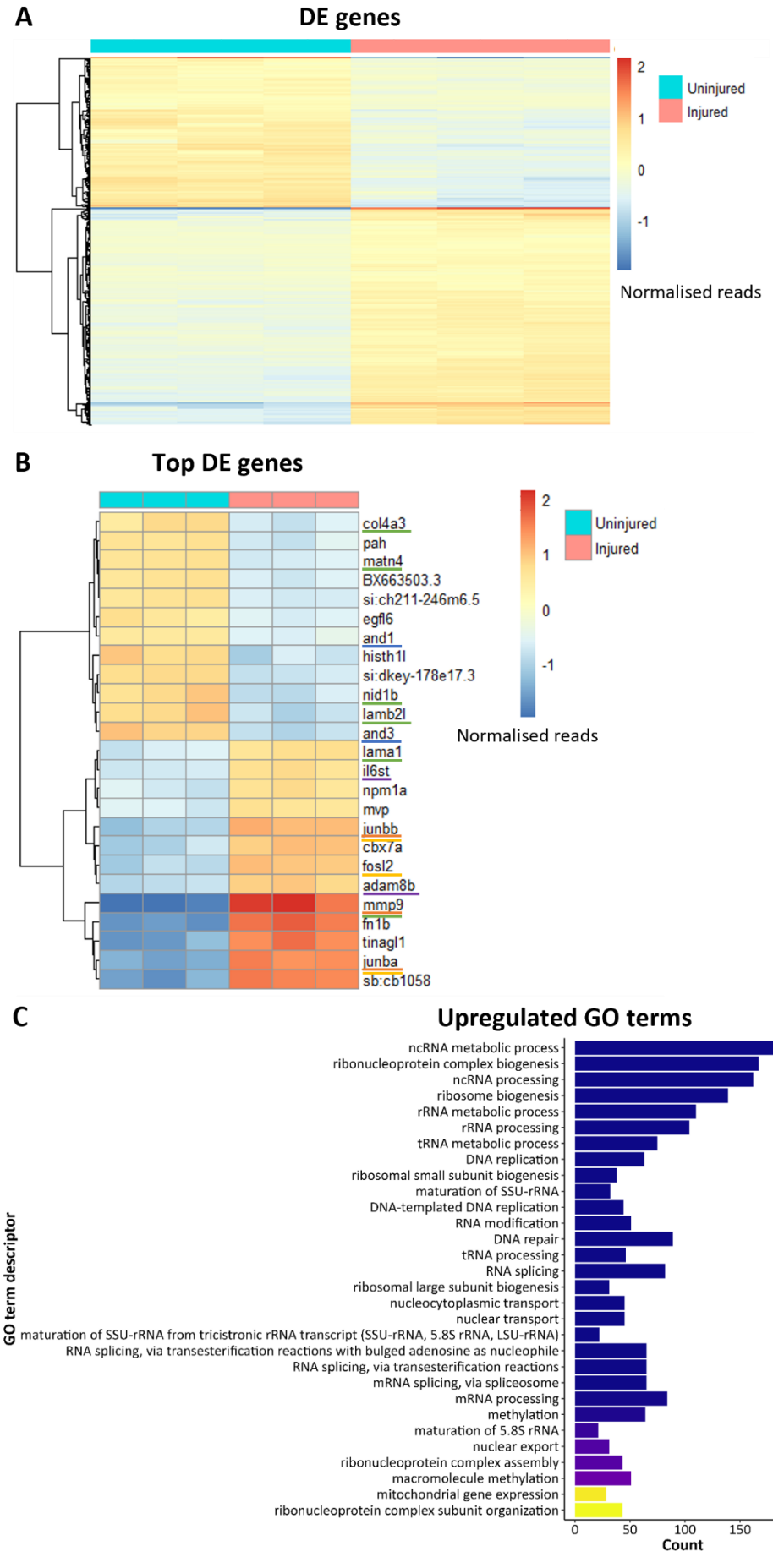
A
DE genes
2
1
0
-1
Uninjured
Injured
Normalised reads
B
Top DE genes
col4a3
pah
matn4
BX663503.3
si:ch211-246m6.5
egfl6
and1
histh1l
si:dkey-178e17.3
nid1b
lamb2l
and3
lama1
il6st
npm1a
mvp
junbb
cbx7a
fosl2
adam8b
mmp9
fn1b
tinagl1
junba
sb:cb1058
2
1
0
-1
Uninjured
Injured
Normalised reads
C
Upregulated GO terms
ncRNA metabolic process
ribonucleoprotein complex biogenesis
ncRNA processing
ribosome biogenesis
rRNA metabolic process
rRNA processing
tRNA metabolic process
DNA replication
ribosomal small subunit biogenesis
maturation of SSU-rRNA
DNA-templated DNA replication
RNA modification
DNA repair
tRNA processing
RNA splicing
ribosomal large subunit biogenesis
nucleocytoplasmic transport
nuclear transport
maturation of SSU-rRNA from tricistronic rRNA transcript (SSU-rRNA, 5.8S rRNA, LSU-rRNA)
RNA splicing, via transesterification reactions with bulged adenosine as nucleophile
RNA splicing, via transesterification reactions
mRNA splicing, via spliceosome
mRNA processing
methylation
maturation of 5.8S rRNA
nuclear export
ribonucleoprotein complex assembly
macromolecule methylation
mitochondrial gene expression
ribonucleoprotein complex subunit organization
GO term descriptor
0
50
100
150
200
Count
p.adjust
1.0e-11
7.5e-12
5.0e-12
2.5e-12

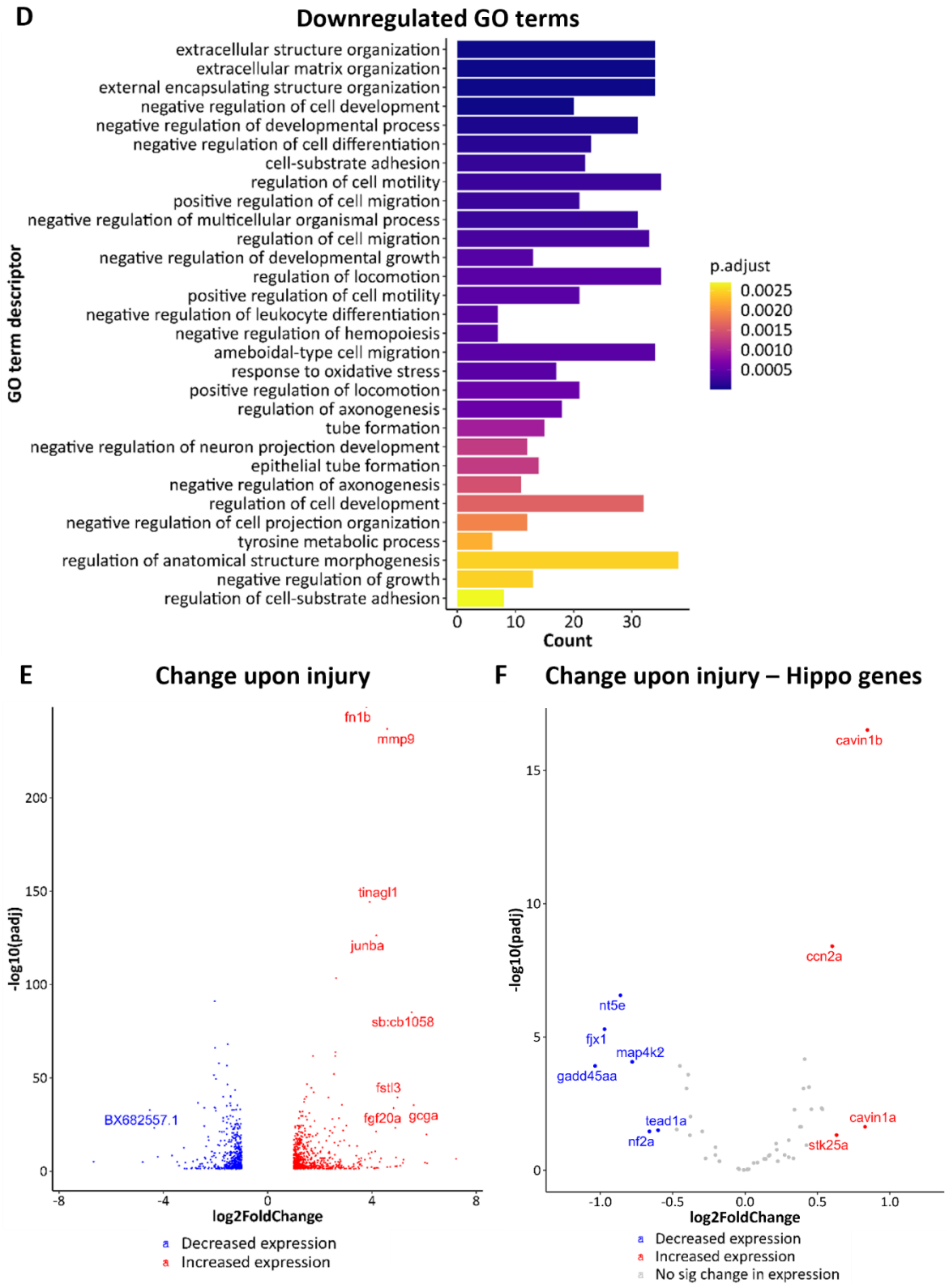

Figure 5.3: Bulk RNAseq data in WT fish after mild tail fin injury

(A) Overview heatmap of all differentially expressed genes upon mild tail fin injury. Expression was consistent between replicates. **(B)** Top 25 most differentially expressed genes upon injury. These are associated with a range of processes, including extracellular matrix, DNA transcription, and fin regeneration. Underline colour represents genes associated with: orange=fin regeneration;

yellow=DNA and cell cycle; green=ECM; blue=fin development; purple=immune system. **(C)** GO terms upregulated upon mild tail fin injury in WT fish. These included processes associated with DNA replication and RNA processes. **(D)** GO terms downregulated upon mild tail fin injury in WT fish. These included cell migration and negative regulation of normal growth. **(E)** Volcano plot of significantly altered genes in WT fish upon injury. Similar results can be seen as shown in B. Cutoff at p(adj)<0.05 and log2FoldChange>1 or <-1. **(F)** Volcano plot of significantly altered Hippo-associated genes in WT fish upon injury. Changes in expression of Yap1/Taz target genes can be observed as both increases and decreases. Cutoff at p(adj)<0.05 and log2FoldChange>0.6 or <-0.6
Raw data taken from Lin et. al. (2021)[214], and processed and analysed for the work presented here. Each column in A+B denotes an independent biological replicate of 50 pooled larvae samples. DE=differentially expressed; GO=gene ontology.

When calculating gene ontology (GO) term enrichment over all differentially expressed genes (Figure 5.3C+D), a similar pattern of gene expression was observed. Upregulated GO terms included those associated with DNA replication and RNA processing (Figure 5.3C), suggesting an increase in cell proliferation, supporting some of the top upregulated genes being associated with DNA transcription. Downregulated GO terms include those associated with cell migration and motility, cell adhesion, and extracellular structure/matrix organisation (Figure 5.3D), which may support the findings in the most differentially expressed genes (see above). There was also a downregulation of GO terms associated with the negative regulation of cell development (i.e. cell maturation), developmental processes, developmental growth, and general growth, suggesting an inhibition of normal growth processes during early regeneration.

Another way to display this data is through volcano plots, which plot the log2 fold change upon injury for each gene against significance (Figure 5.3E). This showed a comparable pattern to the heatmaps of differentially expressed genes, with similar genes showing the largest change (e.g. *fn1b* and *mmp9*). When filtered for Hippo pathway-associated genes only (Figure 5.3F), this showed an interesting pattern. A downregulation of the Yap1/Taz-inhibiting *map4k2* and *nf2a*[18] was seen, suggesting an increase in Yap1/Taz activity. There was no significant change in *yap1* or *wwtr1* mRNA expression themselves, suggesting a change in activity rather than a change in transcription at this timepoint. However, there was both upregulation and downregulation of Yap1/Taz target genes[10,230] (*ccn2a*/*ctgfa*, *cavin1a*, and *cavin1b* and *gadd45aa*, *fjx1*, and *nt5e* respectively). This suggests that Yap1/Taz activity may not be increased in a blanket manner, with Yap1/Taz selectively activating specific target genes, or that these genes may be regulated by multiple pathways[9].

In conclusion, transcriptome changes upon mild tail fin injury revealed changes in ECM organisation and pausing of normal developmental processes. Hippo pathway-specific investigation showed no change in *yap1* or *wwtr1* but changes in their target genes and a downregulation of some inhibitory upstream kinases, highlighting that the Hippo pathway is responsive to mild tail fin injury at a transcriptomic level.

5.3 Severe tail fin injury and CRISPR mutagenesis alters the transcriptome

5.3.1 Overview of gene expression changes after injury

As well as an investigation of the transcriptome following mild tail fin injury, the effect of severe tail fin injury and *yap1*/*wwtr1* mutagenesis was of interest. Therefore, WT, *yap1* CRISPant, and *wwtr1* CRISPant samples were collected at 24 hours post severe tail fin injury or uninjured, and samples were processed as described in 2.18.1. This timepoint is at the beginning of the regenerative outgrowth time window of tail fin regeneration[266] (at a later stage than mild injury), so key transcriptomic changes that support regeneration should occur by this point. Some changes will also reflect the missing tissue and recruited immune cells.

The resulting PCA plot (Figure 5.4A) shows that samples generally clustered within their genotype and injury status, showing consistency between samples. There was a large shift upon injury, showing a dramatic effect of this injury paradigm. *yap1* CRISPant samples were more different from WT than *wwtr1* CRISPants, an effect that was lessened upon injury. This suggests that, upon severe injury, there is a large transcriptomic change in the embryo tail which may not involve the Hippo signalling pathway as a core regulator. It also demonstrates a difference between Yap1 and Taz function on a transcriptomic level.

Figure 5.4B-D shows the transcriptomic changes in WT fish upon injury. There was a general pattern of both increases and decreases in gene expression (Figure 5.4B), in the same manner as mild injury (Figure 5.3E). Samples were consistent within each condition, as shown by the heatmap of differentially expressed (DE) genes (Figure 5.4C). The top 25 most DE genes followed a similar pattern (Figure 5.4D). Significantly downregulated genes upon severe injury included *and2*, a member of the actinodin family of proteins involved in fin development[268]. Others in this family were downregulated in mild tail fin regeneration (see 5.2 above). Significantly upregulated genes also included *acp5a*, *mpeg*, *ctss2.1*, and *ctsk*. These have

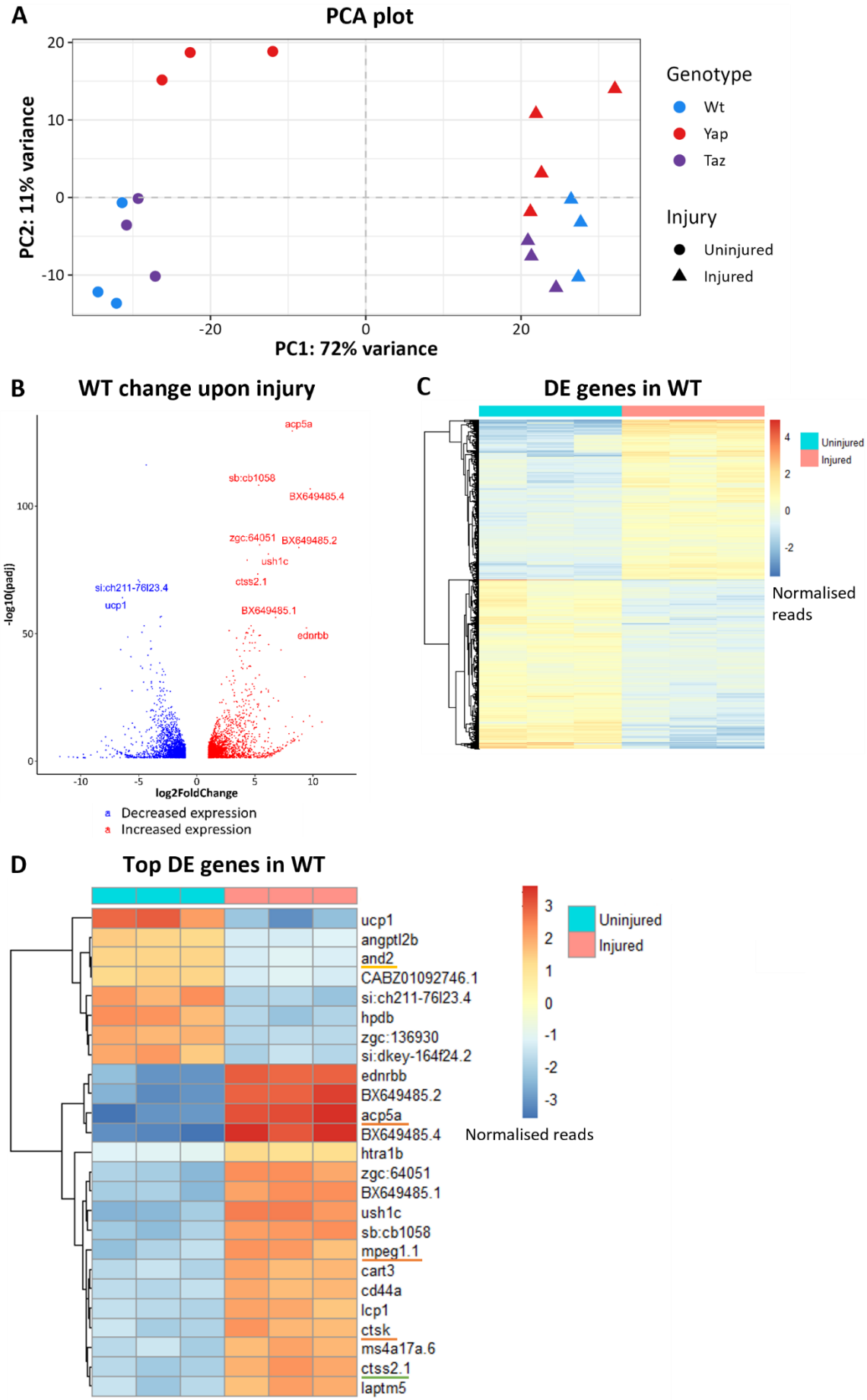
A
PCA plot
PC2: 11% variance
PC1: 72% variance
Genotype
Wt
Yap
Taz
Injury
Uninjured
Injured
B
WT change upon injury
-log10(padj)
log2FoldChange
acp5a
sb:cb1058
BX649485.4
zgc:64051
BX649485.2
ush1c
ctss2.1
si:ch211-76l23.4
ucp1
BX649485.1
ednrbb
Decreased expression
Increased expression
C
DE genes in WT
Uninjured
Injured
Normalised reads
D
Top DE genes in WT
ucp1
angptl2b
and2
CABZ01092746.1
si:ch211-76l23.4
hpdb
zgc:136930
si:dkey-164f24.2
ednrbb
BX649485.2
acp5a
BX649485.4
htra1b
zgc:64051
BX649485.1
ush1c
sb:cb1058
mpeg1.1
cart3
cd44a
lcp1
ctsk
ms4a17a.6
ctss2.1
laptm5
Uninjured
Injured
Normalised reads

E ***yap1*** **CRISPant change upon injury**

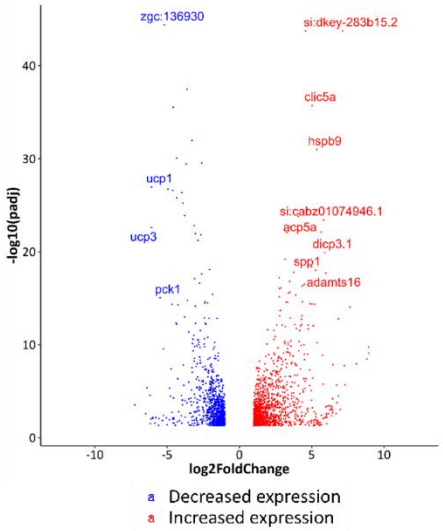

F **DE genes in** ***yap1*** **CRISPant**

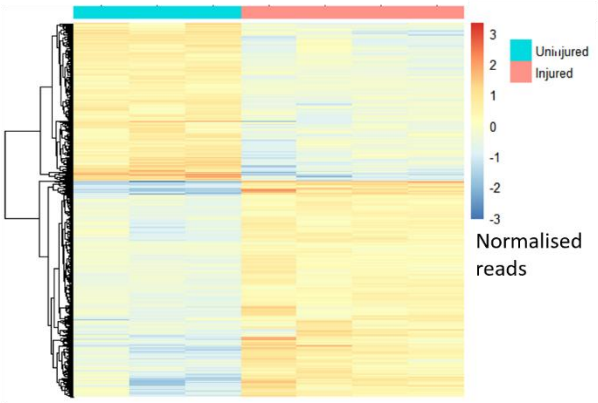

G **Top DE genes in** ***yap1*** **CRISPant**

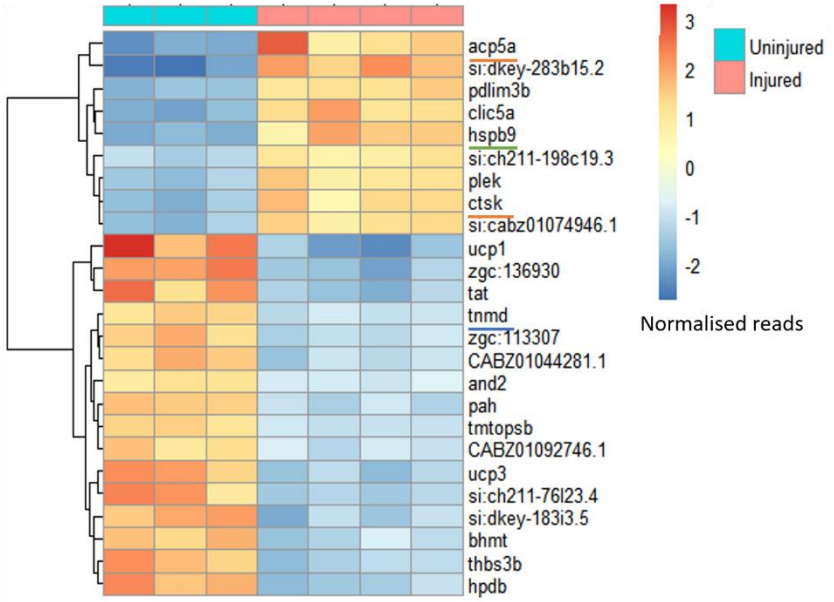

H ***wwtr1*** **CRISPant change upon injury**

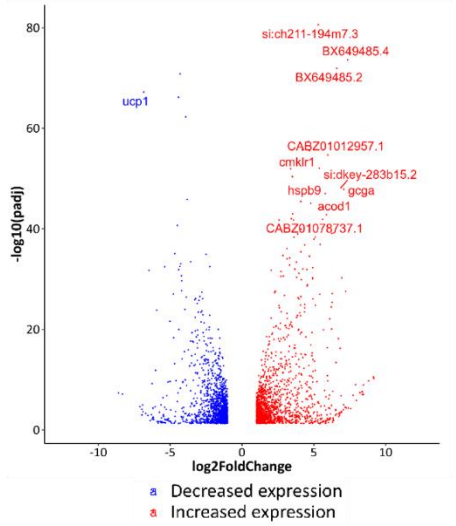

I **DE genes in** ***wwtr1*** **CRISPant**

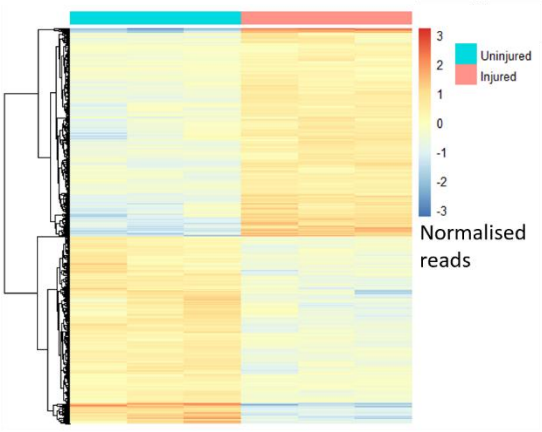

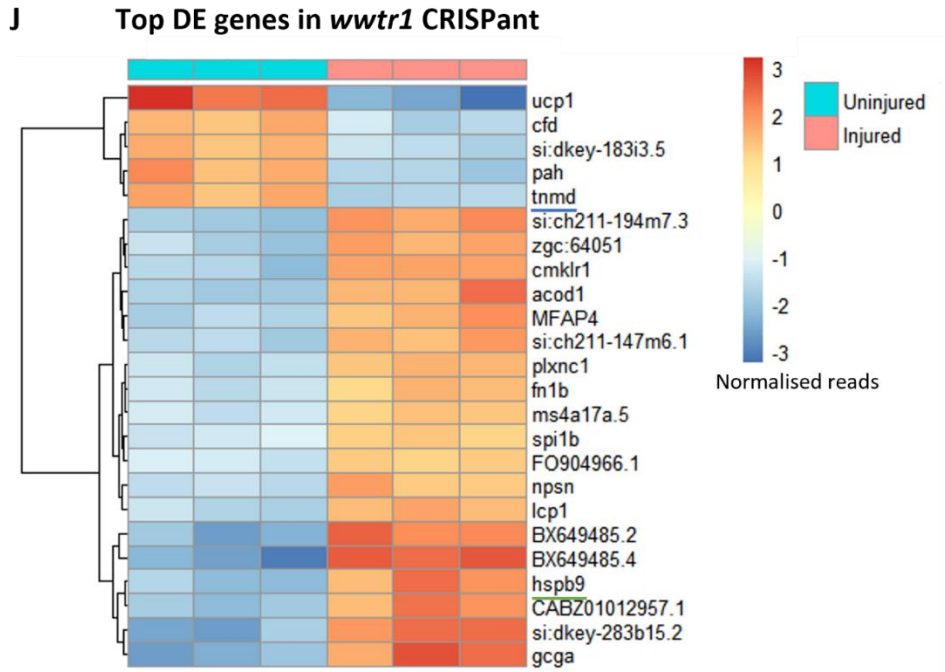

Figure 5.4: Overview of bulk RNAseq data after severe tail fin injury
(A) PCA plot of WT, *yap1* CRISPant, and *wwtr1* CRISPant at both baseline and 24 hours post severe tail fin injury. A large shift was seen upon injury, and *yap1* CRISPant samples varied more in uninjured samples than after injury. **(B)** Volcano plot of significantly upregulated (red) and downregulated (blue) genes in WT fish after severe tail fin injury. **(C)** Overview heatmap of all differentially expressed genes in WT fish after severe tail fin injury. **(D)** The top 25 most differentially expressed genes in WT fish after severe tail fin injury. **(E)** Volcano plot of significantly upregulated (red) and downregulated (blue) genes in *yap1* CRISPant fish after severe tail fin injury. **(F)** Overview heatmap of all differentially expressed genes in *yap1* CRISPant fish after severe tail fin injury. **(G)** The top 25 most differentially expressed genes in *yap1* CRISPant fish after severe tail fin injury. **(H)** Volcano plot of significantly upregulated (red) and downregulated (blue) genes in *wwtr1* CRISPant fish after severe tail fin injury. **(I)** Overview heatmap of all differentially expressed genes in *wwtr1* CRISPant fish after severe tail fin injury. **(J)** The top 25 most differentially expressed genes in *wwtr1* CRISPant fish after severe tail fin injury.
Each column in C, D, F, G, I + J denotes an independent biological replicate of 50 pooled larvae samples. DE=differentially expressed. Cutoff for volcano plots in B, E, and H is p(adj)<0.05 and log2FoldChange>1 or <-1. Underline colour in heatmap genes represents genes associated with: orange=immune system; yellow=fin development; green=apoptosis; blue=stem cell proliferation.

been associated with apoptosis[285] (*ctss2.1*) and the immune system[144,285–289], suggesting an induction of the immune response upon injury, although whether this is a result of immune cell intrinsic alterations or changes in the recruitment of immune cells cannot be determined.

Transcriptomic changes in *yap1* CRISPants upon injury are shown in Figure 5.4E-G. A similar pattern was seen (Figure 5.4E) to that found in WT samples (Figure 5.4B), although there was a slight bias towards increased gene expression. This was consistent between samples (Figure 5.4F). Of the top 25 most DE genes in *yap1* CRISPants (Figure 5.4G) there was some overlap

with WT (Figure 5.4D). Similarly to WT samples after mild and severe injury, there was a decrease in actinodin family members, in this case *and2*. The increase in immune system components in WT fish was replicated in *yap1* CRISPants, although only for two components, *acp5a* and *ctsk*. This could suggest a more blunted immune response upon injury in *yap1* CRISPants, although firmly establishing this requires furthers investigation (see below). Another increased gene of interest was *hspb9*, which has been shown to negatively regulate apoptosis *in vitro*[290], suggesting that apoptosis is decreased in *yap1* CRISPants. This would be a surprising phenotype as YAP1 usually inhibits p53-mediated apoptosis[291,292]. One downregulated gene was *tnmd*. Tnmd is associated with the negative regulation of stem cell proliferation under certain conditions[293], and so its downregulation suggests an increase in stem cell proliferation following injury. This would be expected in WT fish, as regeneration often requires higher rates of proliferation[38]. However, increased YAP/TAZ activity *in vitro* increases proliferation[294], so *yap1* CRISPants might be expected to have decreased proliferation. This topic is discussed further in section 5.4 and 5.8 below.

Similar analysis was performed in *wwtr1* CRISPants (Figure 5.4H-J). Again, this showed both increases and decreases in gene expression (Figure 5.4H), with consistency between samples (Figure 5.4I). Within the top DE genes in *wwtr1* CRISPants (Figure 5.4J), a similar result was observed to those seen in *yap1* CRISPants, i.e. an upregulation of *hspb9*, and a downregulation of *tnmd*. Interestingly, there was no changes in immune genes. Of note, this analysis was limited to only the top 25 most DE genes, so further analysis is required before immune response can be ruled out as impacting on regeneration in *wwtr1* CRISPants.

5.3.2 GO term analysis after severe tail fin injury

GO term analysis is one way to investigate and group the functions of DE genes without a cutoff for numbers as shown in top DE gene heatmaps. Analysis of GO term upregulation following injury within each genotype gave similar results (Figure 5.5). In WT fish, an upregulation of processes involved in DNA replication and cell cycle was seen (Figure 5.5A), suggesting an increase in cell proliferation at this time point of regeneration, which is not unexpected. Downregulated GO terms in WT fish (Figure 5.5B) included those associated with extracellular structure or matrix organisation, suggesting a reduction and/or remodelling of the extracellular matrix during regeneration in a similar manner to mild tail fin injury (Figure

5.3D). GO terms also included the negative regulation of cell development and growth (implying an increase in cell maturation and growth), again similar to mild injury. Bone Morphogenetic Protein (BMP) signalling and response was also downregulated in WT fish. BMP enhances the proliferation and differentiation of osteoblasts in the adult tail fin blastema[295–299]. This might suggest that BMP should be increased following injury rather than the downregulation seen here. However, these papers used adult fish[295–299], where the composition of the fin is different from that of the embryo[300], and used different timepoints following injury, so they are not directly comparable to the data presented here.

In *yap1* and *wwtr1* CRISPants, a similar to WT pattern of upregulation of GO terms associated with cell cycle processes was seen (Figure 5.5C+E). Downregulated GO term processes in CRISPants were also similar to WT, except for no decrease in BMP signalling (Figure 5.5D+F). Previous work in the zebrafish suggests that Yap1 promotes BMP signalling in the proximal blastema after tail fin injury[247]. However, this is balanced by BMP inhibition in the distal blastema[247], and so a change in BMP signalling may not be detected by this technique due to its low spatial resolution within the blastema. *wwtr1* CRISPants also had a reduction in various metabolic and biosynthetic processes (Figure 5.5F), suggesting a *wwtr1*-specific impairment in these. Overall, this GO term-based analysis suggests that *yap1*/*wwtr1* CRISPants are not generally different from WT after injury. However, more direct in depth comparisons of the CRISPants and WT are required to investigate this further, which is described below.

5.3.3 Transcriptomic changes in uninjured fish

A direct comparison of uninjured WT and CRISPant fish is shown in Figure 5.6, demonstrating the effect of CRISPR mutagenesis on the embryos when unchallenged. Comparisons between WT and *yap1* CRISPants are shown in Figure 5.6A-D. A clear bias towards an increase in gene

Figure 5.5: GO term analysis after severe tail fin injury
(A) Upregulated GO terms in WT fish following injury. These included those involved in the cell cycle. **(B)** Downregulated GO terms in WT fish following injury. These included extracellular structure organisation and development. **(C)** Upregulated GO terms in *yap1* CRISPants following injury. Most terms were similar to WT. **(D)** Downregulated GO terms in *yap1* CRISPants following injury. Most terms were similar to WT. **(E)** Upregulated GO terms in *wwtr1* CRISPants following injury. Most terms were similar to WT. **(F)** Downregulated GO terms in *wwtr1* CRISPants following injury. Most terms were similar to WT, but also included a range of biosynthetic and metabolic processes.
GO=gene ontology. Colour of bars denote significance (padj).

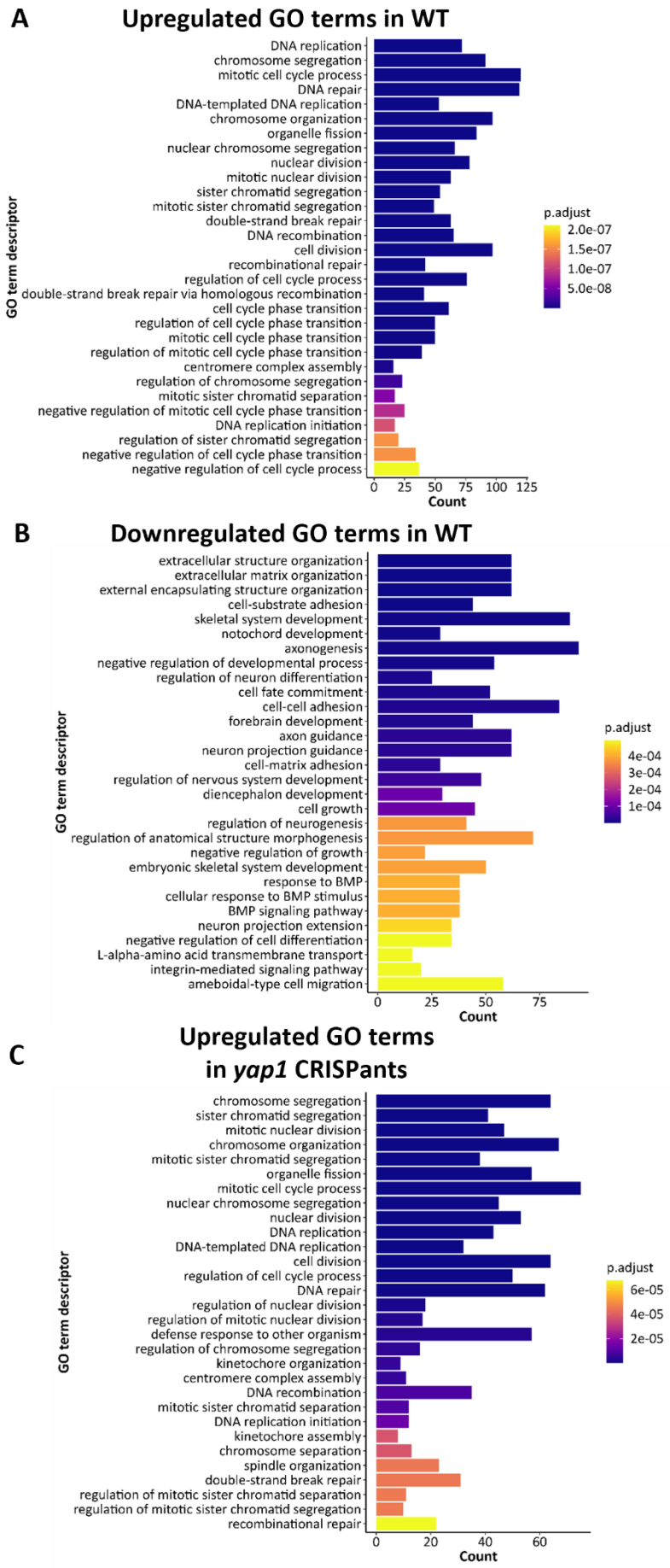
A
Upregulated GO terms in WT
DNA replication
chromosome segregation
mitotic cell cycle process
DNA repair
DNA-templated DNA replication
chromosome organization
organelle fission
nuclear chromosome segregation
nuclear division
mitotic nuclear division
sister chromatid segregation
mitotic sister chromatid segregation
double-strand break repair
DNA recombination
cell division
recombinational repair
regulation of cell cycle process
double-strand break repair via homologous recombination
cell cycle phase transition
regulation of cell cycle phase transition
mitotic cell cycle phase transition
regulation of mitotic cell cycle phase transition
centromere complex assembly
regulation of chromosome segregation
mitotic sister chromatid separation
negative regulation of mitotic cell cycle phase transition
DNA replication initiation
regulation of sister chromatid segregation
negative regulation of cell cycle phase transition
negative regulation of cell cycle process
GO term descriptor
0 25 50 75 100 125
Count
p.adjust
2.0e-07
1.5e-07
1.0e-07
5.0e-08
B
Downregulated GO terms in WT
extracellular structure organization
extracellular matrix organization
external encapsulating structure organization
cell-substrate adhesion
skeletal system development
notochord development
axonogenesis
negative regulation of developmental process
regulation of neuron differentiation
cell fate commitment
cell-cell adhesion
forebrain development
axon guidance
neuron projection guidance
cell-matrix adhesion
regulation of nervous system development
diencephalon development
cell growth
regulation of neurogenesis
regulation of anatomical structure morphogenesis
negative regulation of growth
embryonic skeletal system development
response to BMP
cellular response to BMP stimulus
BMP signaling pathway
neuron projection extension
negative regulation of cell differentiation
L-alpha-amino acid transmembrane transport
integrin-mediated signaling pathway
ameboidal-type cell migration
GO term descriptor
0 25 50 75
Count
p.adjust
4e-04
3e-04
2e-04
1e-04
C
Upregulated GO terms
in yap1 CRISPants
chromosome segregation
sister chromatid segregation
mitotic nuclear division
chromosome organization
mitotic sister chromatid segregation
organelle fission
mitotic cell cycle process
nuclear chromosome segregation
nuclear division
DNA replication
DNA-templated DNA replication
cell division
regulation of cell cycle process
DNA repair
regulation of nuclear division
regulation of mitotic nuclear division
defense response to other organism
regulation of chromosome segregation
kinetochore organization
centromere complex assembly
DNA recombination
mitotic sister chromatid separation
DNA replication initiation
kinetochore assembly
chromosome separation
spindle organization
double-strand break repair
regulation of mitotic sister chromatid separation
regulation of mitotic sister chromatid segregation
recombinational repair
GO term descriptor
0 20 40 60
Count
p.adjust
6e-05
4e-05
2e-05

D

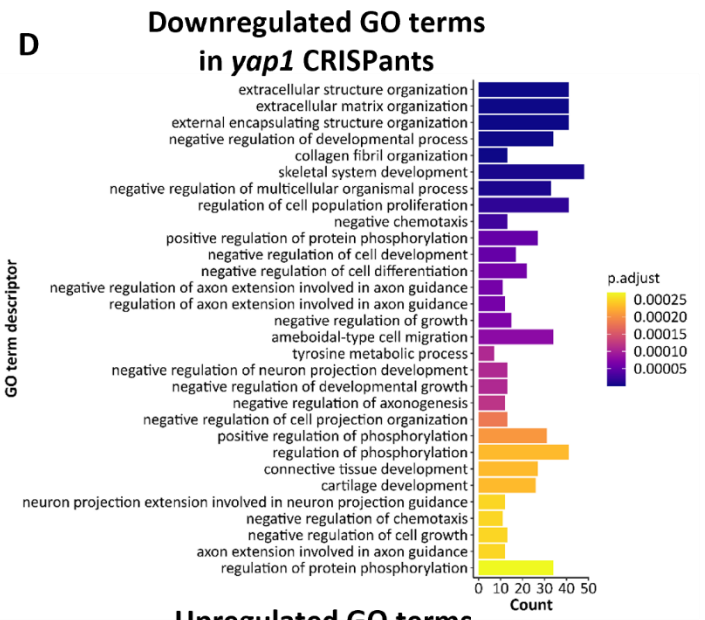
Downregulated GO terms
in yap1 CRISPants
extracellular structure organization
extracellular matrix organization
external encapsulating structure organization
negative regulation of developmental process
collagen fibril organization
skeletal system development
negative regulation of multicellular organismal process
regulation of cell population proliferation
negative chemotaxis
positive regulation of protein phosphorylation
negative regulation of cell development
negative regulation of cell differentiation
negative regulation of axon extension involved in axon guidance
regulation of axon extension involved in axon guidance
negative regulation of growth
ameboidal-type cell migration
tyrosine metabolic process
negative regulation of neuron projection development
negative regulation of developmental growth
negative regulation of axonogenesis
negative regulation of cell projection organization
positive regulation of phosphorylation
regulation of phosphorylation
connective tissue development
cartilage development
neuron projection extension involved in neuron projection guidance
negative regulation of chemotaxis
negative regulation of cell growth
axon extension involved in axon guidance
regulation of protein phosphorylation
GO term descriptor
0 10 20 30 40 50
Count
p.adjust
0.00025
0.00020
0.00015
0.00010
0.00005

E

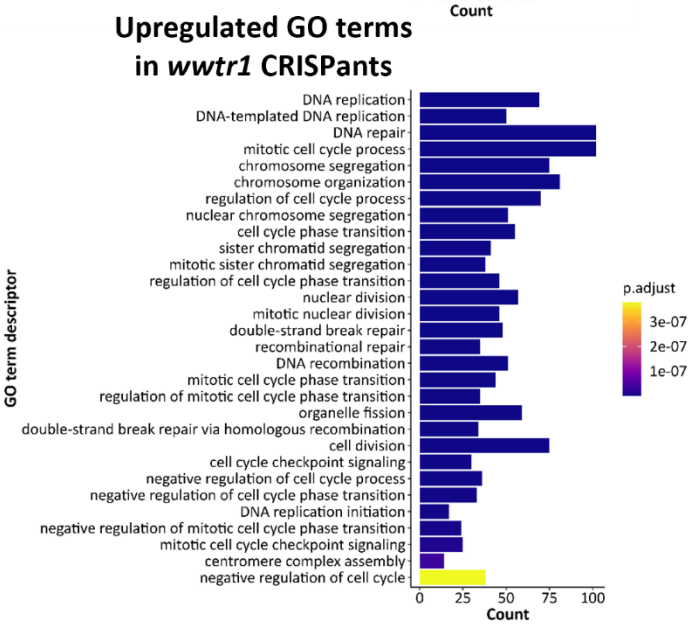
Upregulated GO terms
in wwtr1 CRISPants
DNA replication
DNA-templated DNA replication
DNA repair
mitotic cell cycle process
chromosome segregation
chromosome organization
regulation of cell cycle process
nuclear chromosome segregation
cell cycle phase transition
sister chromatid segregation
mitotic sister chromatid segregation
regulation of cell cycle phase transition
nuclear division
mitotic nuclear division
double-strand break repair
recombinational repair
DNA recombination
mitotic cell cycle phase transition
regulation of mitotic cell cycle phase transition
organelle fission
double-strand break repair via homologous recombination
cell division
cell cycle checkpoint signaling
negative regulation of cell cycle process
negative regulation of cell cycle phase transition
DNA replication initiation
negative regulation of mitotic cell cycle phase transition
mitotic cell cycle checkpoint signaling
centromere complex assembly
negative regulation of cell cycle
GO term descriptor
0 25 50 75 100
Count
p.adjust
3e-07
2e-07
1e-07

F

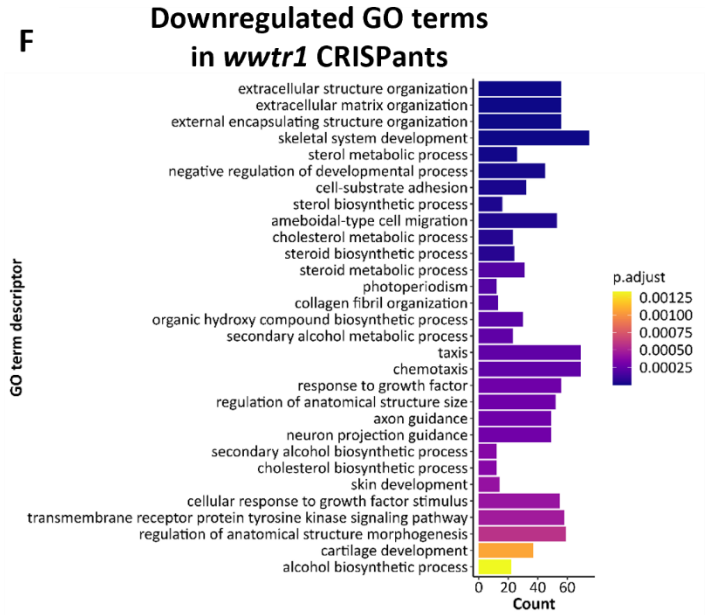
Downregulated GO terms
in wwtr1 CRISPants
extracellular structure organization
extracellular matrix organization
external encapsulating structure organization
skeletal system development
sterol metabolic process
negative regulation of developmental process
cell-substrate adhesion
sterol biosynthetic process
ameboidal-type cell migration
cholesterol metabolic process
steroid biosynthetic process
steroid metabolic process
photoperiodism
collagen fibril organization
organic hydroxy compound biosynthetic process
secondary alcohol metabolic process
taxis
chemotaxis
response to growth factor
regulation of anatomical structure size
axon guidance
neuron projection guidance
secondary alcohol biosynthetic process
cholesterol biosynthetic process
skin development
cellular response to growth factor stimulus
transmembrane receptor protein tyrosine kinase signaling pathway
regulation of anatomical structure morphogenesis
cartilage development
alcohol biosynthetic process
GO term descriptor
0 20 40 60
Count
p.adjust
0.00125
0.00100
0.00075
0.00050
0.00025

expression was observed (Figure 5.6A+B), which was consistent between samples (Figure 5.6B). This suggests a general inhibitory role of Yap1 in embryonic tail development. Of the top 25 most DE genes (all of which were increased in CRISPants), genes were involved in a range of processes, including RNA processing[301,302] (*cpsf6* and *hnrnpaba*), mitosis[303] (*ewsr1b*), metabolism that increases cell growth *in vitro*[304] (*pdhx*), and Wnt signalling[305] (*gsk3ab*) (Figure 5.6C). These groups are supported by the GO term analysis (Figure 5.6D), which highlighted a particular alteration in Wnt signalling processes. However, components associated with both negative and positive regulation of Wnt signalling processes were upregulated, which is investigated in more detail in 5.3.7 below.

Comparison of uninjured WT and *wwtr1* CRISPants are shown in Figure 5.6E-G. Although compared to *yap1* CRISPants (Figure 5.6A) there was a similar bias towards an increase in gene expression, *wwtr1* CRISPants had much fewer DE genes (Figure 5.6E) compared to *yap1* CRISPants, suggesting more similarity of the *wwtr1* CRISPants to WT. Of the top 25 most DE genes, many included those associated with metabolic and biosynthetic processes (Figure 5.6F), which is supported by GO term analysis (Figure 5.6G). This included increased lipid and fatty acid metabolism, particularly in cholesterol synthesis[306–310] (e.g. *fads2*, *scd*, *cyp51*, *tm7sf2*, *hmgcs1*). Of note, the count for these GO terms is small and so may represent noise and implies that the number of altered processes in *wwtr1* CRISPants is low. A change in metabolism, and so processes such as cell growth, proliferation, and differentiation, could underlie the specific tail fin regeneration defect seen in *wwtr1* CRISPants, but further in-depth investigation of this is outside the scope of this thesis.

5.3.4 Transcriptomic changes in injured fish

Analysis was also performed comparing WT and CRISPants after severe injury (Figure 5.7). Results from comparison to *yap1* CRISPants are shown in Figure 5.7A-D. Overall, analysis of DE genes showed fewer genes and lower fold change values (Figure 5.7A) than those seen in uninjured comparisons (Figure 5.6A). This supports the findings presented previously in the PCA plot (Figure 5.4A), where *yap1* CRISPants became more transcriptionally similar to WT fish upon injury. The heatmap of DE genes also showed a general pattern of an increase in gene expression, although the injured *yap1* CRISPant samples were more heterogeneous than uninjured samples (Figure 5.7B+C). GO term analysis also showed fewer altered genes,

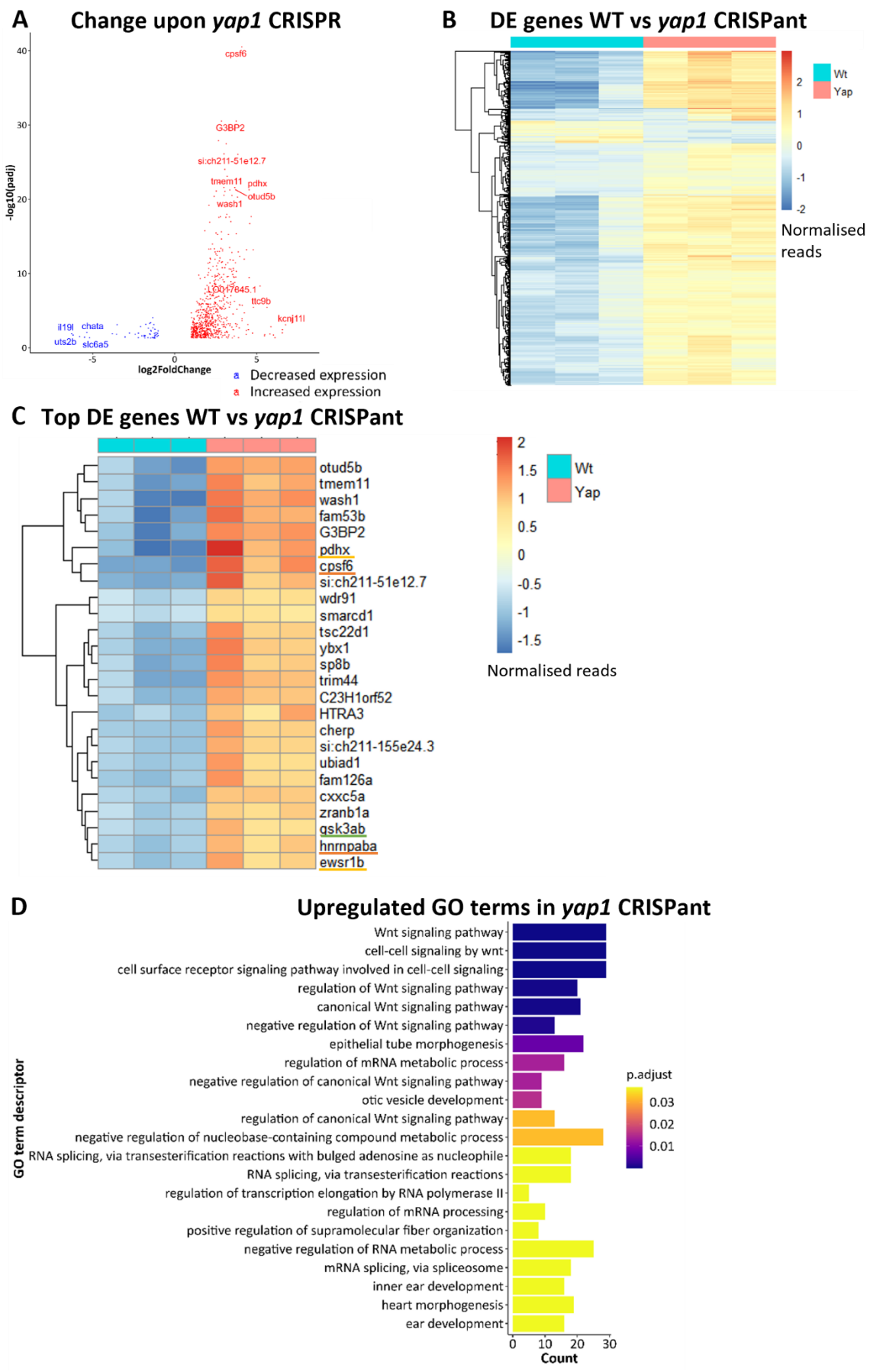
A
Change upon yap1 CRISPR
cpsf6
G3BP2
si:ch211-51e12.7
tmem11
pdhx
otud5b
wash1
LOC417645.1
ttc9b
kcnj11l
il19l
chata
uts2b
slc6a5
-log10(padj)
log2FoldChange
Decreased expression
Increased expression
B
DE genes WT vs yap1 CRISPant
Wt
Yap
Normalised reads
C
Top DE genes WT vs yap1 CRISPant
otud5b
tmem11
wash1
fam53b
G3BP2
pdhx
cpsf6
si:ch211-51e12.7
wdr91
smarcd1
tsc22d1
ybx1
sp8b
trim44
C23H1orf52
HTRA3
cherp
si:ch211-155e24.3
ubiad1
fam126a
cxxc5a
zranb1a
gsk3ab
hnrnpaba
ewsr1b
Wt
Yap
Normalised reads
D
Upregulated GO terms in yap1 CRISPant
Wnt signaling pathway
cell-cell signaling by wnt
cell surface receptor signaling pathway involved in cell-cell signaling
regulation of Wnt signaling pathway
canonical Wnt signaling pathway
negative regulation of Wnt signaling pathway
epithelial tube morphogenesis
regulation of mRNA metabolic process
negative regulation of canonical Wnt signaling pathway
otic vesicle development
regulation of canonical Wnt signaling pathway
negative regulation of nucleobase-containing compound metabolic process
RNA splicing, via transesterification reactions with bulged adenosine as nucleophile
RNA splicing, via transesterification reactions
regulation of transcription elongation by RNA polymerase II
regulation of mRNA processing
positive regulation of supramolecular fiber organization
negative regulation of RNA metabolic process
mRNA splicing, via spliceosome
inner ear development
heart morphogenesis
ear development
GO term descriptor
p.adjust
Count

E **Change upon *wwtr1* CRISPR**

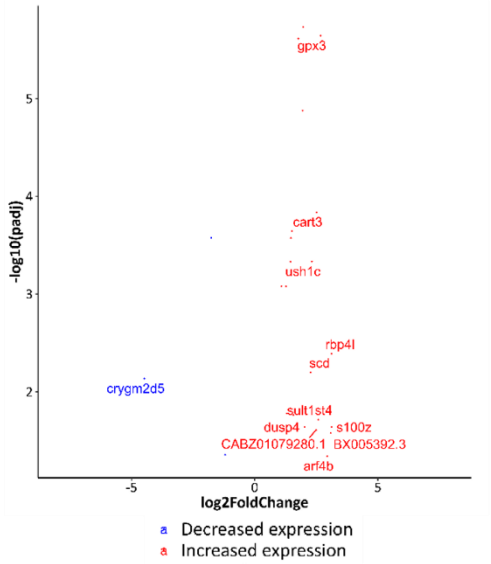

F **Top DE genes WT vs *wwtr1* CRISPant**

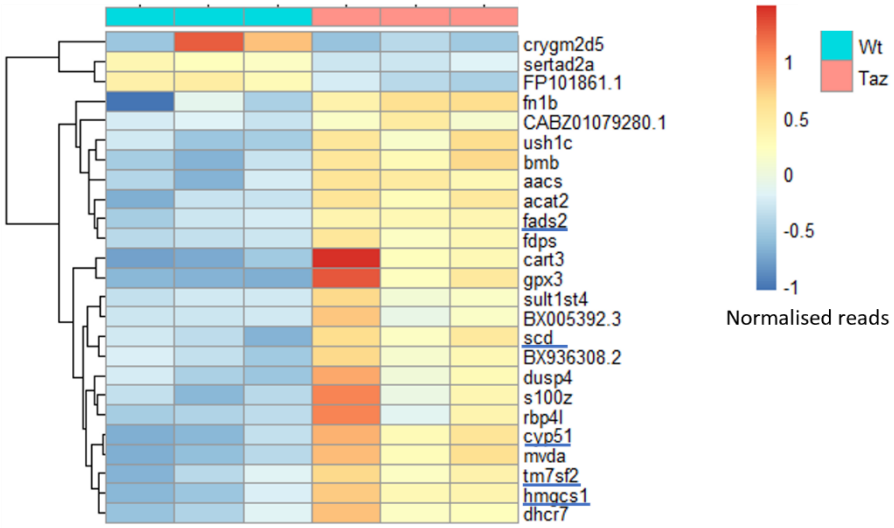

G **Upregulated GO terms in *wwtr1* CRISPant**

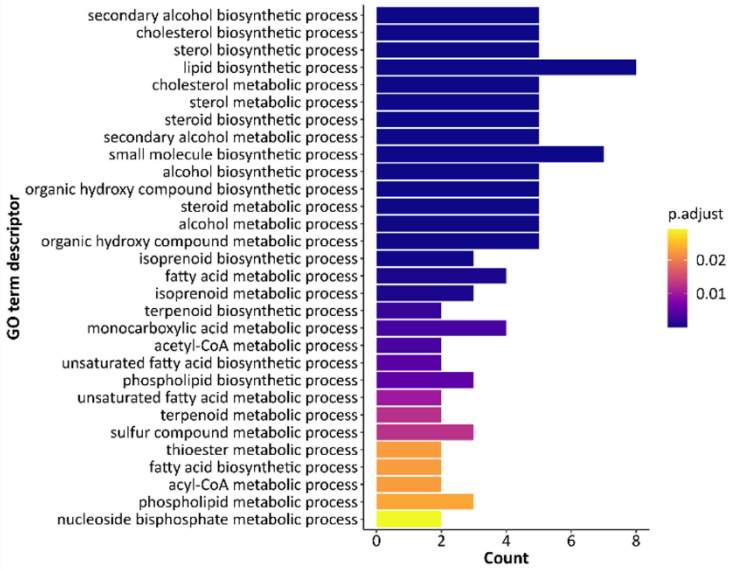

Figure 5.6: Transcriptomic changes in uninjured CRISPant embryos
(A) Volcano plot of significantly upregulated (red) and downregulated (blue) genes in uninjured yap1 CRISPant fish compared to WT. **(B)** Overview heatmap of all differentially expressed genes in uninjured *yap1* CRISPant fish compared to WT. **(C)** The top 25 most differentially expressed genes in uninjured *yap1* CRISPant fish compared to WT. Note all top DE genes are upregulated. **(D)** Upregulated GO terms in uninjured yap1 CRISPant fish compared to WT. Terms included those involved in Wnt signalling. **(E)** Volcano plot of significantly upregulated (red) and downregulated (blue) genes in uninjured *wwtr1* CRISPant fish compared to WT. **(F)** The top 25 most differentially expressed genes in uninjured *wwtr1* CRISPant fish compared to WT. **(G)** Upregulated GO terms in uninjured *wwtr1* CRISPant fish compared to WT. Terms included those involved in metabolism and biosynthesis.
Each column in B, C, + F denotes an independent biological replicate of 50 pooled larvae samples. GO=gene ontology; DE=differentially expressed. Cutoff for volcano plots in A and E is p(adj)<0.05 and log2FoldChange>1 or <-1. Colour of GO term analysis (D+G) bars denotes significance (p.adjust). Underline colour in heatmap genes (C+F) represents genes associated with: orange=RNA processing; yellow=mitosis and cell growth; green=Wnt signalling; blue=lipid and fatty acid metabolism.

although the injured *yap1* CRISPant samples were more heterogeneous than uninjured samples (Figure 5.7B+C). GO term analysis also showed fewer altered processes, with low count values reflecting further similarities between WT and *yap1* CRISPants (Figure 5.7D). Many of the altered processes included metabolic and biosynthetic processes, some of which were reflected in the top most DE genes (Figure 5.7C), such as an increase in *scd*, which is associated with lipid metabolism and fat deposition[309].

Results from comparing injured WT and *wwtr1* CRISPants are shown in Figure 5.7E-H. A similar transcriptomic pattern was seen (Figure 5.7E+F) as in *yap1* CRISPants (Figure 5.7A), namely a trend towards an increase in expression. However, there was more change than uninjured *wwtr1* CRISPants (Figure 5.6E), suggesting a specific defect in the *wwtr1* CRISPant transcriptional response to injury. This pattern was consistent between samples (Figure 5.7F+G). Top most altered genes included chemokines and cytokines[311,312] (*cxcl18b* and *ccl19a.2*) and those involved in lipid metabolism[306,309,310,313–315] (including *sqlea*, *dhcr7*, *fads2*, *scd*, *hmgcra*, and *tm7sf2*, many of which were also altered in uninjured *wwtr1* CRISPants) (Figure 5.7G). This was reflected in the GO term analysis (Figure 5.7H), which showed changes in a range of metabolic and biosynthetic processes, similar to that seen in uninjured fish, and immune cell migration. This suggests that the *wwtr1* CRISPant severe tail fin defect may result from immune cell dysfunction or metabolic dysfunction. Immune response and immune cell function in CRISPants is explored in more detail in sections 5.9 to 5.12 below.

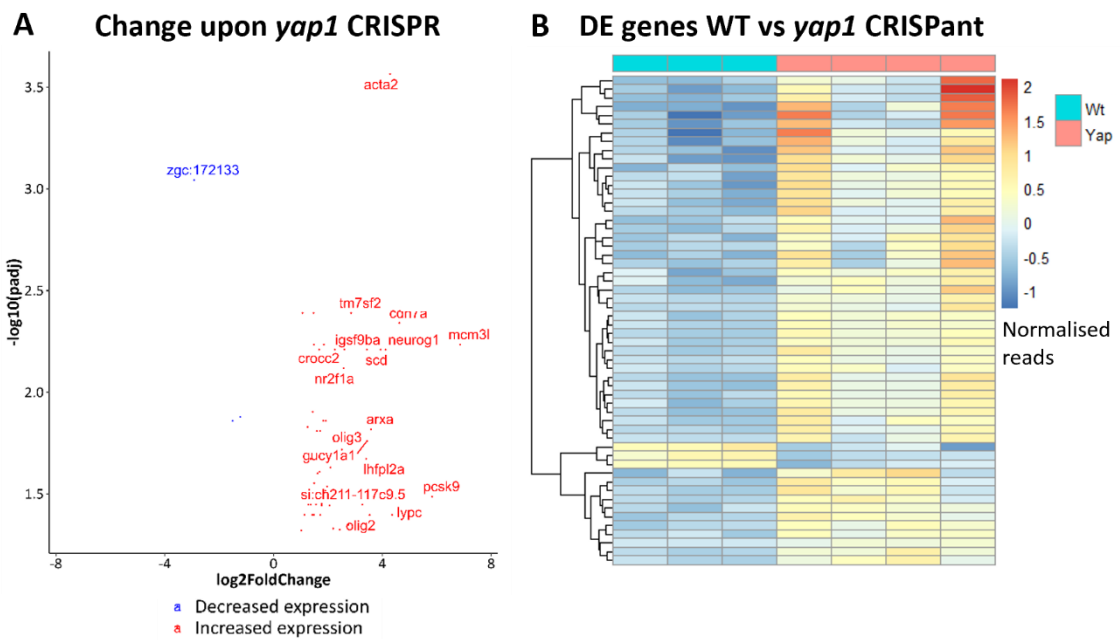
A
Change upon yap1 CRISPR
acta2
zgc:172133
tm7sf2
igsf9ba
neurog1
mcm3l
crocc2
scd
nr2f1a
arxa
olig3
gucy1a1
lhfpl2a
si:ch211-117c9.5
pcsk9
lypc
olig2
-log10(padj)
log2FoldChange
Decreased expression
Increased expression
B
DE genes WT vs yap1 CRISPant
Wt
Yap
Normalised reads

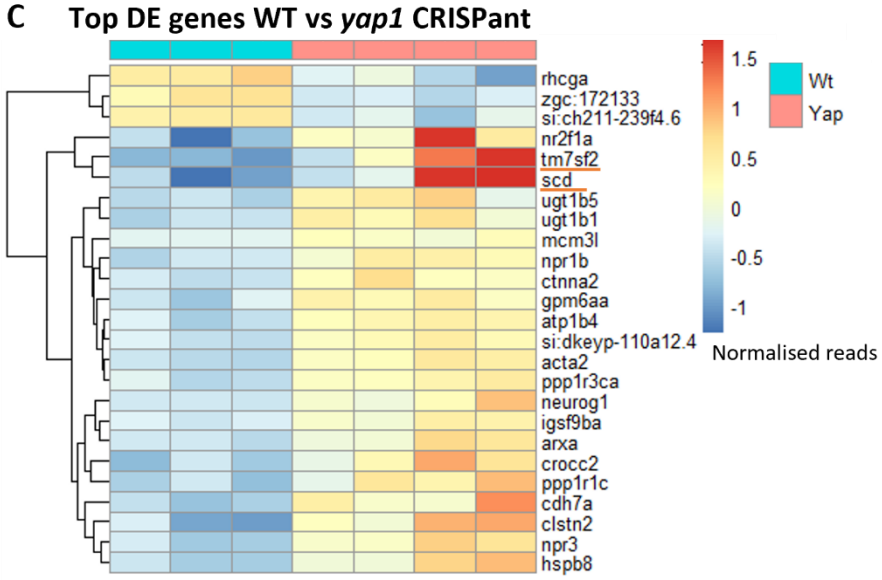
C
Top DE genes WT vs yap1 CRISPant
rhcga
zgc:172133
si:ch211-239f4.6
nr2f1a
tm7sf2
scd
ugt1b5
ugt1b1
mcm3l
npr1b
ctnna2
gpm6aa
atp1b4
si:dkeyp-110a12.4
acta2
ppp1r3ca
neurog1
igsf9ba
arxa
crocc2
ppp1r1c
cdh7a
clstn2
npr3
hspb8
Wt
Yap
Normalised reads

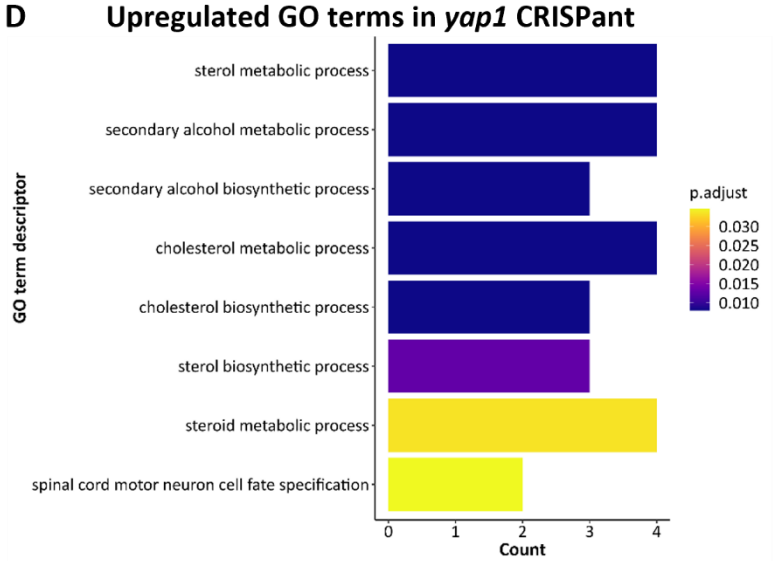
D
Upregulated GO terms in yap1 CRISPant
sterol metabolic process
secondary alcohol metabolic process
secondary alcohol biosynthetic process
cholesterol metabolic process
cholesterol biosynthetic process
sterol biosynthetic process
steroid metabolic process
spinal cord motor neuron cell fate specification
GO term descriptor
Count
p.adjust

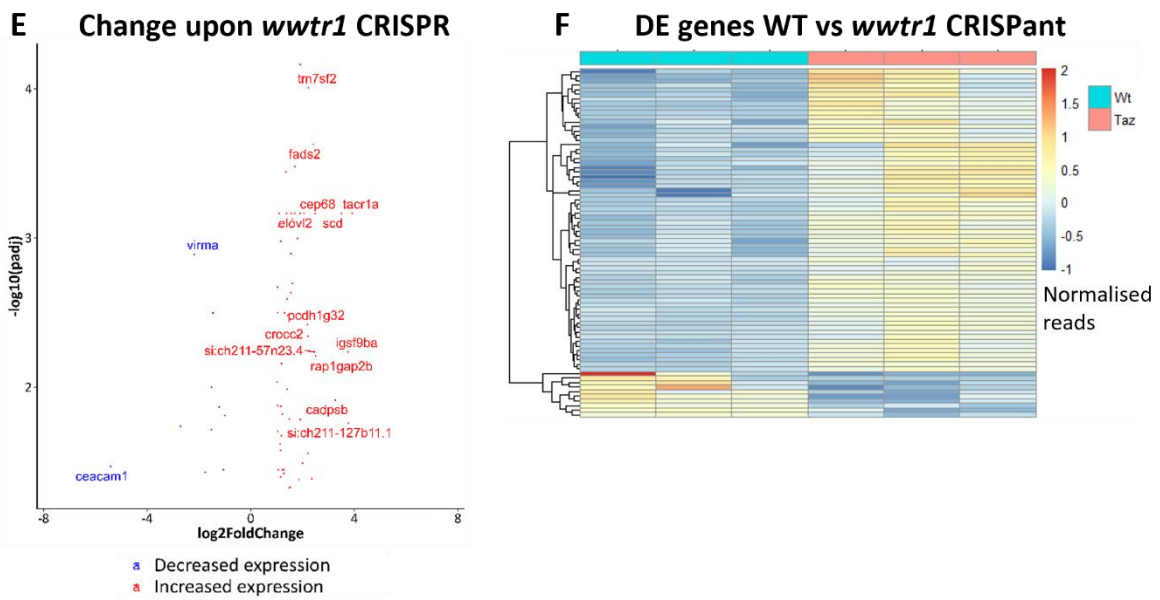
E
Change upon wwtr1 CRISPR
tm7sf2
fads2
cep68
tacr1a
elovl2
scd
virma
pcdh1g32
crocc2
si:ch211-57n23.4
igsf9ba
rap1gap2b
cadpsb
si:ch211-127b11.1
ceacam1
-log10(padj)
log2FoldChange
Decreased expression
Increased expression
F
DE genes WT vs wwtr1 CRISPant
Wt
Taz
Normalised reads

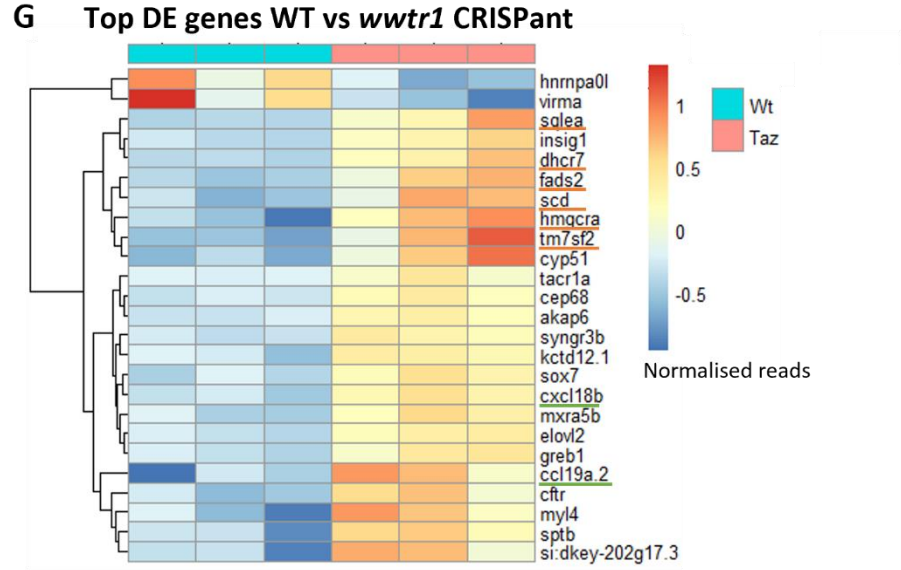
G
Top DE genes WT vs wwtr1 CRISPant
hnrnpa0l
virma
sqlea
insig1
dhcr7
fads2
scd
hmgcra
tm7sf2
cyp51
tacr1a
cep68
akap6
syngr3b
kctd12.1
sox7
cxcl18b
mxra5b
elovl2
greb1
ccl19a.2
cftr
myl4
sptb
si:dkey-202g17.3
Wt
Taz
Normalised reads

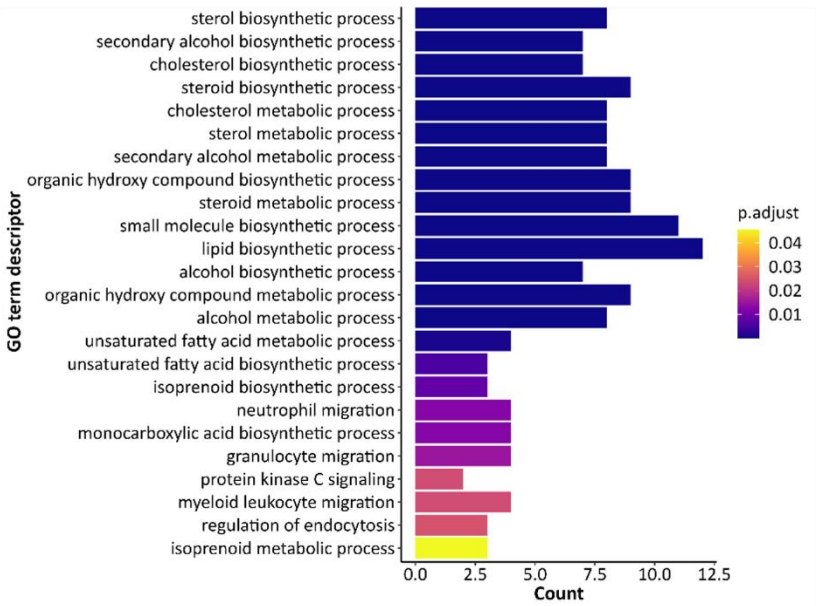
H
Upregulated GO terms in wwtr1 CRISPant
sterol biosynthetic process
secondary alcohol biosynthetic process
cholesterol biosynthetic process
steroid biosynthetic process
cholesterol metabolic process
sterol metabolic process
secondary alcohol metabolic process
organic hydroxy compound biosynthetic process
steroid metabolic process
small molecule biosynthetic process
lipid biosynthetic process
alcohol biosynthetic process
organic hydroxy compound metabolic process
alcohol metabolic process
unsaturated fatty acid metabolic process
unsaturated fatty acid biosynthetic process
isoprenoid biosynthetic process
neutrophil migration
monocarboxylic acid biosynthetic process
granulocyte migration
protein kinase C signaling
myeloid leukocyte migration
regulation of endocytosis
isoprenoid metabolic process
GO term descriptor
Count
p.adjust

Figure 5.7: Transcriptomic changes in CRISPant embryos following severe tail fin injury
(A) Volcano plot of significantly upregulated (red) and downregulated (blue) genes in injured *yap1* CRISPant fish compared to injured WT. **(B)** Overview heatmap of all differentially expressed genes in injured *yap1* CRISPant fish compared to injured WT. **(C)** The top 25 most differentially expressed genes in injured *yap1* CRISPant fish compared to WT. **(D)** Upregulated GO terms in injured *yap1* CRISPant fish compared to injured WT. Terms included those involved in metabolism and biosynthesis. **(E)** Volcano plot of significantly upregulated (red) and downregulated (blue) genes in injured *wwtr1* CRISPant fish compared to injured WT. **(F)** Overview heatmap of all differentially expressed genes in injured *wwtr1* CRISPant fish compared to injured WT. **(G)** The top 25 most differentially expressed genes in injured *wwtr1* CRISPant fish compared to injured WT. **(H)** Upregulated GO terms in uninjured *wwtr1* CRISPant fish compared to injured WT. Terms included those involved in metabolism and biosynthesis and immune cell migration.
Each column in B, C, F, + G denotes an independent biological replicate of 50 pooled larvae samples. GO=gene ontology; DE=differentially expressed. Cutoff for volcano plots in A and E is p(adj)<0.05 and log2FoldChange>1 or <-1. Colour of GO term analysis (D+G) bars denotes significance (p.adjust). Underline colour in heatmap genes (C+F) represents genes associated with: orange=lipid metabolism; green=chemokines and cytokines.

5.3.5 Direct comparison of genotypes upon injury

The above analyses of gene expression changes were unable to directly compare, for example, the differences between the change in transcriptome upon injury in WT and *yap1* CRISPants. The log2 fold change values of the significantly altered genes from DE analysis after injury (as performed in Figure 5.7) was therefore obtained for each genotype and directly plotted against each other (Figure 5.8). Genes that were more than 2 log2 fold change (i.e. a total fold change of 4) higher or lower than the same gene in the other genotype were highlighted as being significantly altered, or if they showed the opposite trend – i.e. an increase in one genotype but a decrease in the other (log2 fold change <-1 in one genotype but >1 in the other, padj <0.05). The resulting genes were then categorised as one of the following (colours in brackets denote the colours used in Figure 5.8): decreased more in WT fish (red), decreased more in CRISPant (orange), increased in WT but decreased in CRISPant (yellow), increased in CRISPant but decreased in WT (green), increased more in WT (blue), and increased more in CRISPant (purple). The graphs for *yap1* CRISPants and *wwtr1* CRISPants are shown in Figure 5.8A and B respectively.

Genes that showed opposite expression patterns were of particular interest. For analysis of *yap1* CRISPants, this included genes that were increased in *yap1* CRISPants but decreased in WT and vice versa (Figure 5.8A). Genes that were increased in *yap1* CRISPants but decreased in WT were *atp1b4*, *myom2a*, and *mettl7a*. These genes have no clear link in function. *atp1b4*

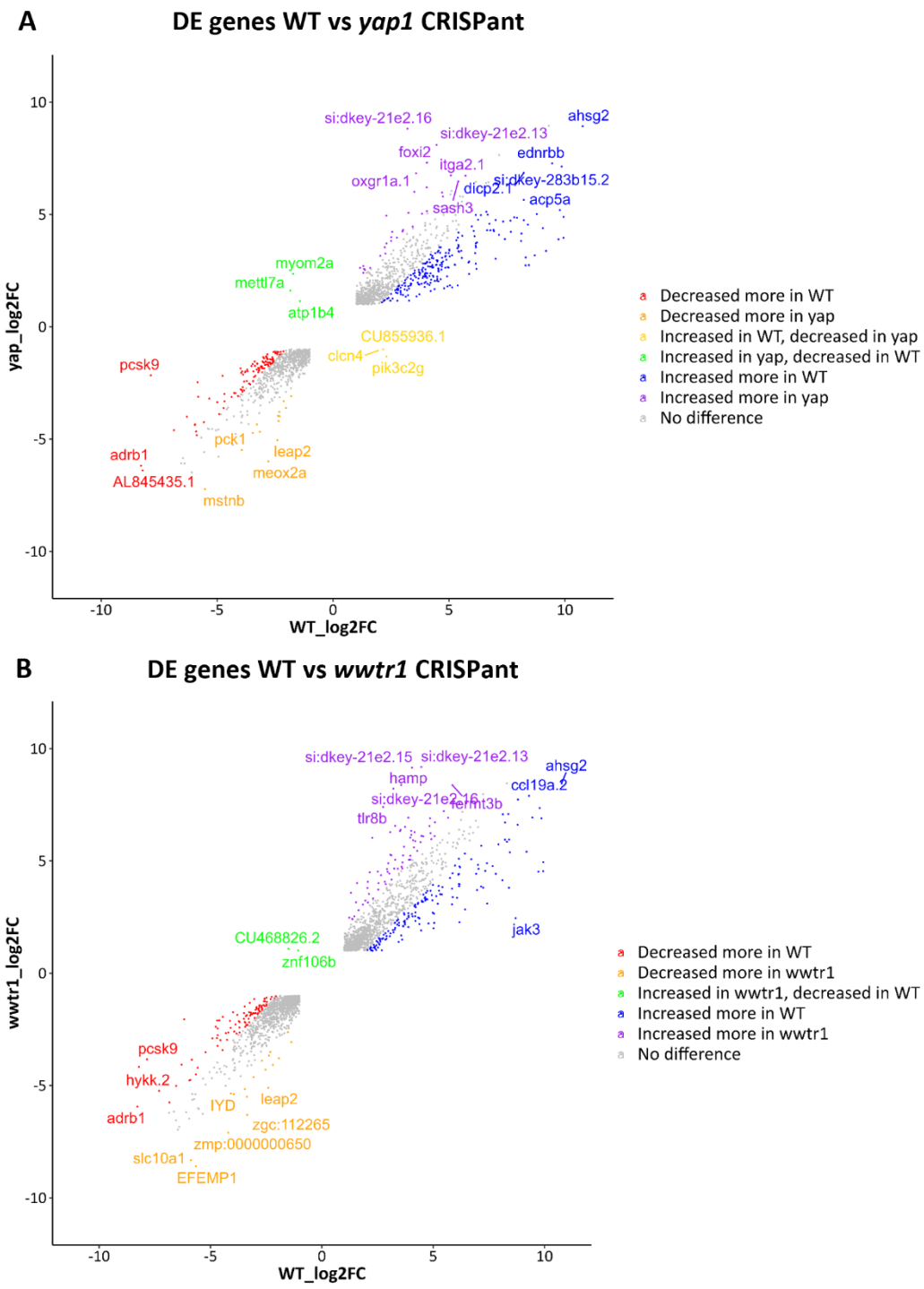

Figure 5.8: Comparison of differentially expressed genes after injury between WT and CRISPants

(A) Comparison of DE genes after injury between WT and *yap1* CRISPants. **(B)** Comparison of DE genes after injury between WT and *wwtr1* CRISPants.

DE=differentially expressed. Red=genes decreased more in WT relative to CRISPant; orange=genes decreased more in CRISPant; yellow=genes increased in WT but decreased in CRISPant; green=genes decreased in WT but increased in CRISPant; blue=genes increased more in WT; purple=genes increased more in CRISPant. Cut off for change upon injury is p(adj)<0.05 and log2FoldChange>1 or <-1. Cut off for change between genotypes is a difference between genotype of more than 2 log2FoldChange.

is associated with potassium and sodium ion transport[316], *myom2a* is linked to muscle development and contraction in humans[317], and *mettl7a* (*tmt1a.1*) is associated with methyltransferase activity[318]. Genes that were increased in WT but decreased in *yap1* CRISPants were similarly disparate. *clcn4* is linked to voltage-gated chloride channel activity[319,320], *pik3c2g* is associated with phosphatidylinositol signalling[321], and *vwa5a* (CU855936.1) has an unknown function, but is a member of a family of von Willebrand factors, which, in humans, has been linked to platelet aggregation[322]. *wwtr1* CRISPants and WT fish also had genes with opposing expression patterns (Figure 5.8B). Genes increased in *wwtr1* CRISPants but decreased in WT are again unrelated. *ano2b* (CU468826.2) is associated with transmembrane chloride transport[323] whilst *znf106b* has RNA binding activity[324]. It is currently unclear what the functional significance of these alterations are. Further analysis of the DE genes in these graphs was limited by time constraints in the project.

Some similarities can be seen between the two graphs in Figure 5.8. For example, *ednrbb* and *insl5b* are increased more in WT fish relative to both CRISPants. In order to compare the two CRISPants more comprehensively, this data was further processed. Lists of genes that were dramatically altered (more than 3 log2 fold change) between genotypes and those with opposite expression patterns (more than 1 log2 fold change) were merged and assigned new categories whether they were altered in the same or different manner in *yap1* or *wwtr1* CRISPants (e.g. “both decreased more WT” and “decreased more in *yap1* CRISPants only). The resulting data is shown in Table 5.1 (unmapped or undefined transcripts were removed from the table). Of note, although there were no genes increased or decreased in both CRISPants indicating differing *yap1*/*wwtr1* function, there were genes that were increased and decreased more in WT fish compared to both CRISPants. These were *pcsk9* (decreased), and increased genes *aqp8b*, *insl5b*, *jak3*, *runx1*, and *sla1a*, which are again seemingly unrelated (see Table 5.1 for a summary of their functions). Of interest, many genes were associated with immune cell function, including *c1qb* and *c4b* of the complement pathway[325] and response to chemokines (*ccl35.1*)[326]. The majority of these had increased expression after injury, as might be expected, and increased more in WT fish. Most were also increased more in WT compared to one CRISPant only, suggesting component-specific defects in the immune response. This is investigated in more detail in 5.9 to 5.12 below.

Table 5.1: Differentially expressed genes when compared between WT and CRISPants

Table showing a list of differentially expressed genes after injury, their predicted or confirmed function, and their human orthologs. Gene list was obtained as described in 5.3.5, and grouped according to their comparative expression: either if increased in one genotype but decreased in another or if the log2 fold change difference between genotypes is more than 3 (i.e. 8-fold).

Comparison	Gene name	Associated with: (from zfin.org/ensembl.org)	Human ortholog
Increased in *yap1* CRISPants and decreased in WT, no change in *wwtr1* CRISPants	*atp1b4*	DNA-templated transcription, potassium ion transport and sodium ion transport[327]	*ATP1B4*
	mettl7a (tmt1a.1)	Methyltransferase activity[328]	*METTL7A*
	myom2a	Muscle development, muscle contraction, and sarcomere organisation[329,330]	*MYOM2*
Increased in *wwtr1* CRISPants and decreased in WT, no change in *yap1* CRISPants	*ano2b*	Calcium activated chloride channel activity and chloride transmembrane transport[331]	*ANO2*
	znf106b	RNA binding activity[332]	*ZNF106*
Increased in WT and decreased in *yap1* CRISPants, no change in *wwtr1* CRISPants	*clcn4*	Voltage-gated chloride channel activity[333]	*CLCN4*
	pik3c2g	Kinase activity, phosphatidylinositol binding activity, phosphatidylinositol phosphate biosynthetic process, and phosphatidylinositol-mediated signalling[334]	*PIK3C2G*
	vwa5a	Platelet adhesion and aggregation[322,335]	*VWA5A*
Both increased more in WT	*aqp8b*	Water transmembrane transporter activity[336]	*AQP8*
	insl5b	G protein-coupled receptor binding activity[337]	*INSL5*
	jak3	Growth hormone receptor binding activity, non-membrane spanning protein tyrosine kinase activity, T cell differentiation in thymus, and natural killer cell differentiation[338]	*JAK3*
	runx1	Cardiac muscle tissue regeneration, positive regulation of collagen biosynthesis, connective tissue replacement, endothelial to haematopoietic transition, and haematopoiesis[339]	*RUNX1*
	sla1a	Epidermal growth factor receptor binding activity, phosphotyrosine residue binding activity, MAPK cascade, and COP9 signalosome[340]	*SLA*
Both decreased more in WT	*pcsk9*	Serine-type endopeptidase activity, central nervous system development, and neurogenesis[341]	*PCSK9*
Increased more in WT relative to *yap1* CRISPants	*abcc12*	ATPase-coupled transmembrane transporter activity and cholangiocyte apoptotic process[342]	Several, including *ABCC12*

	btr29	Zinc ion binding activity[343]	*TRIM41*
	c1qb	Complement activation, classical pathway[344]	*C1QB*
	c4b	Endopeptidase inhibitor activity and complement activation[345]	*C4B*
	cnr2	Cannabinoid receptor activity, haematopoietic stem cell differentiation, haematopoietic stem cell migration to bone marrow, and methionine metabolic process[346]	*CNR2*
	f5	Copper ion binding activity, haemostasis, and bacteria response[347]	*F5*
	ifitm1	Interferon signalling, immune system function, and innate immune response[348,349]	*IFITM1/2/3*
	igfbp6b	Fibronectin binding activity, insulin-like growth factor I and II binding activity, and insulin-like growth factor receptor signalling pathway[350]	*IGFBP6*
	mafbb	Myeloid leukocyte differentiation and skeletal system development[351]	*MAFB*
	nitr2b	Bacteria response[352]	*SIRPB2*
	rasal3	GTPase activator activity and signal transduction[353]	*RASAL3*
	rgs14a	GTPase activator activity and germ cell migration[354]	*RGS141*
	socs3b	1-phosphatidylinositol-3-kinase regulator activity, brain development, and phosphatidylinositol 3-kinase complex[355]	*SOCS3*
Decreased more in WT relative to *yap1* CRISPants	*tlr7*	Inflammatory response and pattern recognition receptor signalling pathway[356]	*FRMPD4*
Increased more in WT relative to *wwtr1* CRISPants	*ccl35.1*	CCR chemokine receptor binding activity and chemokine activity, cellular response to cytokines, leukocyte chemotaxis, positive regulation of ERK1 and ERK2 cascade, and virus response[357]	Several, including *CCL3*, *CCL3L1*, and *CCL3L3*
	gpr132b	G protein-coupled receptor activity and acidic pH response[358]	*GPR132*
	grna.1	Lysosome function, cell migration, and immune cell activation[359,360]	*GRN*
	lepb	Hormone activity, glucose homeostasis, regulation of glucose metabolism, and response to starvation[361]	*LEP*
	mxd	GTPase activity, microtubule binding activity, and virus response[362]	*MX2*
	ocstamp	Response to Tnf, osteoclast differentiation, and proliferation[363,364]	*OCSTAMP*

	odam	Protein phosphorylation, actin cytoskeleton organisation, odontogenesis, positive regulation of epithelial cell proliferation involved in wound healing, inflammatory response, and wound healing[365,366]	*ODAM*
Decreased more in WT relative to *wwtr1* CRISPants	*brinp3a.1*	Response to retinoic acid, negative regulation of mitotic cell cycle, and nervous system development[367]	*BRINP3*
Increased more in *yap1* CRISPants only	*foxi2*	Camera-type eye development[368]	*FOX13*
	oxgr1a.1	G protein-coupled receptor signalling pathway[369]	*OXGR1*
Decreased more in *yap1* CRISPants only	*meox2a*	Regulation of transcription by RNA polymerase II and somite development[370]	*MEOX2*
Increased more in *wwtr1* CRISPants	*cyth4a*	Guanyl-nucleotide exchange factor activity and epiboly formation in gastrulation[371]	*CYTH4*
	hamp	Lipopolysaccharide binding activity, lipoteichoic acid binding activity, peptidoglycan binding activity, response to progesterone, bacteria response, and multicellular organismal-level iron ion homeostasis[372]	*HAMP*
	tlr8b	Pattern recognition receptor activity, I-kappaB kinase/NF-kappaB signalling, positive regulation of interleukin-6 production, toll-like receptor signalling pathway, inflammatory response, and innate immune response[373]	*TLR8*
	tnfsf14	Tumour necrosis factor receptor binding activity and immune response[374]	*TNFSF14*
	vwa11	Platelet adhesion and aggregation [322,375]	None

In conclusion, it was challenging to determine specific expression patterns by comparing DE genes, as many genes grouped in this manner did not appear to have a clear functional association. However, this analysis does show component-specific transcriptomic changes as many genes were only altered in one CRISPant over the other. One point of interest was the increased immune gene expression in WT fish compared to CRISPants, and that there were CRISPant-specific alterations in expression that warrant further investigation.

5.3.6 Changes in the Hippo signalling pathway upon mutagenesis and injury

Surprisingly, none of the GO term or top DE genes analyses indicated a change in Hippo pathway signalling, despite the mutagenesis of the core effectors of the pathway and its important role in regeneration. To investigate this further, the differentially expressed gene dataset was filtered to only show Hippo pathway-associated genes as described in 2.18.3. The resulting volcano plots are shown in Figure 5.9. Upon injury in WT fish, we might expect to see an increase in Yap1/Taz target gene expression and a possible decrease in upstream kinases that would denote an increase in Yap1/Taz activity, as what was broadly seen after mild tail fin injury (Figure 5.3F). However, a more complex picture became apparent after severe tail fin injury (Figure 5.9A). Although there was an increase in the expression of target genes *ankrd1b*, *nuak2*, and *myofl*, there was also a decrease in other target genes[230] (*nt5e*, *amotl2a*, *ccn2a*, *rbms3*, *asap1a*/*asap1b*, and *crim1*). Similarly, as well as a decrease in the upstream kinases *lats2* and *map4k2*/*map4k3a*, there was an increase in others (*stk25a*, *rhoab*/*rhoac*, and CABZ010998833.1 (*MAP4K1* orthologue)). The core DNA-binding transcriptional effectors *tead3a* and *tead1b* were also increased and decreased respectively. Notably, there were no significant changes in *yap1* or *wwtr1* expression. Overall, this could suggest highly specific roles of Yap1/Taz target genes or upstream kinases, or that changes are mostly found outside of the Hippo pathway upon injury. It is also worth highlighting that only some parts of the kinase cascade are regularly transcriptionally regulated[184,376].

A similar analysis was performed in *yap1* CRISPants (Figure 5.9B). Far fewer genes showed significant changes than seen in WT fish, but a similar pattern of both increases (*ankrd1b*, *myofl*, and *cavin1a*/*cavin1b*) and decreases (*amotl2a*, *nt5e*, and *crim1*) in target gene expression was seen. All of these were also found in WT fish (Figure 5.9A), except for an increase in *cavin1a*/*cavin1b* in *yap1* CRISPants. This reduction in number of genes with significant changes could suggest that the absence of Yap1 prevents some of the transcriptional changes taking place in WT fish upon injury, which may imply that Yap1 does mediate these changes. The complex transcription pattern could therefore be a result of highly specific roles of Hippo pathway components, particularly for upstream kinases, and indicate the importance of Yap1 in this process.

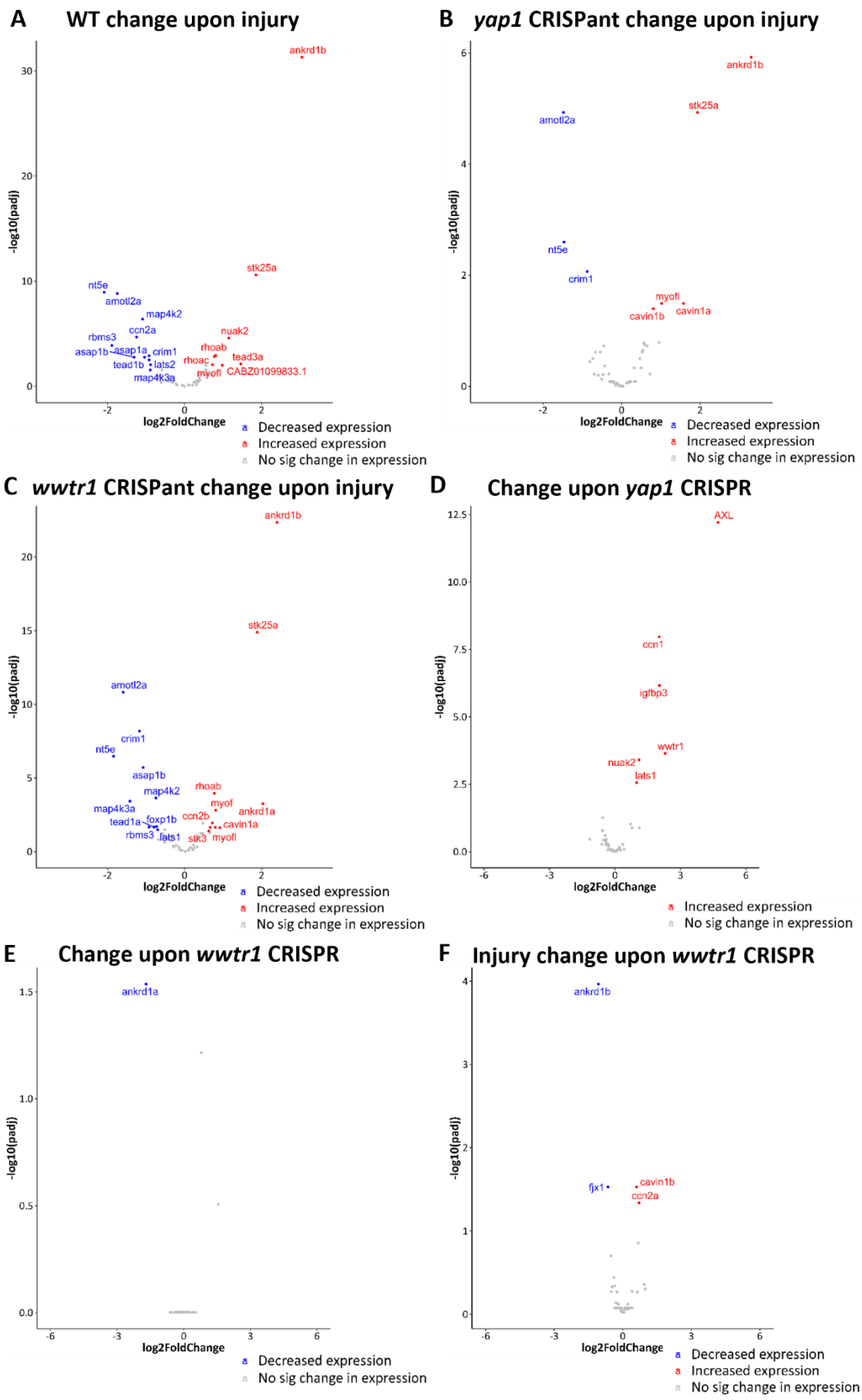
A
WT change upon injury
ankrd1b
stk25a
nt5e
amotl2a
map4k2
ccn2a
rbms3
asap1b
asap1a
crim1
tead1b
lats2
rhoac
rhoab
nuak2
tead3a
myofl
CABZ01099833.1
map4k3a
-log10(padj)
log2FoldChange
Decreased expression
Increased expression
No sig change in expression
B
yap1 CRISPant change upon injury
ankrd1b
stk25a
amotl2a
nt5e
crim1
myofl
cavin1b
cavin1a
-log10(padj)
log2FoldChange
Decreased expression
Increased expression
No sig change in expression
C
wwtr1 CRISPant change upon injury
ankrd1b
stk25a
amotl2a
crim1
nt5e
asap1b
map4k2
rhoab
map4k3a
myof
ankrd1a
tead1a
foxp1b
ccn2b
cavin1a
rbms3
lats1
stk3
myofl
-log10(padj)
log2FoldChange
Decreased expression
Increased expression
No sig change in expression
D
Change upon yap1 CRISPR
AXL
ccn1
igfbp3
wwtr1
nuak2
lats1
-log10(padj)
log2FoldChange
Increased expression
No sig change in expression
E
Change upon wwtr1 CRISPR
ankrd1a
-log10(padj)
log2FoldChange
Decreased expression
No sig change in expression
F
Injury change upon wwtr1 CRISPR
ankrd1b
fjx1
cavin1b
ccn2a
-log10(padj)
log2FoldChange
Decreased expression
Increased expression
No sig change in expression

Figure 5.9: Alterations in Hippo gene signature after mutagenesis and after severe tail fin injury

(A) Volcano plot of significantly upregulated (red) and downregulated (blue) Hippo pathway-associated genes in WT fish after severe tail fin injury. **(B)** Volcano plot of significantly upregulated (red) and downregulated (blue) Hippo pathway-associated genes in *yap1* CRISPants after severe tail fin injury. **(C)** Volcano plot of significantly upregulated (red) and downregulated (blue) Hippo pathway-associated genes in *wwtr1* CRISPants after severe tail fin injury. **(D)** Volcano plot of significantly upregulated (red) Hippo pathway-associated genes in uninjured *yap1* CRISPants compared to WT fish. **(E)** Volcano plot of significantly downregulated (blue) Hippo pathway-associated genes in uninjured *wwtr1* CRISPants compared to WT fish. **(F)** Volcano plot of significantly upregulated (red) and downregulated (blue) Hippo pathway-associated genes in injured *wwtr1* CRISPants compared to WT fish.

Cutoff p(adj)<0.05 and log2FoldChange>0.6 or <-0.6.

---

wwtr1 CRISPants also showed a change in Hippo pathway-associated genes upon injury (Figure 5.9C). The pattern of expression was more similar to WT fish than *yap1* CRISPants, with both increases and decreases in upstream kinases and target genes. This suggests that Yap1 has more of an impact on the Hippo-associated transcriptome changes upon injury than Taz. In order to more directly compare this, CRISPants were compared to WT fish (Figure 5.9D-F). Investigation of uninjured CRISPants confirmed that Yap1 may have more of an impact on Hippo signalling than Taz. Whilst *yap1* CRISPants showed an increase in multiple genes from WT, including the target genes *ccn1*, *nuak2*, *igfbp3*, and *AXL* (Figure 5.9D), *wwtr1* CRISPants showed no change from WT apart from a decrease in the target gene *ankrd1a* (Figure 5.9E), suggesting a Taz-specific role in *ankrd1a* regulation and a Yap1-specific role in regulating others. Interestingly, neither of the CRISPants showed a change in the mRNA targeted by the injected CRISPR guide, suggesting that CRISPR mutagenesis does not alter mRNA levels to an level that is detectable by this method. This indicates a lack of nonsense-mediated decay of the mutant mRNA, but the formation of malformed protein instead. Contrary to RT-qPCR results, which used RNA isolated from whole fish at 24hpf (Figure 3.4M), *yap1* CRISPants showed increased *wwtr1* mRNA (Figure 5.9D), suggesting a level of compensation in the fin.

Analysis of Hippo pathway components after injury in each genotype was also performed. When comparing injured WT and *yap1* CRISPants there were no significantly altered genes (not shown), further supporting the PCA plot findings that *yap1* CRISPants become more similar to WT after injury (Figure 5.4A). Some minor changes were seen when comparing injured WT and *wwtr1* CRISPants (Figure 5.9F). This included an increase in the target

genes[29,230] *cavin1b* and *ccn2a* (*ctgfa*), and a decrease in the target genes *fjx1* and *ankrd1b*, suggesting a Taz-specific role in their regulation after injury.

In summary, after severe injury in WT fish, there was a larger alteration in Hippo pathway-associated gene expression compared to following mild injury. However, there was not a clear change in Hippo pathway signalling as target genes and upstream kinases were both significantly increased and decreased. This could suggest that severe tail fin injury has multiple effects at different levels of the Hippo pathway in different cell types, and that the Hippo pathway has many interconnected levels of regulation such as multiple feedback and feedforward loops or both an inhibitory and promoting-effect of Yap1/Taz on Hippo target genes[184,376]. The effects of *yap1* and *wwtr1* CRISPR mutagenesis on Hippo pathway signalling were similarly complex, with no clear change in expression that might indicate an obvious increase or decrease in Hippo pathway activity. It should be noted that the log2 fold change determined as notable was reduced (0.6 compared to 1) compared to other analyses as the overall changes were lower. This suggests that Hippo pathway components were expressed at generally lower levels than many other components of interest, which could underlie the lack of clear change observed.

5.3.7 Changes in the Wnt signalling pathway upon *yap1* mutagenesis

An interesting observation from this RNAseq data is the GO term increase in canonical Wnt signalling in uninjured *yap1* CRISPants compared to WT fish. In other model systems, the Hippo pathway, and in particular YAP1, has been associated strongly with the Wnt signalling pathway (reviewed in[377–379], for example). YAP1 has been reported to have both positive and negative effects on Wnt signalling, with nuclear YAP1 upregulating β-catenin expression, whilst cytoplasmic YAP1 suppresses β-catenin's activity[379]. In the adult tail fin after injury, Wnt/β-catenin signalling promotes osteoblast dedifferentiation via EMT[298]. *yap1* disruption resulted in the promotion of this Wnt signalling, which, alongside an inhibition of BMP signalling, led to the maintenance of a dedifferentiated osteoprogenitor cell pool and hence disrupted regeneration[247,380]. However, evidence in the larval tail fin suggests that there is no change in Wnt pathway activity during (mild) regeneration[381].

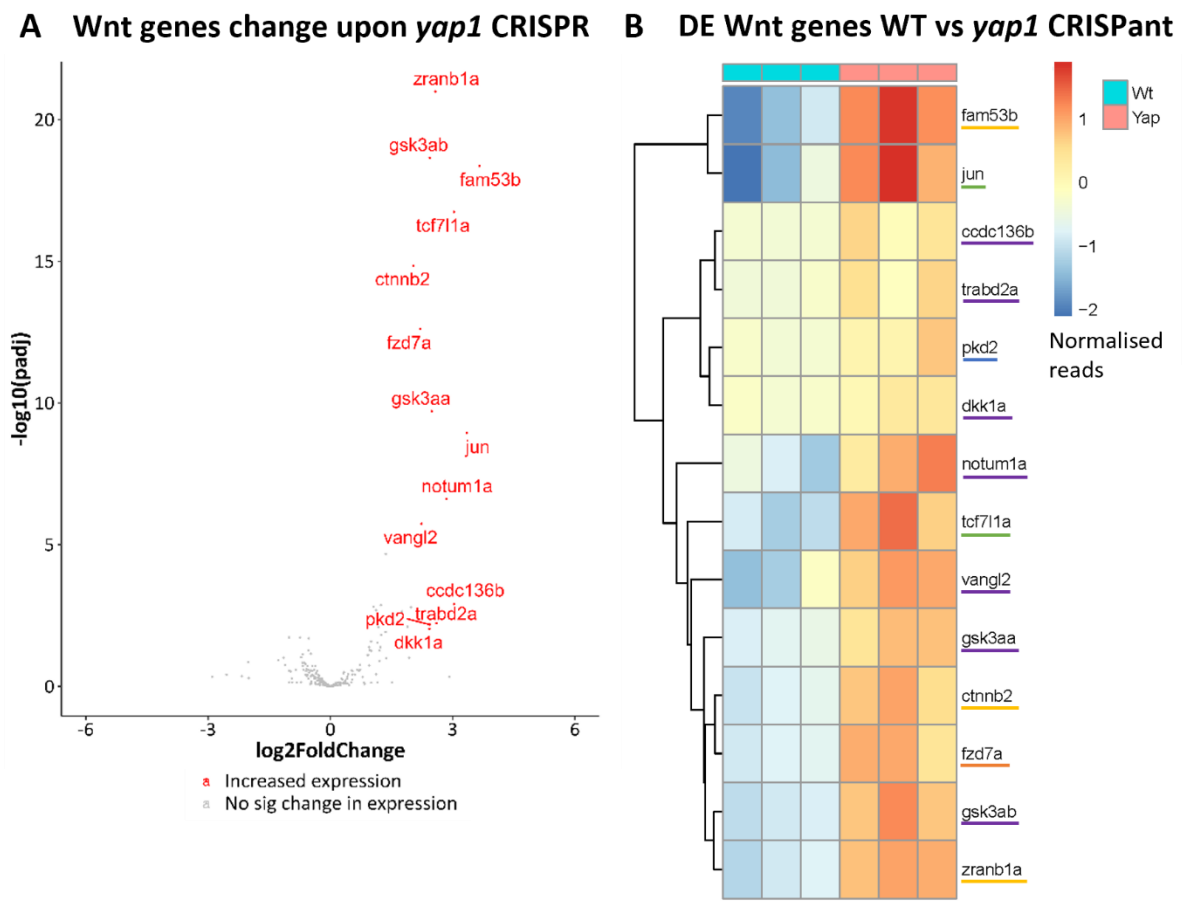

Figure 5.10: Wnt signalling is altered in uninjured *yap1* CRISPants
(A) Volcano plot of significantly upregulated (red) Wnt-associated genes in uninjured *yap1* CRISPant fish compared to WT. **(B)** Overview heatmap of all DE Wnt-associated genes in uninjured *yap1* CRISPant fish compared to WT. Underline colour represents Wnt genes with the function: orange=receptor; yellow=core components; green=transcription factors; blue=target gene; purple=negative regulator. Each column denotes an independent biological replicate of 50 pooled larvae samples.
DE=differentially expressed. Cutoff is p(adj)<0.05 and log2FoldChange>2 or <-2.

In order to investigate this interaction, a list of Wnt pathway-associated genes was obtained from the GO term GO0016055, and the list of DE genes was filtered for those genes only. Results are shown in Figure 5.10. This supports the earlier finding of an increase in Wnt pathway-associated genes. Many of these genes are linked to increased Wnt signalling, such as *ctnnb2*, which encodes the core component of the pathway β-catenin[382], *fzd7a*, which encodes a Frizzled receptor that typically activates the Wnt pathway[382], *fam53b*, which promotes β-catenin nuclear localisation[383], and the transcription factors *jun* and *tcf7l1a*[384,385]. However, there were also increases in genes associated with decreased Wnt signalling, such as *vangl2*[386], *dkk1a*[382,387], and *gsk3aa*/*gsk3ab*[305]. These results suggest that more

investigation is required to elucidate the effect of removing *yap1* on the Wnt pathway in the zebrafish.

5.4 *yap1* and *wwtr1* mRNA expression at baseline in the larval tail fin

Bulk RNA-sequencing was performed to determine transcriptional differences between regenerating tissue in *yap1* and *wwtr1* CRISPants. However, this technique does not contain spatial information of where in the tail fin these differences exist. To begin to resolve this, we used the novel multiplexed high-resolution imaging technique HCR RNA-FISH[388]. This technique utilises probes that are designed to bind to distinct mRNA targets. Amplifiers then bind to the probes to generate fluorescent signal. HCR RNA-FISH therefore bypasses issues from a lack of specific and consistent antibodies for zebrafish protein targets, and allows for multiplexed labelling of multiple targets per sample.

HCR labelling and imaging was performed as described in 2.16. Both *yap1* and *wwtr1* mRNA could be visualised in all conditions (Figure 5.11). During normal development at 96 and 120 hours post fertilisation (hpf), there was an overall widespread pattern of mRNA distribution. This supports the general role of the Hippo pathway in a range of homeostatic and developmental processes, such as cell growth and differentiation[389].

When quantified, there were no significant changes in *yap1* or *wwtr1* fluorescence following mutagenesis, except at 120hpf, where *yap1* CRISPants had increased *wwtr1* signal (Figure 5.11F). Interestingly, this is similar (although the timing is different) to the increase in *wwtr1* mRNA in *yap1* CRISPants as seen in the RNAseq analysis of uninjured fish (Figure 5.6D). The absence of change at baseline in CRISPants might suggest a lack of probe specificity, or an overall low level of expression that is not altered following mutagenesis. CRISPR mutagenesis also does not need to alter mRNA levels to be effective. Stable mutants generated from this CRISPR have lesions that induce multiple early stop codons that result in an absence of protein (see 4.2.1) but not necessarily mRNA.

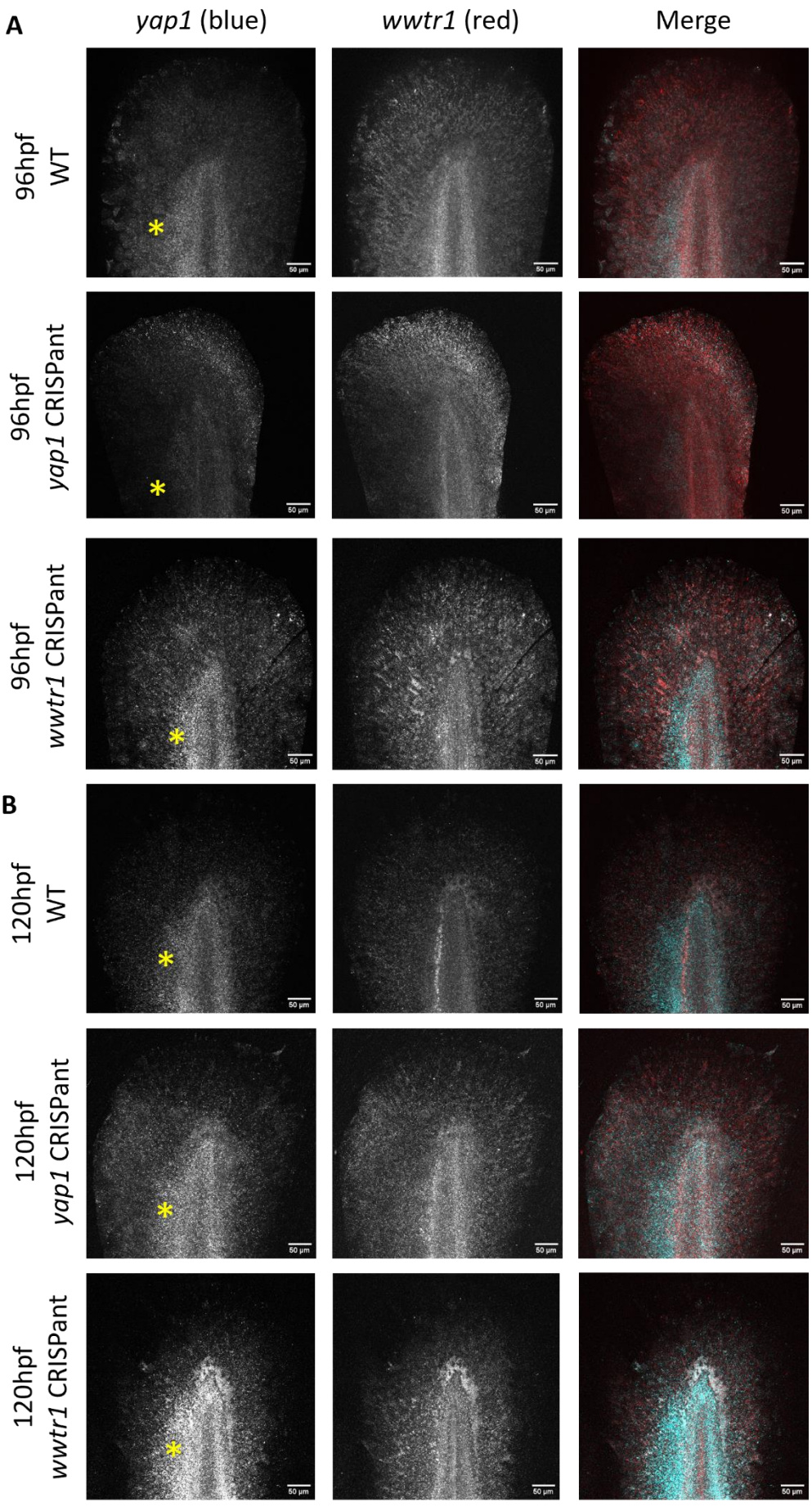
A
yap1 (blue)
wwtr1 (red)
Merge
96hpf WT
96hpf yap1 CRISPant
96hpf wwtr1 CRISPant
B
120hpf WT
120hpf yap1 CRISPant
120hpf wwtr1 CRISPant
50 µm

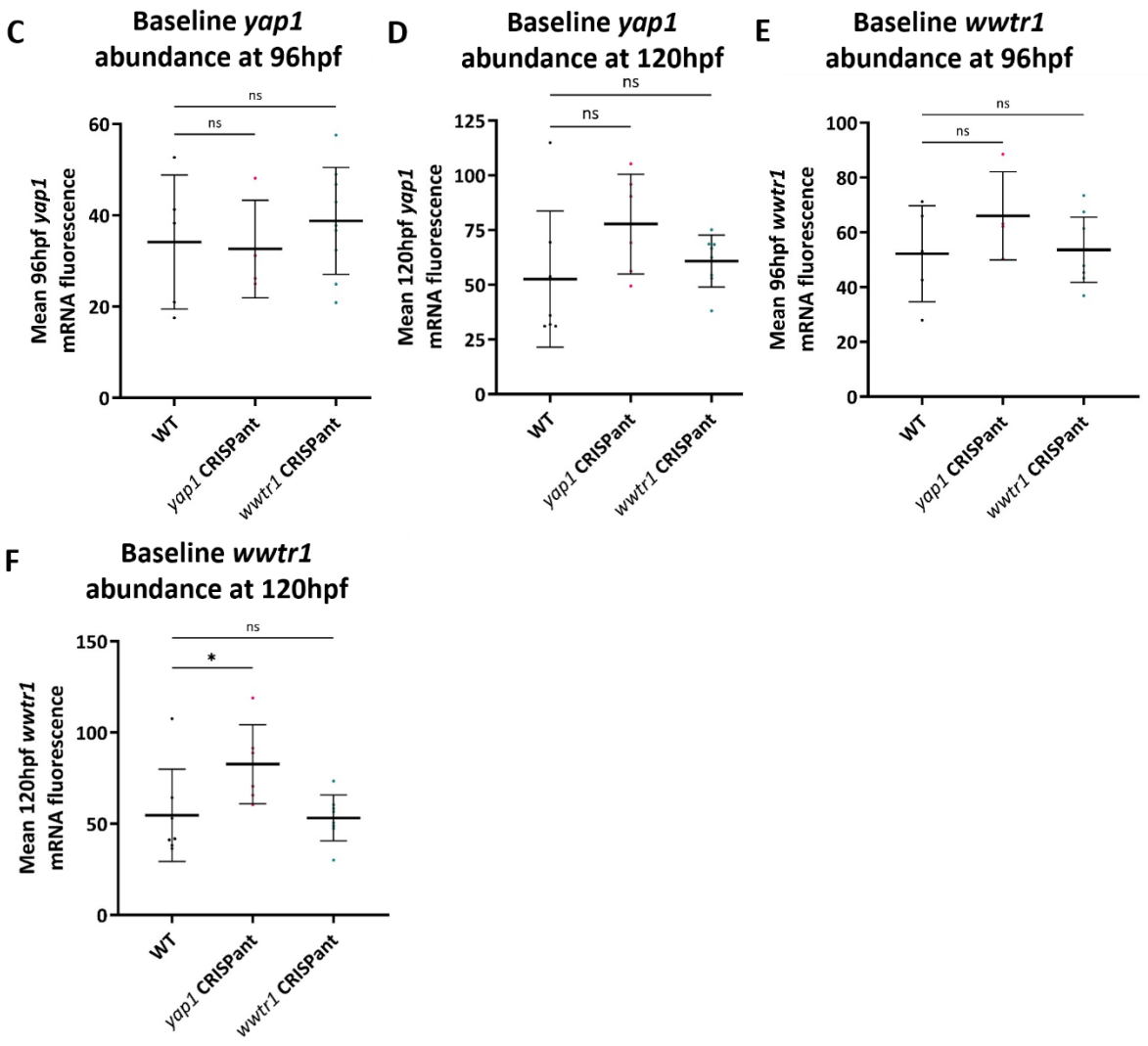

Figure 5.11: *yap1* and *wwtr1* CRISPR mutagenesis has limited impacts on *yap1* and *wwtr1* mRNA fluorescence during embryonic development

(A) Representative WT, *yap1* CRISPant, and *wwtr1* CRISPant images of the developing tail fin at 96 hours post fertilisation. Asterix denotes caudal fin bud. For merged image: cyan=*yap1*, red=*wwtr1*. **(B)** Representative WT, *yap1* CRISPant, and *wwtr1* CRISPant images of the developing tail fin at 120 hours post fertilisation. Asterix denotes caudal fin bud. For merged image: cyan=*yap1*, red=*wwtr1*. **(C)** Quantification of mean *yap1* fluorescence in the uninjured tail fin at 96hpf. No significant changes were observed upon *yap1* or *wwtr1* CRISPR mutagenesis. **(D)** Quantification of mean *yap1* fluorescence in the uninjured tail fin at 120hpf. No significant changes were observed upon *yap1* or *wwtr1* CRISPR mutagenesis. **(E)** Quantification of mean *wwtr1* fluorescence in the uninjured tail fin at 96hpf. No significant changes were observed upon *yap1* or *wwtr1* CRISPR mutagenesis. **(F)** Quantification of mean *wwtr1* fluorescence in the uninjured tail fin at 120hpf. *yap1* CRISPants had an increase in fluorescence. No significant changes were observed upon *wwtr1* CRISPR mutagenesis. Brightness and contrast have been altered for ease of viewing, with the same settings applied to each sample within each experiment. All samples are imaged at 20x. *yap1* and *wwtr1* are labelled. Each dot represents one fish. Results from at least one independent repeat. Significance calculated using one-way ANOVA for C and D, and Kruskal-Wallis test for the remainder, with multiple comparisons. Bars represent mean±SD. *p<0.05; ns=not significant.

One location with elevated *yap1* signal was the caudal fin bud (see asterix in Figure 5.11). This region becomes the adult tail fin[390], and so might be expected to have a high rate of cell proliferation. The Hippo pathway has a well-established role in cell proliferation, with increased YAP1/TAZ activity in mammalian cells increasing proliferation[294]. Interestingly, there wasn't the same enrichment in *wwtr1* mRNA signal, suggesting that the proliferation in this region may only be regulated by Yap1 signalling. This is an example of Yap1 and Taz likely being functionally different in the zebrafish.

wwtr1 mRNA appeared to be more enriched within the fin fold mesenchymal cells, particularly at 96hpf (Figure 5.11A). These cells are vital for the maintenance of actinotrichia and the general development of the larval fin fold[391]. Mesenchymal cells also play a role in tail fin regeneration, as they migrate towards the amputation plane following mild injury, where they are thought to form part of the blastema[248]. Enrichment of *wwtr1* in these cells may suggest a role for Taz in their function, and therefore in the development of the fin fold and in the formation of the blastema.

Both *yap1* and *wwtr1* appeared enriched in the mesenchyme and notochord of the embryo body relative to the fin fold itself (Figure 5.11). This could reflect a slight expression bias away from the epithelial cells of the fin and towards the structural components of the embryo, which give the embryo its rigidity before the formation of the spine, and so is under some mechanical pressure[101]. This supports findings from other models that show mechanical signals are often associated with changes in Hippo signalling[392,393]. The notochord is also a signalling centre during embryonic development[101], and so this suggests an important role for Hippo-Yap1/Taz signalling in this process.

Overall, during development both *yap1* and *wwtr1* are observed throughout the tail fin and are not localised exclusively to any specific structures, apart from a slight bias towards the caudal fin bud, mesenchyme, and notochord, and are unchanged following CRISPR mutagenesis.

5.5 *yap1* and *wwtr1* CRISPR mutagenesis affects *yap1* and *wwtr1* mRNA abundance during regeneration but does not have any clear localisation patterns

During regeneration, a slightly different pattern emerges (representative images in Figure 5.12A+B). Tail fin injury or *yap1* or *wwtr1* CRISPR mutagenesis did not appear to substantially change cell or region-specific expression by eye. One exception was a potential absence of *yap1* signal in the caudal fin bud of *yap1* CRISPants after injury (Figure 5.12A+B), similar to that seen at baseline (Figure 5.11A+B). This could explain why *yap1* CRISPants often have smaller tail fins and reduced regenerative growth, as this growth region may be functionally impaired. Intriguingly, there did not appear to be an enrichment in either *yap1* or *wwtr1* signal in the notochord bead after severe tail fin injury.

CRISPR mutagenesis showed some quantifiable defects. At 24 and 48 hours post injury (hpi) there was a reduction in *yap1* mRNA in *yap1* CRISPants (Figure 5.12C+D), showing a specificity in CRISPR mutagenesis. However, *wwtr1* mRNA was reduced in both *yap1* and *wwtr1* CRISPants at 24hpi (Figure 5.12E), suggesting that there may be a feedback system between Yap1 and Taz at this time point such that a reduction in *yap1* also triggers a reduction in *wwtr1* at an mRNA level. This contrasted an increase in *wwtr1* abundance following *yap1* mutagenesis at 120hpf (Figure 5.11F), which suggested a potential compensatory feedback mechanism where the absence of Yap1 protein causes an increase in *wwtr1* translation to compensate (see 1.6 for a summary of the interactions between Yap1 and Taz). These changes are not thought to be due to off-target effects of the CRISPR mutagenesis as previous work has shown no change in Taz protein in *yap1* CRISPants and vice versa in uninjured fish (Figure 3.5). They could instead be due to a developmental or regenerative time-specific phenomenon. In fact, the reduction in *wwtr1* mRNA in *yap1* CRISPants disappeared by 48hpi, with a specific reduction in *wwtr1* mRNA in *wwtr1* CRISPants only (Figure 5.12F). However, these results are not from three independent repeats, and so further experimentation is required to clarify these apparently contradictory results.

This pattern of *yap1* or *wwtr1* mRNA fluorescence reduction in CRISPants is specific to regenerating fish. As there is little or no change in developing fish (Figure 5.11), it suggests that the effects of CRISPR mutagenesis becomes more obvious when the system is challenged.

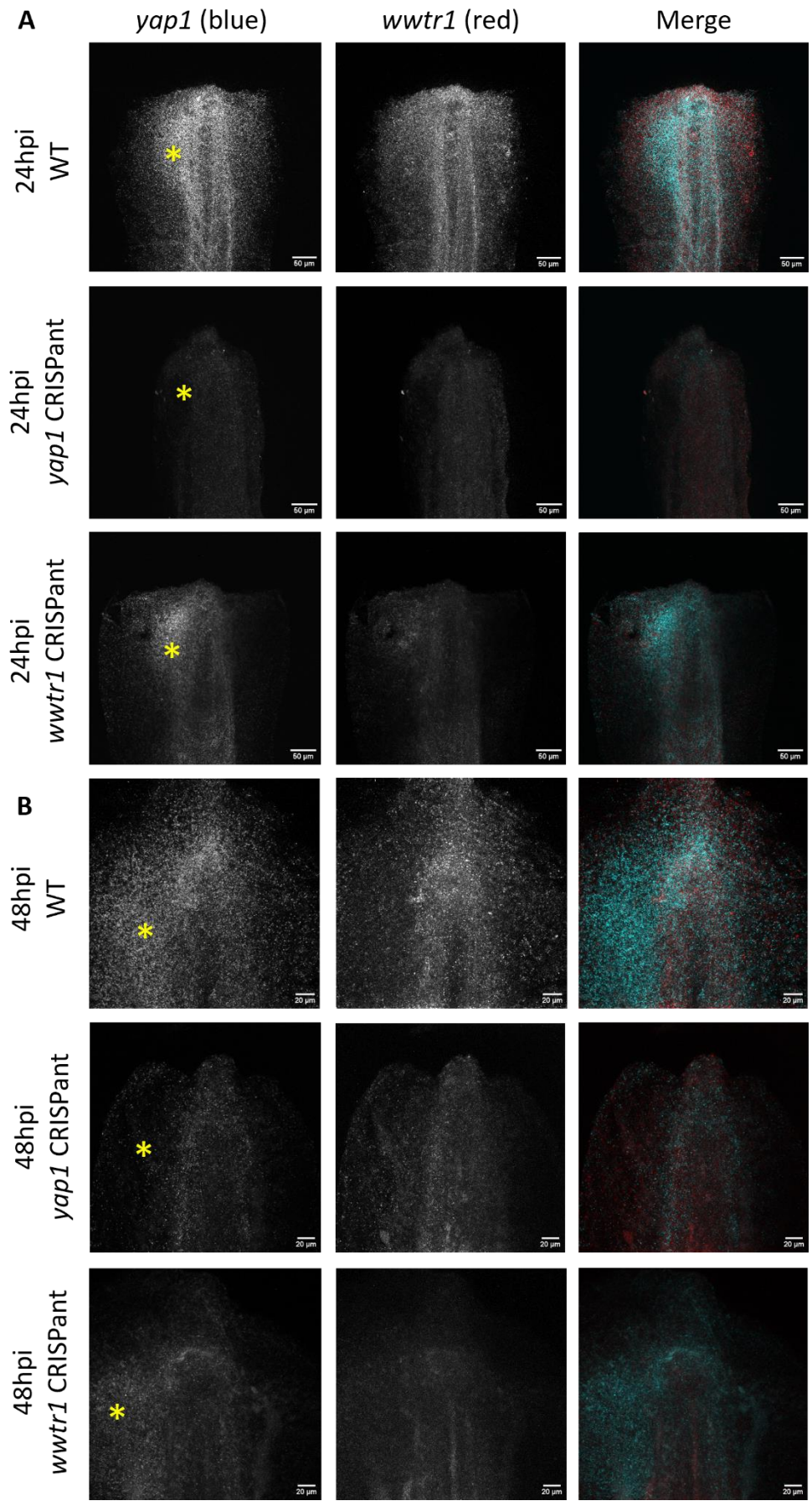
A
yap1 (blue)
wwtr1 (red)
Merge
24hpi WT
24hpi yap1 CRISPant
24hpi wwtr1 CRISPant
B
48hpi WT
48hpi yap1 CRISPant
48hpi wwtr1 CRISPant
50 µm
20 µm

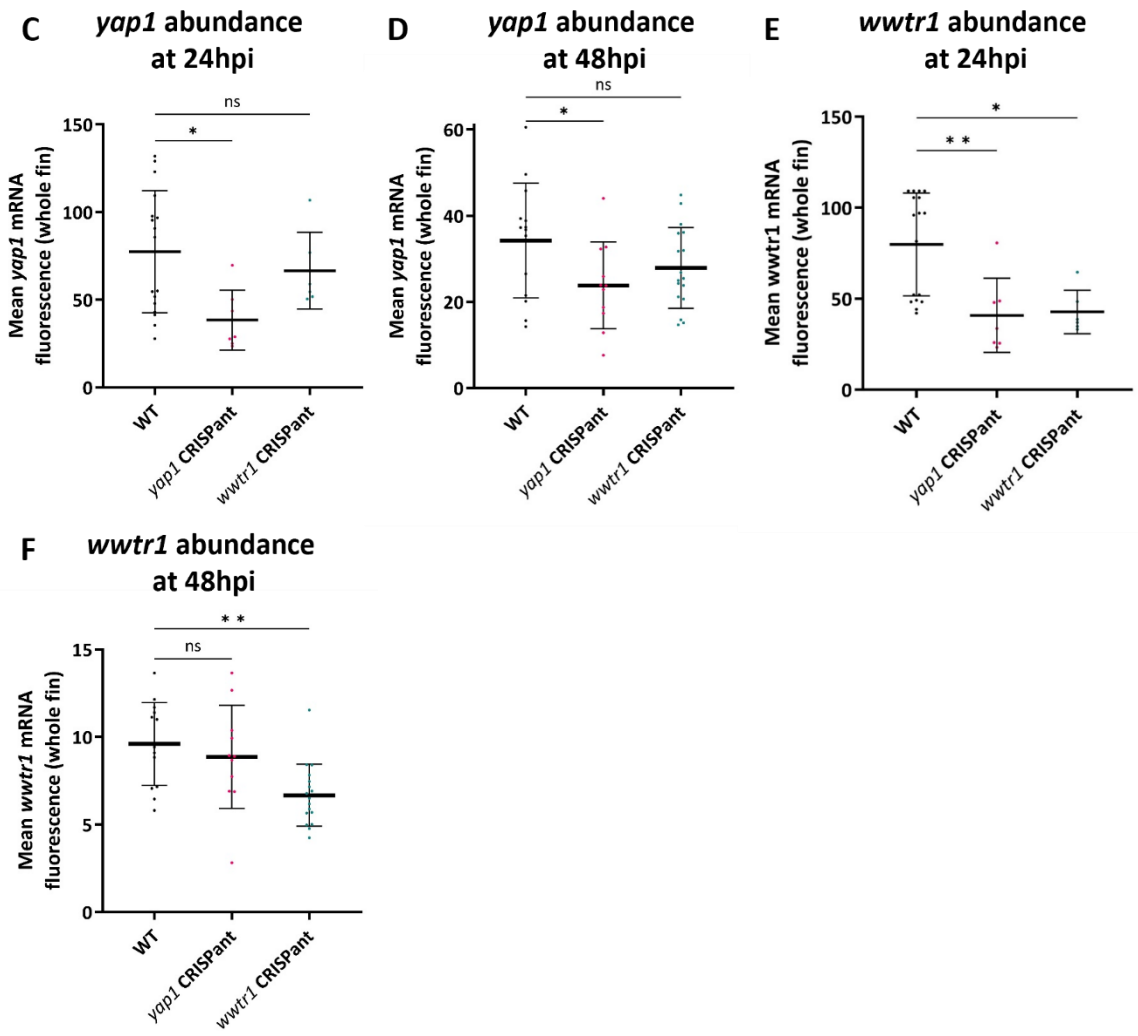

Figure 5.12: Specific reductions in *yap1* and *wwtr1* mRNA in CRISPants during severe tail fin regeneration

(A) Representative WT, *yap1* CRISPant, and *wwtr1* CRISPant images of the regenerating tail fin at 24 hours post injury. Asterix denotes caudal fin bud. For merged image: cyan=*yap1*, red=*wwtr1*. **(B)** Representative WT, *yap1* CRISPant, and *wwtr1* CRISPant images of the regenerating tail fin at 48 hours post injury. Note the change in magnification compared to other samples. Asterix denotes caudal fin bud. For merged image: cyan=*yap1*, red=*wwtr1*. **(C)** Quantification of mean *yap1* fluorescence in the whole fin at 24 hours post severe tail fin injury. *yap1* abundance was reduced in *yap1* but not *wwtr1* CRISPants. **(D)** Quantification of mean *yap1* fluorescence in the whole fin at 48 hours post severe tail fin injury. *yap1* abundance was reduced in *yap1* but not *wwtr1* CRISPants. **(E)** Quantification of mean *wwtr1* fluorescence in the whole fin at 24 hours post severe tail fin injury. *wwtr1* abundance was reduced in both CRISPants. **(F)** Quantification of mean *wwtr1* fluorescence in the whole fin at 48 hours post severe tail fin injury. *wwtr1* abundance was reduced in *wwtr1* but not *yap1* CRISPants.

Brightness and contrast have been altered for ease of viewing, with the same settings applied to each sample within each experiment. All samples are imaged using a 20x air objective. *yap1* and *wwtr1* are labelled. Each dot represents one fish. Results from at least one independent repeat. Significance calculated using Kruskal-Wallis test with multiple comparisons. Bars represent mean±SD. *p<0.05; **p<0.01; ns=not significant.

Potentially, during regeneration there is a large increase in Yap1 and Taz signalling, so normally there would be a concurrent large increase in yap1 and wwtr1 mRNA. However, the increase cannot occur after CRISPR mutagenesis, so a defect is seen in mRNA levels. This further supports a key role of Yap1 and Taz in zebrafish tail fin regeneration.

5.6 *yap1* and *wwtr1* mRNA localisation in a *ctgfa*:GFP transgenic after injury showed slight mutagenesis-induced changes

The HCR RNA-FISH protocol can be modified to amplify antibodies of interest alongside mRNA. A HCR probe was designed to be used in conjunction with an anti-GFP antibody in the *ctgfa*:GFP transgenic zebrafish line (see 4.1 for a summary of this line). However, attempts to utilise the GFP HCR probe had limited success, despite several rounds of optimisation attempts of the protocol (data not shown). The antibody against GFP was determined to have limited penetration into the tissues of interest (blastema, notochord). However, endogenous GFP signal survived the HCR staining protocol, and could be visualised alongside the *yap1* and *wwtr1* HCR probes. This endogenous GFP signal had similar distribution to that seen after confocal imaging of live embryos (e.g. Figure 4.1), and non-GFP fish had no signal (not shown). This live imaging was performed at 24 hours post injury, so HCR imaging at the same time point was performed, and the resulting signals quantified (Figure 5.13).

GFP fluorescence was quantified in various regions of the tail fin following injury: the whole fin (Figure 5.13B), the notochord bead (Figure 5.13C), and in the central notochord region where GFP signal was highest (detected by auto-thresholding in ImageJ, including musculature and notochord bead) (Figure 5.13D). This was performed as the fin fold had low levels of GFP, and there seemed to be regional differences in GFP distribution between CRISPants, with *yap1* CRISPants appearing to have lower signal in the notochord bead, but normal expression in the somites, whereas *wwtr1* CRISPants had the opposite phenotype. When measuring GFP signal in the whole fin, there was a significant reduction after *yap1*, but not *wwtr1*, CRISPR mutagenesis (Figure 5.13B). A similar pattern was seen when measured in the notochord bead, albeit the reduction in the *yap1* CRISPant was not significant (Figure 5.13C). This suggests that Yap1 may regulate *ctgfa* expression more than Taz but contrasts the previous work showing that both *yap1* and *wwtr1* CRISPR mutagenesis reduces *ctgfa*:GFP signal in live imaging following injury (Figure 4.3). However, when analysing GFP in the central

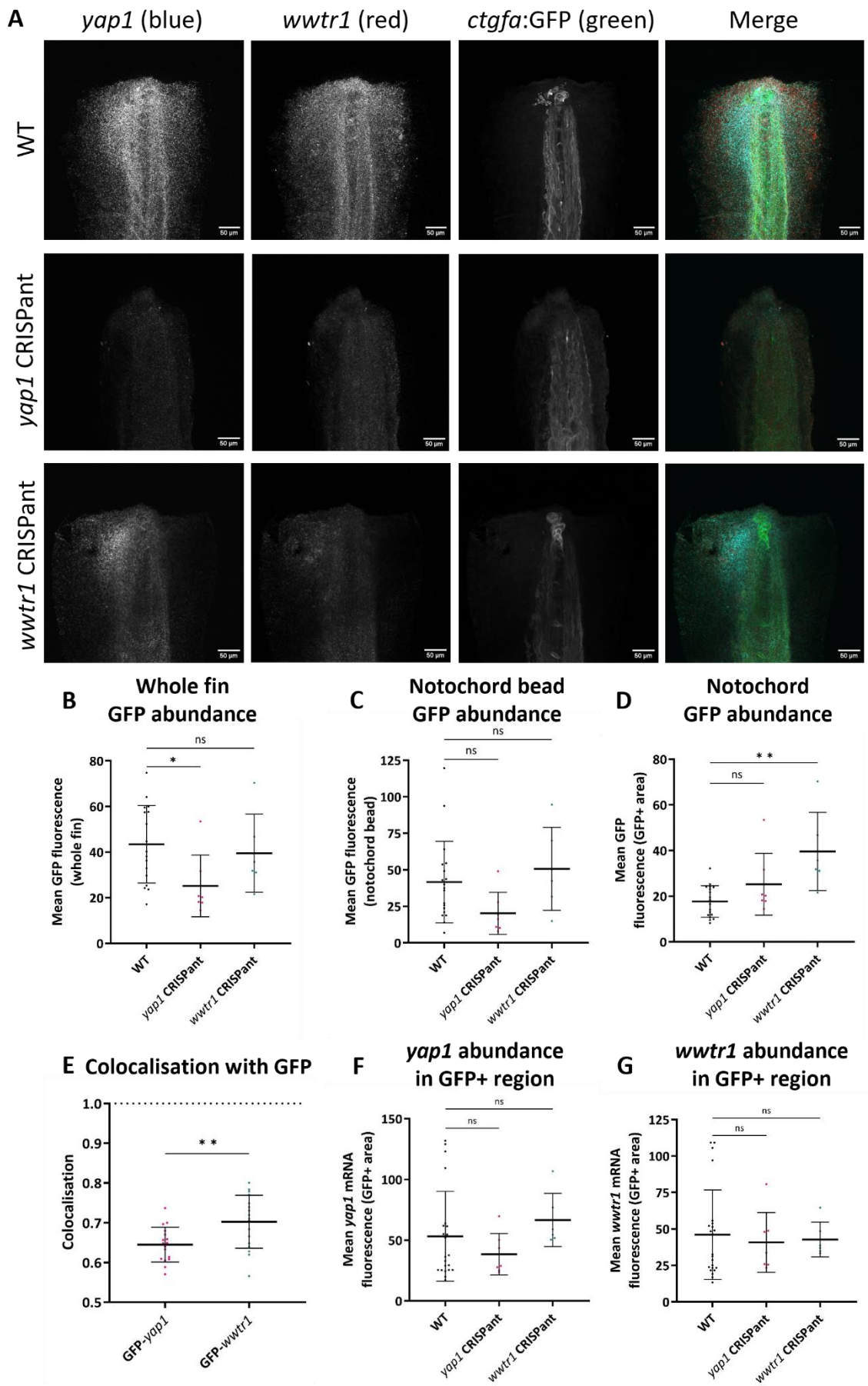
A
yap1 (blue)
wwtr1 (red)
ctgfa:GFP (green)
Merge
WT
yap1 CRISPant
wwtr1 CRISPant
50 µm
B
Whole fin
GFP abundance
Mean GFP fluorescence (whole fin)
ns
*
C
Notochord bead
GFP abundance
Mean GFP fluorescence (notochord bead)
ns
ns
D
Notochord
GFP abundance
Mean GFP fluorescence (GFP+ area)
* *
ns
WT
yap1 CRISPant
wwtr1 CRISPant
E Colocalisation with GFP
Colocalisation
* *
GFP-yap1
GFP-wwtr1
F
yap1 abundance
in GFP+ region
Mean yap1 mRNA fluorescence (GFP+ area)
G
wwtr1 abundance
in GFP+ region
Mean wwtr1 mRNA fluorescence (GFP+ area)

Figure 5.13: Labelling of endogenous GFP signal can be quantified and colocalised with other markers, showing mutagenesis-induced changes

(A) Representative WT, *yap1* CRISPant, and *wwtr1* CRISPant images of the tail fin at 24 hours post injury (hpi) imaged at 20x. *yap1* and *wwtr1* are labelled with HCR probes with endogenous (unlabelled) *ctgfa*:GFP signal. For merged image: cyan=*yap1*, red=*wwtr1*, green=GFP. **(B)** Quantification of mean *ctgfa*:GFP fluorescence in the whole fin at 24hpi. GFP levels were reduced after *yap1* CRISPR mutagenesis only. **(C)** Quantification of mean *ctgfa*:GFP fluorescence in the notochord bead at 24hpi. GFP levels were unchanged after *yap1* and *wwtr1* CRISPR mutagenesis. **(D)** Quantification of mean *ctgfa*:GFP fluorescence in the central notochord and notochord sheath area (defined by auto-thresholding GFP image) at 24hpi. GFP levels were unchanged after *yap1* and increased after *wwtr1* CRISPR mutagenesis. **(E)** Colocalisation of *ctgfa*:GFP signal with *yap1* and *wwtr1* mRNA signal. *wwtr1* colocalised with GFP significantly more than *yap1* mRNA did. **(F)** Quantification of mean *yap1* fluorescence in the GFP+ area at 24hpi. Abundance was not changed following *yap1* or *wwtr1* CRISPR mutagenesis. **(G)** Quantification of mean *wwtr1* fluorescence in the GFP+ area at 24hpi. Abundance was not changed following *yap1* or *wwtr1* CRISPR mutagenesis.

Each dot represents one fish. Results from at least one independent repeat. Significance calculated using unpaired t-test for D, and Kruskal-Wallis test with multiple comparisons for remainder. Bars represent mean±SD. Brightness and contrast have been altered for ease of viewing, with the same settings applied to each sample. *yap1* and *wwtr1* mRNA sample images in A are the same as those shown in Figure 5.12. *p<0.05; **p<0.01; ns=not significant.

notochord region, no change after *yap1* mutagenesis, and an increase in *wwtr1* CRISPants was observed (Figure 5.13D). This was unexpected, and potentially reflects a change in GFP signal localisation upon both *yap1* and *wwtr1* mutagenesis, with a reduction in GFP signal outwith the central region in *yap1* CRISPants and a shift of GFP signal towards the central region in *wwtr1* CRISPants.

Colocalisation analysis of these probes showed that *wwtr1* colocalised more significantly with GFP than *yap1* when measured in the whole fin (Figure 5.13E). This could be a result of higher *yap1* expression in the fin fold, or may suggest that Taz activity regulates *ctgfa* expression to a greater extent than Yap1. These differences may be elucidated after further repeats of this technique, or by analysis of other regions of the fin. *yap1* and *wwtr1* signal in the whole fin after injury has been quantified above (Figure 5.12). Quantification of the signal in the GFP+ region of the tail fin was performed and compared to these results (Figure 5.13F+G). There was no significant change in either *yap1* or *wwtr1* signal in either CRISPant, although there was a trend towards a reduction in *yap1* signal after *yap1* mutagenesis (Figure 5.13F). This does not reflect the results seen in the whole fin and could suggest location-specific changes in both *yap1* and *wwtr1* signal following mutagenesis. Another interesting observation was the lack of enhanced *yap1* and *wwtr1* signal in the 24hpi GFP+ notochord bead, suggesting

that the *ctgfa* expression in this structure may not be driven by Yap1/Taz signalling. This is further discussed in 5.7 below.

In summary, this technique can be used to visualise endogenous levels of fluorophores in transgenic embryos together with mRNAs of interest. In the *ctgfa*:GFP transgenic line, this shows differing contributions of *yap1* and *wwtr1* to *ctgfa* expression, further highlighting that Yap1 and Taz function differently in the developing and regenerating embryo.

5.7 Abundance and localisation of blastema markers at 48 hours post injury is unchanged in CRISPants

Investigation of the structure of the blastema at 48hpi was then performed using markers first described and validated by Sinclair et. al[267]. These structures are shown in the schematic in Figure 5.14C. The central region of the blastema, known as the notochord bead[248,394], is labelled by *col9a2*. Tissue surrounding the notochord bead (the proximal blastema) is labelled by *inhbaa*. The remaining part of the blastema, the distal blastema, is labelled by *aldh1a2*. Blastema markers localised to regions in the same pattern as that previously published[267], showing that the protocol is working as intended (Figure 5.14A+B).

There were no obvious malformations or changes in labelling between WT fish and either CRISPant when inspected by eye. When quantified, this translated to no significant changes in fluorescence (Figure 5.14D-F), although there was a trend towards a reduction in *aldh1a2* signal in both CRISPant samples. The lack of significance in this case may be due to the quantification of the whole fin fluorescence, as there appeared to be a reduction in *aldh1a2* signal outside the notochord bead/trunk, but no change in the notochord bead/trunk region. The lack of significant changes in markers indicates that *yap1* or *wwtr1* mutagenesis alone is not sufficient to disrupt the overall structure of the blastema at 48 hours post injury. It may also suggest that the tail fin regeneration phenotypes in these CRISPants are not due to obvious malformations in the blastema, but instead could be due to other processes such as cell proliferation, differentiation, or immune cell function.

Colocalisation analysis was then performed in WT fish between *yap1* or *wwtr1* signal and blastema markers (Figure 5.14G). This analysis showed that both *yap1* and *wwtr1* colocalised to a much lower extent with *col9a2* (notochord bead) signal, suggesting that Hippo pathway

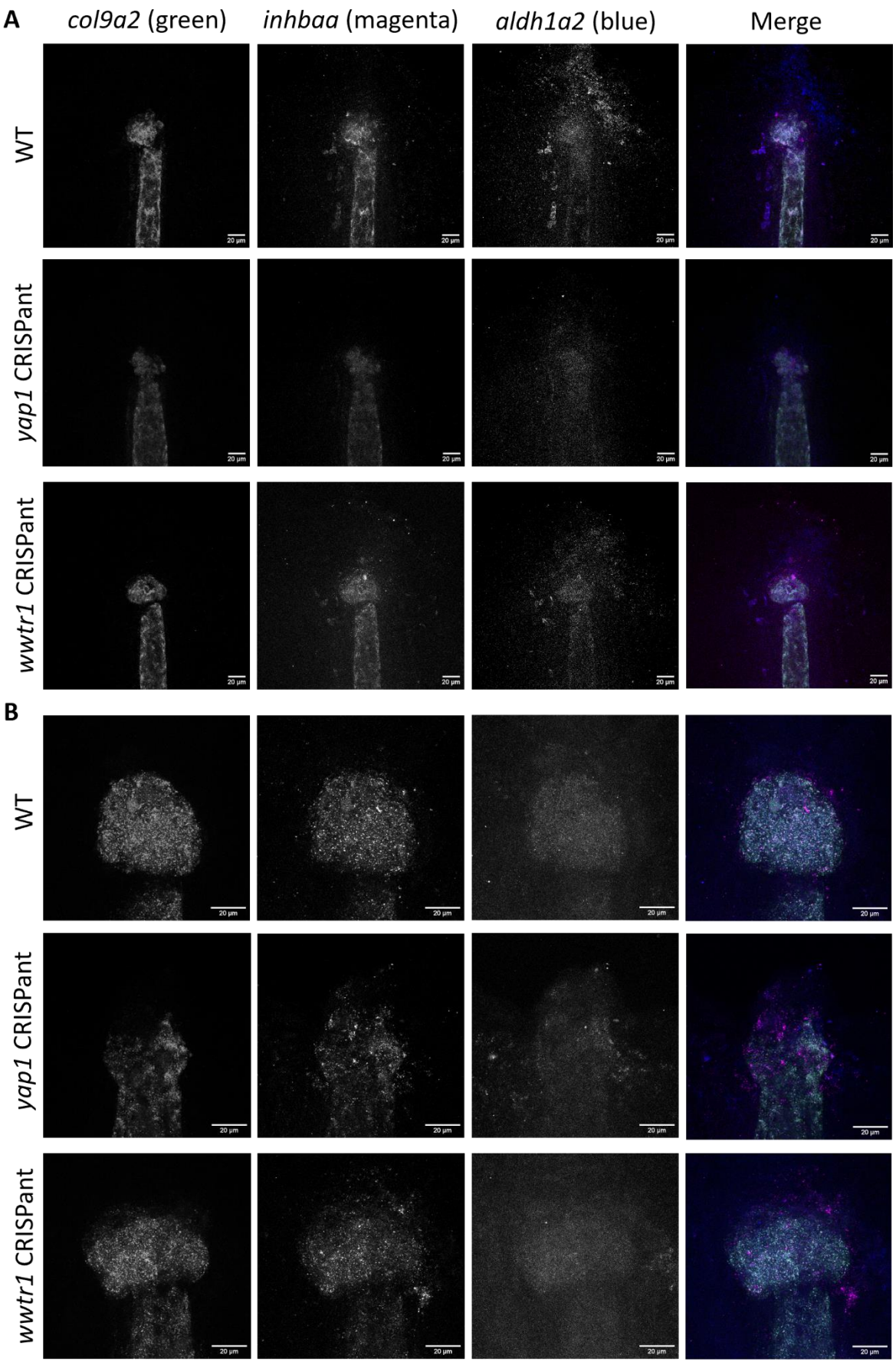
A
col9a2 (green)
inhbaa (magenta)
aldh1a2 (blue)
Merge
WT
yap1 CRISPant
wwtr1 CRISPant
B
WT
yap1 CRISPant
wwtr1 CRISPant
20 µm

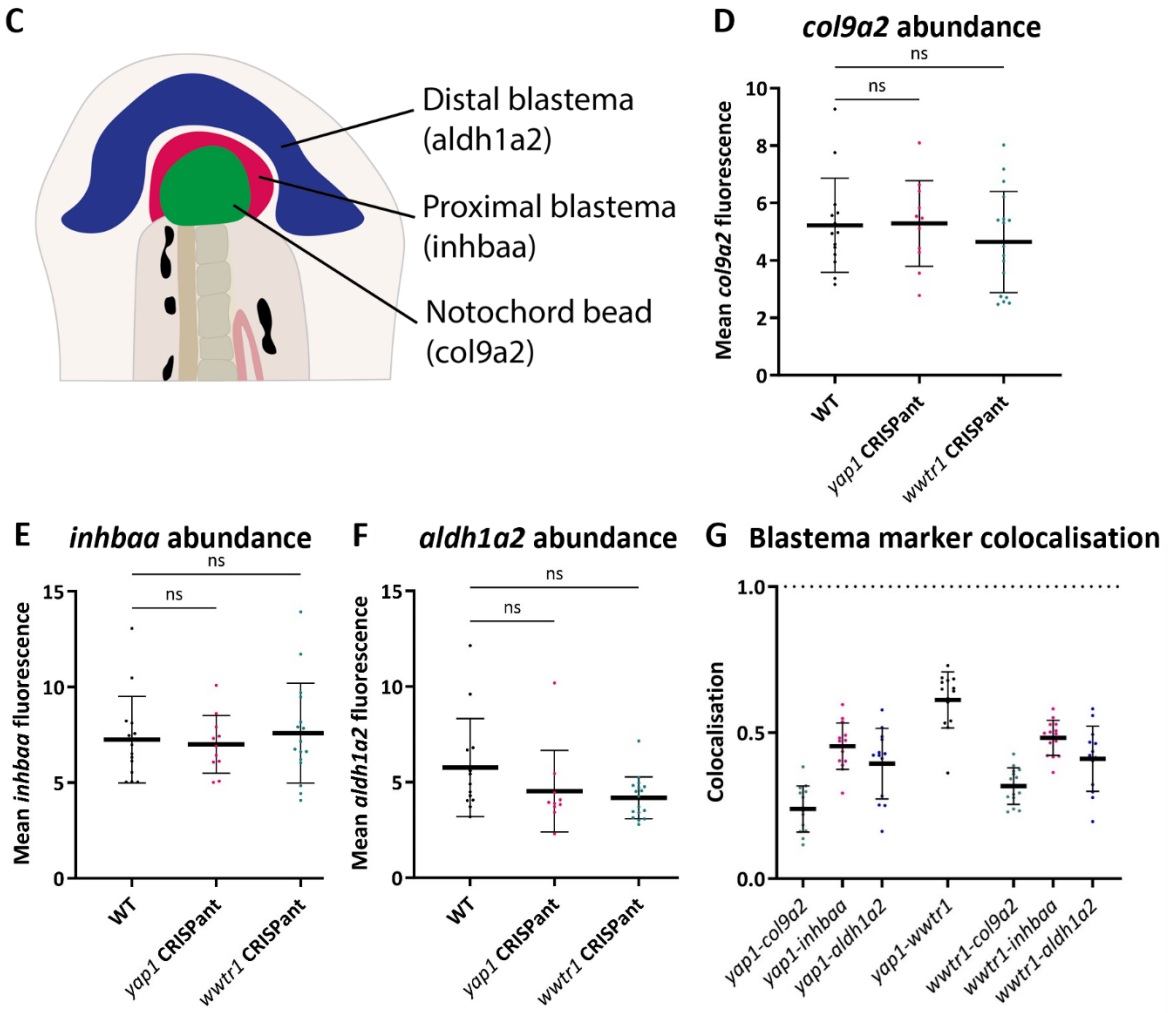

Figure 5.14: Abundance and localisation of blastema markers following severe injury showed no obvious malformations

(A) Representative WT, *yap1* CRISPant, and *wwtr1* CRISPant images of the tail fin at 48 hours post injury imaged at 20x. For merged image: green=*col9a2*, magenta=*inhbaa*, blue=*aldh1a2*. **(B)** Representative images as in Figure 5.14A but taken at 40x. For merged image: green=*col9a2*, magenta=*inhbaa*, blue=*aldh1a2*. **(C)** Schematic showing the areas of the blastema labelled in these samples. *col9a2* labels the notochord bead, *inhbaa* labels the proximal blastema, and *aldh1a2* labels the distal blastema. **(D)** Quantification of mean *col9a2* fluorescence in the whole fin at 48hpi (measured at 20x). Fluorescence was not significantly changed in *yap1* or *wwtr1* CRISPants. **(E)** Quantification of mean *inhbaa* fluorescence in the whole fin at 48hpi (measured at 20x). Fluorescence was not significantly changed in *yap1* or *wwtr1* CRISPants. **(F)** Quantification of mean *aldh1a2* fluorescence in the whole fin at 48hpi (measured at 20x). Fluorescence was not significantly changed in *yap1* or *wwtr1* CRISPants, but a trend towards a reduction in signal was observed in both CRISPants. **(G)** Colocalisation of blastema marker signals with *yap1* and *wwtr1* mRNA in WT fish. Both *yap1* and *wwtr1* colocalised to a lesser extent with *col9a2* than other blastema markers, and *yap1* and *wwtr1* colocalised more with each other than blastema markers. Significance not shown for clarity.

Brightness and contrast has been slightly manipulated for ease of viewing, with the same settings applied to each sample. Each dot represents one fish. Pooled results from three independent repeats. Significance calculated using Kruskal-Wallis test with multiple comparisons. Bars represent mean±SD. ns=not significant

activity is likely most altered outwith the notochord bead. This is also supported by findings above that show a lack of *yap1* and *wwtr1* mRNA signal in this region. The notochord bead is considered to be a signalling centre that orchestrates the formation of the blastema and the regeneration of the zebrafish fin[264]. The relative absence of *yap1*/*wwtr1* mRNA abundance, and therefore Yap1/Taz signalling in this region, suggests that the Hippo pathway may not be a core part of this signalling centre. Instead, Hippo signalling could be altered by signals from the notochord bead to induce regeneration in the proximal and distal blastema. Alternatively, Yap1 and Taz might be post-transcriptionally regulated in the blastema.

There are some limitations of this HCR RNA-FISH technique and the experiments described above. Firstly, more repeats are needed, particularly of the uninjured data and across a greater number of timepoints. Imaging in other parts of the zebrafish would also be of interest. However, the scope for doing these repeats is limited by the relative high cost of the technique. This technique is also somewhat restricted in its ability to analyse CRISPR mutants. CRISPR/Cas9 mutagenesis, by its nature, does not necessarily remove mRNA. DNA lesions often instead induce early stop codons in the mRNA, and this has been confirmed by sequencing of Yap1 and Taz stable mutant lines made from CRISPR-mutagenised embryos, which have multiple early stop codons and an almost complete absence of Yap1 and Taz protein respectively (4.2). Therefore, by imaging mRNA rather than protein, this technique will not always accurately reflect the abundance of functional Yap1 and Taz in the embryo. This may be the reason for some inconsistencies in these results, such as the lack of effect of mutagenesis at baseline. An additional challenge is the presence of WT maternal mRNA in the CRISPants, although this should be limited at the timepoints analysed here. It should also be noted that quantification of these images proved challenging. Mean fluorescence was used to draw conclusions in this thesis, however some claim that it is more appropriate to analyse individual fluorescent points at a higher magnification and resolution.

To summarise, the HCR RNA-FISH technique has allowed the visualisation of GFP, *yap1*, and *wwtr1* in the same sample, which was not possible using standard immunofluorescence. It shows that *yap1* and *wwtr1* are generally expressed throughout the tail fin, and has limited localisation to major regions or cell types. *yap1* does localise more closely with the growth bud of the tail fin than *wwtr1*, suggesting a Yap1-specific role in the proliferation that occurs there. *yap1* and *wwtr1* mutagenesis does not change the morphology of the blastema,

indicating that blastema formation is not dependent on Yap1 or Taz, and that malformation is not a factor driving the impaired regeneration of *yap1* and *wwtr1* CRISPants. Instead, further research is needed to identify or eliminate other processes that might contribute.

5.8 CRISPants have reduced proliferation in the tail fin

The Hippo pathway has been closely linked to cell proliferation in multiple environments[5,28], and proliferation is increased after mild tail fin injury[248]. Therefore, an immunofluorescence protocol was developed to study proliferation in the tail fin for the CRISPants of interest. For this, a marker for phosphohistone H3 (pH3) was used. pH3 labels condensed chromatin before chromosomal segregation, labelling cells in late G2 and therefore mitotically active cells[395]. Both uninjured and injured embryos were analysed (representative images in Figure 5.15A). Notably, in the uninjured fish $pH3^+$ cells were almost exclusively located in the caudal fin bud. This region, mentioned in 5.4 above, is predicted to be an area of high proliferation as it generates cells during the growth of the adult tail fin[390]. As expected, WT fish showed a significant increase in cell proliferation from uninjured levels following severe tail fin injury (Figure 5.15B), which has been reported after mild tail fin injury[248]. Fish also had higher proliferation at later developmental and regenerative timepoints. When uninjured, and when CRISPant proliferation was normalised to WT, there was no change in CRISPant proliferation from WT levels at 96hpf, although this may be due to low numbers of samples analysed (Figure 5.15C). However, by 120hpf, both *yap1* and *wwtr1* CRISPants had significantly reduced rates of proliferation (Figure 5.15C).

Defects in proliferation were also observed after severe tail fin injury. At 24hpi, both CRISPants had significantly reduced proliferation, although at 48hpi only *wwtr1* CRISPants were reduced (Figure 5.15D). This suggests that the *yap1* CRISPant proliferation defect is only at early timepoints whilst the *wwtr1* CRISPant has defects at all timepoints. The lack of reduction in 96hpf uninjured fish but a reduction in injured fish at the same developmental timepoint (24hpi) shows that the reduction at 24hpi is unlikely to be due to developmental defects and is instead specific to regeneration. This proliferation was measured caudal to the start of the pigment gap to the end of the fin, which includes the caudal fin bud mentioned above. In order to measure proliferation only in the regenerating tissue, $pH3^+$ cells were then

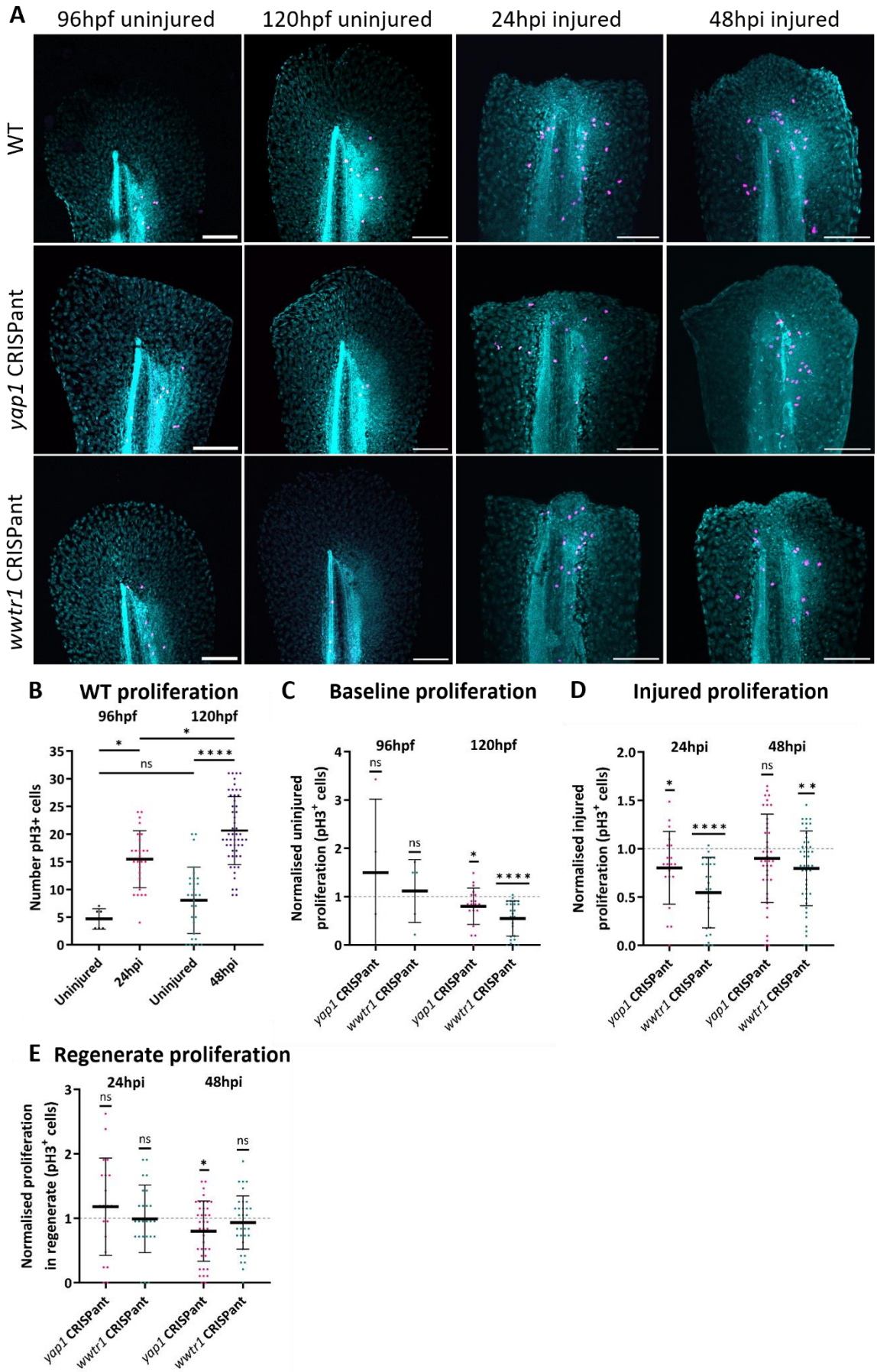
A
96hpf uninjured
120hpf uninjured
24hpi injured
48hpi injured
WT
yap1 CRISPant
wwtr1 CRISPant
B
WT proliferation
96hpf
120hpf
Number pH3+ cells
Uninjured
24hpi
Uninjured
48hpi
C
Baseline proliferation
96hpf
120hpf
Normalised uninjured proliferation (pH3+ cells)
yap1 CRISPant
wwtr1 CRISPant
yap1 CRISPant
wwtr1 CRISPant
D
Injured proliferation
24hpi
48hpi
Normalised injured proliferation (pH3+ cells)
yap1 CRISPant
wwtr1 CRISPant
yap1 CRISPant
wwtr1 CRISPant
E
Regenerate proliferation
24hpi
48hpi
Normalised proliferation in regenerate (pH3+ cells)
yap1 CRISPant
wwtr1 CRISPant
yap1 CRISPant
wwtr1 CRISPant

Figure 5.15: Reduced proliferation in the tail fin at baseline and after severe injury
(A) Representative images of WT, *yap1* CRISPants, and *wwtr1* CRISPants at 96hpf and 120hpf uninjured and 24hpi and 48hpi. Cyan=DAPI, Magenta=pH3. **(B)** Quantification of proliferation in WT fish at both baseline and after severe injury. Injury induced a large increase in cell proliferation relative to uninjured fins. Increased proliferation was observed at 48hpi relative to 24hpi. **(C)** Quantification of uninjured (baseline) cell proliferation at 96hpf, normalised to mean proliferation in uninjured WT fish. Proliferation was unchanged at 96hpf but decreased in both CRISPants at 120hpf. **(D)** Quantification of cell proliferation at 24hpi and 48hpi, normalised to mean proliferation in injured WT fish at the same timepoint. Proliferation was reduced in both CRISPants at 24hpi but *wwtr1* CRISPants only at 48hpi. **(E)** Quantification of cell proliferation in the regenerated area of the fin only at 24hpi and 48hpi, normalised to mean proliferation in injured WT fish at the same timepoint. Proliferation was only reduced in *yap1* CRISPants at 48hpi.
$pH3^+$ cells counted caudal to the start of the pigment gap (B-D) (see Figure 2.6A) or caudal to the approximate cut plane (E) (see Figure 2.6B). Data is normalised to the WT average for that timepoint in C-E. Each dot represents one fish. Pooled results from at least three independent repeats, except 96hpf baseline, where one repeat was performed. Significance calculated using Kruskal-Wallis test with multiple comparisons (B) and one-sample t-test or Wilcoxon test (μ=1) (C-E). Bars represent mean±SD. Brightness and contrast has been slightly manipulated for ease of viewing, with the same settings applied to each sample. *p<0.05; **p<0.01; ****p<0.0001; ns=not significant.

counted only caudal to the approximate cut plane. The pattern of proliferation observed was the opposite of that measured in the whole fin. There was no significant change in proliferation at 24hpi or in *wwtr1* CRISPants at 48hpi, but there was a reduction in *yap1* CRISPants at 48hpi (Figure 5.15E). The difference between results in whole fin and regenerate may suggest that the proliferation defect is localised to the region outwith the regenerated area, such as the caudal fin bud. This could show the importance of the cells that remain after injury in proliferating and regrowing the new fin. Of note, the raw number of proliferating cells in the regenerate was much lower than those in the whole fin, which may have skewed the results.

In summary, regeneration requires an increase in cell proliferation to replace lost cells, and this increase may not be possible in the CRISPants. As mentioned in 5.4 above, increased YAP/TAZ activity *in vitro* increased proliferation[294], and so supports this finding that removing Yap1 and Taz in the zebrafish reduces proliferation. This altered proliferation could therefore be one of the underlying mechanisms by which regeneration is impaired in these CRISPants.

5.9 Immune cells during development

The immune system is vital in many regenerative processes in the zebrafish (see 1.5) In order to investigate the role of Yap1 and Taz in normal immune system development, RNAseq analysis of key immune markers and imaging of uninjured fish was performed to determine

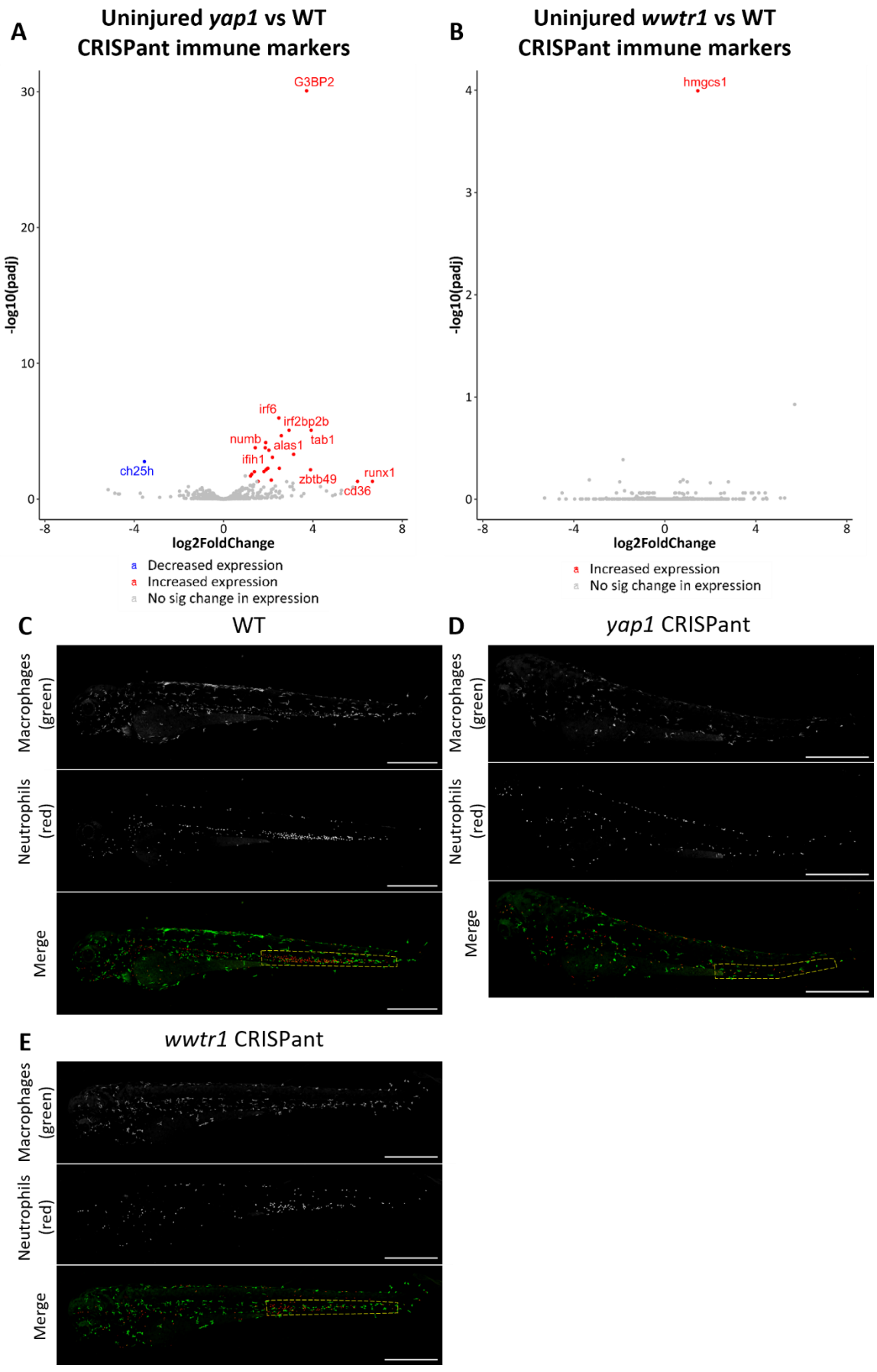
A
Uninjured yap1 vs WT
CRISPant immune markers
G3BP2
irf6
irf2bp2b
numb
alas1
tab1
ifih1
ch25h
zbtb49
runx1
cd36
-log10(padj)
log2FoldChange
Decreased expression
Increased expression
No sig change in expression
B
Uninjured wwtr1 vs WT
CRISPant immune markers
hmgcs1
-log10(padj)
log2FoldChange
Increased expression
No sig change in expression
C
WT
D
yap1 CRISPant
E
wwtr1 CRISPant
Macrophages (green)
Neutrophils (red)
Merge

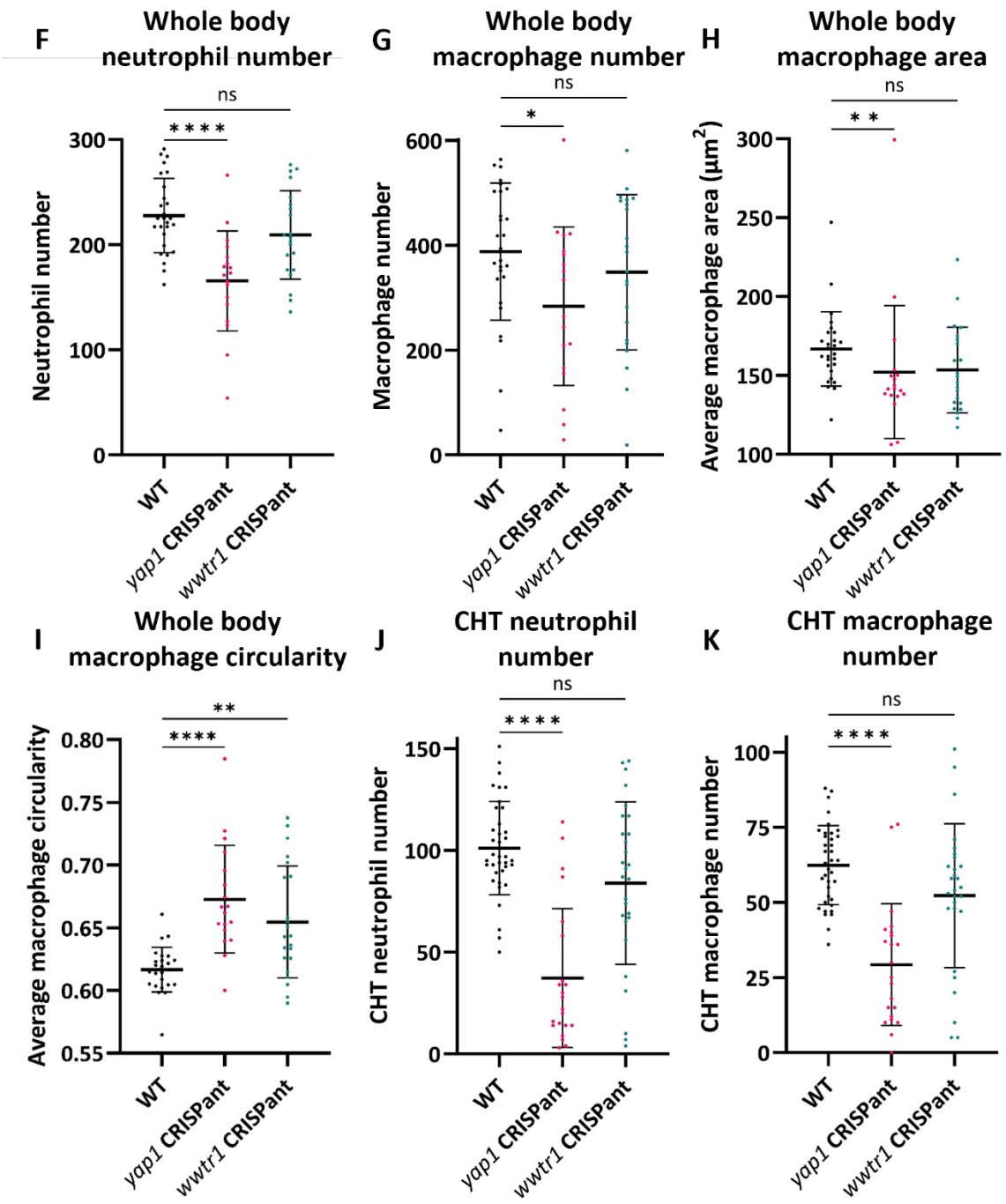

Figure 5.16: Macrophage and neutrophil characteristics in the developing WT and CRISPant embryo

(A) Volcano plot of immune marker expression in uninjured *yap1* CRISPants relative to WT. Red=increased genes; blue=decreased genes. **(B)** Volcano plot of immune marker expression in uninjured *wwtr1* CRISPants relative to WT. Red=increased genes; blue=decreased genes. **(C)** Representative images of macrophages (*mpeg*:GFP) and neutrophils (*lysC*-NLS:mScarlet) in 72hpf WT fish. **(D)** Representative images of macrophages (*mpeg*:GFP) and neutrophils (*lysC*-NLS:mScarlet in 72hpf *yap1* CRISPant fish. **(E)** Representative images of macrophages (*mpeg*:GFP) and neutrophils (*lysC*-NLS:mScarlet) in 72hpf *wwtr1* CRISPant fish. **(F)** Quantification of the number of neutrophils in the whole uninjured fish. *yap1* CRISPants had reduced number. **(G)** Quantification of the number of macrophages in the whole uninjured fish. *yap1* CRISPants had reduced number. **(H)** Quantification of average macrophage area in the whole uninjured fish. *yap1* CRISPants had reduced area. **(I)**

Quantification of average macrophage circularity in the whole uninjured fish. Both *yap1* and *wwtr1* CRISPants had increased circularity. **(J)** Quantification of the number of neutrophils in the CHT. *yap1* CRISPants had reduced number. **(K)** Quantification of the number of macrophages in the CHT. *yap1* CRISPants had reduced number.
Cutoff for volcano plots in A and B is p(adj)<0.05 and log2FoldChange>1 or <-1. Dotted yellow box in C-E denotes the CHT. Scale bar represents 250µm. Bars represent mean±SD. Each dot represents data from one fish. Data from three independent repeats. Significance was calculated by Kruskal-Wallis test (H) or one-way ANOVA (remainder) with multiple comparisons. *p<0.05; **p<0.01; ****p<0.0001; ns=not significant.

---

the characteristics of neutrophils and macrophages in CRISPants. RNAseq analysis of immune markers (gene list obtained from GO term "immune system process" GO0002376) in uninjured fish is shown in Figure 5.16A+B. Overall, *yap1* CRISPants had more differentially expressed (DE) immune genes than *wwtr1* CRISPants, which only showed an increase in the cholesterol synthesis regulator *hmgcs1*[308]. This suggests that, when unchallenged, *yap1* CRISPants have more of a disruption in immune cell development than *wwtr1* CRISPants.

Sample images of uninjured fish positive for macrophage and neutrophil markers are shown in Figure 5.16C-E. Cells were quantified in both the whole body and in the CHT (Figure 5.16F-K). In the whole body, neutrophil and macrophage numbers were significantly decreased in *yap1* CRISPants only (Figure 5.16F+G). This suggests that *yap1* CRISPants have a defect in immune cell development, potentially with the common myeloid progenitor, or due to the defect in proliferation described above. Macrophages also had defective cellular structure in *yap1* CRISPants, with a reduction in average macrophage area (Figure 5.16H). These results support the RNAseq data in Figure 5.16A+B of a greater immune cell defect in *yap1* CRISPants. Interestingly, both *wwtr1* and *yap1* CRISPants showed increased macrophage circularity (Figure 5.16I). Circularity has been associated with macrophage activation[396], suggesting that macrophages are hyperactivated in the CRISPants. Alternatively, it could reflect issues with the cytoskeleton, organisation of which has been associated with Hippo signalling in other model systems[392,397]. A cytoskeletal defect may impair cell migration from the CHT, and so specific investigation of neutrophil and macrophage numbers in the CHT was performed. The CHT showed a similar pattern of reduced neutrophil and macrophage numbers in *yap1* CRISPants only (Figure 5.16J+K respectively). This suggests that the whole-body *yap1* CRISPant defect observed may not be a result of an issue migration of the cells from the CHT, but instead a more general defect in immune cell function or development.

A

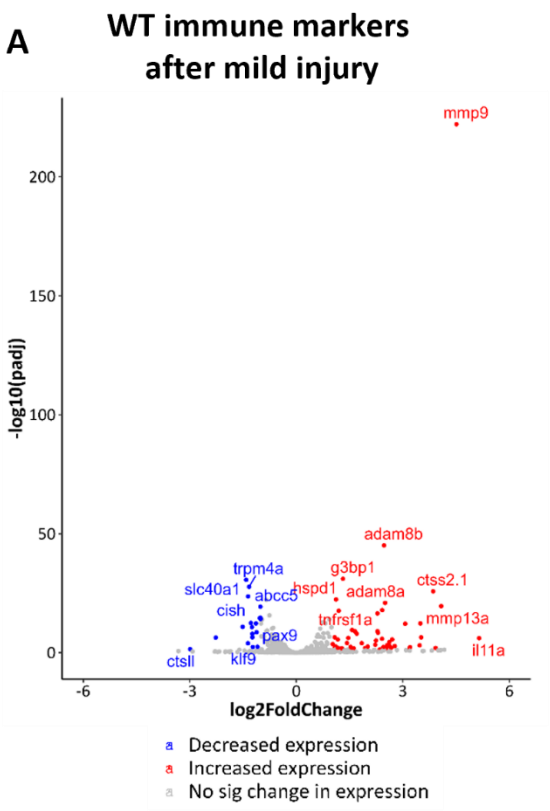
WT immune markers
after mild injury
-log10(padj)
log2FoldChange
mmp9
adam8b
trpm4a
g3bp1
slc40a1
abcc5
hspd1
adam8a
ctss2.1
cish
tnfrsf1a
mmp13a
pax9
il11a
ctsll
klf9
Decreased expression
Increased expression
No sig change in expression

B

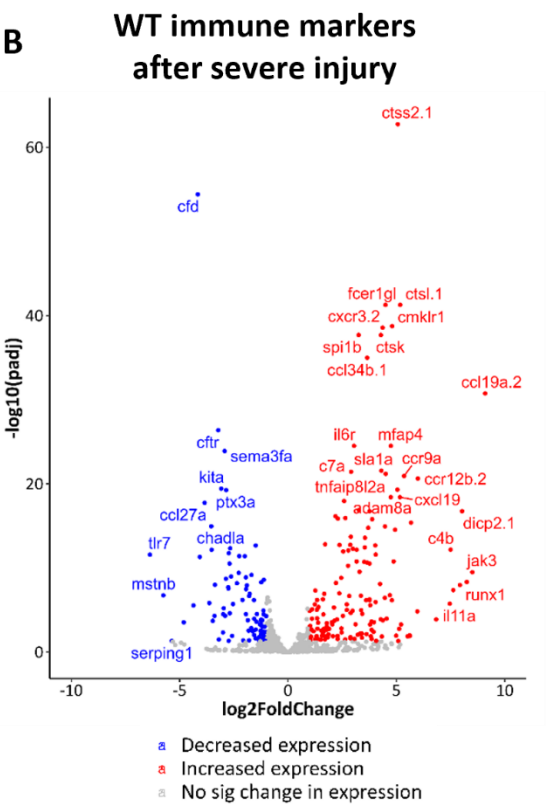
WT immune markers
after severe injury
-log10(padj)
log2FoldChange
ctss2.1
cfd
fcer1gl
ctsl.1
cxcr3.2
cmklr1
spi1b
ctsk
ccl34b.1
ccl19a.2
il6r
mfap4
cftr
sema3fa
c7a
sla1a
ccr9a
kita
tnfaip8l2a
ccr12b.2
ptx3a
cxcl19
ccl27a
adam8a
dicp2.1
tlr7
chadla
c4b
jak3
mstnb
runx1
il11a
serping1
Decreased expression
Increased expression
No sig change in expression

C

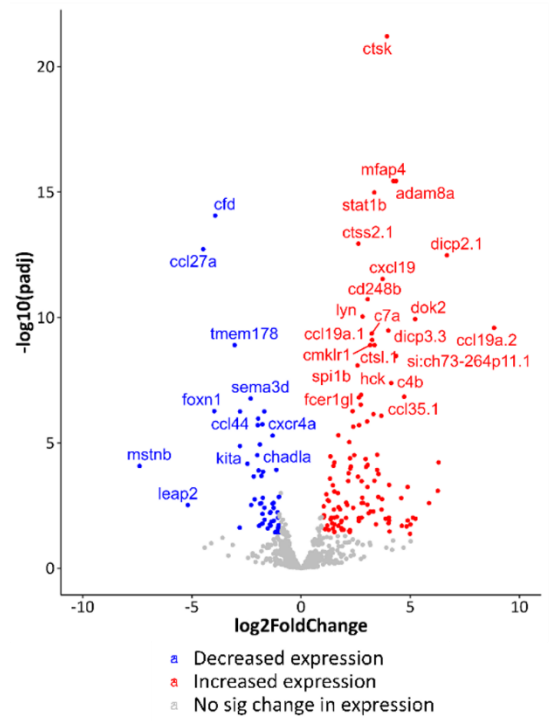
yap1 CRISPant immune
markers after severe injury
-log10(padj)
log2FoldChange
ctsk
mfap4
adam8a
cfd
stat1b
ctss2.1
dicp2.1
ccl27a
cxcl19
cd248b
lyn
c7a
dok2
tmem178
ccl19a.1
dicp3.3
ccl19a.2
cmklr1
ctsl.1
si:ch73-264p11.1
spi1b
hck
c4b
sema3d
foxn1
fcer1gl
ccl35.1
ccl44
cxcr4a
mstnb
kita
chadla
leap2
Decreased expression
Increased expression
No sig change in expression

D

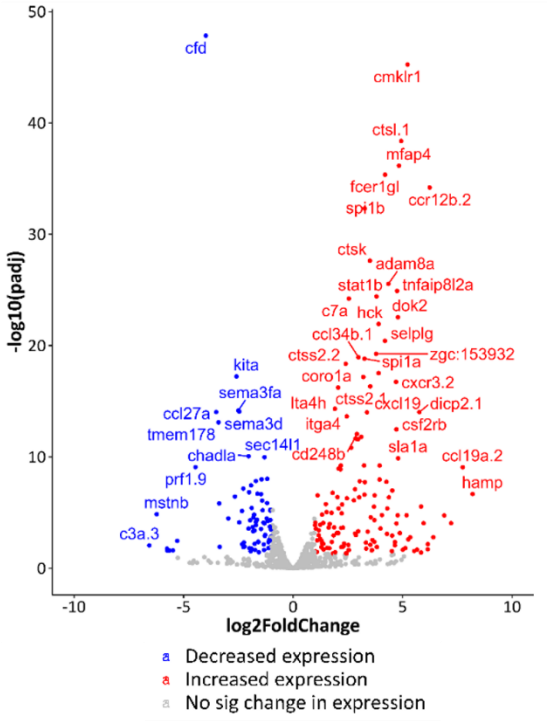
wwtr1 CRISPant immune
markers after severe injury
-log10(padj)
log2FoldChange
cfd
cmklr1
ctsl.1
mfap4
fcer1gl
ccr12b.2
spi1b
ctsk
adam8a
stat1b
tnfaip8l2a
c7a
hck
dok2
ccl34b.1
selplg
ctss2.2
spi1a
zgc:153932
kita
coro1a
cxcr3.2
sema3fa
lta4h
ctss2.1
cxcl19
dicp2.1
ccl27a
sema3d
itga4
csf2rb
tmem178
sec14l1
chadla
cd248b
sla1a
ccl19a.2
prf1.9
hamp
mstnb
c3a.3
Decreased expression
Increased expression
No sig change in expression

E **DE immune genes WT vs *yap1* CRISPant**

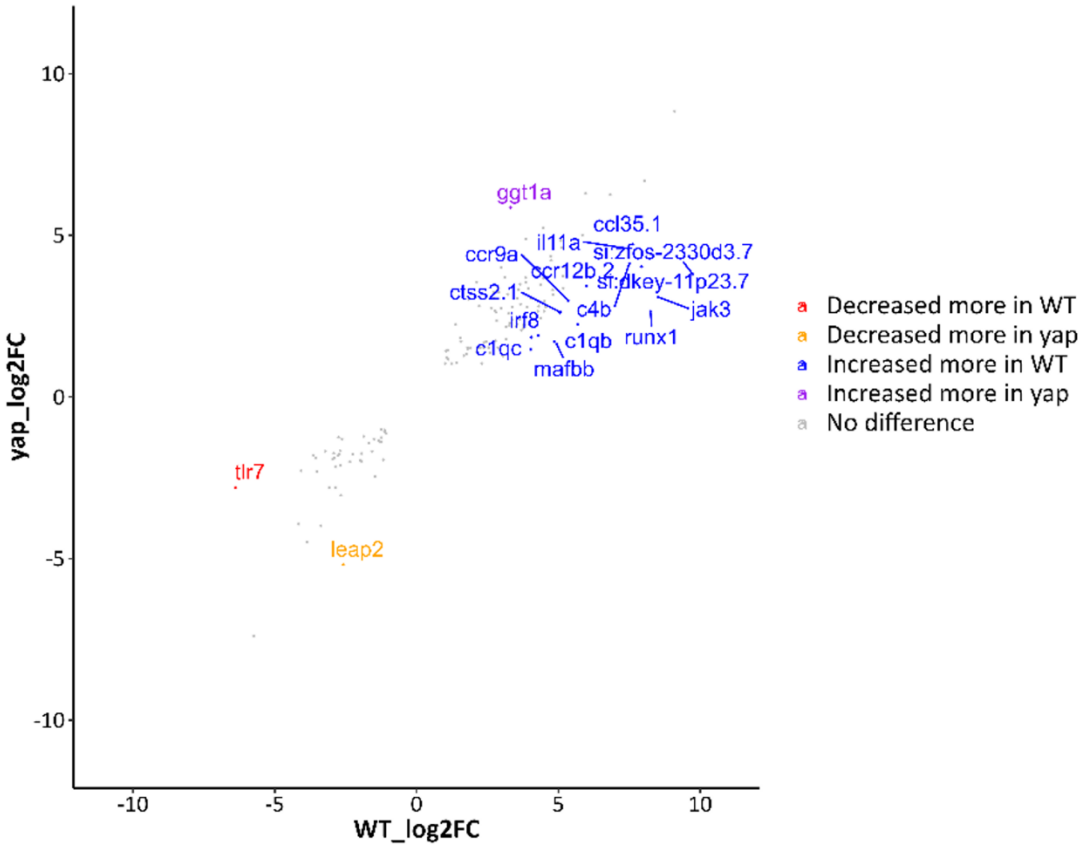

F **DE immune genes WT *vs wwtr1* CRISPant**

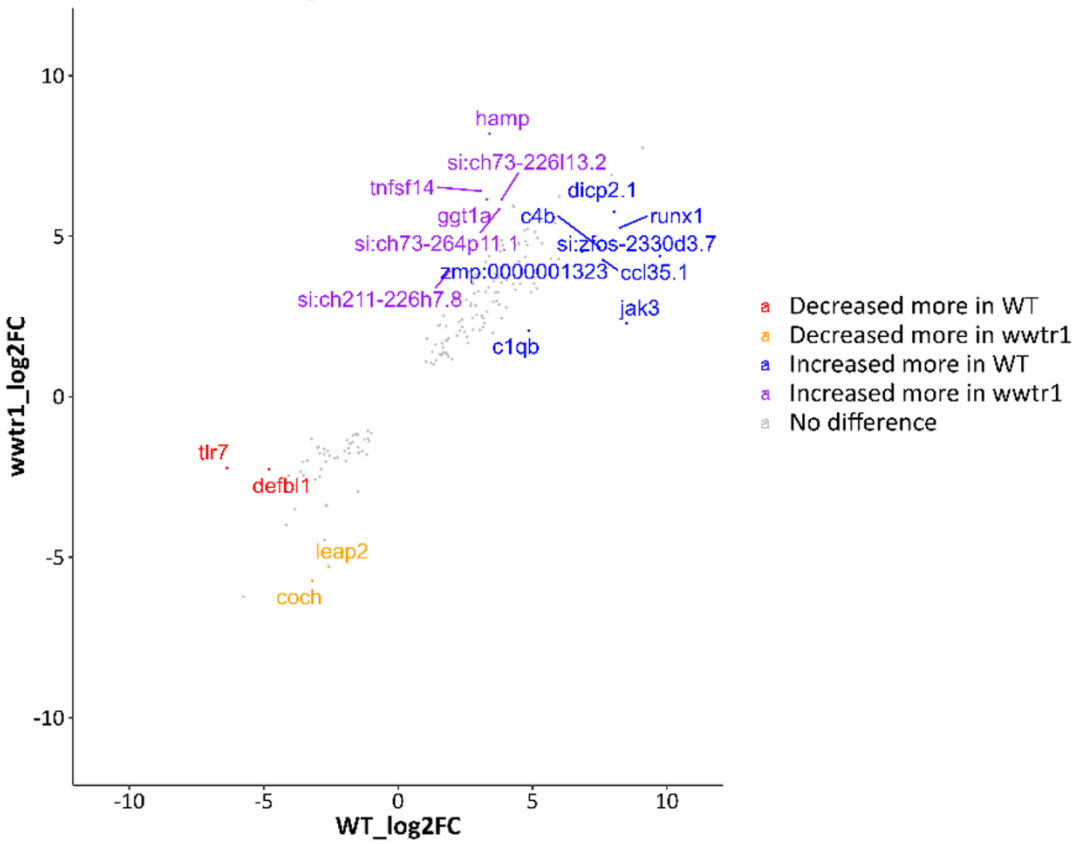

Figure 5.17: RNAseq analysis of immune markers after tail fin injury
(A) Volcano plot of immune markers in WT fish after mild tail fin injury. **(B)** Volcano plot of immune-associated genes in WT fish after severe tail fin injury. **(C)** Volcano plot of immune-associated genes in *yap1* CRISPants after severe tail fin injury. **(D)** Volcano plot of immune-associated genes in *wwtr1* CRISPants after severe tail fin injury. **(E)** Comparison of DE immune genes after severe injury between WT and *yap1* CRISPants. **(F)** Comparison of DE immune genes after severe injury between WT and *wwtr1* CRISPants.
DE=differentially expressed. Cutoff for volcano plots in A-D is p(adj)<0.05 and log2FoldChange>1 or <-1. For A-D, red=increased genes; blue=decreased genes. For E+F, red=genes decreased more in WT relative to CRISPant; orange=genes decreased more in CRISPant; blue=genes increased more in WT; purple=genes increased more in CRISPant. Cut off for change upon injury is p(adj)<0.05 and log2FoldChange>1 or <-1. Cut off for change between genotypes is a difference between genotype of more than 2 log2FoldChange.

5.10 RNAseq analysis of immune markers after tail fin injury

RNAseq analysis of immune-associated genes was then performed in WT and CRISPants after mild and severe tail fin injury (Figure 5.17). In WT fish after mild tail fin injury, there was both increases and decreases in immune gene expression (Figure 5.17A). One notable increase was *mmp9* (4.58 log2 fold change), a matrix metalloproteinase associated with immune cell infiltration[398], suggesting remodelling of the wound environment to allow for immune cell migration and function at the wound. *mmp9* was also increased after severe tail fin injury in WT fish (1.78 log2 fold change) (Figure 5.17B, not labelled), though it was masked in the volcano plot by the higher number of differentially expressed genes. Overall, after severe injury there was a bias towards an increase in immune markers, suggesting an enhancement of immune processes which should be expected. Notable increased genes include chemokines and cytokines from the Ccl, Ccr, and Cxcr families, suggesting a massive increase in immune signalling upon injury. There was also an increase in *spi1b*, a marker that regulates the differentiation of the myeloid progenitor to macrophages and neutrophils[141,147–149], suggesting an increase in innate immune cell production. A similar analysis was performed in *yap1* and *wwtr1* CRISPants after injury (Figure 5.17C+D respectively). A comparable pattern was seen to WT, which is further investigated in Figure 5.17E+F. *spi1b* was increased in CRISPants as well as WT, although *yap1* CRISPants upregulated this expression to a lesser extent than WT and *wwtr1* CRISPants (6.1-fold rather than 9.8-fold), suggesting reduced immune cell production in *yap1* CRISPants.

Table 5.2: Differentially expressed immune-associated genes when compared between WT and CRISPants

Table showing a list of differentially expressed immune-associated genes after injury, their predicted or confirmed function, and their human orthologs. Gene list is obtained as described in 5.10, and grouped according to their comparative expression: either if increased in one genotype but decreased in another or if the log2 fold change difference between genotypes is more than 2 (i.e. 4-fold).

Comparison	Gene name	Associated with: (from zfin.org/ensembl.org)	Human ortholog
Both increased more in WT	*c1qb*	Complement activation, classical pathway[344]	*C1QB*
	c4b	Endopeptidase inhibitor activity and complement activation[345]	*C4B*
	ccl35.1	CCR chemokine receptor binding activity and chemokine activity, cellular response to cytokines, leukocyte chemotaxis, positive regulation of ERK1 and ERK2 cascade, and virus response[357]	Several, including *CCL3* and *CCL3L1*
	jak3	Growth hormone receptor binding activity, non-membrane spanning protein tyrosine kinase activity, T cell differentiation in thymus, and natural killer cell differentiation[338]	*JAK3*
	runx1	Cardiac muscle tissue regeneration, positive regulation of collagen biosynthesis, connective tissue replacement, endothelial to haematopoietic transition, and haematopoiesis[339]	*RUNX1*
Both decreased more in WT	*tlr7*	Inflammatory response and pattern recognition receptor signalling pathway[356]	Several, including *FRMPD4*
Both increased more in CRISPants	*ggt1a*	Glutathione hydrolase activity, glutathione catabolic process, and regulation of inflammatory response[399]	Several, including *GGT1*
Both decreased more in CRISPants	*leap2*	Antimicrobial humoral immune response and defence response to bacterium[400]	*LEAP2*
Increased more in WT relative to *wwtr1* CRISPants	*dicp2.1*	Adaptive immune response, defence response to bacterium, cell adhesion, and positive regulation of NF-kappaB, MAPK, calcium-mediated, and ERK signalling[401,402]	Several, including *CD4*
Decreased more in WT relative to *wwtr1* CRISPants	*defbl1*	Defence response to bacterium and innate immune response[403]	None
Increased more in WT relative to *yap1* CRISPants	*c1qc*	Complement activation, classical pathway[404]	*C1QC*
	ccr12b.2	C-C chemokine binding and receptor activity, calcium-mediated signalling, cell chemotaxis, positive regulation of cytosolic calcium ion concentration, G protein-	None

		coupled receptor signalling pathway, and chemotaxis[405]	
	ccr9a	C-C chemokine binding and receptor activity and lymphoid lineage cell migration into thymus[406]	*CCR9*
	ctss2.1	Cysteine-type endopeptidase activator activity involved in apoptosis, immune response, positive regulation of apoptotic signalling, proteolysis involved in protein catabolic process, and proteolysis[407]	*CTSS*
	il11a	Cytokine activity, growth factor activity, defence response to bacterium, and immune response[408]	*IL11*
	irf8	Microglia development, regulation of macrophage differentiation, and regulation of neutrophil differentiation[409]	*IRF8*
	mafbb	Myeloid leukocyte differentiation and skeletal system development[351]	*MAFB*
Increased more in *wwtr1* CRISPants	*hamp*	Lipopolysaccharide binding activity, lipoteichoic acid binding activity, peptidoglycan binding activity, response to progesterone, bacteria response, and multicellular organismal-level iron ion homeostasis[372]	*HAMP*
	tnfsf14	Tumour necrosis factor receptor binding activity and immune response[374]	*TNFSF14*
Decreased more in *wwtr1* CRISPants	*coch*	Defence response to bacterium, positive regulation of innate immune response, and collagen-containing extracellular matrix[410]	*COCH*

The injury response in WT fish and CRISPants was then compared (Figure 5.17E+F) as described in 5.3.5 above. Results were collated to show differences between genotypes (Table 5.2), albeit with a log2 fold change difference of 2 rather than 3 as used in Table 5.1. When comparing WT and *yap1* CRISPants there was a bias towards a greater number of genes being increased more in WT fish (Figure 5.17E), suggesting that *yap1* CRISPants have a more blunted response to injury than WT fish. This was not seen when WT fish were compared to *wwtr1* CRISPants (Figure 5.17F), which also saw an increase in some genes in *wwtr1* CRISPant, suggesting immune process dysregulation rather than blunting. Table 5.2 shows these differentially altered immune genes, comparing the result of *yap1* and *wwtr1* CRISPR mutagenesis, some of which can also be found in Table 5.1 (which had a more stringent cutoff). Genes increased more in WT fish compared to both CRISPants included chemokines (*ccl35.1*)[326] and complement components (*c4b* and *c1qb*[325]), suggesting a greater

responsiveness of the immune system in WT fish. Many other complement components and chemokines/cytokines were also increased more in WT fish but only relative to *yap1* CRISPants, including *c1qc*, *ccr12b.2*, *ccr9a*, and *il11a*, again suggesting a greater defect in *yap1* CRISPants. Similar to other RNAseq analyses, this also showed metabolic stress with an increase in *ggt1a*[411,412] in both CRISPants compared to WT. *ggt1a* is also an immunosuppressant[413], so increased expression in CRISPants again suggests a dampened or dysregulated immune response. One gene decreased more in WT fish compared to both CRISPants is *tlr7*. This gene usually activates the immune response[414,415], so a greater reduction may suggest that WT fish are beginning to resolve the inflammatory response whilst CRISPants have a disrupted timeline for this to occur. Finally, a marker of macrophage development, *irf8*[149,151], is increased more in WT fish relative to *yap1* CRISPants. Irf8 is also a macrophage marker[151]. This supports the data in 5.9 above of defective macrophage number in *yap1* CRISPants only, indicating an impairment in macrophage development.

5.11 Neutrophils during tail fin regeneration

Innate immune cell function has been investigated after embryonic tail fin injury, most of which were performed in the mild injury paradigm[144,153–155,158–160] (see 1.5). Here, neutrophil numbers were measured during both mild and severe tail fin regeneration using a *lysC*:dsRed transgenic zebrafish line, where neutrophils are labelled with dsRed. Representative images from this analysis are shown in Figure 5.18A (mild) and Figure 5.18B (severe). These numbers were then quantified from the start of the pigment gap to the end of the regenerated fin (Figure 2.6A). Timecourse analysis of WT fish after mild tail fin injury showed a small peak in neutrophil number at 6hpi that plateaued by 24hpi, with no clear difference from CRISPants (Figure 5.18C). When individual timepoints were quantified and genotypes compared, there was no significant change in numbers at 4, 24, or 48hpi (Figure 5.18D, F, G). However, at 6hpi there was a significant reduction in *yap1* CRISPants, and a non-significant trend towards a reduction in *wwtr1* CRISPants as well (Figure 5.18E). This was observed to be the peak of neutrophil infiltration in WT fish, so could suggest that there is a defect in response or infiltration in CRISPants, with the number of neutrophils remaining constant throughout the analysed time period. This defect could be due to defects in the neutrophils themselves, or in the signalling from the tissue to the neutrophils.

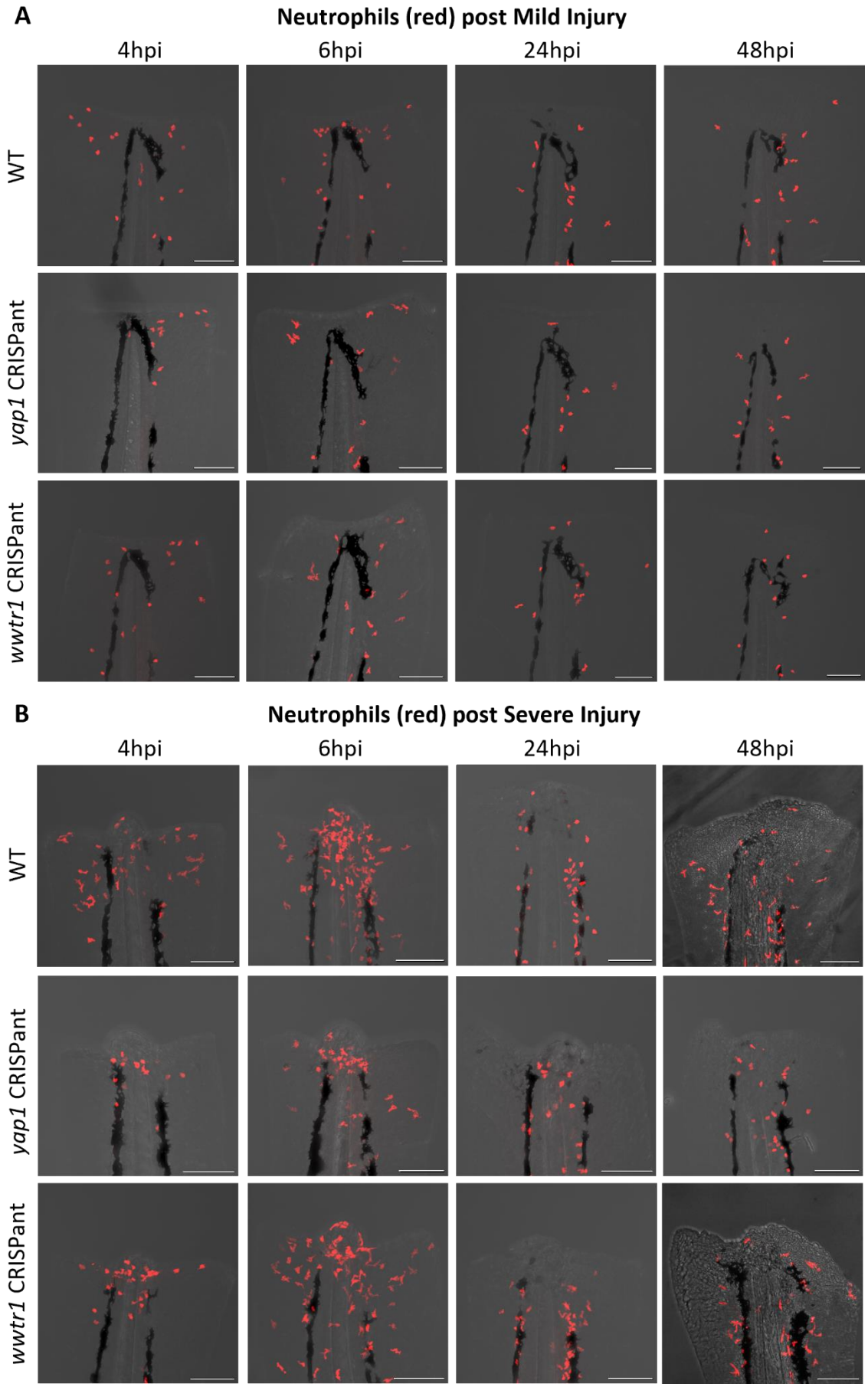
A
Neutrophils (red) post Mild Injury
4hpi
6hpi
24hpi
48hpi
WT
yap1 CRISPant
wwtr1 CRISPant
B
Neutrophils (red) post Severe Injury
4hpi
6hpi
24hpi
48hpi
WT
yap1 CRISPant
wwtr1 CRISPant

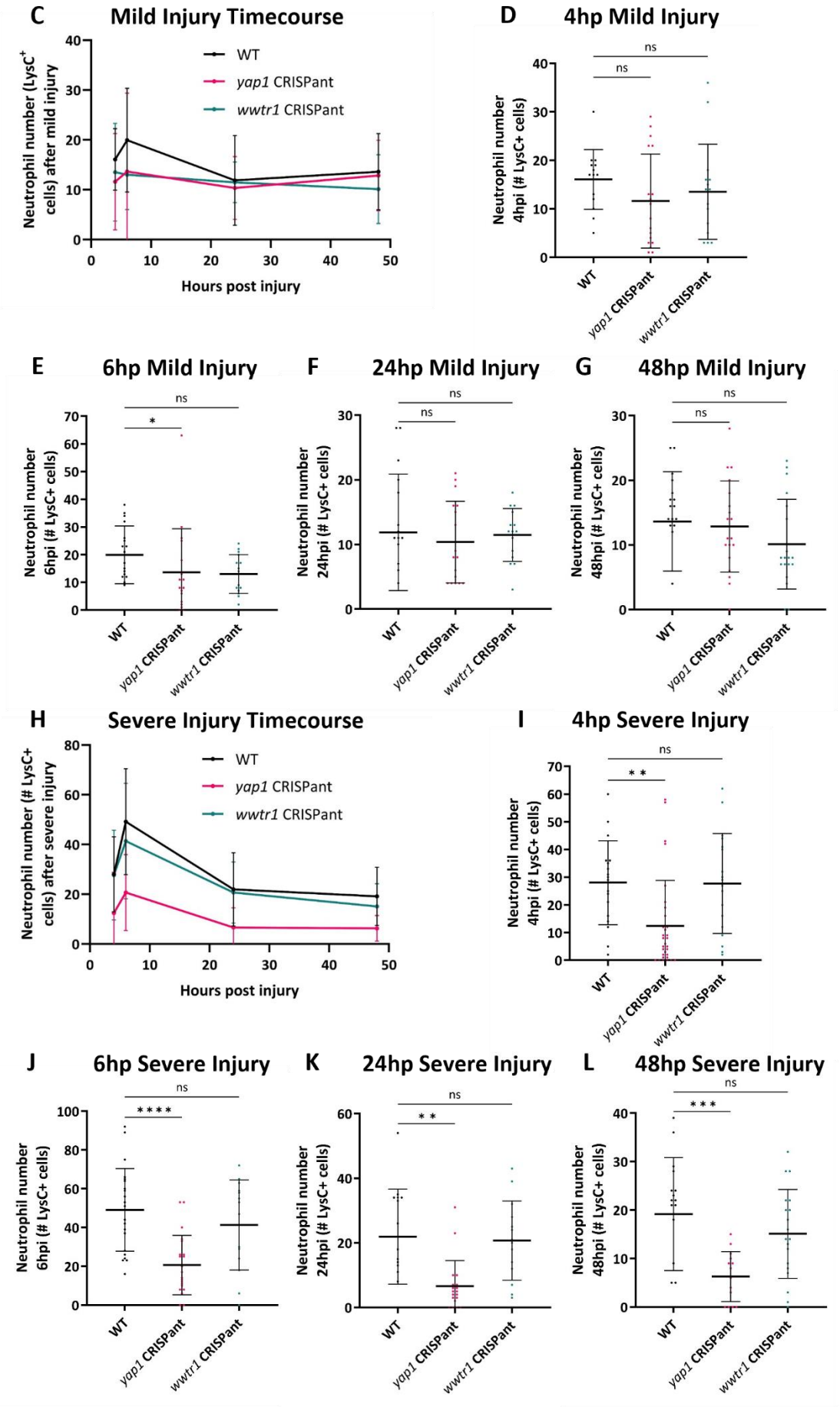
C
Mild Injury Timecourse
Neutrophil number (LysC+ cells) after mild injury
Hours post injury
WT
yap1 CRISPant
wwtr1 CRISPant
D
4hp Mild Injury
Neutrophil number 4hpi (# LysC+ cells)
ns
E
6hp Mild Injury
Neutrophil number 6hpi (# LysC+ cells)
*
F
24hp Mild Injury
Neutrophil number 24hpi (# LysC+ cells)
G
48hp Mild Injury
Neutrophil number 48hpi (# LysC+ cells)
H
Severe Injury Timecourse
Neutrophil number (# LysC+ cells) after severe injury
I
4hp Severe Injury
**
J
6hp Severe Injury
****
K
24hp Severe Injury
L
48hp Severe Injury
***

Figure 5.18: Neutrophil infiltration following tail fin injury
(A) Representative images of neutrophils (*lysC*:dsRed) WT, *yap1* CRISPant, and *wwtr1* CRISPant fins during mild tail fin regeneration. **(B)** Representative images of neutrophils (*lysC*:dsRed) WT, *yap1* CRISPant, and *wwtr1* CRISPant fins during severe tail fin regeneration. **(C)** Timecourse of WT and CRISPant neutrophil numbers during mild tail fin injury regeneration. No obvious changes in CRISPants were observed (significance not calculated). **(D)** Quantification of neutrophil number at 4 hours post mild tail fin injury. CRISPants had no change in number. **(E)** Quantification of neutrophil number at 6 hours post mild tail fin injury. *wwtr1*, but not *yap1*, CRISPants showed a reduction in neutrophil number. **(F)** Quantification of neutrophil number at 24 hours post mild tail fin injury. CRISPants had no change in number. **(G)** Quantification of neutrophil number at 48 hours post mild tail fin injury. CRISPants had no change in number. **(H)** Timecourse of WT and CRISPant neutrophil numbers during severe tail fin injury regeneration. *yap1* CRISPants had reduced numbers throughout the timecourse (significance not calculated). **(I)** Quantification of neutrophil number at 4 hours post severe tail fin injury. *yap1* CRISPants had reduced numbers. **(J)** Quantification of neutrophil number at 6 hours post severe tail fin injury. *yap1* CRISPants had reduced numbers. **(K)** Quantification of neutrophil number at 24 hours post severe tail fin injury. *yap1* CRISPants had reduced numbers. **(L)** Quantification of neutrophil number at 48 hours post severe tail fin injury. *yap1* CRISPants had reduced numbers.
Numbers quantified from the start of the pigment gap to the end of the regenerate (see Figure 2.6A). Scale bar represents 100µm. Bars represent mean±SD. Each dot represents data from one fish. Data from three independent repeats. Significance was calculated by Kruskal-Wallis test (I+K) or one-way ANOVA (remainder) with multiple comparisons. Significance not calculated for timecourse (C+H). *p<0.05; **p<0.01; ***p<0.001; ****p<0.0001; ns=not significant.

Timecourse analysis of neutrophils after severe tail fin injury is shown in Figure 5.18H. The WT numbers followed a similar pattern to that seen after mild injury - namely a peak at 6hpi that plateaus by 24hpi. The overall neutrophil number was however increased relative to mild injury (Figure 5.18C). A pattern also emerged of a reduction in number in *yap1* CRISPants. When quantified at individual timepoints, *yap1* CRISPants had significantly reduced neutrophil numbers at all timepoints measured (Figure 5.18I-L), with no significant change in *wwtr1* CRISPants, suggesting a specific defect in *yap1* CRISPant neutrophils. This reflects the uninjured phenotypes (Figure 5.16), where only *yap1* CRISPants showed neutrophil-associated defects and suggests that the regeneration-associated defect may be due to reduced overall numbers of neutrophils rather than being specific to tail fin injury. However, mild tail fin injury showed no major defect in neutrophil number, suggesting another mechanism may also play a part in the response of neutrophils to injury. The unchanged number of neutrophils in *wwtr1* CRISPants is of interest and suggests that this cell type may not be the underlying issue which causes their defective severe tail fin regeneration.

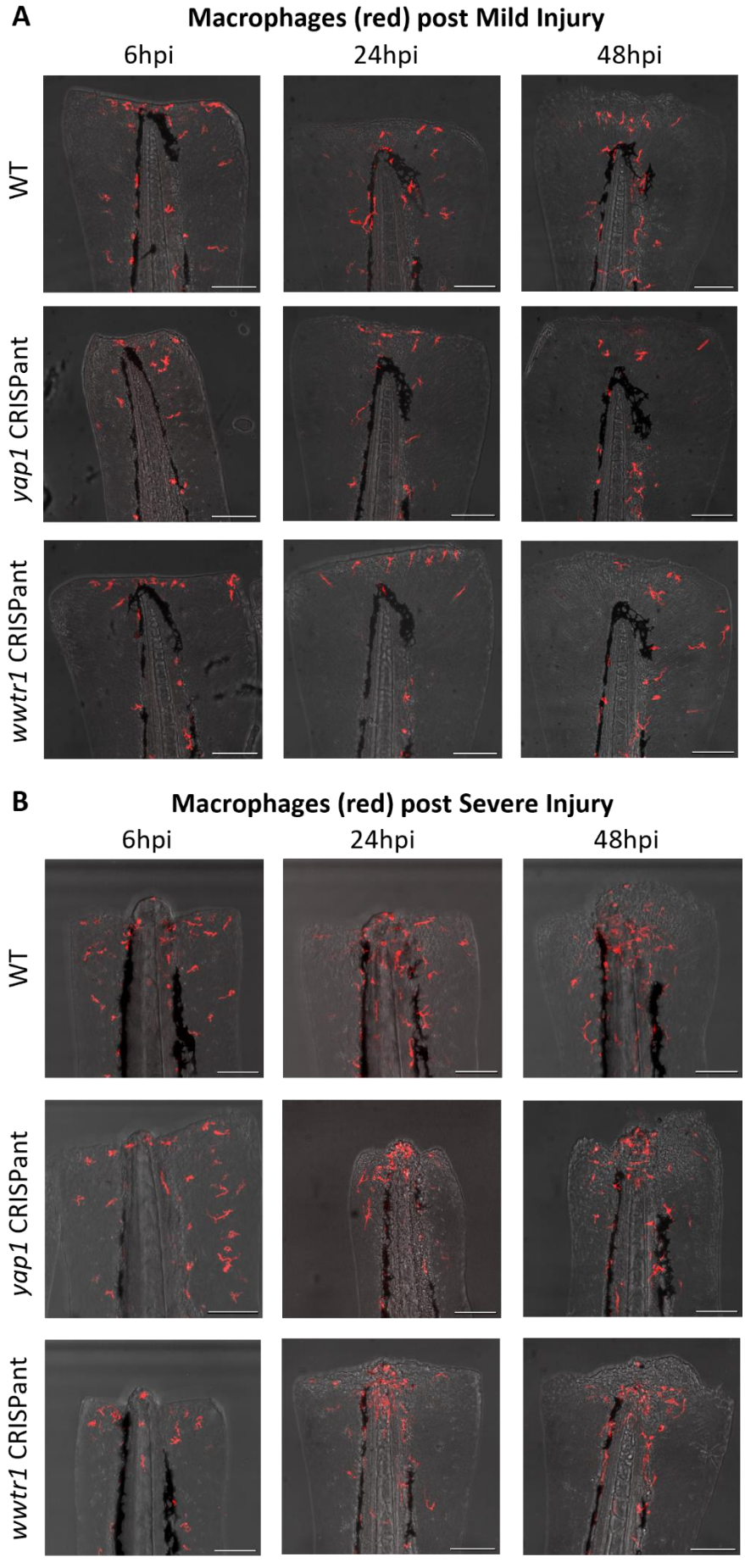
A
Macrophages (red) post Mild Injury
6hpi
24hpi
48hpi
WT
yap1 CRISPant
wwtr1 CRISPant
B
Macrophages (red) post Severe Injury
6hpi
24hpi
48hpi
WT
yap1 CRISPant
wwtr1 CRISPant

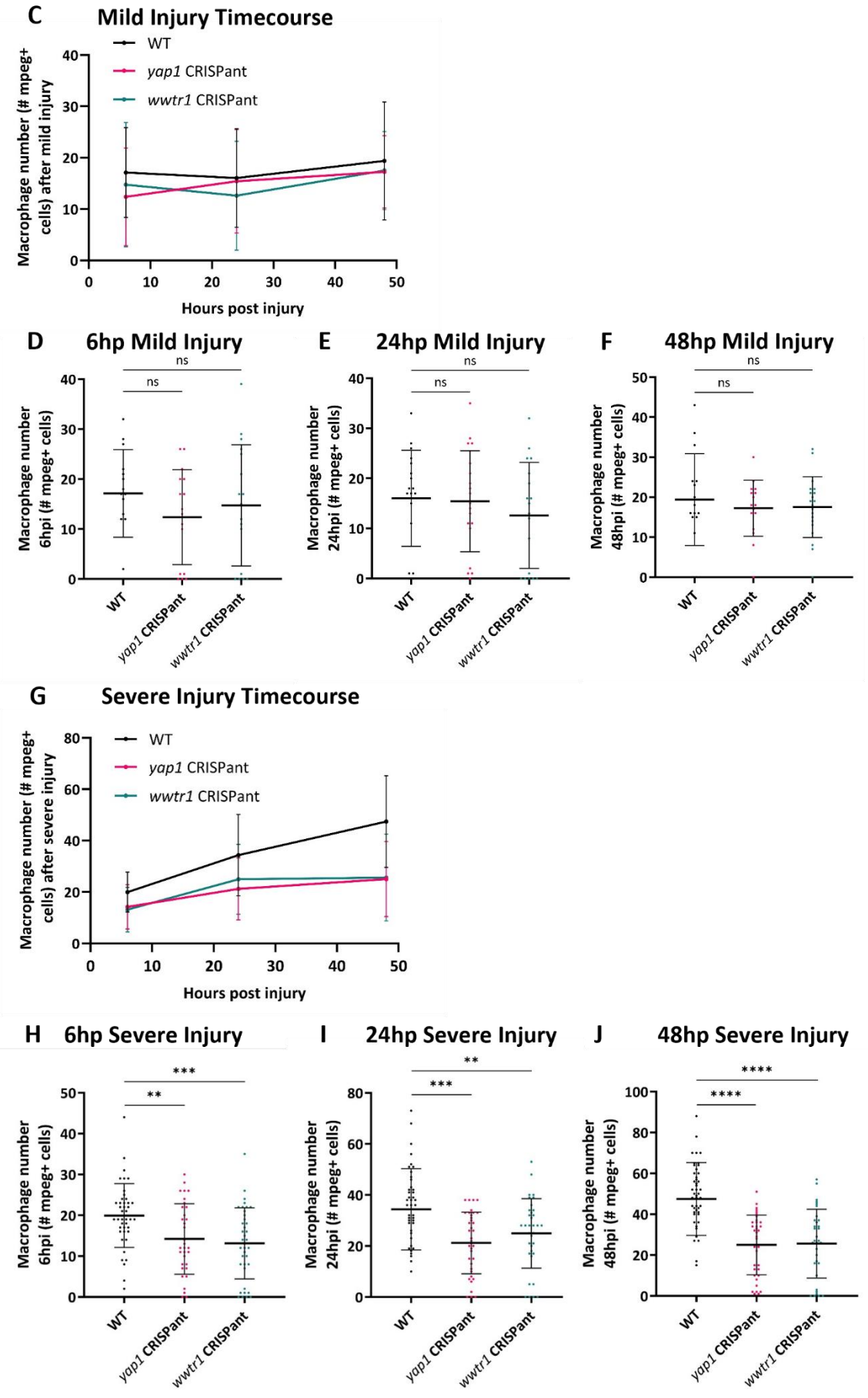
C
Mild Injury Timecourse
WT
yap1 CRISPant
wwtr1 CRISPant
Macrophage number (# mpeg+ cells) after mild injury
Hours post injury
D
6hp Mild Injury
E
24hp Mild Injury
F
48hp Mild Injury
Macrophage number 6hpi (# mpeg+ cells)
Macrophage number 24hpi (# mpeg+ cells)
Macrophage number 48hpi (# mpeg+ cells)
ns
WT
yap1 CRISPant
wwtr1 CRISPant
G
Severe Injury Timecourse
Macrophage number (# mpeg+ cells) after severe injury
H
6hp Severe Injury
I
24hp Severe Injury
J
48hp Severe Injury
**
***
****

Figure 5.19: Macrophage infiltration following tail fin injury
(A) Representative images of macrophages (*mpeg*:mCherry) WT, *yap1* CRISPant, and *wwtr1* CRISPant fins during mild tail fin regeneration. **(B)** Representative images of macrophages (*mpeg*:mCherry) WT, *yap1* CRISPant, and *wwtr1* CRISPant fins during severe tail fin regeneration. **(C)** Timecourse of macrophage number after mild tail fin injury. No obvious changes in CRISPants were observed (significance not calculated). **(D)** Quantification of macrophage number at 6 hours post mild tail fin injury. CRISPants had no change in number. **(E)** Quantification of macrophage number at 24 hours post mild tail fin injury. CRISPants had no change in number. **(F)** Quantification of macrophage number at 48 hours post mild tail fin injury. CRISPants had no change in number. **(G)** Timecourse of macrophage number after severe tail fin injury. Both CRISPants showed reductions in number (significance not calculated). **(H)** Quantification of macrophage number at 6 hours post severe tail fin injury. Both CRISPants show significant reductions in macrophage number. **(I)** Quantification of macrophage number at 24 hours post severe tail fin injury. Both CRISPants show significant reductions in macrophage number. **(J)** Quantification of macrophage number at 48 hours post severe tail fin injury. Both CRISPants show significant reductions in macrophage number.
Numbers quantified from the start of the pigment gap to the end of the regenerate (see Figure 2.6A). Scale bar represents 100µm. Bars represent mean±SD. Each dot represents data from one fish. Data from at least four independent repeats. Significance was calculated by one-way ANOVA with multiple comparisons. Significance not calculated for timecourse (C+G). **p<0.01; ***p<0.001; ****p<0.0001; ns=not significant.

5.12 Macrophages during tail fin regeneration

Previous studies into macrophage function during tail fin regeneration have mainly focussed on the mild injury paradigm and have not investigated the role of the Hippo pathway (see 1.5). Macrophage numbers were analysed using a *mpeg*:mCherry transgenic line, where macrophages are labelled with mCherry[144]. Representative images are shown in Figure 5.19A (mild injury) and Figure 5.19B (severe injury). Similar to neutrophil analyses after mild tail fin injury, a timecourse of macrophage numbers showed no obvious change in macrophage numbers across the imaging time period, and no clear change after CRISPR mutagenesis (Figure 5.19C). This is supported by investigation of the individual timepoints, where there was no significant change in macrophage numbers in CRISPants after mild injury (Figure 5.19D-F). This could suggest a limited role of macrophages in recovery after this injury type, or that the mild injury phenotype observed in *yap1* CRISPants is a result of defects in other cell types.

A markedly different pattern was seen after severe tail fin injury. WT fish showed a steady increase in macrophage numbers following severe injury (Figure 5.19G), an increase that was not seen in CRISPants. When quantified at individual timepoints, there was a significant reduction in number in both CRISPants at all timepoints (Figure 5.19H-J). This suggests a defect in macrophage infiltration or response to severe tail fin injury in *wwtr1* CRISPants,

particularly as data from uninjured fish showed no change in macrophage number (Figure 5.16), giving a possible mechanism for the impaired regeneration in *wwtr1* CRISPants. The defect in *yap1* CRISPants may be a result of the reduced number of macrophages in uninjured fish (Figure 5.16), although, as for neutrophil data (Figure 5.18), there was no change in mild injury so there may be additional processes impacting on this.

Mammalian macrophages can be classified into two subtypes: the pro-inflammatory M1 macrophages and the anti-inflammatory M2 macrophages[416]. Similar subtypes have been observed in the larval zebrafish, which have different roles after mild tail fin injury[158,159,396]. These can be distinguished as M1-like macrophages express *tnfα*, whilst M2-like macrophages do not[159]. The number of M1-like macrophages peaks at 6hpi then reduce over regeneration following mild injury, whilst the number of M2-like macrophages peaks at 6hpi but then plateaus[158]. Recent evidence suggests that these macrophages are recruited in a single wave, and the M1-like macrophages switch both their shape and behaviour to M2-like macrophages at the wound[396]. Tnfα and its receptor Tnfr1 are both also necessary for fin regeneration via activation of blastema cells[158].

Macrophage subtypes were investigated using a *mpeg*:mCherry; *tnfα*:GFP transgenic line, where M1-like macrophages are colabelled with both *mpeg* and *tnfα*, and M2-like macrophages are labelled with *mpeg* only. Because a genotype-induced significant change was only observed after severe injury (Figure 5.19G), these macrophage subtypes were only investigated after severe injury. Representative images are shown in Figure 5.20A (6hpi), Figure 5.20B (24hpi), and Figure 5.20C (48hpi). When quantified, timecourse analyses showed that M1-like macrophage number increased up to 24hpi, then plateaued, with CRISPants having no significant change from WT (Figure 5.20D). M2-like macrophage number showed a steady increase throughout the imaging period in WT fish (Figure 5.20E). In *yap1* CRISPants, M2-like macrophages were significantly reduced from 24hpi, and in *wwtr1* CRISPants M2-like macrophages were decreased at 48hpi. This indicates that these CRISPants may have a defect in the switch from M1-like to M2-like macrophages, suggesting that the defect in regeneration could, at least in part, be a result of an extended pro-inflammatory environment in the tail fin due to defects in the macrophage subtype that would usually resolve it. One hypothesis could be that the *yap1* CRISPant phenotype is a result of a general defect in macrophage function, whilst the

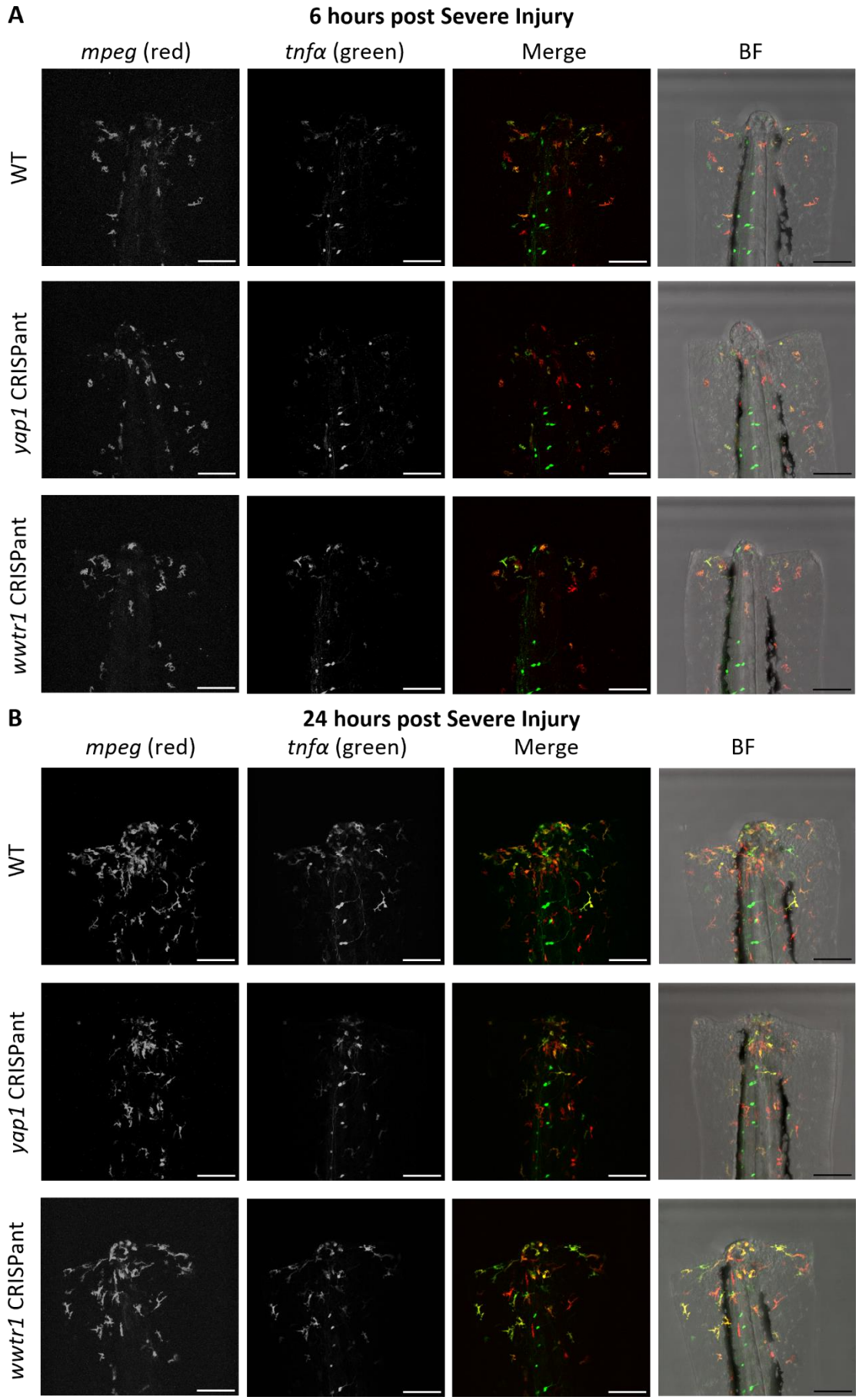
A
6 hours post Severe Injury
mpeg (red)
tnfα (green)
Merge
BF
WT
yap1 CRISPant
wwtr1 CRISPant
B
24 hours post Severe Injury
mpeg (red)
tnfα (green)
Merge
BF
WT
yap1 CRISPant
wwtr1 CRISPant

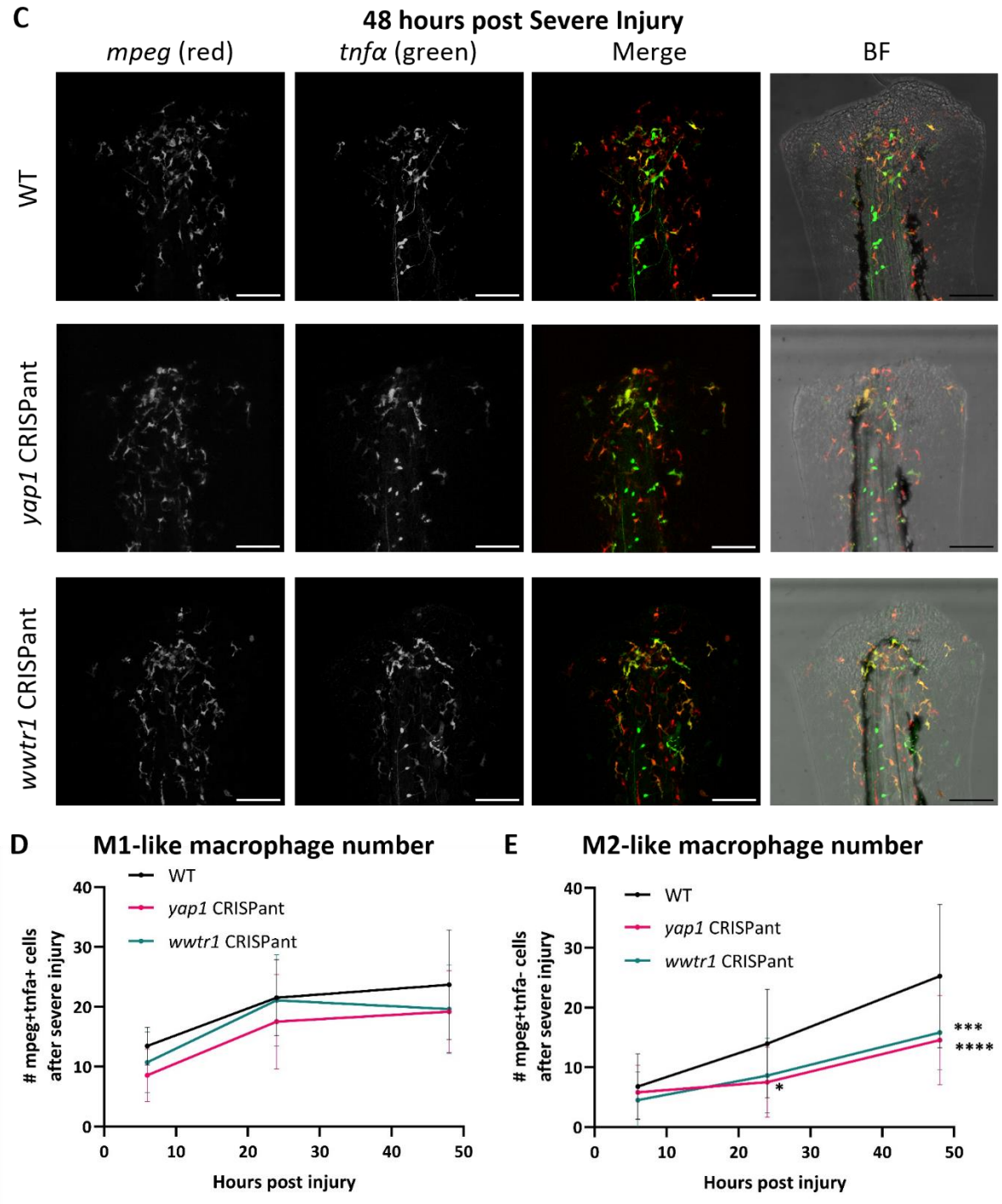

Figure 5.20: Macrophage subtypes are altered after severe tail fin injury

(A) Representative images of *mpeg* (*mpeg*:mCherry) and *tnfα* (*tnfα*:GFP) positive macrophage infiltration in WT, *yap1* CRISPant, and *wwtr1* CRISPant fins at 6 hours post severe tail fin regeneration. **(B)** Representative images of *mpeg* (*mpeg*:mCherry)- and *tnfα* (*tnfα*:GFP)-positive macrophage infiltration in WT, *yap1* CRISPant, and *wwtr1* CRISPant fins at 24 hours post severe tail fin regeneration. **(C)** Representative images of *mpeg* (*mpeg*:mCherry) and *tnfα* (*tnfα*:GFP) positive macrophage infiltration in WT, *yap1* CRISPant, and *wwtr1* CRISPant fins at 48 hours post severe tail fin regeneration. **(D)** Timecourse of number of M1-like ($mpeg^{+}tnf\alpha^{+}$) macrophages during severe injury. CRISPants did not significantly differ from WT at any time point. **(E)** Timecourse of number of M2-like ($mpeg^{+}tnf\alpha^{-}$)

macrophages during severe injury. *yap1* CRISPants had reduced number from 24 to 48hpi, whilst *wwtr1* CRISPants had reduced number at 48hpi only.
Numbers quantified from the start of the pigment gap to the end of the regenerate (see Figure 2.6A). Scale bar represents 100µm. Bars represent mean±SD. Data calculated from three independent repeats. Significance was calculated by two-way ANOVA, with multiple comparisons. *p<0.05; ***p<0.001; ****p<0.0001

---

wwtr1 CRISPant impairment in the M1-like to M2-like switch could be a more specific defect. This can be reflected in the RNAseq analysis (Table 5.2), which shows a *wwtr1* CRISPant-specific increase in *tnfsf14* compared to WT. *tnfsf14* enables Tnf signalling[417,418], and so may reflect the maintenance of the M1-like macrophage population in the tail fin. However, whether the defect in phenotype switching is due to something cell-intrinsic or the external environment is yet to be determined.

In conclusion, there is widespread immune cell dysfunction in *yap1* CRISPants both when uninjured and after severe tail fin injury. This could be due to a multitude of reasons, particularly as these CRISPants show many developmental defects as well, indicating widespread cellular dysfunction. However, the immune dysfunction in *wwtr1* CRISPants is much more specific, with a defect in macrophage function, potentially in the switch to pro-regenerative M2-like macrophages. The cellular phenotype could therefore underlie the highly specific regenerative (but not developmental) defects observed in these CRISPants.

6 Discussion

6.1 Flexibility, utility, and limitations of CRISPR/Cas9 mutagenesis in the embryonic zebrafish to study development and regeneration

6.1.1 Optimisation of a CRISPR/Cas9 zebrafish screen

In this thesis, a CRISPR/Cas9 screen was conceived, optimised, and implemented to investigate the roles of a range of selected Hippo pathway components in zebrafish embryonic development and regeneration (summarised in Figure 3.13). The zebrafish embryo is of particular utility in the design and implementation of an *in vivo* CRISPR/Cas9 screen (see 1.7). External egg fertilisation allows for the injection of CRISPR/Cas9 complexes at the one-cell stage and subsequent quick development enables the study of both regeneration and development within a short period of 5 days. Both fixed and live embryos are also easy to image via light and confocal microscopy, due to their optical transparency, the availability of many different fluorescent transgenic lines, and the ease of administration of drugs and fluorescent markers into the embryo water.

As described in 1.7, there are many key criteria that must be met for a successful CRISPant screen experiment, including a high mutagenesis rate, ease of microinjection mixture generation and administration to one-cell embryos, a quick yet robust identification of phenotypes, and recapitulation of stable mutant phenotypes. The optimised CRISPR/Cas9 screen presented in this thesis met many of these criteria, potentially to a greater extent than some other published screens[201–203,419,420]. A very high efficiency of mutagenesis was achieved with 100% of embryos tested showing target gene mutagenesis induced by each guide RNA (Figure 3.14). This was greater than many other screens, which report around 90% mutagenesis efficiency[203,419,420]. The high rate of mutagenesis was achieved by a combination of careful design and screening of guide RNAs, the use of chemically modified reagents reported to increase efficiency (i.e. Alt-R technology, IDT), and injection methods that ensured full delivery of the CRISPR/Cas9 complexes (see 2.1 for more detail). To ensure full target gene mutagenesis, two guide RNAs were co-injected into each embryo. Increased number of guides (multiplex targeting) has been shown to promote mutagenesis efficiency[421]. However, this also increases the likelihood of off-target effects[202] and might increase the diversity of alleles created in the F0 CRISPant population[420,421], potentially masking CRISPR-

induced phenotypes as a range of proteins with different functionalities might be generated within the same population. This was balanced in this project by the injection of only two guide RNAs, increasing mutagenesis of the target whilst reducing the likelihood of off-target effects, resulting in specific reductions in both mRNA and protein (Figure 3.4 and Figure 3.5). Pre-screening of guide RNAs for those with the highest efficiency can also be performed prior to injection[202], but was not determined to be necessary for the workflow presented here.

Another criterion to be met in the implementation of a CRISPR/Cas9 screen is the ease of microinjection mix generation and administration to the embryo. This reduces the likelihood of toxicity to the embryo whilst increasing the ease and speed of experimentation, required for the analysis of multiple CRISPants. The generation of the CRISPR/Cas9 microinjection mix often varies between different papers, with different levels of involvement. Some reports perform *in vitro* synthesis of Cas9 mRNA and guide RNA[422], a lengthy process that was not required for this study as pre-synthesised reagents were utilised (2.22). These reagents also allowed the generation of Cas9-guide RNA-tracrRNA riboprotein complexes, that are designed to mimic the native *S. pyrogenes* CRISPR/Cas9 system, and so give high efficiency and specificity[194,423]. Reports also differ in the method to mix the CRISPR/Cas9 components. Therefore, a range of temperature of generation was tested (Figure 3.1). It was found that the ideal temperature of mix generation, creating the expected phenotypes with no effects on controls, was at room temperature, which also improved the ease of mixture generation as no heating was required. The amounts of reagents injected and the location of injection also vary between reports. The volume of injection was optimised in this project (Figure 3.2) to ensure that CRISPR mutagenesis could efficiently be performed without toxicity. Importantly, the volume of reagents injected was consistent irrespective of the number of guides injected (i.e. for double versus single CRISPants twice the number of guides were injected but the same volume), which is often not performed in published screens. In order to further increase the ease of experimentation and reduce embryo death, the injection point was the yolk of the single cell embryo, a location much easier to access than the cell. Injection into the cell is typically used to investigate F0 embryo phenotypes, as it has been reported to result in higher mutagenesis efficiency, despite also showing increased embryo death[422]. However, injection into the yolk still resulted in 100% mutagenesis efficiency (Figure 3.14), so this was continued for the whole screen as it increased speed of injection.

Quick and robust investigation of phenotypes is also a requirement for successful CRISPR/Cas9 screens. This was partially achieved in this thesis. Analysis of multiple paradigms could be performed in F0 embryos, which has been previously reported[420]. Some published screens required the use of F1 or F2 embryos to ensure gene mutation and a penetrant phenotype was achieved (for example[201,422]) but this was not required in this project as clear F0 phenotypes were observed. The ability to use the embryo is also of interest, as it reduces the experimental time, cost, and the number of adult animals required, which should always be as low as possible, in keeping with the 3 R's principle of animal research. However, the relatively lengthy hands-on time required for the imaging and analysis of the CRISPant phenotypes meant that a relatively small number of genotypes could be investigated – 13 rather than 100 as reported in other regeneration screens[201]. This limits the practicality of this screen for expansion into the study of other genes, however it was sufficient to identify phenotypes of interest here.

Finally, robust reporting of F0 CRISPant phenotypes would ideally recapitulate stable mutant phenotypes, where the mutation is known and the complete removal of the protein of interest is assumed. Other studies have reported efficient recapitulation of phenotypes[199,419–421], but this was not completely observed in the screen described here. Although *yap1* stable mutants phenocopied *yap1* CRISPants in almost all parameters measured, *wwtr1* stable mutants displayed more severe phenotypes than their CRISPant counterparts (Figure 4.7 to Figure 4.9). However, recapitulation is not always observed, as stable mutants can undergo genetic compensation that alters their transcriptome to potentially also alter their phenotype[424]. Therefore, this phenotypic difference does not negate the utility of the CRISPR/Cas9 screen performed here. In conclusion, this CRISPR/Cas9 screen allowed for the first identification of multiple individual Hippo pathway component CRISPant phenotypes in the zebrafish, some of which were highly specific, and are discussed in further detail below.

6.1.2 A CRISPR/Cas9 screen of Hippo pathway components showed a range of phenotypes that inform knowledge on Hippo pathway function in development and regeneration

Measurements of development at 96hpf gave a range of both expected and unexpected novel phenotypes. As expected from published work (summarised in 1.3), *yap1* CRISPants had reduced length, reduced organ size, developmental delay, and general developmental

disruption (Figure 3.7). When measured at juvenile stages, these phenotypes mostly disappeared (Figure 3.9), suggesting that the most disrupted fish died at post-embryonic stages, or that these embryonic phenotypes can be compensated for in the adult fish. It was of particular interest to compare the pattern of *yap1*-mediated embryonic phenotypes to other CRISPants. One notable comparison is analysis of eye area (Figure 3.15D), which was significantly reduced in *yap1* CRISPants. Conversely, single CRISPants of upstream inhibitory kinase cascade components (*lats1*, *lats2*, *nf2a*, and *nf2b*) had significant eye overgrowth. As inhibiting this kinase cascade reduces Yap1/Taz phosphorylation, increasing their nuclear translocation and so ability to promote transcription, this is thought to demonstrate the effect of increasing Yap1/Taz activity. However, *wwtr1* (gene encoding Taz) CRISPants had no significant change in eye area. This suggests that Taz itself may not regulate eye area in this model, and so the upstream kinase CRISPant phenotypes are potentially the result of predominantly enhancing Yap1. Similarly, single CRISPants for Yap1/Taz target genes (*ctgfa*, *ctgfb*, and *cyr61*) had reduced eye size, suggesting that in this process they are regulated by Yap1 activity more than Taz. Overall, this implies that Yap1 has more of a role in eye size (and potentially organ size in general) regulation than Taz. However, this was not consistent amongst all parameters measured.

One example of this difference was in measurements of swim bladder inflation (reflecting developmental delay) (Figure 3.15C). Whilst *yap1* CRISPants had a decrease in size and *wwtr1* CRISPants had no change in size, similar to eye area measurements, the only upstream component CRISPant with an increase in size was the *lats1* CRISPant and only two target gene CRISPants had a decrease in size (*ctgfa* and *cyr61*). Some upstream components even had the same phenotype as *yap1* CRISPants, such as a decrease in swim bladder inflation in *nf2b* CRISPants. This suggests that there is not a clear opposite effect of constitutively increasing Yap1/Taz activity compared to decreasing it across all cell types, implying the presence of multi-level, and potentially spatiotemporal, regulation of these proteins in these processes.

In general, Hippo pathway target gene CRISPants had similar, but less severe, developmental phenotypes to *yap1* CRISPants. As well as this indicating a greater role for Yap1 than Taz in the regulation of these target genes, this also suggests that a combination of Hippo pathway target genes is required to mediate its function in development rather than a strong role of any individually.

Overall, when comparing each parameter against another (Figure 3.19), fish disrupted in one parameter were often disrupted in another, indicating a role for Hippo pathway components in general development, rather than the specific regulation of a single process, such as heart formation. It was also found that Yap1 had a much greater role in development than Taz as *yap1* CRISPants were significantly more disrupted in all parameters than *wwtr1* CRISPants.

yap1 and *wwtr1* CRISPants also showed differences in regenerative phenotypes. Whilst *yap1* CRISPants showed regeneration defects in almost all parameters measured, *wwtr1* CRISPants lacked regenerative phenotypes apart from after severe tail fin injury. As well as demonstrating another difference between *yap1* and *wwtr1* CRISPants, this highlights that mild and severe tail fin injury clearly have differences in regenerative processes (see 6.4 below for further discussion of this).

Regeneration in upstream inhibitory kinase cascade CRISPants showed different results to those seen during development. Whilst some developmental phenotypes were the opposite to those seen in *yap1* CRISPants, opposite regenerative phenotypes (i.e. enhanced regeneration) were not observed, apart from an increase in neuromast number following injury in *lats1* CRISPants (Figure 3.17E+G). Many phenotypes of upstream kinase cascade components in fact phenocopied *yap1* CRISPants with a defect in regeneration. This suggests that Yap1/Taz activity must be under tight spatio-temporal control within this finely balanced process, and that enhancing regeneration is not as simple as removing an inhibitory factor.

Another interesting comparison is between *ctgfa* and *ctgfb* CRISPants during regeneration. Ctgfa has been associated with promoting regeneration in zebrafish spinal cord and heart regeneration[38]. However, it did not appear to have any role in neuromast regeneration or either tail fin regenerative paradigms in this screen (Figure 3.17 and Figure 3.18), suggesting that the pro-regenerative role is not common to all regeneration types. In contrast, in this screen Ctgfb appeared to have an anti-regenerative effect, as the *ctgfb* CRISPant showed increased regeneration. These fish had an increase in both neuromast area and number at 48hpi (Figure 3.17F+G), and an increase in fin area after severe tail fin injury (Figure 3.18D). The processes behind this effect are unclear, and outside of the scope of this thesis to investigate but may be due to the role of this protein in the extracellular matrix, which can be both pro- and anti-regenerative[425]. The differing function of Ctgfa and Ctgfb is also reflected

in the phenotypes of the *ctgfa*/*ctgfb* double CRISPant. Unlike other double CRISPants, these phenotypes were often not more severe than those of the single CRISPants, suggesting limited compensation between Ctgfa and Ctgfb.

Comparison of other double CRISPants to their single CRISPant counterparts was also of interest. In both development and regeneration, double CRISPants often had a more severe phenotype than either single CRISPant alone. This suggests that many components compensate for their close paralogs. For example, in eye area analysis (Figure 3.15D), both *lats1* and *lats2* single CRISPants showed an increased eye size. However, *lats1*/*lats2* double CRISPants had reduced eye size, suggesting that at least one of the Lats proteins must be present for the overgrowth phenotype to be displayed. The *yap1*/*wwtr1* double CRISPant was also often more severe than each CRISPant alone. This suggests that, despite limited phenotypes in the *wwtr1* CRISPant, Taz still has a role in the processes analysed. It may also imply that Taz loss can be compensated for by Yap1 in *wwtr1* CRISPants, but that Taz alone is not sufficient to compensate for the loss of Yap1 in *yap1* CRISPants, which has also been observed *in vitro*[44]. Notably, in mild tail fin regeneration (Figure 3.18C), the double *yap1*/*wwtr1* CRISPant did not have a more severe defect than *yap1* CRISPants, suggesting that Taz does not function in this regenerative paradigm. This is distinct from severe tail fin regeneration (Figure 3.18D), where the double CRISPant was more defective than either alone, suggesting a role for both Yap1 and Taz in severe regeneration.

6.1.3 Limitations of the CRISPR/Cas9 screen

Despite the many advantages of this CRISPR/Cas9 screen, there are some drawbacks that may limit the conclusions that can be drawn from it. One limitation is the requirement for manual injection, imaging, and quantification, which is labour-intensive, preventing the screen from being high-throughput and limiting the number of embryos that can be analysed in a single repeat. Another limitation is the use of zebrafish, which often have a large variety of phenotypes, even within the same group. When combined with the use of F0 CRISPants, where the mutations induced by CRISPR are varied and not always deleterious or fully penetrant, this creates a group with high variance that therefore requires many samples to reach an appropriate power level for significance. In addition, performing whole-organism disruption of genes that have many functions also creates issues with analyses of

regeneration. Embryos with disrupted development, such as *yap1* CRISPants, are therefore also likely to have disrupted regeneration due to wide-ranging defects in organ and cell function, such as disrupted vasculature, rather than the disruption of a specific regenerative process. It may therefore be interesting in the future to use conditional gene deletions, i.e. only inhibit gene function shortly before regeneration, or cell-specific deletions. Finally, it may be claimed that regeneration during embryonic stages as performed in this screen may differ from "true" adult regeneration, where the fish is not actively growing and so may have a different reaction to injury. Future comparisons with regeneration in the adult CRISPant would therefore be of interest. Overall, there are some limitations to the utility of the CRISPR/Cas9 screen described in this thesis. However, the screen is extremely powerful in its ability to discover a range of *in vivo* phenotypes relatively quickly and in a model organism that has many experimental benefits (see 6.1.1 above), so is still of much utility in this study.

6.1.4 Comparison of CRISPant and stable mutant phenotypes

CRISPant embryos have the advantage over stable mutants in their ease and speed of generation. CRISPR-mediated targeting of *yap1* and *wwtr1* has also shown a very efficient loss of targeted protein (Figure 3.5). However, CRISPant mutagenesis is varied in the exact mutations induced, has a greater likelihood of generating heterozygotes or chimeras, and WT maternal mRNA is still present, affecting early development. These factors are not present in a stable mutant line as fish are genotyped to confirm the presence of a deleterious mutation and bred to homozygosity. It was therefore of interest to generate stable mutant lines from CRISPants of interest and compare their phenotypes. Both *yap1* and *wwtr1* stable mutants were able to be generated (4.2), although they were often difficult to maintain with reduced survival and breeding capacity (particularly *yap1* stable mutants). When put through the same analyses as CRISPants, stable mutants in general showed a more severe phenotype than CRISPants (Figure 4.7 to Figure 4.9). Overall, *yap1* stable mutants robustly phenocopied *yap1* CRISPants, showing defects in almost all parameters measured, confirming the general role of Yap1 in both development and regeneration. However, *wwtr1* stable mutants did not phenocopy *wwtr1* CRISPants in all parameters, showing both developmental and regenerative defects that were not seen in the CRISPants. This could demonstrate the importance of *wwtr1* maternal mRNA or potentially the lower efficiency of deleterious mutagenesis in the CRISPant. It could also be a result of experimental differences, such as the

use of inappropriate controls in the *wwtr1* stable mutant, as WT sibling controls could not be generated. CRISPant and stable mutant experiments were also not conducted at the same time (and so may be affected by experimenter experience and aquaculture conditions), and there was a lower sample size in stable mutants. Of note, stable mutants may also have developed compensatory mechanisms that allow the organism to survive without the targeted gene. However, this could be predicted to result in milder phenotypes than CRISPants, whereas stable mutants here showed a more severe phenotype.

Overall, this data suggests that CRISPR mutagenesis cannot fully replace the generation of stable mutant lines. However, CRISPR mutagenesis provides evidence towards the final phenotype of mutants, and the fast generation time allows for the investigation into the effect of disrupting multiple genes with much less hands-on experimental time required than for stable mutants.

6.2 The role of Taz in embryonic zebrafish

6.2.1 *wwtr1* CRISPR-mediated disruption caused specific defects in severe tail fin injury regeneration

A CRISPant of particular interest is the *wwtr1* CRISPant. These embryos had only slight developmental phenotypes, no significant change in any neuromast measurement (both at baseline and after injury), and no difference in baseline tail fin growth or mild tail fin regeneration (see Figure 3.19 for an overview). One clear phenotype was a defect in tail fin regeneration after severe injury, which became apparent by 48hpi (Figure 5.2). One question arising from this is whether there is a process that occurs around 48hpi that is altered after CRISPR mutagenesis, or whether the defect is caused by changes in processes earlier in development that only impacts the fish at later timepoints. RNAseq analysis was performed at 24hpi to determine if any changes can be observed at a transcriptomic level at this timepoint. A PCA plot showed that all genotypes (WT, *yap1* CRISPant, *wwtr1* CRISPant) had a large shift in transcriptome upon injury (Figure 5.4A). *wwtr1* CRISPants were transcriptionally similar to WT fish both before and after injury, which was also apparent in deeper analysis of differentially expressed genes (5.3). WT and TAZ KO were also transcriptionally similar in RNAseq analysis of uninjured human HEK293A *in vitro* samples[44]. One clear difference in transcriptome between WT and *wwtr1* CRISPant fish was alterations in multiple metabolic

and biosynthetic processes (Figure 5.6F+G). This suggests some cell intrinsic defects in *wwtr1* CRISPants, where metabolic dysregulation causes cell dysfunction, though the exact mechanism of this has not been elucidated. Alterations in metabolism (particularly the Warburg effect/glycolysis) has been previously reported following adult and embryonic (severe) tail fin injury and is vital for regeneration[267,426].

Interestingly, RNAseq analysis of *wwtr1* CRISPants did not show major dysregulation of Hippo signalling (Figure 5.9C+F). When compared to uninjured WT fish, *wwtr1* CRISPants showed only a slight decrease in the expression of Yap1/Taz target gene *ankrd1a*. Comparing injured WT fish to injured *wwtr1* CRISPant samples gave a similar result, with CRISPants having only limited effect on Hippo pathway component expression, i.e. an increase in *cavin1b* and *ccn2a* (*ctgfa*) and a decrease in *ankrd1b* and *fjx1*. Overall, these RNAseq changes suggest a limited but specific effect of removing Taz on the transcriptome.

Cell-based changes in *wwtr1* CRISPants were also investigated to attempt to elucidate the underlying tail fin defect. The blastema appeared to form normally, with key blastema markers localising to the correct regions and being expressed at WT levels (Figure 5.14). However, proliferation in the tail fin was reduced at both baseline and after injury (Figure 5.15). This was similar to *yap1* CRISPants, but the reduction was more severe in *wwtr1* CRISPants, suggesting a potential mechanism for the reduced growth rate after injury. However, proliferation was also reduced in the uninjured fin, which did not show a growth defect, suggesting that the proliferation rate may not impact tail fin growth in a major way.

Another clear phenotype in *wwtr1* CRISPants was a defect in macrophage function. When uninjured, *wwtr1* CRISPants had no defect in macrophage number (Figure 5.16G+K). However, CRISPant macrophages had significantly higher circularity than WT macrophages, which could be due to increased activation or cytoskeletal defects (Figure 5.16I). There were only limited changes in immune marker mRNA expression, including a small increase in *hmgcs1* expression (Figure 5.16B). Altogether, this suggests a limited impact of Taz on macrophages at baseline. After mild tail fin injury in *wwtr1* CRISPants (regeneration of which is not significantly affected), there was also no change in macrophage numbers in the fin (Figure 5.19C-F). However, after severe tail fin injury macrophage numbers were reduced at all timepoints (Figure 5.19H-J). Having no obvious macrophage phenotype when uninjured

suggests that this defect is not due to an overall macrophage reduction during development (as is seen for *yap1* CRISPants), and could instead be specific to the response to severe injury. After injury, *wwtr1* CRISPants also showed expression of many immune markers that differed from WT, suggesting a dysregulation of the immune response (Figure 5.17D+F and Table 5.2).

The *wwtr1* CRISPant macrophage defect may also be specific to M2-like macrophages. Macrophages show both plasticity and heterogeneity in different tissues. Two of these macrophage types involved in tail fin regeneration are M1-like and M2-like macrophages, so named because of their similarity to M1 and M2 mammalian macrophages[159]. M2-like macrophages are broadly considered to be pro-regenerative, and normally switch from a M1-like macrophage phenotype (broadly anti-regenerative), peaking in number at 48hpi[158]. It is therefore of interest as this is around the time a regeneration defect was observed. Whilst M1-like macrophage number was unchanged relative to WT, *wwtr1* CRISPants had reduced M2-like macrophage number, indicating an issue with this phenotypic switch (Figure 5.20D+E). The absence of these pro-regenerative macrophages could therefore underlie the impaired regeneration observed. Whether this macrophage plasticity defect is a result of environmental changes or a cell intrinsic defect to the macrophages is unclear.

6.2.2 Future elucidation of a cell intrinsic versus cell extrinsic role of Taz

The elucidation of a cell intrinsic or cell extrinsic effect of Taz in macrophage function was outside the scope of this thesis, but techniques are available to potentially investigate this in future work. Investigation of cell-intrinsic defects will require single cell RNA analysis, or the isolation of *wwtr1* CRISPant (or stable mutant) macrophages. Many experiments can then be performed *in vitro*, including RNAseq (potentially with a focus on metabolism) and culture of the macrophages. Analysis *in vitro* could include macrophage response to chemokines, migratory ability, investigation of the cytoskeleton, and quantification of protein levels through western blotting or immunofluorescence. A macrophage-specific *wwtr1* deletion would also be of particular interest. Investigation of the environmental impacts on macrophage function could also be performed. This could involve analysis of the mechanical properties of the tail fin, formation of the vasculature (which was observed but not quantified to be disrupted, particularly in *yap1* CRISPants), or determination of signalling pathways such as chemokine release in the tail fin.

6.2.3 Yap1 and Taz cannot be considered to be one entity as they have differing functions in the embryonic zebrafish

A major conclusion from the CRISPR/Cas9 screen and the subsequent analyses was the difference between Yap1 and Taz function. These two proteins are often considered to have greatly overlapping functions or Yap1 is studied as the sole transcriptional effector of the Hippo pathway, although more recent work has begun to elucidate differences in function[44]. *yap1* CRISPants showed major developmental and regenerative defects to the extent that they could be considered a positive control. Discussion of *wwtr1* CRISPant phenotypes is presented above, where the specific severe tail fin injury phenotypes make Taz a promising target to study this regeneration.

Differences between Yap1 and Taz notably include differences in immune cell formation and function and RNAseq differential expression, where *wwtr1* CRISPant samples were more similar to WT samples than *yap1* CRISPant samples. There were also differences in *ctgfa*:GFP fluorescence, where *yap1* CRISPants had reduced fluorescence both when uninjured and after severe injury, whilst *wwtr1* CRISPants were reduced only after severe injury. This reporter expresses GFP under the *ctgfa* promoter and so GFP fluorescence reflects occupation at the *ctgfa* promoter, which is assumed to be mostly through Yap1/Taz. This suggests specific differences in target gene regulation, with Yap1 regulating *ctgfa* expression when uninjured, but both Yap1 and Taz regulating *ctgfa* after severe tail fin injury (Figure 4.3). It is also supported by findings in human HEK293A cells *in vitro*, where YAP was shown to have more of an effect on *CTGF* transcription than TAZ[44].

This comparison of Yap1 and Taz is complicated by the feedback that exists between the two proteins (see 1.6 for a summary of these). These feedback loops may result in compensation after perturbation of *yap1* or *wwtr1*. Investigation of compensation in this thesis showed varied results. Analysis of *yap1* and *wwtr1* CRISPants showed no significant changes in *wwtr1* or *yap1* mRNA respectively at 24hpf (Figure 3.4M+N), and Taz or Yap1 protein at 72hpf (Figure 3.5) However, in mRNA imaging studies using HCR technology (at 120hpf) (Figure 5.11F) and in RNAseq analysis (Figure 5.9D), injured *yap1* CRISPants showed an increase in *wwtr1* mRNA. Conversely, at 24hpi, *yap1* CRISPants had reduced *wwtr1* mRNA by HCR imaging (Figure 5.12E). These discrepancies may be a result of the different time points analysed, or the

different techniques utilised, and so more investigation would be desirable to confirm this compensation effect, such as performing the analyses at more timepoints.

These findings all lead to a hypothesis where Yap1 has major roles in development. Therefore, when disrupted the resulting fish have wide-ranging developmental defects. These defects cause secondary failings in regeneration due to, for example, disrupted vascular system formation or immune cell development. However, Taz has limited roles in development, and so disruption results in phenotypically normal fish, except when measuring severe tail fin regeneration.

6.3 Hippo pathway function in innate immune cell dynamics

The Hippo pathway has been associated with immune cell function in mammals[132,133,139]. In humans, loss of function MST1 mutations result in immunodeficiency, implicating Hippo signalling with immunomodulation[427,428]. Disruptions in other Hippo pathway components (such as YAP1 and TAZ) also cause a dysfunctional immune system in murine models *in vivo*, whilst innate immune signalling also controls Hippo pathway function[132,133,139]. For example, MST1/2 is critical for T cell proliferation, migration, and differentiation (reviewed in Hong et. al., 2018[132]), YAP acts as a link between the biophysical environment and the macrophage inflammatory response[140], and both YAP and TAZ regulate the secretion of inflammatory mediators during tumour development[429,430].

However, in the zebrafish there has been little investigation into the role of the Hippo pathway in the immune system. One finding is that *ctgfa* KO zebrafish had enhanced inflammatory signalling via M1-like macrophages, resulting in reduced heart regeneration[258]. This work provides some initial insights into Yap1 and Taz function into innate immunity in the embryonic zebrafish. *yap1* CRISPants had major defects in both macrophage and neutrophil number, with reduced numbers in uninjured fish (Figure 5.16F-K). This defect was in both the whole fish and in the CHT (the region where haematopoiesis occurs), suggesting an issue with development rather than migration.

This supports previously published work which shows that the Hippo pathway, particularly Yap1, is vital for haematopoiesis in multiple model systems[431], including the zebrafish embryo[72,124]. In the mouse, Hippo signalling is associated with both the maintenance of the

haematopoietic stem and progenitor cell pool and their differentiation into mature immune cells, with Mst1/2 deficiency (predicted to enhance Yap1 activity) resulting in an expanded stem cell pool and altered immune cell populations[432]. Haematopoiesis can also be linked to mechanical properties, which regulates stem cell fate and behaviour[431], and is closely associated with the Hippo pathway[392]. For example, in the zebrafish Yap1-mediated mechanotransduction of cyclic stretch in blood vessels is required to maintain the haematopoietic lineage via Rho-GTPase[124]. The lack of immune cell developmental phenotype observed in *wwtr1* CRISPants suggests that the reported Hippo pathway effects are specific to Yap1.

Reduced immune cell numbers in *yap1* CRISPants were also observed after severe tail fin injury, but interestingly not after mild tail fin injury (Figure 5.18 and Figure 5.19). This could indicate that immune cells are not responding to the mild injury paradigm, even in WT fish. However, published work has shown that mild tail fin injury requires macrophage function for proper regeneration[142,152,153,158,159], suggesting that this is not the case. The lack of change in CRISPants could instead be due to differences in signalling at the injury site that might stimulate the recruitment of different macrophage or neutrophil subtypes. *yap1* CRISPants also had altered immune system-related genes at baseline and after severe injury, further supporting the evidence for a blunted immune response (Figure 5.16A and Figure 5.17C+E). Overall, evidence presented here suggests that Yap1 is vital for immune cell development in the embryonic zebrafish, which likely causes defects in immune cell function after severe tail fin injury. *wwtr1* CRISPants show a slightly different role of Taz in the immune system, which is discussed in detail in 6.2.1 above and includes a much more specific defect in the switch from M1-like to M2-like macrophages after severe tail fin injury, but not in uninjured fish.

In order to fully elucidate the function of Yap1 and Taz in the immune system more investigation is needed. One focus should be on cell intrinsic versus cell extrinsic defects in innate immune cells. It would also be of interest to perform a greater range of timepoints in both the uninjured and injured fish and live timelapses of immune cell infiltration to show migration patterns. Together with single cell RNAseq and cell type-specific mutations, this would give more detailed spatiotemporal insights into Yap1 and Taz function in immunity. Analysis of adaptive immunity in the adult zebrafish could also be performed. In conclusion, although these initial investigations have posited a role for Yap1 and Taz in the innate immune

system, more work is required to define their exact functions during both homeostasis and regeneration.

6.4 Comparing mild and severe tail fin injury paradigms

The embryonic caudal fin anatomy (Figure 3.10A) is relatively simple, particularly when compared to the adult tail fin. The fin fold consists of two epidermal layers containing keratinocytes and an underlying basement membrane enclosing a middle mesenchyme layer. This mesenchyme layer is composed of nerves, actinotrichia that give the fin its structure, and fibroblast-like cells. The fin fold surrounds the posterior trunk containing the neural tube, vasculature, and the notochord. Amputation of just the fin fold (mild injury) and a deeper amputation through the trunk (severe injury) is performed and compared in this thesis (Figure 3.10A).

No published papers directly comparing these different regeneration types could be found at the time of writing. Most studies either focussed on adult tail fin regeneration, which has already been associated with Hippo pathway signalling[247,380,433], or on the mild injury paradigm in the embryo. Both mild and severe injury regeneration require an initial wound healing stage, followed by the formation of a blastemal-like structure (a mass of dedifferentiated cells that may act as a signalling centre and source of new cells), and finally regenerative outgrowth involving enhanced proliferation[434].

Many experiments in this thesis demonstrated differences in mild and severe tail fin injury regeneration, highlighting that a clear distinction is required between these two paradigms. This was first investigated in the CRISPR/Cas9 screen, which showed differences in phenotypes in multiple CRISPants, indicating that Hippo pathway components function differently in these two paradigms (Figure 3.18). Notably, *wwtr1* CRISPants showed no defect after mild tail fin injury but a defect after severe injury. In addition, *ctgfb* CRISPants had reduced regeneration after mild injury but enhanced regeneration after severe injury, whilst *lats2* CRISPants displayed decreased regeneration after mild injury but no change after severe regeneration. A focus was placed on comparing *wwtr1* and *yap1* CRISPant tail fin phenotypes (*yap1* CRISPants had defects in both mild and severe injury). Further differences between mild and severe injury regeneration were observed. This included changes in the transcriptome

(5.2 and 5.3), although this comparison may have been biased by the differences in timepoints analysed (4hpi in mild injury, 24hpi in severe injury). Both mild and severe injury induced the downregulation of genes associated with normal fin development and extracellular matrix and the upregulation of cell cycle, immune system, and apoptosis markers. However, some differences included the downregulation of BMP signalling after severe injury only, and greater downregulation of cell migration and motility after mild injury. A direct comparison between RNAseq results from injury types at more comparable timepoints would be interesting to further investigate these changes and similarities.

Other differences between mild and severe injury regeneration were observed in the analysis of the *ctgfa*:GFP reporter transgenic line after injury (4.1). At early timepoints after mild tail fin injury, there was no induction of GFP at levels higher than baseline, suggesting no response of Yap1/Taz to mild injury. In contrast, at the same timepoint after severe tail fin injury, GFP was increased from baseline levels, suggesting Yap1/Taz response. At later timepoints, GFP was increased from baseline levels in both injury paradigms. However, *yap1* and *wwtr1* CRISPants had no effect on GFP fluorescence levels after mild injury but both reduced fluorescence after severe injury.

Many published works have investigated the innate immune system after mild tail fin injury. These studies have shown that macrophages, but not neutrophils, are necessary for mild tail fin regeneration in the zebrafish[144,153–155,158–160]. However, a limited number of studies have reported on severe tail fin regeneration. Therefore, a comparison between neutrophil and macrophage numbers in both mild and severe injury is of interest for the tail fin regeneration field. In WT fish, neutrophil infiltration after mild tail fin injury peaked at 20 cells at 6hpi, but then plateaued by 24hpi at around 12 cells (Figure 5.18C). This pattern of infiltration was matched after severe injury, but with more than double the number of cells (Figure 5.18H). Macrophage infiltration in WT fish followed a different pattern. After mild tail fin injury there was no noticeable peak or increase in macrophage number, (Figure 5.19C). However, after severe tail fin injury macrophage numbers increased throughout the imaging timecourse from 20 at 6hpi to 50 at 48hpi (Figure 5.19H). The differences in innate cell numbers between mild and severe injury clearly demonstrate a difference in the function or stimulation of these cells between the injury types, and suggest that the severe injury paradigm may be more appropriate for the study of immunity as there was a greater immune cell response.

There is clearly a requirement for diverse processes within these broad regenerative stages as the different paradigms showed varied responses to *yap1* and *wwtr1* manipulation and assays such as immune cell infiltration, and requires the reformation of different cell types. One such difference in regenerative processes could be metabolic reprogramming towards aerobic glycolysis, which is required for severe tail fin regeneration through sustaining TGF-β signalling[267]. The Hippo pathway, particularly Yap1, has been associated with TGF-β signalling[435], which may therefore be a mechanism by which Hippo signalling can alter tail fin regeneration differently in mild and severe injury. However, as always there is more work to be done to further elucidate the differences in these types of regeneration. This could include comparison of proliferation rates, M1-like versus M2-like macrophage function, more in-depth investigation of metabolic changes suggested by RNAseq, and investigation of the blastema.

6.5 Linking the Hippo pathway's role in regeneration and cancer: potential therapeutic insights

The Hippo pathway is perhaps most well-known for its role in cancer, with many cancers having increased YAP/TAZ activity[436,437]. For this reason, some chemotherapy drugs that target the Hippo pathway are being developed, some of which are in preclinical trials (e.g. NCT04665206)[437,438]. However, this link to cancer also associates the Hippo pathway with regeneration, as both require higher than baseline levels of plasticity and proliferation[7]. This crosstalk underlies some of the side effects of chemotherapy (e.g. hair loss) as non-cancerous cells with a normally high level of proliferation (i.e. regenerative cells) are also destroyed. It may also limit regenerative therapies, as treatments that increase proliferation to promote regeneration may also increase the likelihood of cancer. Investigating Hippo pathway function more in depth, elucidating the exact spatiotemporal regulation and function of each component in regeneration and cancer, may therefore allow for the development of treatments with fewer of these deleterious side effects. This thesis has begun this work by identifying Hippo pathway components that affect regeneration without impacting on normal homeostatic function, most notably here Taz. Future work to link this to carcinogenic potential may involve more investigation of proliferation rates and cellular plasticity in the CRISPants, potentially through further immunofluorescence studies to label proliferating cells and utilisation of fluorescent transgenic zebrafish lines. These studies will complement other

work that, when combined, will lead us to the development of highly effective therapies with few, if any, problematic side effects that massively impact on patients' quality of life.

7 Bibliography

1. Twitty, V. C. S. & Josep, L. The growth of eyes and limbs transplanted heteroplastically between two species of Amblystoma. *Journal of Experimental Zoology* **59**, 61–86 (1931).
2. Anderson, R. M. & Higgins, G. M. Experimental Pathology of the liver. I. *Arch Pathot* **12**, 186–202 (1931).
3. Kim, W. & Jho, E. The history and regulatory mechanism of the Hippo pathway. *BMB Rep* **51**, 106–118 (2018).
4. Davis, J. R. & Tapon, N. Hippo signalling during development. *Development* **146**, dev167106 (2019).
5. Huang, J., Wu, S., Barrera, J., Matthews, K. & Pan, D. The Hippo Signaling Pathway Coordinately Regulates Cell Proliferation and Apoptosis by Inactivating Yorkie, the Drosophila Homolog of YAP. *Cell* **122**, 421–434 (2005).
6. Udan, R. S., Kango-Singh, M., Nolo, R., Tao, C. & Halder, G. Hippo promotes proliferation arrest and apoptosis in the Salvador/Warts pathway. *Nat Cell Biol* **5**, 914–920 (2003).
7. Johnson, R. & Halder, G. The two faces of Hippo: targeting the Hippo pathway for regenerative medicine and cancer treatment. *Nat Rev Drug Discov* **13**, 63–79 (2014).
8. Halder, G. & Johnson, R. L. Hippo signaling: growth control and beyond. *Development* **138**, 9–22 (2011).
9. Gram Hansen, C., Moroishi, T. & Guan, K.-L. YAP and TAZ: a nexus for Hippo signaling and beyond. *Trends Cell Biol* **25**, 499–513 (2015).
10. Rausch, V. & Gram Hansen, C. The Hippo Pathway, YAP/TAZ, and the Plasma Membrane. *Trends Cell Biol* **30**, 32–48 (2020).
11. Dupont, S. *et al.* Role of YAP/TAZ in mechanotransduction. *Nature* **474**, 179–185 (2011).
12. Zhao, B. *et al.* Inactivation of YAP oncoprotein by the Hippo pathway is involved in cell contact inhibition and tissue growth control. *Genes Dev* **21**, 2747–2761 (2007).
13. Panciera, T., Azzolin, L., Cordenonsi, M. & Piccolo, S. Mechanobiology of YAP and TAZ in physiology and disease. *Molecular Cell Biology* **18**, 758–770 (2017).
14. Meng, Z., Moroishi, T. & Guan, K.-L. Mechanisms of Hippo pathway regulation. *Genes Dev* **30**, (2016).
15. Moya, I. M. & Halder, G. Hippo–YAP/TAZ signalling in organ regeneration and regenerative medicine. *Nat Rev Mol Cell Biol* **20**, 211–226 (2019).
16. Fulford, A., Tapon, N. & Ribeiro, P. S. Upstairs, downstairs: spatial regulation of Hippo signalling. *Curr Opin Cell Biol* **51**, 22–32 (2017).
17. Ardestani, A., Lupse, B. & Maedler, K. Hippo Signaling: Key Emerging Pathway in Cellular and Whole-Body Metabolism. *Trends in Endocrinology and Metabolism* **29**, 492–509 (2018).
18. Meng, Z. *et al.* MAP4K family kinases act in parallel to MST1/2 to activate LATS1/2 in the Hippo pathway. *Nat Commun* **6**, (2015).
19. Zheng, Y. *et al.* Identification of Happyhour/MAP4K as Alternative Hpo/Mst-like Kinases in the Hippo Kinase Cascade. *Dev Cell* **34**, 642–655 (2015).
20. Lim, S. *et al.* Identification of the kinase STK25 as an upstream activator of LATS signaling. *Nat Commun* **10**, 1547 (2019).
21. Zhao, B., Li, L., Tumaneng, K., Wang, C.-Y. & Guan, K.-L. A coordinated phosphorylation by Lats and CK1 regulates YAP stability through SCF^β-TRCP. *Genes Dev* **22**, 72–85 (2010).
22. Lei, Q.-Y. *et al.* TAZ Promotes Cell Proliferation and Epithelial-Mesenchymal Transition and Is Inhibited by the Hippo Pathway. *Mol Cell Biol* **28**, 2426–2436 (2008).
23. Liu, C.-Y. *et al.* The Hippo Tumor Pathway Promotes TAZ Degradation by Phosphorylating a Phosphodegron and Recruiting the SCF^β-TRCP E3 Ligase. *J Biol Chem* **285**, 37159–37169 (2010).
24. Zhang, H. *et al.* TEAD Transcription Factors Mediate the Function of TAZ in Cell Growth and Epithelial-Mesenchymal Transition. *J Biol Chem* **284**, 13355–13362 (2009).
25. Ota, M. & Sasaki, H. Mammalian Tead proteins regulate cell proliferation and contact inhibition as transcriptional mediators of Hippo signaling. *Development* **135**, 4059–4069 (2008).
26. Zhao, B. *et al.* TEAD mediates YAP-dependent gene induction and growth control. *Genes Dev* **22**, 1962–1971 (2008).

27. Hillmer, R. E. & Link, B. A. The Roles of Hippo Signaling Transducers Yap and Taz in Chromatin Remodeling. *Cells* **8**, (2019).
28. Yu, F.-X., Zhao, B. & Guan, K.-L. Hippo Pathway in Organ Size Control, Tissue Homeostasis, and Cancer. *Cell* **163**, 811–828 (2015).
29. Rausch, V. *et al.* The Hippo Pathway Regulates Caveolae Expression and Mediates Flow Response via Caveolae. *Current Biology* **29**, (2019).
30. Salem, O. & Gram Hansen, C. The Hippo Pathway in Prostate Cancer. *Cells* **8**, (2019).
31. He, M. *et al.* New insights into posttranslational modifications of Hippo pathway in carcinogenesis and therapeutics. *Cell Div* **11**, (2016).
32. Yan, F., Qian, M., He, Q., Zhu, H. & Yang, B. The posttranslational modifications of Hippo-YAP pathway in cancer. *Biochim Biophys Acta Gen Subj* **1864**, (2020).
33. Lapi, E. *et al.* PML, YAP, and p73 Are Components of a Proapoptotic Autoregulatory Feedback Loop. *Mol Cell* **32**, 803–814 (2008).
34. Hata, S. *et al.* A Novel Acetylation Cycle of Transcription Co-activator Yes-associated Protein That Is Downstream of Hippo Pathway Is Triggered in Response to SN2 Alkylating Agents. *Journal of Biological Chemistry* **287**, 22089–22098 (2012).
35. Oudhoff, M. J. *et al.* Control of the Hippo Pathway by Set7-Dependent Methylation of Yap. *Dev Cell* **26**, 188–194 (2013).
36. Fang, L. *et al.* SET1A-Mediated Mono-Methylation at K342 Regulates YAP Activation by Blocking Its Nuclear Export and Promotes Tumorigenesis. *Cancer Cell* **34**, 103-118.e9 (2018).
37. Zhao, W. *et al.* Transcriptional co-activators YAP/TAZ: Potential therapeutic targets for metastatic breast cancer. *Biomedicine and Pharmacotherapy* **133**, (2021).
38. Riley, S. E., Feng, Y. & Gram Hansen, C. Hippo-Yap/Taz signalling in zebrafish regeneration. *NPJ Regen Med* **7**, (2022).
39. Gram Hansen, C., Ng, Y. L. D., Macrina Lam, W.-L., Plouffe, S. W. & Guan, K.-L. The Hippo pathway effectors YAP and TAZ promote cell growth by modulating amino acid signaling to mTORC1. *Cell Res* **25**, 1299–1313 (2015).
40. Mo, J.-S. *et al.* Cellular energy stress induces AMPK-mediated regulation of YAP and the Hippo pathway. *Nat Cell Biol* **17**, 500–510 (2015).
41. Morin-Kensicki, E. M. *et al.* Defects in Yolk Sac Vasculogenesis, Chorioallantoic Fusion, and Embryonic Axis Elongation in Mice with Targeted Disruption of Yap65. *Mol Cell Biol* **26**, 77–87 (2006).
42. Makita, R. *et al.* Multiple renal cysts, urinary concentration defects, and pulmonary emphysematous changes in mice lacking TAZ. *Am J Physiol Renal Physiol* **294**, 542–553 (2008).
43. Mitani, A. *et al.* Transcriptional Coactivator with PDZ-binding Motif Is Essential for Normal Alveolarization in Mice. *Am J Respir Crit Care Med* **180**, 326–338 (2009).
44. Plouffe, S. W. *et al.* The Hippo pathway effector proteins YAP and TAZ have both distinct and overlapping functions in the cell. *Journal of Biological Chemistry* **293**, 11230–11240 (2018).
45. Hossain, Z. *et al.* Glomerulocystic kidney disease in mice with a targeted inactivation of Wwtr1. *Proceedings of the National Academy of Sciences* **104**, 1631–1636 (2007).
46. Kakiuchi-Kiyota, S., Schutten, M. M., Zhong, Y., Crawford, J. J. & Dey, A. Safety Considerations in the Development of Hippo Pathway Inhibitors in Cancers. *Front Cell Dev Biol* **7**, (2019).
47. Hong, A. W., Meng, Z. & Guan, K.-L. The Hippo pathway in intestinal regeneration and disease. *Nat Rev Gastroenterol Hepatol* **13**, 324–337 (2016).
48. Nguyen-Lefebvre, A. T., Selzner, N., Wrana, J. L. & Bhat, M. The hippo pathway: A master regulator of liver metabolism, regeneration, and disease. *FASEB Journal* **35**, e21570 (2021).
49. Camargo, F. D. *et al.* YAP1 Increases Organ Size and Expands Undifferentiated Progenitor Cells. *Current Biology* **17**, 2054–2060 (2007).
50. Dong, J. *et al.* Elucidation of a Universal Size-Control Mechanism in Drosophila and Mammals. *Cell* **130**, 1120–1133 (2007).
51. Bai, H. *et al.* Yes-Associated Protein Regulates the Hepatic Response After Bile Duct Ligation. *Hepatology* **56**, 1097–1107 (2012).
52. Grijalva, J. L. *et al.* Dynamic alterations in Hippo signaling pathway and YAP activation during liver regeneration. *Am J Physiol Gastrointest Liver Physiol* **307**, G196–G204 (2014).
53. Lu, L., Finegold, M. J. & Johnson, R. L. Hippo pathway coactivators yap and taz are required to coordinate mammalian liver regeneration. *Exp Mol Med* **50**, (2018).

54. Fan, F. *et al.* Pharmacological targeting of kinases MST1 and MST2 augments tissue repair and regeneration. *Sci Transl Med* **8**, (2016).
55. Loforese, G. *et al.* Impaired liver regeneration in aged mice can be rescued by silencing Hippo core kinases MST1 and MST2. *EMBO Mol Med* **9**, 46–60 (2017).
56. Xin, M. *et al.* Regulation of insulin-like growth factor signaling by Yap governs cardiomyocyte proliferation and embryonic heart size. *Sci Signal* **4**, (2011).
57. Xin, M. *et al.* Hippo pathway effector Yap promotes cardiac regeneration. *Proceedings of the National Academy of Sciences* **110**, 13839–13844 (2013).
58. Heallen, T. *et al.* Hippo signaling impedes adult heart regeneration. *Development* **140**, 4683–4690 (2013).
59. Heallen, T. *et al.* Hippo Pathway Inhibits Wnt Signaling to Restrain Cardiomyocyte Proliferation and Heart Size. *Science (1979)* **332**, 458–461 (2011).
60. von Gise, A. *et al.* YAP1, the nuclear target of Hippo signaling, stimulates heart growth through cardiomyocyte proliferation but not hypertrophy. *Proceedings of the National Academy of Sciences* **109**, 2394–2399 (2012).
61. Lin, Z. *et al.* Cardiac-Specific YAP Activation Improves Cardiac Function and Survival in an Experimental Murine MI Model. *Circ Res* **115**, 354–363 (2014).
62. Cai, J. *et al.* The Hippo signaling pathway restricts the oncogenic potential of an intestinal regeneration program. *Genes Dev* **24**, 2383–2388 (2010).
63. Azzolin, L. *et al.* YAP/TAZ incorporation in the β-catenin destruction complex orchestrates the Wnt response. *Cell* **158**, 157–170 (2014).
64. Shaw, R. L. *et al.* The Hippo pathway regulates intestinal stem cell proliferation during Drosophila adult midgut regeneration. *Development* **137**, 4147–4158 (2010).
65. Ren, F. *et al.* Hippo signaling regulates Drosophila intestine stem cell proliferation through multiple pathways. *Proceedings of the National Academy of Sciences* **107**, 21064–21069 (2010).
66. Karpowicz, P., Perez, J. & Perrimon, N. The Hippo tumor suppressor pathway regulates intestinal stem cell regeneration. *Development* **138**, 4135–4145 (2010).
67. Gregorieff, A., Liu, Y., Inanlou, M. R., Khomchuk, Y. & Wrana, J. L. Yap-dependent reprogramming of Lgr5+ stem cells drives intestinal regeneration and cancer. *Nature* **526**, 715–718 (2015).
68. Barry, E. R. *et al.* Restriction of intestinal stem cell expansion and the regenerative response by YAP. *Nature* **493**, 106–110 (2013).
69. Davies, P. S., Dismuke, A. D., Powell, A. E., Carroll, K. H. & Wong, M. H. Wnt-reporter expression pattern in the mouse intestine during homeostasis. *BMC Gastroenterol* **8**, (2008).
70. Ashton, G. H. *et al.* Focal Adhesion Kinase is required for intestinal regeneration and tumorigenesis downstream of Wnt/c-Myc signaling. *Dev Cell* **19**, 259–269 (2010).
71. Adhish, M. & Manjubala, I. Effectiveness of zebrafish models in understanding human diseases - A review of models. *Heliyon* **9**, (2023).
72. Hu, J. *et al.* Yes-Associated Protein (Yap) Is Required for Early Embryonic Development in Zebrafish (Danio Rerio). *Int J Biol Sci* **9**, 267–278 (2013).
73. Yi, X. *et al.* The effector of Hippo signaling, Taz, is required for formation of the micropyle and fertilization in zebrafish. *PLoS Genet* **15**, e1007408 (2019).
74. Cox, A. G. *et al.* Yap regulates glucose utilization and sustains nucleotide synthesis to enable organ growth. *EMBO J* **37**, e100294 (2018).
75. Brandt, Z. J., North, P. N. & Link, B. A. Somatic Mutations of lats2 Cause Peripheral Nerve Sheath Tumors in Zebrafish. *Cells* **8**, (2019).
76. Brandt, Z. J., Echert, A. E., Bostrom, J. R., North, P. N. & Link, B. A. Core Hippo pathway components act as a brake on Yap/Taz in the development and maintenance of the biliary network. *Development* **4**, dev.184242 (2020).
77. Loh, S. L. *et al.* Zebrafish yap1 plays a role in differentiation of hair cells in posterior lateral line. *Sci Rep* **4**, (2014).
78. Gee, S. T., Milgram, S. L., Kramer, K. L., Conlon, F. L. & Moody, S. A. Yes-Associated Protein 65 (YAP) Expands Neural Progenitors and Regulates Pax3 Expression in the Neural Plate Border Zone. *PLoS One* **6**, e20309 (2011).
79. Grimm, L. *et al.* Yap1 promotes sprouting and proliferation of lymphatic progenitors downstream of Vegfc in the zebrafish trunk. *Elife* **8**, e42881 (2019).

80. Dooley, C. M. *et al.* The gene regulatory basis of genetic compensation during neural crest induction. *PLoS Genet* **15**, e1008213 (2019).
81. Chen, C.-H., Sun, Y.-H., Pei, D.-S. & Zhu, Z.-Y. Comparative expression of zebrafish Lats1 and Lats2 and their implication in gastrulation movements. *Developmental Dynamics* **238**, 2850–2859 (2009).
82. Fillatre, J. *et al.* TEADS, Yap, Taz, Vgll4s transcription factors control the establishment of left-right asymmetry in zebrafish. *Elife* **8**, e45241 (2019).
83. Huang, H. *et al.* Amotl2 is essential for cell movements in zebrafish embryo and regulates c-Src translocation. *Development* **134**, 979–988 (2007).
84. Li, Z. *et al.* The Amotl2 Gene Inhibits Wnt/β-Catenin Signaling and Regulates Embryonic Development in Zebrafish. *J Biol Chem* **287**, 13005–13015 (2012).
85. Mo, S. *et al.* Caveolin-1 regulates dorsoventral patterning through direct interaction with β -catenin in zebrafish. *Dev Biol* **344**, 210–223 (2010).
86. Nixon, S. J. *et al.* Caveolin-1 is required for lateral line neuromast and notochord development. *J Cell Sci* **120**, 2151–2161 (2007).
87. Pappalardo, A. *et al.* Thyroid development in zebrafish lacking Taz. *Mech Dev* **138**, 268–278 (2015).
88. Park, M.-H. *et al.* CCN1 interlinks integrin and hippo pathway to autoregulate tip cell activity. *Elife* **8**, e46012 (2019).
89. Jiang, L., Romero-Carvajal, A., Haug, J. S., Seidel, C. W. & Piotrowski, T. Gene-expression analysis of hair cell regeneration in the zebrafish lateral line. *Proceedings of the National Academy of Sciences* E1383–E1392 (2014).
90. Fang, P.-K. *et al.* Caveolin-1α and -1β perform nonredundant roles in early vertebrate development. *Am J Pathol* **169**, 2209–2222 (2006).
91. Flinn, M. A., Jeffery, B. E., O'Meara, C. C. & Link, B. A. Yap is required for scar formation but not myocyte proliferation during heart regeneration in zebrafish. *Cardiovasc Res* **115**, 570–577 (2019).
92. Asaoka, Y., Hata, S., Namae, M., Furutani-Seiki, M. & Nishina, H. The Hippo pathway controls a switch between retinal progenitor cell proliferation and photoreceptor cell differentiation in zebrafish. *PLoS One* **9**, e97365 (2014).
93. Chiou, M.-J., Chao, T.-T., Wu, J.-L., Kuo, C.-M. & Chen, J.-Y. The physiological role of CTGF/CCN2 in zebrafish notochond development and biological analysis of the proximal promoter region. *Biochem Biophys Res Commun* **349**, 750–758 (2006).
94. Garcia, J. *et al.* Sheath Cell Invasion and Trans-differentiation Repair Mechanical Damage Caused by Loss of Caveolae in the Zebrafish Notochord. *Current Biology* **27**, 1982-1989.e3 (2017).
95. Lim, Y.-W. *et al.* Caveolae Protect Notochord Cells against Catastrophic Mechanical Failure during Development. *Current Biology* **27**, 1968–1981 (2017).
96. Yi, X. *et al.* Yap1/Taz are essential for the liver development in zebrafish. *Biochem Biophys Res Commun* **503**, 131–137 (2018).
97. Miesfeld, J. B. *et al.* Yap and Taz regulate retinal pigment epithelial cell fate. *Development* **142**, 3021–3032 (2015).
98. Fukui, H. *et al.* Hippo signaling determines the number of venous pole cells that originate from the anterior lateral plate mesoderm in zebrafish. *Elife* **7**, e29106 (2018).
99. Agarwala, S. *et al.* Amotl2a interacts with the Hippo effector Yap1 and the Wnt/β-catenin effector Lef1 to control tissue size in zebrafish. *Elife* **4**, e08201 (2015).
100. Stemple, D. L. *et al.* Mutations affecting development of the notochord in zebrafish. *Development* **123**, 117–128 (1996).
101. Stemple, D. L. Structure and function of the notochord: an essential organ for chordate development. *Development* **132**, 2503–2512 (2005).
102. Dickmeis, T. *et al.* Expression Profiling and Comparative Genomics Identify a Conserved Regulatory Region Controlling Midline Expression in the Zebrafish Embryo. *Genome Res* **14**, 228–238 (2004).
103. Hill, M. M. *et al.* PTRF-Cavin, a Conserved Cytoplasmic Protein Required for Caveola Formation and Function. *Cell* **132**, 113–124 (2008).
104. Jiang, Q. *et al.* Yap Is Required for the Development of Brain, Eyes, and Neural Crest in Zebrafish. *Biochem Biophys Res Commun* **384**, 114–119 (2009).

105. Kimelman, D., Smith, N. L., Lai, J. K. H. & Stainier, D. Y. R. Regulation of posterior body and epidermal morphogenesis in zebrafish by localized Yap1 and Wwtr1. *Elife* **6**, 1–29 (2017).
106. Duan, X. *et al.* Foxc1a regulates zebrafish vascular integrity and brain vascular development through targeting amotl2a and ctnnb1. *Microvasc Res* **143**, (2022).
107. Sadler, K. C., Amsterdam, A., Soroka, C., Boyer, J. & Hopkins, N. A genetic screen in zebrafish identifies the mutants vps18, nf2 and foie gras as models of liver disease. *Development* **132**, 3561–3572 (2005).
108. Xu, D. *et al.* Scribble influences cyst formation in autosomal-dominant polycystic kidney disease by regulating Hippo signaling pathway. *FASEB Journal* **32**, 4394–4407 (2018).
109. Moreno-Mármol, T. *et al.* Stretching of the retinal pigment epithelium contributes to zebrafish optic cup morphogenesis. *Elife* **10**, e63396 (2021).
110. Hong, J.-H. *et al.* TAZ, a transcriptional modulator of mesenchymal stem cell differentiation. *Science (1979)* **309**, 1074–1078 (2005).
111. Lo, H. P. *et al.* The caveolin–cavin system plays a conserved and critical role in mechanoprotection of skeletal muscle. *Journal of Cell Biology* **210**, 833–849 (2015).
112. Kim, M., Kim, M., Lee, M.-S., Kim, C.-H. & Lim, D.-S. The MST1/2-SAV1 complex of the Hippo pathway promotes ciliogenesis. *Nat Commun* **5**, 1–14 (2014).
113. Hildebrand, S. *et al.* The E-cadherin/AmotL2 complex organizes actin filaments required for epithelial hexagonal packing and blastocyst hatching. *Sci Rep* **7**, (2017).
114. Hultin, S. *et al.* Amotl2 links VE-cadherin to contractile actin fibres necessary for aortic lumen expansion. *Nat Commun* **5**, (2014).
115. Flinn, M. A. *et al.* Llgl1 regulates zebrafish cardiac development by mediating Yap stability in cardiomyocytes. *Development* **147**, (2020).
116. Miesfeld, J. B. & Link, B. A. Establishment of transgenic lines to monitor and manipulate Yap/Taz-Tead activity in zebrafish reveals both evolutionarily conserved and divergent functions of the Hippo pathway. *Mech Dev* **133**, 177–188 (2014).
117. Duchemin, A.-L., Vignes, H. & Vermot, J. Mechanically activated piezo channels modulate outflow tract valve development through the Yap1 and Klf2-Notch signaling axis. *Elife* **8**, e44706 (2019).
118. Lai, J. K. H. *et al.* The Hippo pathway effector Wwtr1 regulates cardiac wall maturation in zebrafish. *Development* **145**, (2018).
119. Astone, M. *et al.* Zebrafish mutants and TEAD reporters reveal essential functions for Yap and Taz in posterior cardinal vein development. *Sci Rep* **8**, (2018).
120. Dai, X. *et al.* Phosphorylation of angiomotin by Lats1/2 kinases inhibits F-actin binding, cell migration, and angiogenesis. *J Biol Chem* **288**, 34041–34051 (2013).
121. Nakajima, H. *et al.* Flow-Dependent Endothelial YAP Regulation Contributes to Vessel Maintenance. *Dev Cell* **40**, 523-536.e6 (2017).
122. Nagasawa-Masuda, A. & Terai, K. Yap/Taz transcriptional activity is essential for vascular regression via Ctgf expression and actin polymerization. *PLoS One* **12**, e0174633 (2017).
123. Wang, Y. *et al.* Angiomotin-like2 Gene (amotl2) Is Required for Migration and Proliferation of Endothelial Cells during Angiogenesis. *J Biol Chem* **286**, 41095–41104 (2011).
124. Lundin, V. *et al.* YAP Regulates Hematopoietic Stem Cell Formation in Response to the Biophysical Forces of Blood Flow. *Dev Cell* **52**, (2020).
125. Flinn, M. A., Link, B. A. & O'Meara, C. C. Upstream regulation of the Hippo-Yap pathway in cardiomyocyte regeneration. *Semin Cell Dev Biol* **100**, 11–19 (2020).
126. Grivas, D., González-Rajal, Á., Rodríguez, C. G., Garcia, R. & de la Pompa, J. L. Loss of Caveolin-1 and caveolae leads to increased cardiac cell stiffness and functional decline of the adult zebrafish heart. *Sci Rep* **10**, (2020).
127. Bornhorst, D. *et al.* Biomechanical signaling within the developing zebrafish heart attunes endocardial growth to myocardial chamber dimensions. *Nat Commun* **10**, (2019).
128. Thomas, E. D., Cruz, I. A., Hailey, D. W. & Raible, D. W. There and Back Again: Development and Regeneration of the Zebrafish Lateral Line System. *Wiley Interdiscip Rev Dev Biol.* **4**, (2015).
129. Wang, X. *et al.* Lpar2b Controls Lateral Line Tissue Size by Regulating Yap1 Activity in Zebrafish. *Front Mol Neurosci* **11**, (2018).
130. Kozlovskaja-Gumbrienė, A. *et al.* Proliferation-independent regulation of organ size by Fgf/Notch signaling. *Elife* **6**, e21049 (2017).

131. Mescher, A. L., Neff, A. W. & King, M. W. Inflammation and immunity in organ regeneration. *Dev Comp Immunol* **66**, 98–110 (2017).
132. Hong, L., Li, X., Zhou, D., Geng, J. & Chen, L. Role of Hippo signaling in regulating immunity. *Cell Mol Immunol* **15**, 1003–1009 (2018).
133. Wang, S. *et al.* The Crosstalk Between Hippo-YAP Pathway and Innate Immunity. *Front Immunol* **11**, (2020).
134. Li, W. *et al.* STK4 regulates TLR pathways and protects against chronic inflammation-related hepatocellular carcinoma. *Journal of Clinical Investigation* **125**, 4239–4254 (2015).
135. Boro, M., Singh, V. & Narayanaswamy Balaji, K. Mycobacterium tuberculosis-triggered Hippo pathway orchestrates CXCL1/2 expression to modulate host immune responses. *Sci Rep* **6**, (2016).
136. Geng, J. *et al.* Kinases Mst1 and Mst2 positively regulate phagocytic induction of reactive oxygen species and bactericidal activity. *Nat Immunol* **16**, 1142–1152 (2015).
137. Roh, K.-H. & Choi, E.-J. TRAF2 functions as an activator switch in the reactive oxygen species-induced stimulation of MST1. *Free Radic Biol Med* **91**, 105–113 (2016).
138. Dixit, D., Ghildiyal, R., Anto, N. P. & Sen, E. Chaetocin-induced ROS-mediated apoptosis involves ATM-YAP1 axis and JNK-dependent inhibition of glucose metabolism. *Cell Death Dis* **5**, (2014).
139. Mia, M. M. & Singh, M. K. Emerging roles of the Hippo signaling pathway in modulating immune response and inflammation-driven tissue repair and remodeling. *FEBS J* **289**, 4061–4081 (2022).
140. Meli, V. S. *et al.* YAP-mediated mechanotransduction tunes the macrophage inflammatory response. *Sci Adv* **6**, (2020).
141. Rosowski, E. E. Determining macrophage versus neutrophil contributions to innate immunity using larval zebrafish. *Dis Model Mech* **13**, (2020).
142. Bohaud, C. *et al.* The Role of Macrophages During Zebrafish Injury and Tissue Regeneration Under Infectious and Non-Infectious Conditions. *Front Immunol* **12**, (2021).
143. Renshaw, S. A. & Trede, N. S. A model 450 million years in the making: Zebrafish and vertebrate immunity. *Dis Model Mech* **5**, 38–47 (2012).
144. Ellett, F., Pase, L., Hayman, J. W., Andrianopoulos, A. & Lieschke, G. J. mpeg1 promoter transgenes direct macrophage-lineage expression in zebrafish. *Blood* **117**, (2011).
145. Herbomel, P., Thisse, B. & Thisse, C. Ontogeny and behaviour of early macrophages in the zebrafish embryo. *Development* **126**, 3735–3745 (1999).
146. Le Guyader, D. *et al.* Origins and unconventional behavior of neutrophils in developing zebrafish. *Hematopoiesis* **111**, 132–141 (2008).
147. Lieschke, G. J. *et al.* Zebrafish SPI-1 (PU.1) marks a site of myeloid development independent of primitive erythropoiesis: Implications for axial patterning. *Dev Biol* **246**, 274–295 (2002).
148. Rhodes, J. *et al.* Interplay of pu.1 and Gata1 determines myelo-erythroid progenitor cell fate in zebrafish. *Dev Cell* **8**, 97–108 (2005).
149. Li, L., Jin, H., Xu, J., Shi, Y. & Wen, Z. Irf8 regulates macrophage versus neutrophil fate during zebrafish primitive myelopoiesis. *Blood* **117**, 1359–1369 (2011).
150. Panopoulos, A. D. & Watowich, S. S. Granulocyte colony-stimulating factor: Molecular mechanisms of action during steady state and 'emergency' hematopoiesis. *Cytokine* **42**, 277–288 (2008).
151. Shiau, C. E., Kaufman, Z., Meireles, A. M. & Talbot, W. S. Differential requirement for irf8 in formation of embryonic and adult macrophages in zebrafish. *PLoS One* **10**, (2015).
152. Petrie, T. A., Strand, N. S., Yang, C.-T., Rabinowitz, J. S. & Moon, R. T. Macrophages modulate adult zebrafish tail fin regeneration. *Development* **141**, 2581–2591 (2014).
153. Li, L., Yan, B., Shi, Y.-Q., Zhang, W.-Q. & Wen, Z.-L. Live Imaging Reveals Differing Roles of Macrophages and Neutrophils during Zebrafish Tail Fin Regeneration. *Journal of Biological Chemistry* **287**, 25353–25360 (2012).
154. Hoodless, L. J. *et al.* Genetic and pharmacological inhibition of CDK9 drives neutrophil apoptosis to resolve inflammation in zebrafish in vivo. *Sci Rep* **6**, (2016).
155. Isles, H. M. *et al.* The CXCL12/CXCR4 Signaling Axis Retains Neutrophils at Inflammatory Sites in Zebrafish. *Front Immunol* **10**, (2019).
156. Mathias, J. R. *et al.* Resolution of inflammation by retrograde chemotaxis of neutrophils in transgenic zebrafish. *J Leukoc Biol* **80**, 1281–1288 (2006).

157. Carrillo, S. A. *et al.* Macrophage Recruitment Contributes to Regeneration of Mechanosensory Hair Cells in the Zebrafish Lateral Line. *J Cell Biochem* **117**, 1880–1889 (2016).
158. Nguyen-Chi, M. *et al.* TNF signaling and macrophages govern fin regeneration in zebrafish larvae. *Cell Death Dis* **8**, e2979 (2017).
159. Nguyen-Chi, M. *et al.* Identification of polarized macrophage subsets in zebrafish. *Elife* **4**, (2015).
160. Hasegawa, T., Nakajima, T., Ishida, T., Kudo, A. & Kawakami, A. A diffusible signal derived from hematopoietic cells supports the survival and proliferation of regenerative cells during zebrafish fin fold regeneration. *Dev Biol* **399**, 80–90 (2015).
161. Morales, R. A. & Allende, M. L. Peripheral Macrophages Promote Tissue Regeneration in Zebrafish by Fine-Tuning the Inflammatory Response. *Front Immunol* **10**, (2019).
162. Reggiani, F., Gobbi, G., Ciarrocchi, A. & Sancisi, V. YAP and TAZ Are Not Identical Twins. *Trends Biochem Sci* **46**, 154–168 (2021).
163. Nishioka, N. *et al.* The Hippo Signaling Pathway Components Lats and Yap Pattern Tead4 Activity to Distinguish Mouse Trophectoderm from Inner Cell Mass. *Dev Cell* **16**, 398–410 (2009).
164. Gaffney, C. J. *et al.* Identification, basic characterization and evolutionary analysis of differentially spliced mRNA isoforms of human YAP1 gene. *Gene* **509**, 215–222 (2012).
165. Vrbský, J. *et al.* Evidence for discrete modes of YAP1 signaling via mRNA splice isoforms in development and diseases. *Genomics* **113**, 1349–1365 (2021).
166. Howell, M., Borchers, C. & Milgram, S. L. Heterogeneous nuclear ribonuclear protein U associates with YAP and regulates its co-activation of bax transcription. *Journal of Biological Chemistry* **279**, 26300–26306 (2004).
167. Sudol, M. Yes-associated protein (YAP65) is a proline-rich phosphoprotein that binds to the SH3 domain of the Yes proto-oncogene product. *Oncogene* **9**, 2145–52 (1994).
168. Huang, W. *et al.* The N-terminal phosphodegron targets TAZ/WWTR1 protein for SCF β-TrCP-dependent degradation in response to phosphatidylinositol 3-kinase inhibition. *J Biol Chem* **287**, 26245–26253 (2012).
169. Hau, J. C. *et al.* The TEAD4-YAP/TAZ Protein-Protein Interaction: Expected Similarities and Unexpected Differences. *ChemBioChem* **14**, 1218–1225 (2013).
170. Kaan, H. Y. K. *et al.* Crystal structure of TAZ-TEAD complex reveals a distinct interaction mode from that of YAP-TEAD complex. *Sci Rep* **7**, (2017).
171. Murakami, M., Nakagawa, M., Olson, E. N. & Nakagawa, O. A WW domain protein TAZ is a critical coactivator for TBX5, a transcription factor implicated in Holt-Oram syndrome. *Proceedings of the National Academy of Sciences* **102**, 18034–18039 (2005).
172. Alarcón, C. *et al.* Nuclear CDKs Drive Smad Transcriptional Activation and Turnover in BMP and TGF-β Pathways. *Cell* **139**, 757–769 (2009).
173. Komuro, A., Nagai, M., Navin, N. E. & Sudol, M. WW domain-containing protein YAP associates with ErbB-4 and acts as a co-transcriptional activator for the carboxyl-terminal fragment of ErbB-4 that translocates to the nucleus. *Journal of Biological Chemistry* **278**, 33334–33341 (2003).
174. Haskins, J. W., Nguyen, D. X. & Stern, D. F. Neuregulin 1-activated ERBB4 interacts with YAP to induce Hippo pathway target genes and promote cell migration. *Sci Signal* **7**, (2014).
175. Lai, D., Ho, K. C., Hao, Y. & Yang, X. Taxol resistance in breast cancer cells is mediated by the hippo pathway component TAZ and its downstream transcriptional targets Cyr61 and CTGF. *Cancer Res* **71**, 2728–2738 (2011).
176. Imanaka, Y. *et al.* MicroRNA-141 confers resistance to cisplatin-induced apoptosis by targeting YAP1 in human esophageal squamous cell carcinoma. *J Hum Genet* **56**, 270–276 (2011).
177. Yu, Z., Pestell, T. G., Lisanti, M. P. & Pestell, R. G. Cancer stem cells. *International Journal of Biochemistry and Cell Biology* **44**, 2144–2151 (2012).
178. Cordenonsi, M. *et al.* The Hippo Transducer TAZ Confers Cancer Stem Cell-Related Traits on Breast Cancer Cells. *Cell* **147**, 759–772 (2011).
179. Salem, O., Jia, S., Qian, B.-Z. & Gram Hansen, C. AR activates YAP/TAZ differentially in prostate cancer. *Life Sci Alliance* **6**, e202201620 (2023).
180. Yan, L., Cai, Q. & Xu, Y. Hypoxic conditions differentially regulate TAZ and YAP in cancer cells. *Arch Biochem Biophys* **562**, 31–36 (2014).

181. Totaro, A., Panciera, T. & Piccolo, S. YAP/TAZ upstream signals and downstream responses. *Nat Cell Biol* **20**, 888–899 (2018).
182. Yoo, G., Kim, T., Chung, C., Hwang, D. S. & Lim, D. S. The novel YAP target gene, SGK1, upregulates TAZ activity by blocking GSK3β-mediated TAZ destabilization. *Biochem Biophys Res Commun* **490**, 650–656 (2017).
183. Weiler, S. M. E. *et al.* TAZ target gene ITGAV regulates invasion and feeds back positively on YAP and TAZ in liver cancer cells. *Cancer Lett* **473**, 164–175 (2020).
184. Moroishi, T. *et al.* A YAP/TAZ-induced feedback mechanism regulates Hippo pathway homeostasis. *Genes Dev* **29**, 1271–1284 (2015).
185. Park, G.-S. *et al.* An evolutionarily conserved negative feedback mechanism in the Hippo pathway reflects functional difference between LATS1 and LATS2. *Oncotarget* **7**, 24063–24075 (2016).
186. Kamura, K. *et al.* Obesity in Yap transgenic mice is associated with TAZ downregulation. *Biochem Biophys Res Commun* **505**, 951–957 (2018).
187. Zhang, J., Yuan, S., Vasilyev, A. & Amin Arnaout, M. The transcriptional coactivator Taz regulates proximodistal patterning of the pronephric tubule in zebrafish. *Mech Dev* **138**, 328–335 (2015).
188. Ren, Z., Zhang, Z., Liu, T.-M. & Ge, W. Novel zebrafish polycystic kidney disease models reveal functions of the Hippo pathway in renal cystogenesis. *Dis Model Mech* **10**, (2021).
189. Ishino, Y., Shinagawa, H., Makino, K., Amemura, M. & Nakata, A. Nucleotide Sequence of the iap Gene, Responsible for Alkaline Phosphatase Isozyme Conversion in Escherichia coli, and Identification of the Gene Product. *J Bacteriol* **169**, 5429–5433 (1987).
190. Mojica, F. J. M., Díez-Villaseñor, C., García-Martínez, J. & Soria, E. Intervening sequences of regularly spaced prokaryotic repeats derive from foreign genetic elements. *J Mol Evol* **60**, 174–182 (2005).
191. Marraffini, L. A. & Sontheimer, E. J. CRISPR Interference Limits Horizontal Gene Transfer in Staphylococci by Targeting DNA. *Science (1979)* **322**, 1843–1845 (2008).
192. Brouns, S. J. J. *et al.* Small CRISPR RNAs Guide Antiviral Defense in Prokaryotes. *Science (1979)* **321**, 960–964 (2008).
193. Barrangou, R. *et al.* CRISPR Provides Acquired Resistance Against Viruses in Prokaryotes. *Science (1979)* **315**, 170–172 (2007).
194. Jinek, M. *et al.* A Programmable Dual-RNA-Guided DNA Endonuclease in Adaptive Bacterial Immunity. *Science (1979)* **337**, 816–821 (2012).
195. Jiang, F. & Doudna, J. A. CRISPR-Cas9 Structures and Mechanisms. *Annu Rev Biophys* **46**, 505–529 (2017).
196. Liu, G., Lin, Q., Jin, S. & Gao, C. The CRISPR-Cas toolbox and gene editing technologies. *Mol Cell* **82**, 333–347 (2022).
197. Wang, J. Y. & Doudna, J. A. CRISPR technology: A decade of genome editing is only the beginning. *Science (1979)* **379**, (2023).
198. Doudna, J. A. The promise and challenge of therapeutic genome editing. *Nature* **578**, 229–236 (2020).
199. Cornet, C., Di Donato, V. & Terriente, J. Combining Zebrafish and CRISPR/Cas9: Toward a more efficient drug discovery pipeline. *Front Pharmacol* **9**, (2018).
200. Howe, K. *et al.* The zebrafish reference genome sequence and its relationship to the human genome. *Nature* **496**, 498–503 (2013).
201. Pei, W. *et al.* Guided genetic screen to identify genes essential in the regeneration of hair cells and other tissues. *NPJ Regen Med* **3**, (2018).
202. Keatinge, M. *et al.* CRISPR gRNA phenotypic screening in zebrafish reveals pro-regenerative genes in spinal cord injury. *PLoS Genet* **17**, e1009515 (2021).
203. Klatt Shaw, D. *et al.* Localized EMT reprograms glial progenitors to promote spinal cord repair. *Dev Cell* **56**, (2021).
204. Moroishi, T., Gram Hansen, C. & Guan, K.-L. The emerging roles of YAP and TAZ in cancer. *Nat Rev Cancer* **15**, 73–79 (2015).
205. Benchling. *www.benchling.com*.
206. National Library of Medicine, N. C. for B. I. Primer-BLAST. *ncbi.nlm.nih.gov/tools/primer-blast*.
207. Dewari, P. S. *et al.* An efficient and scalable pipeline for epitope tagging in mammalian stem cells using Cas9 ribonucleoprotein. *Elife* **7**, e35069 (2018).

208. Essner, J. Zebrafish embryo microinjection: Ribonucleoprotein delivery using the Alt-R CRISPR-Cas9 System. *Integrated DNA Technologies* https://eu.idtdna.com/pages/education/decoded/article/protocols-for-crispr-genome-editing-in-your-model-system (2016).
209. Ramazani, Y. *et al.* Connective tissue growth factor (CTGF) from basics to clinics. *Matrx Biology* **68–69**, 44–66 (2018).
210. Link, V., Shevchenko, A. & Heisenberg, C.-P. Proteomics of early zebrafish embryos. *BMC Dev Biol* **6**, (2006).
211. Kinoshita, E., Kinoshita-Kikuta, E. & Koike, T. Separation and detection of large phosphoproteins using Phos-tag SDS-PAGE. *Nat Protoc* **4**, 1513–1521 (2009).
212. University of Queensland. Using ImageJ to Quantify Blots. *di.uq.edu.au/community-and-alumni/sparq-ed/sparq-ed-services/using-imagej-quantify-blots*.
213. Teixidó, E. *et al.* Automated Morphological Feature Assessment for Zebrafish Embryo Developmental Toxicity Screens. *Toxicological Sciences* **167**, 438–449 (2019).
214. Lin, Y.-F., Sam, J. & Evans, T. Sirt1 promotes tissue regeneration in zebrafish through regulating the mitochondrial unfolded protein response. *iScience* **24**, 103118 (2021).
215. Andrews, S. FastQC: A Quality Control Tool for High Throughput Sequence Data [Online]. *http://www.bioinformatics.babraham.ac.uk/projects/fastqc/* (2010).
216. Bolger, A. M., Lohse, M. & Usadel, B. Trimmomatic: A flexible trimmer for Illumina sequence data. *Bioinformatics* **30**, 2114–2120 (2014).
217. Burrows-Wheeler Aligner-MEM. *https://bio-bwa.sourceforge.net/* (2009).
218. Danecek, P. *et al.* Twelve years of SAMtools and BCFtools. *Gigascience* **10**, (2021).
219. Anders, S., Pyl, P. T. & Huber, W. HTSeq - a Python framework to work with high-throughput sequencing data. *Bioinformatics* **31**, 166–169 (2015).
220. Anaconda Inc. Anaconda Software Distribution. *https://docs.anaconda.com*.
221. Kreuger, F. Trim Galore. *https://www.bioinformatics.babraham.ac.uk/projects/trim_galore/* (2012).
222. Love, M. I., Anders, S. & Huber, W. Analyzing RNA-seq data with DESeq2. *http://bioconductor.org/packages/devel/bioc/vignettes/DESeq2/inst/doc/DESeq2.html* (2023).
223. Love, M. I., Huber, W. & Anders, S. Moderated estimation of fold change and dispersion for RNA-seq data with DESeq2. *Genome Biol* **15**, (2014).
224. Yao, B., Huang, Y. & Kang, C. rld: Analyze and Design Repeated Low-Dose Challenge Experiments. *http://cran.nexr.com/web/packages/rld/index.html* (2017).
225. Pagès, H., Carlson, M., Falcon, S. & Li, N. AnnotationDbi: Manipulation of SQLite-based annotations in Bioconductor. R package version 1.62.2. *https://bioconductor.org/packages/AnnotationDbi* (2023).
226. Kolde, R. Package 'pheatmap'; Pretty Heatmaps. *https://cran.r-project.org/web/packages/pheatmap/pheatmap.pdf* (2019).
227. Wickham, H. *et al.* Welcome to the Tidyverse. *J Open Source Softw* **4**, 1686 (2019).
228. Wu, T. *et al.* clusterProfiler 4.0: A universal enrichment tool for interpreting omics data. *The Innovation* **2**, (2021).
229. Carlson, M. org.Dr.eg.db: Genome wide annotation for Zebrafish. R package version 3.8.2. *https://bioconductor.org/packages/release/data/annotation/html/org.Dr.eg.db.html* (2019).
230. Wang, Y. *et al.* Comprehensive Molecular Characterization of the Hippo Signaling Pathway in Cancer. *Cell Rep* **25**, 1304-1317.e5 (2018).
231. Wickham, H. *ggplot2: Elegant Graphics for Data Analysis*. (Springer International Publishing Cham, 2016). doi:10.1007/978-3-319-24277-4.
232. Slowikowski, K. ggrepel: Automatically Position Non-Overlapping Text Labels with 'ggplot2'. R package version 0.9.3. *https://github.com/slowkow/ggrepel* (2023).
233. Chang, W. Package 'extrafont'; Tools for Using Fonts. Version 0.19. *https://github.com/wch/extrafont* (2023).
234. Neuwirth, E. Package RColorBrewer. Version 1.1-2. *https://cran.r-hub.io/web/packages/RColorBrewer/index.html* (2014).
235. Garnier, S. *et al.* viridis(Lite) - Colorblind-Friendly Color Maps for R. *https://sjmgarnier.github.io/viridis/* (2023).
236. He, L. *et al.* Yes-Associated Protein (Yap) Is Necessary for Ciliogenesis and Morphogenesis during Pronephros Development in Zebrafish (Danio Rerio). *Int J Biol Sci* **11**, 935–947 (2015).

237. ZFIN. Swim Bladder. *https://zfin.org/ZFA:0000076*.
238. Sorlien, E. L., Witucki, M. A. & Ogas, J. Efficient production and identification of CRISPR/Cas9-generated gene knockouts in the model system Danio rerio. *Journal of Visualized Experiments* **138**, (2018).
239. Sasagawa, S. *et al.* Downregulation of GSTK1 is a common mechanism underlying hypertrophic cardiomyopathy. *Front Pharmacol* **7**, (2016).
240. Dai, X. *et al.* YAP activates the Hippo pathway in a negative feedback loop. *Cell Res* **25**, 1175–1178 (2015).
241. Kinoshita, E., Kinoshita-Kikuta, E., Takiyama, K. & Koike, T. Phosphate-binding Tag, a New Tool to Visualize Phosphorylated Proteins. *Molecular and Cellular Proteomics* **5**, 749–757 (2006).
242. Cunningham, R. *et al.* YAP/TAZ activation predicts clinical outcomes in mesothelioma and is conserved in in vitro model of driver mutations. *Clin Transl Med* **13**, (2023).
243. Kimmel, C. B., Ballard, W. W., Kimmel, S. R., Ullmann, B. & Schilling, T. F. Stages of embryonic development of the zebrafish. *Developmental Dynamics* **203**, 253–310 (1995).
244. Brand, M. *et al.* Mutations affecting development of the midline and general body shape during zebrafish embryogenesis. *Development* **123**, 129–42 (1996).
245. Marques, I. J., Lupi, E. & Mercader, N. Model systems for regeneration: Zebrafish. *Development* **146**, dev167692 (2019).
246. Sehring, I. M. & Weidinger, G. Recent advancements in understanding fin regeneration in zebrafish. *Wiley Interdiscip Rev Dev Biol* **9**, (2020).
247. Brandão, A. S. *et al.* Yap induces osteoblast differentiation by modulating Bmp signalling during zebrafish caudal fin regeneration. *J Cell Sci* **132**, jcs231993 (2019).
248. Mateus, R. *et al.* In Vivo Cell and Tissue Dynamics Underlying Zebrafish Fin Fold Regeneration. *PLoS One* **7**, (2012).
249. Ye, Z. *et al.* Yap-lin28a axis targets let7-Wnt pathway to restore progenitors for initiating regeneration. *Elife* **9**, e55771 (2020).
250. Mackenzie, S. M. & Raible, D. W. Proliferative Regeneration of Zebrafish Lateral Line Hair Cells after Different Ototoxic Insults. *PLoS One* **7**, (2012).
251. Kelley, M. W. & Meyers, J. R. Hair Cell Regeneration in the Inner Ear and Lateral Line. in *Principles of Regenerative Medicine* 867–885 (Elsevier Inc., 2019).
252. Stengel, D., Zindler, F. & Braunbeck, T. An optimized method to assess ototoxic effects in the lateral line of zebrafish (Danio rerio) embryos. *Comparative Biochemistry and Physiology Part C* **193**, 18–29 (2017).
253. Lush, M. E. & Piotrowski, T. Sensory hair cell regeneration in the zebrafish lateral line. *Developmental Dynamics* **243**, 1187–1202 (2014).
254. Hardy, K. *et al.* Functional development and regeneration of hair cells in the zebrafish lateral line. *Journal of Physiology* **599**, 3913–3936 (2021).
255. Chakraborty, A., Uechi, T., Higa, S., Torihara, H. & Kenmochi, N. Loss of ribosomal protein L11 affects zebrafish embryonic development through a p53-dependent apoptotic response. *PLoS One* **4**, e4152 (2009).
256. Elabd, S. *et al.* Delay in development and behavioural abnormalities in the absence of p53 in zebrafish. *PLoS One* **14**, e0220069 (2019).
257. Mokalled, M. H. *et al.* Injury-induced ctgfa directs glial bridging and spinal cord regeneration in zebrafish. *Science (1979)* **354**, 630–634 (2016).
258. Mukherjee, D. *et al.* Ccn2a is an injury-induced matricellular factor that promotes cardiac regeneration in zebrafish. *Development* **148**, dev193219 (2021).
259. Hergovich, A. Regulation and functions of mammalian LATS/NDR kinases: Looking beyond canonical Hippo signalling. *Cell Biosci* **3**, (2013).
260. Zaykov, V. & Chaqour, B. The CCN2/CTGF interactome: an approach to understanding the versatility of CCN2/CTGF molecular activities. *J Cell Commun Signal* **15**, 567–580 (2021).
261. Hu, X. *et al.* Nuclear condensates of YAP fusion proteins alter transcription to drive ependymoma tumourigenesis. *Nat Cell Biol* **25**, 323–336 (2023).
262. Song, H. *et al.* HIF-1α/YAP Signaling Rewrites Glucose/Iodine Metabolism Program to Promote Papillary Thyroid Cancer Progression. *Int J Biol Sci* **19**, 225–241 (2023).
263. Wu, L. *et al.* ATXN3 promotes prostate cancer progression by stabilizing YAP. *Cell Communication and Signaling* **21**, (2023).

264. Romero, M. M. G., McCathie, G., Jankun, P. & Roehl, H. H. Damage-induced reactive oxygen species enable zebrafish tail regeneration by repositioning of Hedgehog expressing cells. *Nat Commun* **9**, (2018).
265. Bagwell, J. *et al.* Notochord vacuoles absorb compressive bone growth during zebrafish spine formation. *Elife* **9**, (2020).
266. Nguyen-Chi, M. *et al.* Pro-resolving mediator protectin D1 promotes epimorphic regeneration by controlling immune cell function in vertebrates. *Br J Pharmacol* **177**, 4055–4073 (2020).
267. Sinclair, J. W. *et al.* The Warburg effect is necessary to promote glycosylation in the blastema during zebrafish tail regeneration. *NPJ Regen Med* **6**, (2021).
268. Zhang, J. *et al.* Loss of fish actinotrichia proteins and the fin-to-limb transition. *Nature* **466**, 234–237 (2010).
269. LeBert, D. C. *et al.* Matrix metalloproteinase 9 modulates collagen matrices and wound repair. *Development* **142**, 2136–2146 (2015).
270. Yoshinari, N., Ishida, T., Kudo, A. & Kawakami, A. Gene expression and functional analysis of zebrafish larval fin fold regeneration. *Dev Biol* **325**, 71–81 (2009).
271. Ishida, T., Nakajima, T., Kudo, A. & Kawakami, A. Phosphorylation of Junb family proteins by the Jun N-terminal kinase supports tissue regeneration in zebrafish. *Dev Biol* **340**, 468–479 (2010).
272. Kalluri, R. Basement membranes: structure, assembly and role in tumour angiogenesis. *Nat Rev Cancer* **3**, 422–433 (2003).
273. Sztal, T., Berger, S., Currie, P. D. & Hall, T. E. Characterization of the Laminin Gene Family and Evolution in Zebrafish. *Developmental Dynamics* **240**, 422–431 (2011).
274. Bryan, C. D., Chien, C.-B. & Kwan, K. M. Loss of laminin alpha 1 results in multiple structural defects and divergent effects on adhesion during vertebrate optic cup morphogenesis. *Dev Biol* **416**, 324–337 (2016).
275. Kessels, M. Y. *et al.* Proteomics Analysis of the Zebrafish Skeletal Extracellular Matrix. *PLoS One* **9**, e90568 (2014).
276. Zhu, P. *et al.* Short body length phenotype is compensated by the upregulation of nidogen family members in a deleterious nid1a mutation of zebrafish. *Journal of Genetics and Genomics* **44**, 553–556 (2017).
277. Ko, Y.-P., Kobbe, B., Paulsson, M. & Wagener, R. Zebrafish (Danio rerio) matrilins: shared and divergent characteristics with their mammalian counterparts. *Biochemical Journal* **386**, 367–379 (2005).
278. Kubra, K. *et al.* Phylogenetic and Expression Analysis of Fos Transcription Factors in Zebrafish. *Int J Mol Sci* **23**, (2022).
279. Jahangiri, L. *et al.* The AP-1 transcription factor component Fosl2 potentiates the rate of myocardial differentiation from the zebrafish second heart field. *Development* **143**, 113–122 (2016).
280. Piechaczyk, M. & Farràs, R. Regulation and function of JunB in cell proliferation. *Biochem Soc Trans* **36**, 864–867 (2008).
281. Bolli, N. *et al.* Expression of the cytoplasmic NPM1 mutant (NPMc+) causes the expansion of hematopoietic cells in zebrafish. *Blood* **115**, 3329–3340 (2010).
282. Richens, J. *et al.* The detection of ADAM8 protein on cells of the human immune system and the demonstration of its expression on peripheral blood B cells, dendritic cells and monocyte subsets. *Immunobiology* **212**, 29–38 (2007).
283. Su, H., Lei, C.-T. & Zhang, C. Interleukin-6 Signaling Pathway and Its Role in Kidney Disease: An Update. *Front Immunol* **8**, (2017).
284. Duan, J. *et al.* Inflammation–coagulation response and thrombotic effects induced by silica nanoparticles in zebrafish embryos. *Nanotoxicology* **12**, 470–484 (2018).
285. Zhu, H. *et al.* Bacterial Quorum-Sensing Signal DSF Inhibits LPS-Induced Inflammations by Suppressing Toll-Like Receptor Signaling and Preventing Lysosome-Mediated Apoptosis in Zebrafish. *Int J Mol Sci* **23**, (2022).
286. Khrystoforova, I. *et al.* Zebrafish mutants reveal unexpected role of Lrp5 in osteoclast regulation. *Front Endocrinol (Lausanne)* **13**, (2022).
287. Zavašnik-Bergant, T. & Turk, B. Cysteine cathepsins in the immune response. *Tissue Antigens* **67**, 349–355 (2006).

288. Hayman, A. R. *et al.* Mice lacking tartrate-resistant acid phosphatase (Acp 5) have disrupted endochondral ossification and mild osteopetrosis. *Development* **122**, 3151–3162 (1996).
289. Ren, X., Shan, W.-H., Wei, L.-L., Gong, C.-C. & Pei, D.-S. ACP5: Its Structure, Distribution, Regulation and Novel Functions. *Anticancer Agents Med Chem* **18**, 1082–1090 (2018).
290. Xu, Y. J. *et al.* Effect of HSPB9 on Apoptosis of DF-1 Cells. *Biomedical and Environmental Sciences* **32**, 107–120 (2019).
291. Fallahi, E., O'Driscoll, N. A. & Matallanas, D. The MST/Hippo Pathway and Cell Death: A Non-Canonical Affair. *Genes (Basel)* **7**, (2016).
292. Zhang, X., Abdelrahman, A., Vollmar, B. & Zechner, D. The Ambivalent Function of YAP in Apoptosis and Cancer. *Int J Mol Sci* **19**, (2018).
293. Dex, S., Lin, D., Shukunami, C. & Docheva, D. TENOgenic MODULating INsider factor: Systematic assessment on the functions of tenomodulin gene. *Gene* **587**, (2016).
294. Rueda, E. M. *et al.* The Hippo Pathway Blocks Mammalian Retinal Müller Glial Cell Reprogramming. *Cell Rep* **27**, 1637–1649 (2019).
295. Quint, E. *et al.* Bone patterning is altered in the regenerating zebrafish caudal fin after ectopic expression of sonic hedgehog and bmp2b or exposure to cyclopamine. *Proceedings of the National Academy of Sciences* **99**, 8713–8718 (2002).
296. Schebesta, M., Lien, C.-L., Engel, F. B. & Keating, M. T. Transcriptional Profiling of Caudal Fin Regeneration in Zebrafish. *ScientificWorldJournal* **6**, 38–54 (2006).
297. Smith, A., Avaron, F., Guay, D., Padhi, B. K. & Akimenko, M. A. Inhibition of BMP signaling during zebrafish fin regeneration disrupts fin growth and scleroblast differentiation and function. *Dev Biol* **299**, 438–454 (2006).
298. Stewart, S., Gomez, A. W., Armstrong, B. E., Henner, A. & Stankunas, K. Sequential and Opposing Activities of Wnt and BMP Coordinate Zebrafish Bone Regeneration. *Cell Rep* **6**, 482–498 (2014).
299. Murciano, C. *et al.* Ray–Interray Interactions during Fin Regeneration of Danio rerio. *Dev Biol* **252**, 214–224 (2002).
300. van Eeden, F. J. M. *et al.* Genetic analysis of fin formation in the zebrafish, Danio rerio. *Development* **123**, 255–262 (1996).
301. Borini Etichetti, C. M., Tenaglia, A., Arroyo, M. N. & Girardini, J. E. Expression of zebrafish cpsf6 in embryogenesis and role of protein domains on subcellular localization. *Gene Expression Patterns* **36**, (2020).
302. Chaudhury, A., Chander, P. & Howe, P. H. Heterogeneous nuclear ribonucleoproteins (hnRNPs) in cellular processes: Focus on hnRNP E1's multifunctional regulatory roles. *RNA* **16**, 1449–1462 (2010).
303. Azuma, M., Embree, L. J., Sabaawy, H. & Hickstein, D. D. Ewing sarcoma protein Ewsr1 maintains mitotic integrity and proneural cell survival in the zebrafish embryo. *PLoS One* **2**, (2007).
304. Eastlack, S. C., Dong, S., Ivan, C. & Alahari, S. K. Suppression of PDHX by microRNA-27b deregulates cell metabolism and promotes growth in breast cancer. *Mol Cancer* **17**, (2018).
305. Woodgett, J. R. Judging a Protein by More Than Its Name GSK-3. *Science's STKE* **2001**, (2001).
306. Bláhová, Z. *et al.* Partial fads2 Gene Knockout Diverts LC-PUFA Biosynthesis via an Alternative Δ8 Pathway with an Impact on the Reproduction of Female Zebrafish (Danio rerio). *Genes (Basel)* **13**, (2022).
307. Morrison, A. M. S. *et al.* Identification, modeling and ligand affinity of early deuterostome CYP51s, and functional characterization of recombinant zebrafish sterol 14α-demethylase. *Biochim Biophys Acta* **1840**, 1825–1836 (2014).
308. Hernandez, J. A., Castro, V. L., Reyes-Nava, N., Montes, L. P. & Quintana, A. M. Mutations in the zebrafish hmgcs1 gene reveal a novel function for isoprenoids during red blood cell development. *Blood Adv* **3**, 1244–1254 (2019).
309. Zhang, Q., Sun, S., Zhang, Y., Wang, X. & Li, Q. Identification of Scd5 as a functional regulator of visceral fat deposition and distribution. *iScience* **25**, (2022).
310. Gatticchi, L. *et al.* Tm7sf2 gene promotes adipocyte differentiation of mouse embryonic fibroblasts and improves insulin sensitivity. *Biochim Biophys Acta Mol Cell Res* **1868**, (2021).
311. Chen, F., Lu, X.-J., Nie, L., Ning, Y.-J. & Chen, J. Molecular characterization of a CC motif chemokine 19-like gene in ayu (Plecoglossus altivelis) and its role in leukocyte trafficking. *Fish Shellfish Immunol* **72**, 301–308 (2018).

312. Torraca, V., Otto, N. A., Tavakoli-Tameh, A. & Meijer, A. H. The inflammatory chemokine Cxcl18b exerts neutrophil-specific chemotaxis via the promiscuous chemokine receptor Cxcr2 in zebrafish. *Dev Comp Immunol* **67**, 57–65 (2017).
313. Luu, W., Hart-Smith, G., Sharpe, L. J. & Brown, A. J. The terminal enzymes of cholesterol synthesis, DHCR24 and DHCR7, interact physically and functionally. *J Lipid Res* **56**, 888–897 (2015).
314. Padyana, A. K. *et al.* Structure and inhibition mechanism of the catalytic domain of human squalene epoxidase. *Nat Commun* **10**, (2019).
315. Cuccioloni, M. *et al.* Epigallocatechin-3-gallate potently inhibits the in vitro activity of hydroxy-3-methyl-glutaryl-CoA reductase. *J Lipid Res* **52**, 897–907 (2011).
316. Jorgensen, P. L., Håkansson, K. O. & Karlish, S. J. D. Structure and Mechanism of Na,K-ATPase: Functional Sites and Their Interactions. *Annu Rev Physiol* **65**, 817–849 (2003).
317. Auxerre-Plantié, E. *et al.* Identification of MYOM2 as a candidate gene in hypertrophic cardiomyopathy and Tetralogy of Fallot, and its functional evaluation in the Drosophila heart. *Dis Model Mech* **13**, (2020).
318. Tooley, J. G., Catlin, J. P. & Schaner Tooley, C. E. METTLing in Stem Cell and Cancer Biology. *Stem Cell Rev Rep* **19**, 76–91 (2023).
319. Jentsch, T. J. & Pusch, M. CLC Chloride Channels and Transporters: Structure, Function, Physiology, and Disease. *Physiol Rev* **98**, 1493–1590 (2018).
320. Wang, Y.-F., Yan, J.-J., Tseng, Y.-C., Chen, R.-D. & Hwang, P.-P. Molecular Physiology of an Extra-renal Cl- Uptake Mechanism for Body Fluid Cl- Homeostasis. *Int J Biol Sci* **11**, 1190–1203 (2015).
321. Margaria, J. P., Ratto, E., Gozzelino, L., Li, H. & Hirsch, E. Class II PI3Ks at the Intersection between Signal Transduction and Membrane Trafficking. *Biomolecules* **9**, (2019).
322. Harris, N. S., Pelletier, J. P., Marin, M. J. & Winter, W. E. Von Willebrand factor and disease: a review for laboratory professionals. *Crit Rev Clin Lab Sci* **59**, 241–256 (2022).
323. Pedemonte, N. & Galietta, L. J. V. Structure and Function of TMEM16 Proteins (Anoctamins). *Physiol Rev* **94**, 419–459 (2014).
324. Anderson, D. M. *et al.* Severe muscle wasting and denervation in mice lacking the RNA-binding protein ZFP106. *PNAS* **113**, E4494–E4503 (2016).
325. Zhang, S. & Cui, P. Complement system in zebrafish. *Dev Comp Immunol* **46**, 3–10 (2014).
326. Forn-Cuní, G., Varela, M., Pereiro, P., Novoa, B. & Figueras, A. Conserved gene regulation during acute inflammation between zebrafish and mammals. *Sci Rep* **7**, (2017).
327. ZFIN Gene: atp1b4. https://zfin.org/ZDB-GENE-070412-1.
328. ZFIN Gene: tmt1a.1. https://zfin.org/ZDB-GENE-061027-239.
329. Gene: MYOM2 (ENSG00000036448) - Summary - Homo_sapiens - Ensembl genome browser 110. http://www.ensembl.org/Homo_sapiens/Gene/Summary?g=ENSG00000036448;r=8:2045046-2165552.
330. ZFIN Gene: myom2a. https://zfin.org/ZDB-GENE-030131-6201.
331. ZFIN Gene: ano2b. https://zfin.org/ZDB-GENE-060503-62.
332. ZFIN Gene: znf106b. https://zfin.org/ZDB-GENE-091118-24.
333. ZFIN Gene: clcn4. https://zfin.org/ZDB-GENE-061013-353.
334. ZFIN Gene: pik3c2g. https://zfin.org/ZDB-GENE-170327-2.
335. ZFIN Gene: vwa5a. https://zfin.org/ZDB-GENE-040912-181.
336. ZFIN Gene: aqp8b. https://zfin.org/ZDB-GENE-080220-47.
337. ZFIN Gene: insl5b. https://zfin.org/ZDB-GENE-070122-5.
338. ZFIN Gene: jak3. https://zfin.org/ZDB-GENE-070725-4.
339. ZFIN Gene: runx1. https://zfin.org/ZDB-GENE-000605-1.
340. ZFIN Gene: sla1a. https://zfin.org/ZDB-GENE-050904-3.
341. ZFIN Gene: pcsk9. https://zfin.org/ZDB-GENE-060927-1.
342. ZFIN Gene: abcc12. https://zfin.org/ZDB-GENE-050517-25.
343. ZFIN Gene: btr29. https://zfin.org/ZDB-GENE-090512-2.
344. ZFIN Gene: c1qb. https://zfin.org/ZDB-GENE-040801-223.
345. ZFIN Gene: c4b. https://zfin.org/ZDB-GENE-100805-2.
346. ZFIN Gene: cnr2. https://zfin.org/ZDB-GENE-040702-7.
347. ZFIN Gene: f5. https://zfin.org/ZDB-GENE-030131-5531.
348. ZFIN Gene: ifitm1. https://zfin.org/ZDB-GENE-060526-259.

349. Gene: IFITM1 (ENSG00000185885) - Summary - Homo_sapiens - Ensembl genome browser 110. http://www.ensembl.org/Homo_sapiens/Gene/Summary?db=core;g=ENSG00000185885;r=11:310041-315272.
350. ZFIN Gene: igfbp6b. https://zfin.org/ZDB-GENE-090521-2.
351. ZFIN Gene: mafbb. https://zfin.org/ZDB-GENE-010605-4.
352. ZFIN Gene: nitr2b. https://zfin.org/ZDB-GENE-001106-6.
353. ZFIN Gene: rasal3. https://zfin.org/ZDB-GENE-101130-3.
354. ZFIN Gene: rgs14a. https://zfin.org/ZDB-GENE-030131-5579.
355. ZFIN Gene: socs3b. https://zfin.org/ZDB-GENE-040426-2528.
356. ZFIN Gene: tlr7. https://zfin.org/ZDB-GENE-040219-11.
357. ZFIN Gene: ccl35.1. https://zfin.org/ZDB-GENE-081022-33.
358. ZFIN Gene: gpr132b. https://zfin.org/ZDB-GENE-040724-83.
359. Gene: GRN (ENSG00000030582) - Summary - Homo_sapiens - Ensembl genome browser 110. http://www.ensembl.org/Homo_sapiens/Gene/Summary?db=core;g=ENSG00000030582;r=17:44345246-44353106.
360. ZFIN Gene: grna.1. https://zfin.org/ZDB-GENE-060103-1.
361. ZFIN Gene: lepb. https://zfin.org/ZDB-GENE-041210-183.
362. ZFIN Gene: mxd. https://zfin.org/ZDB-GENE-030721-8.
363. ZFIN Gene: ocstamp. https://zfin.org/ZDB-GENE-050327-65.
364. Gene: OCSTAMP (ENSG00000149635) - Summary - Homo_sapiens - Ensembl genome browser 110. http://www.ensembl.org/Homo_sapiens/Gene/Summary?db=core;g=ENSG00000149635;r=20:46540946-46550654;t=ENST00000279028.
365. ZFIN Gene: odam. https://zfin.org/ZDB-GENE-090313-260.
366. Gene: ODAM (ENSG00000109205) - Summary - Homo_sapiens - Ensembl genome browser 110. http://www.ensembl.org/Homo_sapiens/Gene/Summary?db=core;g=ENSG00000109205;r=4:70195725-70204576.
367. ZFIN Gene: brinp3a.1. https://zfin.org/ZDB-GENE-080218-16.
368. ZFIN Gene: foxi2. https://zfin.org/ZDB-GENE-031126-2.
369. ZFIN Gene: oxgr1a.1. https://zfin.org/ZDB-GENE-060421-6734.
370. ZFIN Gene: meox2a. https://zfin.org/ZDB-GENE-080613-1.
371. ZFIN Gene: cyth4a. https://zfin.org/ZDB-GENE-090624-6.
372. ZFIN Gene: hamp. https://zfin.org/ZDB-GENE-050726-1.
373. ZFIN Gene: tlr8b. https://zfin.org/ZDB-GENE-040219-12.
374. ZFIN Gene: tnfsf14. https://zfin.org/ZDB-GENE-101109-3.
375. ZFIN Gene: vwa11. https://zfin.org/ZDB-GENE-141211-58.
376. Park, J. & Gram Hansen, C. Cellular feedback dynamics and multilevel regulation driven by the hippo pathway. *Biochem Soc Trans* (2021).
377. Konsavage, W. M. & Yochum, G. S. Intersection of Hippo/YAP and Wnt/β-catenin signaling pathways. *Acta Biochim Biophys Sin (Shanghai)* **45**, 71–79 (2013).
378. Kim, M. & Jho, E. Cross-talk between Wnt/β-catenin and Hippo signaling pathways: a brief review. *BMB Rep* **47**, 540–545 (2014).
379. Jiang, L., Li, J., Zhang, C., Shang, Y. & Lin, J. YAP-mediated crosstalk between the Wnt and Hippo signaling pathways (Review). *Mol Med Rep* **22**, 4101–4106 (2020).
380. Mateus, R. *et al.* Control of tissue growth by Yap relies on cell density and F-actin in zebrafish fin regeneration. *J Cell Sci* **128**, (2015).
381. Ouyang, X. *et al.* Hyaluronic acid synthesis is required for zebrafish tail fin regeneration. *PLoS One* **12**, e0171898 (2017).
382. Liu, J. *et al.* Wnt/β-catenin signalling: function, biological mechanisms, and therapeutic opportunities. *Signal Transduct Target Ther* **7**, (2022).
383. Kizil, C. *et al.* Simplet/Fam53b is required for Wnt signal transduction by regulating β-catenin nuclear localization. *Development* **141**, 3529–3539 (2014).
384. Gan, X. *et al.* Nuclear Dvl, c-Jun, β-catenin, and TCF form a complex leading to stabilization of β-catenin-TCF interaction. *Journal of Cell Biology* **180**, 1087–1100 (2008).
385. Katoh, M. & Katoh, M. WNT Signaling Pathway and Stem Cell Signaling Network. *Clinical Cancer Research* **13**, 4042–4045 (2007).

386. Bell, I. J., Horn, M. S. & Van Raay, T. J. Bridging the gap between non-canonical and canonical Wnt signaling through Vangl2. *Semin Cell Dev Biol* **125**, 37–44 (2022).
387. Niida, A. *et al.* DKK1, a negative regulator of Wnt signaling, is a target of the β-catenin/TCF pathway. *Oncogene* **23**, 8520–8526 (2004).
388. Schwarzkopf, M. *et al.* Hybridization chain reaction enables a unified approach to multiplexed, quantitative, high-resolution immunohistochemistry and in situ hybridization. *Development* **148**, (2021).
389. Fu, V., Plouffe, S. W. & Guan, K.-L. The Hippo pathway in organ development, homeostasis, and regeneration. *Curr Opin Cell Biol* **49**, 99–107 (2017).
390. Parichy, D. M., Elizondo, M. R., Mills, M. G., Gordon, T. N. & Engeszer, R. E. Normal table of postembryonic zebrafish development: Staging by externally visible anatomy of the living fish. *Developmental Dynamics* **238**, 2975–3015 (2009).
391. Lalonde, R. L. & Akimenko, M.-A. Effects of fin fold mesenchyme ablation on fin development in zebrafish. *PLoS One* **13**, e0192500 (2018).
392. Halder, G., Dupont, S. & Piccolo, S. Transduction of mechanical and cytoskeletal cues by YAP and TAZ. *Nat Rev Mol Cell Biol* **13**, 591–600 (2012).
393. Gaspar, P. & Tapon, N. Sensing the local environment: actin architecture and Hippo signalling. *Curr Opin Cell Biol* **31**, 74–83 (2014).
394. Scott, C. A., Carney, T. J. & Amaya, E. Aerobic glycolysis is important for zebrafish larval wound closure and tail regeneration. *Wound Repair and Regeneration* **30**, 665–680 (2022).
395. Kim, J.-Y. *et al.* The value of phosphohistone H3 as a proliferation marker for evaluating invasive breast cancers: A comparative study with Ki67. *Oncotarget* **8**, 65064–65076 (2017).
396. Sipka, T. *et al.* Macrophages undergo a behavioural switch during wound healing in zebrafish. *Free Radic Biol Med* **192**, 200–212 (2022).
397. Sun, S. & Irvine, K. D. Cellular Organization and Cytoskeletal Regulation of the Hippo Signaling Network. *Trends Cell Biol* **26**, 694–704 (2016).
398. Li, S. *et al.* COL3A1 and MMP9 Serve as Potential Diagnostic Biomarkers of Osteoarthritis and Are Associated With Immune Cell Infiltration. *Front Genet* **12**, (2021).
399. ZFIN Gene: ggt1a. https://zfin.org/ZDB-GENE-040426-1388.
400. ZFIN Gene: leap2. https://zfin.org/ZDB-GENE-081022-131.
401. ZFIN Gene: dicp2.1. https://zfin.org/ZDB-GENE-120306-16.
402. Gene: CD4 (ENSG00000010610) - Summary - Homo_sapiens - Ensembl genome browser 110. http://www.ensembl.org/Homo_sapiens/Gene/Summary?db=core;g=ENSG00000010610;r=12:6786858-6820799.
403. ZFIN Gene: defbl1. https://zfin.org/ZDB-GENE-070207-1.
404. ZFIN Gene: c1qc. https://zfin.org/ZDB-GENE-041010-51.
405. ZFIN Gene: ccr12b.2. https://zfin.org/ZDB-GENE-070301-2.
406. ZFIN Gene: ccr9a. https://zfin.org/ZDB-GENE-060130-125.
407. ZFIN Gene: ctss2.1. https://zfin.org/ZDB-GENE-050522-559.
408. ZFIN Gene: il11a. https://zfin.org/ZDB-GENE-051019-1.
409. ZFIN Gene: irf8. https://zfin.org/ZDB-GENE-040718-367.
410. ZFIN Gene: coch. https://zfin.org/ZDB-GENE-030616-403.
411. Lim, J.-S. *et al.* Is serum γ-glutamyltransferase inversely associated with serum antioxidants as a marker of oxidative stress? *Free Radic Biol Med* **37**, 1018–1023 (2004).
412. Lee, D.-H., Blomhoff, R. & Jacobs, D. R. Is Serum Gamma Glutamyltransferase a Marker of Oxidative Stress? *Free Radic Res* **38**, 535–539 (2004).
413. Xie, Z. *et al.* Targeting GGT1 Eliminates the Tumor-Promoting Effect and Enhanced Immunosuppressive Function of Myeloid-Derived Suppressor Cells Caused by G-CSF. *Front Pharmacol* **13**, (2022).
414. Liu, B. *et al.* Innate immune memory and homeostasis may be conferred through crosstalk between the TLR3 and TLR7 pathways. *Sci Signal* **9**, (2016).
415. Pietretti, D. & Wiegertjes, G. F. Ligand specificities of Toll-like receptors in fish: Indications from infection studies. *Dev Comp Immunol* **43**, 205–222 (2014).
416. Yunna, C., Mengru, H., Lei, W. & Weidong, C. Macrophage M1/M2 polarization. *Eur J Pharmacol* **877**, (2020).
417. Holbrook, J., Lara-Reyna, S., Jarosz-Griffiths, H. & McDermott, M. Tumour necrosis factor signalling in health and disease. *F1000Res* **8**, (2019).

418. Tian, A. *et al.* Isolation and characterization of LIGHT (TNFSF14) gene homologue in zebrafish (Danio rerio). *Int Immunopharmacol* **14**, 629–634 (2012).
419. Shaw, D. K. & Mokalled, M. H. Efficient CRISPR/Cas9 mutagenesis for neurobehavioral screening in adult zebrafish. *G3: Genes, Genomes, Genetics* **11**, (2021).
420. Kroll, F. *et al.* A simple and effective F0 knockout method for rapid screening of behaviour and other complex phenotypes. *Elife* **10**, e59683 (2021).
421. Jobst-Schwan, T. *et al.* Acute multi-sgRNA knockdown of KEOPS complex genes reproduces the microcephaly phenotype of the stable knockout zebrafish model. *PLoS One* **13**, (2018).
422. Varshney, G. K. *et al.* A high-throughput functional genomics workflow based on CRISPR/Cas9-mediated targeted mutagenesis in zebrafish. *Nat Protoc* **11**, 2357–2375 (2016).
423. Hoshijima, K. *et al.* Highly Efficient CRISPR-Cas9-Based Methods for Generating Deletion Mutations and F0 Embryos that Lack Gene Function in Zebrafish. *Dev Cell* **51**, 645-657.e4 (2019).
424. Buglo, E. *et al.* Genetic compensation in a stable slc25a46 mutant zebrafish: A case for using F0 CRISPR mutagenesis to study phenotypes caused by inherited disease. *PLoS One* **15**, e0230566 (2020).
425. Moretti, L., Stalfort, J., Barker, T. H. & Abebayehu, D. The interplay of fibroblasts, the extracellular matrix, and inflammation in scar formation. *Journal of Biological Chemistry* **298**, 101530 (2022).
426. Brandão, A. S. *et al.* A regeneration-triggered metabolic adaptation is necessary for cell identity transitions and cell cycle re-entry to support blastema formation and bone regeneration. *Elife* **11**, (2022).
427. Abdollahpour, H. *et al.* The phenotype of human STK4 deficiency. *Blood* **119**, 3450–3457 (2012).
428. Nehme, N. T. *et al.* MST1 mutations in autosomal recessive primary immunodeficiency characterized by defective naive T-cell survival. *Blood* **119**, 3458–3468 (2012).
429. Zhang, W. *et al.* Downstream of Mutant KRAS, the Transcription Regulator YAP Is Essential for Neoplastic Progression to Pancreatic Ductal Adenocarcinoma. *Sci Signal* **7**, (2014).
430. Hagenbeek, T. J. *et al.* The Hippo pathway effector TAZ induces TEAD-dependent liver inflammation and tumors. *Sci Signal* **11**, (2018).
431. Kim, I., Park, T., Noh, J.-Y. & Kim, W. Emerging role of Hippo pathway in the regulation of hematopoiesis. *BMB Rep* **56**, 417–425 (2023).
432. Lee, D.-H., Kim, T.-S., Lee, D. & Lim, D.-S. Mammalian sterile 20 kinase 1 and 2 are important regulators of hematopoietic stem cells in stress condition. *Sci Rep* **8**, (2018).
433. Moro, A. *et al.* MicroRNA-dependent regulation of biomechanical genes establishes tissue stiffness homeostasis. *Nat Cell Biol* **21**, 348–358 (2019).
434. Kawakami, A., Fukazawa, T. & Takeda, H. Early fin primordia of zebrafish larvae regenerate by a similar growth control mechanism with adult regeneration. *Developmental Dynamics* **231**, 693–699 (2004).
435. Luo, K. Signaling cross talk between TGF-β/Smad and other signaling pathways. *Cold Spring Harb Perspect Biol* **9**, (2017).
436. Plouffe, S. W., Hong, A. W. & Guan, K.-L. Disease implications of the Hippo/YAP pathway. *Trends Mol Med* **21**, 212–222 (2015).
437. Cunningham, R. & Gram Hansen, C. The Hippo pathway in cancer: YAP/TAZ and TEAD as therapeutic targets in cancer. *Clin Sci* **136**, 197–222 (2022).
438. ClinicalTrials.gov. NCT04665206: Study to Evaluate VT3989 in Patients With Metastatic Solid Tumors Enriched for Tumors With NF2 Gene Mutations. *https://www.clinicaltrials.gov/study/NCT04665206* (2023).

8 Appendix

The following literature review is from[38]: Riley, S.E., Feng, Y., and Hansen, C.G., Hippo-Yap/Taz signalling in zebrafish regeneration, *npj* Regenerative Medicine, published 2022 in partnership with Australian Regenerative Medicine Institute.

This review forms part of the Introduction in section 1.4.

npj | Regenerative Medicine

www.nature.com/npjregenmed

REVIEW ARTICLE OPEN

Check for updates

Hippo-Yap/Taz signalling in zebrafish regeneration

Susanna E. Riley[1], Yi Feng[1] and Carsten Gram Hansen[1]✉

The extent of tissue regeneration varies widely between species. Mammals have a limited regenerative capacity whilst lower vertebrates such as the zebrafish (*Danio rerio*), a freshwater teleost, can robustly regenerate a range of tissues, including the spinal cord, heart, and fin. The molecular and cellular basis of this altered response is one of intense investigation. In this review, we summarise the current understanding of the association between zebrafish regeneration and Hippo pathway function, a phosphorylation cascade that regulates cell proliferation, mechanotransduction, stem cell fate, and tumorigenesis, amongst others. We also compare this function to Hippo pathway activity in the regenerative response of other species. We find that the Hippo pathway effectors Yap/Taz facilitate zebrafish regeneration and that this appears to be latent in mammals, suggesting that therapeutically promoting precise and temporal YAP/TAZ signalling in humans may enhance regeneration and hence reduce morbidity.

npj Regenerative Medicine (2022)7:9 ; https://doi.org/10.1038/s41536-022-00209-8

INTRODUCTION

Many different organisms have the ability to regenerate, although the robustness, efficiency, and scope of this regeneration is varied. Invertebrates such as planarians and Hydra regenerate their entire body such that, when cut in half, each section forms an entire new organism[1–4]. At the other end of the scale, mammalian regeneration is limited, with adult animals often responding to injury with fibrotic scarring rather than regeneration[5,6]. Some mammalian tissues do regenerate, including the skin, intestine, liver, peripheral nervous system, and blood[7–11], as well as foetal tissues[12] but this capability is impaired in ageing systems[13,14], which, along with a general lack of regenerative ability in most tissues, causes high morbidity in humans.

Midway on the scale from complete (invertebrate) to limited (mammalian) regeneration are lower vertebrates, including amphibians and fish. The zebrafish *Danio rerio* has the potential to completely regenerate multiple adult and embryonic organs, including the heart, fin, and many nervous system components[15–20]. First explored in the 1980s by Streisinger[21,22], the zebrafish is regularly utilised in the study of adult and embryonic regeneration due to their rapid external development, relative low cost, ease of genetic manipulation, scalability, transparent juveniles, and high rate of regeneration, none of which are present in the mouse.

The cellular and molecular drivers of zebrafish regeneration have been the subject of intense research[5,19]. Effective replacement of lost or damaged cells requires a large pool of available healthy cells. Cell pools can be formed by multiple sources, including the activation of resident stem or progenitor cells (differentiation), the reversion of differentiated cells to a more immature pluripotent state (dedifferentiation), or the conversion of one differentiated cell type into another mature cell type (transdifferentiation)[5,23]. On a molecular level, these can be driven by epigenetic and gene expression changes, such as alterations in DNA methylation[5,23–25], histone modifications[5,26–29], regeneration-responsive enhancers[28,30–33], and the activation of a range of key developmental signalling pathways, including Bmp, Fgf, Notch, RA, Shh, and Wnt/β-catenin (summarised in Table 1)[34–77]. In recent years, it has become evident that Hippo signalling (Fig. 1) plays a critical role in developmental and regenerative processes in both zebrafish and mammals. This is associated with the Hippo pathway's role in regulating cell proliferation and migration, detecting and responding to changes in tissue tension, extracellular matrix, chemical cues, which consequently alter cell fates[78–82].

The core Hippo signalling pathway is comprised of a serine/threonine kinase phosphorylation cascade (Fig. 1), most of which were identified in genetic screens of *Drosophila melanogaster* for tumour suppressor genes[83,84]. Activity of this pathway is regulated by a range of stimuli, including mechanical signalling, cell shape, ECM stiffness, cell polarity, metabolism, and cell:cell contacts[78,79,82,85–90], which are integrated to stimulate key kinases MST1/2 (the fly Hippo orthologs), STK25, and MAP4Ks when the Hippo pathway is active[87,89,91–93]. These kinases then phosphorylate, and so activate, LATS1/2, which phosphorylate the core Hippo effectors transcriptional co-activator YAP1 and its paralog TAZ on multiple conserved serine residues[86,87,91,92,94,95]. YAP1/TAZ phosphorylation triggers their retention in the cytoplasm via binding to protein 14-3-3, or ubiquitin-mediated degradation[86,87,94–97]. When the Hippo pathway is inactive these phosphorylations do not occur, resulting in YAP1/TAZ nuclear localisation, where they outcompete VGLL4 and bind to transcription factors TEAD1-4[87,98–101]. Binding to TEADs stimulate the expression of a range of pro-proliferative, -oncogenic, -stemness, and -EMT genes, such as *CTGF* and *CYR61*[78,87,90,98–100,102–104]. Additional YAP1/TAZ transcription factors have also been identified[87], but the most extensively studied are the TEADs. Zebrafish Hippo pathway genes have high genetic orthology to human genes, suggesting that this is an appropriate model in which to study Hippo pathway function (Fig. 2). Here we review the role of the Hippo pathway in the regeneration of a range of organs, including heart, spinal cord, tail fin, lateral line, and liver regeneration, with a focus on the zebrafish.

Heart regeneration

Cardiovascular diseases are the primary cause of morbidity and mortality globally, with around half of these deaths caused by

[1]University of Edinburgh Centre for Inflammation Research, Institute for Regeneration and Repair, Queen's Medical Research Institute, Edinburgh bioQuarter, 47 Little France Crescent, Edinburgh EH16 4TJ, UK. ✉email:

Table 1. A summary of major non-Hippo signalling pathways involved in zebrafish regeneration.

Signalling pathway	Model	Role of pathway
BMP	Heart[34]	Promotes CM proliferation and dedifferentiation
	Tail Fin[239–241,35,36]	Enhances proliferation and differentiation of osteoblasts in the blastema
Calcineurin	Tail Fin[37]	Regulates regeneration rate for positional information
Fgf	Spinal Cord[188,38]	Increases glial bridge formation, neuronal proliferation, and neurite outgrowth
	Tail Fin[229,39–41]	Promotes blastema formation and regenerative outgrowth Regulates regenerative growth rate
	Lateral Line[42]	Promotes support cell differentiation
Igf	Heart[43]	Enhances CM proliferation
	Tail Fin[44]	Promotes blastema cell proliferation and basal epithelium maintenance
Jak/Stat3	Heart[45]	Promotes CM proliferation
	Lateral Line[46]	Increases progenitor cell proliferation and differentiation
	Liver[47]	Necessary for appropriate timing of progenitor cell-to-hepatocyte differentiation Establishes the correct number of biliary epithelial cells during regeneration
NF-κB	Heart[48]	Promotes CM proliferation and dedifferentiation
Notch	Heart[49]	Enhances CM proliferation
	Spinal Cord[50]	Inhibits motor neuron neurogenesis
	Tail Fin[51,52]	Maintains blastema cells in a proliferative undifferentiated state
	Lateral Line[274,53,54]	Reduces support cell proliferation
	Liver[55–57]	Enhances biliary cell to hepatocyte conversion and differentiation of progenitor cells to biliary epithelial cells
Nrg	Heart[58]	Promotes CM proliferation
RA	Heart[59,60]	Enhances CM proliferation and wound epithelium formation
	Tail Fin[59,61–63]	Increases blastema and basal epidermis formation and patterning during regenerative outgrowth Restricts osteoprogenitor cells to boy ray regions
ROS	Heart[64]	Recruits immune cells and primes heart for regeneration
	Tail Fin[65]	Promotes proliferation of stump epidermal cells
Shh	Heart[43]	Increases CM proliferation
	Spinal Cord[66,67]	Activates motor neuron neurogenesis
	Tail Fin[35]	Promotes proliferation and differentiation of osteoblasts in the blastema
Tgfβ	Tail Fin[41,68]	Enhances cell migration and blastemal proliferation during outgrowth
	Heart[43,69,70]	Promotes CM proliferation and transient scar formation
Wnt/β-catenin	Spinal Cord[185,190]	Increases glial progenitor differentiation into neurons, axonal regrowth, and deposition of pro-regenerative collagen
	Tail Fin[212,239,71–73]	Enhances blastemal cell proliferation and osteoblast dedifferentiation
	Lateral Line[279,53,74]	Promotes support cell dedifferentiation and proliferation, and hair cell formation
	Liver[55,75–77]	Increases differentiation of biliary-derived progenitor cells into hepatocytes

ischaemic heart disease leading to heart failure[105]. This is due to the limited regeneration capacity of the adult human heart, which responds to heart muscle damage with fibrosis and scarring rather than the reformation of contractile muscle[106]. A similar response is seen in other mammals (such as the mouse), which also show limited cardiac regeneration after experimental injury paradigms[107]. An exception is an enhanced heart regeneration potential in neonatal mice, but this is transient and is lost within the first week of life[108], coinciding with a decrease in YAP1 transcriptional activity[78], and the withdrawal of cardiomyocytes (CMs) from the cell cycle[109]. However, this regenerative ability in neonatal mice[108] highlights that there may be therapeutic potential in reactivating the regenerative capacity in humans.

In contrast to restricted mammalian regeneration, both adult and embryonic zebrafish regenerate their heart fully following injury and even after multiple insults[5,6,15,19,110–113] (Fig. 3). This extensive heart regeneration is the result of two key characteristics: a high level of existing CM proliferation (around 3% per week, compared to <1% per year in adult mice[114] and humans[115]), and a permissive extracellular environment that stimulates it[19,116]. One major hurdle and pathological driver in mammalian heart regeneration is the formation of a fibrotic scar and non-permissive ECM at the injury area, replacing dead CMs with non-contractile elements such as collagen or fibroblasts rather than new CMs[106,117] (Fig. 3B). However, in the zebrafish, although collagen and fibronectin does accumulate and a scar is formed, it is eliminated to allow effective regeneration[113,118–120]. This scarring is regulated by Hippo signalling, with *cav-1*, *yap1*, and *ctgfa* mutants having disrupted scar formation and hence regeneration[121–123] (see Table 2 for a summary of these phenotypes). Heart injury promotes Ctgfa secretion into the ECM from endocardial cells, where it promotes the expression of pro-regenerative ECM genes (such as fibronectins and collagens)[121]. This expression allows for a transient scar, as shown by *ctgfa* mutants having a larger and more persistent scar, whilst *ctgfa* overexpression speeds scar resolution[121]. Similarly, *yap1* mutants have an altered ECM composition at the injury site, resulting in increased scarring and impaired regeneration at early time points[122]. This alteration of the scar microenvironment by secretion of Hippo pathway transcriptional targets

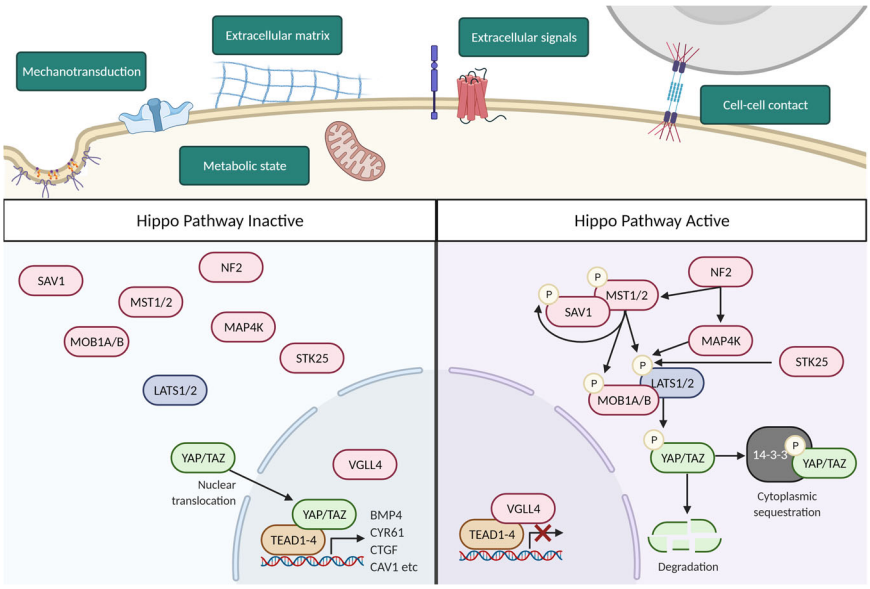

Fig. 1 Summary of the Hippo pathway signalling cascade and its stimuli. The Hippo pathway is regulated by the integration of a range of upstream stimuli. This includes mechanotransductive elements (such as caveolae and Piezo signalling), metabolism, extracellular matrix and integrin signalling, transduction of extracellular stimuli via mitogenic growth factor signalling and GPCRs, cell polarity and cell–cell contacts. Activation of the Hippo pathway triggers a phosphorylation cascade that leads to the phosphorylation of the Hippo pathway effectors YAP/TAZ. Phosphorylation of YAP/TAZ redistributes YAP/TAZ to the cytoplasm, blocking TEAD-mediated gene expression. Hippo pathway inactivation prevents YAP/TAZ phosphorylation, allowing their nuclear translocation and hence TEAD-mediated gene expression. Note that MST1/2 (mammalian STE20-like kinase1/2) are encoded by *STK4/3*, and TAZ by *WWTR1*. Figure 1 is created in BioRender.com.

suggests that Hippo signalling may also indirectly regulate the infiltration and proliferation of CMs through a cell non-autonomous mechanism.

The immune system creates a permissive microenvironment for regeneration (Fig. 3C). This is clearly demonstrated in the medaka, a teleost species closely related to the zebrafish. The medaka displays limited heart regeneration, a finding that is surprising considering their evolutionary similarity to the zebrafish[124,125]. This limited regeneration is, at least in part, due to the medaka's delay in macrophage recruitment to the injury site[124]. When recapitulated in the zebrafish by clodronate liposome-mediated macrophage depletion, these macrophage defects cause compromised neovascularisation and CM proliferation and consequently severe defects in heart regeneration[124]. This is due to the role of macrophages and other immune cell components such as T_{reg} cells in many areas of cardiac regeneration, including enhancing neovascularisation, CM proliferation, and scar resolution via the production of pro-regenerative factors, with inhibition of inflammation and timely immune cell recruitment inhibiting regeneration[124,126–129].

However, this pro-regenerative effect of the immune system is not simple. Yap1-Ctgfa signalling, shown to enhance cardiac regeneration, also negatively regulates the migration and infiltration of macrophages into the injury site[121,122], suggesting that inhibiting macrophage infiltration promotes cardiac regeneration. Similarly, *yap1* KO fish have increased macrophage infiltration in the scar and increased monocyte chemotactic gene expression[122], and *ctgfa* KO promotes the chemokine receptor gene *cxcr3.1* in the heart to increase M1 macrophage polarisation and so enhance inflammatory signalling[121], and both KO lines have defective regeneration. This apparent contradiction may be due to differences between experimental paradigms in investigating immune cell function in regeneration—it has been shown that the type of immune cells recruited, and the different regenerative stages alter the functional role of the immune system in regeneration[128]. An alternative explanation for this apparent discrepancy could be due to the requirement for tight spatio-temporal control of the immune system function during regeneration. This is shown by disruption of reparative regeneration after both immune system hyperactivation[121,122] and excessive inhibition[124,126,127,129]. Another potential reason for the inconsistency is that various immune cell types likely react differently to the injury, and so the Hippo pathway may respond in a range of ways to the same trigger. Therefore, the extent of activation or inhibition in these studies will greatly impact the results. Further in-depth studies are needed in order to fully elucidate the detailed spatiotemporal inflammatory response including revealing the exact immune cell types involved in regeneration and thereby the role of the Hippo pathway in the immune system's contribution to cardiac regeneration.

Hippo pathway signalling has also been linked to the epicardium, which is activated after heart injury in the zebrafish (Fig. 3C)[15,130]. The epicardium promotes regeneration, potentially by functioning as a cellular scaffold that generates epicardial-derived cells which differentiate into myofibroblasts and perivascular fibroblasts in the injured myocardium[131]. This may then act in a paracrine manner to induce CM proliferation and neoangiogenesis[131]. Epicardial activation has not yet been linked to the Hippo pathway in zebrafish heart regeneration. However, in the developing mouse, Hippo components are expressed in both the proepicardium and epicardium, and deletion of either Yap or Taz in the mouse gives coronary defects and impacts on epicardial cell proliferation, EMT, and specification of cell fate[132]. Similar developmental cardiac defects can be seen in a range of Hippo pathway component mutants in the zebrafish[112,133–152], suggesting that this role of the Hippo pathway may be conserved between mammals and teleosts.

After injury, existing differentiated CMs undergo limited dedifferentiation, upregulate the embryonic cardiogenesis gene *gata4*, and proliferate[113,153–156]. These CMs migrate to the injury site along newly-formed coronary vasculature[157–162] (Fig. 3E), where they proliferate further and differentiate to replace dead CMs and form new functional heart muscle[163] (Fig. 3F). CM proliferation is promoted by a range of signalling pathways, including Nrg, Tgfβ, Igf, and the Hippo pathway (Table 1). Disruption of the Hippo pathway-regulated genes *cav-1a* and

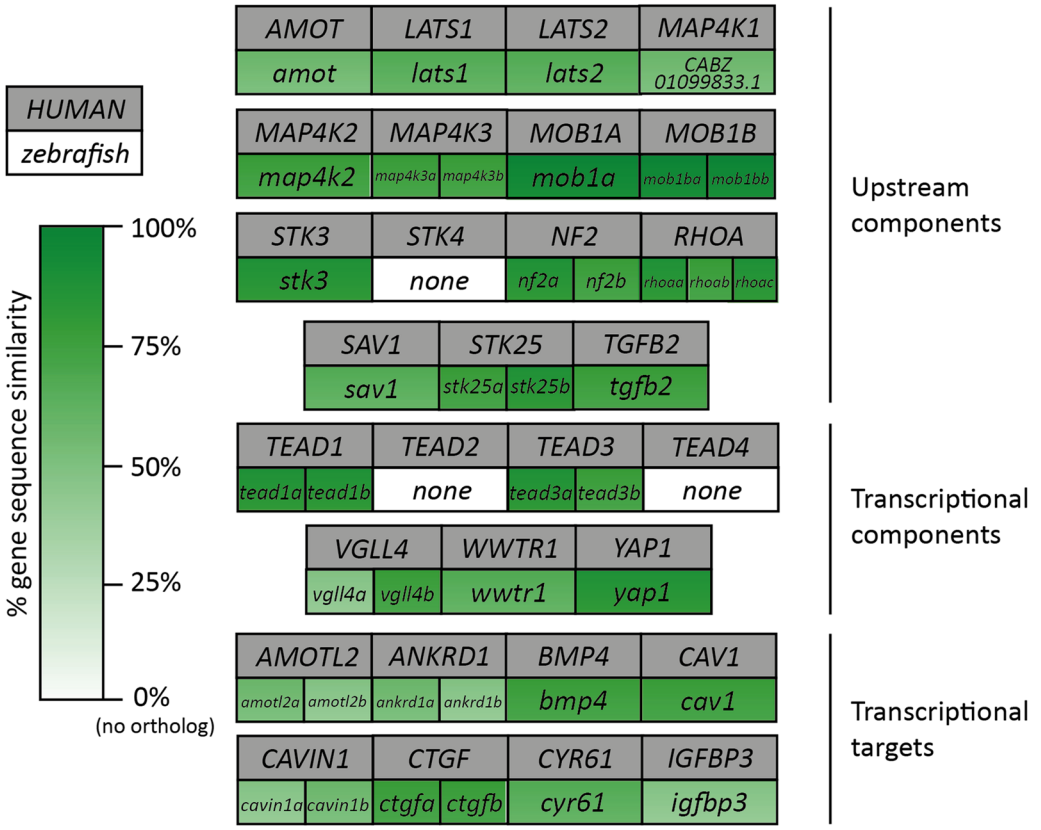

Fig. 2 Similarity between selected human and zebrafish Hippo pathway genes. Direct gene sequence comparison between a sample of human and zebrafish Hippo pathway members and transcriptional targets shows a range of similarity scores, emphasizing a high degree of similarities between fish and human genes, while also highlighting that some Hippo pathway components appear to have no direct orthologs present in both species. *WWTR1* encodes TAZ. *STK4* encodes MST1 and *STK3* encodes MST2 (in accordance with the consensus of the Hippo pathway field). *CYR61* is also known as *CCN1* and *CTGF* as *CCN2*. % gene sequence similarity identified using ensembl.org under orthology tab. *ctgfb*, *nf2b*, *map4k2*, and *rhoaa-c* could not be identified as orthologues in this manner, so manual BLAST comparison of genomic sequence (from GRCz11) was performed to give the values indicated.

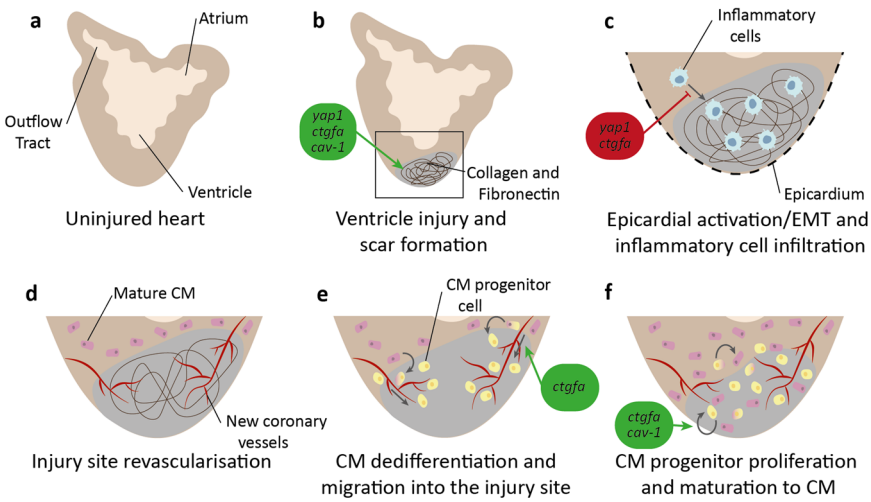

Fig. 3 Overview of zebrafish heart regeneration. a Structure of the uninjured zebrafish adult heart. **b** Injury at the ventricle apex induces collagen and fibronectin deposition and scar formation. *yap1*, *ctgfa*, and *cav-1* promote appropriate and transient scar formation. **c** Heart epicardium undergoes EMT and inflammatory cells (blue) infiltrate into the scar. *yap1* and *ctgfa* inhibit inflammatory cell infiltration. **d** New coronary vessels form to revascularize the injury site. **e** Mature cardiomyocytes (CMs) (pink) dedifferentiate into progenitor cells (yellow) and migrate along the new coronary vessels into the injury site. *ctgfa* promotes CM migration. **f** CM progenitors proliferate to create a progenitor cell pool, which matures back to CMs to reform the heart muscle. *ctgfa* and *cav-1* promote cell proliferation.

Table 2. Overview of zebrafish phenotypes seen when Hippo pathway components are disrupted.

Gene	Activity level	Disruption method	Allele created	Model	Phenotype
amotl2a	–	MO/TALEN	N/A/*fu45*, *fu46*	LL development[261]	Overproliferation in trailing edge of pLLP Increased pLLP size and cell number Reduced pLLP migration speed Increased number of neuromasts
cav-1a	–	TALEN	*pd1094*, *pd1104*	Heart regeneration[123]	Impaired recovery after injury, injury-induced CM proliferation, and scar resolution
		MO	N/A	LL development[136]	Reduced number and maturation of hair cells and neuromasts
ctgfa	–	TALEN	*bns50*	Heart regeneration[121]	Reduced CM proliferation, expression of pro-regenerative ECM genes, and CM migration along the coronary vasculature to repopulate the wound Increased collagenous scarring
				SC regeneration[197]	Reduced functional recovery after injury, glial cell proliferation and bridging, and axon regeneration
	+	hsp70:*ctgfa* OE plasmid	*pd97*	Heart regeneration[121]	Increased recovery after injury, CM proliferation, resolution of collagen deposition, and expression of pro-regenerative ECM genes
				SC regeneration[197]	Enhanced functional recovery after injury, glial bridging, and axon growth
		CRISPR	*zf3090*	Tail fin regeneration[234]	Increased tissue stiffness, contractility, and ECM deposition
lats2	–	CRISPR	*mw87*	Cancer[311]	Increased lethality Formation of peripheral nerve sheath tumours by 3mpf
nf2a	–	MO	N/A	Liver development[299]	Hepatomegaly, dilated bile duct, and extrahepatic choledochal cysts
sav1	–	CRISPR	*mw95*	Liver development[301]	Biliary dysgenesis, altered hepatocyte morphology and polarity, and biliary cell dysplastic morphology and increased expansion
stk3	–	TALEN	*mw96*	Liver development[301]	Biliary dysgenesis, altered hepatocyte morphology and polarity, and biliary cell dysplastic morphology and increased expansion
wwtr1	–	MO	N/A	Tail fin regeneration[149]	Lack of skeletal ossification
yap1	–	TALEN	*mw48*	Heart regeneration[122]	Improper scar formation Reduced ability to secrete collagen at the injury site Increased macrophage infiltration in the scar, monocyte chemotactic gene expression, space between the epicardium and myocardium, and CM proliferation
				LL regeneration[277]	Reduced progenitor cell maturation and proliferation
				Liver development[147]	Reduced liver size
		hsp70:DN-Yap plasmid	*zf621*	SC regeneration[193]	Impaired functional recovery after injury, axon growth, and glial bridging
				Tail fin regeneration[232,233]	Reduced recovery after injury, cell proliferation, and osteoprogenitor differentiation into osteoblasts Defects in bone formation
		5 µM verteporfin	N/A	LL regeneration[277]	Defective supporting cell, hair cell and mantle cell proliferation and hair cell maturation
				LL development[259–262]	Reduced number of neuromasts and hair cells, pLLP size, number of cells in the pLLP, mechanoreceptor differentiation, and Wnt signalling component expression
	+	Tol2 (myl7:3SA-myc *yap1*)	N/A	Heart regeneration[122]	Increased CM proliferation
		hsp70:CA-Yap plasmid	*zf622*	Tail fin regeneration[232]	Impaired recovery after injury, increased cell proliferation
		CA-Yap1 mRNA injection (in *lpar2b* MO)	N/A	LL development[262]	Increased pLLP size, and number of neuromasts and proliferating cells in the pLLP
		I-SceI (*lf:Yap1*)	N/A	Liver development[300]	Hepatomegaly
yap1;wwtr1	–	CRISPR	N/A	SC regeneration[193]	Impaired functional recovery after injury

This table is non-exhaustive and primarily covers developmental and regenerative phenotypes described in this review. Many other Hippo pathway mutants and morphants exist (e.g. *wwtr1* alleles *bns35*, *swu46*, *swu47*, *va4*, *mw49*, *ncv114*, and *fu55*). See individual gene pages on zfin.org for a complete list.

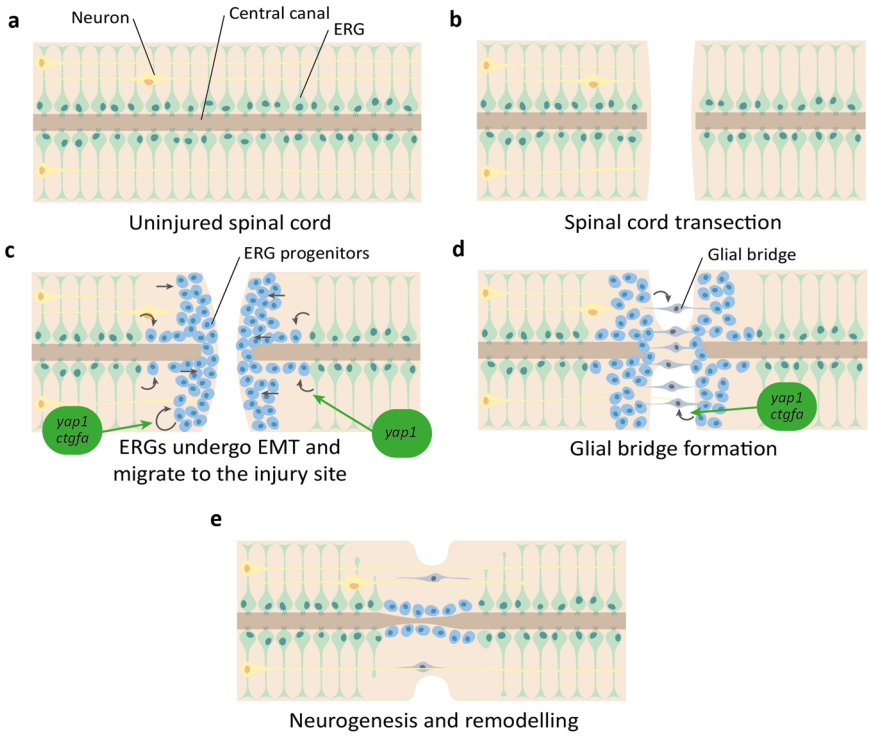

Fig. 4 Overview of zebrafish spinal cord regeneration. a Structure of the uninjured spinal cord, with ependymal radial glia (ERG) (green) lining the central canal and motor neurons (yellow). **b** Spinal cord transection disrupts neuronal processes. **c** ERGs undergo EMT to form ERG progenitors (blue) and migrate to the site of injury. *yap1* promotes EMT of ERGs, and *yap1* and *ctgfa* promote progenitor proliferation. **d** ERG progenitors extend processes across the injury site to form a glial bridge (grey). *yap1* and *ctgfa* promote the formation of the glial bridge. **e** Neuronal processes extend across the injury site, guided by the glial bridge to promote remodelling and reformation of the spinal cord.

ctgfa inhibits CM proliferation and repopulation of the injury area[121,123]. Similarly, TGFβ-mediated activation of regulatory elements upstream of *ctgfa* promotes CM proliferation at the injury site[32]. *cav-1a* and *ctgfa* are induced after injury in epicardial and endocardial cells respectively, suggesting a role for these cells in cell non-autonomous regulation of CM function, such as in ECM secretion in response to extracellular stimuli[121,123]. Disruption of *cav-1a* and *ctgfa* results in defective heart regeneration[121,123], whilst overexpression of *ctgfa* and *yap1* has the opposite effect[121,122]. Disrupting Hippo signalling in mammals gives comparable results. In pigs, CM-specific knockdown of *Sav* (which results in increased YAP activity[164,165]) increases CM proliferation and improves heart function after myocardial infarction[165]. Similar outcomes are observed when *Yap1* is disrupted in mice, causing heart regeneration defects through decreased CM proliferation[166–171], whilst heart regeneration (and CM proliferation) is stimulated after *Yap1* activation[167–169], potentially due to the Hippo pathway's link to cytoskeletal and ECM regulation[170]. However, the opposite effect is observed when Hippo signalling is disrupted in murine cardiac fibroblasts[172,173]. Deletion of *Yap1/Taz* in these fibroblasts results in improved cardiac function after myocardial infarction through modulation of the fibrotic and fibroinflammatory response[172]. Enhanced Yap1/Taz signalling (through either Yap1 overexpression or *Lats1/2* deletion) has the opposing effect, with mice displaying elevated fibrotic responses[173,172]. This apparent contradiction between the role of the Hippo pathway in CMs and cardiac fibroblasts supports a model where the Hippo pathway functions differently in different cell types.

CMs in zebrafish *ctgfa* mutants also fail to migrate along the coronary vasculature to infiltrate the wound, despite no changes in revascularisation, potentially as a result of alterations in cytoskeletal gene expression in a cell autonomous regulation of CM infiltration[121,123]. Supporting this, data using in vitro primary rat cultures of cardiac fibroblasts show that *Yap1* siRNA-mediated knockdown reduces expression of factors associated with cytoskeletal motility and ECM adhesion, although these results have not been recapitulated in zebrafish, CMs, or in vivo[122].

In summary, the Hippo signalling pathway enhances cardiac regeneration by temporal activation of Yap1/Taz and promotes normal cardiovascular development. Yap1/Taz promote appropriate scar formation and potentially prevent overactivation of the immune response, which, when combined, increase scar resolution, spatio-temporal CM proliferation, and thereby cardiac regeneration. Taking advantage of this regenerative capacity may hold therapeutic potential in the treatment of human MI. For example, pharmacological regulation of the Hippo pathway could modulate CM proliferation and fate plasticity[156,174], promoting scarless healing in the adult heart and reducing disease burden. Recent work disrupting Hippo signalling in pigs after myocardial infarction[165] suggests, in a clinically relevant model system, that this could be possible. However, precise cell type-specific modulation of the Hippo pathway will be vital to realise its full potential, as the Hippo pathway has been shown to have different functions in the cell types involved. For example, heart function is improved after injury in mammals when YAP activity is increased in CMs[165] but also when *Yap1/Taz* is deleted in cardiac fibroblasts[172].

Spinal cord regeneration

The Hippo pathway is also associated with regeneration after spinal cord injury (SCI) in the zebrafish. After SCI in humans and other mammals, the affected axons and neurons are destroyed and a non-permissive scar is formed in the place of new cells, commonly resulting in lifelong disability[175–177]. However, both adult and larval zebrafish robustly and effectively regenerate their spinal cords after injury, with viable axon regrowth over the lesion site and return of full swimming function within weeks after injury[18,19,178–182] (Fig. 4).

For functional recovery in the spinal cord, new and existing cells must proliferate, migrate to the injury site, bridge the lesion, and differentiate to reintegrate with existing distal neuronal circuitry[183]. Neurogenesis from tissue-resident progenitors is a vital step for this to occur in zebrafish, which is promoted by multiple signalling pathways, including Wnt/β-catenin, Fgf, Shh, and is inhibited by Notch signalling (Table 1). The tissue-resident progenitors responsible for cell proliferation and bridging are thought to be the ventral ependymal radial glia (ERG)[181,184–186]. These cells have general functions during development and adulthood in maintaining spinal cord homoeostasis such as sealing the blood-brain barrier and maintaining ion balance, but also proliferate and differentiate into a range of neuronal cell types after injury[181,183,187].

To allow new cell processes to traverse the lesion site, a glial bridge is formed. After injury, ERGs migrate to the lesion and elongate to form an astroglial bridge over the lesion, along which axons can grow to innervate distal targets (Fig. 4C–E). This is driven by pro-regenerative gene expression (e.g. *col12a1a/b* and *tenascin-c*), interactions with other cell types such as Schwann cells, and additional environmental cues[180,182,184,188–190]. Zebrafish glial bridging shares clear morphological and functional similarities with the bridging observed during mammalian peripheral nerve regeneration (which occurs to a much greater extent than mammalian CNS regeneration)[183,191–193], indicating that this common process may be manipulated in the human for therapeutic benefit.

In order to induce glial cells to undergo bridging, ventral ERGs undergo an epithelial-to-mesenchymal transition (EMT)[193] (Fig. 4C). EMT is a common feature of many cells activated by injury, and is linked to stem cell activation, increased cellular plasticity, and tissue remodelling[194–196]. Glial EMT is both necessary and sufficient to induce glial bridging, and is linked to Yap1-Ctgfa signalling[193,197]. *yap1*, *wwtr1* (gene encoding Taz), and *ctgfa* are upregulated following SCI, with *yap1* and *ctgfa* expression localised to bridging glia and ventral ERGs[193,197]. As well as inducing *ctgfa* expression in ventral ERGs, Yap1 promotes *twist1a* expression[193]. *twist1a* is an established EMT marker, activation of which directs a mesenchymal transition in Ctgfa^{+} ERGs, promoting glial bridging and functional spinal cord repair[193].

Similar to heart regeneration, one major difference between the zebrafish and mammalian response to SCI is the formation of a glial scar. SCI causes vascular damage, oedema, and inflammation, resulting in widespread gliosis, necrosis, and apoptosis that eventually forms a glial/fibrotic scar in mammals, stretching beyond the site of the initial trauma and acting to prevent secondary damage but also preventing axon regrowth[176,198,199]. There is no significant scarring in the zebrafish, so there is no experimental work linking the Hippo pathway in zebrafish to scar resolution, however siRNA-mediated knockdown of the YAP1/TAZ-TEAD target gene *Ctgf* in rats reduces the glial scar and hence improves regeneration after SCI[200], suggesting that YAP1/TAZ signalling may promote scar formation or impair scar resolution and outlining a potential therapeutic target for SCI treatment in mammals.

Loss of function mutations of *yap1*, *wwtr1*, and *ctgfa* all result in impaired functional recovery after SCI, with *ctgfa* and *yap1* disruption causing a glia-specific cell proliferation reduction, resulting in impaired bridging and axon regeneration across the lesion site[193,197]. Exogenous administration of human CTGF to these *ctgfa* mutants reversed this defect[197]. This finding, and the similar finding that heart scar formation is larger and more persistent in *ctgfa, yap1*, and *cav-1* mutants[121–123] appears in contrast to that seen in the rat glial scar[200], which found that knockdown of CTGF increased recovery through the clearance of scarring, and the current clinical trials which are targeting CTGF to reduce fibrosis and scarring[201]. This may be due to species differences in the function of the Hippo pathway, but this is not supported by the relatively high translatability of other studies between rodent and zebrafish. An alternative explanation might be that Yap/Taz-Ctgfa signalling has opposing effects at different stages of spinal cord regeneration, or that strictly regulated temporal activation/repression of signalling is key, although studies of this in mammals must be performed after the scar has been resolved, which currently presents an experimental challenge.

Yap1 signalling is also associated with the regenerative role of glial cells in other parts of the CNS, such as the retina. In the zebrafish, retinal damage induces reprogramming events where Müller glia are converted to a highly proliferative progenitor-like state, dividing asymmetrically to replace lost photoreceptors[202–207]. *Yap1* knockdown blocks Müller glial cell proliferation and neurogenesis after light damage of the zebrafish retina[208], suggesting a common role for *yap1* in the regenerative functions of glial cells. Mammalian retinas usually do not have a proliferative, pro-regenerative, Müller glia response to injury. However, in the mouse, YAP promotes glial reprogramming, with YAP activation inducing Müller glia reprogramming to a highly proliferative, progenitor-like cell[202,204]. This suggests that promoting Yap1 signalling therapeutically may also promote CNS regeneration in humans.

These findings propose a model in which Yap1 senses the mechanical stress caused by SCI, enhancing *ctgfa* and *twist1a* expression to activate a pro-EMT and pro-proliferative transcriptional programme in ventral ERGs, promoting glial bridging, axon regeneration, and, consequently, functional recovery[193]. This model suggests that enhancing scar resolution, promoting EMT, enhancing CTGF signalling at later stages of regeneration, and identifying CTGF-responsive spinal cord cells may allow for the identification of a therapeutic target to promote mammalian spinal cord regeneration[197]. Targeting CTGF has been investigated in a variety of preclinical and clinical trials for multiple conditions, including muscular dystrophy and pancreatic cancer. For example, the monoclonal antibody Pamrevlumab has shown promise in trials for idiopathic pulmonary fibrosis[209,210]. However, these trials involve the inhibition of CTGF activity, rather than the enhancement that may be required to promote recovery[201,211]. Consequently, further insights must be obtained before translating these findings into an effective treatment option in humans.

Tail fin regeneration

Zebrafish and other teleosts regenerate their fins completely after multiple consecutive amputations[212], a phenomenon that was studied as early as the 18th century[213], and by the regeneration pioneer T. H. Morgan at the turn of the 20th century[214–216]. Fin regeneration occurs through epimorphic regeneration, a process characterised by the presence of a blastema early in regeneration (Fig. 5). This mass of undifferentiated proliferating progenitor cells at the site of injury is formed by mature cell dedifferentiation, which can then differentiate back into mature cells to generate an actively growing tissue that replaces the lost appendage[217].

There is not yet direct evidence for a role for the Hippo pathway in dedifferentiation in the zebrafish caudal fin blastema, but in other in vivo models, both mammalian and invertebrate, the Hippo pathway maintain stemness, promote proliferation, and revert differentiated cells to a progenitor cell state[81,218–224]. In the zebrafish, dedifferentiated cells proliferate to form a large pool of progenitor cells in the blastema (Fig. 5D).

Blastema formation is enhanced and maintained by a range of developmental signalling pathways, including Hippo, Wnt/β-catenin, Igf, Notch, Fgf, Shh, Tgfβ, (Table 1) as well as inflammatory signals such as Il1β and Hsp90α[225–227]. The concentration gradient of these signalling pathways gives positional information along the proximodistal axis of the injured tissue, ensuring that structures are reformed at the correct location and that the tissue grows at an appropriate rate, halting

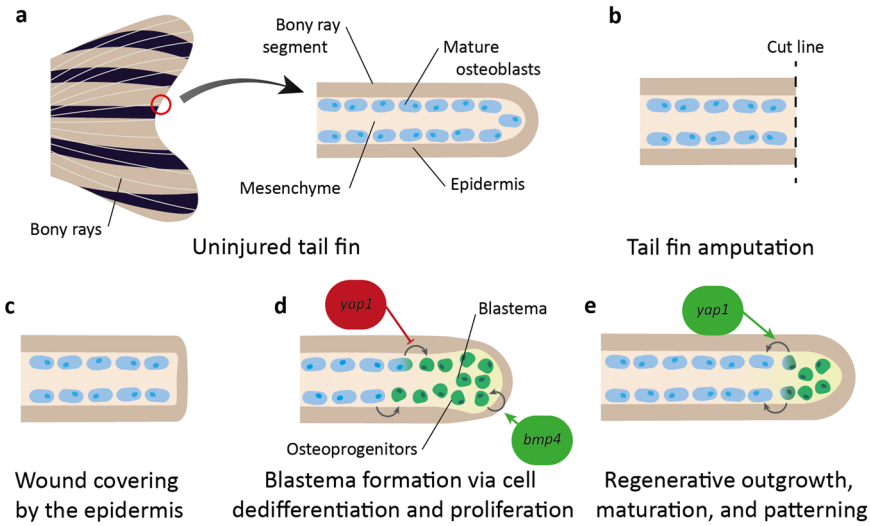

Fig. 5 Overview of zebrafish tail fin regeneration (adult), focussing on osteoblast regeneration of bony rays. a The uninjured tail fin of the adult zebrafish is formed of many bony rays, which each consist of epidermis surrounding mature osteoblasts (purple) in the mesenchyme. **b** Amputation of the tail fin disrupts the bony ray segment. **c** In the initial stages of tail fin regeneration the epidermis covers the wound. **d** Osteoblasts and other mature cells dedifferentiate and proliferate at the wound tip to form a blastema with osteoprogenitors (green). *yap1* inhibits osteoblast dedifferentiation and *bmp4* enhances blastema cell proliferation. **e** The bony ray segment extends through maturation of the progenitor cells back to their original cell type. *yap1* promotes osteoprogenitor maturation.

when the previous size and shape is reached[16,228–231]. Hippo signalling is one such signalling pathway with activity changes in proximodistal expression. In the high cell density distal blastema, Yap1 is mainly cytoplasmic (and so inactive), whilst in the low density proximal blastema, it becomes mainly nuclear (active)[232]. Yap1 is also localised to α-catenin and F-actin when in the cytoplasm[232]. This suggests that the heterogeneous cell densities within the blastema could be transduced through cell junctions and the cytoskeleton[232]. These mechanical properties then impact Yap1 localisation, which alters the regenerative capacity of the fin[232]. For example, *yap1* disruption impairs cell proliferation and alters key signalling pathways, including promoting Wnt and reducing Bmp signalling after fin injury[232,233]. This results in an accumulation of osteoprogenitors and prevention of osteoblast differentiation, and so defective regeneration[233]. Ctgfa levels are also increased following fin injury, and disruption of its regulatory sequences induces increased tissue stiffness and ECM deposition[234].

Tail fin progenitor cells are not multipotent. Instead, cells remain lineage restricted[235,236]. The osteoblast is one such cell type. After injury, these cells dedifferentiate, proliferate, and mature to only give rise to osteoblasts in the regenerate (Fig. 5)[236–238]. More specifically, injury induces differentiated mature osteoblasts close to the injury site, which usually form the bony rays of the fin, to lose expression of late and intermediate osteoblast differentiation markers (such as *osteocalcin* and *osterix*) and undergo a Wnt/β-catenin-mediated EMT to gain progenitor markers and generate osteoprogenitor cells, which migrate to the blastema and proliferate in a Fgf-dependent manner[237,239]. These progenitors then undergo Bmp-mediated maturation into osteoblasts[239] (Fig. 5D), a process that is associated with the Hippo pathway[233,239]. This link to osteoblast formation and function is most dramatically illustrated by *wwtr1* disruption in embryonic zebrafish, which results in a complete lack of skeletal ossification[149]. Similarly, disruption of *yap1* results in major bone defects and impaired fin regeneration, caused by an inhibition of osteoprogenitor cell maturation, giving an increased osteoprogenitor pool with a downregulation of intermediate and mature gene markers[233]. These defects are mediated by a reduction in Bmp signalling (which usually promotes maturation into osteoblasts[239]). In wild-type fish, Yap1 promotes Bmp signalling in a cell non-autonomous manner, restricting osteoprogenitors to the distal blastema (where Yap1 is inactive), and promotes osteoblast formation in the proximal blastema (where Yap1 is active)[233]. *bmp4* is also associated with tail fin regeneration. Bmp4 is expressed in the distal blastema, and its inhibition reduces fin outgrowth after injury due to reduced proliferation of blastema cells[240,241]. This data suggests that Yap1 functions in the blastema to mechanotransduce tension changes and control the fate and migration of specific cell types in the amputated fin, regulating the precise control of tissue growth, potentially through the expression of ECM factors such as Ctgfa[232,234].

The Hippo pathway is also associated with the differentiation of osteoblasts from mesenchymal stem cells (MSCs) during development, which generate neurons, adipocytes, skeletal muscle, and osteoblasts[242]. In vitro studies, TAZ promotes osteoblast differentiation from MSCs via activation of Runx2-dependent gene transcription whilst inhibiting adipocyte differentiation via repression of PPARγ signalling[149]. CTGF also promotes osteoblast differentiation from MSCs in vitro[243]. Similar data are observed in mice, where YAP1 and TAZ promote bone formation and repair through their regulation of the osteoblast lineage[244,245]. Osteoblast lineage-specific *Yap1* KO mice have reduced osteoblast differentiation and increased adipocyte formation, an effect that is diminished following increased β-catenin expression, demonstrating the importance of Wnt/β-catenin signalling in this process[245]. However, the role of the Hippo pathway in osteoblast differentiation is contested, with some in vitro studies suggesting that YAP1/TAZ suppress osteoblast differentiation and bone formation, and increase adipogenesis[246,247], so more work is required to elucidate this complexity.

Zebrafish tail fin regeneration is most closely associated with limb regeneration, which does not occur in mammals or other higher vertebrates, although the mouse has been found in some instances to regenerate the digit tip in both newborns and adults[248]. Appendage regeneration does occur in certain amphibians such as salamanders as well as some invertebrates, and the *Drosophila yap1* ortholog *yki* has been shown to promote wing disc regeneration[249]. Regeneration of an entire limb in mammals appears unlikely, but work in the zebrafish tail fin and other systems suggests that Hippo signalling may play an important role and promoting it could enhance regenerative capacity of specific

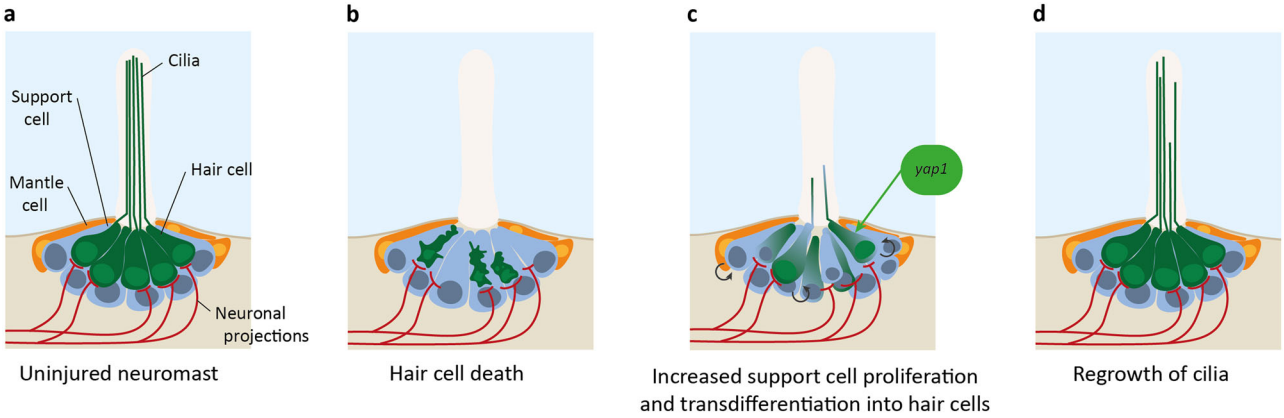

Fig. 6 Overview of neuromast regeneration. a Uninjured neuromasts consist of hair cells (green) with cilia projecting into the external liquid, support cells (blue), mantle cells (orange), and afferent sensory neurons (red) that project to the brain. **b** Administration of aminoglycosides or Cu^{2+} causes specific hair cell death. **c** Support cell proliferation increases and cells transdifferentiate into hair cells. *yap1* promotes support cell transdifferentiation. **d** Hair cell cilia regrowth restores neuromast function.

aspects of limb regeneration, such as enhanced bone regeneration after breaks.

Hair cell regeneration in the lateral line

The lateral line is a mechanosensitive organ in fish and other aquatic amphibians that detects motion of the external liquid, aiding feeding and social behaviour as well as orientation in currents. In zebrafish, this rapidly developing organ is formed of sixty small clusters of cells (termed neuromasts) in adulthood (expanded from an initial eight in larvae)[250], located along with the head (anterior lateral line) and trunk (posterior lateral line, pLL) in stereotyped positions[17]. Neuromasts consist of a group of hair cells with stereocilia projecting out of the skin and into the surrounding water, mechanical movement of which triggers sensation, and surrounding interdigitating supporting cells and mantle cells (Fig. 6A). Hair cells are innervated by ribbon synapses with afferent sensory neurons[17] that project to the hindbrain, where they exhibit a somatotopy similar to the tonotopy seen in mammalian cochlear afferent projections[251].

During early zebrafish development, a pLL primordium (pLLP) is generated behind the otic vesicle, forming a mass of cells that migrates along the flank beneath the skin, depositing proto-neuromasts at periodic intervals[252–255]. The deposition of protoneuromasts and their development into mature neuromasts is mediated by Wnt/β-catenin, Notch, and Fgf signalling pathways, and is reviewed elsewhere[17,256]. These migrating cells must maintain a cohesive structure through high levels of expression of E-cadherin and tight junctions. In mammalian epithelial cells, E-Cadherin is a key upstream regulator of YAP1/TAZ[257,258], indicating a potential role for Hippo signalling in this process. In fact, the Hippo pathway is linked to lateral line development in the zebrafish, as indicated by the induced expression of Yap1, Amotl2a, and Cav-1α in the developing lateral line[136,259–261], and how disrupting these proteins functions impact lateral line formation. Downregulation of Cav-1α reduces the number of neuromasts formed[136] and disruption of *yap1* triggers a range of phenotypes, including a reduction in primordium size, reduced number of neuromasts, and a decrease in hair cell number[259–262]. Amotl2a negatively regulates Yap1 in the developing lateral line, limiting proliferation and so restricting the size of the pLLP, coupling with Notch signalling (which upregulates Yap1 to promote proliferation) to ensure correct pLLP size is reached[259,261].

Analysis of the transcriptome of *yap1*-deficient embryos shows multiple gene expression changes, including those involved in the Wnt/β-catenin signalling pathway[260], and lysophosphatidic acid (LPA)[262]. One of these factors is Prox1a, a target of β-catenin that aids hair cell differentiation in the lateral line[260,263]. Analysis of *yap1*- and *prox1a*-deficient embryos shows that *yap1* deficiency recapitulates the *prox1a* deficiency phenotype of reduced hair cell number and impaired mechanoreceptor differentiation. These *yap1* phenotypes are rescued by the administration of *prox1a* mRNA, suggesting that Yap1 functions by promoting Prox1a activity, so regulating hair cell maturation[260]. In the lateral line, the LPA receptor Lpar2b is expressed in the pLL and neuromasts, and its loss-of-function phenocopies *yap1* KD[262]. LPA inhibits the Hippo kinase module, consequently activating YAP1/TAZ[264,265] and stimulating cell proliferation, migration, and differentiation[262,266]. In the zebrafish specifically, LPA affects early development, promoting vascular and midline development, left-right patterning, and cell migration during gastrulation, amongst others[267–270]. In the pLL Lpar2b regulates Yap1 phosphorylation, suggesting that LPA signalling controls both primordium size and neuromast number by regulating Yap1 activity[262]. These results suggest that the Hippo pathway promotes appropriate size and cell function in lateral line development through a range of signalling pathways, many of which are also associated with other developmental processes.

The high regenerative capacity of the amphibian lateral line was first observed in the salamander[271,272] but has since been observed in multiple organisms, including the zebrafish[273] (Fig. 6). This is in contrast to the limited regeneration of mammalian hair cells, e.g. of the inner ear[256]. The majority of regenerated lateral line hair cells are formed by symmetric asynchronous division of support cells in the first 20 hours post injury[254,274,275], where mitotic division of one support cell gives rise to two hair cells[276] (Fig. 6C). The molecular and cellular triggers of this regeneration include pathways involved in lateral line development—Wnt/β-catenin, Notch, and Fgf signalling—as well as novel factors such as the Jak/Stat3 pathway (Table 1), which balance self-renewal, hair cell differentiation, and the risk of overgrowth.

The Hippo pathway links to lateral line regeneration[277]. The expression pattern of supporting cells during regeneration is reminiscent of expression in the migrating primordium during lateral line development, which is silenced when leading progenitors differentiate into mature supporting cells and hair cells[259,278,279]. This includes the expression of Hippo components *cav-1* and *ctgfa*, which are upregulated in the support cells of both the zebrafish lateral line and the mouse inner ear[280]. In addition, after severe hair cell injury, Yap1 is activated in hair cell precursors, and regeneration is impaired in *yap1* mutants[277]. Yap1 activation may occur through cell junction damage and resulting loss of junction-associated proteins such as Amotl2a, which usually

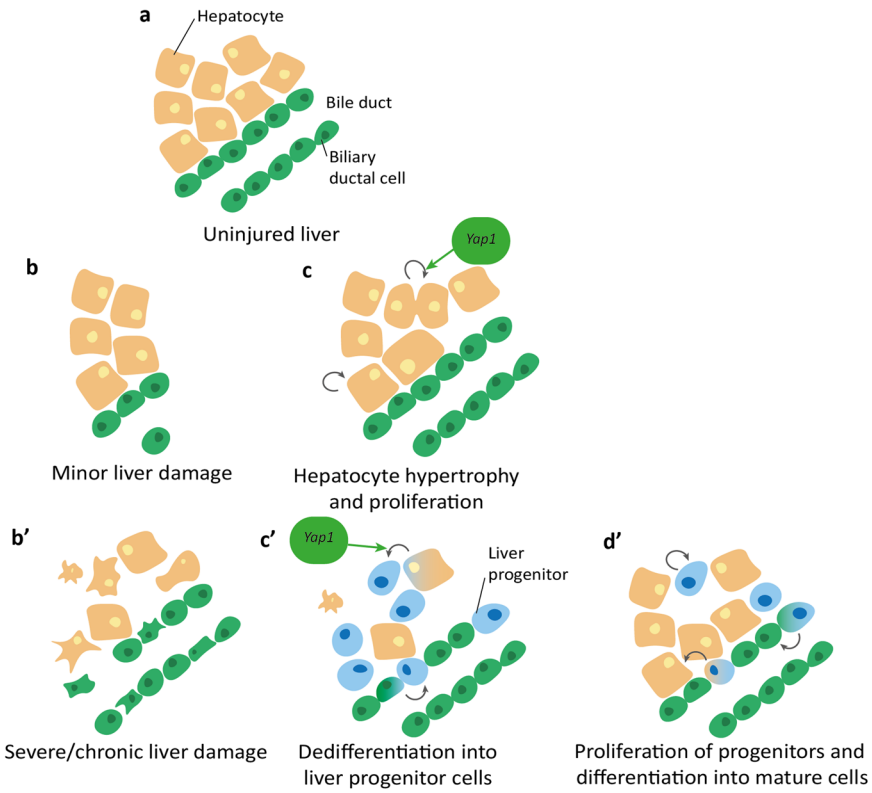

Fig. 7 Overview of liver regeneration after minor (b, c) and severe (b', c', d') injury. a Healthy (uninjured) zebrafish liver consists of multiple cell types hepatocytes (orange) and bile ducts comprising of biliary ductal cells (green). **b** Minor liver injury such as partial hepatectomy removes portions of the liver and the associated cells. **c** Liver recovery after minor liver damage involves hypertrophy and increased proliferation of remaining cells. *Yap1* promotes hepatocyte proliferation. **b'** Chronic or severe liver damage causes widespread cell death and necrosis. **c'** Remaining cells dedifferentiate into liver progenitor cells, promoted by *Yap1*. **d'** Progenitor cells proliferate then differentiate into mature hepatocytes and biliary ductal cells.

restricts Yap1 activity in the lateral line[261,277]. Activated Yap1 upregulates *lin28a* transcription, an RNA-binding protein that regulates the translation of mRNAs involved in developmental timing, pluripotency and metabolism[281]. This promotes a Yap1-lin28a-let7-Wnt signalling axis that is both necessary and sufficient to promote progenitor cell activation and hence neuromast regeneration. The Yap1-lin28a-let7-Wnt signalling axis has other roles in dedifferentiation, including zebrafish retinal regeneration, mammalian embryonic inner ear development, and in vitro reprogramming of stem cell cultures[282–285].

In summary, Yap1/Taz signalling in progenitor support cells is triggered after hair cell injury, promoting their differentiation towards hair cells via a Wnt signalling pathway, and enhancing recovery. Promoting Yap1/Taz signalling may also have therapeutic benefits in humans. The hair cells of the inner ear do not regenerate[256] but have high similarity to zebrafish lateral line hair cells. This includes similar expression patterns of mechanosensitive ion channel and tip link genes and responses to key signalling pathways and ototoxic insults[256,286–290], and so targeting the Hippo pathway to promote the regeneration of inner ear hair cells to combat age-related hearing decline may be a viable approach.

Liver regeneration

Despite limited mammalian regeneration of many organs, both mammals and zebrafish can regenerate their livers efficiently through the proliferation of differentiated hepatocytes, regaining liver function through epimorphic regrowth and compensatory enlargement of liver lobes[291,292] (Fig. 7). However, this capacity of hepatocytes to repopulate the liver in humans can be overwhelmed by chronic or severe injury, resulting in liver failure that is only treatable by liver transplantation. There are many functional, cellular, and structural similarities between mammalian and zebrafish liver, both of which can regenerate their liver after more chronic insults,[292] making the zebrafish a useful model to study the development and regeneration of the liver. However, limited research has been performed investigating the role of the Hippo pathway in zebrafish liver regeneration, although much work on this topic has been performed in the mouse. After experimental murine liver injury, YAP1 protein levels increase, with increased nuclear localisation in the liver and enhanced expression of downstream YAP1/TAZ target genes[220,293,294]. In a mouse model with *Yap* deletion in hepatocytes, bile duct ligation results in hepatic necrosis, reduced hepatocyte proliferation, and increased mortality[220,295] compared to wild-type mice, suggesting a key role for Hippo signalling in mammalian liver regeneration.

One method posited to promote liver regeneration is the recapitulation of developmental processes to generate progenitor-like cells that repopulate the liver after hepatocyte loss. Supporting this, after severe liver injury biliary cells have been shown to transdifferentiate into hepatocytes via a dedifferentiated progenitor-like state to repopulate the liver[291,292]. Hippo signalling is implicated in multiple cell fate transitions during liver regeneration in the mouse[296,297]. This includes YAP signalling activation by the alteration of cholangiocytes' epigenome and transcriptome to aid their restoration of normal hepatocyte and cholangiocyte number[296]. YAP also associates with factors such as Arid1a to promote the induction of liver progenitor-like cell-enriched genes[297].

The Hippo pathway is linked to liver development in both mammalian and zebrafish livers, and likely regulates cell fate plasticity in this process. In mice, YAP1 overexpression causes

hepatomegaly that is reversible upon cessation of YAP1 signalling, suggesting a function for YAP1 in regulation of cell proliferation and hepatocyte function[221,298]. Hepatomegaly is also observed in the zebrafish after Yap1 overexpression or *nf2a* disruption[299,300], whilst conversely *yap1*$^{-/-}$ fish have reduced liver size[147]. Other structural defects observed when disrupting upstream Hippo pathway components in the zebrafish include dilated bile ducts[299], biliary dysgenesis[301], and extrahepatic choledochal cysts[299]. Yap1 has also been linked to metabolism in the zebrafish liver, where it stimulates nucleotide biosynthesis to promote tissue growth through increasing glutamine synthetase and glucose transporter *glut1* expression[147,300,302].

The Hippo pathway's role in hepatocyte development is thought to be vital in its role in the liver as hepatocytes are the predominant cell type in the liver and are key to liver function[292]. Appropriate Hippo pathway function is essential in the maintenance of mature hepatocytes, with hepatocyte-specific *Nf2* loss in mice leading to hepatocyte dedifferentiation into highly renewable progenitors[303], and overexpression causing a dysplastic hepatocyte morphology[221]. YAP1 is also associated with the formation of bile ducts in the developing mouse[304], and with the function of the bile ducts (which promote immune cell recruitment and function) in the regenerating adult mouse liver[305]. Similarly, *stk3* and *sav1* zebrafish mutants (which both result in increased Yap1 activity) display altered hepatocyte morphology and polarity alongside biliary cell disruption[301]. Overall, these data suggest a conserved role for the Hippo pathway in structural liver, hepatocyte and biliary cell function between mammals and zebrafish. This implies that the Hippo pathway may also have a role in zebrafish liver regeneration, although this research is still in its infancy and will need further detailed investigation before conclusions can be drawn.

CONCLUSION

The zebrafish is a powerful model system for the study of regeneration due to their rapid external development, relative low cost, transparent juvenile stages and robust reparative regeneration as well as the availability of a range of established genetic tools and other experimental procedures to study these. In this review, the role of the Hippo pathway in zebrafish regeneration is summarised, with the finding that Yap1/Taz signalling often enhances regeneration through the promotion of cell proliferation, progenitor cell dedifferentiation and maturation, EMT, and scar resolution, as well as linking to key developmental pathways. The phenotypes resulting from the disruption of Hippo pathway components is summarised in Table 2.

The positive effect of Yap1/Taz signalling on regeneration in the zebrafish, which appears to be latent in mammals, suggests some therapeutic potential in promoting YAP/TAZ signalling to enhance mammalian regeneration. However, this must be carefully investigated, as many of the processes associated with enhanced regeneration are linked to an increased risk of cancer, such as an elevated cell proliferation rate, cellular heterogeneity, and increased stemness[306]. In fact, dysregulation of the Hippo pathway and thereby pathological hyperactivation of YAP1/TAZ promotes carcinogenesis in most, if not all, types of solid tumours[102,307,308]. The zebrafish may therefore be vital in the elucidation of this association between cancer and regeneration, which could allow us to manipulate regenerative potential without impacting carcinogenesis or vice versa. One way to do this could be through the utilisation of zebrafish Hippo pathway-induced cancer models, which recapitulate human findings in that manipulation of Hippo signalling can trigger tumour formation[309–311]. However, the field of Hippo signalling in the zebrafish is still relatively new, and so much work must be performed to bridge the gaps that are currently preventing its translation to the clinic, particularly the study of the molecular and cellular drivers of the Hippo pathway's effects on both regeneration and development (Box 1).

Box 1: Outstanding questions

1. What are the interactions and feedback between Hippo signalling and the immune system in regeneration that result in the current contradictory observations described? Does the Hippo pathway function differently in distinct immune processes, or are these apparent contradictions simply due to differences in experimental design?
2. Enhanced Yap1/Taz signalling is linked to increased risk of tumorigenesis. Is there a way to activate Yap1/Taz signalling spatiotemporally and precisely in specific cell types to promote regeneration without increasing cancer risk?
3. Can these findings be translated to humans? If so, can they be manipulated for therapeutic purposes, such as triggering regeneration in non-regenerating organs (e.g. heart and CNS) or promoting regeneration after chronic injury (e.g. liver)?
4. Zebrafish are an attractive model to study Hippo pathway dynamics in vivo, as it is amenable to live imaging with genetically encoded biosensors and tagged proteins. What are the dynamics of the Hippo pathway components in different cell types in vivo during development and regeneration in vertebrae?

Received: 7 July 2021; Accepted: 14 December 2021;
Published online: 27 January 2022

REFERENCES

1. Wittlieb, J., Khalturin, K., Lohmann, J. U., Anton-Erxleben, F. & Bosch, T. C. G. Transgenic Hydra allow in vivo tracking of individual stem cells during morphogenesis. *Proc. Natl. Acad. Sci. USA* **103**, 6208–6211 (2006).
2. van Wolfswinkel, J. C., Wagner, D. E. & Reddien, P. W. Single-cell analysis reveals functionally distinct classes within the planarian stem cell compartment. *Cell Stem Cell* **15**, 326–339 (2014).
3. Ivankovic, M. et al. Model systems for regeneration: planarians. *Development* **146**, dev167684 (2019).
4. Vogg, M. C., Galliot, B. & Tsiairis, C. D. Model systems for regeneration: Hydra. *Development* **146**, dev177212 (2019).
5. Zhao, A., Qin, H. & Fu, X. What determines the regenerative capacity in animals? *Bioscience* **66**, 735–746 (2016).
6. Poss, K. D., Keating, M. T. & Nechiporuk, A. Tales of regeneration in zebrafish. *Dev. Dyn.* **226**, 202–210 (2003).
7. Mao, S. A., Glorioso, J. M. & Nyberg, S. L. Liver regeneration. *Transl. Res.* **163**, 352–362 (2014).
8. Plikus, M. V. et al. Epithelial stem cells and implications for wound repair. *Semin. Cell Dev. Biol.* **23**, 946–953 (2012).
9. Hong, A. W., Meng, Z. & Guan, K.-L. The Hippo pathway in intestinal regeneration and disease. *Nat. Rev. Gastroenterol. Hepatol.* **13**, 324–337 (2016).
10. Scheib, J. & Höke, A. Advances in peripheral nerve regeneration. *Nat. Rev. Neurol.* **9**, 668–676 (2013).
11. Flach, J. & Milyavsky, M. Replication stress in hematopoietic stem cells in mouse and man. *Mutat. Res. - Fundam. Mol. Mech. Mutagen.* **808**, 74–82 (2018).
12. Larson, B. J., Longaker, M. T. & Lorenz, H. P. Scarless fetal wound healing: a basic science review. *Plast. Reconstr. Surg.* **126**, 1172–1180 (2010).
13. Sousounis, K., Baddour, J. A. & Tsonis, P. A. Aging and regeneration in vertebrates. *Curr. Top. Dev. Biol.* **108**, 217–246 (2014).
14. Yun, M. H. Changes in regenerative capacity through lifespan. *Int. J. Mol. Sci.* **16**, 25392–25432 (2015).
15. Smith, K. A. & Mommersteeg, M. T. M. Talkin' 'bout regeneration: new advances in cardiac regeneration using the zebrafish. *Curr. Opin. Physiol.* **14**, 48–55 (2020).
16. Sehring, I. M. & Weidinger, G. Recent advancements in understanding fin regeneration in zebrafish. Wiley Interdiscip. *Rev. Dev. Biol.* **9**, e367 (2020).
17. Thomas, E. D., Cruz, I. A., Hailey, D. W. & Raible, D. W. There and back again: development and regeneration of the zebrafish lateral line system. *Wiley Interdiscip. Rev. Dev. Biol.* **4**, 1–16 (2015).
18. Cigliola, V., Becker, C. J. & Poss, K. D. Building bridges, not walls: spinal cord regeneration in zebrafish. *Dis. Model. Mech.* **13**, dmm044131 (2020).
19. Gemberling, M., Bailey, T. J., Hyde, D. R. & Poss, K. D. The zebrafish as a model for complex tissue regeneration. *Trends Genet.* **29**, 611 (2013).
20. Marques, I. J., Lupi, E. & Mercader, N. Model systems for regeneration: zebrafish. *Development* **146**, dev167692 (2019).

21. Streisinger, G., Singer, F., Walker, C., Knauber, D. & Dower, N. Segregation analyses and gene-centromere distances in zebrafish. *Genetics* **112**, 311–319 (1986).
22. Streisinger, G., Walker, C., Dower, N., Knauber, D. & Singer, F. Production of clones of homozygous diploid zebra fish (Brachydanio rerio). *Nature* **291**, 293–296 (1981).
23. Jopling, C., Boue, S. & Belmonte, J. C. I. Dedifferentiation, transdifferentiation and reprogramming: three routes to regeneration. *Nat. Rev. Mol. Cell Biol.* **12**, 79–89 (2011).
24. Powell, C., Grant, A. R., Cornblath, E. & Goldman, D. Analysis of DNA methylation reveals a partial reprogramming of the Müller glia genome during retina regeneration. *Proc. Natl. Acad. Sci. USA* **110**, 19814–19819 (2013).
25. Hirose, K., Shimoda, N. & Kikuchi, Y. Transient reduction of 5-methylcytosine and 5-hydroxymethylcytosine is associated with active DNA demethylation during regeneration of zebrafish fin. *Epigenetics* **8**, 899–906 (2013).
26. Stewart, S., Tsun, Z.-Y. & Belmonte, J. C. I. A histone demethylase is necessary for regeneration in zebrafish. *Proc. Natl. Acad. Sci. USA* **106**, 19889–19894 (2009).
27. Pfefferli, C., Müller, F., Jazwinska, A. & Wicky, C. Specific NuRD components are required for fin regeneration in zebrafish. *BMC Biol.* **12**, 30 (2014).
28. Goldman, J. A. et al. Resolving heart regeneration by replacement histone profiling. *Dev. Cell* **40**, 392–404 (2017).
29. Golenberg, N. et al. Citrullination regulates wound responses and tissue regeneration in zebrafish. *J. Cell Biol.* **219**, e201908164 (2020).
30. Wang, W. et al. Changes in regeneration-responsive enhancers shape regenerative capacities in vertebrates. *Science* **309**, eaaz3090 (2020).
31. Kang, J. et al. Modulation of tissue repair by regeneration enhancer elements. *Nature* **532**, 201–206 (2016).
32. Pfefferli, C. & Jazwinska, A. The careg element reveals a common regulation of regeneration in the zebrafish myocardium and fin. *Nat. Commun.* **8**, 15151 (2017).
33. Thompson, J. D. et al. Identification and requirements of enhancers that direct gene expression during zebrafish fin regeneration. *Development* **147**, dev191262 (2020).
34. Wu, C.-C. et al. Spatially Resolved Genome-wide Transcriptional Profiling Identifies BMP Signaling as Essential Regulator of Zebrafish Cardiomyocyte Regeneration. *Dev. Cell* **36**, 36–49 (2016).
35. Quint, E. et al. Bone patterning is altered in the regenerating zebrafish caudal fin after ectopic expression of sonic hedgehog and bmp2b or exposure to cyclopamine. *Proc. Natl Acad. Sci.* **99**, 8713–8718 (2002).
36. Schebesta, M., Lien, C.-L., Engel, F. B. & Keating, M. T. Transcriptional Profiling of Caudal Fin Regeneration in Zebrafish. *ScientificWorldJournal* **6**, 38–54 (2006).
37. Kujawski, S. et al. Calcineurin Regulates Coordinated Outgrowth of Zebrafish Regenerating Fins. *Dev. Cell* **28**, 573–587 (2014).
38. Goldshmit, Y. et al. Different Fgfs have distinct roles in regulating neurogenesis after spinal cord injury in zebrafish. Neural Dev. 13, (2018).
39. Poss, K. D. et al. Roles for Fgf Signaling during Zebrafish Fin Regeneration. *Dev. Biol.* **222**, 347–358 (2000).
40. Whitehead, G. G., Makino, S., Lien, C.-L. & Keating, M. T. fgf20 is essential for initiating zebrafish fin regeneration. *Sci. (80-.).* **310**, 1957–1960 (2005).
41. König, D., Page, L., Chassot, B. & Jazwinska, A. Dynamics of actinotrichia regeneration in the adult zebrafish fin. *Dev. Biol.* **433**, 416–432 (2018).
42. Lee, S. G. et al. Myc and Fgf Are Required for Zebrafish Neuromast Hair Cell Regeneration. *PLoS One* **11**, e0157768 (2016).
43. Choi, W.-Y. et al. In vivo monitoring of cardiomyocyte proliferation to identify chemical modifiers of heart regeneration. *Development* **140**, 660–666 (2013).
44. Chablais, F. & Jazwinska, A. IGF signaling between blastema and wound epidermis is required for fin regeneration. *Development* **137**, 871–879 (2010).
45. Fang, Y. et al. Translational profiling of cardiomyocytes identifies an early Jak1/Stat3 injury response required for zebrafish heart regeneration. *Proc. Natl Acad. Sci.* **110**, 13416–13421 (2013).
46. Liang, J. et al. The stat3/socs3a Pathway Is a Key Regulator of Hair Cell Regeneration in Zebrafish stat3/socs3a Pathway: Regulator of Hair Cell Regeneration. *J. Neurosci.* **32**, 10662–10673 (2012).
47. Khaliq, M. et al. Stat3 Regulates Liver Progenitor Cell-Driven Liver Regeneration in Zebrafish. *Gene Expr.* **18**, 157–170 (2018).
48. Karra, R., Knecht, A. K., Kikuchi, K. & Poss, K. D. Myocardial NF-κB activation is essential for zebrafish heart regeneration. *Proc. Natl Acad. Sci.* **112**, 13255–13260 (2015).
49. Zhao, L. et al. Notch signaling regulates cardiomyocyte proliferation during zebrafish heart regeneration. *Proc. Natl Acad. Sci.* **111**, 1403–1408 (2014).
50. Dias, T. B., Yang, Y.-J., Ogai, K., Becker, T. & Becker, C. G. Notch Signaling Controls Generation of Motor Neurons in the Lesioned Spinal Cord of Adult Zebrafish. *J. Neurosci.* **32**, 3245–3252 (2012).
51. Grotek, B., Wehner, D. & Weidinger, G. Notch signaling coordinates cellular proliferation with differentiation during zebrafish fin regeneration. *Development* **140**, 1412–1423 (2013).
52. Münch, J., González-Rajal, A. & de la Pompa, J. L. Notch regulates blastema proliferation and prevents differentiation during adult zebrafish fin regeneration. *Development* **140**, 1402–1411 (2013).
53. Romero-Carvajal, A. et al. Regeneration of Sensory Hair Cells Requires Localized Interactions between the Notch and Wnt Pathways. *Dev. Cell* **34**, 267–282 (2015).
54. Pinto-Teixeira, F. et al. Inexhaustible hair-cell regeneration in young and aged zebrafish. *Biol. Open* **4**, 903–909 (2015).
55. Huang, M. et al. Antagonistic Interaction Between Wnt and Notch Activity Modulates the Regenerative Capacity of a Zebrafish Fibrotic Liver Model. *Hepatology* **60**, 1753–1766 (2014).
56. He, J., Lu, H., Zou, Q. & Luo, L. Regeneration of Liver After Extreme Hepatocyte Loss Occurs Mainly via Biliary Transdifferentiation in Zebrafish. *Gastroenterology* **146**, 789–800 (2014).
57. Ko, S. et al. Hdac1 Regulates Differentiation of Bipotent Liver Progenitor Cells During Regeneration via Sox9b and Cdk8. *Gastroenterology* **156**, 187–202 (2019).
58. Gemberling, M., Karra, R., Dickson, A. L. & Poss, K. D. Nrg1 is an injury-induced cardiomyocyte mitogen for the endogenous heart regeneration program in zebrafish. *Elife* **4**, e05871 (2015).
59. Mathew, L. K. et al. Comparative expression profiling reveals an essential role for Raldh2 in epimorphic regeneration. *J. Biol. Chem.* **284**, 33642–33653 (2009).
60. Kikuchi, K. et al. Retinoic Acid Production by Endocardium and Epicardium Is an Injury Response Essential for Zebrafish Heart Regeneration. *Dev. Cell* **20**, 397–404 (2011).
61. Blum, N. & Begemann, G. Retinoic acid signaling controls the formation, proliferation and survival of the blastema during adult zebrafish fin regeneration. *Development* **139**, 107–116 (2012).
62. Blum, N. & Begemann, G. Osteoblast de- and redifferentiation are controlled by a dynamic response to retinoic acid during zebrafish fin regeneration. *Development* **142**, 2894–2918 (2015).
63. Blum, N. & Begemann, G. Retinoic acid signaling spatially restricts osteoblasts and controls ray-interray organization during zebrafish fin regeneration. *Development* **142**, 2888–2893 (2015).
64. Han, P. et al. Hydrogen peroxide primes heart regeneration with a derepression mechanism. *Cell Res.* **24**, 1091–1107 (2014).
65. Gauron, C. et al. Sustained production of ROS triggers compensatory proliferation and is required for regeneration to proceed. Sci. Rep. 3, (2013).
66. Reimer, M. M. et al. Sonic hedgehog is a polarized signal for motor neuron regeneration in adult zebrafish. *J. Neurosci.* **29**, 15073–15082 (2009).
67. Reimer, M. M. et al. Dopamine from the Brain Promotes Spinal Motor Neuron Generation during Development and Adult Regeneration. *Dev. Cell* **25**, 478–491 (2013).
68. Jazwinska, A., Badakov, R. & Keating, M. T. Activin-βA Signaling Is Required for Zebrafish Fin Regeneration. *Curr. Biol.* **17**, 1390–1395 (2007).
69. Chablais, F. & Jazwinska, A. The regenerative capacity of the zebrafish heart is dependent on TGFβ signaling. *Development* **139**, 1921–1930 (2012).
70. Dogra, D. et al. Opposite effects of Activin type 2 receptor ligands on cardiomyocyte proliferation during development and repair. Nat. Commun. 8, (2017).
71. Kawakami, Y. et al. Wnt/β-catenin signaling regulates vertebrate limb regeneration. *Genes Dev.* **20**, 3232–3237 (2006).
72. Stoick-Cooper, C. L. et al. Distinct Wnt signaling pathways have opposing roles in appendage regeneration. *Development* **134**, 479–489 (2007).
73. Wehner, D. et al. Wnt/β-catenin Signaling Defines Organizing Centers that Orchestrate Growth and Differentiation of the Regenerating Zebrafish Caudal Fin. *Cell Rep.* **6**, 467–481 (2014).
74. Head, J. R., Gacioch, L., Pennisi, M. & Meyers, J. R. Activation of Canonical Wnt/Beta-Catenin Signaling Stimulates Proliferation in Neuromasts in the Zebrafish Posterior Lateral Line. *Dev. Dyn.* **242**, 832–846 (2013).
75. Poulain, M. & Ober, E. A. Interplay between Wnt2 and Wnt2bb controls multiple steps of early foregutderived organ development. *Development* **138**, 3557–3568 (2011).
76. Goessling, W. et al. APC mutant zebrafish uncover a changing temporal requirement for wnt signaling in liver development. *Dev. Comp. Immunol.* **320**, 161–174 (2008).
77. Choi, T.-Y., Ninov, N., Stainier, D. Y. R. & Shin, D. Extensive Conversion of Hepatic Biliary Epithelial Cells to Hepatocytes After Near Total Loss of Hepatocytes in Zebrafish. *Gastroenterology* **146**, 776–788 (2014).
78. Moya, I. M. & Halder, G. Hippo–YAP/TAZ signalling in organ regeneration and regenerative medicine. *Nat. Rev. Mol. Cell Biol.* **20**, 211–226 (2019).
79. Panciera, T., Azzolin, L., Cordenonsi, M. & Piccolo, S. Mechanobiology of YAP and TAZ in physiology and disease. *Nat. Publ. Gr.* **18**, 758–770 (2017).
80. Fu, V., Plouffe, S. W. & Guan, K.-L. The Hippo pathway in organ development, homeostasis, and regeneration. *Curr. Opin. Cell Biol.* **49**, 99–107 (2017).

81. Zhao, B., Tumaneng, K. & Guan, K.-L. The Hippo pathway in organ size control, tissue regeneration and stem cell self-renewal. *Nat. Cell Biol.* **13**, 877–883 (2011).
82. Ardestani, A., Lupse, B. & Maedler, K. Hippo signaling: key emerging pathway in cellular and whole-body metabolism. *Trends Endocrinol. Metab.* **29**, 492–509 (2018).
83. Kim, W. & Jho, E. The history and regulatory mechanism of the Hippo pathway. *BMB Rep.* **51**, 106–118 (2018).
84. Davis, J. R. & Tapon, N. Hippo signalling during development. *Development* **146**, dev167106 (2019).
85. Dupont, S. et al. Role of YAP/TAZ in mechanotransduction. *Nature* **474**, 179–185 (2011).
86. Zhao, B. et al. Inactivation of YAP oncoprotein by the Hippo pathway is involved in cell contact inhibition and tissue growth control. *Genes Dev.* **21**, 2747–2761 (2007).
87. Gram Hansen, C., Moroishi, T. & Guan, K.-L. YAP and TAZ: a nexus for Hippo signaling and beyond. *Trends Cell Biol.* **25**, 499–513 (2015).
88. Meng, Z., Moroishi, T. & Guan, K.-L. Mechanisms of Hippo pathway regulation. Genes Dev. **30**, 1–17 (2016).
89. Fulford, A., Tapon, N. & Ribeiro, P. S. Upstairs, downstairs: spatial regulation of Hippo signalling. *Curr. Opin. Cell Biol.* **51**, 22–32 (2017).
90. Rausch, V. & Gram Hansen, C. The Hippo pathway, YAP/TAZ, and the plasma membrane. *Trends Cell Biol.* **30**, 32–48 (2020).
91. Meng, Z. et al. MAP4K family kinases act in parallel to MST1/2 to activate LATS1/2 in the Hippo pathway. *Nat. Commun.* **6**, 8357 (2015).
92. Zheng, Y. et al. Identification of happyhour/MAP4K as alternative Hpo/Mst-like kinases in the Hippo kinase cascade. *Dev. Cell* **34**, 642–655 (2015).
93. Lim, S. et al. Identification of the kinase STK25 as an upstream activator of LATS signaling. *Nat. Commun.* **10**, 1547 (2019).
94. Zhao, B., Li, L., Tumaneng, K., Wang, C.-Y. & Guan, K.-L. A coordinated phosphorylation by Lats and CK1 regulates YAP stability through SCF^β-TRCP. *Genes Dev.* **22**, 72–85 (2010).
95. Lei, Q.-Y. et al. TAZ Promotes cell proliferation and epithelial-mesenchymal transition and is inhibited by the Hippo pathway. *Mol. Cell. Biol.* **28**, 2426–2436 (2008).
96. Liu, C.-Y. et al. The Hippo tumor pathway promotes TAZ degradation by phosphorylating a phosphodegron and recruiting the SCF^β-TRCP E3 ligase. *J. Biol. Chem.* **285**, 37159–37169 (2010).
97. Wang, S. et al. YAP antagonizes innate antiviral immunity and is targeted for lysosomal degradation through IKKε-mediated phosphorylation. *Nat. Immunol.* **18**, 733–743 (2017).
98. Zhang, H. et al. TEAD transcription factors mediate the function of TAZ in cell growth and epithelial-mesenchymal transition. *J. Biol. Chem.* **284**, 13355–13362 (2009).
99. Ota, M. & Sasaki, H. Mammalian Tead proteins regulate cell proliferation and contact inhibition as transcriptional mediators of Hippo signaling. *Development* **135**, 4059–4069 (2008).
100. Zhao, B. et al. TEAD mediates YAP-dependent gene induction and growth control. *Genes Dev.* **22**, 1962–1971 (2008).
101. Hillmer, R. E. & Link, B. A. The roles of Hippo signaling transducers Yap and Taz in chromatin remodeling. *Cells* **8**, 502 (2019).
102. Salem, O. & Gram Hansen, C. The Hippo pathway in prostate cancer. *Cells* **8**, 370 (2019).
103. Yu, F.-X., Zhao, B. & Guan, K.-L. Hippo pathway in organ size control, tissue homeostasis, and cancer. *Cell* **163**, 811–828 (2015).
104. Rausch, V. et al. The Hippo pathway regulates caveolae expression and mediates flow response via caveolae. *Curr. Biol.* **29**, 1–14 (2019).
105. Riching, A. S. & Song, K. Cardiac regeneration: new insights into the frontier of ischemic heart failure therapy. *Front. Bioeng. Biotechnol.* **8**, 637538 (2021).
106. St. John Sutton, M. G. & Sharpe, N. Left ventricular remodeling after myocardial infarction: pathophysiology and therapy. *Circulation* **101**, 2981–2988 (2000).
107. Engel, F. B., Hsieh, P. C. H., Lee, R. T. & Keating, M. T. FGF1/p38 MAP kinase inhibitor therapy induces cardiomyocyte mitosis, reduces scarring, and rescues function after myocardial infarction. *Proc. Natl. Acad. Sci. USA* **103**, 15546–15551 (2006).
108. Porrello, E. R. et al. Transient regenerative potential of the neonatal mouse heart. *Science* **331**, 1078–1080 (2011).
109. Li, F., Wang, X., Capasso, J. M. & Gerdes, A. M. Rapid transition of cardiac myocytes from hyperplasia to hypertrophy during postnatal development. *J. Mol. Cell. Cardiol.* **28**, 1737–1746 (1996).
110. Bise, T., Sallin, P., Pfefferli, C. & Jazwinska, A. Multiple cryoinjuries modulate the efficiency of zebrafish heart regeneration. *Sci. Rep.* **10**, 11551 (2020).
111. Sehring, I. M., Jahn, C. & Weidinger, G. Zebrafish fin and heart: what's special about regeneration? *Curr. Opin. Genet. Dev.* **40**, 48–56 (2016).
112. Wang, J. et al. The regenerative capacity of zebrafish reverses cardiac failure caused by genetic cardiomyocyte depletion. *Development* **138**, 3421–3430 (2011).
113. Poss, K. D., Wilson, L. G. & Keating, M. T. Heart regeneration in zebrafish. *Science* **298**, 2188–2190 (2002).
114. Senyo, S. E. et al. Mammalian heart renewal by pre-existing cardiomyocytes. *Nature* **493**, 433–436 (2013).
115. Bergmann, O. et al. Dynamics of cell generation and turnover in the human heart. *Cell* **161**, 1566–1575 (2015).
116. Foglia, M. J. & Poss, K. D. Building and re-building the heart by cardiomyocyte proliferation. *Development* **143**, 729–740 (2016).
117. Bassat, E. et al. The extracellular matrix protein agrin promotes heart regeneration in mice. *Nature* **547**, 179–184 (2017).
118. González-Rosa, J. M., Martín, V., Peralta, M., Torres, M. & Mercader, N. Extensive scar formation and regression during heart regeneration after cryoinjury in zebrafish. *Development* **138**, 1663–1674 (2011).
119. Wang, J., Karra, R., Dickson, A. L. & Poss, K. D. Fibronectin is deposited by injury-activated epicardial cells and is necessary for zebrafish heart regeneration. *Dev. Biol.* **382**, 427–435 (2013).
120. Lowe, V. et al. Neuropilin 1 mediates epicardial activation and revascularization in the regenerating zebrafish heart. *Development* **146**, dev174482 (2019).
121. Mukherjee, D. et al. Ccn2a is an injury-induced matricellular factor that promotes cardiac regeneration in zebrafish. *Development* **148**, dev193219 (2021).
122. Flinn, M. A., Jeffery, B. E., O'Meara, C. C. & Link, B. A. Yap is required for scar formation but not myocyte proliferation during heart regeneration in zebrafish. *Cardiovasc. Res.* **115**, 570–577 (2019).
123. Cao, J. et al. Single epicardial cell transcriptome sequencing identifies caveolin 1 as an essential factor in zebrafish heart regeneration. *Development* **143**, 232–243 (2016).
124. Lai, S.-L. et al. Reciprocal analyses in zebrafish and medaka reveal that harnessing the immune response promotes cardiac regeneration. *Elife* **6**, e25605 (2017).
125. Furutani-Seiki, M. & Wittbrodt, J. Medaka and zebrafish, an evolutionary twin study. *Mech. Dev.* **121**, 629–637 (2004).
126. Huang, W.-C. et al. Treatment of Glucocorticoids inhibited early immune responses and impaired cardiac repair in adult zebrafish. *PLoS One* **8**, e66613 (2013).
127. de Preux Charles, A.-S., Bise, T., Baier, F., Marro, J. & Jazwinska, A. Distinct effects of inflammation on preconditioning and regeneration of the adult zebrafish heart. *Open Biol.* **6**, 160102 (2016).
128. Godwin, J. W., Pinto, A. R. & Rosenthal, N. A. Chasing the recipe for a pro-regenerative immune system. *Semin. Cell Dev. Biol.* **61**, 71–79 (2017).
129. Hui, S. P. et al. Zebrafish regulatory T cells mediate organ-specific regenerative programs. *Dev. Cell* **43**, 659–672 (2017). e5.
130. Stewart, K. M. R., Walker, S. L., Baker, A. H., Riley, P. R. & Brittan, M. Hooked on heart regeneration: the zebrafish guide to recovery. *Cardiovasc. Res.* https://doi.org/10.1093/cvr/cvab214 (2021).
131. González-Rosa, J. M., Peralta, M. & Mercader, N. Pan-epicardial lineage tracing reveals that epicardium derived cells give rise to myofibroblasts and perivascular cells during zebrafish heart regeneration. *Dev. Biol.* **370**, 173–186 (2012).
132. Singh, A. et al. Hippo signaling mediators Yap and Taz are required in the epicardium for coronary vasculature development. *Cell Rep.* **15**, 1384–1393 (2016).
133. Miesfeld, J. B. et al. Yap and Taz regulate retinal pigment epithelial cell fate. *Development* **142**, 3021–3032 (2015).
134. Hildebrand, S. et al. The E-cadherin/AmotL2 complex organizes actin filaments required for epithelial hexagonal packing and blastocyst hatching. *Sci. Rep.* **7**, 9540 (2017).
135. Hultin, S. et al. Amotl2 links VE-cadherin to contractile actin fibres necessary for aortic lumen expansion. *Nat. Commun.* **5**, 3743 (2014).
136. Nixon, S. J. et al. Caveolin-1 is required for lateral line neuromast and notochord development. *J. Cell Sci.* **120**, 2151–2161 (2007).
137. Flinn, M. A. et al. Llgl1 regulates zebrafish cardiac development by mediating Yap stability in cardiomyocytes. *Development* **147**, dev193581 (2020).
138. Fang, P.-K. et al. Caveolin-1α and -1β perform nonredundant roles in early vertebrate development. *Am. J. Pathol.* **169**, 2209–2222 (2006).
139. Dai, X. et al. Phosphorylation of angiomotin by Lats1/2 kinases inhibits F-actin binding, cell migration, and angiogenesis. *J. Biol. Chem.* **288**, 34041–34051 (2013).
140. Nagasawa-Masuda, A. & Terai, K. Yap/Taz transcriptional activity is essential for vascular regression via Ctgf expression and actin polymerization. *PLoS One* **12**, e0174633 (2017).
141. Nakajima, H. et al. Flow-dependent endothelial YAP regulation contributes to vessel maintenance. *Dev. Cell* **40**, 523–536 (2017). e6.
142. Astone, M. et al. Zebrafish mutants and TEAD reporters reveal essential functions for Yap and Taz in posterior cardinal vein development. *Sci. Rep.* **8**, 1–15 (2018).
143. Grimm, L. et al. Yap1 promotes sprouting and proliferation of lymphatic progenitors downstream of Vegfc in the zebrafish trunk. *Elife* **8**, e42881 (2019).

144. Xu, D. et al. Scribble influences cyst formation in autosomal-dominant polycystic kidney disease by regulating Hippo signaling pathway. *FASEB J.* **32**, 4394–4407 (2018).
145. Park, M.-H. et al. CCN1 interlinks integrin and hippo pathway to autoregulate tip cell activity. *Elife* **8**, e46012 (2019).
146. Dooley, C. M. et al. The gene regulatory basis of genetic compensation during neural crest induction. *PLOS Genet.* **15**, e1008213 (2019).
147. Cox, A. G. et al. Yap regulates glucose utilization and sustains nucleotide synthesis to enable organ growth. *EMBO J.* **37**, e100294 (2018).
148. Pappalardo, A. et al. Thyroid development in zebrafish lacking Taz. *Mech. Dev.* **138**, 268–278 (2015).
149. Hong, J.-H. et al. TAZ, a transcriptional modulator of mesenchymal stem cell differentiation. *Sci. (80-.)* **309**, 1074–1078 (2005).
150. Yi, X. et al. The effector of Hippo signaling, Taz, is required for formation of the micropyle and fertilization in zebrafish. *PLoS Genet.* **15**, e1007408 (2019).
151. Lo, H. P. et al. The caveolin–cavin system plays a conserved and critical role in mechanoprotection of skeletal muscle. *J. Cell Biol.* **210**, 833–849 (2015).
152. Kim, M., Kim, M., Lee, M.-S., Kim, C.-H. & Lim, D.-S. The MST1/2-SAV1 complex of the Hippo pathway promotes ciliogenesis. *Nat. Commun.* **5**, 1–14 (2014).
153. Jopling, C. et al. Zebrafish heart regeneration occurs by cardiomyocyte dedifferentiation and proliferation. *Nature* **464**, 606–609 (2010).
154. Kikuchi, K. et al. Primary contribution to zebrafish heart regeneration by gata4+ cardiomyocytes. *Nature* **464**, 601–605 (2010).
155. Gupta, V. et al. An injury-responsive gata4 program shapes the zebrafish cardiac ventricle. *Curr. Biol.* **23**, 1221–1227 (2013).
156. Zhang, R. et al. In vivo cardiac reprogramming contributes to zebrafish heart regeneration. *Nature* **498**, 497–502 (2013).
157. Harrison, M. R. M. et al. Chemokine-guided angiogenesis directs coronary vasculature formation in zebrafish. *Dev. Cell* **33**, 442–454 (2015).
158. Kikuchi, K. et al. tcf21+ epicardial cells adopt non-myocardial fates during zebrafish heart development and regeneration. *Development* **138**, 2895–2902 (2011).
159. Kim, J. et al. PDGF signaling is required for epicardial function and blood vessel formation in regenerating zebrafish hearts. *Proc. Natl Acad. Sci. USA* **107**, 17206–17210 (2010).
160. Marín-Juez, R. et al. Coronary revascularization during heart regeneration is regulated by epicardial and endocardial cues and forms a scaffold for cardiomyocyte repopulation. *Dev. Cell* **51**, 503–515 (2019).
161. Marín-Juez, R. et al. Fast revascularization of the injured area is essential to support zebrafish heart regeneration. *Proc. Natl Acad. Sci. USA* **113**, 11237–11242 (2016).
162. Lepilina, A. et al. A dynamic epicardial injury response supports progenitor cell activity during zebrafish heart regeneration. *Cell* **127**, 607–619 (2006).
163. Itou, J. et al. Migration of cardiomyocytes is essential for heart regeneration in zebrafish. *Development* **139**, 4133–4142 (2012).
164. Tapon, N. et al. Salvador promotes both cell cycle exit and apoptosis in drosophila and is mutated in human cancer cell lines. *Cell* **110**, 467–478 (2002).
165. Liu, S. et al. Gene therapy knockdown of Hippo signaling induces cardiomyocyte renewal in pigs after myocardial infarction. *Sci. Transl. Med.* **13**, eabd6892 (2021).
166. Del Re, D. P. et al. Yes-associated protein isoform 1 (Yap1) promotes cardiomyocyte survival and growth to protect against myocardial ischemic injury. *J. Biol. Chem.* **288**, 3977–3988 (2013).
167. von Gise, A. et al. YAP1, the nuclear target of Hippo signaling, stimulates heart growth through cardiomyocyte proliferation but not hypertrophy. *Proc. Natl Acad. Sci. USA* **109**, 2394–2399 (2012).
168. Xin, M. et al. Hippo pathway effector Yap promotes cardiac regeneration. *Proc. Natl. Acad. Sci. USA* **110**, 13839–13844 (2013).
169. Lin, Z. et al. Cardiac-specific YAP activation improves cardiac function and survival in an experimental murine MI model. *Circ. Res.* **115**, 354–363 (2014).
170. Morikawa, Y., Heallen, T., Leach, J., Xiao, Y. & Martin, J. F. Dystrophin-glycoprotein complex sequesters Yap to inhibit cardiomyocyte proliferation. *Nature* **547**, 227–231 (2017).
171. Mia, M. M. & Singh, M. K. The Hippo signaling pathway in cardiac development and diseases. *Front. Cell Dev. Biol.* **7**, 211 (2019).
172. Mia, M. M. et al. Loss of Yap/Taz in cardiac fibroblasts attenuates adverse remodelling and improves cardiac function. *Cardiovasc. Res*. https://doi.org/10.1093/cvr/cvab205 (2021).
173. Xiao, Y. et al. Hippo pathway deletion in adult resting cardiac fibroblasts initiates a cell state transition with spontaneous and self-sustaining fibrosis. *Genes Dev.* **33**, 1491–1505 (2019).
174. Tian, Y. et al. A microRNA-Hippo pathway that promotes cardiomyocyte proliferation and cardiac regeneration in mice. *Sci. Transl. Med.* **7**, 279ra38 (2015).
175. Courtine, G. & Sofroniew, M. V. Spinal cord repair: advances in biology and technology. *Nat. Med.* **25**, 898–908 (2019).
176. Tran, A. P., Warren, P. M. & Silver, J. The biology of regeneration failure and success after spinal cord injury. *Physiol. Rev.* **98**, 881–917 (2018).
177. Hilton, B. J., Moulson, A. J. & Tetzlaff, W. Neuroprotection and secondary damage following spinal cord injury: concepts and methods. *Neurosci. Lett.* **652**, 3–10 (2017).
178. Becker, T., Wullimann, M. F., Becker, C. G., Bernhardt, R. R. & Schachner, M. Axonal regrowth after spinal cord transection in adult zebrafish. *J. Comp. Neurol.* **377**, 577–595 (1997).
179. Becker, C. G. et al. L1.1 is involved in spinal cord regeneration in adult zebrafish. *J. Neurosci.* **24**, 7837–7842 (2004).
180. Becker, T. & Becker, C. G. Dynamic cell interactions allow spinal cord regeneration in zebrafish. *Curr. Opin. Physiol.* **14**, 64–69 (2020).
181. Becker, C. G. & Becker, T. Neuronal regeneration from ependymo-radial glial cells: cook, little pot, cook! *Dev. Cell* **32**, 516–527 (2015).
182. Rasmussen, J. P. & Sagasti, A. Learning to swim, again: axon regeneration in fish. *Exp. Neurol.* **287**, 318–330 (2017).
183. Ghosh, S. & Hui, S. P. Regeneration of zebrafish CNS: adult neurogenesis. *Neural Plast.* **2016**, 5815439 (2016).
184. Reimer, M. M. et al. Motor neuron regeneration in adult zebrafish. *J. Neurosci.* **28**, 8510–8516 (2008).
185. Briona, L. K., Poulain, F. E., Mosimann, C. & Dorsky, R. I. Wnt/ß-catenin signaling is required for radial glial neurogenesis following spinal cord injury. *Dev. Biol.* **403**, 15–21 (2015).
186. Ohnmacht, J. et al. Spinal motor neurons are regenerated after mechanical lesion and genetic ablation in larval zebrafish. *Development* **143**, 1464–1474 (2016).
187. Kuscha, V. et al. Lesion-induced generation of interneuron cell types in specific dorsoventral domains in the spinal cord of adult zebrafish. *J. Comp. Neurol.* **520**, 3604–3616 (2012).
188. Goldshmit, Y. et al. Fgf-dependent glial cell bridges facilitate spinal cord regeneration in Zebrafish. *J. Neurosci.* **32**, 7477–7492 (2012).
189. Yu, Y.-M. et al. The extracellular matrix glycoprotein tenascin-C promotes locomotor recovery after spinal cord injury in adult zebrafish. *Neuroscience* **183**, 238–250 (2011).
190. Wehner, D. et al. Wnt signaling controls pro-regenerative Collagen XII in functional spinal cord regeneration in zebrafish. *Nat. Commun.* **8**, 126 (2017).
191. Gomez-Sanchez, J. A. et al. After nerve injury, lineage tracing shows that myelin and Remak Schwann cells elongate extensively and branch to form repair Schwann cells, which shorten radically on remyelination. *J. Neurosci.* **37**, 9086–9099 (2017).
192. Parrinello, S. et al. EphB signaling directs peripheral nerve regeneration through Sox2-dependent Schwann cell sorting. *Cell* **143**, 145–155 (2010).
193. Klatt Shaw, D. et al. Localized EMT reprograms glial progenitors to promote spinal cord repair. *Dev. Cell* **56**, 613.e7–626.e7(2021).
194. Wilson, M. M., Weinberg, R. A., Lees, J. A. & Guen, V. J. Emerging mechanisms by which EMT programs control stemness. *Trends Cancer* **6**, 775–780 (2020).
195. Ye, X. & Weinberg, R. A. Epithelial-mesenchymal plasticity: a central regulator of cancer progression. *Trends Cell Biol.* **25**, 675–686 (2015).
196. Jessen, K. R. & Arthur-Farraj, P. Repair Schwann cell update: adaptive reprogramming, EMT, and stemness in regenerating nerves. *Glia* **67**, 421–437 (2019).
197. Mokalled, M. H. et al. Injury-induced ctgfa directs glial bridging and spinal cord regeneration in zebrafish. *Science* **354**, 630–634 (2016).
198. Bradbury, E. J. & Burnside, E. R. Moving beyond the glial scar for spinal cord repair. *Nat. Commun.* **10**, 3879 (2019).
199. Hu, R. et al. Glial scar and neuroregeneration: histological, functional, and magnetic resonance imaging analysis in chronic spinal cord injury. *J. Neurosurg.* **13**, 169–180 (2010).
200. Wang, Y. et al. Lentivirus-mediated silencing of the CTGF gene suppresses the formation of glial scar tissue in a rat model of spinal cord injury. *Spine J.* **18**, 164–172 (2018).
201. NIH, U. S. National Library of Medicine. *ClinicalTrials.gov* https://clinicaltrials.gov/ct2/results?cond=&term=ctgf&cntry=&state=&city=&dist (2021).
202. Hamon, A. et al. Linking YAP to Müller glia quiescence exit in the degenerative retina. *Cell Rep.* **27**, 1712–1725 (2019).
203. Hamon, A., Roger, J. E., Yang, X.-J. & Perron, M. Müller glial cell-dependent regeneration of the neural retina: an overview across vertebrate model systems. *Dev. Dyn.* **245**, 727–738 (2016).
204. Rueda, E. M. et al. The Hippo pathway blocks mammalian retinal Müller glial cell reprogramming. *Cell Rep.* **27**, 1637–1649 (2019).
205. Wan, J. & Goldman, D. Retina regeneration in zebrafish. *Curr. Opin. Genet. Dev.* **40**, 41–47 (2016).
206. Bernardos, R. L., Barthel, L. K., Meyers, J. R. & Raymond, P. A. Late-stage neuronal progenitors in the retina are radial Müller glia that function as retinal stem cells. *J. Neurosci.* **27**, 7028–7040 (2007).
207. Thummel, R., Kassen, S. C., Montgomery, J. E., Enright, J. M. & Hyde, D. R. Inhibition of Müller glial cell division blocks regeneration of the light-damaged zebrafish retina. *Dev. Neurobiol.* **68**, 492–408 (2008).

208. Hoang, T. et al. Gene regulatory networks controlling vertebrate retinal regeneration. *Science* **370**, eabb8598 (2020).
209. Richeldi, L. et al. Pamrevlumab, an anti-connective tissue growth factor therapy, for idiopathic pulmonary fibrosis (PRAISE): a phase 2, randomised, double-blind, placebo-controlled trial. *Lancet Respir. Med.* **8**, 25–33 (2020).
210. Raghu, G. et al. FG-3019 anti-connective tissue growth factor monoclonal antibody: results of an open-label clinical trial in idiopathic pulmonary fibrosis. *Eur. Respir. J.* **47**, 1481–1491 (2016).
211. Ramazani, Y. et al. Connective tissue growth factor (CTGF) from basics to clinics. *Matrx Biol.* **68–69**, 44–66 (2018).
212. Azevedo, A. S., Grotek, B., Jacinto, A., Weidinger, G. & Saúde, L. The regenerative capacity of the zebrafish caudal fin is not affected by repeated amputations. *PLoS One* **6**, e22820 (2011).
213. Broussonet, M. Observations sur la regeneration de quelques parties du corps des poissons. *Hist. d. l'Acad. R. des Sci.* **105**, 625–641 (1786).
214. Morgan, T. H. *Regeneration* (Macmillan, 1901).
215. Morgan, T. H. Regeneration in teleosts. *Arch. f.ür. Entwickslungsmech Org.* **10**, 120–131 (1900).
216. Sunderland, M. E. Regeneration: Thomas hunt Morgan's window into development. *J. Hist. Biol.* **43**, 325–361 (2010).
217. Pfefferli, C. & Jazwinska, A. The art of fin regeneration in zebrafish. *Regeneration* **2**, 72–83 (2015).
218. Cao, X., Pfaff, S. L. & Gage, F. H. YAP regulates neural progenitor cell number via the TEA domain transcription factor. *Genes Dev.* **22**, 3320–3334 (2008).
219. Panciera, T. et al. Induction of expandable tissue-specific stem/progenitor cells through transient expression of YAP/TAZ. *Cell Stem Cell* **19**, 725–737 (2016).
220. Patel, S. H., Camargo, F. D. & Yimlamai, D. Hippo signaling in the liver regulates organ size, cell fate, and carcinogenesis. *Gastroenterology* **152**, 533–545 (2017).
221. Camargo, F. D. et al. YAP1 increases organ size and expands undifferentiated progenitor cells. *Curr. Biol.* **17**, 2054–2060 (2007).
222. Karpowicz, P., Perez, J. & Perrimon, N. The Hippo tumor suppressor pathway regulates intestinal stem cell regeneration. *Development* **138**, 4135–4145 (2010).
223. Mo, J.-S., Park, H. W. & Guan, K.-L. The Hippo signaling pathway in stem cell biology and cancer. *EMBO Rep.* **15**, 642–656 (2014).
224. Lian, I. et al. The role of YAP transcription coactivator in regulating stem cell self-renewal and differentiation. *Genes Dev.* **24**, 1106–1118 (2010).
225. Hasegawa, T. et al. Transient inflammatory response mediated by interleukin-1β is required for proper regeneration in zebrafish fin fold. *Elife* **6**, e22716 (2017).
226. Li, J. et al. Expression analysis of Hsp90α and cytokines in zebrafish caudal fin regeneration. *Dev. Comp. Immunol.* **116**, 103922 (2021).
227. Nguyen-Chi, M. et al. TNF signaling and macrophages govern fin regeneration in zebrafish larvae. *Cell Death Dis.* **8**, e2979 (2017).
228. Tornini, V. A. et al. Live monitoring of Blastemal cell contributions during appendage regeneration. *Curr. Biol.* **26**, 2981–2991 (2016).
229. Lee, Y., Grill, S., Sanchez, A., Murphy-Ryan, M. & Poss, K. D. Fgf signaling instructs position-dependent growth rate during zebrafish fin regeneration. *Development* **132**, 5173–5183 (2005).
230. Shibata, E., Liu, Z., Kawasaki, T., Sakai, N. & Kawakami, A. Robust and local positional information within a fin ray directs fin length during zebrafish regeneration. *Dev. Growth, Differ.* **60**, 354–364 (2018).
231. Nechiporuk, A. & Keating, M. T. A proliferation gradient between proximal and msxb-expressing distal blastema directs zebrafish fin regeneration. *Development* **129**, 2607–2617 (2002).
232. Mateus, R. et al. Control of tissue growth by Yap relies on cell density and F-actin in zebrafish fin regeneration. *J. Cell Sci.* **128**, e1.2–e1.2 (2015).
233. Brandão, A. S. et al. Yap induces osteoblast differentiation by modulating Bmp signalling during zebrafish caudal fin regeneration. *J. Cell Sci.* **132**, jcs231993 (2019).
234. Moro, A. et al. MicroRNA-dependent regulation of biomechanical genes establishes tissue stiffness homeostasis. *Nat. Cell Biol.* **21**, 348–358 (2019).
235. Stewart, S. & Stankunas, K. Limited dedifferentiation provides replacement tissue during zebrafish fin regeneration. *Dev. Biol.* **365**, 339–349 (2012).
236. Tu, S. & Johnson, S. L. Fate restriction in the growing and regenerating zebrafish fin. *Dev. Cell* **20**, 725–732 (2011).
237. Knopf, F. et al. Bone regenerates via dedifferentiation of osteoblasts in the zebrafish fin. *Dev. Cell* **20**, 713–724 (2011).
238. Sousa, S. et al. Differentiated skeletal cells contribute to blastema formation during zebrafish fin regeneration. *Development* **138**, 3897–3905 (2011).
239. Stewart, S., Gomez, A. W., Armstrong, B. E., Henner, A. & Stankunas, K. Sequential and opposing activities of Wnt and BMP coordinate zebrafish bone regeneration. *Cell Rep.* **6**, 482–498 (2014).
240. Smith, A., Avaron, F., Guay, D., Padhi, B. K. & Akimenko, M. A. Inhibition of BMP signaling during zebrafish fin regeneration disrupts fin growth and scleroblast differentiation and function. *Dev. Biol.* **299**, 438–454 (2006).
241. Murciano, C. et al. Ray–interray interactions during fin regeneration of Danio rerio. *Dev. Biol.* **252**, 214–224 (2002).
242. Halder, G., Dupont, S. & Piccolo, S. Transduction of mechanical and cytoskeletal cues by YAP and TAZ. *Nat. Rev. Mol. Cell Biol.* **13**, 591–600 (2012).
243. Luo, Q. et al. Connective tissue growth factor (CTGF) is regulated by Wnt and bone morphogenetic proteins signaling in osteoblast differentiation of mesenchymal stem cells. *J. Biol. Chem.* **279**, 55958–55968 (2004).
244. Kegelman, C. D. et al. Skeletal cell YAP and TAZ combinatorially promote bone development. *FASEB J.* **32**, 2706–2721 (2018).
245. Pan, J.-X. et al. YAP promotes osteogenesis and suppresses adipogenic differentiation by regulating β-catenin signaling. *Bone Res.* **6**, 18 (2018).
246. Seo, E. et al. SOX2 regulates YAP1 to maintain stemness and determine cell fate in the osteo-adipo lineage. *Cell Rep.* **3**, 2075–2087 (2013).
247. Xiong, J., Almeida, M. & O'Brien, C. A. The YAP/TAZ transcriptional co-activators have opposing effects at different stages of osteoblast differentiation. *Bone* **112**, 1–9 (2018).
248. Rinkevich, Y., Lindau, P., Ueno, H., Longaker, M. T. & Weissman, I. L. Germ-layer and lineage-restricted stem/progenitors regenerate the mouse digit tip. *Nature* **476**, 409–414 (2011).
249. Grusche, F. A., Degoutin, J. L., Richardson, H. E. & Harvey, K. F. The Salvador/Warts/Hippo pathway controls regenerative tissue growth in Drosophila melanogaster. *Dev. Biol.* **350**, 255–266 (2011).
250. Nuñez, V. A. et al. Postembryonic development of the posterior lateral line in the zebrafish. *Evol. Dev.* **11**, 391–404 (2009).
251. Alexandre, D. & Ghysen, A. Somatotopy of the lateral line projection in larval zebrafish. *Proc. Natl. Acad. Sci. USA* **96**, 7558–7562 (1999).
252. Ledent, V. Postembryonic development of the posterior lateral line in zebrafish. *Development* **129**, 597–604 (2002).
253. Sarrazin, A. F., Nuñez, V. A., Sapède, D., Tassin, V. & Dambly-Chaudière, C. Origin and early development of the posterior lateral line system of zebrafish. *J. Neurosci.* **30**, 8234–8244 (2010).
254. Lush, M. E. & Piotrowski, T. Sensory hair cell regeneration in the zebrafish lateral line. *Dev. Dyn.* **243**, 1187–1202 (2014).
255. Lecaudey, V., Cakan-Akdogan, G., Norton, W. H. J. & Gilmour, D. Dynamic Fgf signaling couples morphogenesis and migration in the zebrafish lateral line primordium. *Development* **135**, 2695–2705 (2008).
256. Atkinson, P. J., Huarcaya Najarro, E., Sayyid, Z. N. & Cheng, A. G. Sensory hair cell development and regeneration: similarities and differences. *Development* **142**, 1561–1571 (2015).
257. Kim, N.-G., Koh, E., Chen, X. & Gumbiner, B. M. E-cadherin mediates contact inhibition of proliferation through Hippo signaling-pathway components. *Proc. Natl. Acad. Sci. USA* **108**, 11930–11935 (2011).
258. Benham-Pyle, B. W., Pruitt, B. L. & Nelson, W. J. Mechanical strain induces E-cadherin-dependent Yap1 and β-catenin activation to drive cell cycle entry. *Science* **348**, 1024–1027 (2015).
259. Kozlovskaja-Gumbriene, A. et al. Proliferation-independent regulation of organ size by Fgf/Notch signaling. *Elife* **6**, e21049 (2017).
260. Loh, S. L. et al. Zebrafish yap1 plays a role in differentiation of hair cells in posterior lateral line. *Sci. Rep.* **4**, 1–9 (2014).
261. Agarwala, S. et al. Amotl2a interacts with the Hippo effector Yap1 and the Wnt/β-catenin effector Lef1 to control tissue size in zebrafish. *Elife* **4**, e08201 (2015).
262. Wang, X. et al. Lpar2b controls lateral line tissue size by regulating Yap1 activity in zebrafish. *Front. Mol. Neurosci.* **11**, 34 (2018).
263. Pistocchi, A. et al. The zebrafish prospero homolog prox1 is required for mechanosensory hair cell differentiation and functionality in the lateral line. *BMC Dev. Biol.* **9**, 58 (2009).
264. Yung, Y. C., Stoddard, N. C. & Chun, J. LPA receptor signaling: pharmacology, physiology, and pathophysiology. *J. Lipid Res.* **55**, 1192–1214 (2014).
265. Yu, F.-X. et al. Regulation of the Hippo-YAP pathway by G-protein-coupled receptor signaling. *Cell* **150**, 780–791 (2012).
266. Okudaira, S., Yukiura, H. & Aoki, J. Biological roles of lysophosphatidic acid signaling through its production by autotaxin. *Biochimie* **92**, 698–706 (2010).
267. Lai, S.-L. et al. Autotaxin/Lpar3 signaling regulates Kupffer's vesicle formation and left-right asymmetry in zebrafish. *Development* **139**, 4439–4448 (2012).
268. Frisca, F. et al. Role of ectonucleotide pyrophosphatase/phosphodiesterase 2 in the midline axis formation of zebrafish. *Nature* **6**, 37678 (2016).
269. Yukiura, H. et al. Autotaxin regulates vascular development via multiple Lysophosphatidic Acid (LPA) receptors in zebrafish. *J. Biol. Chem.* **286**, 43972–43983 (2011).
270. Lee, S.-J. et al. LPA1 is essential for lymphatic vessel development in zebrafish. *FASEB J.* **22**, 3706–3715 (2008).
271. Stone, L. S. The development of lateral-line sense organs in amphibians observed in living and vital-stained preparations. *J. Comp. Neurol.* **57**, 507–540 (1933).
272. Stone, L. S. Further experimental studies of the development of lateral-line sense organs in amphibians observed in living preparations. *J. Comp. Neurol.* **68**, 83–115 (1937).

273. Dijkgraaf, S. The functional and significance of the lateral-line organs. *Biol. Rev.* **38**, 51–105 (1962).
274. Ma, E. Y., Rubel, E. W. & Raible, D. W. Notch signaling regulates the extent of hair cell regeneration in the zebrafish lateral line. *J. Neurosci.* **28**, 2261–2273 (2008).
275. Namdaran, P., Reinhart, K. E., Owens, K. N., Raible, D. W. & Rubel, E. W. Identification of modulators of hair cell regeneration in the zebrafish lateral line. *J. Neurosci.* **32**, 3516–3528 (2012).
276. López-Schier, H. & Hudspeth, A. J. A two-step mechanism underlies the planar polarization of regenerating sensory hair cells. *Proc. Natl. Acad. Sci. USA* **103**, 18615–18620 (2006).
277. Ye, Z. et al. Yap-lin28a axis targets let7-Wnt pathway to restore progenitors for initiating regeneration. *Elife* **9**, e55771 (2020).
278. Aman, A. & Piotrowski, T. Wnt/β-catenin and Fgf signaling control collective cell migration by restricting chemokine receptor expression. *Dev. Cell* **15**, 749–761 (2008).
279. Jiang, L., Romero-Carvajal, A., Haug, J. S., Seidel, C. W. & Piotrowski, T. Gene-expression analysis of hair cell regeneration in the zebrafish lateral line. *Proc. Natl. Acad. Sci. USA* **111**, E1383–E1392 (2014). https://doi.org/10.1073/pnas.1402898111
280. Giffen, K. P., Liu, H., Kramer, K. L. & He, D. Z. Expression of protein-coding gene orthologs in zebrafish and mouse inner ear non-sensory supporting cells. *Front. Neurosci.* **13**, 1117 (2019).
281. Jin, J. et al. Evidence that Lin28 stimulates translation by recruiting RNA helicase A to polysomes. *Nucleic Acids Res.* **39**, 3724–3734 (2011).
282. Yu, J. et al. Induced pluripotent stem cell lines derived from human somatic cells. *Sci. (80-.)* **318**, 1917–1920 (2007).
283. Zhang, J. et al. LIN28 regulates stem cell metabolism and conversion to primed pluripotency. *Cell Stem Cell* **19**, 66–80 (2016).
284. Golden, E. J., Benito-Gonzalez, A. & Doetzlhofer, A. The RNA-binding protein LIN28B regulates developmental timing in the mammalian cochlea. *Proc. Natl. Acad. Sci. USA* **112**, E3864–E3873 (2015).
285. Ramachandran, R., Fausett, B. V. & Goldman, D. Ascl1a regulates Müller glia dedifferentiation and retinal regeneration through a Lin-28-dependent, let-7 microRNA signalling pathway. *Nat. Cell Biol.* **12**, 1101–1107 (2010).
286. Corey, D. P. et al. TRPA1 is a candidate for the mechanosensitive transduction channel of vertebrate hair cells. *Nature* **432**, 723–730 (2004).
287. Siemens, J. et al. Cadherin 23 is a component of the tip link in hair-cell stereocilia. *Nature* **428**, 950–955 (2004).
288. Söllner, C. et al. Mutations in cadherin 23 affect tip links in zebrafish sensory hair cells. *Nature* **428**, 955–959 (2004).
289. Santos, F., Macdonald, G., Rubel, E. W. & Raible, D. W. Lateral line hair cell maturation is a determinant of aminoglycoside susceptibility in zebrafish (Danio rerio). *Hear. Res.* **213**, 25–33 (2006).
290. Buck, L. M. J., Winter, M. J., Redfern, W. S. & Whit, T. T. Ototoxin-induced cellular damage in neuromasts disrupts lateral line function in larval zebra fish. *Hear. Res.* **284**, 67–81 (2012).
291. Forbes, S. J. & Newsome, P. N. Liver regeneration—mechanisms and models to clinical application. *Nat. Rev. Gastroenterol. Hepatol.* **13**, 473–485 (2016).
292. Wang, S., Miller, S. R., Ober, E. A. & Sadler, K. C. Making it new again: insight into liver development, regeneration, and disease from zebrafish. *Curr. Top. Dev. Biol.* 124, 161–195 (2017).
293. Wang, C. et al. Differences in Yes-associated protein and mRNA levels in regenerating liver and hepatocellular carcinoma. *Mol. Med. Rep.* **5**, 410–414 (2012).
294. Grijalva, J. L. et al. Dynamic alterations in Hippo signaling pathway and YAP activation during liver regeneration. *Am. J. Physiol. Gastrointest. Liver Physiol.* **307**, G196–G204 (2014).
295. Bai, H. et al. Yes-associated protein regulates the hepatic response after bile duct ligation. *Hepatology* **56**, 1097–1107 (2012).
296. Aloia, L. et al. Epigenetic remodelling licences adult cholangiocytes for organoid formation and liver regeneration. *Nat. Cell Biol.* **21**, 1321–1333 (2019).
297. Li, W. et al. A homeostatic arid1a-dependent permissive chromatin state licenses hepatocyte responsiveness to liver-injury-associated YAP signaling. *Cell Stem Cell* **25**, 54–68 (2019).
298. Dong, J. et al. Elucidation of a universal size-control mechanism in Drosophila and mammals. *Cell* **130**, 1120–1133 (2007).
299. Sadler, K. C., Amsterdam, A., Soroka, C., Boyer, J. & Hopkins, N. A genetic screen in zebrafish identifies the mutants vps18, nf2 and foie gras as models of liver disease. *Development* **132**, 3561–3572 (2005).
300. Cox, A. G. et al. Yap reprograms glutamine metabolism to increase nucleotide biosynthesis and enable liver growth. *Nat. Cell Biol.* **18**, 886–896 (2016).
301. Brandt, Z. J., Echert, A. E., Bostrom, J. R., North, P. N. & Link, B. A. Core Hippo pathway components act as a brake on Yap/Taz in the development and maintenance of the biliary network. *Development* **4**, dev.184242 (2020).
302. Driskill, J. H. & Pan, D. The Hippo pathway in liver homeostasis and pathophysiology. *Annu. Rev. Pathol. Mech. Dis.* **16**, 299–322 (2021).
303. Yimlamai, D. et al. Hippo pathway activity influences liver cell fate. *Cell* **157**, 1324–1338 (2014).
304. Molina, L. M. et al. Compensatory hepatic adaptation accompanies permanent absence of intrahepatic biliary network due to YAP1 loss in liver progenitors. *Cell Rep.* **36**, 109310 (2021).
305. Verboven, E. et al. Regeneration defects in Yap and Taz mutant mouse livers are caused by bile duct disruption and cholestasis. *Gastroenterology* **160**, 847–862 (2021).
306. MacCarthy-Morrogh, L. & Martin, P. The hallmarks of cancer are also the hallmarks of wound healing. *Sci. Signal.* **13**, eaay8690 (2020).
307. Moroishi, T., Gram Hansen, C. & Guan, K.-L. The emerging roles of YAP and TAZ in cancer. *Nat. Rev. Cancer* **15**, 73–79 (2015).
308. Johnson, R. & Halder, G. The two faces of Hippo: targeting the Hippo pathway for regenerative medicine and cancer treatment. *Nat. Rev. Drug Discov.* **13**, 63–79 (2014).
309. Merkes, C. et al. Ewing sarcoma Ewsa protein regulates chondrogenesis of Meckel's Cartilage through modulation of Sox9 in zebrafish. *PLoS One* **10**, e0116627 (2015).
310. Mayrhofer, M. et al. A novel brain tumour model in zebrafish reveals the role of YAP activation in MAPK- and PI3K-induced malignant growth. *Dis. Model. Mech.* **10**, 15–28 (2017).
311. Brandt, Z. J., North, P. N. & Link, B. A. Somatic mutations of lats2 cause peripheral nerve sheath tumors in zebrafish. *Cells* **8**, 972 (2019).

ACKNOWLEDGEMENTS

Work ongoing in the Gram Hansen lab is supported by a University of Edinburgh Chancellor's Fellowship as well as by Worldwide Cancer Research (19-0238) and LifeArc-CSO. Additional funding has been obtained from the Bone Cancer Research Trust (BCRT), Sarcoma UK (SUK202.2016), the Wellcome Trust-University of Edinburgh Institutional Strategic Support Fund (ISSF3). Y.F. received a Wellcome Trust Sir Henry Dale Fellowship (100104/Z/12/Z); Cancer Research UK early detection project award (C38363/A26931) and a Cancer Research UK pioneering award (C38363/A25107). S.E.R. is funded by a Wellcome Trust PhD studentship [108906/Z/15/Z]. Figures, besides Fig. 1, created in Adobe Illustrator.

AUTHOR CONTRIBUTIONS

S.E.R. and C.G.H. drafted the manuscript. S.E.R., Y.F., and C.G.H. revised the manuscript. C.G.H. and Y.F. supervised the project. S.E.R. prepared the figures.

COMPETING INTERESTS

The authors declare no competing interests.

ADDITIONAL INFORMATION

Correspondence and requests for materials should be addressed to Carsten Gram Hansen.

Reprints and permission information is available at http://www.nature.com/reprints

Publisher's note Springer Nature remains neutral with regard to jurisdictional claims in published maps and institutional affiliations.

Open Access This article is licensed under a Creative Commons Attribution 4.0 International License, which permits use, sharing, adaptation, distribution and reproduction in any medium or format, as long as you give appropriate credit to the original author(s) and the source, provide a link to the Creative Commons license, and indicate if changes were made. The images or other third party material in this article are included in the article's Creative Commons license, unless indicated otherwise in a credit line to the material. If material is not included in the article's Creative Commons license and your intended use is not permitted by statutory regulation or exceeds the permitted use, you will need to obtain permission directly from the copyright holder. To view a copy of this license, visit http://creativecommons.org/licenses/by/4.0/.

© The Author(s) 2022